

# CLINICAL AND EXPERIMENTAL OPTOMETRY

SPECIAL ISSUE **VISUAL OPTICS: LOOKING BEYOND 2020**

**Modern spectacle lens design**  
**Stand magnifiers for low vision**  
**Multifocal optics**  
**Aberration-controlling lenses for keratoconus**  
**Optical changes with orthokeratology**  
**Optical regulation of eye growth**  
**Aberrations and refractive error development**  
**Peripheral refraction and aberrations**  
**Aberrations and accommodation**  
**Blur adaptation**  
**Adaptive optics vascular imaging**  
**Orthokeratology compression factor**

Official Journal of:



The Hong Kong Society of  
Professional Optometrists



NEW ZEALAND ASSOCIATION  
OF OPTOMETRISTS INC.



SINGAPORE OPTOMETRIC ASSOCIATION

**Impact Factor:** 1.559 ISI Journal Citation Reports®  
Ranking: 2018: 40/59 (Ophthalmology)

**Aims and Scope:** *Clinical and Experimental Optometry* is a peer reviewed journal listed by ISI and abstracted by PubMed, Science Citation Index and Current Contents. It publishes original research papers and reviews in clinical optometry and vision science. Debate and discussion of controversial scientific and clinical issues is encouraged and letters to the Editor and short communications expressing points of view on matters within the Journal's areas of interest are welcome. *Clinical and Experimental Optometry* also welcomes papers that explore the history of optometry and vision science.

**OnlineOpen:** *Clinical and Experimental Optometry* accepts articles for Open Access publication. Please visit <https://authorservices.wiley.com/author-resources/Journal-Authors/open-access/onlineopen.html> for further information about OnlineOpen.

**Address for Editorial Correspondence:**

Editor, *Clinical and Experimental Optometry*,  
Suite 101, 68–72 York Street, South Melbourne,  
Victoria 3205, Australia. E-mail: [cxo.editor@optometry.org.au](mailto:cxo.editor@optometry.org.au); Tel: +61 3 9668 8500;  
Fax: +61 3 9682 0928.

**Disclaimer:** The Publisher, Optometry Australia (OA), New Zealand Association of Optometrists (NZAO), Hong Kong Society of Professional Optometrists (HKSP), Singapore Optometric Association (SOA) and Editor cannot be held responsible for errors or any consequences arising from the use of information contained in this journal; the views and opinions expressed do not necessarily reflect those of the Publisher, OA, NZAO, HKSP, SOA and Editor, neither does the publication of advertisements constitute any endorsement by the Publisher, OA, NZAO, HKSP, SOA and Editor of the products advertised.

**Copyright © 2020 Optometry Australia**

Wiley is a founding member of the UN-backed HINARI, AGORA, and OARE initiatives. They are now collectively known as Research4Life, making online scientific content available free or at nominal cost to researchers in developing countries. Please visit Wiley's Content Access – Corporate Citizenship site: <http://www.wiley.com/WileyCDA/Section/id-390082.html>.

ISSN 0816-4622 (Print)  
ISSN 1444-0938 (Online)

Cover image: Lisa Breayley, MedPIC,  
The Royal Victorian Eye and Ear Hospital

**EDITOR**

Emeritus Professor Nathan Efron AC

**DEPUTY EDITOR**

Dr Maria Markoulli

**EDITORIAL BOARD**

Associate Professor Nicola Anstice  
(Associate Editor)  
University of Canberra, Australia

Dr Lauren Ayton (Associate Editor)  
The University of Melbourne, Australia

Dr Alex Black (Associate Editor)  
Queensland University of Technology,  
Australia

Dr Mei-Ying Boon (Associate Editor)  
University of New South Wales, Australia

Ms Lyn Brodie  
Optometry Australia, Australia

Associate Professor Bang Bui  
(Associate Editor)  
The University of Melbourne, Australia

Dr Andrew Carkeet (Associate Editor)  
Queensland University of Technology,  
Australia

Dr Nicole Carnt (Associate Editor)  
University of New South Wales, Australia

Dr Holly Chinnery (Associate Editor)  
The University of Melbourne, Australia

Emeritus Professor H Barry Collin AM  
(Emeritus Editor)  
University of New South Wales, Australia

Dr Cirous Dehghani (Associate Editor)  
The University of Melbourne, Australia

Dr Laura Downie (Associate Editor)  
The University of Melbourne, Australia

Dr Katie Edwards (Associate Editor)  
Queensland University of Technology,  
Australia

Emeritus Professor Nathan Efron AC  
(Editor and Chairman)  
Queensland University of Technology,  
Australia

Dr Lesley Frederikson  
New Zealand Association of Optometrists,  
New Zealand

Associate Professor Ian Gutteridge  
(Associate Editor)  
The University of Melbourne, Australia

Associate Professor Isabelle Jalbert  
(Associate Editor)  
University of New South Wales, Australia

Associate Professor Andrew Lam  
Hong Kong Polytechnic University, Hong  
Kong SAR, China

Dr Angelica Ly  
University of New South Wales, Australia

Associate Professor Michele Madigan  
(Associate Editor)  
University of New South Wales, Australia

Dr Maria Markoulli (Deputy Editor)  
University of New South Wales, Australia

Dr Lisa Nivison-Smith (Associate Editor)  
University of New South Wales, Australia

Dr Nicola Pritchard (Associate Editor)  
Queensland University of Technology,  
Australia

Dr Kah Ooi Tan  
Singapore Optometric Association, Singapore

Dr Phil Turnbull (Associate Editor)  
The University of Auckland, New Zealand

Associate Professor Stephen Vincent  
(Associate Editor)  
Queensland University of Technology,  
Australia

**INTERNATIONAL ADVISORY BOARD**

Dr Waleed AlGhamdi  
Qassim University, Saudi Arabia

Professor Raymond Applegate  
University of Houston, USA

Associate Professor Reiko Arita  
University of Tokyo, Japan

Professor David Atchison  
Queensland University of Technology,  
Australia

Professor Sharon Bentley  
Queensland University of Technology,  
Australia

Dr Paul Constable  
Flinders University, Australia

Professor Stephen Dain  
University of New South Wales, Australia

Professor Steven Dakin  
The University of Auckland, New Zealand

Professor Erica Fletcher  
The University of Melbourne, Australia

Professor Alex Gentle  
Deakin University, Australia

Professor Robert F Hess  
McGill University, Canada

Professor Michael Ibbotson  
National Vision Research Institute, Australia

Professor Michael Kalloniatis  
Centre for Eye Health, Australia

Professor Lisa Keay  
University of New South Wales, Australia

Professor Allison McKendrick  
The University of Melbourne, Australia

Professor Eric Papas  
University of New South Wales, Australia

Dr Konrad Pesudovs  
Optometry consultant, South Australia

Professor Jacob Sivak  
University of Waterloo, Canada

Professor Fiona Stapleton  
University of New South Wales, Australia

Professor Chi-ho To  
Hong Kong Polytechnic University, Hong  
Kong SAR, China

Professor James Wolffsohn  
Aston University, United Kingdom

Publications Manager: Jessica Donald

## Looking and seeing beyond 2020

*Clin Exp Optom* 2020; 103: 1–2

DOI:10.1111/cxo.12993

**Stephen J Vincent**  PhD

**Scott A Read**  PhD

Contact Lens and Visual Optics Laboratory, School of Optometry and Vision Science, Queensland University of Technology, Brisbane, Australia  
E-mail: sj.vincent@qut.edu.au

Submitted: 7 October 2019

Accepted for publication: 8 October 2019

The inaugural issue of *Clinical and Experimental Optometry* (then *The Commonwealth Optometrist*), ran to a grand total of 12 pages. While a modest beginning, this first publication provides important insights into the state of our profession in the early twentieth century. For example, the first issue published in March 1919 included a brief note,<sup>1</sup> directed at optometrists, explaining the correct pronunciation of the word 'Optometry'; *'...emphasis should be put on the second syllable 'tom'... pronunciation should be universal, so as not to confuse the public.'*

In an era of restricted scope of practice, prior to gaining access to diagnostic and therapeutic agents or even legislation to protect the public and define the profession,<sup>2</sup> it is perhaps not surprising that optical matters predominated this first issue of the journal. Included under the banner heading *'Visual Optics'* was an overview of clinical techniques employed during subjective refraction,<sup>3</sup> still utilised to this day, such as gradual fogging to relax accommodation in the latent hyperope. Here the author emphasised the importance of practitioners having a clear understanding of both the qualitative and quantitative effects of imposed defocus upon the visual system: *'We must know what effects should result from the application of certain lenses under certain conditions and check up our diagnosis thereby.'*

Another section titled *'Practical Optics'* included an homage of sorts to the 'Kryptok'<sup>a</sup> –

a combination bifocal consisting of a flint glass inset of higher refractive index embedded within a crown glass spectacle lens.<sup>4</sup> While our scope of practice has expanded substantially over the past century from sight testing opticians to primary health-care providers, optics remains at the heart of the optometric profession. In this special issue of *Clinical and Experimental Optometry*, international leaders critically examine the current state of the field, encompassing recent advances in ophthalmic and physiological optics, with an eye to the future, beyond 2020.

In contrast to the Kryptok of 1919, Jalie<sup>5</sup> (a name synonymous with ophthalmic optics) reviews modern spectacle lens designs including free-form manufacturing techniques to minimise the visual impact of spectacle lens aberrations. Carkeet<sup>6</sup> also examines the optics of stand magnifiers, a commonly prescribed low vision aid despite significant advances in electronic devices in recent years.<sup>7</sup> A novel method utilising digital photography to determine the equivalent viewing distance of stand magnifiers is also described.

In recent years, a range of new contact lens designs have emerged for the correction of presbyopia, irregular corneal astigmatism, and for the control of childhood myopia. Kolbaum and Bradley<sup>8</sup> tackle the often clinically challenging task of providing clear vision over a range of vergence demands in presbyopic patients and examine the strengths and limitations of the different strategies used to generate multifocal optics. Another technically challenging optical correction in contact lens practice is minimising the visual sequelae of elevated higher order aberrations in keratoconic eyes despite optimal standard contact lens correction. Jinabhai<sup>9</sup> reviews experimental approaches and commercially available customised contact lens solutions to address this issue including customised wavefront-guided soft and scleral contact lenses.

While it is now well accepted that overnight orthokeratology treatment significantly slows

myopia progression in children,<sup>10</sup> the underlying optical mechanism remains unclear. Nti and Berntsen<sup>11</sup> review the optics of modern overnight reverse geometry orthokeratology lens designs including their effects on accommodation, peripheral refraction and on axis higher order aberrations. Lau et al.<sup>12</sup> also report on the change in the higher order aberration profile by modifying the Jessen factor in paediatric orthokeratology for myopia control.

Given the well-documented increase in the prevalence of myopia over the past century, understanding the optical effects of potential interventions to slow myopia progression and axial eye growth in children is a current global research priority. Chakraborty et al.<sup>13</sup> provide a detailed overview of the animal model literature examining how optical factors influence eye growth. The contributions of this body of work to the current understanding of how visual experience influences myopia development and progression, and the translation into interventions to control myopia in the human eye are discussed. Hughes et al.<sup>14</sup> examine the potential role of higher order aberrations upon eye growth with respect to myopia development and control through both optical and pharmaceutical interventions in humans.

In parallel with technological advances in manufacturing, our understanding of the natural optics of the eye and the visual effects of optical corrections has continued to evolve. Romashchenko et al.<sup>15</sup> analyse data from over 2,000 eyes and describe in detail the change in refraction, higher order aberrations, and image quality across the visual field. Del Aguila-Carrasco et al.<sup>16</sup> review work examining the changes in higher order aberrations associated with accommodation, and reciprocally, the changes in the accommodation response when specific higher order aberrations are manipulated. Cufflin and Mallen<sup>17</sup> also investigate the adaptive changes in the visual system in response to imposed blur. These papers are particularly relevant to optical interventions

<sup>a</sup>A derivation of the Greek "Kryptos" meaning hidden or secret.

designed to manipulate the visual experience and slow eye growth in children which alter peripheral refraction, higher order aberrations, visual quality and potentially the accommodation response.

While a century ago, the examination of the posterior eye was exclusively the remit of the ocularist (ophthalmologist), significant developments in ocular imaging now allow vision scientists to examine the retina non-invasively with exquisite detail, to the level of individual photoreceptors. Bedggood and Metha<sup>18</sup> describe the current state of adaptive optics imaging to visualise both the structure and function of the microvasculature of the retina, and how this technology can influence clinical practice for a range of systemic diseases such as diabetes, stroke, and dementia.

Advances in our understanding of visual optics and numerous research discoveries and developments have changed the practice of optometry over the past century. Practitioners now have a wide range of state-of-the-art optical solutions available to

correct simple ametropia, and in the case of childhood myopia, control its progression. New contact lens technologies are also improving visual outcomes for patients with irregular corneal astigmatism, and adaptive optics continues to expand our knowledge of the visual system, with the potential for more widespread clinical impact in years to come. In 2020 and beyond, visual optics will no doubt remain the cornerstone of the optometric profession.

#### REFERENCES

1. Optometry. *Commonwealth Optom* 1919; 1: 6.
2. Vincent SJ. Sydney barber Josiah Skertchly (1850-1926): scientist, educator and advocate for Queensland optometry. *Clin Exp Optom* 2017; 100: 402-406.
3. Cumberland JK. Subjective sight-testing. *Commonwealth Optom* 1919; 1: 7-8.
4. The Kryptok. *Commonwealth Optom* 1919; 1: 5-6.
5. Jalie M. Modern spectacle lens design. *Clin Exp Optom* 2020; 103: 3-10.
6. Carkeet A. Stand magnifiers for low vision: description, prescription, assessment. *Clin Exp Optom* 2020; 103: 11-20.
7. Chong MF, Jackson AJ, Wolffsohn JS et al. An update on the characteristics of patients attending the Kooyong low vision clinic. *Clin Exp Optom* 2016; 99: 555-558.
8. Kollbaum PS, Bradley A. Correction of presbyopia: old problems with old (and new) solutions. *Clin Exp Optom* 2020; 103: 21-30.
9. Jinabhai AN. Customised aberration-controlling corrections for keratoconic patients using contact lenses. *Clin Exp Optom* 2020; 103: 31-43.
10. Cho P, Tan Q. Myopia and orthokeratology for myopia control. *Clin Exp Optom* 2019; 102: 364-377.
11. Nti AN, Berntsen DA. Optical changes and visual performance with orthokeratology. *Clin Exp Optom* 2020; 103: 44-54.
12. Lau JK, Vincent SJ, Cheung SW et al. The influence of orthokeratology compression factor on ocular higher-order aberrations. *Clin Exp Optom* 2020; 103: 123-128.
13. Chakraborty R, Ostrin LA, Benavente-Perez A et al. Optical mechanisms regulating emmetropisation and refractive errors: evidence from animal models. *Clin Exp Optom* 2020; 103: 55-67.
14. Hughes RPJ, Vincent SJ, Read SA et al. Higher order aberrations, refractive error development and myopia control: a review. *Clin Exp Optom* 2020; 103: 68-85.
15. Romashchenko D, Rosen R, Lundstrom L. Peripheral refraction and higher order aberrations. *Clin Exp Optom* 2020; 103: 86-94.
16. Del Aguila-Carrasco AJ, Kruger PB, Lara F et al. Aberrations and accommodation. *Clin Exp Optom* 2020; 103: 95-103.
17. Cufflin MP, Mallen EAH. Blur adaptation: clinical and refractive considerations. *Clin Exp Optom* 2020; 103: 104-111.
18. Bedggood P, Metha A. Adaptive optics imaging of the retinal microvasculature. *Clin Exp Optom* 2020; 103: 112-122.

## Modern spectacle lens design

*Clin Exp Optom* 2020; 103: 3–10

DOI:10.1111/cxo.12930

**Mohammed Jalie** DSc SMSA FBDO (Hons)  
SLD HonFCOptom HonFCGI MCIM

Department of Biomedical Science, Ulster University,  
Coleraine, Northern Ireland, UK  
E-mail: mojalie@aol.com

Ophthalmic lens design concerns the control of spectacle lens aberrations which occur when the eye rotates away from the optical centre of the lens. The most significant aberrations are oblique astigmatism and mean oblique error (power error). A brief review of these aberrations is given, explaining how the lens designer can control them using just the bending of the lens, and what results can be achieved using simple spherical and toroidal surfaces. Before 1985, aspherical surfaces were used only for post-cataract spectacle lenses and high-power magnifiers. Today, aspherical surfaces are used by all major lens manufacturers to produce thinner, lighter and more attractive best-form lenses in the normal power range. Aspherical surfaces are employed because the surface itself is astigmatic and the surface astigmatism is used to combat aberrational astigmatism due to oblique incidence. The various types of aspherical surface and how the surface astigmatism arises is described, before considering how this feature is used to produce flatter, thinner lenses. In the case of astigmatic prescriptions, the surface requires different asphericities along its principal meridians and the geometry of these atoroidal surfaces is also described. The advent of free-form manufacturing techniques requires the lens designer to convert the surface description to the  $(x,y,z)$  co-ordinates needed to generate the surface. Examples of how these co-ordinates can be obtained from the equation to the surface are given for toroidal and aspherical surfaces. In the case of free-form progressive surfaces, the pre-determined  $z$ -co-ordinates must be added to the  $z$ -co-ordinates of the prescription surface to obtain the final free-form surface. In the case of optimised prescription surfaces, on-board software will analyse the result by ray tracing to obtain the final  $z$ -co-ordinates.

Submitted: 28 March 2019

Revised: 29 April 2019

Accepted for publication: 29 April 2019

**Key words:** aberrations, aspherical surfaces, atoroidal surfaces, oblique astigmatism, power error

When the eye is viewing along the optical axis of a spectacle lens, the form of the lens does not matter. The image formed by the lens is not afflicted with any defects or aberrations that might affect its sharpness or shape. However, in practice the eye turns behind the lens to view through off-axis visual points and it is then that the lens form assumes importance. Ideally, the off-axis performance of the lens should be the same as its performance at the optical centre. In general, this is not the case, with the off-axis images being afflicted with various aberrations which spoil the quality of the images formed by the lens.

### Spectacle lens aberrations

As the eye rotates about its centre of rotation, the macula and the far point of the eye also rotate, the latter tracing out a

spherical surface concentric with the centre of rotation of the eye upon which the far point remains. This surface is referred to as the far point sphere. The aim of spectacle lens design for distance vision lenses is to enable the lens to form point images of distant point objects on the far point sphere. In reality, the images are afflicted with various aberrations and those which are of significance to the spectacle wearer<sup>1–7</sup> are:

- transverse chromatic aberration
- oblique astigmatism
- curvature of field
- distortion.

### **Transverse chromatic aberration**

Transverse chromatic aberration (TCA) is due to the lens material. It is caused by the fact that the refractive index of the lens material varies with the wavelength of the incident light. This effect is expressed by the

Abbe number of the material denoted by the  $V$ -value, defined as:

$$V\text{-value} = (n_d - 1) / (n_F - n_C),$$

where  $n_d$ ,  $n_F$  and  $n_C$  represent the refractive indices of the material for yellow, blue and red light, respectively. In conditions of high contrast, its effect is to cause coloured fringes to be seen surrounding the image of a high-contrast target.

Under conditions of low contrast, colour fringing may not be noticed. Instead, the effect of TCA is to cause a reduction in visual acuity. This effect is referred to as off-axis blur and often gives rise to the complaint by patients that 'the lenses are fine when I look through the centres but are blurred when I look through the edge!'

To a good approximation, the magnitude of the TCA at any given point on a lens is found by calculating the prismatic effect,  $P$ ,

at the point and dividing this by the Abbe number,  $V$ , that is,

$$TCA = P/V. \quad [1]$$

It is generally considered that the threshold value for TCA is  $0.1^\Delta$ . TCA less than  $0.1^\Delta$  is unlikely to give rise to complaints. The  $V$ -value for normal-index materials in which the refractive index is in the region of 1.50 (for example, crown glass and CR 39), is about 60 and the prismatic effect at the visual point would need to be about  $6^\Delta$  before the threshold is reached. Using paraxial theory, this amount of prism would be encountered at a point 15 mm from the optical centre of a +4.00 D lens. Materials in which  $V$ -values are in the region of 40 would give rise to  $0.1^\Delta$  of TCA at a point where the prismatic effect is  $4^\Delta$  – for example, 10 mm away from the optical centre of a +4.00 D lens. It is for this reason that it is wise to select a material with the highest available Abbe number.

### Oblique astigmatism

When a narrow pencil of rays is refracted obliquely by a spherical surface, the refracted pencil becomes astigmatic. Instead of the rays re-uniting in a single image point, they form two-line foci at right angles to one another and between them, where the refracted pencil has its least cross-sectional area – a disc of least confusion. The plane containing the optical axis of the surface is referred to as the tangential plane and the plane at right angles to this is referred to as the sagittal plane. The tangential and sagittal oblique vertex sphere powers of a spectacle lens are determined by accurate trigonometric ray tracing through the lens. The chief ray passes through the centre of rotation of the eye which is supposed to lie on the optical axis of the lens. It is also assumed that the primary line of sight coincides with the optical axis.<sup>5</sup> When it does not, as would be the case when the lens is tilted or decentered before the eye – for example, when a pantoscopic or face form tilt is applied to the lens – more complicated ray tracing techniques must be applied, which invariably requires the use of computer software to trace skew rays through the lens.<sup>5</sup>

Before the arrival of the computer, third-order equations were employed to determine the best form of spectacle lenses.<sup>8</sup> More recently, fifth-order equations have been published to determine the optimum

forms for spectacle lenses,<sup>9</sup> but the authors conclude that the resulting forms differ by negligible amounts from their third-order equivalents. In any case, the arrival of the computer has rendered these approximate analytical methods redundant.

The effect of oblique astigmatism is to produce a blurring of the image as though an unwanted spherocylinder had been interposed between the lens and the eye. The reduction of oblique astigmatism is very important in the design of spectacle lenses and it will be seen later that this may be achieved by a suitable choice of lens bending or by the use of an aspherical surface.

### Curvature of field

In the design of a camera lens, curvature of the image plane should be zero, allowing the image plane to correspond with the flat film plane. In the case of a spectacle lens, the curvature of the image is usually insufficient to match the curvature of the far point sphere. There is a mismatch between the axial power and the mean oblique power of the lens, known as mean oblique error or power error.

### Distortion

Distortion affects the shape of the image rather than its sharpness and is caused by the fact that the power of a spherical surface increases toward its periphery, with the change in shape increasing as the eye uses wider and wider zones of a spherical lens.

### PINCUSHION DISTORTION

Plus lenses produce pincushion distortion, which is the type of distortion typically seen when a strong plus lens is used as a magnifier. The characteristic pincushion-shape image also gives the impression that the object being viewed is concave, whereby the centre of the object seems further from the eye than the edges.

### BARREL DISTORTION

Minus lenses produce barrel distortion and is often reported by myopes who view through peripheral zones of their lenses. An object afflicted with barrel distortion gives rise to a convex appearance of the target; the centre of the target appears to be closer than the edges.

When the form of a lens is changed, the amount of distortion that is exhibited by the lens also changes and is probably the chief cause of the perceptual problems that occur

when a subject is given new lenses of a different form.

## Field diagrams

A 'best-form', or 'corrected curve', spectacle lens is one with surface powers that have been specially computed to eliminate, or at least minimise, certain stated defects in its image-forming properties. Of the four aberrations described above, transverse chromatism can only be eliminated by constructing an achromatic lens; that is, a pair of lenses bonded together, in which the chromatism of one component neutralises the chromatism of the second. Such devices are too bulky to be used as spectacle lenses. Ordinarily, chromatism is a function of the Abbe number of the lens material and is minimised for a given power by selecting a material with the highest available Abbe number.

For most people, the brain readily adapts to distortion and usually, this aberration is an ongoing problem only in cases where there has been a significant change in the prescription, or in the lens form. It is possible to reduce distortion and eliminate either oblique astigmatism or mean oblique error by supplying lenses of very steeply curved form, but such lenses are expensive to produce and appear very bulbous.

The two aberrations that remain – over which the designer can exert some influence – are oblique astigmatism and curvature of field. A useful guide to the effects of oblique astigmatism and curvature of field in a given spectacle lens is obtained by studying a field diagram for the lens form. A field diagram (Figure 1A) is a plot of the tangential and sagittal oblique vertex sphere powers against the ocular rotation of the eye viewing through the lens. In the case of a perfect lens – such as the +4.00 D design that has an ideal field diagram illustrated in Figure 1A – the tangential and sagittal oblique vertex sphere powers remain +4.00 D for all zones of the lens. Unfortunately, this performance is impossible to obtain in a single lens with just two surfaces, at least for this power.

The performance of a +4.00 D design made in plano-convex form is shown in Figure 1B. When the eye views along the optical axis of the lens, the power of the lens is indeed +4.00 D. However, when the eye rotates through  $35^\circ$  from the optical axis, the real effect of the lens is +4.25 D in the sagittal meridian and +5.75 D in the tangential meridian. This effect can be expressed as

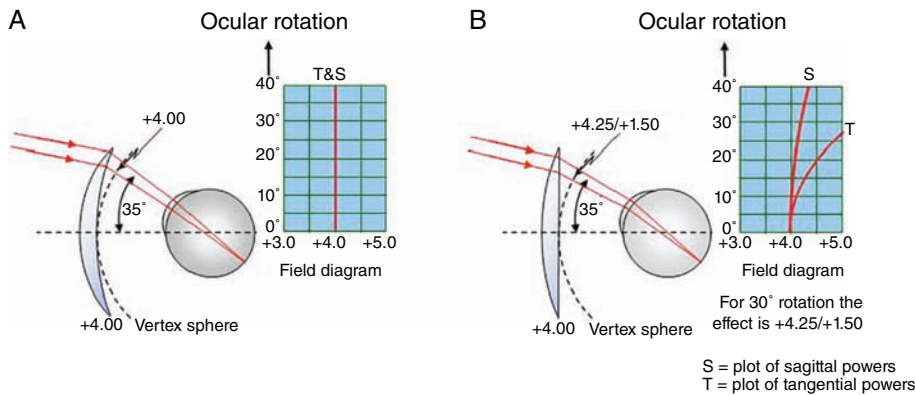


**Figure 1. A:** Field diagram for an ideal +4.00 D lens. The graph indicates that the tangential (T) and sagittal (S) oblique vertex sphere powers remain +4.00 D for all directions of gaze. **B:** Field diagram for +4.00 D lens made in plano-convex form. The graph shows that the lens is afflicted with aberrational astigmatism which increases as the eye rotates away from the optical axis of the lens.

being equivalent to a power +4.25 D sphere with a +1.50 D cylinder, and is so different from the paraxial power that it cannot be ignored. Clearly, a plano-convex design for a lens of power +4.00 D is a poor choice.

In general, the surface powers which are chosen for any given lens are those which make the power obtained during oblique gaze as close as possible to the power obtained when the eye looks along the optical axis of the lens.<sup>10</sup> Although a +4.00 D lens for which the power remains the same for all directions of gaze cannot be made, the performance shown in Figure 1B can certainly be improved upon.

### Best-form spectacle lenses

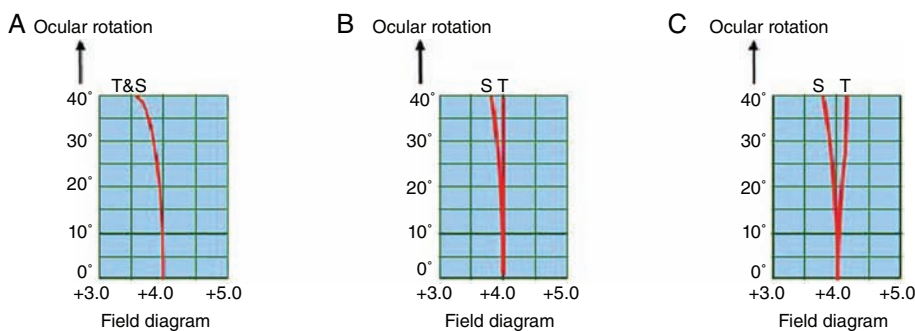
The control which the designer can exercise over these two aberrations is illustrated in

Figure 2, which shows how the off-axis performance of +4.00 D lenses varies for three curved forms with front curves +9.62 D, +8.12 D and +7.62 D.

In Figure 2A, the lens has been bent into a form where the oblique astigmatic error has been entirely eliminated. Such a form is described as a point-focal lens form, from the German word Punktal, which means 'point-forming'. This of course is the name still used by Carl Zeiss to describe their classic series of point-focal lenses.

At 35°, the power of the lens has dropped to +3.70 D; that is, when the astigmatism is fully corrected, the mean oblique power of the lens changes by -0.30 D. The lens has a mean oblique error at 35° of -0.30 D.

If the form of the lens is flattened from the point-focal bending, the tangential power increases. For the +8.12 D bending depicted in Figure 2B, it is now the same as



**Figure 2. Field diagrams for +4.00 D lens designs made in various best forms. A:** Point-focal form, where oblique astigmatic error = 0. **B:** Minimum tangential error form, where  $F_T = F_V$ . **C:** Percival-form, where mean oblique power =  $F_V$  and hence mean oblique error = 0.

the back vertex power of the lens. Such a form is described as a minimum tangential error form<sup>11</sup> and is seen to suffer from an ever-increasing amount of aberrational astigmatism, albeit small, as the eye rotates away from the optical axis. The oblique astigmatic error amounts to about +0.25 D at 35° and the blurring effect of this small cylinder is certain to be less than the 0.25 D sphere blur found in the point-focal form depicted in Figure 2A.

In Figure 2C, the bending of the lens has been reduced still further to a +7.62 D base curve. It can be seen in the field diagram that the tangential and sagittal oblique vertex sphere powers have increased to just the point where the focal lines within the eye would lie either side of, and equidistant from, the retina. At 35° the off-axis power of the lens is +3.85 DS/+0.30 DC, the tangential power is +4.15 D and the sagittal power +3.85 D, compared with the paraxial power which is +4.00 DS. The mean oblique power of the lens is +4.00 D. This form of lens is known as a Percival lens design and is free from mean oblique error for the zone in question.

Today, most best-form lens series are designed to be free from tangential error when fitted at an average vertex distance. When minimum T-error-form lenses are fitted at a longer vertex distance than normal, they tend to perform like point-focal lenses. However, when fitted at a shorter vertex distance, that is, closer to the eye, they tend to perform like Percival-form lenses.

The same principles are involved in the design of minus spectacle lenses. The tangential ( $F'_T$ ) and sagittal ( $F'_S$ ) oblique vertex sphere powers are given in Tables 1-3 for -4.00 D lenses made in point-focal form (+4.70 D base curve), minimum tangential error form (+3.70 D base curve) and Percival-form (+3.25 D base curve) for ocular rotations out to 35°.

### Aspherical surfaces

The term 'aspherical surface' usually refers to a surface that is rotationally symmetrical but at the same time, not spherical. The simplest aspherical surfaces are the conicoids, obtained by rotating a conic section about the z-axis. The conic sections are illustrated in Figure 3A. They differ from one another by their degree of asphericity, which is denoted in the diagram by the

Ocular rotation	$F_T$	$F_S$	OAE	MOP	MOE
35°	-3.75	-3.78	+0.03	-3.77	+0.23
30°	-3.85	-3.85	0.00	-3.85	+0.15
25°	-3.92	-3.90	-0.02	-3.91	+0.09
20°	-3.96	-3.94	-0.02	-3.95	+0.05
15°	-3.98	-3.99	-0.01	-3.99	+0.01
10°	-3.99	-3.99	0.00	-3.99	+0.01
5°	-4.00	-4.00	0.00	-4.00	0.00
0°	-4.00	-4.00	0.00	-4.00	0.00

MOE: mean oblique error, MOP: mean oblique power, OAE: oblique astigmatic error.

**Table 1. Aberrational data for -4.00 D lens made in point-focal form,  $F_1 = +4.70$ ,  $t_c = 1.5$  mm,  $n = 1.50$ , centre of rotation distance = 27 mm. All aberrations expressed in dioptres.**

Ocular rotation	$F_T$	$F_S$	OAE	MOP	MOE
35°	-3.95	-3.84	-0.11	-3.89	+0.11
30°	-4.00	-3.90	-0.10	-3.95	+0.05
25°	-4.02	-3.93	-0.09	-3.98	+0.02
20°	-4.02	-3.96	-0.06	-3.99	+0.01
15°	-4.02	-3.98	-0.04	-4.00	0.00
10°	-4.01	-3.99	-0.02	-4.00	0.00
5°	-4.00	-4.00	0.00	-4.00	0.00
0°	-4.00	-4.00	0.00	-4.00	0.00

MOE: mean oblique error, MOP: mean oblique power, OAE: oblique astigmatic error.

**Table 2. Aberrational data for -4.00 D lens made in Min. T-Error form,  $F_1 = +3.70$ ,  $t_c = 1.5$  mm,  $n = 1.50$ , centre of rotation distance = 27 mm. All aberrations expressed in dioptres.**

Ocular rotation	$F_T$	$F_S$	OAE	MOP	MOE
35°	-4.05	-3.88	-0.17	-3.97	+0.03
30°	-4.08	-3.92	-0.16	-4.00	0.00
25°	-4.07	-3.95	-0.12	-4.02	-0.02
20°	-4.06	-3.97	-0.09	-4.02	-0.02
15°	-4.04	-3.99	-0.05	-4.02	-0.02
10°	-4.02	-3.99	-0.03	-4.01	-0.01
5°	-4.00	-4.00	0.00	-4.00	0.00
0°	-4.00	-4.00	0.00	-4.00	0.00

MOE: mean oblique error, MOP: mean oblique power, OAE: oblique astigmatic error.

**Table 3. Aberrational data for -4.00 D lens made in Percival-form,  $F_1 = +3.25$ ,  $t_c = 1.5$  mm,  $n = 1.50$ , centre of rotation distance = 27 mm. All aberrations expressed in dioptres.**

$p$ -value for each member of the family. Other methods for expressing the asphericity include the eccentricity,  $e$ , which is related to  $p$  by the equation:

$$e = \sqrt{1 - p^2}$$

or by  $K$  (or  $Q$ ), where:

$$K \text{ (or } Q) = (p - 1).$$

A typical aspherical surface is the ellipsoid illustrated in Figure 3B, which would be generated by an ellipse rotating about its major diameter. The ellipsoid is one member of a family of aspherical surfaces known collectively as the conicoids, since they result

from the rotation of a conic section about its  $z$ -axis (Figure 3A). The spherical surface is also a member of the family. An ellipse rotated about its  $z$ -axis produces an ellipsoid. If the major axis of the ellipse is horizontal, the solid is referred to as a prolate ellipsoid. If the minor axis is horizontal, the solid is referred to as an oblate ellipsoid.

A parabola rotated about the  $z$ -axis generates a paraboloid and a hyperbola generates a hyperboloid. These conicoidal surfaces are astigmatic at every point on the surface except at the vertex, and their use enables the designer to make a lens of any power, in any bending, free from aberrational astigmatism by choosing an aspherical surface the asphericity of which neutralises the astigmatism of oblique incidence.

The designer is not limited to conicoidal surfaces. If the equation for a conic section is written in the form:

$$z = y^2 / \left\{ r_0 + \sqrt{(r_0^2 - py^2)} \right\} \quad [2]$$

where  $r_0$  represents the radius of curvature of the surface at the vertex, and expanded by the binomial theorem, the following series is obtained:

$$z = Ay^2 + By^4 + Cy^6 + Dy^8 + \dots \quad [3]$$

where:  $A = 1/2r_0$ ,  $B = p/(2^2 \cdot 2!r_0^3)$ ,  $C = 3p^2/2^3 \cdot 3!r_0^5$ ,  $D = 15p^3/2^4 \cdot 4!r_0^7$ .

By altering the co-efficients  $A$ ,  $B$ ,  $C$ ,  $D$  and so on, the designer can configure the surfaces to deform them from their pure conicoidal forms. These deformed conicoids are often referred to as polynomial or higher-order aspherical surfaces.

### Aspheric lenses for the correction of aphakia

The field diagrams illustrated in Figure 4 show the off-axis performances of +12.00 D lenses made in various forms. Figure 4A illustrates the field diagram for a form that employs spherical surfaces. The increase in tangential power of the lens and the large amount of aberrational astigmatism are seen in the diagram. The sagittal power remains about +12.00 D, but the tangential power increases, reaching about +14.00 D at 35° from the optical axis. At 35°, the real effect of this form with spherical surfaces is +11.91 D with a +2.00 D cylinder – not the



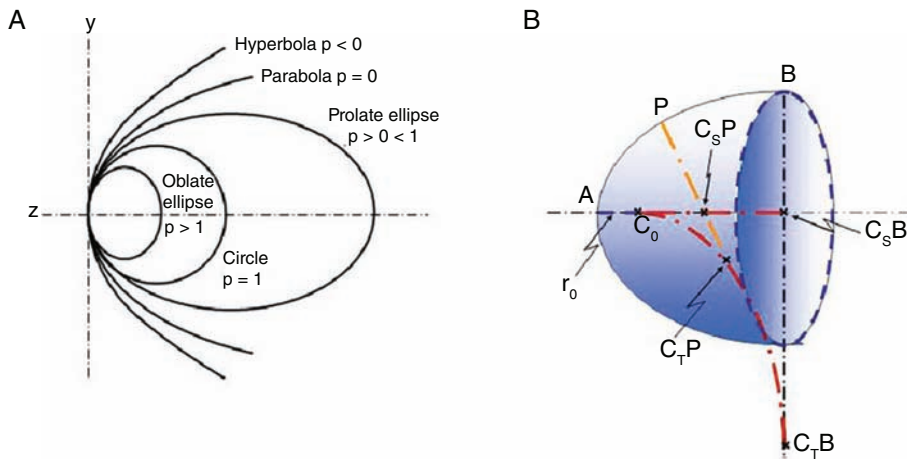


**Figure 3. A: The conic sections. B: How an ellipsoidal surface corrects aberrational astigmatism.** A is the vertex of the curve. C<sub>0</sub> is the centre of curvature of the surface at the vertex. AC<sub>0</sub> is the radius of curvature of the surface at the vertex, r<sub>0</sub>. P is a point on the curve. PC<sub>T</sub>P is the radius of curvature of the surface at point P in the tangential meridian, which is the plane of the diagram. C<sub>T</sub>P lies on the evolute, C<sub>0</sub>C<sub>T</sub>B, which is the locus of the tangential centres of curvature of the surface between points A and B. PC<sub>S</sub>P is the radius of curvature of the surface at point P in the sagittal meridian, which lies at right angles to the plane of the diagram. C<sub>S</sub>P lies on the evolute, C<sub>0</sub>C<sub>S</sub>B, which is the locus of the sagittal centres of curvature of the surface between points A and B.

+12.00 D sphere intended. At this point, the lens exhibits 2.00 D of unwanted astigmatism.

When the designer is not limited to the use of spherical surfaces, oblique astigmatism can be eliminated to provide an increase in the field of useful vision. This is achieved by employing a surface which itself is astigmatic, with the surface astigmatism varying in just the right way to counteract the astigmatism of oblique incidence.

One of the simplest surfaces to provide the correct variation in neutralising astigmatism is the ellipsoid. It is easy to see how this surface introduces neutralising astigmatism by considering how the surface alters in shape as the eye rotates away from the pole of the curve. Figure 3B illustrates the instantaneous centres of curvature for the point, P, on the surface of a convex prolate ellipsoidal surface. The evolutes for the section AB are also shown and it is seen that

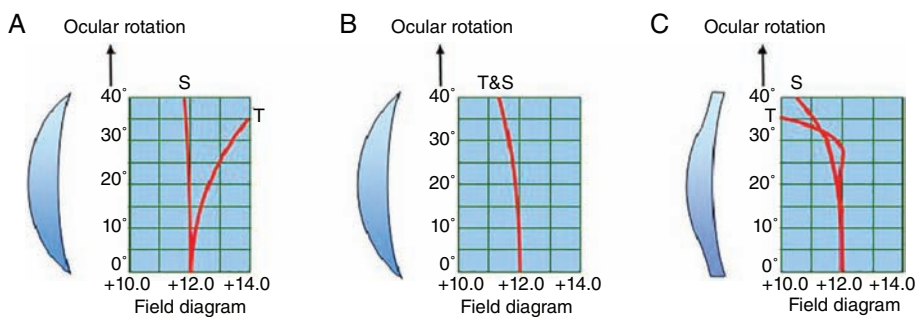


**Figure 4. Field diagrams for +12.00 D lenses made in various forms. A: +12.00 D lens made with spherical surfaces. Note that for a 20° rotation of the eye, the effective prescription is +12.00/+0.56 and at 30°, the effective prescription is +11.93/+1.37. B: +12.00 D lens made with convex prolate ellipsoidal surface. At 30° the effective prescription is +11.33 DS. C: +12.00 D lens made with convex polynomial surface. At 30° the effective prescription is +11.55/+0.09.**

both the tangential and the sagittal radii of curvature for the surface increase, with the tangential radius changing at a faster rate than the sagittal radius. Inspection of the field diagram in Figure 4B confirms that this is just what is required to combat the aberrational astigmatism for this form of lens – a greater decrease in the tangential power of the lens.

By careful choice of eccentricity for the ellipsoid it is possible to eliminate oblique astigmatism for wide zones of the lens. Aspheric lenses of the type needed for the correction of aphakia usually employ a convex prolate ellipsoidal surface to eliminate aberrational astigmatism in the post-cataract range of prescriptions.

The improvement in off-axis performance can be judged from the field diagram shown in Figure 4B, which illustrates the zonal variation in oblique vertex sphere powers for a point-focal +12.00 D lens made with a –3.00 D back curve and a suitably chosen ellipsoidal front surface, whose p-value is +0.65. It can be seen for this design that the tangential and sagittal oblique vertex sphere powers remain the same for all zones out to 40°, but the lens performance is by no means perfect. The mean oblique power, which now is the same as the tangential and sagittal oblique vertex sphere powers, drops off rapidly as the eye rotates away from the optical axis of the lens.

This loss in power, the mean oblique error, amounts to almost 1.00 D at 35° from the optical axis, but at least the error in off-axis performance is a spherical one. It goes without saying that, ideally, the designer would like the marginal power of the aspheric design to increase in order to provide a constant correction for all zones of the lens.

The large drop in tangential power does provide the advantage for lens powers in this range, in that there is a reduction in distortion compared with the spherical design.

Figure 4C illustrates the zonal variation in oblique vertex sphere powers for a +12.00 D lens made with a convex polynomial surface. The astigmatism is zero out to about 20°, then increases slightly before dropping to zero at about 32°. Beyond 35°, there is a rapid drop in tangential power as the surface becomes concave in this zone of the lens.

### Aspheric lenses for the normal power range

Aspherical surfaces are now employed for lenses of low power, as required for the

Refractive index	Front curve	Form of front curve	Back curve	Centre thickness
1.50	+8.25 D	Sphere	-4.45 D	4.4 mm
1.50	+5.42 D	Hyperboloid $p = -1.4$	-1.50 D	3.9 mm
1.50	+3.96 D	Hyperboloid $p = -10.5$	0.00	3.7 mm

**Table 4. +4.00 D lenses made in CR 39 in various forms at 60 mm diameter with 0.5 mm edge thickness**

Ocular rotation	$F'_T$	$F'_S$	OAE	MOP	MOE
35°	+3.94	+3.79	+0.15	+3.86	-0.14
30°	+4.00	+3.86	+0.14	+3.93	-0.07
25°	+4.02	+3.91	+0.11	+3.97	-0.03
20°	+4.02	+3.95	+0.07	+3.98	-0.02
15°	+4.02	+3.97	+0.05	+3.99	-0.01
10°	+4.01	+3.99	+0.02	+4.00	0.00
5°	+4.00	+4.00	0.00	+4.00	0.00
0°	+4.00	+4.00	0.00	+4.00	0.00

MOE: mean oblique error, MOP: mean oblique power, OAE: oblique astigmatic error.

**Table 5. Aberrational data for +4.00 D lens made in Min. T-Error form,  $F_2 = -1.50$ ,  $t_c = 3.9$  mm,  $n = 1.50$ , centre of rotation distance = 27 mm. All aberrations expressed in dioptres.**

usual range of prescriptions.<sup>12</sup> The use of aspheric forms for the low to medium power range allows the production of thinner and lighter lenses for this range of prescriptions. The reduction in thickness is the result of a two-stage process. First, the lens is made much flatter in form by employing a shallower base curve.

The mechanical details of a series of +4.00 D uncut lenses made in CR 39 material at 60 mm diameter, all with an edge thickness of 0.5 mm, is shown in Table 4. Note that the first form is a standard CR 39 lens made with spherical surfaces. The second form is a typical CR 39 aspheric lens with a shallow inside curve and the third form is plano-convex in form with the tangential error neutralised by the hyperboloidal front surface. It can be seen that by flattening and aspherising the lens form, a saving in centre thickness is obtained. The flatter the lens, the thinner it becomes.

When spherical surfaces are used for flatter-form lenses, aberrational astigmatism arises when the eye views through off-axis portions of the lens. To eliminate the tangential error and greatly reduce the

astigmatism, an aspherical surface can be employed, the form of which is such that it introduces negative surface astigmatism to neutralise the increase in tangential power, or if required, produce a point-focal lens.

If the error in tangential power,  $\delta T$ , is known for a given incidence height,  $y_1$ , at the front surface of radius,  $r_1$  and power  $F_1$ , then the necessary asphericity,  $p$ , to eliminate the tangential error can be found from:<sup>13</sup>

$$p = 1 + (r_1/y_1)^2 \cdot \{1 - [F_1/(F_1 - \delta T)]^{2/3}\} \quad [4]$$

Refractive index	Front curve	Form of front curve	Back curve	Centre thickness
1.60	+5.45 D	Hyperboloid $p = -3.35$	-1.50 D	3.2 mm
1.67	+5.45 D	Hyperboloid $p = -5.0$	-1.50 D	2.9 mm
1.74	+5.45 D	Hyperboloid $p = -6.9$	-1.50 D	2.7 mm

**Table 6. +4.00 D lenses made in various materials at 60 mm diameter with 0.5 mm edge thickness**

This expression enables the correct asphericity to be found to produce a best-form lens for any chosen bending.

Table 5 gives the off-axis performance of the second +4.00 D lens described in Table 4, made with a -1.50 D back surface power and a convex aspherical surface whose  $p$ -value has been chosen to eliminate tangential error. This form has a very small degree of aberrational astigmatism. The surface is a convex hyperboloid whose  $p$ -value is -1.4.

An even greater saving in thickness is obtained when a higher refractive index material is employed. If the same base curve is used the saving is two-fold. First, there is the obvious reduction in the sags of the curves, since longer radii of curvature are employed. Second, since the use of the same power base curve on a higher refractive index material requires a longer radius of curvature at the vertex, the lens is flatter still and requires greater asphericity for the surface to restore the off-axis performance.

This is illustrated in Table 6, which shows how the centre thickness of 60 mm diameter +4.00 D lenses would reduce when made in 1.60, 1.67 and 1.74 index materials. The asphericity of the convex surfaces indicated in the figure has been chosen to provide the same off-axis performance for each lens.

Another important advantage of these low-power aspheric designs for hypermetropia can be gleaned from Table 6. They lend themselves far better to a system of supply of large diameter plus uncut lenses, which are subsequently edged to smaller diameters depending upon the choice of shape and size of the lens.

### Aspheric lenses for myopia

The principle of flattening a curved lens form to make it thinner and then

aspherising one surface to restore the off-axis performance of the flatter-form lens can be applied equally to minus lenses.

In the days when the concave surface of a spectacle lens incorporated any cylindrical correction, aspheric minus lens series originally employed a convex aspherical surface, the purpose of which was to increase the convexity of the front surface toward the edge of the lens. With the advent of free-form production techniques, concave aspherical surfaces designed to flatten the surface toward its edge have become the norm. In the case of astigmatic prescriptions, concave atoroidal surfaces may be employed.

In cases of very high myopia, the principle of blending has been applied to the workshop-flattened lenticular, to produce a blended concave lenticular with a truly invisible dividing line.

These blended lenticulars for myopia, such as the Wrobel Super-lenti and the Rodenstock Lentilux designs, enjoy excellent cosmetic properties and allow very high minus prescriptions, even in excess of -20.00 D, to be dispensed in relatively thin and lightweight form. Several manufacturers now offer these designs under various trade names.

### Astigmatic lenses

A best-form astigmatic lens would have the correct principal powers and an equal cylindrical effect along each meridian of the lens.

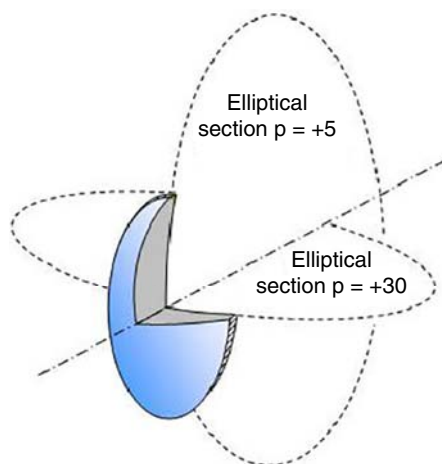


**Figure 5. Concave atoroidal surface in which principal meridians are oblate ellipses**

This ideal is difficult to achieve with the usual form of toroidal surface where it is impossible to optimise each principal meridian and maintain the correct cylindrical effect for all zones of the lens. Most designers agree that a best-form astigmatic lens is one where the cylinder power is the same for each principal meridian even though the power is not maintained along these meridians. In practice, this is best achieved for plus astigmatic lenses when the convex surface is toroidal and of barrel form. For minus astigmatic lenses, the cylinder should be included on the concave surface. Once again, the barrel form is preferred.

Free-form production techniques allow the asphericity to be varied between the principal meridians of the lens, resulting in an atoroidal surface and atoric lenses (one surface being atoroidal), which offer the best solution for astigmatic prescriptions.<sup>14</sup>

An isometric view of a concave atoroidal surface is illustrated in Figure 5. When used with the flatter forms which are employed for low-power aspheric lenses, a concave atoroidal surface may be combined with an aspherical front surface when the design becomes bi-aspheric in form. In addition to reducing the cylinder error, this form of construction produces a small saving in thickness. However, there is little advantage to be gained by using a bi-aspheric construction for purely spherical prescriptions. This is because – in the case of point-focal lenses – although there is a slight decrease in mean oblique error, this is accompanied by a slight increase in distortion and the saving in thickness is negligible.

### Free-form surface description

When a surface is to be produced by means of computer numerical control machining, the surface curves must be translated to three-dimensional co-ordinates (x,y,z). This is a simple matter for the surfaces considered so far, for which equations would be known to the designer. For example, an aspherical surface whose p-value is known, is described by the equation:

$$x^2 + y^2 + pz^2 - 2r_0z = 0 \tag{5}$$

and solving for z for any given (x,y) co-ordinates enables the on-board computer to generate the z-heights for the surface.

The equation to a toroidal surface is:

$$x^2 + y^2 + z^2 - 2r_Ez + 2(r_E - r_T) \left( r_T - \sqrt{r_T^2 - y^2} \right) \tag{6}$$

where  $r_E$  is the equatorial radius of curvature and  $r_T$  is the transverse radius of curvature of the surface. Again, solving for z for any given (x,y) co-ordinates enables the on-board computer to produce the surface. The form in which the information should be presented to the generator is described in the Vision Council Data communication standard, entry 5.6.3.1, SURFMT.

### Progressive lenses

The first commercially successful progressive power lens was developed by Bernard Maitenz of Essel, one of the founding members of Essilor International, and introduced in Europe under the trade name Varilux in 1959.<sup>15</sup> It was pointed out in 1963 by the German scientist Minkwitz<sup>16</sup> that a surface in which power increased across its face must also have an astigmatic effect, whereby the astigmatism increases at twice the rate of change in power and lies at right angles to the direction of the change in power. Since that time, the goal of progressive lens design has been to minimise the effects of so-called Minkwitz astigmatism.

In 1995 a patent was taken out by Kelch et al.<sup>17</sup> describing a progressive lens which had a convex progressive power surface and an aspherical (for spherical prescriptions) or atoroidal (for astigmatic prescriptions) concave surface. This strategy optimised the design for the required prescription in that the design criterion is restored to the lens, no matter what prescription or cylinder axis direction is prescribed.

Before the advent of free-form production techniques, one convex base curve with its given near addition was expected to be used for powers covering a range of perhaps four dioptres or so in spherical power and also cylinders in 0.25 intervals up to 4.00 D with any prescribed axis direction. The progressive surface would have been optimised for a single spherical power in the middle of this range. If the prescription deviated from the power for which the surface was designed, the symmetry of the isocylinder lines would be destroyed and they would then encroach upon the areas which were supposed to provide clear vision. The Kelch patent described a method whereby

the combination of the progressive surface and the aspherical concave prescription surface restored the iso-cylinder lines to their previous ideal design position.

The modern method used by most major lens manufacturers to produce free-form progressive surfaces is to provide a database containing the (x,y,z) co-ordinates for the initial design of a progressive surface. Then, the z-co-ordinates for the prescription surface are computed for the same values of x and y and simply added to the z-co-ordinates for the progressive surface. For their flagship designs, an optimisation ray tracing routine may be run to ensure that the finished lens performs in the manner which the designer intended.<sup>18</sup>

In recent years, a series of low-addition progressive power lenses has been introduced, mainly for intermediate and near vision use, when only some 50 per cent of the full near addition is required.<sup>16</sup> These so-called degressive lenses are especially useful when worn at the computer where, mainly, only mid-distance and near vision is required. Some manufacturers promote very low-addition progressive power lenses for use by pre-presbyopes, suggesting that they may help to relieve computer vision syndrome at the workstation. Needless to say, because the addition is very small, and the corridor length so long, the Minkwitz astigmatism exhibited by these lenses is very small, with the designs offering wide fields of clear vision.

Several patents have also appeared for vocational progressive designs which have not yet reached the market. For example, a progressive design can be employed where

the practitioner stipulates which area of the lens should be optimised for various occupations.<sup>19</sup> Also, a progressive design with the upper portion devoted to distance vision and the lower portion to intermediate vision<sup>20</sup> is claimed to be ideal for use at a computer workstation.

Prism-controlled designs have been described which incorporate – in addition to an increase in power from distance to near – an increasing horizontal prism as the eye rotates down from distance to near.<sup>21</sup> With the advent of free-form production techniques, it is possible to supply progressive designs with different cylinder powers and/or axes in the distance and near portions.<sup>22</sup> Another interesting progressive design has an additional intermediate portion below the near portion to enable subjects to clearly see steps and the ground at their feet.<sup>23</sup>

#### REFERENCES

1. Henker O. *Introduction to the Theory of Spectacles*. Jena: Jena Optikerschule, 1924.
2. Emsley HH, Swaine W. *Ophthalmic Lenses*, 6th ed. London: Hatton Press, 1961.
3. Emsley HH. *Aberrations of Thin Lenses*. London: Constable, 1956.
4. Kingslake R. *Lens Design Fundamentals*. London: Academic Press Inc, 1978.
5. Jalie M. *The Principles of Ophthalmic Lenses*, 5th ed. London: ABDO, 2016.
6. Fannin TE, Grosvenor T. *Clinical Optics*. Boston: Butterworths, 1987.
7. Atchison DA, Smith G. *Optics of the Human Eye*. Edinburgh: Butterworths, 2000.
8. Atchison DA. Third-order theory and aspheric spectacle lens design. *Ophthalmic Physiol Opt* 1984; 4: 179–186.
9. Miks A, Novak J. Fifth order theory of the astigmatism of thin spectacle lenses. *Optom Vis Sci* 2011; 88: 1369–1374.

10. Fry GA. Choosing the base curve for an ophthalmic lens. *Am J Optom Physiol Opt* 1978; 55: 238–248.
11. Davis JK, Fernald HG, Rayner AW. An analysis of ophthalmic lens design. *Am J Optom Arch Am Acad Optom* 1964; 41: 400–421.
12. Jalie M, inventor, Ophthalmic Spectacle Lenses Having a Hyperbolic Surface. United States patent US 4289387. 1981 Sep 15.
13. Davis JK, Fernald HG, Inventors; American Optical Corporation, assignee. Ophthalmic Lens Series. United States patent US 3960442. 1976 Jun 1.
14. Jalie M, Inventor; Opticorp Inc., Assignee. Aspheric Lenses. United States patent US 5083859. 1992 Jan 28.
15. Cretin-Maitenaz B, Inventor; Societe Industrielle et commerciale des Ouvriers Lunetiers, assignee. Multifocal Lens Having a Locally Variable Power. United States patent US 2869422. 1959 Jan 20.
16. Minkwitz G. On the surface astigmatism of a fixed symmetrical aspheric surface. *Opt Acta (Lond)* 1963; 10: 223–227.
17. Kelch G, Lahres H, Wietschorke H, Inventors; Carl-Zeiss-Stiftung, assignee. Spectacle Lens. United States patent US 544503. 1995 Aug 22.
18. Hof A, Hanssen A, Inventors; Carl-Zeiss-Stiftung, Assignee. A Spectacle Lens with Spherical Front Side and Multifocal Back Side and Process for its Production. United States patent US 6089713. 2000 Jul 18.
19. Baumbach P, Esser G, Mueller W, et al., Inventors; Optische Werke G Rodenstock (DE) Assignee. Method of Manufacturing Ophthalmic Lenses. United States patent US 6685316 B2. 2004 Feb 3.
20. Dorsch R, Haimerle W, Inventors; Rodenstock GmbH Assignee. Progressive Spectacle Lens For Seeing Objects at a Large or Average Distance. United States patent US 7033022 B2. 2006 Apr 25.
21. Poulain I, Drobe B, Haro C, et al., Inventors; Essilor International (Companie Generale d'Optique) Assignee. Ophthalmic Lens with Progressive Addition of Power and Prism. United States patent US 7216977 B2. 2007 May 15.
22. Donetti B, Petignaud C, Hernandez M, Inventors; Essilor International (Companie Generale d'Optique) Assignee. Method for Determination of an Ophthalmic Lens Using an Astigmatic Prescription for Far Sight and for Near Sight. United States Patent US 7249850 B2. 2007 Jul 31.
23. Giraudet G, Poulain I, Inventors; Essilor International (Companie Generale d'Optique) Assignee. Progressive Lens for Ophthalmic Spectacles having an Additional Zone for Intermediate Vision. United States Patent US 8061838 B2. 2011 Nov 22.

## Stand magnifiers for low vision: description, prescription, assessment

*Clin Exp Optom* 2020; 103: 11–20

DOI:10.1111/cxo.12948

**Andrew Carkeet**  BAppSci (Optom) MSc  
BA PhD

School of Optometry and Vision Science, and Institute  
of Health and Biomedical Innovation, Queensland  
University of Technology, Brisbane, Queensland,  
Australia  
E-mail: a.carkeet@qut.edu.au

Submitted: 11 April 2019

Revised: 3 July 2019

Accepted for publication: 3 July 2019

Stand magnifiers are still one of the most commonly prescribed classes of low vision devices. Their performance can be difficult to understand because stand magnifiers usually do not give an image at infinity. This review summarises the methods of describing image enlargement for stand magnifiers, emphasising their relationship to equivalent viewing distance (EVD). This is done in terms of the underlying optical equations, and measurement methods, and methods of prescribing. In the past, methods of determining EVD have been somewhat indirect, requiring accurate measurement of lens power, and image position. The use of digital photography provides an alternative, more direct, simpler method of determining EVD, which can be accomplished in-office. This method is described and it is demonstrated how it gives comparable results to older methods with small, clinically non-meaningful differences, that may be due to differences in image distance reference planes. Describing the performance of stand magnifiers in terms of their dioptric power, or in terms of 'nominal magnification' or 'trade magnification', is imprecise and misleading. It is better to use indices such as equivalent viewing power and EVD, which take into account the magnifier dioptric power, the image position of the magnifier and the distance a patient is from the magnifier. While EVD is a useful index for prescribing stand magnifiers, manufacturers do not always provide sufficient technical details to determine EVD for their stand magnifiers, and available tables of EVDs are more than a decade old and are likely to need updating. Photographic comparison provides a method for determining EVD, and this method can also be applied to other low vision devices.

**Key words:** equivalent viewing distance, low vision, magnification, stand magnifiers

Stand magnifiers are still commonly used for low vision management. Although there is an increasing use of optoelectronic devices, which may sometimes yield better reading performance,<sup>1,2</sup> many patients still find a use for stand magnifiers, because of their low cost, portability, and ease of use. In one tertiary hospital low vision clinic, stand magnifier prescription was relatively stable over three decades until 2003, with the use of illuminated magnifiers becoming more common. In a study of outreach low vision clinics in 2004, they were the most frequently prescribed near low vision device for adult patients.<sup>3</sup> A 2016 study in a paediatric low vision population found that stand magnifiers were the most commonly prescribed near low vision device.<sup>4</sup> They are easy for patients to learn to use although patients may sometimes have difficulty scanning text with a stand magnifier<sup>5</sup> and in-office practice may improve reading

speed with stand magnifiers in age-related macular degeneration patients.<sup>6</sup>

However, nearly all stand magnifiers form images which are not located at infinity. If a patient is emmetropic, or is wearing a distance spectacle correction, then additional positive focusing power must be used with the magnifier to form a clear image on the retina of the patient. This is either in the form of accommodation, or if the patient is presbyopic (as most are), in the form of a spectacle addition.

Practitioners, then, must consider stand magnifier prescription in terms of providing an optical system comprised of the magnifier itself and the potential spectacle addition along with the distance prescription of a patient. The power of the addition will be determined by how far the image is formed behind the magnifier, the distance from the eye of the patient to the magnifier, and the residual accommodation of the patient.

Also, for a patient, the relative image enlargement provided by the system will depend on the dioptric power of the magnifier, the exit vergence of the magnifier, and the distance from the eye of the patient to the magnifier.

The optical principles behind stand magnifiers might seem complicated to apply in low vision practice, but there are concepts which make their prescription easier. This paper will review the optical principles underpinning stand magnifiers; the various clinical descriptions of image enlargement – in particular, equivalent viewing distance (EVD), the accuracy of the specifications of the manufacturer for stand magnifiers, in-office methods of assessing clinical parameters of stand magnifiers, and required near additions. Where possible, these topics will be distilled into clinically useful prescribing principles for low vision stand magnifiers.

## Optics of stand magnifiers

Figure 1 illustrates the optical principles behind stand magnifiers. The object is placed at the base of the stand magnifier, at the object distance  $\ell$  from the magnifier lens. Its image will be formed at the image distance  $\ell'$  from the magnifier lens. Most stand magnifiers are constructed so that the image is closer than infinity and  $\ell'$  is negative. Useful relationships are given by standard paraxial refraction equations. Object vergence  $L = \frac{1}{\ell}$  and image vergence will be negative (divergent) with  $L' = \frac{1}{\ell'}$ . The image size  $h'$  and object size  $h$  are related by the lateral magnification equations:

$$m = \frac{h'}{h} = \frac{\ell'}{\ell} = \frac{L}{L'} \quad [1]$$

(Note: for this, Fincham's notation  $m$  for lateral magnification<sup>7</sup> has been used. Bailey et al.<sup>8</sup> use ER, enlargement ratio, to describe lateral magnification, that is  $m = ER$ , as do others.)<sup>9</sup>

The stand magnifier dioptric power is denoted as  $F_{SM}$ , then

$$L' = F_{SM} + L \quad [2]$$

The distance from the magnifier lens to the eye is  $z$  and the eye-image distance  $EID = z - \ell'$ .

(Note: the subscript  $SM$  is used to denote variables pertaining to the specific case of stand magnifiers throughout. When variables apply to magnifiers in general, for example hand magnifiers, the subscript  $M$  is used.)<sup>9</sup>

If the patient is presbyopic and has no accommodation, then they will need a spectacle addition to see the image which is a distance of  $z - \ell'$  from the eye, that is a spectacle addition of power  $Add_{Max}$  (the maximum addition required if no accommodation is used) is indicated where:

$$Add_{Max} = \frac{1}{EID} = \frac{1}{z - \ell'} = -\frac{L'}{1 - zL'} \quad [3]$$

To summarise, a stand magnifier will produce an enlarged image, and that image will be at a distance from the patient. Both those factors, lateral magnification and image position, need to be considered when assessing the potential value to a patient of a stand magnifier. There are a number of clinical metrics that have been used to do this.

### EVD

Probably the most useful of these metrics is EVD, described by Bailey et al.<sup>8,10</sup> The EVD is defined as the distance at which an object would need to be from the unaided eye, to subtend the same angle that it would when viewed through the magnifier. For example, from the tables of Bailey et al.,<sup>8</sup> if a COIL #4210 (specified 10 x 36 D) stand magnifier is used with eye-lens distance  $z$  of 10 cm, the EVD is 3.8 cm. In other words when viewing through the magnifier, objects will subtend the same angle as if the patient had viewed, unaided, the object at 3.8 cm. EVD is the EID divided by the lateral magnification of the image:

$$EVD = \frac{EID}{m} = \frac{z - \ell'}{m} \quad [4]$$

For stand magnifiers, and the image distance  $\ell'$  is often known with appropriate precision, as is the power of the magnifier  $F_{SM}$ . Lateral magnification can be calculated from those two values:

$$m = \frac{\ell'}{\ell} = \frac{\ell'}{\frac{1}{L}} = \frac{\ell' L}{1 - F_{SM}} = \ell' (L' - F_{SM}) = \ell' \left( \frac{1}{\ell} - F_{SM} \right) \quad [5]$$

So for a given combination of  $\ell'$ ,  $F_{SM}$  and  $z$

$$EVD = \frac{z - \ell'}{\ell' \left( \frac{1}{\ell} - F_{SM} \right)} \quad [6]$$

EVD might appear difficult to calculate, but as seen below it is easy to determine with photographic methods, and provides a common metric that can be applied to other near magnifier types such as hand magnifiers, and electronic devices.

### Other metrics for stand magnifiers

#### Equivalent viewing power

Equivalent viewing power (EVP)<sup>11-13</sup> can be thought of as the spectacle addition (or accommodation required) for an object actually positioned at the EVD. It is the reciprocal of EVD, that is

$$EVP = \frac{1}{EVD} \quad [7]$$

EVP can also be considered and calculated as the equivalent power of a lens system made up of the stand magnifier lens, and the maximum addition (or required accommodation) separated by the eye-lens distance  $z$ . Thus, based on the equivalent power equation:

$$EVP = F_{SM} + Add_{Max} - zF_{SM}Add_{Max} \quad [8]$$

For the COIL #4210 used at  $z = 10$  cm,  $Add_{Max}$  would be 2.08 D and EVP would be 26.4 D.

If the lateral magnification  $m$  for the stand magnifier is known then EVP can be calculated.

$$EVP = m \times Add_{Max} \quad [9]$$

Given the EVD and EVP are reciprocals of each other, the two indices should be

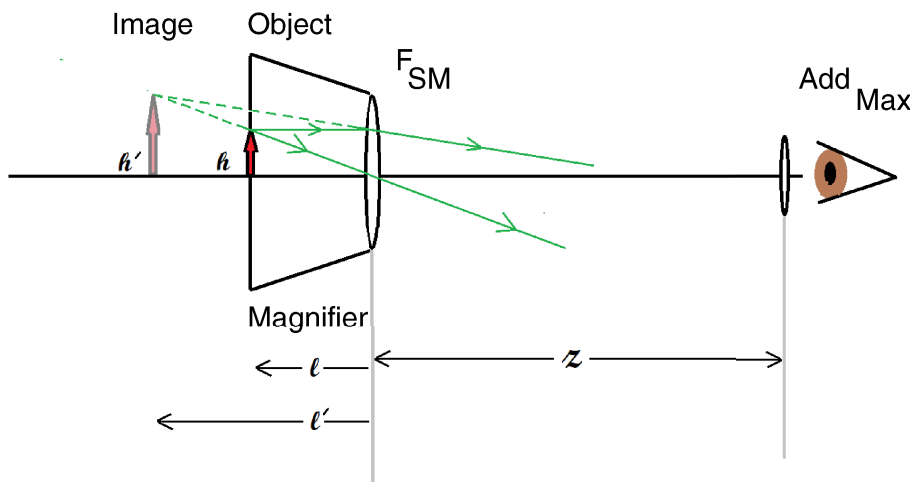


Figure 1. Object image relationship stand magnifier of power  $F_{SM}$ . Object distance is  $\ell$ , image distance  $\ell'$ , object height  $h$ , image height  $h'$  and eye-lens distance  $z$ .

similarly useful from a clinical point of view. Tables using one method can be easily converted to the other.

### Dioptric power

Most manufacturers will specify a dioptric power for stand magnifiers. That power is nearly always a misleading indicator of the image enlarging properties of a stand magnifier.

First, it is often inaccurate. For the example above – a COIL #4210 stand magnifier – the specified dioptric power was +36.00 D, but previous authors<sup>8</sup> measured equivalent power of the magnifier as actually +30.70 D. This issue with inaccurate power specification given by the manufacturer is well-known and has been reported by a number of authors. Bailey et al.<sup>8</sup> measured the equivalent power of a series of 82 stand magnifiers of which 40 had labelled dioptric powers designated by the manufacturer; of those, 27 had powers that differed by 0.50 D from the labelled powers. Of those there were three magnifiers with labelled power underestimating actual power, and for 24 magnifiers the manufacturer overestimated the power of the magnifier. Of those, 21 were from the one manufacturer – COIL – although it should be noted that 25 per cent of COIL magnifiers (Equation 6) had labelled powers that matched actual powers to within 0.50 D. This issue with COIL magnifiers had been observed by others. Chung and Johnston<sup>14</sup> also noted differences between measured and manufacturer-specified powers for COIL stand magnifiers, as did Bullimore and Bailey,<sup>10</sup> who found that manufacturer-specified powers were overstated in nearly all COIL stand magnifiers they measured, by between zero and 28 per cent.

Second, that power can be difficult to measure. Stand magnifier equations assume thin lenses, but the stand magnifier lenses are often thick enough so that assumption will be problematic. While it is more appropriate to specify equivalent lens power,  $F_e$ , for  $F_{SM}$ , that power is referenced to principal planes, which are imaginary planes associated with the lens.  $F_e$  needs to be determined indirectly, for example using methods that measure image magnification for known object distances. Sometimes it is easier to measure back vertex power of the lens ( $F_v$  or BVP), which is referenced to the back surface of the lens, a real physical structure. Some manufacturers may designate power in terms of BVP<sup>14</sup> instead of the more appropriate  $F_e$ .

Third, the use of power alone ignores parameters which will affect the functional performance of a stand magnifier. For a stand magnifier, the lateral magnification will be constant, but as can be seen from Equation 6, EVD depends also on the image distance  $\ell'$  from the lens and the eye to lens distance,  $z$ . In the example above – the COIL #4210 –  $\ell'$  was measured by Bailey et al.<sup>8</sup> as –38 cm. If a patient had positioned their eye close to the lens (at  $z = 2.5$  cm) the EVD would be 3.2 cm. If a patient used the stand magnifier from further away (at  $z = 25$  cm) the EVD would be 5.0 cm. That represents a change in performance of about 0.2 log units. If the reading threshold of a patient was N6 in the first position, it would be expected to be N10 in the second eye-lens distance. This is something that cannot be predicted from stand magnifier power alone.

### Near 'relative magnification'

There is a long-standing convention in which near magnification is specified in terms of the ratio of the angular subtense  $\alpha'$  of an image viewed through a magnifier, to the angular subtense  $\alpha_{25}$  of an object viewed at a standard distance, usually 25 cm (or 10 inches).<sup>7</sup> Bailey refers to this as 'relative magnification' (M), and this paper adopts that use. Relative magnification is usually denoted by an uppercase M to distinguish near relative magnification M,<sup>7</sup> from lateral magnification  $m$ .

For a magnifier (for example, a hand magnifier) of power  $F_M$  and a focal length  $f'_M$  with the object at its primary focal point, and the image at infinity, this equation can be written as:

$$M = \frac{\alpha'}{\alpha_{25}} = \frac{0.25}{f'_M} = \frac{F_M}{4} \quad [10]$$

This definition is sometimes referred to as 'nominal magnification'.<sup>9,15</sup>

The equation is sometimes modified to allow for some accommodation by the patient, traditionally an amount of 4.00 D, and to assume that the eye of the observer is so close to the magnifier that working distance  $z$  is approximately zero. Under those circumstances the magnifier can be considered as having a power of  $F_M + 4.00$  D. If that is the case, then:

$$M = \frac{F_M + 4}{4} = \frac{F_M}{4} + 1 \quad [11]$$

M calculated by this method is sometimes referred to as 'trade magnification'.<sup>9,15</sup> This equation is based on an arbitrary reference distance of 25 cm. It assumes the exit vergence from the magnifier is –4.00 D and that eye-lens distance  $z = 0$ . These assumptions are almost never appropriate for stand magnifiers and so the equations are inappropriate for stand magnifiers.

For a given lens power, trade magnification gives a higher value, by one, than does nominal magnification. Perhaps for this reason trade magnification is more often used by manufacturers to designate the enlargement properties of stand magnifiers. However, whether trade or nominal magnification is used to label a stand magnifier, they are nearly always misleading and usually overstate the magnification of the device.

Brown et al.<sup>9</sup> surveyed 66 stand magnifiers, 48 of which were labelled with trade magnification and 18 were labelled with nominal magnification. With  $z = 0$ , that is the eye coincident with the magnifier plane, all of those labelled with nominal magnification underestimated the enlargement performance of the device, because none had an image located at infinity. However, the image would need additional accommodation or a spectacle addition to be in focus. Of the 48 labelled with trade magnification, only nine had images acceptably close to 25 cm from the lens, 31 had images closer than 25 cm from the lens (and trade magnification would therefore underestimate performance), and eight had images further than 25 cm from the lens (and trade magnification would therefore overestimate performance). If a reasonable working distance  $z$  of 25 cm was used for any device, any trade or nominal magnification greater than one overestimated performance.

However, one can accurately use EVD to calculate M for a stand magnifier image (that is,  $M_{SM}$ ), compared with an object at 25 cm. Because EVD is the distance that the object would subtend the same angle that it would when viewed through the magnifier, then:

$$M_{SM} = \frac{0.25}{EVD} \quad [12]$$

$$M_{SM} = \frac{0.25}{\ell' \left( \frac{1}{z} - F_{SM} \right)} \quad [13]$$

$$M_{SM} = \frac{\ell' \left( \frac{1}{\ell'} - F_{SM} \right)}{4(z - \ell')} \quad [14]$$

Smith et al.<sup>16</sup> have expressed this in terms of vergence exiting the magnifier lens (instead of image position):

$$M_{SM} = \frac{g(F_{SM} - L')}{(1 - zL')} \quad [15]$$

where  $g = 0.25$  m.

By way of example, the stand magnifier previously discussed – the COIL #4210 – was described by the manufacturer as having a power of +36.00 D and a magnification M of 10X, which comes from the definition  $M = F/4 + 1$ . In fact, the stand magnifier was measured as having a power of 30.70 D, so applying the trade magnification equation  $M = F/4 + 1$  would give an M of  $34.7/4 = 8.7X$ . But actual  $M_{SM} = 0.25/EVD$ . For an eye-lens distance  $z$  of 2.5 cm, the EVD was 3.2 cm (0.032 m), so  $M_{SM} = 0.25/0.032 = 7.8X$ . For  $z = 10$  cm, EVD was 3.8 cm (0.038 m) and  $M_{SM} = 6.6X$ . For  $z = 25$  cm, EVD was 5.0 cm, so  $M_{SM} = 5.0X$ . This is half the M specified by the manufacturer (trade magnification).

Although 25 cm is the most commonly used reference distance for industry calculations of M, some authors use additional reference distances<sup>7</sup> including 40 cm.<sup>7,17</sup> Bailey<sup>17</sup> differentiates near relative magnification specified by different reference distances by using subscripts (that is,  $M_{0.25}$  or  $M_{0.40}$ ) and shows magnification equations for the later reference distance.

In summary, manufacturers nearly always describe their stand magnifiers in terms of trade magnification. But irrespective of whether trade magnification or nominal magnification is used, it almost always overestimates performance, especially for larger eye-lens distances.

### Stand magnifier field of view

The linear extent of a field that is visible through a stand magnifier ( $FoV_{SM}$ ) with an aperture A can be shown to be:<sup>18,19</sup>

$$FoV_{SM} = \frac{A}{EVP \times z} \quad [16]$$

which can be written in terms of EVD:<sup>8</sup>

$$FoV_{SM} = \frac{A \times EVD}{z} \quad [17]$$

Some authors (for example, Wolffsohn<sup>13</sup>) have erroneously reported the equation for

hand magnifiers (which assumes an infinite image for the magnifier), as the equation for a stand magnifier. For a hand magnifier held with the object at its primary focal point and an image at infinity<sup>12</sup>

$$FoV_M = \frac{A}{F_M \times z} \quad [18]$$

There can be significant errors in estimates of field size if Equation 18 is used for a stand magnifier.

For the COIL #4210 mentioned above ( $F_{SM} = +30.70$  D,  $\ell' = -38$  cm, with  $A = 36$  mm), used at an eye-lens distance of  $z = 25$  cm, then Equation 18 gives a field size of 4.7 mm. However, the correct equation – Equation 17 – (EVD of 5.0 cm) gives a field size of 7.2 mm, so using the wrong equation significantly underestimates field of view. If a close working distance,  $z = 2.5$  cm, is used, then using the incorrect equation (Equation 18) gives a field size of 47 mm, which slightly overestimates the value given by the correct equation (Equation 17) of 46 mm.

It should be noted that the calculations for field of view (Equations 16–18) depend on the assumptions that thin lenses are used, that pupil size is negligibly small, and that the full extent of the lens can be used.<sup>8,14,19</sup> The usable field of the magnifier, that can be seen clearly through the magnifier, may be different. This is because magnifier lenses probably do not have negligible thickness, and are likely to be aspheric. Also, for very close working distances, the base of the magnifier may act as the field stop and limit how much text can be seen. In addition, there are at least two possible reference planes from which the eye position can be judged when calculating field size. Stationary field of view should be judged (and  $z$  calculated) with respect to the pupil of the patient, approximately 3 mm<sup>20</sup> behind the corneal plane. For field of fixation, the field which can be viewed with a preferred locus of fixation,  $z$ , of the patient should be calculated from the centre of rotation of the eye, approximately 15 mm behind the cornea.<sup>21</sup>

Chung and Johnston<sup>14,19</sup> noted discrepancies between measured and calculated field sizes for very close observation distances where the base of the magnifier limits the field, and measured field could be as low as 17 per cent of the calculated field. However, even for larger distances, it was not uncommon for calculated field to overestimate and underestimate measured field by 10–20 per cent.

### Using EVD for prescribing stand magnifiers

As shown above, EVD is a useful measurement for describing image enlargement in low vision. It is a common metric that can be calculated for stand magnifiers, near additions, hand magnifiers, and near electronic magnifiers. Bailey et al.<sup>8</sup> suggested the following steps for determining the appropriate EVD for a patient based on near tasks and acuity.

1. Decide on a goal print size. This will be task-related. For example, a patient may wish to read regular print books of N12. Bailey et al.<sup>8</sup> initially set this as the goal print size, because it was believed that setting a goal close to threshold was optimal because it maximised the amount of text that could be fitted into the field.<sup>22</sup> More recently it has been demonstrated that increasing print size above threshold improves reading rates in normal and low vision patients.<sup>23–27</sup> It is considered appropriate to modify this goal print size to allow for an acuity reserve so that the patient is not working at threshold. Researchers<sup>28,29</sup> have suggested that an acuity reserve of two-fold would give fluent reading, with larger acuity reserves giving higher reading rates, although Legge et al. have suggested individual testing at different print sizes to establish fluency rates.<sup>30,31</sup> Using an acuity reserve of 2X goal print size would be N6 (N12/2).
2. Test reading threshold at a known working distance with an appropriate near correction (the addition is to ensure optimal performance). For example, a reading threshold was obtained of N18 at a working distance of 40 cm with a 2.5 D addition.
3. Determine a required EVD as:

$$EVD = \frac{\text{Goal reading print size}}{\text{Threshold print size}} \times \text{Test distance} \quad [19]$$

In this case EVD would be N6/N18 x 40 cm = 13.3 cm.

4. Choose a device which gives that EVD at appropriate eye-lens distance. Tables of appropriate optical devices with their EVDs can be found in Bailey et al.,<sup>8</sup> Bullimore et al.,<sup>10</sup> and Lovie-Kitchin and Whittaker.<sup>28</sup> Tables provided by Chung and Johnston<sup>14,19</sup> use similar tables for EVP. Table 1 is taken from Lovie-Kitchin and Whittaker<sup>28</sup> (their table 5). Suppose the patient wanted a device to use at



Manufacturer and ID#	Description of manufacturer	Measured $F_{SM}$ D	Predict performance (z = eye-lens distance)					
			z = 2.5 cm		z = 10 cm		z = 25 cm	
			EVD	Eye-image (cm)	EVD	Eye-image (cm)	EVD	Eye-image (cm)
COIL 5213	8D/3X Hi-power aspheric tilt	7.9	9.0	24.9	11.7	32.4	17.1	47.4
Eschenbach 2050	10D/2.5X hand mag, converts to stand	9.0	7.1	12.9	11.2	20.4	19.4	35.4
Eschenbach 2630	10D/3.5X aspheric, tilt, 75 x 50 mm	9.4	7.6	20.8	10.4	28.3	15.9	43.3
Schweizer 320/90	12D/3X, Visolette, paperweight, 90 mm	10.8	5.4	9.4	9.7	16.9	18.3	31.9
COIL 5214	12D/4X Hi-power aspheric tilt	10.8	8.4	69.5	9.3	77.0	11.2	92.0
Eschenbach 1420	Bright field, paperweight, 65 mm	15.6	4.1	7.1	8.5	14.6	17.3	29.6
Schweizer 320/65	16D/4X, Visolette, paperweight, 65 mm	15.6	4.2	7.6	8.4	15.1	16.8	30.1
Eschenbach 1421	Bright field, paperweight, 65 mm	17.2	4.0	7.1	8.2	14.6	16.5	29.6
Schweizer 320/40	24D/6X, Visolette, paperweight, 40 mm	23.2	3.2	5.0	7.9	12.5	17.4	27.5
COIL 4206	20D/6X Hi-power aspheric	18.7	5.1	51.6	5.8	59.1	7.3	74.1
Eschenbach 2626	23D/6X, aspheric	23.0	4.1	32.8	5.0	40.3	6.9	55.3
COIL 4208	28D/6X Hi-power aspheric	23.4	4.2	73.0	4.6	80.5	5.5	95.5
Peak 1961	40D/10X Loup	29.2	3.3	23.3	4.4	30.8	6.5	45.8
Eschenbach 1153	32D/8X aplanatic	28.9	3.4	44.5	4.0	52.0	5.1	67.0
COIL 4212	44D/12X Hi-power	35.1	3.0	22.5	4.0	30.0	6.1	45.0
COIL 4210	36D/10X Hi-power	30.7	3.2	40.5	3.8	48.0	5.0	63.0
COIL 4215	56D/15X Hi-power focusable	40.3	2.5	18.1	3.5	25.6	5.6	40.6
Eschenbach 2628	38D/10X, aspheric	37.1	2.7	44.2	3.1	51.7	4.0	66.7
Peak 1962	15X Loup	45.3	2.2	20.9	3.0	28.4	4.7	43.4
Peak 1964	22X Loup	64.9	1.7	10.1	3.0	17.6	5.5	32.6
COIL 4220	76D/20X Hi-power	53.6	1.9	15.9	2.9	23.4	4.7	38.4

†For most of the higher-powered devices (for example EVD < 6 cm), an eye-lens distance of 25 cm is not practical because the field of view is too small.

**Table 1. Table of equivalent viewing distances (EVDs) for stand magnifiers taken from Lovie-Kitchin and Whittaker<sup>28</sup>**

an eye-lens distance  $z$  of 10 cm. COIL 5213 has an EVD of 11.7 (slightly better than the required EVD) and an EID of 32.4 cm.

5. Trial the selected magnifier with the appropriate spectacle addition at the appropriate eye-lens distance. In this case the EID is 32.4 cm, which would correspond to an addition power of +3.00 D. If fluency is not achieved at the appropriate print size (N12) then other devices can be tried, based on the patient's actual performance.

Prescribing magnification using EVD in this way is one of a number of similar methods which can be based on the patient's near acuity.<sup>32</sup>

### Measurement of EVD and image position

More recent tables of EVDs for low vision devices are difficult to obtain. It is possible

to determine EVD and associated spectacle additions from parameters provided by some manufacturers, or by careful measurements of the stand magnifiers themselves. At a minimum, a good estimate of  $F_{SM}$  and image position  $\ell'$  can be used to determine EVD, but there are other methods to determine EVD. Eschenbach provides good detail about their stand magnifier products on their websites,<sup>33</sup> including  $F_{SM}$ ,  $L'$  and lateral magnification  $m$ , which make calculating EVD easy. But for other companies, the data are more difficult to obtain; however, the EVD can be relatively easily measured.

Bailey<sup>34</sup> described simple in-office measurements which can be used to determine magnifier lens power, and the image position for the lens. To determine  $F_{SM}$ , a bright object of known size  $h_t$  is positioned at a long-distance  $\ell_t$  from the lens. (The subscript  $t$  is used to indicate that this is a

set-up for testing the stand magnifier). At that large object distance, the small uncertainty in the location of the first principal plane of the lens is insignificant (Figure 2A). The author uses two bright LED pen-torches shone through pinholes (Figure 2A), positioned at an object distance  $-4$  m. This is imaged on a suitable translucent object. Bailey<sup>34</sup> suggested using translucent tape on a graticule for a loupe. The image size can be read off the loupe graticule. The author uses tape on a ruler as the image screen and measures image size from pixels on a photograph (Figure 2C). The image size  $h_t'$  is carefully measured. From Equation 1  $m_t$  can be calculated and therefore  $\ell_t'$  can be calculated:

$$\frac{h_t'}{m_t} = m_t \text{ and } \ell_t' = m_t \ell_t \quad [1b] [1c]$$

The paraxial refraction equation can be used to determine  $F_{SM}$ :

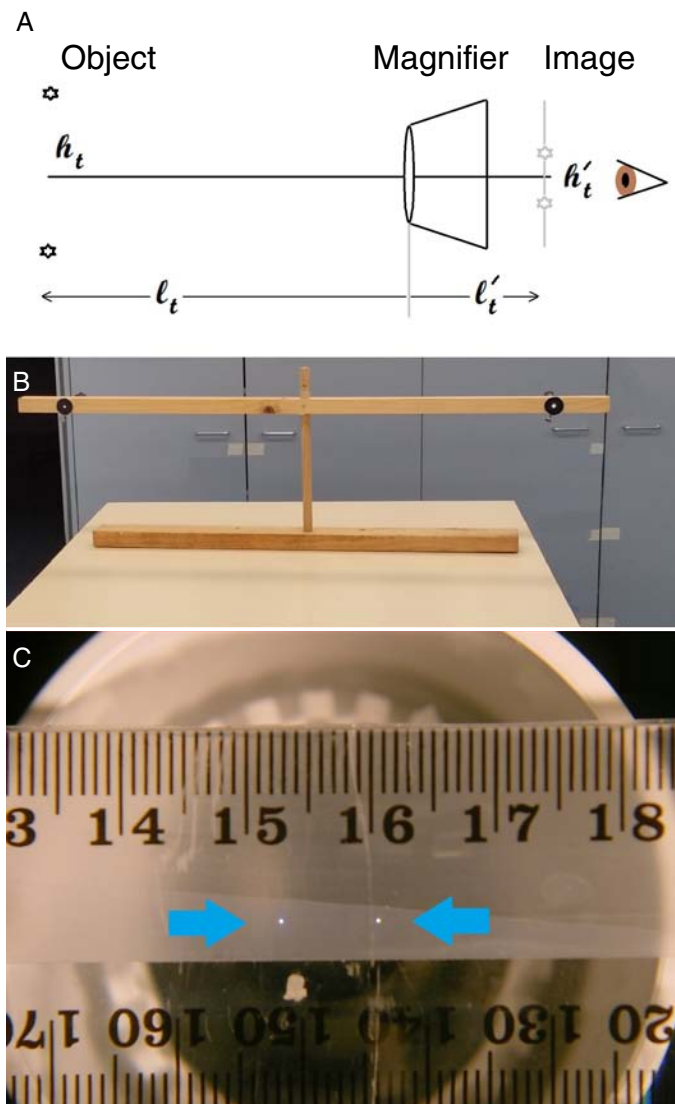


**Figure 2.** Bailey<sup>34</sup> method for determining power of a stand magnifier. **A:** Optical set up with  $-l > > l'$ . **B:** Object, two lights shone through pinhole. **C:** Image, shown by two arrows, formed on translucent tape on a ruler.

$$F_{SM} = L'_t - L_t = \frac{1}{l'_t} - \frac{1}{l_t} \quad [2b]$$

Variants of this method have been used in a number of studies for determining stand magnifier dioptric power.<sup>8,10,11,14,19,35</sup>

To determine EVP and to determine the appropriate spectacle addition at different eye-lens positions, an estimate of the image position  $l'$  is required. Bailey<sup>34</sup> suggested using a retinoscopy rack or trial lenses at the magnifier lens face, to focus light from the base of the magnifier for an emmetropic eye viewing with relaxed accommodation through the magnifier. The power of the lens neutralising the exit vergence of the

magnifier will provide an estimate of its exit vergence. To improve this judgement, the observer can look through the stand magnifier and trial lens using a telescope focused for distance.<sup>36</sup>

Alternatively, light from a distant object can be refracted through the lens in reverse, to form an image onto a translucent screen at the base of the magnifier. The retinoscopy rack can be adjusted until an image is formed on the screen, and the exit vergence will be equal and opposite in power to the retinoscopy rack lens. These methods will provide a sufficiently precise estimate of exit vergence to determine the appropriate

spectacle addition at different working distances, but it is unlikely to give a precise enough estimate of image position  $l'$  to estimate EVD using Equation 6.

Bailey<sup>37</sup> later suggested an alternative, more precise, method using a travelling near-focusing telescope. The telescope is first focused on the exit surface of the magnifier, then moved until it is focused on the image formed by the magnifier, and the distance through which the telescope is moved provides an estimate of  $l'$ . This method has been used to measure image position in most subsequent studies of stand magnifier parameters.<sup>8,10,14,19,35</sup>

### Measuring EVD using photographic comparison

Using information about stand magnifier power  $F_{SM}$  and image position  $l'$  is an indirect way to determine EVD. Recently Carkeet et al.<sup>38</sup> used a photographic technique to measure EVD. This technique is illustrated in Figure 3, showing measurements of an Eschenbach System Vario Plus 155339 used at eye-lens distance  $z$  of 25 cm. A digital camera was used, but as an in-office technique, the resolution of a modern smart phone camera or tablet camera will usually be adequate. The camera should be focused, set at infinity, because allowing the camera to autofocus may change image size in unknown ways.

For some smart phones and tablets, this may require the use of an additional application. The focus is adjusted for near objects by placing different lenses of different powers in front of the camera lens, simulating a spectacle addition. Although the camera is placed close to the trial lens, that trial lens is used as the reference plane for the measurements, on the assumption that vergence exiting that lens will be zero, and the distance from the trial lens to the camera does not affect image size. Pilot work showed this to be true. The trial lens power is adjusted until the image on the screen is clear. This can be done reliably to the nearest 0.25 D, giving an estimate of  $Add_{Max}$  for a given set of conditions. 'z' is defined as the distance from the stand magnifier exit surface to the centre of the trial lens (that is, the 'spectacle plane').

The technique is simple and intuitive. Objects of known scale are used – graph paper in this case – and a reference

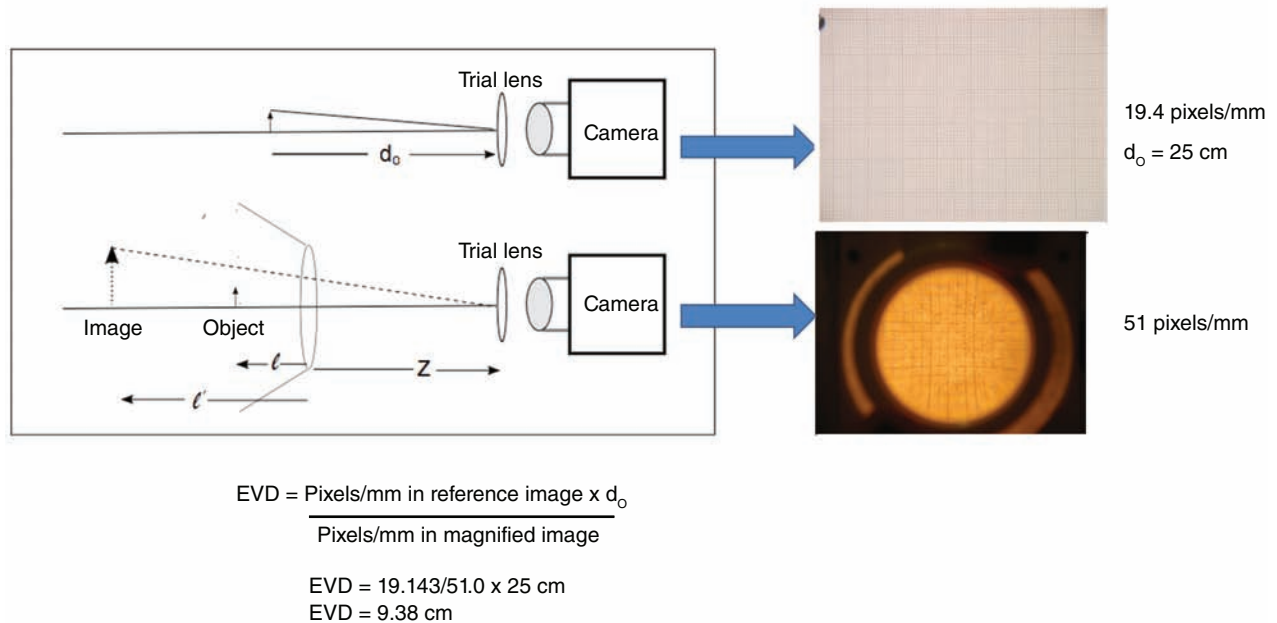


**Figure 3. Arrangement for photographic determination of equivalent viewing distance (EVD). In the example an image is taken of the object, at a reference distance of  $d_o$  (in this case 25 cm) (19.413 pixels/mm). An image is also taken at a distance  $z$  from the stand magnifier (51 pixels/mm). From Equation 20,  $EVD = 19.413/51 \times 25 \text{ cm} = 9.38 \text{ cm}$ .**

photograph is taken at a known distance  $d_o$ . In the example,  $d_o$  was set at 25 cm, but it could be at another distance which gives sufficient image quality. The trial lens is adjusted to give a clear image on the camera. As a check it should be equal to the reciprocal of  $d_o$ . An image is taken. The appropriate stand magnifier is positioned over the object and the camera is set up at the desired distance  $z$ . The trial lens which gives the clearest screen image is inserted. The image through the magnifier is photographed. An appropriate section of the image can be selected to be analysed.

For high-powered magnifiers with peripheral distortion, a clear section of the image at the centre of the magnifier is chosen. The number of pixels per millimetre in the image seen through the stand magnifier is determined (the cursor functions on Microsoft Paint are used for this) as is the number of pixels per millimetre in the reference image. This allows comparison of the relative scales of the images. Then EVD can be calculated as

$$EVD = \frac{\text{pixels/mm in reference image} \times d_o}{\text{pixels/mm in magnifier image}} \quad [20]$$

In the example, 19.143 pixels/mm was measured in the reference image at a

reference distance  $d_o = 25 \text{ cm}$  and 51 pixels/mm was measured in the magnifier image. This gives an EVD value of 9.38 cm.

This 'photo comparison' method with Equation 20 was used to determine EVD values for the Eschenbach System Vario Plus series of stand magnifiers, for  $z = 2.5 \text{ cm}$ , 10 cm, and 25 cm, along with the appropriate spectacle additions. For comparison, EVDs were determined based on  $F_{SM}$  measured using Bailey's magnification method<sup>8,10,14,19,34</sup> and  $\ell'$  measured using the telescope method<sup>10,14,19,34,37</sup> referenced to the exit surface of the magnifier, and Equation 6, along with  $Add_{Max}$  calculated using Equation 3. Eschenbach provides considerable technical information about these magnifiers in their catalogue,<sup>33</sup> including  $F_{SM}$  and  $L'$  which was used to derive  $\ell'$  and these were used to calculate EVDs, again using Equation 6, along with  $Add_{Max}$  calculated using Equation 3.

These results are shown in Table 2. Figure 4 shows difference-versus-mean plots to compare the photo comparison EVDs with the Bailey method EVDs (upper frame) and the photo comparison EVDs with the EVDs taken from catalogue specifications (lower frame). The dashed straight line on both plots represents inter-method differences of five per

cent. The photo comparison method and the Bailey method EVDs agree to close to five per cent, which would be acceptable from a clinical point of view, being a difference of only 0.02 log units.

The data in the upper plot are very close to the five per cent difference line and show that the photo comparison method yields slightly higher estimates of EVD (that is, less image enlargement) than the Bailey method. Some of that difference between the two measurements is expected because the reference plane used to calculate exit vergence in the Bailey method is the surface of the lens and a more appropriate reference plane is the second principal point of the magnifier lens, which lies closer to the image and object.

From the data of Chung and Johnston<sup>19</sup> on COIL stand magnifiers, the second principal plane lay, on average, 1 cm from the lens surface. If the second principal plane of the Eschenbach magnifiers in Table 2 lies at a similar position then it can be calculated that lateral magnification  $m$  for the Bailey method would be overestimated by 3.5 per cent, resulting in EVD measurements being 3.5 per cent too low. Thus, the position of the reference plane for exit vergence is likely to account for a considerable amount of the difference between the two methods.

Catalogue number	z = 2.5 cm		z = 10 cm		z = 25 cm	
	EVD (cm)	Add <sub>Max</sub> (D)	EVD (cm)	Add <sub>Max</sub> (D)	EVD (cm)	Add <sub>Max</sub> (D)
Eschenbach System Vario Plus						
15806 – 3 × 7.6D	8.80	+5.50	12.43	+3.75	19.78	+2.25
15817 – 3.9 × 11.4D	7.79	+4.50	10.56	+3.50	15.85	+2.25
15826 – 2.8 × 7D	8.79	+6.00	12.86	+4.00	20.63	+2.25
15599 – 3 × 12D	6.70	+6.00	9.83	+4.00	15.79	+2.50
15549 – 4 × 16D	5.95	+4.25	7.85	+3.25	11.90	+2.00
15539 – 5 × 20D	4.99	+3.75	6.48	+2.75	9.38	+1.75
15527 – 6 × 24 D	4.39	+3.25	5.49	+2.75	7.98	+1.75
15516 – 7 × 28D	3.71	+2.75	4.54	+2.25	6.14	+1.50
15507 – 10 × 38D	2.67	+3.25	3.44	+2.50	4.93	+1.75
15577 – 12.5 × 50D	2.18	+3.25	2.55	+2.50	3.60	+1.75
Bailey method						
15806 – 3 × 7.6D	8.35	+5.47	11.78	+3.88	18.63	+2.45
15817 – 3.9 × 11.4D	7.33	+4.64	9.89	+3.44	14.99	+2.27
15826 – 2.8 × 7D	8.37	+6.09	12.20	+4.18	19.85	+2.57
15599 – 3 × 12D	6.43	+6.07	9.36	+4.17	15.21	+2.57
15549 – 4 × 16D	5.66	+4.33	7.50	+3.27	11.17	+2.19
15539 – 5 × 20D	4.78	+3.87	6.17	+3.00	8.95	+2.07
15527 – 6 × 24 D	4.14	+3.70	5.29	+2.90	7.59	+2.02
15516 – 7 × 28D	3.58	+2.86	4.34	+2.35	5.87	+1.74
15507 – 10 × 38D	2.65	+3.53	3.35	+2.79	4.75	+1.97
15577 – 12.5 × 50D	2.06	+3.39	2.59	+2.70	3.64	+1.92
Catalogue						
15806 – 3 × 7.6D	8.18	+5.71	11.68	+4.00	18.69	+2.5
15817 – 3.9 × 11.4D	6.86	+4.44	9.15	+3.33	13.72	+2.22
15826 – 2.8 × 7D	8.54	+5.71	12.20	+4.00	19.51	+2.50
15599 – 3 × 12D	6.25	+5.71	8.93	+4.00	14.29	+2.50
15549 – 4 × 16D	5.50	+3.64	7.00	+2.86	10.00	+2.00
15539 – 5 × 20D	4.60	+3.51	5.81	+2.78	8.23	+1.96
15527 – 6 × 24 D	3.96	+3.08	4.88	+2.5	6.71	+1.82
15516 – 7 × 28D	3.47	+2.74	4.18	+2.27	5.61	+1.69
15507 – 10 × 38D	2.62	+2.60	3.13	+2.17	4.16	+1.64
15577 – 12.5 × 50D	2.03	+2.60	2.42	+2.17	3.21	+1.64

**Table 2. Eschenbach stand magnifier equivalent viewing distances (EVDs) and Add<sub>Max</sub> for different eye-lens differences z determined using the photo comparison method, Bailey method<sup>34,37</sup> and from parameters in the Eschenbach catalogue<sup>33</sup>**

Estimates of spectacle additions using the Bailey telescope method match those from the photographic method to within 0.50 D for the different techniques. Catalogue estimates match less precisely, to within 0.65 D. This is probably sufficient for low vision purposes. Legge et al.<sup>39</sup> observed tolerance to defocus increased with defocus, patients whose acuity was 6/12 having depth of focus of 0.50 D and those with acuity of 6/120 having depth of focus between 1.50 D and 5.00 D. Tucker and Charman<sup>40</sup> observed a similar relationship. Jacobs and Johnston<sup>41</sup> trialled different stand magnifiers with different spectacle additions on a

single patient with 6/150 acuity obtaining depth of focus levels between  $\pm 1.00$  D and  $\pm 3.00$  D. However, there is no current study of how defocus with real-world use of stand magnifiers affects parameters such as reading speed.

Empirically, assessing field of view has been usually accomplished by an observer positioned at the appropriate distance, and there can be a mismatch between empirical field of view and calculated field of view.<sup>19</sup> Photographic methods modified from those used in Figure 3 could also be used. The appropriate reference plane for this is the entrance pupil of the camera, and the measurement could

be taken with a smart phone with autofocus. Field of view does influence reading performance<sup>23,24</sup> with optimum recommended field of view for reading being 16–20 characters.<sup>25</sup> Fine et al.<sup>42</sup> have shown that reading performance increases with stand magnifiers even when there are already 13 characters in the field. Some patients show a reduction in reading rate with magnifiers when print size gets too large.<sup>27</sup> Field of view may therefore be a useful addition to tables of EVDs as incorporated by other authors,<sup>14,19,43</sup> allowing practitioners to distinguish between devices of similar EVDs.

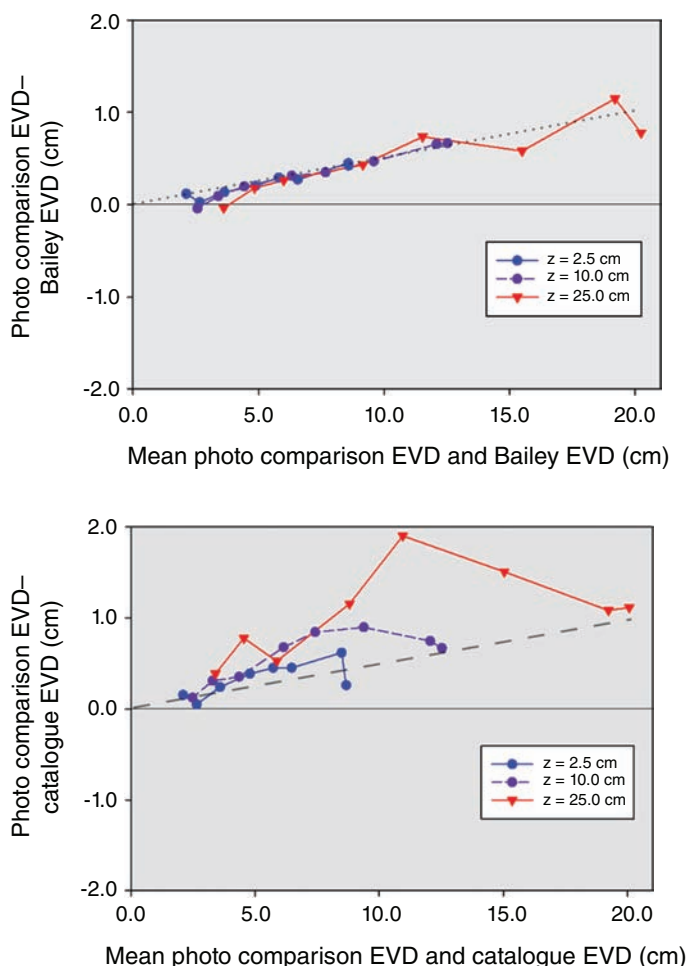


**Figure 4. Difference-versus-mean plots comparing equivalent viewing distance (EVD) calculated by photo comparison with Bailey<sup>34,37</sup> method (upper frame) and with EVD from catalogue measurements (lower frame), for a series of Eschenbach stand magnifiers. The dashed line denotes a five per cent difference.**

## Conclusions

The labels of manufacturers on stand magnifiers are nearly always misleading, in terms of their enlarging properties. Measures such as EVD or EVP will be more useful for prescribing devices. Some manufacturers provide sufficient information about their stand magnifiers to estimate EVD, but many do not. EVD tables are therefore likely to be useful for the practitioner.

It should be noted that Table 2 is the first table of EVDs for stand magnifiers published in reviewed literature in 20 years. More recent tables are available online,<sup>43</sup> updated in 2006, containing EVDs for stand magnifiers, prism spectacles, hand magnifiers and electronic magnifiers. For EVD to remain useful, such tables must be made readily available and regularly updated as new

products become available. There is currently a need for an updated set of measurements for commonly used stand magnifiers, and indeed other forms of near devices. If practitioners need to characterise the EVD of a stand magnifier that is not catalogued then the photographic method described above is sufficiently simple to be used in-office.

Most tables of EVDs for stand magnifiers specify EID for different  $z$  values.<sup>8,10,28</sup> Table 2 expresses this parameter as its reciprocal,  $Add_{Max}$ . This is likely to be easier for practitioners to use than EID, as many vision-impaired patients will have presbyopia. For them, it may be simplest to use  $Add_{Max}$  to prescribe a spectacle addition or to compare with an existing addition. For non-presbyopic patients, for example children using stand magnifiers,<sup>44,45</sup>  $Add_{Max}$  will be an estimate of accommodative demand

required for viewing clearly through the magnifier. It must be stressed that there has been no research on whether using a spectacle addition has an effect on reading performance with stand magnifiers and this may be an area for further research. From a clinical perspective, practitioners can trial appropriate additions to see if patients report subjective improvement with a stand magnifier. Presbyopic practitioners may find it quicker and easier to measure the addition on themselves, looking through the magnifier at the appropriate working distance.

Table 2 does not contain estimates of field of view. This is likely to be a useful parameter as well, and should be included if available. Where possible, such field of view measurements should be based on empirical measurements. Again, this could be done with photographic methods, but using the magnifier at the appropriate distance, with a ruler as an object, which will usually be sufficiently accurate for in-office measurements.

The photo comparison method for determining EVD for stand magnifiers works well. It could be adapted to measuring EVD (and field of view) in other near devices such as hand magnifiers, near telescopes, prism spectacles, and electronic magnifiers, as well as measuring the magnification in distance telescopes.

## REFERENCES

- Virgili G, Acosta R, Grover LL et al. Reading aids for adults with low vision. *Cochrane Database Syst Rev* 2013; CD003303.
- Peterson RC, Wolffsohn JS, Rubinstein M et al. Benefits of electronic vision enhancement systems (EVES) for the visually impaired. *Am J Ophthalmol* 2003; 136: 1129–1135.
- Lindsay J, Bickerstaff D, McGlade A et al. Low vision service delivery: an audit of newly developed outreach clinics in Northern Ireland. *Ophthalmic Physiol Opt* 2004; 24: 360–368.
- Gao G, Yu M, Dai J et al. Demographic and clinical characteristics of a paediatric low vision population in a low vision clinic in China. *Clin Exp Optom* 2016; 99: 274–279.
- Bowers A, Cheong AM, Lovie-Kitchin JE. Reading with optical magnifiers: page navigation strategies and difficulties. *Optom Vis Sci* 2007; 84: 9–20.
- Cheong AM, Lovie-Kitchin JE, Bowers AR et al. Short-term in-office practice improves reading performance with stand magnifiers for people with AMD. *Optom Vis Sci* 2005; 82: 114–127.
- Fincham WHA, Freeman MH. The principles of optical instruments. In: *Optics*, 8th ed. London: Butterworths, 1980. pp. 155–174.
- Bailey IL, Bullimore MA, Greer RB et al. Low vision magnifiers—their optical parameters and methods for prescribing. *Optom Vis Sci* 1994; 71: 689–698.
- Brown WL, Siemsen DW. Magnification labels for stand magnifiers: always misleading and usually unachievable. *Optometry* 2008; 79: 9–17.
- Bullimore MA, Bailey IL. Stand magnifiers: an evaluation of new optical aids from COL. *Optom Vis Sci* 1989; 66: 766–773.
- Johnston AW. Understanding how simple magnifiers provide image enlargement. *Clin Exp Optom* 2003; 86: 403–408.

12. Rumney NJ. Hand magnifiers. In: Jackson JA, Wolffsohn JS, Bailey IL, eds. *Low Vision Manual*. Edinburgh: Butterworth Heinemann Elsevier, 2007. pp. 198–209.
13. Wolffsohn JS. Stand magnifiers. In: Jackson JA, Wolffsohn JS, Bailey IL, eds. *Low Vision Manual*. Edinburgh: Butterworth Heinemann Elsevier, 2007. pp. 210–222.
14. Chung ST, Johnston AW. New stand magnifiers do not meet rated levels of performance. *Clin Exp Optom* 1990; 73: 194–199.
15. International Standards Organization. 15253. *Ophthalmic Optics and Instruments- Optical Devices for Enhancing Low Vision*. Geneva, Switzerland, 2000.
16. Smith G, Jacobs RJ, Johnston AW. Procedures for the optical assessment of low vision aids. *Aust J Optom* 1979; 62: 195–200.
17. Bailey IL. Magnification for near vision. *Optom Mon* 1980; 71: 73–76.
18. Johnston AW. Technical note: the relationship between magnification and field of view for simple magnifiers. *Aust J Optom* 1982; 65: 74–77.
19. Chung ST, Johnston AW. Practical options for magnification and field of view of stand magnifiers. *Clin Exp Optom* 1989; 72: 140–147.
20. Smith G, Atchison DA. A3 schematic eyes. In: *The Eye and Visual Optical Instruments*. Cambridge: Cambridge University Press, 1997. pp. 777–792.
21. Smith G, Atchison DA. The eye. In: *The Eye and Visual Optical Instruments*. Cambridge: Cambridge University Press, 1997. pp. 291–316.
22. Lovie-Kitchin J, Bowman KJ. *Senile Macular Degeneration-Management and Rehabilitation*, 1st ed. Boston: Butterworths, 1985. p. 96.
23. Legge GE, Pelli DG, Rubin GS et al. Psychophysics of reading—I. Normal vision. *Vision Res* 1985; 25: 239–252.
24. Legge GE, Rubin GS, Pelli DG et al. Psychophysics of reading—II. Low vision. *Vision Res* 1985; 25: 253–265.
25. Whittaker SG, Lovie-Kitchin J. Visual requirements for reading. *Optom Vis Sci* 1993; 70: 54–65.
26. Bullimore MA, Bailey IL. Reading and eye movements in age-related maculopathy. *Optom Vis Sci* 1995; 72: 125–138.
27. Cheong AC, Lovie-Kitchin JE, Bowers AR. Determining magnification for reading with low vision. *Clin Exp Optom* 2002; 85: 229–237.
28. Lovie-Kitchin JE, Whittaker SG. Prescribing near magnification for low vision patients. *Clin Exp Optom* 1999; 82: 214–224.
29. Lovie-Kitchin J. Reading with low vision: the impact of research on clinical management. *Clin Exp Optom* 2011; 94: 121–132.
30. Ahn SJ, Legge GE, Luebker A. Printed cards for measuring low-vision reading speed. *Vision Res* 1995; 35: 1939–1944.
31. Legge GE, Ross JA, Isenberg LM et al. Psychophysics of reading. Clinical predictors of low-vision reading speed. *Invest Ophthalmol Vis Sci* 1992; 33: 677–687.
32. Wolffsohn JS, Eperjesi F. Predicting prescribed magnification. *Ophthalmic Physiol Opt* 2004; 24: 334–338.
33. Eschenbach. Eschenbach Products Stand Magnifiers 2013. Available at: <https://eschenbach.com/products/illuminated-stand-magnifiers.asp>. Accessed 19/07/2019.
34. Bailey IL. Verifying near vision magnifiers- part 2. *Optom Mon* 1981; 72: 34–38.
35. Rumney NJ. New range of stand magnifiers based on standardized image position. *Ophthalmic Physiol Opt* 1994; 14: 419–422.
36. Dillehay SM, Pensyl CD. Low vision aids and the presbyope. *J Am Optom Assoc* 1991; 62: 704–710.
37. Bailey IL. Low vision- locating the image in stand magnifiers - an alternative method. *Optom Wkly* 1983; 74: 487–488.
38. Carkeet A, Gambrill B, Harding M et al. Measurement of stand magnifier equivalent viewing distance, using digital photography. Poster. *Annual Meeting of the American Academy of Optometry Seattle*, 2013.
39. Legge GE, Mullen KT, Woo GC et al. Tolerance to visual defocus. *J Opt Soc Am A* 1987; 4: 851–863.
40. Tucker J, Charman WN. The depth-of-focus of the human eye for Snellen letters. *Am J Optom Physiol Opt* 1975; 52: 3–21.
41. Jacobs RJ, Johnston AW. Evaluation of low vision aids. *Aust J Optom* 1982; 65: 213–216.
42. Fine EM, Kirschen MP, Peli E. The necessary field of view to read with an optimal stand magnifier. *J Am Optom Assoc* 1996; 67: 382–389.
43. Bailey IL. Berkeley Yellow Pages- Bailey, Catalog of Optical Parameters of Low Vision Aids 2018. Available at: [https://www.researchgate.net/publication/329105246\\_Berkeley\\_Yellow\\_Pages\\_Bailey](https://www.researchgate.net/publication/329105246_Berkeley_Yellow_Pages_Bailey). Accessed 19/07/2019.
44. Liebrand-Schurink J, Cox RF, van Rens GH et al. Effective and efficient stand magnifier use in visually impaired children. *Front Psych* 2016; 7: 944.
45. Liebrand-Schurink J, Boonstra FN, van Rens GH et al. Shape of magnifiers affects controllability in children with visual impairment. *Acta Ophthalmol* 2016; 94: 761–767.

## Correction of presbyopia: old problems with old (and new) solutions

*Clin Exp Optom* 2020; 103: 21–30

DOI:10.1111/cox.12987

**Pete S Kollbaum** OD PhD FAAO

**Arthur Bradley** PhD

School of Optometry, Indiana University, Bloomington,  
Indiana, USA

E-mail: kollbaum@indiana.edu

Submitted: 13 July 2019

Revised: 5 September 2019

Accepted for publication: 20 September  
2019

We live in a three-dimensional world and the human eye can focus images from a wide range of distances by adjusting the power of the eye's lens (accommodation). Progressive senescent changes in the lens ultimately lead to a complete loss of this ability by about age 50, which then requires alternative strategies to generate high-quality retinal images for far and close viewing distances. This review paper highlights the biomimetic properties and underlying optical mechanisms of induced anisometropia, small apertures, dynamic lenses, and multi-optic lenses in ameliorating the visual consequences of presbyopia. Specifically, the advantages and consequences of non-linear neural summation leveraged in monovision treatments are reviewed. Additionally, the value of a small pupil is quantified, and the impact of pinhole pupil location and their effects on neural sensitivity are examined. Different strategies of generating multifocal optics are also examined, and specifically the interaction between ocular and contact or intraocular lens aberrations and their effect on resulting image quality are simulated. Interestingly, most of the novel strategies for aiding presbyopic and pseudophakic eyes (for example, monovision, multifocality, pinhole pupils) have emerged naturally via evolution in a range of species.

**Key words:** accommodation, anisometropia, aspheric, multifocal, presbyopia, pupil, spherical aberration

We live in a three-dimensional world, and with monofocal optics, only one object distance can generate a focused image at any given time.<sup>1,2</sup> Therefore, most of the retinal image is likely to be out of focus most of the time. However, optical defocus can be catastrophic for human vision<sup>3</sup> and may also be a stimulus for failed emmetropisation and the continued eye growth that underlies myopia.<sup>4–6</sup>

Most vertebrate eyes focus images on the retina by adjusting the optical power of the eye as stimulus distance changes by either moving the eye's lens (for example, fish<sup>7–9</sup> and cats<sup>10</sup>), adjusting the power of the eye's lens (for example, humans), or adjusting the power of the cornea (for example, chameleons).<sup>11–13</sup> However, less common strategies are employed that use a pinhole pupil to expand the depth of field (for example, nautilus<sup>14</sup>), multifocal optics (for example, fish<sup>15</sup>), and different powers in different eyes (for example, chameleons<sup>16</sup>). Variants of these less common strategies are now being utilised by older humans who have lost the ability to adjust power of their lenses (presbyopes and pseudophakes<sup>17,18</sup>), a senescent trait also observed in non-human primates and

other mammals.<sup>18,19</sup> This paper builds upon recent comprehensive reviews<sup>20,21</sup> to examine the optical implications of current and potential strategies to focus the retinal image despite the loss of accommodative ability.

### **Induced anisometropia**

Although different distances can be focused by employing different optical powers in each eye (for example, chameleons<sup>16</sup>), evolution has not developed this approach for humans for whom anisometropia is rare and a possible cause of visual cortical disruption if present in early life (amblyopia, loss of stereopsis).<sup>22</sup> However, inducing anisometropia in older presbyopic or pseudophakic patients ('monovision') has been shown to expand the binocular depth of field by generating clear bifocality of the binocular visual system,<sup>23–26</sup> and high-quality vision at two distances (Figure 1).<sup>27</sup> The success of monovision hinges on the observation that vision with one focused and one defocused eye is dominated by the focused image,<sup>28</sup> as shown quantitatively in studies of contrast sensitivity<sup>23–25</sup> and

visual acuity.<sup>26,29</sup> The improvement in near vision created by correcting one eye can be dramatic, but monovision does not replicate the range of high-quality vision observed in young adults (Figure 1). There is a small reduction of peak acuity and contrast sensitivity down to levels observed with monocular vision.<sup>30,31</sup> Additionally, intermediate distance vision (where neither eye has a focused image) is significantly degraded, an effect that is exacerbated by high add powers<sup>23,26</sup> (Figure 1). Also, because monocular defocus is especially detrimental to stereopsis,<sup>32,33</sup> patients fit with monovision corrections have compromised stereo acuity<sup>34,35</sup> and discrimination of suprathreshold horizontal disparities.<sup>36</sup> Furthermore, in binocularly vulnerable patients monovision can induce strabismus.<sup>37</sup>

Unlike a bifocal lens which simultaneously produces focused and defocused images that add optically (and therefore linearly) at the retina, a monovision patient must employ binocular neural summation to add focused and defocused images in the cortex where non-linear summation<sup>38</sup> or cross-eye neural inhibition<sup>39</sup> is thought to reduce the visibility of the defocused image.<sup>28</sup>

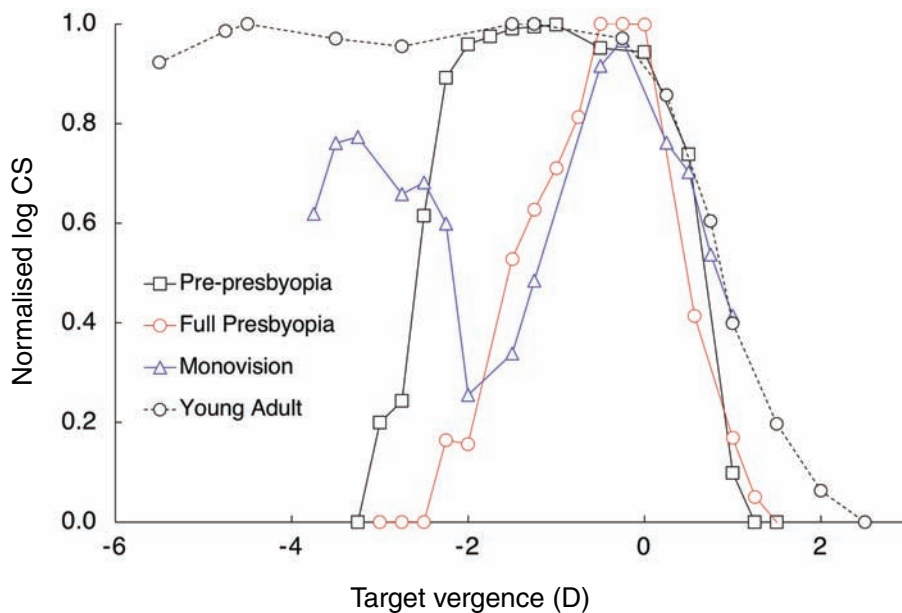


**Figure 1.** Contrast sensitivity plotted as a function of target vergence (dioptres) for four different subjects: A young adult (24 years of age; circle symbols and black dashed line), a pre-presbyope not yet requiring a reading add (44 years of age; square symbols and black solid line), a full presbyope who had been using a reading add for several years (44 years of age; red circle symbols and red solid line), and a full presbyope wearing a +3.00 D add in front of one eye (blue triangle symbols and blue solid line). Y-axis is log normalised CS (log CS/best corrected binocular single vision log contrast sensitivity).

### Small aperture optics

The need for multiple optical powers can be avoided by employing pinhole optics, which can expand the depth of field of the eye<sup>21,40,41</sup> because the blur resulting from defocus is approximately proportional to pupil diameter.<sup>42</sup> The invertebrate nautilus employs this type of pinhole eye design, achieving imaging and depth of field with a small pupil,<sup>14</sup> and to a lesser extent, there is some argument that human vision also employs this small pupil strategy. Pupil size generally decreases over the age of 50,<sup>43</sup> and the retention of near vision pupil miosis in older eyes<sup>44,45</sup> can further reduce pupil size for the near viewing conditions where defocus is more likely. The smaller pupils in older eyes effectively correct for the increased aberrations found in these eyes.<sup>46,47</sup> However, the senescent decrease in photopic and mesopic pupil diameters in 65 year old eyes (for example, ranging from 4.7 to 3.8 photopically and 6.8 to 4.9 mm mesopically<sup>43</sup>) fails to provide sufficient expansion of the depth of field for older

observers, who typically require some optical correction to read at near.<sup>48</sup>

The impact of pupil size on depth of field can be seen in Figure 2 where image quality (visual Strehl ratio on optical transfer function)<sup>49–51</sup> is plotted as a function of target vergence (adapted from Xu et al.<sup>41</sup>) assuming high photopic light levels and a typically aberrated older eye. The depth of field versus diffraction blur trade-off can be seen. The impact of diffraction is striking once the pupil size is reduced to under 2 mm, and peak image quality for the 0.5 mm pupil is less than 10 per cent of that achieved with mid-sized pupils. However, for near distances between 100 and 50 cm, the 1 mm pupil provides the best image quality, and it outperforms the 0.5 mm pupil over more than a 3.5 D range. The degradation in image quality due to the added spherical aberration reduces peak image quality for the largest pupil (7 mm) to that observed with a 1 mm pupil. Maximum peak image quality is observed with pupil diameters between 2.5 and 4.5 mm. For this aberrated eye that is paraxially emmetropic, there is a small myopic shift as the pupil is dilated due to positive spherical aberration.

Clinical strategies that employ pinhole pupils to expand the eye's depth of field have a long history (for example, Daza de Valdes, 1591, cited in a recent review by Charman<sup>21</sup>). Three key parameters must be selected: pupil axial location, pupil size, and whether to employ a fixed pupil or one that varies with light level.

Small pupils have been introduced into the spectacle plane,<sup>52–54</sup> corneal plane<sup>55,56</sup> and iris plane.<sup>57</sup> Placing a small pupil into the spectacle plane will expand the eye's depth of field (as proposed by Donders), but will also drastically reduce the field of view (for example, a 1 mm pinhole placed 17 mm in front of the eye's entrance pupil will start vignetting the retinal image for field eccentricities of about  $\pm 3$  degrees),<sup>52,53</sup> which limits the clinical utility of such an approach. One strategy to deal with this field restriction has been to employ multiple pinholes in the spectacle plane, obtaining some depth of field expansion and each individual pinhole allowing light to reach the retina from different field locations producing a complex patchwork of images and scotomas.<sup>53</sup> Placing the pinhole into the corneal plane either surgically<sup>58–60</sup> or with a contact lens<sup>61</sup> reduces the field constriction effect. However, light from the mid-periphery will still be blocked from entering the eye,<sup>62–66</sup> and total peripheral field occlusion can only be avoided by employing an annular 'iris', which for large field angles allows light to enter the eye around the outside of the inlay.<sup>63</sup> These field constriction problems can be avoided by placing the pinhole pupil into or very close to the iris plane (for example, by employing pharmacological miotics),<sup>67–70</sup> or including a small aperture into the anterior surface of an intraocular lens (IOL),<sup>55,57,71</sup> or piggy-back implantation of a pinhole aperture.<sup>72</sup>

Selection of pinhole pupil size is affected by many factors, but a balance must be struck between improving the defocused near vision without compromising focused distance vision.<sup>73</sup> The value of pinhole optics for presbyopic vision occurs because blur resulting from defocus will approximately scale in proportion to the amount of defocus and pupil diameter,<sup>42</sup> for example, the blur present in the retinal image when a distance-corrected presbyope views a stimulus at 50 cm through a 6 mm pupil can be halved by adding a +1.00 D correcting lens, or reducing pupil diameter to 3 mm. However, this proportionality rule ignores the impact of diffraction and optical aberrations.



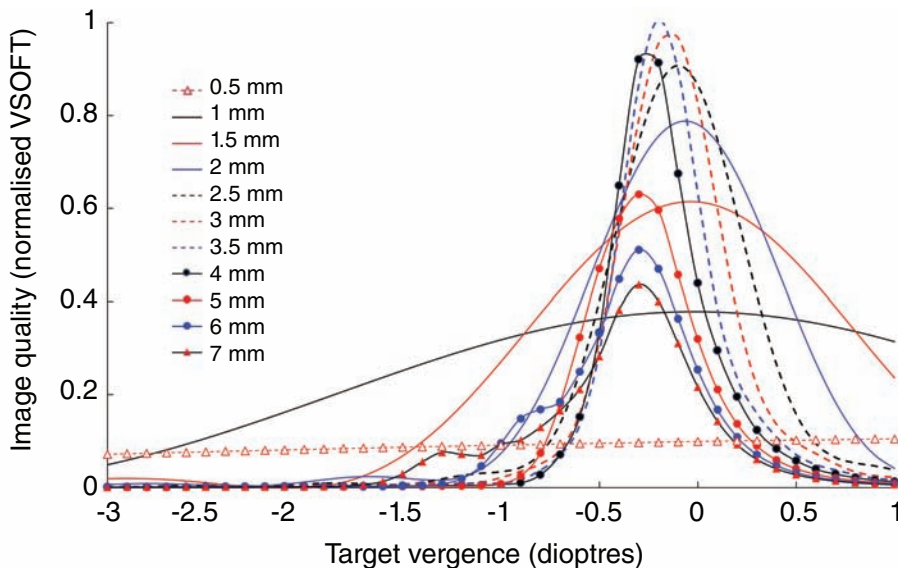


**Figure 2. Image quality for different pupil diameters is plotted as a function of target vergence (dioptries) for a model eye with 0.2 microns of primary spherical aberration ( $C_4^0$ ). Image quality is quantified by the visual Strehl ratio on optical transfer function metric<sup>49-51</sup> normalised to the diffraction limited value observed with a 3 mm diameter pupil.**

It also fails to capture the significant impact of pupil constriction on retinal illuminance and vision.<sup>73</sup> As pupil size decreases, the role of diffraction blur in degrading image quality is amplified,<sup>41</sup> but the impact of higher-order aberrations is reduced, which produces a peak image quality in a focused eye for pupil diameters between 2 and 3 mm.<sup>73,74</sup> At high light levels, where Weber's law is effective, the accompanying drop in retinal illuminance produced by pupil constriction has no effect on vision.<sup>75</sup> However, at low photopic and mesopic light levels, reducing retinal illuminance lowers contrast sensitivity due to photon noise effects,<sup>73,76</sup> and the combined effects of diffraction and reductions in retinal illuminance can significantly impair distance vision when pupil diameters are decreased below 2.5 mm.<sup>74</sup> These studies emphasise that, as is the case for normal human vision,<sup>77,78</sup> the optimum pupil diameter for presbyopia treatment is larger at low environmental light levels.<sup>74</sup> Interestingly, in highly aberrated eyes, depth of focus can be expanded by either constricting the pupil (pinhole pupil effect) or dilating the pupil (multifocal optics effect).<sup>41</sup>

Pinhole spectacle devices have employed pupils less than 1 mm (for example, 0.9 mm<sup>52,53</sup>), with a resulting diffraction limit of < 30 cpd, which predictably impairs

focused vision in the central field at photopic light levels.<sup>53</sup> For example, the KAMRA corneal inlays employ a 1.6 mm artificial pupil, which has proven effective at providing reading at near in photopic conditions.<sup>60,79</sup> Pharmacological pupil miotics have reduced pupil diameters to between 1–2 mm at photopic light levels, providing significant improved near vision and effective near reading.<sup>68</sup> However, laboratory studies reveal that such small pupils will significantly degrade focused (distance) vision when lighting drops to low photopic and mesopic levels.<sup>73,74</sup> Balancing the need for expanded depth of field with the need to avoid loss of distance vision may require a small pupil approach that adjusts with light level, and this behaviour is generally observed with miotics drugs.<sup>80</sup> As pointed out by Charman,<sup>21</sup> effectiveness of expanding the eye's depth of field may also be enhanced if the eye is slightly myopic.

### Lens mobility

Similar to the approach taken by some fish<sup>7-9</sup> and cats,<sup>10</sup> multifocality can also be achieved by adjusting the position of the eye's lens. This approach lies at the heart of strategies to re-establish accommodation in pseudophakic eyes. In particular, the Food

and Drug Administration approved Crystalens (Bausch and Lomb, Rochester, NY, USA) employs a hinged haptic to try to utilise existing ciliary muscle activity to move the lens axially in pseudophakic eyes.<sup>81</sup> However, despite the addition of aspheric optics to the most recent lens design (Crystalens AO) aimed at creating spherical aberration-free surfaces,<sup>82</sup> inadequate axial movement has prevented this device from being widely successful.<sup>83</sup>

### Lens power variations

Multifocality can also be achieved by non-dynamic methods. Similar to some fish,<sup>15</sup> optical corrections in which optical power varies with spatial location across the pupil have been implemented in modern multifocal IOLs<sup>84-86</sup> and contact lenses.<sup>87-90</sup> Radially symmetric or concentric design multifocal lenses are most common,<sup>20</sup> but early multifocal contact lenses employed a segmented geometry inherited from spectacle lenses,<sup>91-93</sup> as did the earliest bifocal IOL (a variant of which is still produced).<sup>94</sup> Segmented bifocal contact lenses, however, suffered from rotational instabilities,<sup>92</sup> and are now typically only implemented as gas-permeable lens designs utilised for a select patient group.<sup>20</sup> Optical modelling reveals, however, that meridionally segmented optical designs may offer superior optical performance.<sup>95,96</sup>

The core principle of a concentric multifocal design is that it will be rotationally insensitive and include two or more powers contained in geometrically separate zones located at different distances from the lens centre<sup>97</sup> (Figure 3). Designs that incorporate two powers in alternating annular zones often also include significant regions of the lens in which there is a gradual power change with increasing radial distance.<sup>98,99</sup> For example, in Figure 3, which shows high-resolution Shack-Hartmann two-dimensional power maps and radially averaged power profile maps, this can be seen in both the centre-distance (top left) and centre-near (lower left) designs, and to a lesser extent in the concentric ring design (top right). Manufacturing limitations may necessitate a spatial spread of the transition in optical power, thereby adding multiple powers, and thus authenticating 'multifocal' labelling despite the fact that the lens design may have been strictly bifocal. This manufacturing by-product is

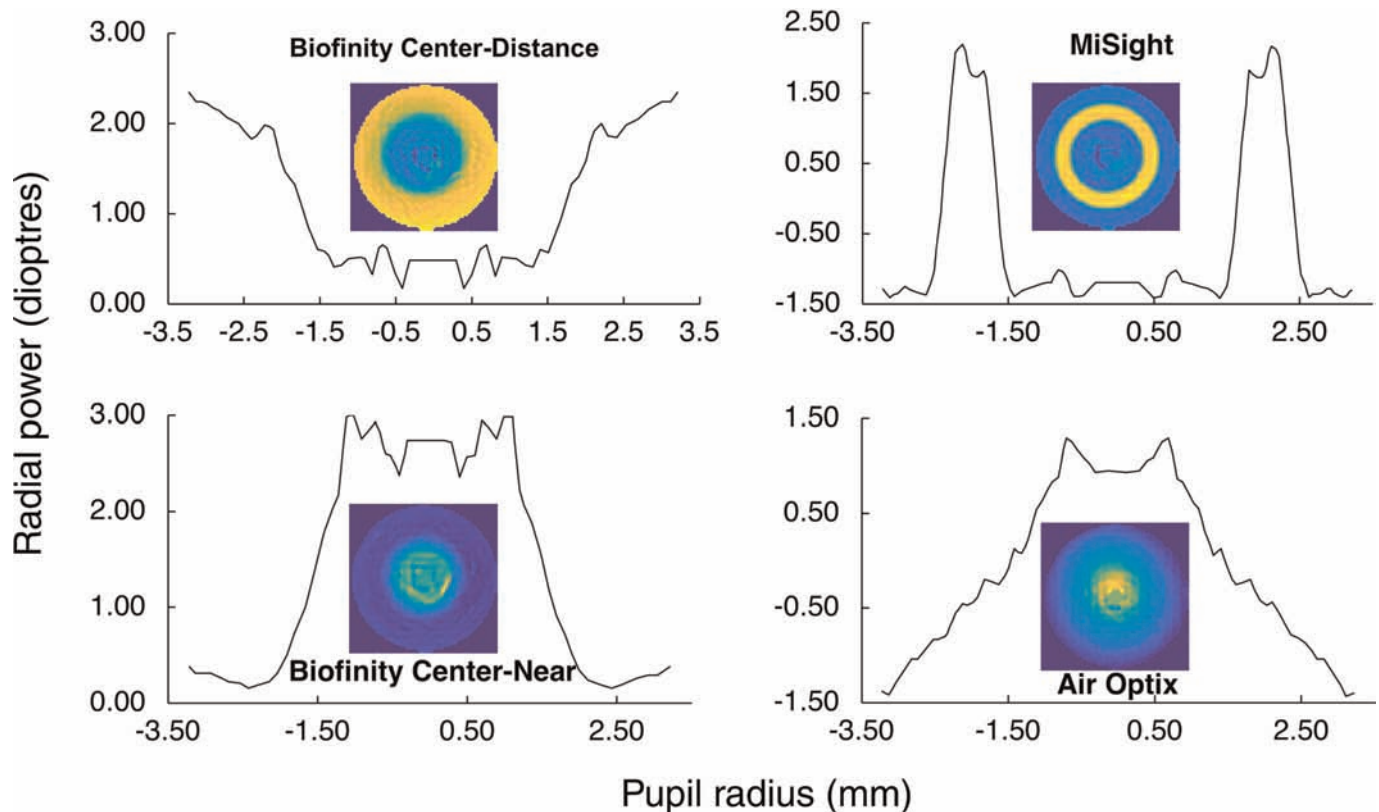


**Figure 3.** This figure shows power profiles of four multifocal contact lenses, two centre-distance designs (Biofinity CD and MiSight, both CooperVision, Pleasanton, CA, USA), and two centre-near designs (Biofinity CN and AirOptix, CooperVision and Alcon, Ltd, Fort Worth, TX, USA, respectively). Radial power was computed from wavefront slope data collected over a 7 mm analysis diameter (Power = slope/radius<sup>178,179</sup>) measured with a validated<sup>129</sup> Clear Wave (Lumetrics, Inc., Rochester, NY, USA) single pass Shack-Hartmann aberrometer (sample spacing of 0.104 mm). To avoid exaggerated computational noise errors near to the lens centre, power computations are not made in the central 0.6 mm, so this very centre data should be ignored. Colour maps show the radial symmetry of these four designs. In each colour map, the mean power is assigned green colour, and positive and negative deviations are coded by warm (yellow, orange) and cold (cyan, blue) colours, respectively.

quite different from a multifocal design containing a spatially extensive power gradient (similar to adding spherical aberration) from the lens centre to its periphery (Figure 3, lower right).

Another type of multifocal lens employs many concentric zones that each introduce half wavelength (or other fractional wavelength) optical path length steps between zones. These are usually referred to as diffractive lenses because their imaging properties rely on specific optical path length changes between zones<sup>100,101</sup> and result in constructive interference (images) at focal distances determined by the ring geometry.<sup>102</sup> In these lenses, a half wavelength ( $\pi$ ) phase shift between each zone produces a lens with two powers, a bifocal<sup>26,101,103</sup> and other phase step combinations can be used to generate trifocal

designs.<sup>104–106</sup> These diffractive designs can be distinguished from the previously described concentric refractive lenses because every location across the lens contributes to each power, and thus these lenses are often referred to as ‘full aperture’ designs,<sup>107–110</sup> in which the relative amount of energy in the distance and near images does not necessarily vary with pupil size, as it does with concentric refracting designs.<sup>97–99</sup> Diffractive optics have been incorporated into several IOLs,<sup>26,101,103,106,111,112</sup> but have had limited commercial success as contact lenses (for example, Echelon<sup>113,114</sup> and Diffrax<sup>115</sup>).

The pupil size dependency of concentric refractive designs can be considered either a liability or an attractive feature of the design,<sup>97</sup> and indeed, several IOLs have specifically modified the standard diffractive

design to generate a pupil size dependency in which the add optical power produced by the diffractive optical element contributes a higher proportion of the light in the image with small pupils and a much smaller proportion for large pupils. This ‘centre-near’ approach biases the optics toward the near add for near viewing (due to near viewing pupil miosis, which is present in older eyes<sup>116,117</sup>) but biases the optics to distance vision at night.<sup>101,112</sup> For example, a centre-near two-zone design with a central 3 mm diameter zone may become effectively a monofocal near correction at high light levels<sup>97,98,118</sup> resulting in all of the image energy being defocused when viewing distant objects. Similar to the diffractive lenses, an alternative design approach that varies power across meridians and not as a function of radius<sup>95</sup> may also have optical

characteristics that are approximately invariant as pupil size changes. Also, such designs avoid the inherently poor optical quality available from thin annular apertures<sup>97</sup> resulting in generally superior optical quality of the meridionally varying designs.<sup>95</sup> Such meridionally varying lenses were first introduced into IOLs by cementing together half lenses with differing powers.<sup>94</sup>

## Eye's inherent multifocality

Although the presbyopic eye is often considered as a monofocal optical system to be augmented with multifocal lenses in presbyopia and pseudophakia, the eye's optics are actually multifocal. For example, ocular longitudinal chromatic aberration (LCA) of the human eye generates approximately a 2.5 D difference in refractive state at the two extremes of the visible spectrum. Whitefoot and Charman<sup>119</sup> examined the impact on depth of focus by doubling or correcting LCA. Depth of focus increased by 0.50 D when doubling LCA and decreased by 0.30 D when correcting LCA. Some diffractive lens designs have the opposite sign of longitudinal chromatic aberration to refractive optics (more power at long wavelength versus short),<sup>102,103,115</sup> Therefore, the reverse LCA in the first diffractive order used to contribute bifocal add power can mostly correct the ocular LCA,<sup>103</sup> providing improved polychromatic image quality. These studies reveal that the multifocality of human eyes due to the wavelength dependence of refractive index offers little true multifocality for polychromatic stimuli, as expected due to the large visual attenuation of the spectral margins.<sup>120</sup>

The human eye also exhibits significant multifocality at each wavelength, primarily due to spherical aberration and coma. The former produces optical power that varies with radius squared, typically resulting in a myopic shift of about 2.00 D at the edge of an 8 mm diameter pupil.<sup>121</sup> Coma, on the other hand, can create a meridional linear ramp of power across the pupil. Therefore, the typical eye has both inherent radial and meridional multifocality, but as most presbyopes can attest, these levels of inherent multifocality remain insufficient to provide the depth of focus required to navigate our three-dimensional world. However, the naturally occurring changes in refractive state across the pupil will add to (or subtract from) any multifocality provided by a

contact lens or IOL.<sup>97,122</sup> Therefore, the significant positive spherical aberration exhibited by older eyes,<sup>123–125</sup> and the corneas of pseudophakes<sup>126</sup> may augment any centre-distance multifocal that also contributes more positive power with increasing radial distance from the lens centre (positive spherical aberration). However, in the case of centre-near designs which inherently contain negative spherical aberration,<sup>27,98,99,122</sup> ocular positive spherical aberration will subtract from the add power provided by the multifocal lens containing negative spherical aberration.<sup>97</sup> Importantly, ocular spherical aberration may be either a help or hindrance depending on the type of design being fit, and may likely contribute to the variable patient responses often experienced with these multifocal designs.<sup>127</sup>

Therefore, to achieve a desired level of multifocality in the corrected eye requires larger radially varying power changes (spherical aberration) in the correcting lens of a centre-near design than of a centre-distance design.<sup>27,97,122</sup> Although it is a simple matter to add the extra radially varying power needed for the centre-near designs, high levels of spherical aberration in a contact lens will introduce more coma as the lens decentres,<sup>128,129</sup> a problem well documented in the contact lens<sup>44,130–133</sup> and IOL<sup>134–140</sup> literature. Because many commercially available multifocal contact lenses and IOLs employ centre-near designs this problem is likely to be commonplace.

Figure 4 quantifies this issue by examining the impact of lens decentration when the

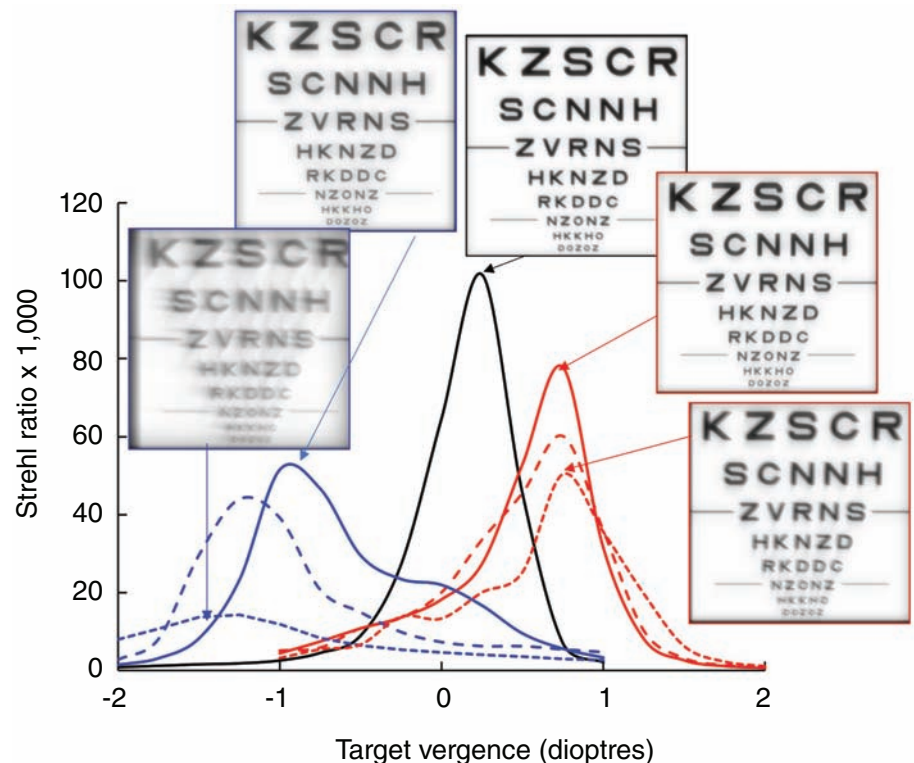


**Figure 4. Impact on image quality of adding spherical aberration to achieve multifocality.** The graph plots the Strehl Ratio image quality metric  $\times 1,000$  as a function of target vergence in dioptres for an aberrated presbyopic eye with a 6 mm pupil and  $+0.2$  microns of  $C_4^0$  (black curve), and for the same eye after spherical aberration has been added to give the eye+contact lens either  $+0.4$  microns of  $C_4^0$  spherical aberration (centre-distance model, red) or  $-0.4$  microns of  $C_4^0$  spherical aberration (centre-near model, blue). Further, 0.5 mm or 1.0 mm of lens decentration was introduced into the same centre-distance and centre-near models (dashed and dotted lines, respectively). Images of logMAR letter charts show the peak image quality achievable with and without 1 mm contact lens decentration.

added lens is designed to achieve a net spherical aberration level of 0.4 microns across a 6 mm pupil. The model included the reported higher-order aberrations of older eyes,<sup>141</sup> with a baseline spherical aberration level ( $C_4^0$ ) of +0.2 microns. To achieve matching eye+lens resultant positive and negative multifocality levels of positive or negative ( $C_4^0$ ) of 0.4 microns, the centre-distance lens must add +0.2 microns to the eye's +0.2 microns, but the centre-near lens must add -0.6 microns. The resulting peak image quality is slightly higher for the centre-distance model, but the impact of lens decentration is now much more dramatic for the centre-near model because the coma introduced by decentration scales with the magnitude of the spherical aberration levels within the contact lens.<sup>128</sup> Peak image quality (Figure 4, see inserts) and overall image quality ultimately is affected more by lens decentration in the centre-near design because of the higher levels of lens spherical aberration required to achieve multifocality.

**Problem of the simultaneously present defocused images**

Although zonal, diffractive bifocal, and multifocal lenses provide the different powers required to focus distance and near stimuli on the retina, the focused image is always coupled with a defocused image produced by the optical power inappropriate for the stimulus distance (for example, near optic and distant target). The amount of defocused light in a simple two-zone concentric design will vary systematically with pupil size<sup>97,98,122</sup> (Figure 5A). When the outer zone of a two-zone concentric design is defocused, the defocused point spread function will be an annulus.<sup>97,142,143</sup> In this case, the resulting annular 'halo' will increase in size as the pupil dilates and be most visible when the stimulus contrast is highest, as it is when viewing lights at night (a common source of visual disturbance clinically reported with multifocal optics). In addition to reducing the size of these haloes by reducing the add power (described as either low add multifocal lenses or 'extended depth of focus' lenses),<sup>144</sup> two alternative strategies have been proposed to minimise the visibility of these haloes. In one, the size of the defocused halo is reduced by coupling positive defocus with negative spherical aberration (that is,

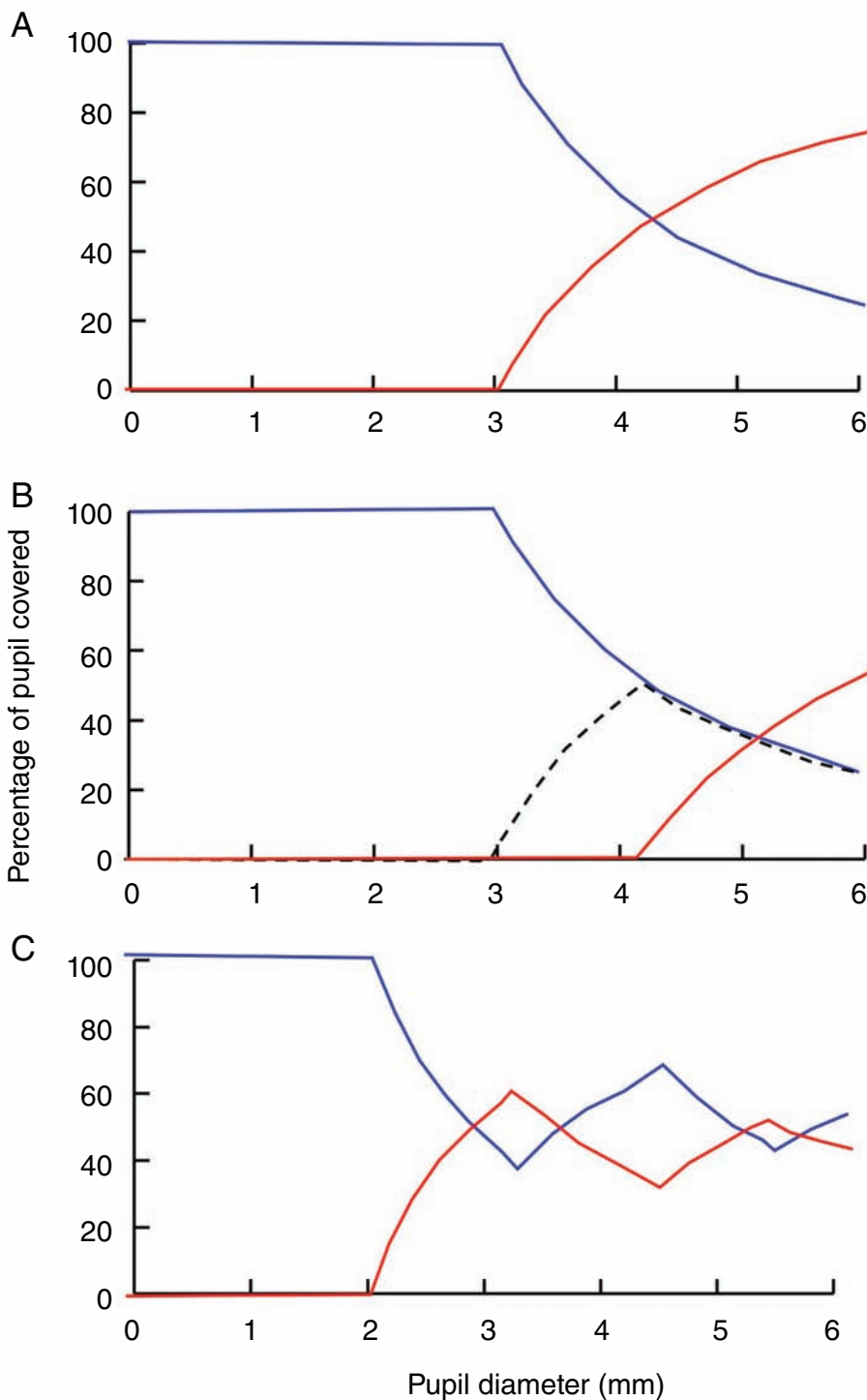


**Figure 5.** Three examples showing the relationship between pupil diameter (x-axis, mm) and the proportion of light imaged by each optic (y-axis) of radially varying zonal lenses. In each plot, the proportion of pupil covered by the distance (blue), near (red) and transition (black dashed) optics are plotted as a function of pupil diameter in mm for three centre-distance designs. Specifically, A: a lens with a 3 mm centre zone and an abrupt change to the add power, B: a centre-distance design with a 3 mm centre zone surrounded by 1.2 mm annulus across which power gradually changed to the near add power, and C: a five zone design with alternating distance (zones one, three, and five) and near (zones two and four) powers. Adapted from Bradley et al.<sup>97</sup> and Altoaimi et al.<sup>98</sup>

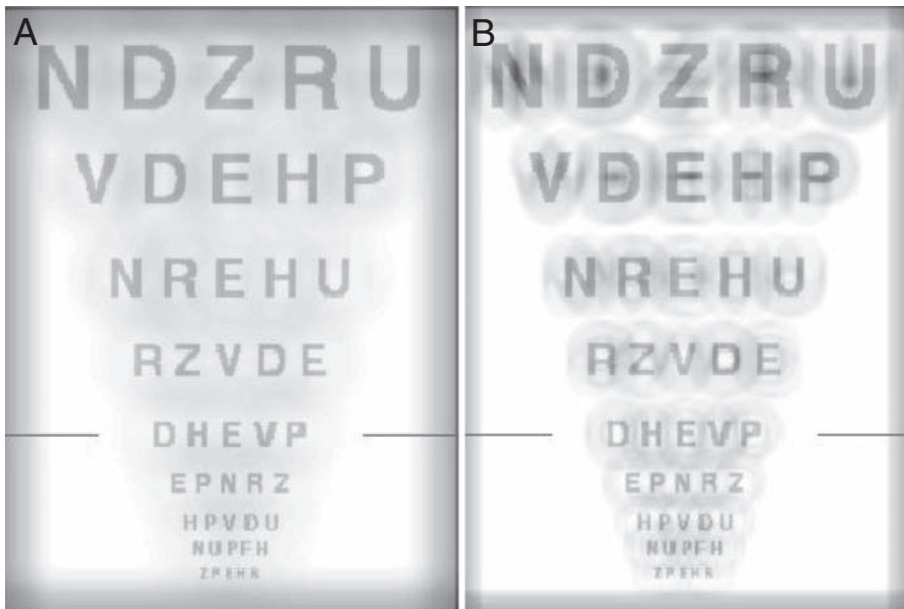


**Figure 6. Simulated retinal images generated by a radially varying zonal bifocal lens when the centre zone is focused, and the add zone is nominally +2.00 D defocused. Centre zone diameter is 3 mm, pupil diameter is 6 mm. In A: 0.15 microns of positive spherical aberration was added to the add zone, and in B: negative spherical aberration was added.**

including negative spherical aberration in the add zone) and vice versa. This produces a smaller but higher contrast halo. Alternatively, contrast of ghost images can be reduced by coupling positive spherical aberration with positive defocus (including positive spherical aberration in the add zone) and vice versa, which generates larger but lower contrast haloes with now clear edges.<sup>145</sup> The results of these two aberration-based strategies are simulated in Figure 6 for two designs of centre-distance optics with distance targets. On the left (Figure 6A), positive spherical aberration has been added to the near add zone increasing the size of the blur, but reducing its contrast, whereas on the right (Figure 6B), negative spherical aberration has been added to the add zone reducing the blur size but increasing its contrast. When positive defocus is generated by the add zone for distance stimuli, adding opposite sign negative spherical aberration creates high contrast phase reversed regions of the spatial frequency spectrum<sup>103</sup> which can disrupt the spatial structure of the focused image. This phase effect can be easily seen by comparing the phase correct but low contrast images in Figure 6A with the higher contrast but phase altered image in Figure 6B. Which would be more disruptive to a patient?

### Adopting multifocal optical designs for the control of myopia

Although multifocal optical designs were originally developed to provide increased depth of focus for eyes lacking autofocus capability (presbyopic and pseudophakic eyes) as described above, recent experiments on infant monkeys have shown that adding some extra plus power to an otherwise hyperopic eye will slow the growth of the vitreal chamber resulting in reduced myopia.<sup>146–148</sup> Significantly, Smith et al. also showed that added plus power could be restricted to the peripheral retina and have a similar impact.<sup>149</sup> These two results have led to a rapid proliferation of optical interventions to control myopia development that employ added plus power, notably into the peripheral retina.<sup>150–154</sup> Plus power can be added to the peripheral retinal image using some of the same approaches described above, such as by several types of centre-distance concentric ring designs (for example, MiSight; CooperVision, Pleasanton, CA, USA) or annular (Biofinity Multifocal, CooperVision). The axial separation of the cornea and contact lens from the eye's entrance pupil necessitates that rays

entering the pupil from the peripheral field must pass through the peripheral optics of the contact lens.<sup>63,155–158</sup> Of course, a similar variation in refractive state across the visual field may also potentially be created by aspheric lenses containing significant positive spherical aberration.<sup>159</sup> Likewise, orthokeratology also produces an eye with myopia in the peripheral optics or equivalently an eye with positive corneal plane spherical aberration.<sup>27,160–162</sup> Consistent with the hypothesis of removing peripheral hyperopia from the retinal image, these multifocal concentric ring<sup>163</sup> and annular<sup>164–166</sup> contact lens designs and the multifocal orthokeratology corneas have generally shown promise at slowing myopia development.<sup>163,167–173</sup>

### Lessons from evolution

Evolution developed some of the multifocal strategies now used to correct presbyopia, and the need for improved surrogates for accommodation grows every day as the presbyopic population grows toward an estimated 1.8 billion by 2050.<sup>174,175</sup> Additionally, the value of multifocal optics has expanded due to its ability to slow myopia progression.<sup>163,167–173</sup> As work continues to optimise these designs, there may be as yet untried evolutionary strategies that can be adapted. The true long-term solution, and where much of our future research likely may need to occur may be in preventing the onset of presbyopia in the first place.<sup>176</sup> Or, better yet, maybe even preventing ageing from occurring in the first place.<sup>177</sup> However, until then, a key understanding of the strengths and limitations of accommodation surrogates and how they might be applied in our clinical practices to aid our patients is critical.

### REFERENCES

1. Flitcroft DJ. The complex interactions of retinal, optical and environmental factors in myopia aetiology. *Prog Retin Eye Res* 2012; 31: 622–660.
2. Hoffman DM, Banks MS. Focus information is used to interpret binocular images. *J Vis* 2010; 10: 13.
3. Thorn F, Schwartz F. Effects of dioptric blur on Snellen and grating acuity. *Optom Vis Sci* 1990; 67: 3–7.
4. Raviola E, Wiesel TN. Effect of dark-rearing on experimental myopia in monkeys. *Invest Ophthalmol Vis Sci* 1978; 17: 485–488.
5. Smith EL 3rd. Spectacle lenses and emmetropization: the role of optical defocus in regulating ocular development. *Optom Vis Sci* 1998; 75: 388–398.
6. Smith EL 3rd, Hung LF. The role of optical defocus in regulating refractive development in infant monkeys. *Vision Res* 1999; 39: 1415–1435.
7. Schwab IR, Dubielzig RR, Schober C. *Evolution's Witness: How Eyes Evolved*. New York: Oxford University Press, 2012.

8. Schwab IR, Hart N. Cover illustration. More than black and white. *Br J Ophthalmol* 2006; 90: 406.
9. Khorramshahia O, Schartau JM, Krogera RHH. A complex system of ligaments and a muscle keep the crystalline lens in place in the eyes of boy fishes (teleosts). *Vision Res* 2008; 48: 1503–1508.
10. Hughes A. Observing accommodation in the cat. *Vision Res* 1973; 13: 481–482.
11. Alevogt R, Alevogt R. Studien zur Kinematik der Chamaeleonzung. *Z Vgl Physiol* 1954; 36: 66–77.
12. Flanders M. Visually guided head movement in the African chameleon. *Vision Res* 1985; 25: 935–942.
13. Kirmse W, Kirmse R, Milev E. Visuomotor operation in transition from object fixation to prey shooting in chameleons. *Biol Cybern* 1994; 71: 209–214.
14. Muntz WRA, Raj U. On the visual system of Nautilus Pompilius. *J Exp Biol* 1984; 109: 253–263.
15. Gagnon Y, Soderberg B, Kroger R. Optical advantages and function of multifocal spherical fish lenses. *J Opt Soc Am A Opt Image Sci Vis* 2012; 29: 1786–1793.
16. Ott M, Schaeffel F, Kirmse W. Binocular vision and accommodation in prey-catching chameleons. *J Comp Physiol A* 1998; 182: 319–330.
17. Duane A. An attempt to determine the normal range of accommodation at various ages, being a revision of Donder's experiments. *Trans Am Ophthalmol Soc* 1908; 11: 634–641.
18. Howland HC, Sivak JG. Penguin vision in air and water. *Vision Res* 1984; 24: 1905–1909.
19. Bito LZ, Kaufman PL, DeRousseau CJ et al. Presbyopia: an animal model and experimental approaches for the study of the mechanism of accommodation and ocular ageing. *Eye (Lond)* 1987; 1: 222–230.
20. Wolffsohn JS, Davies LN. Presbyopia: effectiveness of correction strategies. *Prog Retin Eye Res* 2019; 68: 124–143.
21. Charman WN. Pinholes and presbyopia: solution or sideshow? *Ophthalmic Physiol Opt* 2019; 39: 1–10.
22. Barrett BT, Bradley A, Candy TR. The relationship between anisometropia and amblyopia. *Prog Retin Eye Res* 2013; 36: 120–158.
23. Legras R, Hornain V, Monot A et al. Effect of induced anisometropia on binocular through-focus contrast sensitivity. *Optom Vis Sci* 2001; 78: 503–509.
24. Vandermeer G, Legras R, Gicquel JJ et al. Quality of vision with traditional monovision versus modified monovision. *Acta Ophthalmol Suppl* 2013; 91: S085.
25. Vandermeer G, Rio D, Gicquel JJ et al. Subjective through-focus quality of vision with various versions of modified monovision. *Br J Ophthalmol* 2015; 99: 997–1003.
26. Ravikumar S, Bradley A, Bhardwaj S et al. Expanding binocular depth of focus by combining monovision with diffractive bifocal intraocular lenses. *J Cataract Refract Surg* 2016; 42: 1288–1296.
27. Kollbaum PS. Optical aberrations of contact lenses and eyes corrected with contact lenses. In: *Optometry: Indiana University*. Bloomington, Indiana, 2007. pp. 196–233.
28. Schor C, Landsman L, Erickson P. Ocular dominance and the interocular suppression of blur in monovision. *Am J Optom Physiol Opt* 1987; 64: 723–730.
29. Fernandez EJ, Schwarz C, Prieto PM et al. Impact on stereo-acuity of two presbyopia correction approaches: monovision and small aperture inlay. *Biomed Opt Express* 2013; 4: 822–830.
30. Loshin DS. Binocular summation with monovision contact lens correction for presbyopia. *Int Contact Lens Clinic* 1982; 9: 161–173.
31. Collins M, Goode A, Brown B. Distance visual acuity and monovision. *Optom Vis Sci* 1993; 70: 723–728.
32. Lit A. Presentation of experimental data. *J Am Optom Assoc* 1968; 39: 1098–1099.
33. Westheimer G, McKee SP. Stereoscopic acuity with defocused and spatially filtered retinal images. *JOSA* 1980; 70: 772–778.
34. Back A, Grant T, Hine N. Comparative visual performance of three presbyopic contact lens corrections. *Optom Vis Sci* 1992; 69: 474–480.
35. Freeman MH, Charman WN. An exploration of modified monovision with diffractive bifocal contact lenses. *Cont Lens Anterior Eye* 2007; 30: 189–196.
36. Smith CE, Allison RS, Wilkinson F et al. Monovision: consequences for depth perception from large disparities. *Exp Eye Res* 2019; 183: 62–67.
37. Pollard ZF, Greenberg MF, Bordenca M et al. Strabismus precipitated by monovision. *Am J Ophthalmol* 2011; 152: 479–482 e471.
38. Legge GE, Rubin GS. Binocular interactions in suprathreshold contrast perception. *Percept Psychophys* 1981; 30: 49–61.
39. Ding J, Sperling G. A gain-control theory of binocular combination. *Proc Natl Acad Sci U S A* 2006; 103: 1141–1146.
40. Hickenbotham A, Tiruveedhula P, Roorda A. Comparison of spherical aberration and small-pupil profiles in improving depth of focus for presbyopic corrections. *J Cataract Refract Surg* 2012; 38: 2071–2079.
41. Xu R, Wang H, Jaskulski M et al. Small-pupil versus multifocal strategies for expanding depth of focus of presbyopic eyes. *J Cataract Refract Surg* 2019; 45: 647–655.
42. Smith G. Angular diameter of defocus blur discs. *Am J Optometry and Physiol Optics* 1982; 59: 885–889.
43. Winn B, Whitaker D, Elliott DB et al. Factors affecting light-adapted pupil size in normal human subjects. *Invest Ophthalmol Vis Sci* 1994; 35: 1132–1137.
44. Chateau N, De Brabander J, Bouchard F et al. Infrared pupillometry in presbyopes fitted with soft contact lenses. *Optom Vis Sci* 1996; 73: 733–741.
45. Xu R, Gil D, Dibas M et al. The effect of light level and small pupils on presbyopic reading performance. *Invest Ophthalmol Vis Sci* 2016; 57: 5656–5664.
46. Elliott SL, Choi SS, Doble N et al. Role of high-order aberrations in senescent changes in spatial vision. *J Vis* 2009; 9: 24.1–16.
47. Guirao A, Gonzalez C, Redondo M et al. Average optical performance of the human eye as a function of age in a normal population. *Invest Ophthalmol Vis Sci* 1999; 40: 203–213.
48. Pointer JS. The presbyopic add. I. Magnitude and distribution in a historical context. *Ophthalmic Physiol Opt* 1995; 15: 235–240.
49. Cheng X, Thibos LN, Bradley A. Estimating visual quality from wavefront aberration measurements. *J Refract Surg* 2003; 19: S579–S584.
50. Cheng X, Bradley A, Thibos LN. Predicting subjective judgment of best focus with objective image quality metrics. *J Vis* 2004; 4: 310–321.
51. Thibos LN, Hong X, Bradley A et al. Accuracy and precision of objective refraction from wavefront aberrations. *J Vis* 2004; 4: 329–351.
52. Kim WS, Park IK, Chun YS. Quantitative analysis of functional changes caused by pinhole glasses. *Invest Ophthalmol Vis Sci* 2014; 55: 6679–6685.
53. Kim WS, Park IK, Park YK et al. Comparison of objective and subjective changes induced by multiple-pinhole glasses and single-pinhole glasses. *J Korean Med Sci* 2017; 32: 850–857.
54. Wittenberg S. Pinhole eyewear systems: a special report. *J Am Optom Assoc* 1993; 64: 112–116.
55. Dick HB. Small-aperture strategies for the correction of presbyopia. *Curr Opin Ophthalmol* 2019; 30: 236–242.
56. Seyeddain O, Hohensinn M, Riha W et al. Small-aperture corneal inlay for the correction of presbyopia: 3-year follow-up. *J Cataract Refract Surg* 2012; 38: 35–45.
57. Srinivasan S. Small aperture intraocular lenses: the new kids on the block. *J Cataract Refract Surg* 2018; 44: 927–928.
58. Campos M, Beer S, Nakano EM et al. Complete depigmentation of a small aperture corneal inlay implanted for compensation of presbyopia. *Arq Bras Oftalmol* 2017; 80: 52–56.
59. Göt W. Correction of presbyopia with a small aperture corneal inlay. *J Refract Surg* 2011; 27: 842–845.
60. Dexl AK, Seyeddain O, Riha W et al. Reading performance after implantation of a small-aperture corneal inlay for the surgical correction of presbyopia: two-year follow-up. *J Cataract Refract Surg* 2011; 37: 525–531.
61. Freeman E. Pinhole contact lenses. *Am J Optom Arch Am Acad Optom* 1952; 29: 347–352.
62. Albarran Diego C, Montes-Mico R, Pons AM et al. Influence of the luminance level on visual performance with a disposable soft cosmetic tinted contact lens. *Ophthalmic Physiol Opt* 2001; 21: 411–419.
63. Atchison DA, Blazaki S, Suheimat M et al. Do small-aperture presbyopic corrections influence the visual field? *Ophthalmic Physiol Opt* 2016; 36: 51–59.
64. Langenbacher A, Goebels S, Szentmary N et al. Vignetting and field of view with the KAMRA corneal inlay. *Biomed Res Int* 2013; 2013: 154593.
65. Nau A. A contact lens model to produce reversible visual field loss in healthy subjects. *J Am Optom Assoc* 2012; 83: 279–284.
66. Carkeet A. Field restriction and vignetting in contact lenses with opaque peripheries. *Clin Exp Optom* 1998; 81: 151–158.
67. Renna A, Alio JL, Vejarano LF. Pharmacological treatments of presbyopia: a review of modern perspectives. *Eye Vis (Lond)* 2017; 4: 3.
68. Abdelkader A. Improved presbyopic vision with miotics. *Eye Contact Lens* 2015; 41: 323–327.
69. Abdelkader A, Kaufman HE. Clinical outcomes of combined versus separate carbachol and brimonidine drops in correcting presbyopia. *Eye Vis (Lond)* 2016; 3: 31.
70. Benozzi J, Benozzi G, Orman B. Presbyopia: a new potential pharmacological treatment. *Med Hypothesis Discov Innov Ophthalmol* 2012; 1: 3–5.
71. Dick HB, Piovella M, Vukich J et al. Prospective multicenter trial of a small-aperture intraocular lens in cataract surgery. *J Cataract Refract Surg* 2017; 43: 956–968.
72. Trindade C. Small aperture (pinhole) intraocular implant to increase depth of focus. In: *Application UP ed. US*, 2014.
73. Xu R, Wang H, Thibos LN et al. Interaction of aberrations, diffraction, and quantal fluctuations determine the impact of pupil size on visual quality. *J Opt Soc Am A Opt Image Sci Vis* 2017; 34: 481–492.
74. Xu R, Thibos L, Bradley A. Effect of target luminance on optimum pupil diameter for presbyopic eyes. *Optom Vis Sci* 2016; 93: 1409–1419.
75. Van Nes F, Baouman M. Spatial modulation transfer in the human eye. *JOSA* 1967; 57: 401–406.
76. Banks MS, Geisler WS, Bennett PJ. The physical limits of grating visibility. *Vision Res* 1987; 27: 1915–1924.
77. Campbell FW, Gregory AH. Effect of size of pupil on visual acuity. *Nature* 1960; 187: 1121–1123.
78. Woodhouse JM. The effect of pupil size on grating detection at various contrast levels. *Vision Res* 1975; 15: 645–648.
79. Seyeddain O, Riha W, Hohensinn M et al. Refractive surgical correction of presbyopia with the AcuFocus small aperture corneal inlay: two-year follow-up. *J Refract Surg* 2010; 26: 707–715.
80. McDonald JE 2nd, El-Moatassem Kotb AM, Decker BB. Effect of brimonidine tartrate ophthalmic solution 0.2% on pupil size in normal eyes under different luminance conditions. *J Cataract Refract Surg* 2001; 27: 560–564.
81. Marchini G, Pedrotti E, Sartori P et al. Ultrasound biometric changes during accommodation in eyes with accommodating intraocular lenses: pilot study and hypothesis for the mechanism of accommodation. *J Cataract Refract Surg* 2004; 30: 2476–2482.
82. Incorporated BaL. Bausch and Lomb Crystalens Accommodating Posterior Chamber Intraocular Lens Device Description. [Cited 07 Jan 2019] Available at: <https://www.bausch.com/ecp/our-products/cataract-surgery/lens-systems/crystalens-a0>, 2016.
83. Marcos S, Ortiz S, Perez-Merino P et al. Three-dimensional evaluation of accommodating intraocular lens shift and alignment in vivo. *Ophthalmology* 2014; 121: 45–55.
84. McNeely RN, Pazo E, Spence A et al. Visual quality and performance comparison between 2 refractive rotationally asymmetric multifocal intraocular lenses. *J Cataract Refract Surg* 2017; 43: 1020–1026.

85. Tan N, Zheng D, Ye J. Comparison of visual performance after implantation of 3 types of intraocular lenses: accommodative, multifocal, and monofocal. *Eur J Ophthalmol* 2014; 24: 693-698.
86. Lane SS, Morris M, Nordan L et al. Multifocal intraocular lenses. *Ophthalmol Clin North Am* 2006; 19: 89-105 vi.
87. Legras R, Rio D. Simulation of commercial vs theoretically optimised contact lenses for presbyopia. *Ophthalmic Physiol Opt* 2017; 37: 297-304.
88. Monsalvez-Romin D, Dominguez-Vicent A, Garcia-Lazaro S et al. Power profiles in multifocal contact lenses with variable multifocal zone. *Clin Exp Optom* 2018; 101: 57-63.
89. Kim E, Bakaraju RC, Ehrmann K. Power profiles of commercial multifocal soft contact lenses. *Optom Vis Sci* 2017; 94: 183-196.
90. Wagner S, Conrad F, Bakaraju RC et al. Power profiles of single vision and multifocal soft contact lenses. *Cont Lens Anterior Eye* 2015; 38: 2-14.
91. Robboy M, Erickson P. Performance comparison of current hydrophilic alternating vision bifocal contact lenses. *Int Contact Lens Clinic* 1987; 14: 237-243.
92. Borish IM, Soni S. Bifocal contact lenses. *J Am Optom Assoc* 1982; 53: 219-229.
93. Tshida H, Takahashi K, Sado K et al. Bifocal contact lenses: history, types, characteristics, and actual state and problems. *Clin Ophthalmol* 2008; 2: 869-877.
94. Hoffer KJ, Savini G. Multifocal intraocular lenses: historical perspective. In: Alió JL, Joseph P, eds. *Multifocal Intraocular Lenses: The Art and the Practice, Essentials in Ophthalmology*. Switzerland: Springer, 2014. pp. 5-28.
95. de Gracia P, Hartwig A. Optimal orientation for angularly segmented multifocal corrections. *Ophthalmic Physiol Opt* 2017; 37: 610-623.
96. de Gracia P, Dorronsoro C, Marcos S. Multiple zone multifocal phase designs. *Opt Lett* 2013; 38: 3526-3529.
97. Bradley A, Nam J, Xu R et al. Impact of contact lens zone geometry and ocular optics on bifocal retinal image quality. *Ophthalmic Physiol Opt* 2014; 34: 331-345.
98. Altoaimi BH, Kollbaum P, Meyer D et al. Experimental investigation of accommodation in eyes fit with multifocal contact lenses using a clinical auto-refractor. *Ophthalmic Physiol Opt* 2018; 38: 152-163.
99. Plainis S, Atchison DA, Charman WN. Power profiles of multifocal contact lenses and their interpretation. *Optom Vis Sci* 2013; 90: 1066-1077.
100. Klein SA. Understanding the diffractive bifocal contact lens. *Optom Vis Sci* 1993; 70: 439-460.
101. Davison JA, Simpson MJ. History and development of the apodized diffractive intraocular lens. *J Cataract Refract Surg* 2006; 32: 849-858.
102. Buralli D, Morris G, Rogers J. Optical performance of holographic kinoforms. *Appl Optics* 1989; 28: 976-983.
103. Ravikumar S, Bradley A, Thibos LN. Chromatic aberration and polychromatic image quality with diffractive multifocal intraocular lenses. *J Cataract Refract Surg* 2014; 40: 1192-1204.
104. Lee S, Choi M, Xu Z et al. Optical bench performance of a novel trifocal intraocular lens compared with a multifocal intraocular lens. *Clin Ophthalmol* 2016; 10: 1031-1038.
105. Alió JL, Plaza-Puche AB, Alió Del Barrio JL et al. Clinical outcomes with a diffractive trifocal intraocular lens. *Eur J Ophthalmol* 2018; 28: 419-424.
106. Cochener B, Boutillier G, Lamard M et al. A comparative evaluation of a new generation of diffractive trifocal and extended depth of focus intraocular lenses. *J Refract Surg* 2018; 34: 507-514.
107. Barton K, Freeman MH, Woodward EG et al. Diffractive bifocal contact lenses in aphakia and pseudophakia. *A pilot study Eye (Lond)* 1991; 5: 344-347.
108. Schwiegerling J. Analysis of the optical performance of presbyopia treatments with the defocus transfer function. *J Refract Surg* 2007; 23: 965-971.
109. Choi J, Schwiegerling J. Optical performance measurement and night driving simulation of ReSTOR, ReZoom, and Tecnis multifocal intraocular lenses in a model eye. *J Refract Surg* 2008; 24: 218-222.
110. Zheleznyak L, Kim MJ, MacRae S et al. Impact of corneal aberrations on through-focus image quality of presbyopia-correcting intraocular lenses using an adaptive optics bench system. *J Cataract Refract Surg* 2012; 38: 1724-1733.
111. Simpson MJ. Re: assessing the optical performance of multifocal (diffractive) intraocular lenses. *Ophthalmic Physiol Opt* 2009; 29: 207.
112. Simpson MJ. Diffractive multifocal intraocular lens image quality. *Appl Optics* 1992; 31: 3621-3626.
113. Atchison DA, Ye M, Bradley A et al. Chromatic aberration and optical power of a diffractive bifocal contact lens. *Optom Vis Sci* 1992; 69: 797-804.
114. Bradley A, Abdul Rahman H, Soni PS et al. Effects of target distance and pupil size on letter contrast sensitivity with simultaneous vision bifocal contact lenses. *Optom Vis Sci* 1993; 70: 476-481.
115. Freeman M, Stone J. A new diffractive bifocal contact lens. *Trans BCLA* 1987; 10: 15-22.
116. Radhakrishnan H, Charman WN. Age-related changes in static accommodation and accommodative miosis. *Ophthalmic Physiol Opt* 2007; 27: 342-352.
117. Altoaimi BH, Almutairi MS, Kollbaum P et al. Accommodative behavior of eyes wearing aspheric single vision contact lenses. *Optom Vis Sci* 2017; 94: 971-980.
118. Charman WN, Radhakrishnan H. Accommodation, pupil diameter and myopia. *Ophthalmic Physiol Opt* 2009; 29: 72-79.
119. Whitefoot HD, Charman WN. Hyperchromatic lenses as potential aids for the presbyope. *Ophthalmic Physiol Opt* 1995; 15: 13-22.
120. Bradley A, Glenn A. Fry Award Lecture 1991: perceptual manifestations of imperfect optics in the human eye: attempts to correct for ocular chromatic aberration. *Optom Vis Sci* 1992; 69: 515-521.
121. Thibos LN, Ye M, Zhang X et al. Spherical aberration of the reduced schematic eye with elliptical refracting surface. *Optom Vis Sci* 1997; 74: 548-556.
122. Kollbaum PS, Bradley A, Thibos LN. Comparing the optical properties of soft contact lenses on and off the eye. *Optom Vis Sci* 2013; 90: 924-936.
123. Guirao A, Redondo M, Artal P. Optical aberrations of the human cornea as a function of age. *J Opt Soc Am A Opt Image Sci Vis* 2000; 17: 1697-1702.
124. Artal P, Berrio E, Guirao A et al. Contribution of the cornea and internal surfaces to the change of ocular aberrations with age. *J Opt Soc Am A Opt Image Sci Vis* 2002; 19: 137-143.
125. Brunette I, Bueno JM, Harissi-Dagher M et al. Optical quality of the eye with the Artisan phakic lens for the correction of high myopia. *Optom Vis Sci* 2003; 80: 167-174.
126. Wang L, Santaella RM, Booth M et al. Higher-order aberrations from the internal optics of the eye. *J Cataract Refract Surg* 2005; 31: 1512-1519.
127. Bakaraju RC, Ehrmann K, Ho A et al. Inherent ocular spherical aberration and multifocal contact lens optical performance. *Optom Vis Sci* 2010; 87: 1009-1022.
128. Guirao A, Williams DR, Cox IG. Effect of rotation and translation on the expected benefit of an ideal method to correct the eye's higher-order aberrations. *J Opt Soc Am A Opt Image Sci Vis* 2001; 18: 1003-1015.
129. Kollbaum P, Jansen M, Thibos L et al. Validation of an off-eye contact lens Shack-Hartmann wavefront aberrometer. *Optom Vis Sci* 2008; 85: E817-E828.
130. Belda-Salmeron L, Drew T, Hall L et al. Objective analysis of contact lens fit. *Cont Lens Anterior Eye* 2015; 38: 163-167.
131. Woods RL, Saunders JE, Port MJ. Optical performance of decentered bifocal contact lenses. *Optom Vis Sci* 1993; 70: 171-184.
132. Wake E, Tienda JB, Uyekawa PM et al. Centration and coverage of hydrogel contact lenses. *Am J Optom Physiol Opt* 1981; 58: 302-308.
133. Mackie IA, Mason D, Perry BJ. Factors influencing corneal contact lens centration. *Br J Physiol Opt* 1970; 25: 87-103.
134. Holladay JT, Calogero D, Hilmantel G et al. Special report: American academy of ophthalmology task force summary statement for measurement of tilt, decentration, and chord length. *Ophthalmology* 2017; 124: 144-146.
135. Monestam E. Frequency of intraocular lens dislocation and pseudophacodonesis, 20 years after cataract surgery - a prospective study. *Am J Ophthalmol* 2019; 198: 215-222.
136. Perez-Merino P, Marcos S. Effect of intraocular lens decentration on image quality tested in a custom model eye. *J Cataract Refract Surg* 2018; 44: 889-896.
137. Schroder S, Schreckner J, Daas L et al. Impact of intraocular lens displacement on the fixation axis. *J Opt Soc Am A Opt Image Sci Vis* 2018; 35: 561-566.
138. Uzel MM, Ozates S, Koc M et al. Decentration and tilt of intraocular lens after posterior capsulotomy. *Semin Ophthalmol* 2018; 33: 766-771.
139. Zhu X, He W, Zhang Y et al. Inferior decentration of multifocal intraocular lenses in myopic eyes. *Am J Ophthalmol* 2018; 188: 1-8.
140. Zhu X, Zhang Y, He W et al. Tilt, decentration, and internal higher-order aberrations of sutured posterior-chamber intraocular lenses in patients with open globe injuries. *J Ophthalmol* 2017; 2017: 3517461.
141. Wang L, Koch DD. Ocular higher-order aberrations in individuals screened for refractive surgery. *J Cataract Refract Surg* 2003; 29: 1896-1903.
142. Charman WN. Theoretical aspects of concentric varifocal lenses. *Ophthalmic Physiol Opt* 1982; 2: 75-86.
143. Charman WN, Murray IJ, Nacer M et al. Theoretical and practical performance of a concentric bifocal intraocular implant lens. *Vision Res* 1998; 38: 2841-2853.
144. Gatinel D, Loicq J. Clinically relevant optical properties of bifocal, trifocal, and extended depth of focus intraocular lenses. *J Refract Surg* 2016; 32: 273-280.
145. Bradley A, Kollbaum PS, Thibos LN. Multifocal correction providing improved quality of vision. In: *USPTO ed. United States*, 2012.
146. Arumugam B, Hung LF, To CH et al. The effects of simultaneous dual focus lenses on refractive development in infant monkeys. *Invest Ophthalmol Vis Sci* 2014; 55: 7423-7432.
147. Arumugam B, Hung LF, To CH et al. The effects of the relative strength of simultaneous competing defocus signals on emmetropization in infant rhesus monkeys. *Invest Ophthalmol Vis Sci* 2016; 57: 3949-3960.
148. Smith EL 3rd, Hung LF, Huang J et al. Effects of local myopic defocus on refractive development in monkeys. *Optom Vis Sci* 2013; 90: 1176-1186.
149. Smith EL 3rd, Ramamirtham R, Qiao-Grider Y et al. Effects of foveal ablation on emmetropization and form-deprivation myopia. *Invest Ophthalmol Vis Sci* 2007; 48: 3914-3922.
150. Mutti DO, Sinnott LT, Reuter KS et al. Peripheral refraction and eye lengths in myopic children in the bifocal lenses in nearsighted kids (BLINK) study. *Transl Vis Sci Technol* 2019; 8: 17.
151. Liu Y, Wildsoet C. The effect of two-zone concentric bifocal spectacle lenses on refractive error development and eye growth in young chicks. *Invest Ophthalmol Vis Sci* 2011; 52: 1078-1086.
152. Charman WN, Mountford J, Atchison DA et al. Peripheral refraction in orthokeratology patients. *Optom Vis Sci* 2006; 83: 641-648.
153. Smith EL 3rd, Hung LF, Huang J. Relative peripheral hyperopic defocus alters central refractive development in infant monkeys. *Vision Res* 2009; 49: 2386-2392.
154. Shen J, Clark CA, Soni PS et al. Peripheral refraction with and without contact lens correction. *Optom Vis Sci* 2010; 87: 642-655.
155. Almutleb ES, Bradley A, Jedlicka J et al. Simulation of a central scotoma using contact lenses with an opaque centre. *Ophthalmic Physiol Opt* 2018; 38: 76-87.


156. Fedtke C, Manns F, Ho A. The entrance pupil of the human eye: a three-dimensional model as a function of viewing angle. *Opt Express* 2010; 18: 22364–22376.
157. Mathur A, Gehrman J, Atchison DA. Pupil shape as viewed along the horizontal visual field. *J Vis* 2013; 13: 3.
158. Spring KH, Apparent Shape SWS. Size of the pupil viewed obliquely. *Br J Ophthalmol* 1948; 32: 347–354.
159. Cheng X, Xu J, Chehab K et al. Soft contact lenses with positive spherical aberration for myopia control. *Optom Vis Sci* 2016; 93: 353–366.
160. Hiraoka T, Matsumoto Y, Okamoto F et al. Corneal higher-order aberrations induced by overnight orthokeratology. *Am J Ophthalmol* 2005; 139: 429–436.
161. Hiraoka T, Okamoto C, Ishii Y et al. Contrast sensitivity function and ocular higher-order aberrations following overnight orthokeratology. *Invest Ophthalmol Vis Sci* 2007; 48: 550–556.
162. Gifford P, Li M, Lu H et al. Corneal versus ocular aberrations after overnight orthokeratology. *Optom Vis Sci* 2013; 90: 439–447.
163. Chamberlain P, Peixoto-de-Matos P, Logan NS et al. A three-year randomized clinical trial of misight lenses for myopia control. *Optom Vis Sci* 2019; 96: 556–567.
164. Smith MJ, Walline JJ. Controlling myopia progression in children and adolescents. *Adolesc Health Med Ther* 2015; 6: 133–140.
165. Walline JJ, Greiner KL, McVey ME et al. Multifocal contact lens myopia control. *Optom Vis Sci* 2013; 90: 1207–1214.
166. Walline JJ, Lindsley K, Vedula SS et al. Interventions to slow progression of myopia in children. *Cochrane Database Syst Rev* 2011: CD004916.
167. Cho P, Cheung SW, Edwards M. The longitudinal orthokeratology research in children (LORIC) in Hong Kong: a pilot study on refractive changes and myopic control. *Curr Eye Res* 2005; 30: 71–80.
168. Walline JJ, Jones LA, Sinnott LT. Corneal reshaping and myopia progression. *Br J Ophthalmol* 2009; 93: 1181–1185.
169. Kakita T, Hiraoka T, Oshika T. Influence of overnight orthokeratology on axial elongation in childhood myopia. *Invest Ophthalmol Vis Sci* 2011; 52: 2170–2174.
170. Santodomingo-Rubido J, Villa-Collar C, Gilmartin B et al. Myopia control with orthokeratology contact lenses in Spain: refractive and biometric changes. *Invest Ophthalmol Vis Sci* 2012; 53: 5060–5065.
171. Cho P, Cheung SW. Retardation of myopia in Orthokeratology (ROMIO) study: a 2-year randomized clinical trial. *Invest Ophthalmol Vis Sci* 2012; 53: 7077–7085.
172. Hiraoka T, Kakita T, Okamoto F et al. Long-term effect of overnight orthokeratology on axial length elongation in childhood myopia: a 5-year follow-up study. *Invest Ophthalmol Vis Sci* 2012; 53: 3913–3919.
173. Churm J, Cho P. High myopia-partial reduction ortho-k: a 2-year randomized study. *Optom Vis Sci* 2013; 90: 530–539.
174. Holden BA, Fricke TR, Ho SM et al. Global vision impairment due to uncorrected presbyopia. *Arch Ophthalmol* 2008; 126: 1731–1739.
175. Frick KD, Joy SM, Wilson DA et al. The global burden of potential productivity loss from uncorrected presbyopia. *Ophthalmology* 2015; 122: 1706–1710.
176. Tsuneyoshi Y, Higuchi A, Negishi K et al. Suppression of presbyopia progression with pirenixine eye drops: experiments on rats and non-blinded, randomized clinical trial of efficacy. *Sci Rep* 2017; 7: 6819.
177. Lai RW, Lu R, Danthi PS et al. Multi-level remodeling of transcriptional landscapes in aging and longevity. *BMB Rep* 2019; 52: 86–108.
178. Southwell WH. Wave-front estimation from wave-front slope measurements. *J Opt Soc Am* 1980; 70: 998–1006.
179. Himebaugh NL, Nam J, Bradley A et al. Scale and spatial distribution of aberrations associated with tear breakup. *Optom Vis Sci* 2012; 89: 1590–1600.



# Customised aberration-controlling corrections for keratoconic patients using contact lenses

*Clin Exp Optom* 2020; 103: 31–43

DOI:10.1111/cox.12937

**Amit Navin Jinabhai**  PhD BSc (Hons)  
MCOptom FBCLA FEAEO FHEA

Division of Pharmacy and Optometry, School of Health Sciences, Faculty of Biology Medicine and Health, The University of Manchester, Manchester, UK  
E-mail: amit.jinabhai@manchester.ac.uk

Submitted: 8 April 2019

Revised: 20 May 2019

Accepted for publication: 23 May 2019

Technological advancements in the design of soft and scleral contact lenses have led to the development of customised, aberration-controlling corrections for patients with keratoconus. As the number of contact lens manufacturers producing wavefront-guided corrections continues to expand, clinical interest in this customisable technology is also increasing among both patients and practitioners. This review outlines key issues surrounding the measurement of ocular aberrations for patients with keratoconus, with a particular focus on the possible factors affecting the repeatability of Hartmann-Shack aberrometry measurements. This review also discusses and compares the relative successes of studies investigating the design and fitting of soft and scleral customised contact lenses for patients with keratoconus. A series of key limitations that should be considered before designing customised contact lens corrections is also described. Despite the challenges of producing and fitting customised lenses, improvements in visual performance and comfortable wearing times, as provided by these lenses, could help to reduce the rate of keratoplasty in keratoconic patients, thereby significantly reducing clinical issues related to corneal graft surgery. Furthermore, enhancements in optical correction, provided by customised lenses, could lead to increased independence, particularly among young adult keratoconic patients, therefore leading to improvements in quality of life.

**Key words:** aberration-controlling lenses, customised scleral lenses, customised soft lenses, higher-order aberrations, keratoconus, vertical coma

Keratoconus is an ectatic disease of the cornea, typically characterised by stromal tissue thinning causing the cornea to take on a steepened, conical shape.<sup>1</sup> Such alterations occur due to significant changes in the biomechanical properties of the cornea,<sup>2</sup> resulting in the stromal lamellar matrix no longer following a highly regularised, orthogonal pattern. Instead, there are distinct areas of poorly aligned collagen intermixed with collagen that is arranged in the conventional quasiregular fashion.<sup>3</sup> Subsequently, the keratoconic corneal shape becomes more easily distorted and typically shows a high degree of protrusion. The keratoconic cornea can also develop apical scarring, which may typically be attributed to rigid corneal contact lens wear and/or disease progression over time.<sup>4</sup> As the retina usually remains unaffected in keratoconus, the reduced visual performance found, compared to normal eyes, is directly attributable to a combination of irregular astigmatism,<sup>5</sup> higher-order aberrations (HOAs)<sup>6–8</sup> and,

where present, corneal scarring, which induces unwanted light scatter.<sup>9</sup>

Although keratoconus is most usually bilateral, inter-ocular asymmetry is common, with Nichols et al.<sup>10</sup> reporting that the degree of asymmetry is usually largest in patients with more advanced disease.

Unlike other ectatic conditions, such as pellucid marginal corneal degeneration,<sup>11</sup> keratoconus characteristically affects the inferior-central two-thirds of the cornea;<sup>12</sup> however, reports of centrally,<sup>13</sup> inferiorly,<sup>14</sup> inferior-nasally<sup>15</sup> and superiorly positioned cone apices<sup>16</sup> have also been published. Other studies indicate that the cone apex is most commonly displaced inferior-temporally in keratoconus.<sup>17,18</sup> Overall, the nature and exact location of the corneal steepening is unique for each keratoconic eye.

Alterations in the profile of the keratoconic cornea (Figure 1) induce large magnitudes of HOAs,<sup>6,19</sup> which differ significantly from those measured in healthy eyes.<sup>20–22</sup> Vertical coma (Z (3,-1)) is most commonly found to

be significantly elevated in keratoconic eyes,<sup>8,21,23–26</sup> as the maximal stromal thinning classically occurs at either the inferior<sup>5</sup> or inferior-temporal position.<sup>17,18</sup> Light waves arriving at the keratoconic eye, from a distant source, will be distorted by comparatively differing amounts at the (flatter) superior and (steeper) inferior cornea.<sup>20,27</sup> The keratoconic cone apex also distorts incoming light waves by 'rotating' them,<sup>27</sup> thereby inducing trefoil (or triangular astigmatic) aberrations.<sup>28,29</sup> Furthermore, the steepened cone also induces spherical aberration.<sup>20,28,29</sup> These notable differences in HOA terms, compared to normal eyes, have supported the use of aberrometry measurements as a useful tool to detect subclinical keratoconus<sup>25,28</sup> as well as to grade its severity.<sup>30</sup>

Despite these uses, a debatable issue, in relation to the measurement of HOAs in keratoconic patients, is their repeatability, particularly when compared to repeated aberration measurements made in normal

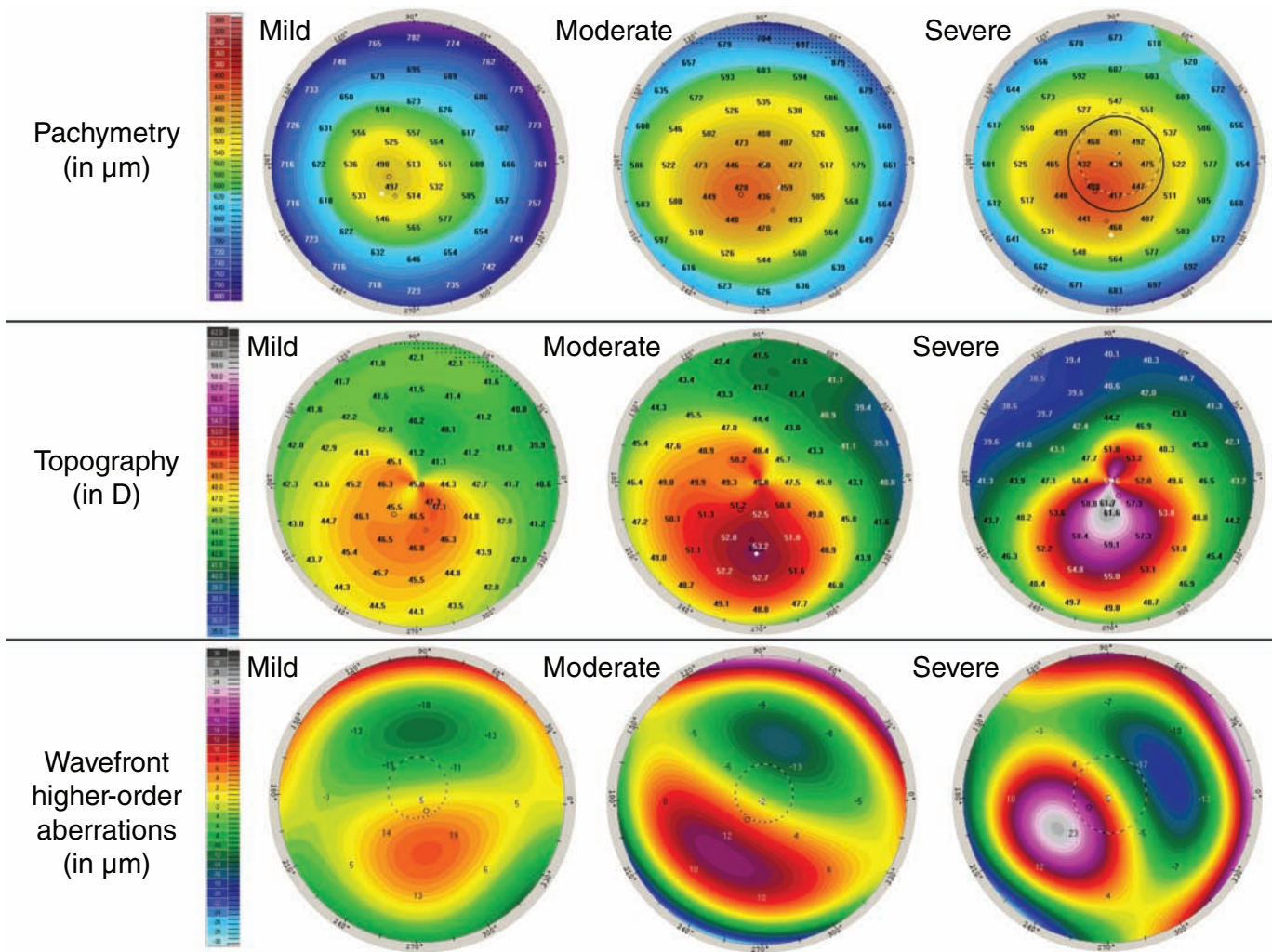


**Figure 1.** A collection of Pentacam data images highlighting the progression of keratoconus between three different keratoconic patients; specifically, an eye with ‘mild’ keratoconus (left-hand column), an eye with ‘moderate’ keratoconus (central column) and an eye with ‘severe’ keratoconus (right-hand column). The upper row presents pachymetry maps (numerical data are shown in microns [μm]), the middle row presents topography maps (numerical data are shown in dioptres [D]) and the lower row presents corneal wavefront higher-order aberration maps (numerical data are shown in microns [μm]).

eyes. Using a Scheimpflug-based topographer, both Shankar et al.<sup>29</sup> and Sideroudi et al.<sup>31</sup> have previously reported poor repeatability of anterior and posterior corneal surface aberrations, respectively. This finding was further supported by Jinabhai et al.,<sup>32</sup> who reported poor repeatability of ocular HOA measurements made using the Hartmann-Shack technique. In contrast, Bayhan et al.<sup>33</sup> reported comparable levels of intra-examiner repeatability between anterior corneal aberrations measured in 41 keratoconic eyes and 31 normal eyes using a combined Scheimpflug-Placido topographer. However, the authors’ data indicate that the repeatability of their posterior corneal aberration measurements was

comparatively poorer in the same group of keratoconic patients. Interestingly, Ortiz-Toquero et al.<sup>34</sup> have reported that anterior corneal HOA measurements, made using a Placido-based topographer, were actually more repeatable in 36 keratoconic eyes than measurements made in 36 normal eyes. Correspondingly, Shetty et al.<sup>35</sup> suggested that using a programmable, liquid-crystal-on-silicon phase modulating adaptive optics set-up, to evaluate ocular HOAs, yielded a high intra-session repeatability for eyes with mild to moderate keratoconus.

As the broad aim of this review is to consider HOA measurements with respect to their potential optical correction, discussion of the issues surrounding the measurement

of ocular aberrations would be of greater importance than just anterior corneal surface aberrations alone. This is due to the fact that the eye’s internal optics (the posterior corneal surface and the crystalline lens) are known to partly compensate for the aberrations of the anterior cornea in both normal<sup>36,37</sup> and keratoconic eyes.<sup>19,22,38,39</sup> In fact, Chen and Yoon<sup>38</sup> proposed that in keratoconus, some level of compensation exists between the coma root-mean-square (RMS) error aberrations of the anterior and posterior corneal surfaces. Their results indicated that the level of compensation seemed to vary with the severity of disease; on average 22, 24 and 14 per cent of the anterior surface’s coma RMS error

aberrations were compensated for by the posterior surface in severe, moderate and mild keratoconic eyes, respectively. In contrast, no such compensatory effects for coma RMS error were found in their normal subjects.

The majority of the studies that have explored the correction of ocular HOAs in keratoconic patients, using either soft, rigid corneal or rigid scleral contact lenses, have used the Hartmann-Shack principle to measure their patient's aberrations,<sup>23,26,40-56</sup> whereas comparatively fewer studies have used either skiascopic methods<sup>7,57-59</sup> or the laser ray-tracing method.<sup>60</sup>

Due to its comparative popularity, some key contributors that are likely to impact on the repeatability of ocular aberration measurements made using the Hartmann-Shack technique, in keratoconic patients, include:

- spot-imaging errors at the wavefront sensor
- computational limitations
- small (fixational) eye movements during measurements
- changes in aberrations due to micro-fluctuations in accommodation and/or changes in the tear film during measurements.

### Spot-imaging issues

For the Hartmann-Shack technique, the aberrated wavefront emerging from the eye is relayed onto a micro-lenslet array (Figure 2, lower image) thereby generating a pattern of multiple spot images, which is then analysed by computerised software. By measuring the displacement of the spot image, with respect to a fixed 'reference' point (Figure 3), the software then attempts to reconstruct the original aberrated wavefront falling onto the lenslet array (Figure 4, lower image).

When attempting to evaluate the optical quality of the keratoconic eye using the Hartmann-Shack technique, the fundamental problem lies in acquiring the spot images at the wavefront sensor, as the cornea may often be very distorted or even scarred (particularly in severe cases of keratoconus). The measurement performance of the wavefront sensor directly depends on how accurately the centre of each spot can be detected by the sensor's centroiding algorithm.<sup>61</sup> In general, data derived from a Hartmann-Shack sensor does not consider the 'optical quality' of the individual spots formed by the lenslet array.

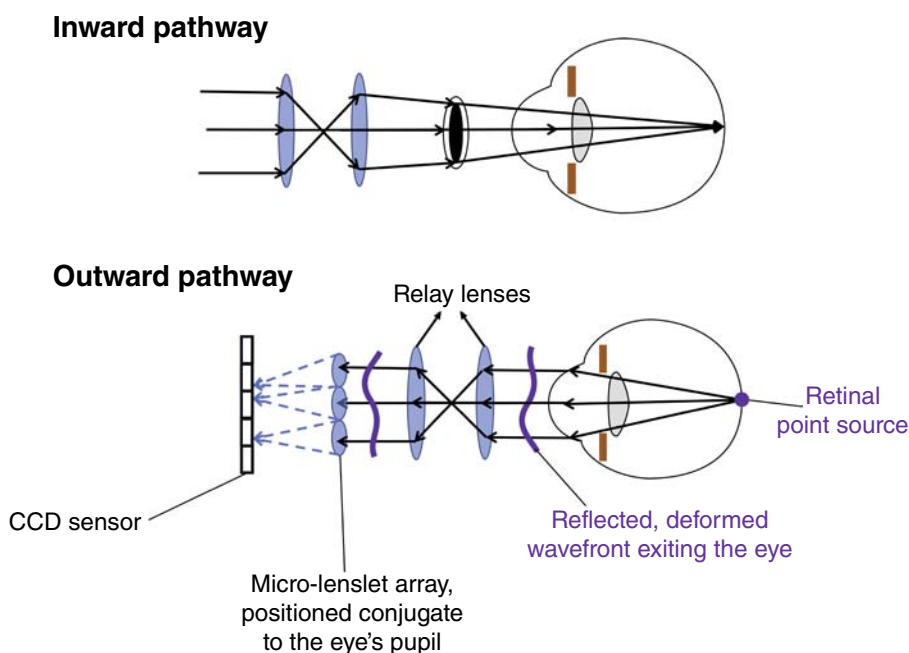


**Figure 2. Upper:** a diagram depicting the optical path that light takes through the Hartmann-Shack aberrometer as it enters the eye under investigation. **Lower:** a diagram depicting the optical path that light waves, reflecting off the retina, take on their way outward, toward the micro-lenslet array, before being imaged onto the charge-coupled device (CCD) sensor.

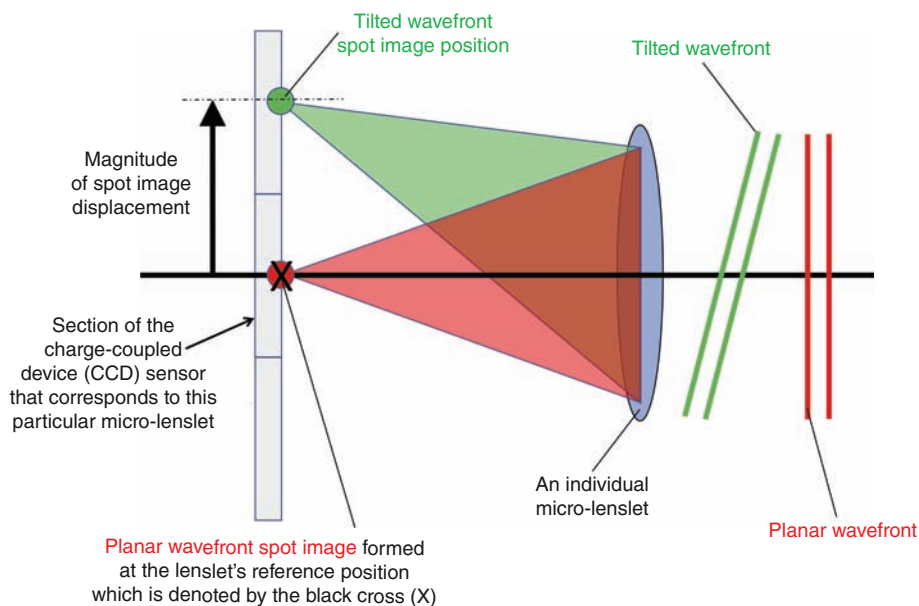


**Figure 3. A schematic diagram depicting the local wavefront slope formed at the Hartmann-Shack wavefront sensor. The planar wavefront (shown in red) passing through the micro-lenslet forms a spot image along its optical axis. The centroid position of the spot image is defined as the 'reference' position for the micro-lenslet (denoted by the black cross, X). The tilted wavefront (shown in green) passing through the micro-lenslet forms a spot image which is displaced away from the reference position (X) and corresponds to the local slope (shown in green) formed in front of the micro-lenslet.**

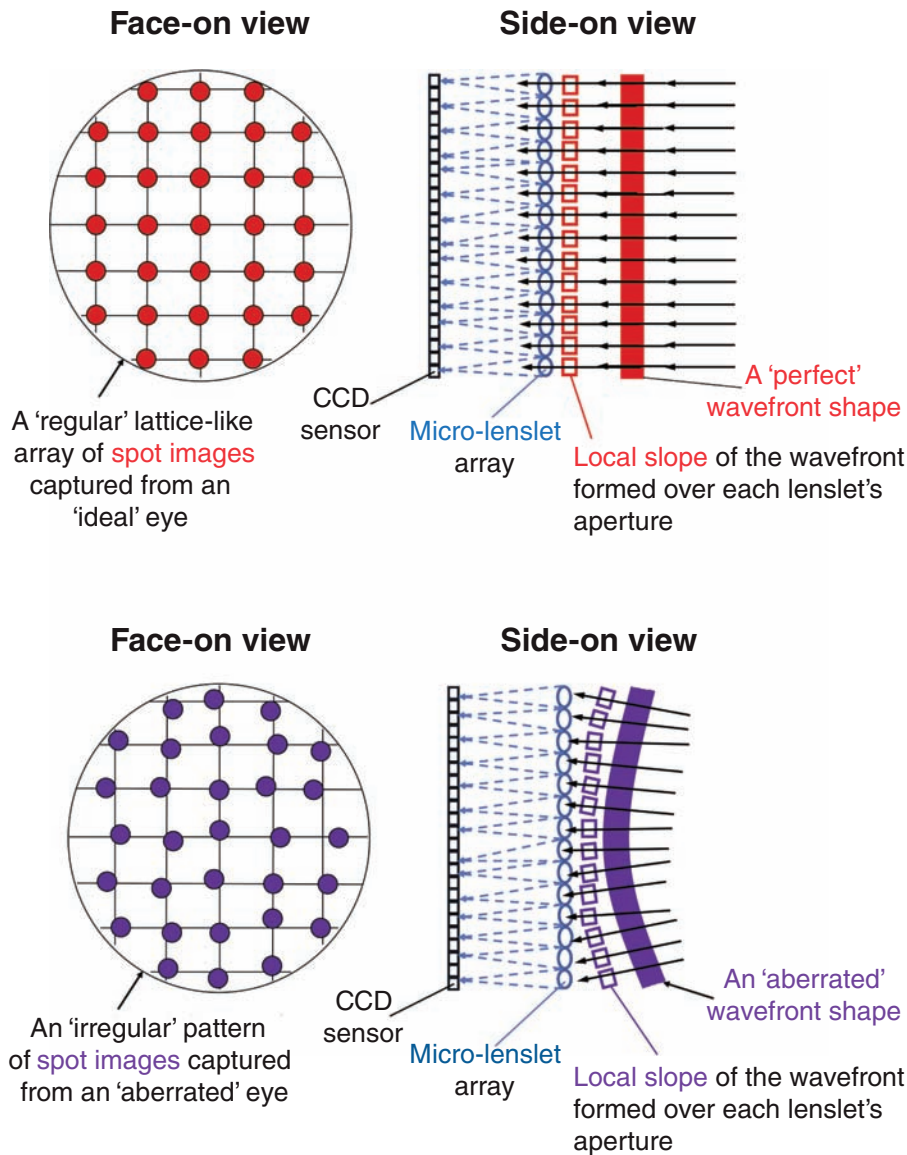


**Figure 4.** The imaging principles underpinning the Hartmann-Shack aberrometry technique for a perfect (upper) and an aberrated eye (lower). Upper: the Hartmann-Shack device's micro-lenslet array (where individual lenslets are typically between 0.3 to 0.5 mm in diameter) effectively subdivides the wavefront into multiple beams. The 'local slope' of the wavefront, over each individual lenslet's aperture, will determine the location of each individual spot image on the charge-coupled device (CCD) sensor. The upper illustration depicts the results for an 'ideal' eye, where the solid red line shows a 'perfect' wavefront. Lower: an aberrated wavefront produces an irregular pattern of spots on the CCD sensor. Displacement of each spot from the corresponding lenslet's axis gives a measure of the 'local slope' of the wavefront. The lower illustration depicts the results of an 'aberrated' eye where the wavy purple line shows an 'aberrated' wavefront.

Only the degree of their 'displacement' is needed to compute the local wavefront slope over each lenslet aperture (Figure 3). However, it is important to note that the optical quality of these spot images can vary greatly between normal and keratoconic eyes.<sup>62,63</sup>

A fundamental limitation of the Hartmann-Shack sensor is the requirement that each spot image, generated by any given micro-lenslet, must land within the 'virtual sub-aperture' of a certain photon detector at the charge-coupled device (CCD). To this end, the 'dynamic range' of a Hartmann-Shack aberrometer is somewhat restricted by the diameter of each individual micro-lenslet, which typically ranges somewhere between 0.3 to 0.5 mm,<sup>64</sup> but can be as large as 0.75 mm.<sup>65</sup>

The computerised software typically used in commercially available Hartmann-Shack aberrometers is not usually capable of correctly identifying the following spot image registration issues:<sup>56,61,66</sup>

- when two (or more) separate spot images are formed at the same CCD photon detector sub-aperture (Figure 5A)
- a spot image which perfectly overlaps with another, formed by an adjacent micro-lenslet (Figure 5B)
- a spot image that 'crosses over' the allocated path of another spot (Figure 5C)
- missing spot images – when one or more spot images are formed in an area that falls entirely outside of the CCD sensor (Figure 5D).

While a 'displaced' spot image is obviously aberrant from the 'chief' or 'reference' ray, the magnitude of this displacement provides no indication of the image's quality. On the other hand, a blurry spot image may actually contain more aberration, optical scatter and refractive blur compared to a sharper spot image.<sup>62,63</sup> Figure 6 shows a typical example of the appearance of the Hartmann-Shack spot images captured from an eye with severe keratoconus, while Figure 7 depicts the reconstruction of a highly aberrated wavefront derived from a grossly distorted spot image array formed at the CCD array, as is typically found in patients with keratoconus.

With the Hartmann-Shack technique, the CCD sensor assumes that all of the spot images will lie 'flat' over the finite diameter of the lenslet in question.<sup>67</sup> This assumption begins to break down even for coarse, lower-order aberrations when the magnitude of those aberrations is large. In such cases, the wavefront is significantly curved over the lenslet's aperture, resulting in a

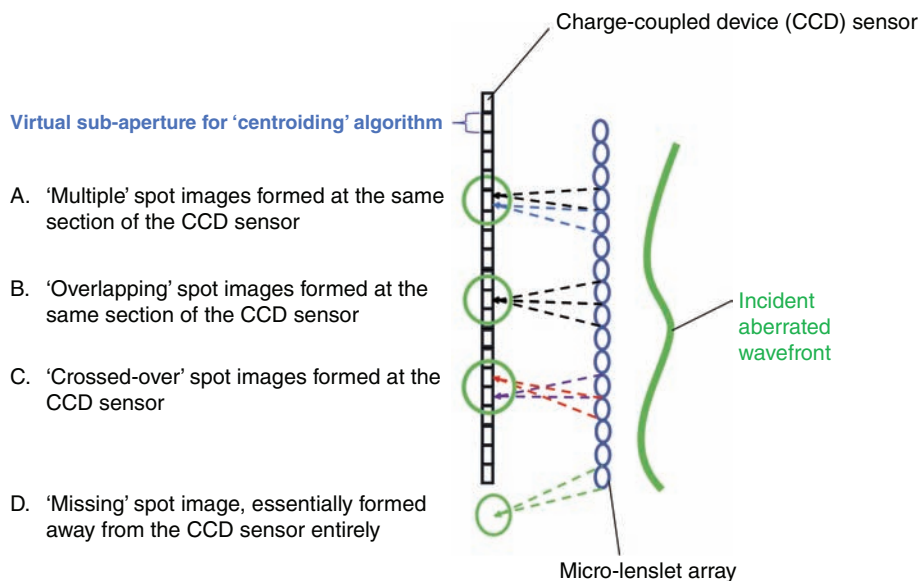


**Figure 5. Examples of spot-imaging issues impacting on the Hartmann-Shack technique, including: A: ‘multiple’ spot images, B: ‘overlapping’ spot images, C: ‘crossed-over’ spot images and D: a ‘missing’ spot image**

blurry spot, which is difficult to localise because its centre cannot always be accurately located.<sup>67</sup> If the aberrations are large enough, these blurry spots can even overlap, which considerably complicates the analysis.

It is also possible that ‘micro-aberrations’ may exist within the spot images, which are too small to be detected by the wavefront sensor’s detector.<sup>67</sup> These micro-aberrations could still be detrimental to the retinal image quality as they may contribute to the

inducement of a ‘hazy’ image of the spot, rather than a true geographical deviation of the spot image.<sup>9,63</sup> Although these blurry spot images are problematic, they contain useful information about the degree and location of optical scatter sources within the eye.<sup>63</sup>

Fundamentally, a simple solution to help decrease the amount of ‘crossover’ or ‘overlapping’ of the aberrated spot images would be to reduce the physical amount of spot displacement possible. This may be achieved

simply by using a micro-array of lenslets with a shorter second focal length.<sup>61,66</sup> However, this concept is somewhat flawed, as higher-powered micro-lenses would result in a reduction in sensitivity, that is, a decrease in the sensor’s ability to detect differences between differing magnitudes of aberration. Conversely, increasing the micro-lenses’ second focal length could provide permissible sensitivity, which may still be clinically useful; however, this adjustment limits the sensor’s dynamic range.<sup>61</sup> Another option would be to rearrange the physical spacing of the lenslets to allow maximum resolution;<sup>68</sup> however, this is not easily achieved with most commercially available Hartmann-Shack aberrometers and would likely impact on the spatial resolution of the wavefront.

Rarer and more complex methods have been suggested to help reduce the loss of data for the Hartmann-Shack technique, which include using:

- complex ‘unwrapping’ algorithms in the computational spot detection process; mathematical modifications to assign spots to their corresponding lenslet, even if deviated outside their sub-aperture<sup>69</sup>
  - astigmatic lenses in the micro-lenslet array, which produce ‘line’ rather than ‘spot’ images, all the cylindrical lenses are orientated at a multitude of different angles allowing simpler recognition of the line image from a given cylindrical aperture lens<sup>70</sup>
  - a spatial modulator array; this device is placed in front of the lenslet array and allows the selective switching ‘on’ and ‘off’ of certain sub-apertures, allowing a definite assignment of the spots to their corresponding sub-apertures onto the CCD sensor<sup>71</sup>
  - an image-processing algorithm, alongside an astigmatic lenslet array, that is capable of tracing line foci which fall outside the bounds of the conventional search<sup>72</sup>
  - a ‘spot searching’ method, which involves fitting an astigmatic micro-lenslet to the centre of every group of 2-x-2 spherical micro-lenslets within the overall array (also known as a dual micro-lenslet array). This optical set-up allows the generation of both spot and line images, which creates a unique discernible pattern which is then processed using binary computations and mask processing.<sup>64</sup>
- However, it is worth noting that most commercially available Hartmann-Shack aberrometers do not easily allow any of the

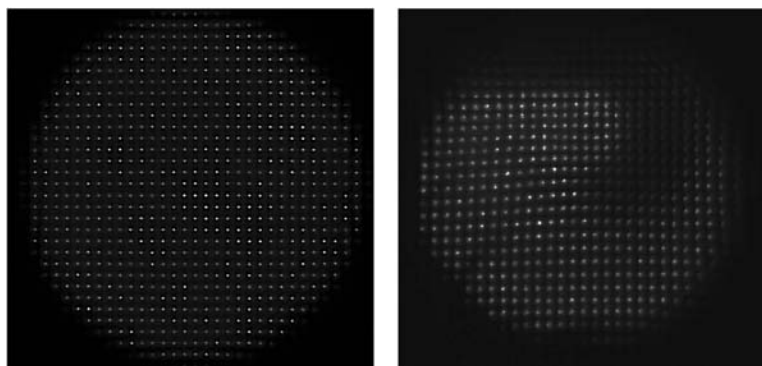


**Figure 6. A comparison of the raw Hartmann-Shack spot images (formed at the charge-coupled device) between a healthy normal eye (left) and an eye with severe keratoconus (right). While the left-hand image shows a regular series of spot images arranged into a lattice-like array, the right-hand image shows substantial spot image irregularities, such as missing spot images as well as fainter, blurrier spot images.**

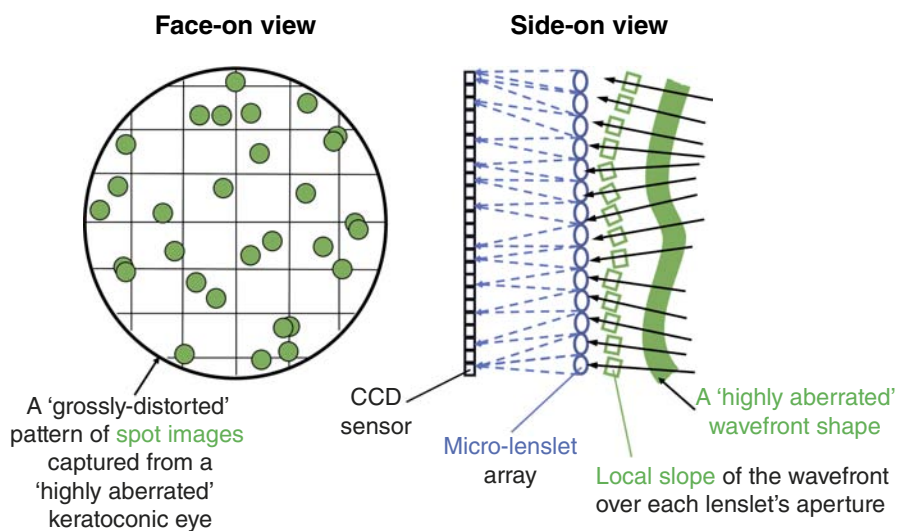


**Figure 7. A highly aberrated wavefront produces a grossly distorted pattern of spots on the charge-coupled device (CCD) sensor (left-hand image). Displacement of each spot from the corresponding lenslet's axis gives a measure of the 'local slope' of the wavefront. The illustration above depicts the results from a 'highly aberrated' keratoconic eye, where the wavy green line shows a highly aberrated wavefront (right-hand image).**

above modifications to be made to the devices' original set-up; as a result, these modifications are not routinely used in clinical investigations.

Compared to the aforementioned studies, the use of a 'translatable grid' has been implemented as a more practical approach for increasing the Hartmann-Shack method's 'dynamic range' – the maximum measurable wavefront slope of an aberrated ray.<sup>73,74</sup> The translatable grid increases the width of the area that any given aberrated spot can fall onto, by blocking every other neighbouring lenslet, for any given lenslet. Yoon et al.<sup>74</sup> used this translatable grid device on four normal human eyes, a keratoconic eye and an aberrated phase plate, and reported no difference in sensitivity, repeatability or accuracy compared to measurements made without the grid. Pantanelli et al.<sup>73</sup> successfully used this method on 190 normal control subjects, as well as 19 eyes with keratoconus. They found higher levels of negative vertical coma, third-order trefoil and fourth-order spherical aberration in the keratoconic eyes than in the normal eyes. Nonetheless, there are limitations to using a translatable grid, in that inaccuracies and errors could arise due to the longer data acquisition times required when using this technique, as the grid needs to

be moved several times during data capture. Additionally, neither study discusses that some spots, due to gross corneal distortion/scarring, will become deviated away from the aberrometer's CCD sensor altogether, nor do they clarify if their translating-grid method could possibly account for this. Finally, it is entirely plausible that some spot images, no matter how many times the grid is moved, are likely to fall onto the grid itself, causing 'lost' data (as no image will be registered at the CCD sensor). Nevertheless, the results from Pantanelli et al.<sup>73</sup> provided a possible solution for evaluating highly aberrated eyes. Translatable grids can only usually be used in custom-built aberrometers, as commercially available instruments will not permit such adaptations of their micro-lenslet array.

### Computational limitations

The aberration co-efficients recorded by an aberrometer are mathematically reconstructed from a discrete number of sampling points and are therefore *not* the perfect mirror image of the true aberrant wavefront.<sup>61,74,75</sup> The mathematical approach classically used in aberrometry employs the Zernike polynomial expansion series, which is based on the expansion of the derivatives of the wavefront aberration. Zernike polynomials are extremely popular in wavefront

analysis, primarily due to their orthogonality over a circular pupil and their representation of 'classic' Seidel aberration terms such as coma and spherical aberration.<sup>76</sup> Computation of the Zernike co-efficients requires a set of discrete orthogonal polynomials to be constructed using the Gram-Schmidt method, where the co-efficients are calculated by 'fitting' the wavefront slope gradients and orthogonal polynomials using a 'least-squares' method.<sup>77</sup> This methodology essentially describes how each aberration coefficient makes up a proportion of the total wavefront and aims to minimise the absolute error between the measured sampled points and the Zernike terms which are fitted to the data. However, investigators should be wary that the number of sampling points available from the Hartmann-Shack aberrometer will typically be far greater than the number of Zernike polynomial terms that can be fitted to the wavefront to describe its shape.<sup>67</sup> This has led to other research exploring newer methods to reconstruct and compute HOAs.<sup>78</sup>

Unfortunately, the direct subtraction or comparison of 'corneal' and 'total ocular' aberrations is not usually possible and can give rise to major inaccuracies, purely because different reference axes may have been used during the topography and aberrometry measurements. Most commercially available wavefront aberrometers measuring the total ocular aberrations tend to use the patient's line of sight as the reference axis. Aberrations measured with respect to this axis therefore have the pupil centre as the Cartesian origin.<sup>79</sup> On the other hand, corneal topographers generally align the videokeratographic axis with the corneal sighting centre (the intersection of the line of sight with the corneal surface).<sup>80</sup> Such inaccuracies in comparing corneal versus ocular aberrations may be accounted for (both mathematically and geometrically) and may be minimised by using an instrument that can take simultaneous corneal and ocular aberration measurements.<sup>20,22,24</sup>

### Small (fixational) eye movements

From the results of their reliability study of normal eyes, Cheng et al.<sup>81</sup> suggested that small fixational eye movements, which may have occurred during the measurement process, could induce variability in aberration measurements. Therefore, it is highly likely, for eyes with keratoconus, that any

such small eye movements during the measurement stage would induce larger variations in aberrations. This point is of particular importance as the magnitude of fixational eye movements are likely to be larger in keratoconic patients, than in normal subjects, due to poorer levels of acuity. While this suggestion currently remains unexplored, it is worth noting that both Mihaltz et al.<sup>82</sup> and Tan et al.<sup>6</sup> have demonstrated that the magnitude of the lower-order and HOAs measured in keratoconic eyes will be greatly influenced by the location of the cone apex.

### Changes in aberrations due to micro-fluctuations in accommodation or changes in the tear film

In normal eyes, other possible sources of variance in HOA measurements include changes in aberrations due to micro-fluctuations in accommodation<sup>83</sup> or variations in the tear film<sup>84</sup> during the measurement process. However, in patients with moderate keratoconus, Radhakrishnan et al.<sup>85</sup> found that while HOAs did alter with accommodation and tear film changes immediately post-blink; the magnitude of these changes were relatively small compared to their patients' manifest aberrations. In support of these results, Chen et al.<sup>48</sup> proposed that tear film-induced variations in aberrations could be somewhat countered by standardising aberration measurements, by ensuring that all readings are taken two seconds post-blink.

### Correcting ocular aberrations in keratoconic patients

#### VISUAL BENEFIT

Despite potential issues regarding their repeatability, Williams et al.<sup>86</sup> have proposed there is usually an identifiable and significant 'visual benefit' (VB) to correcting the ocular HOAs of the keratoconic eye measured using the Hartmann-Shack method. The authors calculated their VB scores as the ratio of the modulation transfer function (MTF) measured with a 'customised aberration correction' in place (that is, a correction that specifically corrected for all lower-order and HOA terms), to the MTF found with just the second-order aberrations corrected – all of their MTFs were computed for a pupil diameter of 5.7 mm and a spatial frequency of 16 cycles/degree.<sup>86</sup> Accordingly, their VB scores indicated the potential increase in retinal image contrast by correcting all of the monochromatic HOAs

(in white light), rather than just defocus and astigmatism alone. Scores of > 1.0 represent a positive VB, indicating a gain in visual performance through aberration correction, whereas eyes with a score of 1.0 would gain no VB from correction. Williams et al.<sup>86</sup> found that the VB in 109 normal eyes ranged from 1.5 to 8.0, whereas the VB for their four keratoconic eyes varied between 2.5 to 25.0. Similar magnitudes of positive VB scores were also found for four keratoconic patients by Guiaro et al.,<sup>87</sup> at MTF spatial frequencies of 16 and 32 cycles/degree. Furthermore, using their translatable grid-integrated Hartmann-Shack wavefront aberrometer to increase dynamic range,<sup>74</sup> Pantanelli et al.<sup>73</sup> also reported encouraging VB scores (ranging from 2.5 to 10.5) for 15 keratoconic patients. The authors calculated their VB scores using the metric of volume under the MTF across spatial frequencies of zero to 60 cycles/degree. Overall, these three studies each highlighted that the theoretical benefit of using customised correction methods for keratoconic eyes was far superior to that of normal eyes.

#### DO ALL ABERRATION TERMS NEED CORRECTING?

The literature indicates that correcting every single aberration term may not be beneficial, as lens decentrations are likely to hinder the VB yielded for both normal<sup>87,88</sup> and keratoconic eyes.<sup>40,89,90</sup> Furthermore, due to changes with accommodation and variations in the tear film, it is also widely accepted that very few HOA terms are completely stable in either normal<sup>81,83,84,91</sup> or keratoconic eyes.<sup>32,51,85</sup> Nonetheless, López-Gil et al.<sup>92</sup> reported that the aberrations created through decentration of customised lenses were likely to be smaller than the difference between the total RMS error measured with and without customised lenses in place for two normal eyes. Thus López-Gil et al.<sup>92</sup> hypothesised that, "wearing a customised contact lens over a course of time will show a clear benefit... especially for patients with moderate to high amounts of aberration". On the other hand, Marsack et al.<sup>75</sup> proposed that correction of all the HOA terms of the keratoconic eye are not worthwhile. The authors suggested that only correcting between the third and up to the fifth Zernike orders would give most keratoconic eyes better visual performance and lessen the likelihood of inducing superfluous aberrations due to lens decentrations. However,

when interpreting the data presented by Marsack et al.,<sup>75</sup> it is important to note that the authors assumed a 'perfect' on-eye alignment of their 'customised lens' correction (that is, a contact lens that was custom-designed to correct lower-order aberrations, while also simultaneously reducing some of the HOAs associated with keratoconus). However, this is an unrealistic assumption for even a prism-ballasted toric soft lens, which typically moves vertically by 0.3 to 1.0 mm upon blink,<sup>93,94</sup> with approximately 2–15 degrees of rotation.<sup>95</sup> The results of modelling simulation by Marsack et al.<sup>75</sup> showed that mild and moderate cases of keratoconus would theoretically benefit more than those with severe keratoconus if the number of Zernike radial orders that are corrected are truncated. This finding was perhaps to be expected, as severe to advanced keratoconic patients are more likely to show larger magnitudes of aberrations at the higher radial orders. Therefore, in order to successfully correct aberrations in keratoconus, with aberration-controlling customised lenses, it may be necessary to modify the strategy of correction depending on each individual patient's disease severity.

### The use of non-customised contact lenses to correct aberrations

To date, a number of studies have investigated the use of non-customised soft lenses,<sup>43,57,58</sup> rigid corneal lenses<sup>7,23,40,42,46,47,54,57</sup> and rigid scleral lenses<sup>51,55,59</sup> to reduce the magnitude of manifest HOAs in keratoconic patients, with each demonstrating varying degrees of success, as well as revealing some important findings.

Perhaps rather predictably, both Jinabhai et al.<sup>43</sup> and Abdu et al.<sup>57</sup> agreed that non-customised corneal lenses provided better visual performance and superior aberration correction than non-customised soft contact lenses. Compared to soft lenses, corneal lenses can mask the manifest corneal aberrations, induced through keratoconus, by effectively 'replacing' the irregular corneal surface with smooth and regular refractive surfaces.<sup>96,97</sup>

However, both Jinabhai et al.<sup>43</sup> and Abdu et al.<sup>57</sup> confirmed that even with corneal lenses *in situ*, there were still some residual HOAs present, which were typically larger in magnitude than the aberrations measured in normal, healthy eyes.<sup>91,98</sup> These findings corroborated the results of other previous studies of keratoconic patients habitually wearing corneal lenses<sup>7,23,46,47</sup> or scleral

lenses.<sup>59</sup> Other authors have proposed that these residual aberrations are most likely attributable to irregularities of the posterior corneal surface,<sup>22,38,39</sup> which is also known to become significantly distorted in keratoconus.<sup>99</sup>

To investigate the potential impact of correcting such residual aberrations on visual performance, Yang et al.<sup>54</sup> used a customised adaptive optics visual simulator (a 37-actuator deformable mirror) to measure contrast sensitivity function (using sine-wave gratings, presented at five different spatial frequencies) with corneal contact lenses *in situ* for 20 eyes of 19 keratoconic patients. Compared to without it, the authors reported improved contrast sensitivity function with their simulator, particularly at low (two cycles/degree) and intermediate spatial frequencies (four, eight and 16 cycles/degree). Overall, the results from this study highlighted that better correction of residual aberrations could likely improve visual performance in keratoconic patients.<sup>54</sup>

### The use of customised corrections for keratoconic patients

Ahead of discussing individual studies, it is important to acknowledge that the majority of the literature regarding the design and use of customised lenses,<sup>26,41,44,45,48-50</sup> phase plates<sup>49</sup> or adaptive optics (typically in the form of a deformable mirror)<sup>54,100-103</sup> is largely limited to 'non-surgical' keratoconic corneas only, which typically show no apical scarring. While this is not representative of the full spectrum of keratoconic patients, such studies provide key information about the impact of correcting optical aberrations without the confounding factor of 'optical scattering' due to the presence of corneal scarring.

Contact lenses are discrete, simple to use and relatively inexpensive to manufacture, and therefore represent a suitable device with which to correct HOAs. This idea was first proposed by Smirnov<sup>104</sup> who acknowledged that "it is possible to manufacture a lens compensating for the wave(front) aberrations of the eye" and that "these lenses must obviously be contact ones". As corneal lenses will typically show significant magnitudes of on-eye decentration with blinking, a number of studies have investigated the use of soft contact lenses for providing a customised correction of aberrations.<sup>26,41,44,45,48-50</sup> A soft lens design, which could achieve maximum on-eye lens comfort as well as providing optimal

visual performance, would be appealing to many keratoconic patients and practitioners alike. Ideally, this hydrogel contact lens would be silicone-based, of a regular thickness and would have the capabilities to reduce the manifest ocular HOAs associated with keratoconus.

### SIMULATIONS

de Brabander et al.<sup>90</sup> simulated the visual performance achieved by using a customised soft lens to correct HOAs in nine moderate keratoconic eyes and reported large improvements in the MTF with the 'perfect' alignment of a customised lens. Like the results of Guirao et al.,<sup>88,105</sup> de Brabander et al.<sup>90</sup> reported that decentrations of their customised soft lens led to a partial loss in the VB gained for keratoconic patients. However, it should be noted that the authors calculated the effects of rotation and translation separately from each other. Clinically, it is widely accepted that soft lenses will translate and rotate upon blinking, simultaneously,<sup>93,94</sup> and that these movements are not mutually exclusive. Nonetheless, the results of de Brabander et al.<sup>90</sup> showed that rotations up to a maximum of five degrees and translations up to a maximum of 1 mm, upon blinking would be permissible to still yield a benefit from a customised lens.

Yoon and Jeong<sup>106</sup> simulated the decentration of customised contact lenses for two post-penetrating keratoplasty and two keratoconic eyes. They found that compared to normal eyes (VB = 3), a customised correction gave their highly aberrated eyes a threefold improvement in visual performance (VB = 9). The authors' results also suggested that highly aberrated eyes were more tolerant to decentrations than normal eyes; for a 0.2 mm translation vertically, the VB gained was reduced by only a third for highly aberrated eyes, but by half in normal eyes.

### CUSTOMISED SOFT LENSES

Jeong and Yoon<sup>49</sup> manufactured a front-surface, customised aberration-controlling soft lens for a patient with advanced keratoconus. On-eye lens decentration was accounted for by first fitting a conventional soft 'trial' lens and monitoring its centration using an infrared pupil camera linked to their aberrometer. The aberration correction was transferred onto the final customised lens, accounting for any on-eye

lens translation/rotation observed with the 'trial' lens. Their customised lens reduced uncorrected higher-order RMS (HORMS) error by 67 per cent; however, the authors did not measure visual acuity as part of their experiment. The authors proposed that their residual aberrations could have been induced by variations in the tear film, or even on-eye vertical translation and/or rotation of the customised lens with blinks.

Sabesan et al.<sup>50</sup> conducted a comparison study for three keratoconic eyes (two severe and one moderate) investigating the effectiveness of front-surface, customised soft lenses versus conventional soft and corneal lenses. The authors accounted for possible soft lens decentrations by fitting 'trial' lenses with three different base curves and assessed their fittings to ascertain which was the most stable for each eye, ahead of manufacturing their customised soft lenses. In the most successful case, the uncorrected HORMS error was reduced by 75 per cent with the customised lens, but only by 17 per cent with a conventional soft lens. Compared to the conventional lenses, the customised lenses gave improved low-contrast (20 per cent) logarithm of the minimum angle of resolution (logMAR) acuities, by an average of 2.1 lines. For one of their severe cases, the customised lens gave an improvement of three lines of low-contrast logMAR acuity compared to the patient's habitual corneal lens. For high-contrast (100 per cent) acuity there was very little difference between the subject's corneal lens and the customised lens; however, the customised lens still performed best. In agreement with Jeong and Yoon<sup>49</sup>, Sabesan et al.<sup>50</sup> also noted that some small residual errors persisted even with their customised lenses *in situ*.

Marsack et al.<sup>45</sup> produced a front-surface, customised aberration-controlling soft lens for a patient with moderate keratoconus and compared this to the patient's habitual, conventional soft contact lens. The results showed that both high-contrast (87 per cent) and low-contrast (four per cent) logMAR acuity were improved with the customised lens compared to with the habitual soft lens. In contrast to the results of Sabesan et al.,<sup>50</sup> Marsack et al.<sup>45</sup> found that high-contrast logMAR acuity was improved (by 1.5 lines;  $p = 0.03$ ) more than low-contrast logMAR acuity (which only improved by one line of letters;  $p = 0.11$ ); however, such differences may be due to the differing contrast levels used between these two studies.



Interestingly, although Marsack et al.<sup>45</sup> noted that the habitual lenses typically translated on-eye with blinks, they did not incorporate this factor into the design of their final customised lenses. Nonetheless, their customised lens successfully reduced the uncorrected HORMS error from 0.99  $\mu\text{m}$  to 0.37  $\mu\text{m}$  over a 5 mm pupil (compared to 0.77  $\mu\text{m}$  found with the habitual conventional soft lens).

Chen et al.<sup>48</sup> proposed a method of enhancing the fitting of aberration-controlling soft lenses by custom-designing the lens' back surface (using topographical data) to help reduce residual aberrations induced through lens translations/rotations. The authors reported that compared to conventional lenses, their customised lenses reduced both horizontal and vertical translations by a factor of two and reduced rotations by a factor of five. However, the authors' customised lenses only successfully reduced uncorrected HORMS error for one of their three patients with moderate keratoconus, from 1.66  $\pm$  0.06  $\mu\text{m}$  to 0.61  $\pm$  0.04  $\mu\text{m}$ , whereas for one patient, the author's customised lens actually induced a significant increase in HORMS error, from 1.17  $\pm$  0.04  $\mu\text{m}$  (when uncorrected) to 1.30  $\pm$  0.10  $\mu\text{m}$ , which was largely attributed to overcorrection of a majority of Zernike terms with their customised lens *in situ*. For the remaining patient, there was no significant change in HORMS error (uncorrected: 0.70  $\pm$  0.03  $\mu\text{m}$ , versus with the customised lens: 0.69  $\pm$  0.08  $\mu\text{m}$ ).

Unfortunately, Chen et al.<sup>48</sup> did not measure either high- or low-contrast visual acuity in their study. However, because they measured both corneal surfaces' aberrations as well as the total ocular aberrations, they were able to partly model the magnitude of the aberrations of the eye's internal optics. Their modelling results indicated that the posterior corneal surface and crystalline lens were also responsible for some of the residual aberrations measured with their customised lenses on-eye for their three keratoconic patients. Chen et al.<sup>48</sup> also acknowledged that their customised lenses only had a central 5 mm optical zone of aberration correction, which would likely cause problems with glare if the lenses were worn in scotopic conditions.

Marsack et al.<sup>44</sup> compared visual performance and ocular aberrations using bespoke wavefront-guided soft contact lenses versus the subject's own habitual corneal lenses. The authors produced

customised lenses for three keratoconic eyes (one severe and two moderate cases) and reported that all three customised lenses provided better logMAR acuities compared to the patients' habitual corneal lenses. For their patient with severe keratoconus, their habitual corneal lens provided a high-contrast (91 per cent) acuity of 0.04  $\pm$  0.09 log units, whereas their customised lens gave an improved acuity of  $-0.05 \pm 0.05$  log units. Conversely, the patient's habitual corneal lens provided a low-contrast (52 per cent) acuity of 0.58  $\pm$  0.04 log units, whereas the customised lens yielded an acuity of 0.61  $\pm$  0.04 log units. Encouragingly, the mean uncorrected HORMS error was reduced from 1.57  $\pm$  0.03  $\mu\text{m}$  to 0.76  $\pm$  0.03  $\mu\text{m}$  with the customised lens, and to 0.50  $\pm$  0.15  $\mu\text{m}$  with the habitual corneal lens. Similarly, for one of their moderate cases, the uncorrected HORMS error was reduced from 0.61  $\pm$  0.02  $\mu\text{m}$  to 0.39  $\pm$  0.02  $\mu\text{m}$  using their habitual corneal lens, and to 0.38  $\pm$  0.07  $\mu\text{m}$  with the customised lens. The high-contrast (91 per cent) acuity for this particular patient was 0.20  $\pm$  0.02 log units with their habitual corneal lens, which reduced to 0.14  $\pm$  0.02 log units with the customised lens. However, the patient's habitual corneal lens provided a low-contrast (37 per cent) acuity of 0.58  $\pm$  0.04 log units, whereas the customised lens yielded an acuity of 0.59  $\pm$  0.04 log units. Nonetheless, these two cases highlighted that customised soft lenses have the potential to provide comparable results to corneal lenses in terms of low-contrast acuity, yet superior results in terms of high-contrast acuity.

Katsoulos et al.<sup>26</sup> used a rather different approach to producing customised soft lenses for eight mild to moderate keratoconic eyes; their lenses were designed to correct for around 75 per cent of the eye's manifest third-order negative vertical coma aberration, as well the second-order Zernike terms extracted directly from their aberrometry data for a 4 mm pupil diameter. In all eight cases, a reduction in uncorrected HORMS error was seen (the largest reduction was from 0.86  $\mu\text{m}$  to 0.42  $\mu\text{m}$ ); however, the authors did not explain if the mean differences were significant. On the other hand, Katsoulos et al.<sup>26</sup> reported a significant reduction in the magnitude of uncorrected vertical coma aberration with their customised lenses ( $p < 0.005$ ). The largest reduction reported

was from  $-0.56 \mu\text{m}$  to  $-0.15 \mu\text{m}$ . These reductions in HOAs were believed to have contributed to the improvements in high-contrast (100 per cent) logMAR visual acuities measured with the customised lenses, compared to the patient's best-corrected spectacle acuities (the largest improvement reported was from 0.52 to 0.06 log units). In broad agreement with the results of Sabesan et al.,<sup>50</sup> Katsoulos et al.<sup>26</sup> also found greater improvements in low-contrast (50 per cent) logMAR visual acuities compared to best-corrected spectacle acuities (the largest improvement was from 1.00 to 0.10 log units). The authors' rationale for using a 75 per cent correction was based on previous studies which had shown that decentrations of a partial wavefront aberration correction, rather than the full correction, would still yield a helpful VB compared to conventional contact lenses.<sup>90,105</sup> Acknowledging that not all keratoconic cones are always decentred in the same position away from the individual eye's line of sight,<sup>6,82</sup> Katsoulos et al.<sup>26</sup> also proposed that more centrally located cones could require the correction of spherical aberration in order to achieve optimal visual performance.

Building on the approach used by Katsoulos et al.,<sup>26</sup> Jinabhai et al.<sup>41</sup> explored the effectiveness of aberration correction provided by customised lenses that gave either a 50 per cent or a 100 per cent correction of both vertical and horizontal third-order coma, over a natural 4 mm pupil. The authors' rationale for using a 'partial' correction was based on previous studies which confirmed that decentration of a 'full' wavefront-guided correction (through either rotation and/or translation) induces superfluous residual aberrations,<sup>40,60,89,90</sup> thereby diminishing visual performance. Jinabhai et al.<sup>41</sup> compared their two customised lenses to non-customised, conventional toric soft lenses and the patient's habitual corneal lenses. Unlike in previous studies, the authors used a subjective over-refraction result to determine the lower-order powers of both their customised and non-customised soft toric lenses. This was because both Katsoulos et al.<sup>26</sup> and Jinabhai et al.<sup>8</sup> had previously demonstrated that the lower-order sphere and cylinder terms, measured objectively using Hartmann-Shack aberrometry, did not readily correspond with the sphere and cylinder powers measured during a subjective refraction for keratoconic patients. Such variability between these methods may be attributable to errors at the wavefront sensor.<sup>61</sup>

Jinabhai et al.<sup>41</sup> reported significant changes in mean third-order vertical coma aberration for 12 keratoconic eyes, from  $-0.93 \pm 0.34 \mu\text{m}$  when uncorrected, to  $+0.18 \pm 0.39 \mu\text{m}$  with the '100 per cent lenses' ( $p = 0.002$ ); to  $-0.17 \pm 0.30 \mu\text{m}$  with the '50 per cent lenses' ( $p = 0.002$ ) and to  $+0.39 \pm 0.14 \mu\text{m}$  with the patient's habitual corneal lenses ( $p = 0.002$ ). In contrast, their non-customised toric lenses did not significantly reduce vertical coma ( $-0.66 \pm 0.43 \mu\text{m}$ ). While both the '100 per cent lenses' and the habitual corneal lenses produced a 'positive shift' in vertical coma, the differences between these two modes of correction were not statistically significant. The authors also found no significant differences in horizontal third-order coma measurements between these five measurement conditions.

In spite of the apparent improvements in vertical coma aberration with their two customised lenses, Jinabhai et al.<sup>41</sup> reported that the patient's habitual corneal lenses provided significantly better distance high-contrast (95 per cent) logMAR acuity, distance low-contrast (15 per cent) logMAR acuity and near vision SKILL card<sup>107</sup> scores compared to the '100 per cent lenses' ( $p \leq 0.002$ ). However, the authors found no significant differences in high-contrast, low-contrast or SKILL card scores measured with the '50 per cent lenses', versus either the habitual corneal lenses or the '100 per cent lenses'. While it was clear that the corneal lenses provided the best visual performance scores of all the possible lens options that were investigated, the authors also noted that the '50 per cent lenses' generally provided better visual performance scores compared to the '100 per cent lenses'.

The authors acknowledged that their customised lenses' visual performance results were likely to have been affected by small on-eye lens translations (despite on-eye rotations being accounted for during the manufacturing process), as well as differences between the patient's natural pupil size (during the visual performance measurements) and the size of the zone of customisation of both their '50 per cent' and '100 per cent' lenses. These clinical findings corroborated the results of the authors' previous study,<sup>40</sup> which modelled the effects of customised lens translations and rotations on the correction of aberrations in keratoconic patients, where the theoretical customised lens was designed to fully correct all high-order Zernike terms, up to the fifth order. Using computerised simulations,

Jinabhai et al.<sup>40</sup> demonstrated that, depending on their magnitude as well as the eye's inherent wavefront error, superfluous lower-order and HOAs, induced through unwanted customised lens decentrations, can reduce the effectiveness of the wavefront correction. These induced, residual aberrations are typically proportional to the amount of displacement, as well the magnitude of the displaced aberration.<sup>88,108</sup> Of particular importance, Jinabhai et al.<sup>40</sup> reported that vertical translations typically induced larger residual spherical and cylindrical errors than horizontal translations. The authors' results suggested that vertical translations of a full, customised HOA correction might be limited to no more than 0.1 mm.

### CUSTOMISED SCLERAL LENSES

Compared to customised soft lenses, which typically induce superfluous aberrations due to their unavoidable degree of 'on-eye' movement and their variable conformity to the keratoconic corneal profile, customised scleral contact lenses are likely to offer a greater degree of on-eye stability for keratoconic patients.<sup>52,53,109</sup> Moreover, scleral lenses also have the added benefit of improving optical performance, by providing a 'regular', rigid first optical surface, while also simultaneously increasing lens wear comfort by allowing a majority of the lens' weight to bear onto the conjunctiva.<sup>110</sup>

Sabesan et al.<sup>52</sup> designed customised scleral lenses, for six keratoconic patients (11 eyes), by first identifying their 'best-fitting' conventional lenses. These 'best-fitting' lenses each had a 'central optic', the corrective properties of which were purely spherical, and a 'customisable periphery' which had toric properties, and also allowed quadrant-specific adjustments to be made (where necessary) to stabilise the lens while simultaneously minimising compression/impingement on the conjunctiva. With these 'best-fitting' lenses *in situ*, the authors carefully evaluated and accounted for both on-eye rotation and translations after measuring ocular lower-order and HOAs (via Hartmann-Shack aberrometry) through the lenses. Using the 'best-fitting' lens parameters as a starting point, the authors used their aberration measurements to create front-surface, customised scleral lenses, manufactured using a sub-micron-precision lathe. Once verified and fitted on-eye, the customised scleral lenses were found to provide good temporal stability, showing no more than two degrees of

on-eye rotation and less than 200  $\mu\text{m}$  of on-eye translations with blinks over a 20-second period. Sabesan et al.<sup>52</sup> found that, compared with the 'best-fitting' spherical optic lenses ( $1.17 \pm 0.57 \mu\text{m}$ ), the customised scleral lenses significantly reduced the mean HORMS error (to  $0.37 \pm 0.19 \mu\text{m}$ ;  $p < 0.05$ ) for their keratoconic patients. Equally, the authors also reported a significant improvement in mean monocular, distance high-contrast logMAR visual acuity between the study lenses, by an average of 1.9 lines ( $p < 0.05$ ), in addition to significant improvements in sinusoidal grating-based contrast sensitivities at four (increased by a factor of 2.4), eight (increased by a factor of 1.8) and 12 cycles/degree (increased by a factor of 1.4), respectively. While these results indicate that the reduction of aberrations was fairly successful, it is worth noting that residual aberrations still remained even with the customised scleral lenses *in situ*; these were most likely due to the small lens movements observed immediately after blinking, or even due to keratoconus-induced distortions at the posterior corneal surface and/or the crystalline lens.<sup>38</sup> Another contributing factor could have been the slight mismatch between the pupil size at which the HOAs were measured with the Hartmann-Shack aberrometer (6 mm) and the actual size of the zone of customisation within the scleral lenses (which varied between patients, from 7.0 to 8.5 mm).

In accordance with Sabesan et al.,<sup>52</sup> Marsack et al.<sup>53</sup> also utilised a posterior surface scleral toric landing zone in their peripheral lens designs to help provide on-eye rotational stability. However, in contrast to the approach used by Sabesan et al.,<sup>52</sup> Marsack et al.<sup>53</sup> designed their 'best-fitting' conventional, or 'intermediate', scleral lenses to incorporate a 'spherical equivalent' defocus power within the central optic, which was derived from a subjective refraction routine; this was to produce a starting lens the weight of which would be more closely matched to that of the 'final' customised lens. This allowed for more accurate measurements of 'on-eye' lens rotation and/or translations of the 'intermediate' lens ahead of designing and manufacturing the customisation zone of their 'final' lenses. Marsack et al.<sup>53</sup> used this approach to design lenses for seven keratoconic patients (14 eyes). Once the 'intermediate' lens had settled, a Hartmann-Shack aberrometer was used to evaluate

aberrations through the lens, over a 7 mm pupil diameter, from the second to the fifth order (inclusive); these measurements were then used to design the final customised lens optic. Specifically, Marsack et al.<sup>53</sup> explained that the 'final' customised scleral lenses contained the baseline level of defocus correction that was previously incorporated into the 'intermediate' lens, plus compensation for the residual objective lower-order and HOAs measured via aberrometry. Measurements of the 'intermediate' lens' on-eye decentrations were made using a customised camera system; however, unlike Sabesan et al.,<sup>52</sup> Marsack et al.<sup>53</sup> only measured their lens' decentrations over a period of 10 seconds.

Overall, Marsack et al.<sup>53</sup> reported that, compared to the 'intermediate' lenses, the 'final' customised lenses provided significantly lower magnitudes of residual mean lower-order RMS error ( $p < 0.001$ ) and residual mean HORMS error ( $p < 0.02$ ), over a 6 mm pupil, for all 14 eyes. However, the authors' individual patient data revealed that three (designed for two patients) of their 14 'final' customised lenses actually induced more residual aberrations than the 'intermediate' lenses. The most likely reason for these anomalies was proposed to be on-eye lens decentration, resulting in the wavefront-compensating optical zone becoming misaligned with respect to the patient's pupil. Nonetheless, the authors reported that, on average, 10 of the 14 eyes achieved a mean improvement of 1.5 lines of high-contrast monocular logMAR acuity, compared to their habitual mode of correction, which was similar to the findings of Sabesan et al.<sup>52</sup>

Even with their customised scleral lenses *in situ*, both Sabesan et al.<sup>52</sup> and Marsack et al.<sup>53</sup> noted that a significant reduction in HOAs did not always yield a significant improvement in visual performance. This key finding suggests there might be a degree of post-receptor neural deficit present in keratoconic patients, which limits the degree of visual improvement possible, even with the near-normal or better than normal levels of optical quality, as is provided by wearing a well-aligned customised wavefront correction. Such a deficit may be attributable to long-term exposure to an asymmetrically blurry retinal image.<sup>103</sup> Further studies are needed to explore this concept; for example, it is currently unclear if the degree of neural deficit is related to the severity of the patient's disease and/or age, or whether

such deficits could be overcome through regular perceptual learning/training.<sup>111</sup> At present, only one study has explored the impact of allowing keratoconic patients to habituate to a wavefront-guided, customised scleral lens correction for a substantial time period.<sup>109</sup> Using the customisation methodology outlined in their previous investigation,<sup>53</sup> Hastings et al.<sup>109</sup> conducted a randomised study, which included a crossover design, allowing comparisons between 'conventional' scleral lenses (acting as a control) and 'customised' scleral lenses, over two eight-week (approximate) periods, for eight patients with keratoconus. Although the authors reported that both sets of lenses were worn on a 'daily' basis, for each eight-week period, specific data on how many hours of lens wear per day were not presented in their paper. Expectedly, Hastings et al.<sup>109</sup> found that the mean HORMS error reduced from  $+0.46 \pm 0.24 \mu\text{m}$  with the conventional lenses, to  $+0.26 \pm 0.08 \mu\text{m}$  with the customised lenses ( $p = 0.004$ ). However, although improved, the difference in the mean area under the log contrast sensitivity function did not reach statistical significance between the two lens types (conventional lenses =  $13.91 \pm 2.20$  log units, customised lenses  $15.82 \pm 2.34$  log units [ $p = 0.09$ ]). Similarly, a non-significant improvement was also reported for mean high-contrast logMAR acuity (conventional lenses =  $-0.03 \pm 0.09$  log units, customised lenses  $-0.09 \pm 0.10$  log units [ $p = 0.07$ ]).

#### FURTHER LIMITATIONS TO THE USE OF CUSTOMISED LENSES

While some limitations of using either soft or scleral customised contact lenses have already been discussed in this review (for example, on-eye lens decentration), there are other more general limitations that also need to be considered, with respect to the correction of HOAs, which include:

- optical limits that are set by diffraction; these are related to the patient's pupil size
- the limit of the photoreceptors' 'packing density' at the foveola centralis
- any errors in the manufacturing process of incorporating the required aberration magnitudes onto the customised lenses<sup>48,52</sup>
- potential light scattering and/or glare effects from the boundaries of the lens' customisation zone (more likely to be noticeable in scotopic conditions)
- changes in the patient's habitual lower-order and/or HOAs due to disease progression would mean that the customised

lenses need to be redesigned/modified and refitted on a regular basis, which could prove to be financially inconvenient to the patient, while also requiring substantial clinical chair time

- poor customised lens care by the patient (for example damage to the contact lenses during cleaning, storing or handling)
- customised contact lenses can only optically correct HOAs at one given pupil size. When the patient's pupil increases beyond this size, the effectiveness of the aberration control will begin to reduce; however, the patient might still experience some degree of benefit.

Another issue to overcome in manufacturing customised scleral/soft contact lenses is the need for highly specialised equipment. The cost of buying and maintaining micron-precision lathe machines is typically high, which therefore significantly increases the cost of producing customised lenses. A further challenge is the requirement of specialist training for practitioners, to enable them to carry out the assessment, fitting and subsequent modification of these complex lens designs.

In order to gain the maximum benefit from HOA customised corrections, another difficulty to overcome is the need to improve the efficacy of correcting lower-order terms with customised lenses, as any under- or overcorrection of these terms may potentially diminish, or even eliminate, any benefits gained by correcting the comparatively smaller-magnitude HOA terms.

Nonetheless, further technological advances in the field of scleral/soft lens design are likely to promote the emergence of customised aberration-controlling lenses for keratoconic patients, particularly as improvements in visual performance and comfortable wearing times, provided by such lenses, could reduce the rate of keratoplasty in keratoconic patients, thereby significantly reducing clinical issues related to corneal graft surgery. Additionally, enhancements in optical correction, provided by customised lenses, could lead to increased independence, particularly among young adult keratoconic patients, thereby contributing to improvements in quality of life.

#### REFERENCES

1. Rabinowitz YS. Keratoconus. *Surv Ophthalmol* 1998; 42: 297-319.
2. Shah S, Laiquzzaman M, Bhojwani R et al. Assessment of the biomechanical properties of the cornea with the ocular response analyzer in normal and

- keratoconic eyes. *Invest Ophthalmol Vis Sci* 2007; 48: 3026–3031.
3. Meek KM, Tuft SJ, Huang Y et al. Changes in collagen orientation and distribution in keratoconus corneas. *Invest Ophthalmol Vis Sci* 2005; 46: 1948–1956.
  4. Barr JT, Wilson BS, Gordon MO et al. Estimation of the incidence and factors predictive of corneal scarring in the Collaborative Longitudinal Evaluation of Keratoconus (CLEK) study. *Cornea* 2006; 25: 16–25.
  5. Zadnik K, Barr JT, Gordon MO et al. Biomicroscopic signs and disease severity in keratoconus. *Cornea* 1996; 15: 139–146.
  6. Tan B, Baker K, Chen YL et al. How keratoconus influences optical performance of the eye. *J Vis* 2008; 8: 1–10.
  7. Negishi K, Kumanomido T, Utsumi Y et al. Effect of higher-order aberrations on visual function in keratoconic eyes with a rigid gas permeable contact lens. *Am J Ophthalmol* 2007; 144: 924–929.
  8. Jinabhai A, O'Donnell C, Radhakrishnan H. A comparison between subjective refraction and aberrometry-derived refraction in keratoconus patients and control subjects. *Curr Eye Res* 2010; 35: 703–714.
  9. Jinabhai A, O'Donnell C, Radhakrishnan H et al. Forward light scatter and contrast sensitivity in keratoconic patients. *Cont Lens Anterior Eye* 2012; 35: 22–27.
  10. Nichols JJ, Steger-May K, Edrington TB et al. The relation between disease asymmetry and severity in keratoconus. *Br J Ophthalmol* 2004; 88: 788–791.
  11. Jinabhai A, Radhakrishnan H, O'Donnell C. Pellucid corneal marginal degeneration: a review. *Cont Lens Anterior Eye* 2011; 34: 56–63.
  12. Romero-Jiménez M, Santodomingo-Rubido J, Wolffsohn JS. Keratoconus: a review. *Cont Lens Anterior Eye* 2010; 33: 157–166.
  13. Jafri B, Lichter H, Stulting RD. Asymmetric keratoconus attributed to eye rubbing. *Cornea* 2004; 23: 560–564.
  14. Lafond G, Bazin R, Lajoie C. Bilateral severe keratoconus after laser in situ keratomileusis in a patient with forme fruste keratoconus. *J Cataract Refract Surg* 2001; 27: 1115–1118.
  15. Maguire LJ, Lowry JC. Identifying progression of sub-clinical keratoconus by serial topography analysis. *Am J Ophthalmol* 1991; 112: 41–45.
  16. Weed KH, McGhee CN, MacEwen CJ. Atypical unilateral superior keratoconus in young males. *Cont Lens Anterior Eye* 2005; 28: 177–179.
  17. Auffarth GU, Wang L, Völcker HE. Keratoconus evaluation using the Orbscan topography system. *J Cataract Refract Surg* 2000; 26: 222–228.
  18. Demirbas N, Pflugfelder S. Topographic pattern and apex location of keratoconus on elevation topography maps. *Cornea* 1998; 17: 476–484.
  19. Barbero S, Marcos S, Merayo-Llloves J et al. Validation of the estimation of corneal aberrations from videokeratography in keratoconus. *J Refract Surg* 2002; 18: 263–270.
  20. Maeda N, Fujikado T, Kuroda T et al. Wavefront aberrations measured with Hartmann-Shack sensor in patients with keratoconus. *Ophthalmol* 2002; 109: 1996–2003.
  21. Lim L, Wei R, Tan D et al. Evaluation of higher order ocular aberrations in patients with keratoconus. *J Refract Surg* 2007; 23: 825–828.
  22. Schlegel Z, Lteif Y, Bains HS et al. Total, corneal, and internal ocular optical aberrations in patients with keratoconus. *J Refract Surg* 2009; 25: S951–S957.
  23. Kosaki R, Maeda N, Bessho K et al. Magnitude and orientation of Zernike terms in patients with keratoconus. *Invest Ophthalmol Vis Sci* 2007; 48: 3062–3068.
  24. Shah S, Naroo S, Hosking S et al. Nidek OPD-scan analysis of normal, keratoconic, and penetrating keratoplasty eyes. *J Refract Surg* 2003; 19: S255–S259.
  25. Bühren J, Kühne C, Kohnen T. Defining subclinical keratoconus using corneal first-surface higher-order aberrations. *Am J Ophthalmol* 2007; 143: 381–389.
  26. Katsoulos C, Karageoriadis L, Vasileiou N et al. Customized hydrogel contact lenses for keratoconus, incorporating correction for vertical coma aberration. *Ophthalmic Physiol Opt* 2009; 29: 321–329.
  27. Jinabhai A, Radhakrishnan H, O'Donnell C. Higher-order aberrations in keratoconus: a review. *Optom Pract* 2009; 10: 141–160.
  28. Gobbe M, Guillon M. Corneal wavefront aberration measurements to detect keratoconus patients. *Cont Lens Anterior Eye* 2005; 28: 57–66.
  29. Shankar H, Taranath D, Santhirathelagan CT et al. Repeatability of corneal first-surface wavefront aberrations measured with Pentacam corneal topography. *J Cataract Refract Surg* 2008; 34: 727–734.
  30. Alio J, Shabayek M. Corneal higher order aberrations: a method to grade keratoconus. *J Refract Surg* 2006; 22: 539–545.
  31. Sideroudi H, Labiris G, Giarmoulakis A et al. Repeatability, reliability and reproducibility of posterior curvature and wavefront aberrations in keratoconic and cross-linked corneas. *Clin Exp Optom* 2013; 96: 547–556.
  32. Jinabhai A, Radhakrishnan H, O'Donnell C. Repeatability of ocular aberration measurements in patients with keratoconus. *Ophthalmic Physiol Opt* 2011; 31: 588–594.
  33. Bayhan HA, Aslan Bayhan S, Muhafiz E et al. Repeatability of aberrometric measurements in normal and keratoconus eyes using a new Scheimpflug-Placido topographer. *J Cataract Refract Surg* 2014; 40: 269–275.
  34. Ortiz-Toquero S, Rodriguez G, de Juan V et al. repeatability of wavefront aberration measurements with a placido-based topographer in normal and keratoconic eyes. *J Refract Surg* 2016; 32: 338–344.
  35. Shetty R, Kochar S, Grover T et al. Repeatability of a commercially available adaptive optics visual simulator and aberrometer in normal and keratoconic eyes. *J Refract Surg* 2017; 33: 769–772.
  36. Artal P, Benito A, Taberero J. The human eye is an example of robust optical design. *J Vis* 2006; 6: 1–7.
  37. Artal P, Guirao A, Berrio E et al. Compensation of corneal aberrations by the internal optics in the human eye. *J Vis* 2001; 1: 1–8.
  38. Chen M, Yoon G. Posterior corneal aberrations and their compensation effects on anterior corneal aberrations in keratoconic eyes. *Invest Ophthalmol Vis Sci* 2008; 49: 5645–5652.
  39. Nakagawa T, Maeda N, Kosaki R et al. Higher-order aberrations due to the posterior corneal surface in patients with keratoconus. *Invest Ophthalmol Vis Sci* 2009; 50: 2660–2665.
  40. Jinabhai A, Charman WN, O'Donnell C et al. Optical quality for keratoconic eyes with conventional RGP lens and simulated, customised contact lens corrections: a comparison. *Ophthalmic Physiol Opt* 2012; 32: 200–212.
  41. Jinabhai A, O'Donnell C, Tromans C et al. Optical quality and visual performance with customised soft contact lenses for keratoconus. *Ophthalmic Physiol Opt* 2014; 34: 528–539.
  42. Jinabhai A, Radhakrishnan H, O'Donnell C. Visual acuity and ocular aberrations with different rigid gas permeable lens fittings in keratoconus. *Eye Contact Lens* 2010; 36: 233–237.
  43. Jinabhai A, Radhakrishnan H, Tromans C et al. Visual performance and optical quality with soft lenses in keratoconus patients. *Ophthalmic Physiol Opt* 2012; 32: 100–116.
  44. Marsack JD, Parker KE, Applegate RA. Performance of wavefront-guided soft lenses in three keratoconus subjects. *Optom Vis Sci* 2008; 85: 1172–1178.
  45. Marsack JD, Parker KE, Niu Y et al. On-eye performance of custom wavefront-guided soft contact lenses in a habitual soft lens-wearing keratoconic patient. *J Cataract Refract Surg* 2007; 23: 960–964.
  46. Marsack JD, Parker KE, Pesudovs K et al. Uncorrected wavefront error and visual performance during RGP wear in keratoconus. *Optom Vis Sci* 2007; 84: 463–470.
  47. Choi J, Wee W, Lee J et al. Changes of ocular higher order aberration in on-and off-eye of rigid gas permeable contact lenses. *Optom Vis Sci* 2007; 84: 42–51.
  48. Chen M, Sabesan R, Ahmad K et al. Correcting anterior corneal aberration and variability of lens movements in keratoconic eyes with back-surface customized soft contact lenses. *Opt Lett* 2007; 32: 3203–3205.
  49. Jeong TM, Yoon G. Customized correction of wavefront aberrations in abnormal human eyes by using a phase plate and a customized contact lens. *J Korean Physical Soc* 2006; 49: 121–125.
  50. Sabesan R, Jeong TM, Carvalho LA et al. Vision improvement by correcting higher-order aberrations with customized soft contact lenses in keratoconic eyes. *Opt Lett* 2007; 32: 1000–1002.
  51. Yildiz E, Toklu MT, Vural ET et al. Change in accommodation and ocular aberrations in keratoconus patients fitted with scleral lenses. *Eye Contact Lens* 2018; 44: S50–S53.
  52. Sabesan R, Johns L, Tomashevskaya O et al. Wavefront-guided scleral lens prosthetic device for keratoconus. *Optom Vis Sci* 2013; 90: 314–323.
  53. Marsack JD, Ravikumar A, Nguyen C et al. Wavefront-guided scleral lens correction in keratoconus. *Optom Vis Sci* 2014; 91: 1221–1230.
  54. Yang B, Liang B, Liu L et al. Contrast sensitivity function after correcting residual wavefront aberrations during RGP lens wear. *Optom Vis Sci* 2014; 91: 1271–1277.
  55. Montalt JC, Porcar E, Espana-Gregori E et al. Visual quality with corneo-scleral contact lenses for keratoconus management. *Cont Lens Anterior Eye* 2018; 41: 351–356.
  56. Shi Y, Queener HM, Marsack JD et al. Optimizing wavefront-guided corrections for highly aberrated eyes in the presence of registration uncertainty. *J Vis* 2013; 13: 1–15.
  57. Abdu M, Mohidin N, Mohd-Ali B. Visual performance and aberration associated with contact lens wear in patients with keratoconus: a pilot study. *Clin Optom* 2014; 6: 47–57.
  58. Gumus K, Kahraman N. A new fitting approach for providing adequate comfort and visual performance in keratoconus: soft HydroCone (Toris K) lenses. *Eye Contact Lens* 2016; 42: 225–230.
  59. Gumus K, Gire A, Pflugfelder SC. The impact of the Boston ocular surface prosthesis on wavefront higher-order aberrations. *Am J Ophthalmol* 2011; 151: 682–690.e2.
  60. Marsack JD, Rozema JJ, Koppen C et al. Template-based correction of high-order aberration in keratoconus. *Optom Vis Sci* 2013; 90: 324–334.
  61. Yoon G, Pantanelli S, MacRae S. Optimising the Shack-Hartmann wavefront sensor. In: Krueger RR, Applegate RA, MacRae S, eds. *Wavefront Customized Visual Correction - The Quest for SuperVision 2, Chapter 16*. Thorofare, New Jersey: Slack Inc., 2004. pp. 131–136.
  62. Lombardo M, Lombardo G. New methods and techniques for sensing the wave aberrations of human eyes. *Clin Exp Optom* 2009; 92: 176–186.
  63. Mihashi T, Hirohara Y, Bessho K et al. Intensity analysis of Hartmann-Shack images in cataractous, keratoconic, and normal eyes to investigate light scattering. *Jpn J Ophthalmol* 2006; 50: 323–333.
  64. Shinto H, Saita Y, Nomura T. Shack-Hartmann wavefront sensor with large dynamic range by adaptive spot search method. *Appl Optics* 2016; 55: 5413–5418.
  65. de Oliveira OG, de Lima Monteiro DW. Optimization of the Hartmann-Shack microlens array. *Opt Lasers Eng* 2011; 49: 521–525.
  66. Thibos LN, Hong X. Clinical applications of the Shack-Hartmann Aberrometer. *Optom Vis Sci* 1999; 76: 817–825.
  67. Thibos LN, Applegate RA. Assessment of optical quality. In: Krueger RR, Applegate RA, MacRae S, eds. *Customized Corneal Ablation - The Quest for SuperVision*,

- Chapter 6. Thorofare, New Jersey: Slack Inc., 2001. pp. 55–63.
68. Llorente L, Marcos S, Dorronsoro C et al. Effect of sampling on real ocular aberration measurements. *J Opt Soc Am A Opt Image Sci Vis* 2007; 24: 2783–2796.
  69. Pfund J, Lindlein N, Schwider J. Dynamic range expansion of a Shack–Hartmann sensor by use of a modified unwrapping algorithm. *Opt Lett* 1998; 23: 995–997.
  70. Lindlein N, Pfund J, Schwider J. Expansion of the dynamic range of a Shack–Hartmann sensor by using astigmatic microlenses. *Opt Eng* 2000; 39: 2220–2225.
  71. Lindlein N, Pfund J, Schwider J. Algorithm for expanding the dynamic range of a Shack–Hartmann sensor by using a spatial light modulator array. *Opt Eng* 2001; 40: 837–840.
  72. Ares M, Royo S, Caum J. Shack–Hartmann sensor based on a cylindrical microlens array. *Opt Lett* 2007; 32: 769–771.
  73. Pantanelli S, MacRae S, Jeong TM et al. Characterizing the wave aberration in eyes with keratoconus or penetrating keratoplasty using a high–dynamic range wavefront sensor. *Ophthalmol* 2007; 114: 2013–2021.
  74. Yoon G, Pantanelli S, Nagy LJ. Large-dynamic-range Shack–Hartmann wavefront sensor for highly aberrated eyes. *J Biomed Opt* 2006; 11: 0305021–0305023.
  75. Marsack JD, Pesudovs K, Sarver E et al. Impact of Zernike-fit error on simulated high- and low-contrast acuity in keratoconus: implications for using Zernike-based corrections. *J Opt Soc Am A Opt Image Sci Vis* 2006; 23: 769–776.
  76. Born M, Wolf E. Geometrical theory of aberrations. In: *Principles of Optics, Chapter 5*, 7th ed. Cambridge, UK: Cambridge University Press, 1999. pp. 228–260.
  77. Ríos S, Acosta E, Bará S. Hartmann sensing with Albrecht grids. *Opt Commun* 1997; 133: 443–453.
  78. Gatinel D, Malet J, Dumas L. Polynomial decomposition method for ocular wavefront analysis. *J Opt Soc Am A Opt Image Sci Vis* 2018; 35: 2035–2045.
  79. Thibos LN, Applegate RA, Schwiegerling JT et al. VSIA-taskforce-members. Standards for reporting the optical aberrations of eyes. In: Lakshminarayan V, ed. *Vision Sciences and Its Applications. Vol 35 of OSA Trends in Optics and Photonics Series*. Washington, DC: Optical Society of America, 2000. pp. 232–244.
  80. Mandell RB, Chiang CS, Klein SA. Location of the major corneal reference points. *Optom Vis Sci* 1995; 72: 776–784.
  81. Cheng X, Himebaugh N, Kollbaum PS et al. Test-retest reliability of clinical Shack–Hartmann measurements. *Invest Ophthalmol Vis Sci* 2004; 45: 351–360.
  82. Mihaltz K, Kranitz K, Kovacs I et al. Shifting of the line of sight in keratoconus measured by a Hartmann–Shack sensor. *Ophthalmol* 2010; 117: 41–48.
  83. Ninomiya S, Fujikado T, Kuroda T et al. Changes of ocular aberration with accommodation. *Am J Ophthalmol* 2002; 134: 924–926.
  84. Montés-Micó R, Alió JL, Muñoz G et al. Temporal changes in optical quality of air-tear film Interface at anterior cornea after blink. *Invest Ophthalmol Vis Sci* 2004; 45: 1752–1757.
  85. Radhakrishnan H, Jinabhai A, O'Donnell C. Dynamics of ocular aberrations in keratoconus. *Clin Exp Optom* 2010; 93: 164–174.
  86. Williams DR, Yoon GY, Porter J et al. Visual benefit of correcting higher order aberrations of the eye. *J Refract Surg* 2000; 16: S554–S559.
  87. Guirao A, Porter J, Williams DR et al. Calculated impact of higher-order monochromatic aberrations on retinal image quality in a population of human eyes: erratum. *J Opt Soc Am A* 2002; 19: 620–628.
  88. Guirao A, Williams DR, Cox I. Effect of rotation and translation on the expected benefit of an ideal method to correct the eye's higher-order aberrations. *J Opt Soc Am A Opt Image Sci Vis* 2001; 18: 1003–1015.
  89. López-Gil N, Castejón-Mochón JF, Fernández-Sánchez V. Limitations of the ocular wavefront correction with contact lenses. *Vision Res* 2009; 49: 1729–1737.
  90. de Brabander J, Chateau N, Marin G et al. Simulated optical performance of custom Wavefront soft contact lenses for keratoconus. *Optom Vis Sci* 2003; 80: 637–643.
  91. Radhakrishnan H, Charman WN. Age-related changes in ocular aberrations with accommodation. *J Vis* 2007; 7: 1–21.
  92. López-Gil N, Castejón-Mochón JF, Benito A et al. Aberration generation by contact lenses with aspheric and asymmetric surfaces. *J Refract Surg* 2002; 18: S603–S609.
  93. Tomlinson A, Ridder WH, Watanabe R. Blink-induced variations in visual performance with Toric soft contact lenses. *Optom Vis Sci* 1994; 71: 545–549.
  94. Young G, McIlraith R, Hunt C. Clinical evaluation of factors affecting soft Toric lens orientation. *Optom Vis Sci* 2009; 86: E1259–E1266.
  95. Edrington TB. A literature review: the impact of rotational stabilization methods on toric soft contact lens performance. *Cont Lens Anterior Eye* 2011; 34: 104–110.
  96. Griffiths M, Zahner K, Collins MJ et al. Masking of irregular corneal topography with contact lenses. *CLAO J* 1998; 24: 76–81.
  97. Charman WN. Rigid lens optics. In: Efron N, ed. *Contact Lens Practice, Chapter 14*. Oxford, London: Butterworth-Heinemann, 2002. pp. 171–176.
  98. Hartwig A, Atchison DA. Analysis of higher-order aberrations in a large clinical population. *Invest Ophthalmol Vis Sci* 2012; 53: 7862–7870.
  99. de Sanctis U, Loiacono C, Richiardi L et al. Sensitivity and specificity of posterior corneal elevation measured by Pentacam in discriminating keratoconus/subclinical keratoconus. *Ophthalmol* 2008; 115: 1534–1539.
  100. Rocha KM, Vabre L, Chateau N et al. Enhanced visual acuity and image perception following correction of highly aberrated eyes using an adaptive optics visual simulator. *J Refract Surg* 2010; 26: 52–56.
  101. Sabesan R, Ahmad K, Yoon G. Correcting highly aberrated eyes using large-stroke adaptive optics. *J Refract Surg* 2007; 23: 947–952.
  102. Sabesan R, Yoon G. Visual performance after correcting higher order aberrations in keratoconic eyes. *J Vis* 2009; 9: 1–10.
  103. Sabesan R, Yoon G. Neural compensation for long-term asymmetric optical blur to improve visual performance in keratoconic eyes. *Invest Ophthalmol Vis Sci* 2010; 51: 3835–3839.
  104. Smirnov MS. Measurement of the wave aberration of the human eye. *Biophys J* 1962; 7: 766–795.
  105. Guirao A, Cox I, Williams DR. Method for optimizing the correction of the eye's higher-order aberrations in the presence of decentrations. *J Opt Soc Am A Opt Image Sci Vis* 2002; 19: 126–128.
  106. Yoon G, Jeong TM. Effect of the movement of customized contact lens on visual benefit in abnormal eyes. *J Vis* 2003; 3: 38.
  107. Haegerstrom-Portnoy G, Brabyn J, Schneck ME et al. The SKILL card. An acuity test of reduced luminance and contrast. Smith-Kettlewell Institute low luminance. *Invest Ophthalmol Vis Sci* 1997; 38: 207–218.
  108. Kollbaum PS, Jansen M, Thibos LN et al. Validation of an off-eye contact lens Shack–Hartmann wavefront aberrometer. *Optom Vis Sci* 2008; 85: E817–E828.
  109. Hastings GD, Applegate RA, Nguyen LC et al. Comparison of wavefront-guided and best conventional scleral lenses after habituation in eyes with corneal ectasia. *Optom Vis Sci* 2019; 96: 238–247.
  110. Ticak A, Marsack JD, Koenig DE et al. A comparison of three methods to increase scleral contact lens on-eye stability. *Eye Contact Lens* 2015; 41: 386–390.
  111. Sabesan R, Barbot A, Yoon G. Enhanced neural function in highly aberrated eyes following perceptual learning with adaptive optics. *Vision Res* 2017; 132: 78–84.

## Optical changes and visual performance with orthokeratology

*Clin Exp Optom* 2020; 103: 44–54

DOI:10.1111/cxo.12947

**Augustine N Nti** OD

**David A Berntsen** OD PhD

The Ocular Surface Institute, College of Optometry,  
University of Houston, Houston, Texas, USA

E-mail: dberntsen@uh.edu

Orthokeratology has undergone drastic changes since first described in the early 1960s. The original orthokeratology procedure involved a series of lenses to flatten the central cornea and was plagued by variable results. The introduction of highly oxygen-permeable lens materials that can be worn overnight, corneal topography, and reverse-geometry lens designs revolutionised this procedure. Modern overnight orthokeratology causes rapid, reliable, and reversible reductions in refractive error. With modern designs, patients can wear lenses overnight, remove them in the morning, and see clearly throughout the day without the need for daytime refractive correction. Modern reverse-geometry lens designs cause central corneal flattening and mid-peripheral corneal steepening that provides clear foveal vision while simultaneously causing a myopic shift in peripheral retinal defocus. The peripheral myopic retinal defocus caused by orthokeratology is hypothesised to be responsible for reductions in myopia progression in children fitted with these lenses. This paper reviews the changes in orthokeratology lens design that led to the reverse-geometry orthokeratology lenses that are used today and the optical changes these lenses produce. The optical changes reviewed include changes in refractive error and their time course, high- and low-contrast visual acuity changes, changes in higher-order aberrations and visual quality metrics, changes in accommodation, and changes in peripheral defocus caused by orthokeratology. The use of orthokeratology for myopia control in children is also reviewed, as are hypothesised connections between orthokeratology-induced myopic peripheral defocus and slowed myopia progression in children, and safety and complications associated with lens wear. A better understanding of the ocular and optical changes that occur with orthokeratology will be beneficial to both clinicians and patients in making informed decisions regarding the utilisation of orthokeratology. Future research directions with this lens modality are also discussed.

Submitted: 2 April 2019

Revised: 17 June 2019

Accepted for publication: 18 June 2019

**Key words:** aberrations, myopia, myopia control, orthokeratology, visual acuity

Uncorrected refractive errors were the leading global cause of moderate or severe vision impairment in 2015.<sup>1</sup> Flaxman et al.<sup>1</sup> noted that although the prevalence of uncorrected refractive error is declining, the total number of people with vision impairment due to uncorrected refractive error increased from 6.2 million in 1990 to 7.4 million in 2015. Options to correct refractive errors include spectacles, contact lenses, and refractive surgery.

Orthokeratology, a specialty contact lens option, is the temporary 'reduction, modification or elimination of refractive anomalies by the programmed application of contact lenses or other related procedures'.<sup>2</sup> Myopic orthokeratology involves fitting lenses flatter than the flat meridian to reduce the curvature of the central cornea. While orthokeratology is predominantly used to correct

myopia, the procedure can also be used to temporarily reduce hyperopia using steeper-fitting contact lenses that increase central corneal curvature. Toric orthokeratology can also be used to temporarily correct moderate-to-high levels of astigmatism (greater than 1.25 D).

Attempts to manipulate the cornea to reduce or correct refractive error goes far back to the early Japanese who placed small bags of shot on the eyelids overnight to reduce myopia.<sup>3</sup> However, it was not until the 1950s that clinicians realised that flat fitted rigid contact lenses produced corneal changes that could eliminate myopia. Early work on traditional orthokeratology was pioneered by Jessen in 1962 when he wrote a paper on 'orthofocus techniques', which described how rigid contact lenses can be used to correct myopia.

Traditional orthokeratology involved wearing a series of flatter-fitting rigid lenses during the day that gradually flattened the central cornea further with each lens until myopia was eliminated. After the targeted reduction in myopia was achieved, lens wear was gradually reduced. With time, this wearing schedule allowed for periods in the day during which no lenses were worn. These early attempts at orthokeratology unfortunately produced variable results, unpredictable vision, and did not gain widespread acceptance and usage.

In 1989, Wlodyga and Stoyan produced the first reverse-geometry orthokeratology lenses.<sup>4</sup> These lenses had a secondary curve that was steeper than the base curve. This design allowed for better centration of the lens and more rapid reduction in refractive

error, leading to the term 'accelerated orthokeratology'.

This paper reviews the optical changes that occur with orthokeratology, the effect of orthokeratology on vision, and future directions involving the use of orthokeratology.

## Modern orthokeratology

Four developments significantly influenced modern orthokeratology: reverse-geometry designs, highly oxygen-permeable lens materials, corneal topography, and computer-controlled lathing, which allowed for consistent manufacturing of highly specialised lenses.

Since the introduction of reverse-geometry lens designs in 1989, all modern orthokeratology lenses use some modification of this design. 'Reverse geometry' refers to the first back peripheral curve radius being steeper than the base curve (Figure 1).

Newer lens materials with high oxygen permeability have enabled modern orthokeratology lenses to be worn safely overnight, thus the term 'overnight orthokeratology'. These lenses mould or reshape the cornea overnight and provide patients with clear unaided vision during the day after lens removal. These corneal changes are reversible, and patients wear their lenses each night to maintain clear unaided vision during waking hours. The widespread availability of corneal topographers allows practitioners to measure the centration and effects of orthokeratology lenses on the cornea and appropriately modify treatment.

Although orthokeratology can be used to correct astigmatism, hyperopia and myopia, orthokeratology is predominantly used to reduce myopia. Much of the rest of this review will focus on myopic orthokeratology.

## Corneal changes

### Myopic orthokeratology

The goal of myopic orthokeratology is to flatten the central cornea to reduce myopia, and the mid-peripheral cornea is steepened in the process. Figure 2 shows corneal topography for a patient before and after orthokeratology and the resulting corneal power changes. Based on studies measuring corneal changes, the flattening of the

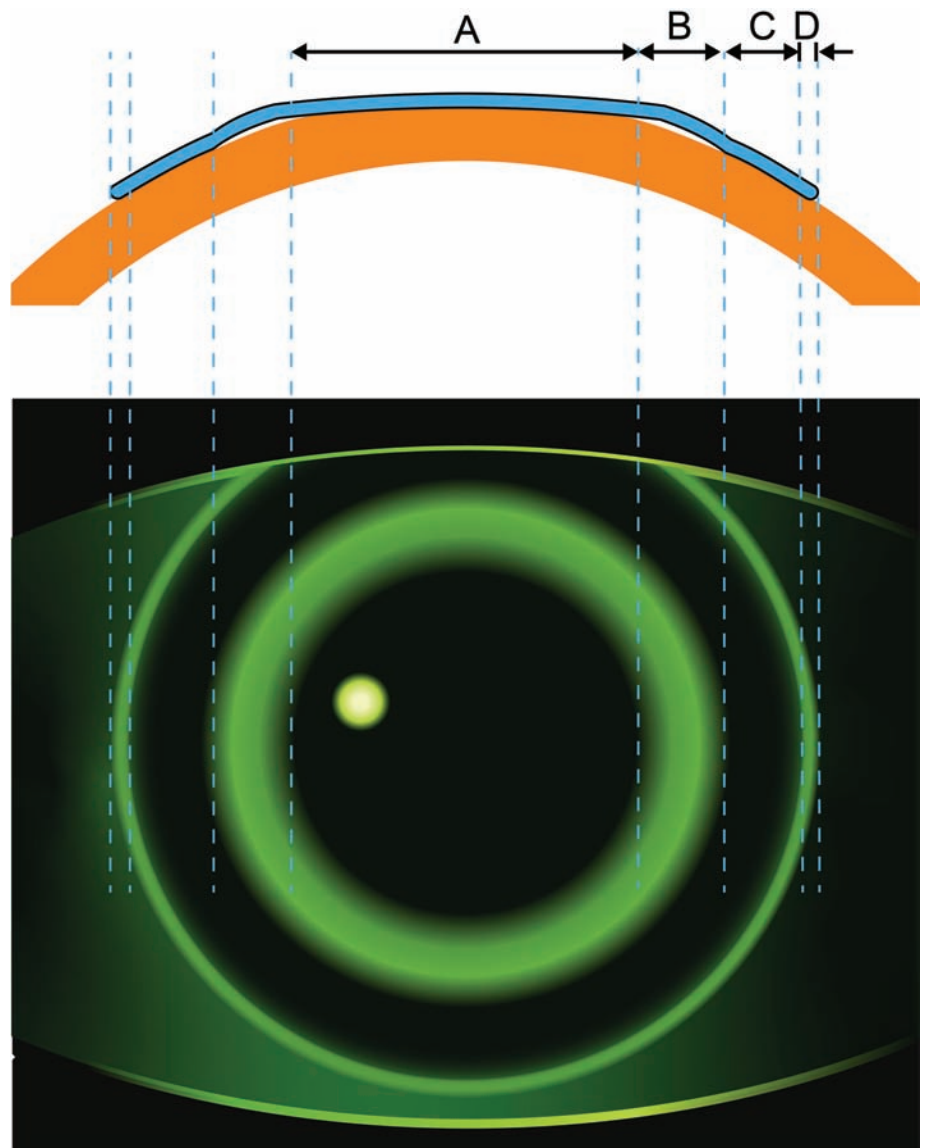


**Figure 1. Representative cross-section and fluorescein pattern of a well-fitted orthokeratology reverse-geometry lens (not drawn to scale). Note that some lens designs may have additional back-surface curves beyond what is shown. The back-surface curves are labelled as follows. A: Base curve. B: Reverse curve. C: Alignment curve. D: Peripheral curve.**

cornea happens mostly in the anterior portion of the cornea.<sup>5-10</sup> The central corneal epithelium thins, while the mid-peripheral cornea thickens.<sup>5,9,11,12</sup>

Orthokeratology can also lead to asymmetric changes in the cornea.<sup>13</sup> In a retrospective study, Maseedupally et al.<sup>13</sup> reported that after 14 days of orthokeratology, there was greater flattening in the temporal sector of the central cornea compared with the nasal sector. In the paracentral corneal

annulus, there was greater steepening of the temporal sector compared with the nasal sector. They found no asymmetries in the vertical sectors.

Based on histological sectioning of cat corneas after being fitted with orthokeratology, Choo et al.<sup>14</sup> reported that mid-peripheral corneal thickening occurs in the epithelium; however, other studies suggest this thickening is stromal in origin.<sup>11,15,16</sup> Although some studies reported

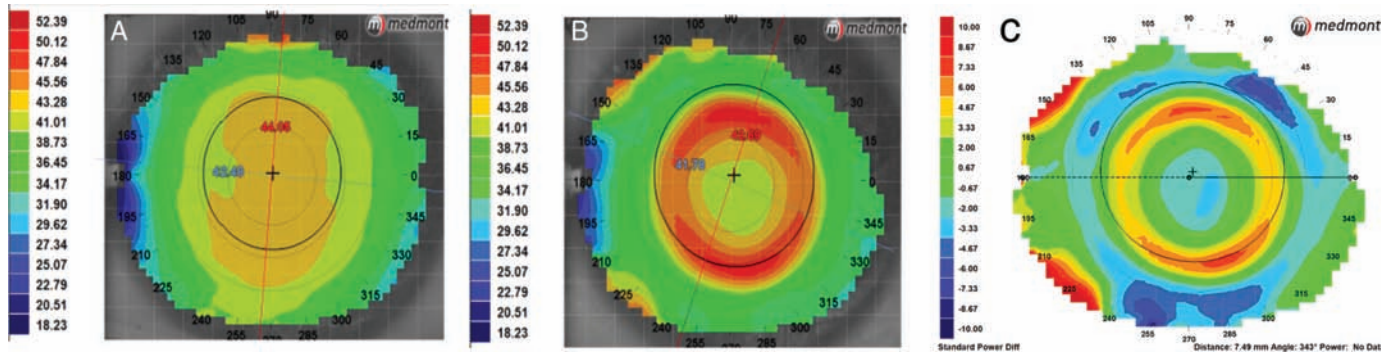


**Figure 2.** Corneal topography tangential maps of an eye **A:** before being fitted with orthokeratology and **B:** after orthokeratology fitting. **C:** A power difference map shows the changes in corneal power after being fitted with orthokeratology. Warmer colours represent higher corneal power. Topography maps courtesy of Maria Walker, OD MS.

flattening of the posterior cornea,<sup>15,16</sup> it is generally accepted that orthokeratology primarily causes flattening of the anterior cornea without bending the whole cornea.<sup>5,7,10,17</sup>

Significant corneal changes occur as early as 10 minutes after an orthokeratology lens is worn.<sup>6</sup> Thus, just one night of orthokeratology improves visual acuity and reduces myopia,<sup>9,17,18</sup> providing a rapid and reversible means of correcting myopia. A meta-analysis by Li et al.<sup>19</sup> found that the reduction in corneal thickness occurs within the first week of orthokeratology and remains stable thereafter.

Studies suggest that the rate of corneal changes with orthokeratology depends on the amount of targeted refractive change; orthokeratology lenses targeted to correct higher amounts of myopia cause faster corneal changes than lenses to correct lower amounts of myopia.<sup>8,20</sup> However, how long it takes the cornea to return to its normal shape depends on the duration of treatment. The longer orthokeratology lenses are used, the longer it takes the cornea to fully return to its normal shape,<sup>21</sup> and reversibility may be slower in some children.<sup>22</sup>

### Hyperopic orthokeratology

Hyperopic orthokeratology induces a myopic shift in refractive error by steepening the central cornea.<sup>23,24</sup> Hyperopic orthokeratology flattens the mid-peripheral cornea<sup>23,24</sup> by thickening the central corneal epithelium and thinning the mid-peripheral corneal epithelium.<sup>25</sup> Similar to myopic orthokeratology, corneal changes are rapid (significant changes after one night of lens wear) and reversible.<sup>23</sup>

### Optical changes with myopic orthokeratology

#### Refractive error changes and stability of changes

Multiple studies have evaluated refractive error changes and their stability using overnight orthokeratology.<sup>18,26–39</sup> Nichols et al.<sup>39</sup> conducted a prospective study of refractive error changes in patients undergoing overnight orthokeratology and found that most of the reduction in myopia occurred during the first seven days of overnight lens wear. There was no significant reduction in myopia after the seventh day. Other studies have similarly reported that most of the refractive error reduction occurs within the first week of orthokeratology.<sup>18,30</sup>

Orthokeratology lenses generally have approval to correct myopia up to  $-5.00$  D to  $-6.00$  D, although this varies by country and lens design. Eye-care providers may choose to fit lenses off-label to correct higher amounts of myopia depending on the laws of the country in which they practise. For patients with myopia higher than the approved limits of a particular lens design, an option is partial-reduction orthokeratology, where a portion of the myopia is corrected by orthokeratology with the residual myopia corrected by spectacles during the day to provide clear vision.<sup>40</sup>

Overnight orthokeratology using spherical lens designs is generally indicated for patients with low-to-moderate ( $-1.50$  D or less) astigmatism. This indication is because moderate-to-high astigmatism can cause decentration of orthokeratology lenses which can lead to decentred treatment, poor vision, and may induce astigmatism.<sup>41</sup>

Orthokeratology generally does not induce astigmatism in patients with spherical refractive errors.<sup>42,43</sup> In myopic patients with astigmatism, standard spherical orthokeratology does not consistently change the amount of astigmatism. Some studies have reported that orthokeratology causes significant changes in astigmatism<sup>43–45</sup> while others have found no significant change in astigmatism.<sup>29,31</sup>

For patients with moderate-to-high levels of astigmatism (more than  $-1.50$  D), toric orthokeratology is effective at reducing the amount of astigmatism. One of the earliest case reports utilising toric orthokeratology reported reductions in astigmatism of up to  $-2.50$  D three weeks after the start of treatment, although there was variability in residual astigmatism over time.<sup>46</sup> Subsequent studies have shown the effectiveness of toric orthokeratology. Chen et al.<sup>47</sup> reported a 79 per cent reduction in refractive astigmatism after one month of toric orthokeratology in myopic children with moderate-to-high astigmatism ( $-1.25$  up to  $-3.50$  D of astigmatism).

Since myopic orthokeratology temporarily flattens the central cornea, there is a gradual myopic regression over the course of the day once orthokeratology lenses are removed and the cornea slightly steepens; however, this myopic regression is minimal and accounted for by targeting a refractive error of roughly  $+0.50$  D in the morning. After 28 days of orthokeratology in a group of myopic subjects, Sorbara et al.<sup>33</sup> found only a  $-0.32$  D change in refractive error over a 14-hour period after removing lenses in the morning. Comparable results were reported by Soni et al.,<sup>18</sup> who found a  $-0.37$  D change in refractive error over a



12-hour period after lens removal in myopic subjects who had been wearing orthokeratology lenses for 30 days. Similarly, Stillitano et al.<sup>48</sup> found a  $-0.33$  D change in refractive error over a 10-hour period after six months of orthokeratology in myopic subjects.

Importantly, the refractive changes are reversible. Kobayashi et al.<sup>36</sup> reported that after one year of orthokeratology, the changes in refractive error were reversible. In their study, 15 myopic subjects wore orthokeratology lenses for 52 weeks and then discontinued lens wear. Spherical equivalent refractive error returned to baseline one month after discontinuation of lens wear, demonstrating that the corneal changes are not permanent.

### Higher-order aberration changes

While orthokeratology causes a significant reduction in myopia, the combination of central corneal flattening and mid-peripheral corneal steepening leads to a significant increase in higher-order aberrations.<sup>31,32,34,48-51</sup> Joslin et al.<sup>28</sup> conducted one of the earliest studies that measured the effect of reverse-geometry orthokeratology lenses on higher-order aberrations. They found a significant increase in higher-order aberrations after one month of wear for both a 3-mm and 6-mm pupil diameter. For the 6-mm pupil diameter, mean higher-order root-mean-square (RMS) wavefront error increased by  $0.425\ \mu\text{m}$ , with the highest individual Zernike term increase of  $0.306\ \mu\text{m}$  being for spherical aberration ( $Z_4^0$ ).

Similarly, Berntsen et al.<sup>31</sup> reported an average increase in higher-order RMS for a 5-mm pupil diameter after one month of orthokeratology lens wear of  $0.180\ \mu\text{m}$  and an increase in spherical aberration of up to  $0.186\ \mu\text{m}$ . They also reported that while orthokeratology caused significant increases in third- through sixth-order RMS for a 5-mm pupil, the increase in positive spherical aberration was a major contributor to the increase in higher-order aberrations. As well, Stillitano et al.<sup>52</sup> later reported a  $0.39\ \mu\text{m}$  increase in higher-order aberrations for a 6.5 mm pupil diameter, also reporting a significant increase in spherical aberration after orthokeratology. Most higher-order aberrations have been reported to stabilise within one week of beginning orthokeratology treatment.<sup>53</sup>

Higher-order aberration levels throughout the day after one month or more of

successful orthokeratology wear have been reported to be relatively stable. Although two studies reported minor fluctuations in spherical aberration over the course of the day, the other higher-order aberration terms were stable.<sup>31,48</sup> While some studies have reported increases in horizontal coma after orthokeratology, others have found no increase in coma.<sup>28,31,32</sup> This discrepancy in whether horizontal coma is increased by orthokeratology may be attributable to differences in lens centration between studies.

### Visual acuity and visual quality metrics

As expected, orthokeratology leads to significant improvements in uncorrected high- and low-contrast visual acuity due to the elimination of uncorrected myopia.<sup>27,33,39</sup> These improvements in uncorrected high-contrast visual acuity are relatively stable throughout the day, with very little regression. After 30 days of orthokeratology, Nichols et al.<sup>39</sup> observed less than a 0.02 logMAR (one letter) reduction in uncorrected high-contrast visual acuity over eight hours. Other researchers have reported similar results.<sup>18,33</sup> Orthokeratology can also provide unaided high-contrast visual acuity that is comparable to spectacles. In a study by Sorbara et al.,<sup>33</sup> 89 per cent of subjects wearing spectacles had 6/6 or better visual acuity while 83 per cent of the orthokeratology subjects achieved the same level of vision without correction. Similarly, after 28–60 days of successful orthokeratology, uncorrected low-contrast visual acuity is also stable throughout the day with decreases of between two to three letters.<sup>33,39</sup>

As described earlier, patients wearing orthokeratology lenses for one year had their refractive error return to baseline levels within one month of discontinuing orthokeratology. As expected, the same study also reported that uncorrected visual acuity returned to baseline values roughly one month after discontinuing orthokeratology.<sup>36</sup>

Best-corrected high-contrast visual acuity before and during orthokeratology are also not significantly different, demonstrating that increased higher-order aberrations due to orthokeratology do not have a clinically meaningful effect on high-contrast acuity.<sup>31,35,54</sup> However, best-corrected low-contrast visual acuity is reduced by up to 0.12 logMAR (six letters) due to orthokeratology when compared to spectacle correction. This reduction in low-contrast visual

acuity after orthokeratology is associated with increases in spherical aberration. These reductions in low-contrast visual acuity are also greater as pupil size increases.<sup>31</sup>

As one would expect based on increased higher-order aberrations and reduced low-contrast visual acuity reported after orthokeratology, retinal image quality is affected. Berntsen<sup>55</sup> reported retinal image quality in 20 myopic subjects before and one month after orthokeratology using six single-valued retinal image quality metrics previously reported to be highly correlated with low-contrast visual acuity. All six metrics showed a significant reduction in retinal image quality after orthokeratology. Five of the six image quality metrics were correlated with increases in positive spherical aberration and reductions in low-contrast visual acuity after orthokeratology. An example of a point spread function before and after orthokeratology is shown in Figure 3. Although high-contrast visual acuity is not affected by orthokeratology, these results demonstrate that increased higher-order aberrations due to orthokeratology influence visual performance.

### Accommodation changes

Several studies have examined accommodative changes with orthokeratology. Felipe-Marquez et al.<sup>56</sup> conducted a prospective study of 21 young adults wearing spectacles and 51 similar adults wearing orthokeratology lenses. After three months of orthokeratology treatment, there were no significant changes in negative relative accommodation, positive relative accommodation, amplitude of accommodation, accommodative lag, or monocular accommodative facility, and no differences in these accommodative measurements between



**Figure 3. Higher-order aberration point spread functions (PSFs) from an eye with  $-3.00$  D of spherical myopia at baseline (left) and one month after orthokeratology (right). Change in spherical aberration =  $0.24$  microns (5 mm pupil diameter).<sup>55</sup>**

spectacle and orthokeratology-wearing subjects. Kang et al.<sup>57</sup> also examined the effect of orthokeratology on accommodative facility in 15 myopic young adults and found no significant change in facility after 28 nights of orthokeratology.

However, Gifford et al.<sup>58</sup> found a lower accommodative lag in orthokeratology subjects compared with control subjects wearing single-vision contact lenses in a retrospective study. In a subsequent 12-month prospective study, Gifford et al.<sup>59</sup> reported improved accommodative responses with orthokeratology. They measured negative relative accommodation, positive relative accommodation, and accommodative lag in myopic children and young adults. Baseline measurements were performed while wearing single-vision contact lenses, and measurements were repeated after one month and 12 months of orthokeratology lens wear. There was no significant change in negative relative accommodation from baseline; however, there was a significant increase in positive relative accommodation in both children and adults beginning one month after starting orthokeratology. Accommodative lag decreased after one month of orthokeratology in children, and after 12 months in adults.

The strongest evidence of changes in accommodation with orthokeratology comes from a randomised study of 240 myopic children conducted by Han et al.<sup>60</sup> Children were randomly assigned to wear either single-vision spectacles (n = 90), orthokeratology (n = 90), or multifocal spectacles (n = 60) with concentric rings designed to reduce paracentral defocus. In children wearing orthokeratology, accommodative lag was significantly lower after one year when compared to baseline and to the single-vision control group. Accommodative facility also improved in the orthokeratology group. These results demonstrate that long-term orthokeratology improves accommodative accuracy and facility. Gifford et al.<sup>61</sup> reported that increased accommodation in myopic young adults undergoing orthokeratology could be an adaptation to counteract the increase in positive spherical aberration caused by orthokeratology.

**Peripheral optics**

Myopic eyes generally have relative peripheral hyperopia in the horizontal meridian, meaning refractive error in the periphery is more hyperopic (light focused behind the

retina) compared with central refraction along the line of sight.<sup>62</sup> This relative peripheral hyperopia has been hypothesised to promote myopia progression.<sup>63</sup> Studies measuring peripheral refraction of myopic eyes before and after orthokeratology have found that while orthokeratology corrects central myopia, mid-peripheral steepening of the cornea yields a myopic shift in peripheral refractive error that results in peripheral myopic defocus after orthokeratology (light focused in front of the retina).

Queiros et al.<sup>37</sup> measured peripheral refraction along the horizontal meridian of 28 myopic subjects before and after one month of orthokeratology. They reported a hyperopic change in central refractive error (elimination of uncorrected myopia) within the central ±20° of retinal eccentricity, no change in mean spherical equivalent at 25° eccentricity, and a myopic shift in spherical equivalent beyond 25°. They also found that treating greater amounts of myopia with orthokeratology resulted in greater myopic shifts in peripheral refractive error at eccentricities of 20° or more.

Multiple studies have also reported that the reshaping of the cornea with orthokeratology results in a conversion of relative peripheral hyperopic defocus in the horizontal meridian before orthokeratology to

relative peripheral myopic defocus after orthokeratology.<sup>37,38,64-67</sup> The simultaneous creation of peripheral myopic defocus while still providing clear foveal vision has been hypothesised to be the reason why orthokeratology lenses have been reported to slow the progression of myopia. Changes in relative peripheral refraction reported in some of these studies are shown in Figure 4.

These changes in peripheral refraction occur rapidly after the start of orthokeratology. Kang and Swarbrick<sup>65</sup> measured the time course of changes in peripheral refraction with orthokeratology over two weeks, and reported that the most significant change in mean peripheral refraction occurred after the first night of lens wear. They also found no significant differences between the mean spherical equivalent refraction measured after seven nights of orthokeratology lens wear and those measured after 14 nights of lens wear.

Kang et al.<sup>64</sup> also conducted a study to determine whether changing the optic zone diameter or peripheral tangent curve of an orthokeratology lens alters changes observed in peripheral refraction. They measured peripheral refraction of 17 myopic subjects after wearing orthokeratology lenses for two weeks. After a washout

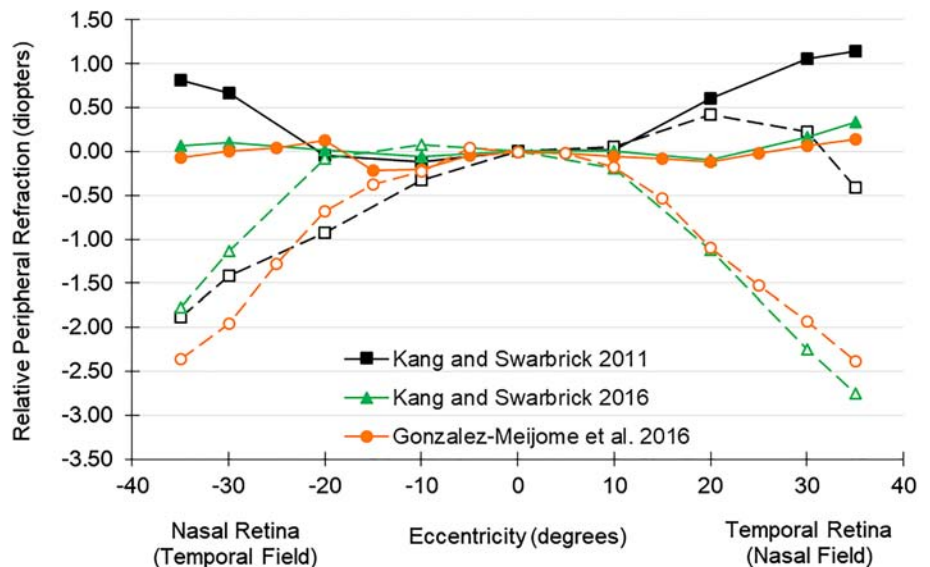


**Figure 4. Spherical equivalent relative peripheral refraction (in dioptres) measured by autorefraction across the horizontal meridian of the eye from several studies before orthokeratology (solid lines with filled symbols) and after orthokeratology (dashed lines with open symbols). Square symbols = Kang and Swarbrick<sup>38</sup> (n = 16), triangle symbols = Kang and Swarbrick<sup>67</sup> (n = 19), circle symbols = Gonzalez-Mejome et al.<sup>66</sup> (n = 34).**

period, subjects wore a similar orthokeratology lens with a smaller optic zone diameter on one eye and a steeper peripheral tangent curve on the other eye. They reported that the change in optic zone diameter and peripheral tangent curve did not lead to significant changes in peripheral refraction when compared with the pattern of peripheral refraction produced by the original lenses. Kang and Swarbrick<sup>68</sup> also found no evidence of differences in peripheral refraction when comparing three different orthokeratology lens designs. The lenses differed in the total diameter, sphericity of the base curve, the number of reverse curves, and the design of both the reverse and alignment curves.

Although most studies have only evaluated changes in peripheral refraction in the horizontal meridian, myopic shifts in refraction with orthokeratology have also been reported in the vertical meridian.<sup>67,69</sup> Kang and Swarbrick<sup>67</sup> measured peripheral refraction along the vertical meridian in 19 myopic subjects before and after 14 nights of orthokeratology. Subjects had peripheral myopia in the vertical meridian at baseline, and orthokeratology caused a myopic shift in peripheral refraction that increased the amount of peripheral myopic defocus.

## **Effects on visual quality of life**

Another aspect of orthokeratology that is important to understand is its effect on vision-related quality of life and on vision-related tasks. One of the early studies reporting vision-related quality of life between orthokeratology and soft contact lenses was conducted by Lipson et al.<sup>70</sup> Study participants were randomly assigned to wear orthokeratology lenses or soft contact lenses for eight weeks. After a washout period, subjects wore the other lens type for another eight weeks. After each lens-wear period, participants completed the National Eye Institute Refractive Error Quality of Life Instrument – 42 questionnaire.<sup>71</sup> Participants, on average, rated orthokeratology as having fewer activity limitations, fewer symptoms, and less dependence on correction than soft contact lenses. Compared to orthokeratology, soft contact lenses resulted in less glare. Additionally, 68 per cent of the participants preferred orthokeratology to soft contact lenses as a form of correction.

A similar result was reported by Ritchey et al.,<sup>72</sup> in which orthokeratology was reported to reduce dependence on correction versus extended-wear soft contact lenses. Berntsen et al.<sup>73</sup> found that compared to their habitual correction of either spectacles or soft contact lenses, dependence on correction and visual symptoms of participants were reduced after one month of orthokeratology, although glare increased.

Santodomingo-Rubido et al.<sup>74</sup> administered a paediatric refractive error profile questionnaire to children assigned to wear orthokeratology or single-vision spectacles and found they rated orthokeratology as being better than spectacles in terms of overall vision, far distance vision, symptoms, appearance, satisfaction, effect on activities, academic performance, handling, and peer perceptions. Zhao et al.<sup>75</sup> also reported higher vision-related quality of life with orthokeratology compared to spectacles in myopic children with 75 per cent of the participants preferring orthokeratology to spectacles. Additional studies have reported subjective satisfaction with orthokeratology on a visual analogue scale, with participants rating vision as 7.8/10 in one study<sup>76</sup> and 9.1/10 in another.<sup>77</sup> These study results demonstrate that most patients using orthokeratology lenses are satisfied with the vision it provides.

## **Myopia control**

Various interventions have been shown to be effective at slowing the progression of myopia. These include pharmaceuticals such as atropine and pirenzepine, and optical interventions such as bifocal and progressive addition spectacles, bifocal and multifocal contact lenses and orthokeratology.<sup>78</sup> Overnight orthokeratology lenses were initially produced to flatten the central cornea overnight and provide clear unaided vision throughout the day. Although the approved indication for orthokeratology lenses is to temporarily correct myopia, research evaluating the efficacy of this lens modality for slowing the progression of myopia in children has gained considerable traction.

As described above, the central corneal flattening and mid-peripheral corneal steepening created by modern reverse-geometry orthokeratology lens designs produce a myopic shift in refraction in the peripheral

retina. Several results from animal studies have shown that peripheral hyperopic defocus can lead to myopia progression, while peripheral myopic defocus can slow myopia progression.<sup>79</sup> Based on these studies, it is thought that the peripheral myopic defocus created by orthokeratology serves as a signal to slow the growth of the eye, reducing the progression of myopia. There has also been a suggestion that visual signals from different meridians of the retina may be differentially effective in influencing central refractive error changes,<sup>80</sup> but it is still unclear whether myopic defocus in specific meridians of the retina are more effective at slowing myopia progression. Work in this area over the last two decades has progressed from case reports<sup>81</sup> and pilot studies to randomised, controlled clinical trials evaluating the efficacy of overnight orthokeratology for slowing the progression of myopia in children. Figure 5 summarises the myopia control effects reported.

Cho et al.<sup>82</sup> conducted the first pilot study to evaluate whether orthokeratology could potentially slow eye growth in myopic children. Their study found that after two years of orthokeratology, axial elongation was reduced by 46 per cent in myopic children compared with spectacle-wearing historical controls. Although this pilot study used historical controls, their work provided initial evidence supporting further research to determine whether orthokeratology was effective in slowing myopia progression.

Walline et al.<sup>83</sup> also reported a 55 per cent reduction in axial growth over two years in myopic children wearing orthokeratology when compared with soft contact lens-wearing historical controls. Studies were subsequently published in which myopic children were followed for two years wearing either orthokeratology lenses or spectacles lenses. Although children and parents could self-select the modality their child would receive, these studies also reported two-year reductions in eye growth of between 32 to 36 per cent in children wearing orthokeratology lenses.<sup>84,85</sup>

The first randomised, controlled clinical trial evaluating the efficacy of orthokeratology in slowing myopia progression in children was the Retardation of Myopia in Orthokeratology (ROMIO) study. Cho and Cheung<sup>86</sup> randomly assigned 102 myopic children into orthokeratology or single-vision spectacles and followed them for two years. Of the 78 subjects who completed the study, those wearing orthokeratology

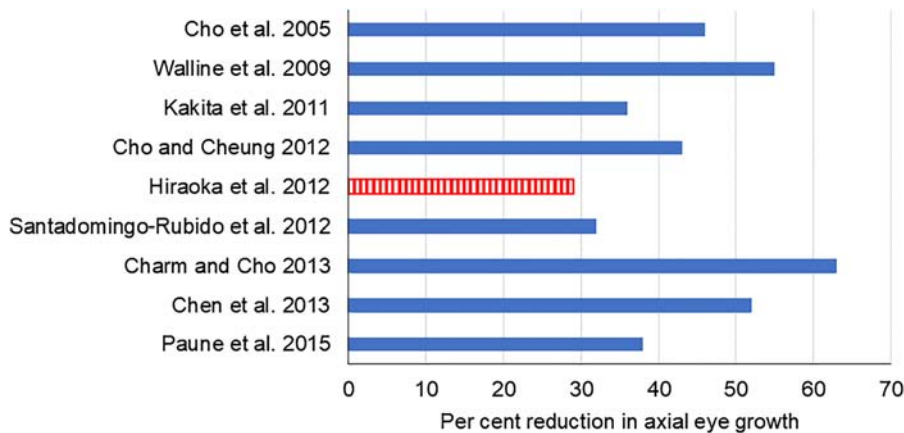


**Figure 5. Percent reduction in axial eye growth in subjects fitted with orthokeratology versus control subjects wearing spectacles or soft contact lenses from several studies.<sup>40,47,82-88</sup> Subjects were followed for two years (blue solid bars) or five years (red striped bar).**

lenses had 43 per cent less axial elongation compared with the single-vision spectacle control group. Axial length was measured every six months. For each six-month period of the study, there was a significant reduction in axial elongation in children wearing orthokeratology lenses compared with spectacle-wearing controls, demonstrating a continued treatment effect over the two-year period.

The studies described above evaluated the effect of orthokeratology on myopic children with low-to-moderate myopia. Charm and Cho<sup>40</sup> also investigated the myopia control effect of partial-reduction orthokeratology in highly myopic children (–5.75 D or more spherical equivalent myopia) over two years. In their study, orthokeratology lenses were used to treat 4.00 D of myopia, and the residual myopia was corrected with single-vision spectacles worn during the day. They found that in this group of highly myopic subjects, partial-reduction orthokeratology reduced myopia progression by 63 per cent over two years compared with children in the control group wearing single-vision spectacles to correct all of their myopia. However, this study had a relatively high dropout rate (37 per cent in the orthokeratology group and 16 per cent in the control group) which could potentially introduce bias in their results.

Toric orthokeratology is indicated for patients with high amounts of corneal astigmatism. A non-randomised prospective study by Chen et al.<sup>47</sup> evaluated axial

elongation between myopic children with moderate-to-high astigmatism (–1.25 to –3.50 D) wearing toric orthokeratology lenses and single-vision spectacles. Of the 35 myopic children who completed the study, Chen et al.<sup>47</sup> found that the children wearing toric orthokeratology lenses had 52 per cent slower axial eye elongation compared with spectacle-wearing controls over a two-year period.

Longer retrospective studies have been published reporting myopia progression in children wearing orthokeratology lenses. A study by Downie and Lowe<sup>89</sup> reported that orthokeratology slowed myopia progression for up to eight years, while another study by Lee et al.<sup>90</sup> reported significantly slower myopia progression in children wearing orthokeratology lenses up to six years after the start of treatment. One limitation of both studies, apart from the fact that they were retrospective record reviews, is that both studies measured myopia progression by over-refraction over the orthokeratology lenses as opposed to measuring changes in axial length.

Long-term data from a prospective study was reported by Santodomingo-Rubido et al.<sup>91</sup> They recruited subjects for a two-year study comparing the effect of orthokeratology (n = 29) versus single-vision spectacles (n = 24) on axial growth. Orthokeratology slowed axial elongation by 32 per cent over two years compared to spectacles. Five years after their initial study ended, roughly half of the subjects who had continued with a

modality similar to their original assignment (orthokeratology [n = 14] versus either spectacles or soft contact lenses [n = 16]) returned. Seven years after starting initial treatment, orthokeratology had slowed axial elongation by 33 per cent compared with single-vision corrections.

The longest prospective study of orthokeratology for myopia control was conducted by Hiraoka et al.<sup>87</sup> over a five-year period. They reported statistically significant accrual of a treatment effect over the first three years. There was no statistically significant difference in axial elongation between the orthokeratology and control groups in years four and five, but there was also no evidence of loss of the previously accrued treatment effect. This prospective study suggests that the myopia control effect of orthokeratology lenses is greatest in the initial years of wear with reduced efficacy over time. This finding may be because as the myopic children become older during the later stages of these long-term studies, their myopia progression naturally decreases, making it more difficult to find a significant difference in the rate of myopia progression between the orthokeratology and control groups.

The treatment effects reported in these studies are an average across all children. Individual progression results vary, with some children having greater treatment effects than others. One explanation that has been proposed for these differences in myopia control is differences in pupil size. Chen et al.<sup>92</sup> conducted a non-randomised study where myopic children wore either orthokeratology lenses or single-vision spectacles. They evaluated the effect of pupil size on myopia progression and found a significant association between larger pupils and slower myopia progression in children wearing orthokeratology lenses, proposing that larger pupils allowed a larger area of the peripheral retina to experience myopic defocus. Children wearing orthokeratology lenses who had larger pupils (greater than 6.43 mm) experienced significantly slower axial elongation over two years ( $0.36 \pm 0.22$  mm) compared to orthokeratology-wearing children with smaller pupils ( $0.74 \pm 0.32$  mm). However, it is perplexing that children wearing orthokeratology lenses with smaller pupils had faster axial elongation than children wearing single-vision spectacle lenses with small pupils who progressed only  $0.47 \pm 0.21$  mm over two years. Given this discrepancy, the

influence of pupil size should be studied further.

Apart from pupil size, Santodomingo-Rubido et al.<sup>93</sup> proposed other factors that were correlated with the inhibitory effects of orthokeratology on myopia progression. They included gender, age, age at myopia onset, rate of myopia progression, baseline amount of myopia, anterior chamber depth, corneal power and shape, iris diameter, and refractive error of the parents. However, subsequent studies found no correlation between reduction in myopia progression with orthokeratology and baseline amount of myopia, gender and corneal toricity.<sup>40,86</sup> Further work is needed to better understand the factors that are necessary to identify myopic children who may benefit most from orthokeratology and those who may be better suited for other myopia control methods.

There is evidence suggesting the potential for a rebound increase in axial elongation when myopic children discontinue orthokeratology treatment. In a contralateral eye crossover study conducted by Swarbrick et al.,<sup>94</sup> myopic children were randomly fitted with a rigid gas-permeable lens in one eye for daytime wear and overnight orthokeratology in the other eye. After six months, the lens allocation was swapped between eyes after a two-week recovery period, and the children were followed for another six months. The rate of axial elongation after eyes that had been wearing orthokeratology were switched to rigid gas-permeable lenses was greater than the rate of axial elongation in fellow eyes originally fitted with rigid gas-permeable lenses.

In another study by Cho and Cheung,<sup>95</sup> a subset of orthokeratology-wearing children from two previous studies agreed to be randomly assigned to either continue wearing orthokeratology for 14 months or to discontinue orthokeratology for seven months and then resume orthokeratology for another seven months. The authors found an increase in axial elongation in children who discontinued orthokeratology lens wear compared to both children still in orthokeratology and children who had never worn orthokeratology. Fortunately, eye elongation slowed again once children resumed orthokeratology. Further controlled studies are needed to explore the potential for an axial growth rebound after discontinuing orthokeratology.

Finally, a meta-analysis of the myopia control effect of orthokeratology by Si et al.<sup>96</sup> showed that compared to controls,

orthokeratology was effective at slowing axial eye growth by 0.26 mm (95% CI 0.21 to 0.31) over a two-year period. Sun et al.,<sup>97</sup> in another meta-analysis, also reported a 0.27 mm (95% CI 0.22 to 0.32) reduction in axial elongation compared to controls over two years, representing approximately 45 per cent reduction in axial elongation.

A network meta-analysis of published randomised controlled trials on interventions to slow myopia progression by Huang et al.<sup>98</sup> found that compared with controls, orthokeratology reduced axial elongation by 0.15 mm per year (95% CI 0.08 to 0.22). This myopia control effect of orthokeratology was similar to low-dose (0.01%) atropine (0.15 mm per year; 95% CI 0.05 to 0.25) and multifocal contact lenses (0.11 mm per year; 95% CI 0.03 to 0.20), but lower than high dose (1.0 or 0.5%) atropine (0.21 mm per year; 95% CI 0.16 to 0.28).

While orthokeratology and soft multifocal contact lenses for myopia control had similar effects on slowing eye growth, fitting orthokeratology typically requires more chair time. In a case series of 110 myopia control patients, Turnbull et al.<sup>99</sup> reported that children undergoing orthokeratology had a significantly higher number of clinic visits and chair time compared with children wearing multifocal contact lenses. The greater number of visits and potential need for morning visits during school time could influence a parent's decision regarding a myopia control modality.

### **Safety and complications**

With the growing use of orthokeratology for myopia correction and control, there is great interest in the safety of orthokeratology. Complications from orthokeratology range from easily treatable, low-grade corneal staining to potentially sight-threatening microbial keratitis. Other complications such as central corneal epitheliopathy,<sup>100</sup> recurrent binding of the contact lens to the cornea,<sup>101</sup> and corneal bubble and dimple formation<sup>102</sup> have also been reported. The majority of these complications are minor, easily managed, and do not lead to a reduction in visual acuity.<sup>103</sup>

### **Infectious keratitis**

Although cases of microbial keratitis have also been reported,<sup>104–106</sup> with *Pseudomonas aeruginosa* and *acanthamoeba* being the most prevalent causative organisms,<sup>104</sup> the highest number of infections occurred in

the late 1990s and early 2000s in China and have been attributed to the use of non-gas-permeable lens materials, improperly trained practitioners, and the use of tap water to clean and store lenses.<sup>107</sup> When good clinical practice guidelines are followed, the incidence of adverse events in clinical practice is the same for orthokeratology lenses as it is for other overnight contact lens modalities.<sup>103,105</sup> In the USA, the overall estimated incidence of microbial keratitis with orthokeratology is 7.7 per 10,000 years of wear (95% CI 0.9 to 27.8).<sup>108</sup> It is important that practitioners discuss possible complications with their patients and emphasise the importance of strict adherence to appropriate lens hygiene practices.

### **Iron deposition**

Corneal iron deposition has been reported during orthokeratology. These iron rings are benign and have no effect on vision but may represent some change in corneal physiology. They occur in both myopic<sup>109,110</sup> and hyperopic<sup>111</sup> orthokeratology, as early as one week<sup>109</sup> or as late as three and a half years<sup>111</sup> after starting orthokeratology. Cho et al.<sup>109</sup> reported that the rings resolved two months after discontinuing orthokeratology.

### **Future directions**

With the current interest in orthokeratology by researchers, clinicians, and patients, the future of orthokeratology looks very promising. There have been suggestions that multifocal orthokeratology designs could be developed to further increase the benefit of this lens modality for myopia control,<sup>112</sup> although no trials have been published on such a lens design. Additional studies are needed to determine if optimisation of the orthokeratology lens design could lead to a better myopia control effect.

Depending on the refractive error of a patient, both myopic and hyperopic orthokeratology can be used to create monovision correction in presbyopes. In a small cohort of 16 emmetropic presbyopes, Gifford and Swarbrick<sup>113</sup> used hyperopic orthokeratology to cause a 1.11 D myopic change in refractive error, essentially providing these presbyopes a roughly 1.00 D add. Although this study was published about five years ago, there has been little else published on this topic. The field would benefit from future work determining whether

a greater add can be created in emmetropic patients or if this is a viable option in patients with low hyperopia.

Another future application involves combining orthokeratology with atropine for myopia control. Since atropine and orthokeratology are thought to slow myopia progression through different mechanisms, combining the two treatments could lead to a greater reduction in myopia progression than orthokeratology alone. The greater effect of the combined treatment could also be from low-dose atropine causing slight increases in pupil size,<sup>114</sup> exposing a greater area of the retina to the myopic defocus.

Two published reports provide evidence supporting this synergistic effect.<sup>115,116</sup> Children in both studies who received orthokeratology and low-dose atropine progressed more slowly than children in orthokeratology alone; however, one study was only three months in length,<sup>115</sup> and the other was retrospective.<sup>116</sup> There is currently an ongoing two-year randomised clinical trial in which children were randomly assigned to either orthokeratology alone or orthokeratology with 0.01% atropine that should shed more light on the efficacy of this combined therapy for myopia control.<sup>117</sup>

Finally, future research is needed to understand how axial eye growth changes in myopic children after discontinuing orthokeratology. Overall, one should expect to continue hearing of new developments regarding the use of this contact lens modality.

## Conclusions

Overnight orthokeratology can temporarily reduce myopia, hyperopia, and astigmatism. This reduction in refractive error leads to improvements in uncorrected high- and low-contrast visual acuity with very little regression throughout the day. Orthokeratology also increases higher-order aberrations and can improve accommodative accuracy. Specifically, myopic orthokeratology increases positive spherical aberration.

Although high-contrast visual acuity with orthokeratology is similar to visual acuity with spectacles, increased higher-order aberrations reduce best-corrected low-contrast visual acuity and retinal image quality. Mid-peripheral corneal steepening with myopic orthokeratology also causes a myopic shift in peripheral refraction and is hypothesised to contribute to observed reductions in myopia

progression. There is continued research into optimising the design of orthokeratology lenses in attempts to potentially improve visual quality and myopia control effects, and to find new applications for these lenses.

## REFERENCES

1. Flaxman SR, Bourne RRA, Resnikoff S et al. Global causes of blindness and distance vision impairment 1990-2020: a systematic review and meta-analysis. *Lancet Glob Health* 2017; 5: e1221-e1234.
2. Brungardt TF. Orthokeratology: an analysis. *Int Contact Lens Clin* 1976; 3: 56-58.
3. Kerns RL. Research in orthokeratology. Part I: introduction and background. *J Am Optom Assoc* 1976; 47: 1047-1051.
4. Wlodyga RJ, Bryla C. Corneal molding: the easy way. *Contact Lens Spectrum* 1989; 4: 58-65.
5. Swarbrick HA, Wong G, O'Leary DJ. Corneal response to orthokeratology. *Optom Vis Sci* 1998; 75: 791-799.
6. Sridharan R, Swarbrick H. Corneal response to short-term orthokeratology lens wear. *Optom Vis Sci* 2003; 80: 200-206.
7. Tsukiyama J, Miyamoto Y, Higaki S et al. Changes in the anterior and posterior radii of the corneal curvature and anterior chamber depth by orthokeratology. *Eye Contact Lens* 2008; 34: 17-20.
8. Villa-Collar C, Gonzalez-Mejome JM, Queiros A et al. Short-term corneal response to corneal refractive therapy for different refractive targets. *Cornea* 2009; 28: 311-316.
9. Zhong X, Chen X, Xie RZ et al. Differences between overnight and long-term wear of orthokeratology contact lenses in corneal contour, thickness, and cell density. *Cornea* 2009; 28: 271-279.
10. Yoon JH, Swarbrick HA. Posterior corneal shape changes in myopic overnight orthokeratology. *Optom Vis Sci* 2013; 90: 196-204.
11. Alharbi A, Swarbrick HA. The effects of overnight orthokeratology lens wear on corneal thickness. *Invest Ophthalmol Vis Sci* 2003; 44: 2518-2523.
12. Wang J, Fonn D, Simpson TL et al. Topographical thickness of the epithelium and total cornea after overnight wear of reverse-geometry rigid contact lenses for myopia reduction. *Invest Ophthalmol Vis Sci* 2003; 44: 4742-4746.
13. Maseedupally V, Gifford P, Lum E et al. Central and paracentral corneal curvature changes during orthokeratology. *Optom Vis Sci* 2013; 90: 1249-1258.
14. Choo JD, Caroline PJ, Harlin DD et al. Morphologic changes in cat epithelium following continuous wear of orthokeratology lenses: a pilot study. *Cont Lens Anterior Eye* 2008; 31: 29-37.
15. Owens H, Garner LF, Craig JP et al. Posterior corneal changes with orthokeratology. *Optom Vis Sci* 2004; 81: 421-426.
16. Gonzalez-Mesa A, Villa-Collar C, Lorente-Velazquez A et al. Anterior segment changes produced in response to long-term overnight orthokeratology. *Curr Eye Res* 2013; 38: 862-870.
17. Chen D, Lam AK, Cho P. Posterior corneal curvature change and recovery after 6 months of overnight orthokeratology treatment. *Ophthalmic Physiol Opt* 2010; 30: 274-280.
18. Soni PS, Nguyen TT, Bonanno JA. Overnight orthokeratology: visual and corneal changes. *Eye Contact Lens* 2003; 29: 137-145.
19. Li F, Jiang ZX, Hao P et al. A meta-analysis of central corneal thickness changes with overnight orthokeratology. *Eye Contact Lens* 2016; 42: 141-146.
20. Kim WK, Kim BJ, Ryu IH et al. Corneal epithelial and stromal thickness changes in myopic orthokeratology and their relationship with refractive change. *PLoS One* 2018; 13: e0203652.

21. Kang SY, Kim BK, Byun YJ. Sustainability of orthokeratology as demonstrated by corneal topography. *Korean J Ophthalmol* 2007; 21: 74-78.
22. Wu R, Stapleton F, Swarbrick HA. Residual corneal flattening after discontinuation of long-term orthokeratology lens wear in Asian children. *Eye Contact Lens* 2009; 35: 333-337.
23. Lu F, Sorbara L, Simpson T et al. Corneal shape and optical performance after one night of corneal refractive therapy for hyperopia. *Optom Vis Sci* 2007; 84: 357-364.
24. Gifford P, Swarbrick HA. Time course of corneal topographic changes in the first week of overnight hyperopic orthokeratology. *Optom Vis Sci* 2008; 85: 1165-1171.
25. Gifford P, Alharbi A, Swarbrick HA. Corneal thickness changes in hyperopic orthokeratology measured by optical pachometry. *Invest Ophthalmol Vis Sci* 2011; 52: 3648-3653.
26. Mountford J. An analysis of the changes in corneal shape and refractive error induced by accelerated orthokeratology. *Int Contact Lens Clin* 1997; 24: 128-144.
27. Rah MJ, Jackson JM, Jones LA et al. Overnight orthokeratology: preliminary results of the lenses and overnight orthokeratology (LOOK) study. *Optom Vis Sci* 2002; 79: 598-605.
28. Joslin CE, Wu SM, McMahon TT et al. Higher-order wavefront aberrations in corneal refractive therapy. *Optom Vis Sci* 2003; 80: 805-811.
29. Koffler BH, Smith VM. Myopia reduction using corneal refractive therapy contact lenses. *Eye Contact Lens* 2004; 30: 223-226.
30. Soni PS, Nguyen TT, Bonanno JA. Overnight orthokeratology: refractive and corneal recovery after discontinuation of reverse-geometry lenses. *Eye Contact Lens* 2004; 30: 254-262.
31. Berntsen DA, Barr JT, Mitchell GL. The effect of overnight contact lens corneal reshaping on higher-order aberrations and best-corrected visual acuity. *Optom Vis Sci* 2005; 82: 490-497.
32. Hiraoka T, Matsumoto Y, Okamoto F et al. Corneal higher-order aberrations induced by overnight orthokeratology. *Am J Ophthalmol* 2005; 139: 429-436.
33. Sorbara L, Fonn D, Simpson T et al. Reduction of myopia from corneal refractive therapy. *Optom Vis Sci* 2005; 82: 512-518.
34. Hiraoka T, Okamoto C, Ishii Y et al. Time course of changes in ocular higher-order aberrations and contrast sensitivity after overnight orthokeratology. *Invest Ophthalmol Vis Sci* 2008; 49: 4314-4320.
35. Hiraoka T, Okamoto C, Ishii Y et al. Mesopic contrast sensitivity and ocular higher-order aberrations after overnight orthokeratology. *Am J Ophthalmol* 2008; 145: 645-655.
36. Kobayashi Y, Yanai R, Chikamoto N et al. Reversibility of effects of orthokeratology on visual acuity, refractive error, corneal topography, and contrast sensitivity. *Eye Contact Lens* 2008; 34: 224-228.
37. Queiros A, Gonzalez-Mejome JM, Jorge J et al. Peripheral refraction in myopic patients after orthokeratology. *Optom Vis Sci* 2010; 87: 323-329.
38. Kang P, Swarbrick H. Peripheral refraction in myopic children wearing orthokeratology and gas-permeable lenses. *Optom Vis Sci* 2011; 88: 476-482.
39. Nichols JJ, Marsich MM, Nguyen M et al. Overnight orthokeratology. *Optom Vis Sci* 2000; 77: 252-259.
40. Charm J, Cho P. High myopia-partial reduction ortho-k: a 2-year randomized study. *Optom Vis Sci* 2013; 90: 530-539.
41. Chan B, Cho P, Cheung SW. Orthokeratology practice in children in a university clinic in Hong Kong. *Clin Exp Optom* 2008; 91: 453-460.
42. Walline JJ, Rah MJ, Jones LA. The children's overnight orthokeratology investigation (COOKI) pilot study. *Optom Vis Sci* 2004; 81: 407-413.
43. Cheung SW, Cho P, Chan B. Astigmatic changes in orthokeratology. *Optom Vis Sci* 2009; 86: 1352-1358.

44. Mountford J, Pesudovs K. An analysis of the astigmatic changes induced by accelerated orthokeratology. *Clin Exp Optom* 2002; 85: 284–293.
45. Hiraoka T, Furuya A, Matsumoto Y et al. Quantitative evaluation of regular and irregular corneal astigmatism in patients having overnight orthokeratology. *J Cataract Refract Surg* 2004; 30: 1425–1429.
46. Chan B, Cho P, de Vecht A. Toric orthokeratology: a case report. *Clin Exp Optom* 2009; 92: 387–391.
47. Chen C, Cheung SW, Cho P. Myopia control using toric orthokeratology (TO-SEE study). *Invest Ophthalmol Vis Sci* 2013; 54: 6510–6517.
48. Stillitano I, Schor P, Lipener C et al. Stability of wavefront aberrations during the daytime after 6 months of overnight orthokeratology corneal reshaping. *J Refract Surg* 2007; 23: 978–983.
49. Lian Y, Shen M, Huang S et al. Corneal reshaping and wavefront aberrations during overnight orthokeratology. *Eye Contact Lens* 2014; 40: 161–168.
50. Santolaria-Sanz E, Cervino A, Gonzalez-Mejome JM. Corneal aberrations, contrast sensitivity, and light distortion in orthokeratology patients: 1-year results. *J Ophthalmol* 2016; 2016: 8453462.
51. Santodomingo-Rubido J, Villa-Collar C, Gilmartin B et al. Short- and long-term changes in corneal aberrations and axial length induced by orthokeratology in children are not correlated. *Eye Contact Lens* 2017; 43: 358–363.
52. Stillitano IG, Chalita MR, Schor P et al. Corneal changes and wavefront analysis after orthokeratology fitting test. *Am J Ophthalmol* 2007; 144: 378–386.
53. Stillitano I, Schor P, Lipener C et al. Long-term follow-up of orthokeratology corneal reshaping using wavefront aberrometry and contrast sensitivity. *Eye Contact Lens* 2008; 34: 140–145.
54. Johnson KL, Carney LG, Mountford JA et al. Visual performance after overnight orthokeratology. *Cont Lens Anterior Eye* 2007; 30: 29–36.
55. Berntsen DA. Retinal image quality after orthokeratology. *Invest Ophthalmol Vis Sci* 2018; 59: 1748.
56. Felipe-Marquez G, Nombela-Palomo M, Cacho I et al. Accommodative changes produced in response to overnight orthokeratology. *Graefes Arch Clin Exp Ophthalmol* 2015; 253: 619–626.
57. Kang P, Watt K, Chau T et al. The impact of orthokeratology lens wear on binocular vision and accommodation: a short-term prospective study. *Cont Lens Anterior Eye* 2018; 41: 501–506.
58. Gifford K, Gifford P, Hendicott PL et al. Near binocular visual function in young adult orthokeratology versus soft contact lens wearers. *Cont Lens Anterior Eye* 2017; 40: 184–189.
59. Gifford KL, Gifford P, Hendicott PL et al. Zone of clear single binocular vision in myopic orthokeratology. *Eye Contact Lens* 2019. <https://doi.org/10.1097/ICL.0000000000000614>.
60. Han X, Xu D, Ge W et al. A comparison of the effects of orthokeratology lens, medcall lens, and ordinary frame glasses on the accommodative response in myopic children. *Eye Contact Lens* 2018; 44: 268–271.
61. Gifford P, Li M, Lu H et al. Corneal versus ocular aberrations after overnight orthokeratology. *Optom Vis Sci* 2013; 90: 439–447.
62. Mutti DO, Sholtz RI, Friedman NE et al. Peripheral refraction and ocular shape in children. *Invest Ophthalmol Vis Sci* 2000; 41: 1022–1030.
63. Smith EL 3rd, Hung LF, Huang J. Relative peripheral hyperopic defocus alters central refractive development in infant monkeys. *Vision Res* 2009; 49: 2386–2392.
64. Kang P, Gifford P, Swarbrick H. Can manipulation of orthokeratology lens parameters modify peripheral refraction? *Optom Vis Sci* 2013; 90: 1237–1248.
65. Kang P, Swarbrick H. Time course of the effects of orthokeratology on peripheral refraction and corneal topography. *Ophthalmic Physiol Opt* 2013; 33: 277–282.
66. Gonzalez-Mejome JM, Faria-Ribeiro MA, Lopes-Ferreira DP et al. Changes in peripheral refractive profile after orthokeratology for different degrees of myopia. *Curr Eye Res* 2016; 41: 199–207.
67. Kang P, Swarbrick H. New perspective on myopia control with orthokeratology. *Optom Vis Sci* 2016; 93: 497–503.
68. Kang P, Swarbrick H. The influence of different OK lens designs on peripheral refraction. *Optom Vis Sci* 2016; 93: 1112–1119.
69. Queiros A, Amorim-de-Sousa A, Lopes-Ferreira D et al. Relative peripheral refraction across 4 meridians after orthokeratology and LASIK surgery. *Eye Vis (Lond)* 2018; 5: 12.
70. Lipson MJ, Sugar A, Musch DC. Overnight corneal reshaping versus soft disposable contact lenses: vision-related quality-of-life differences from a randomized clinical trial. *Optom Vis Sci* 2005; 82: 886–891.
71. National Eye Institute. NEI Refractive Error Quality of Life Instrument-42 (NEI RQL-42) (Internet). [Cited 17 Jun 2013.] Available at: <https://nei.nih.gov/catalog/nei-refractive-error-quality-life-instrument-42-nei-rql-42>
72. Ritchey ER, Barr JT, Mitchell GL. The comparison of overnight lens modalities (COLM) study. *Eye Contact Lens* 2005; 31: 70–75.
73. Berntsen DA, Mitchell GL, Barr JT. The effect of overnight contact lens corneal reshaping on refractive error-specific quality of life. *Optom Vis Sci* 2006; 83: 354–359.
74. Santodomingo-Rubido J, Villa-Collar C, Gilmartin B et al. Myopia control with orthokeratology contact lenses in Spain: a comparison of vision-related quality-of-life measures between orthokeratology contact lenses and single-vision spectacles. *Eye Contact Lens* 2013; 39: 153–157.
75. Zhao F, Zhao G, Zhao Z. Investigation of the effect of orthokeratology lenses on quality of life and behaviors of children. *Eye Contact Lens* 2018; 44: 335–338.
76. Hiraoka T, Okamoto C, Ishii Y et al. Patient satisfaction and clinical outcomes after overnight orthokeratology. *Optom Vis Sci* 2009; 86: 875–882.
77. Santolaria E, Cervino A, Queiros A et al. Subjective satisfaction in long-term orthokeratology patients. *Eye Contact Lens* 2013; 39: 388–393.
78. Wildsoet CF, Chia A, Cho P et al. IMI - interventions for controlling myopia onset and progression report. *Invest Ophthalmol Vis Sci* 2019; 60: M106–M131.
79. Smith EL 3rd. Prentice award lecture 2010: a case for peripheral optical treatment strategies for myopia. *Optom Vis Sci* 2011; 88: 1029–1044.
80. Schmid GF. Association between retinal steepness and central myopic shift in children. *Optom Vis Sci* 2011; 88: 684–690.
81. Cheung SW, Cho P, Fan D. Asymmetrical increase in axial length in the two eyes of a monocular orthokeratology patient. *Optom Vis Sci* 2004; 81: 653–656.
82. Cho P, Cheung SW, Edwards M. The longitudinal orthokeratology research in children (LORIC) in Hong Kong: a pilot study on refractive changes and myopic control. *Curr Eye Res* 2005; 30: 71–80.
83. Walline JJ, Jones LA, Sinnott LT. Corneal reshaping and myopia progression. *Br J Ophthalmol* 2009; 93: 1181–1185.
84. Kakita T, Hiraoka T, Oshika T. Influence of overnight orthokeratology on axial elongation in childhood myopia. *Invest Ophthalmol Vis Sci* 2011; 52: 2170–2174.
85. Santodomingo-Rubido J, Villa-Collar C, Gilmartin B et al. Myopia control with orthokeratology contact lenses in Spain: refractive and biometric changes. *Invest Ophthalmol Vis Sci* 2012; 53: 5060–5065.
86. Cho P, Cheung SW. Retardation of myopia in orthokeratology (ROMIO) study: a 2-year randomized clinical trial. *Invest Ophthalmol Vis Sci* 2012; 53: 7077–7085.
87. Hiraoka T, Kakita T, Okamoto F et al. Long-term effect of overnight orthokeratology on axial length elongation in childhood myopia: a 5-year follow-up study. *Invest Ophthalmol Vis Sci* 2012; 53: 3913–3919.
88. Paune J, Morales H, Armengol J et al. Myopia control with a novel peripheral gradient soft lens and orthokeratology: a 2-year clinical trial. *Biomed Res Int* 2015; 2015: 507572.
89. Downie LE, Lowe R. Corneal reshaping influences myopic prescription stability (CRIMPS): an analysis of the effect of orthokeratology on childhood myopic refractive stability. *Eye Contact Lens* 2013; 39: 303–310.
90. Lee YC, Wang JH, Chiu CJ. Effect of orthokeratology on myopia progression: twelve-year results of a retrospective cohort study. *BMC Ophthalmol* 2017; 17: 243.
91. Santodomingo-Rubido J, Villa-Collar C, Gilmartin B et al. Long-term efficacy of orthokeratology contact lens wear in controlling the progression of childhood myopia. *Curr Eye Res* 2017; 42: 713–720.
92. Chen Z, Niu L, Xue F et al. Impact of pupil diameter on axial growth in orthokeratology. *Optom Vis Sci* 2012; 89: 1636–1640.
93. Santodomingo-Rubido J, Villa-Collar C, Gilmartin B et al. Factors preventing myopia progression with orthokeratology correction. *Optom Vis Sci* 2013; 90: 1225–1236.
94. Swarbrick HA, Alharbi A, Watt K et al. Myopia control during orthokeratology lens wear in children using a novel study design. *Ophthalmology* 2015; 122: 620–630.
95. Cho P, Cheung SW. Discontinuation of orthokeratology on eyeball elongation (DOEE). *Cont Lens Anterior Eye* 2017; 40: 82–87.
96. Si JK, Tang K, Bi HS et al. Orthokeratology for myopia control: a meta-analysis. *Optom Vis Sci* 2015; 92: 252–257.
97. Sun Y, Xu F, Zhang T et al. Orthokeratology to control myopia progression: a meta-analysis. *PLoS One* 2015; 10: e0124535.
98. Huang J, Wen D, Wang Q et al. Efficacy comparison of 16 interventions for myopia control in children: a network meta-analysis. *Ophthalmology* 2016; 123: 697–708.
99. Turnbull PR, Munro OJ, Phillips JR. Contact lens methods for clinical myopia control. *Optom Vis Sci* 2016; 93: 1120–1126.
100. Ng LH. Central corneal epitheliopathy in a long-term, overnight orthokeratology lens wearer: a case report. *Optom Vis Sci* 2006; 83: 709–714.
101. Chui W, Cho P. Recurrent lens binding and central island formations in a fast-responding orthokeratology lens wearer. *Optom Vis Sci* 2003; 80: 490–494.
102. Stillitano I, Maidana E, Lui M et al. Bubble and corneal dimple formation after the first overnight wear of an orthokeratology lens: a case series. *Eye Contact Lens* 2007; 33: 253–258.
103. Liu YM, Xie P. The safety of orthokeratology - a systematic review. *Eye Contact Lens* 2016; 42: 35–42.
104. Kam KW, Yung W, Li GKH et al. Infectious keratitis and orthokeratology lens use: a systematic review. *Infection* 2017; 45: 727–735.
105. Hiraoka T, Sekine Y, Okamoto F et al. Safety and efficacy following 10-years of overnight orthokeratology for myopia control. *Ophthalmic Physiol Opt* 2018; 38: 281–289.
106. Li W, Sun X, Wang Z et al. A survey of contact lens-related complications in a tertiary hospital in China. *Cont Lens Anterior Eye* 2018; 41: 201–204.
107. Watt KG, Swarbrick HA. Trends in microbial keratitis associated with orthokeratology. *Eye Contact Lens* 2007; 33: 373–377.
108. Bullimore MA, Sinnott LT, Jones-Jordan LA. The risk of microbial keratitis with overnight corneal reshaping lenses. *Optom Vis Sci* 2013; 90: 937–944.
109. Cho P, Chui WS, Cheung SW. Reversibility of corneal pigmented arc associated with orthokeratology. *Optom Vis Sci* 2003; 80: 791–795.

110. Rah MJ, Barr JT, Bailey MD. Corneal pigmentation in overnight orthokeratology: a case series. *Optometry* 2002; 73: 425–434.
111. Kirkwood BJ, Rees IH. Central corneal iron line arising from hyperopic orthokeratology. *Clin Exp Optom* 2011; 94: 376–379.
112. Loertscher M. Multifocal orthokeratology associated with rapid shortening of vitreous chamber depth in eyes of myopic children. *Cont Lens Anterior Eye* 2013; 36: e2.
113. Gifford P, Swarbrick HA. Refractive changes from hyperopic orthokeratology monovision in presbyopes. *Optom Vis Sci* 2013; 90: 306–313.
114. Kaymak H, Fricke A, Mauritz Y et al. Short-term effects of low-concentration atropine eye drops on pupil size and accommodation in young adult subjects. *Graefes Arch Clin Exp Ophthalmol* 2018; 256: 2211–2217.
115. Kinoshita N, Konno Y, Hamada N et al. Additive effects of orthokeratology and atropine 0.01% ophthalmic solution in slowing axial elongation in children with myopia: first year results. *Jpn J Ophthalmol* 2018; 62: 544–553.
116. Wan L, Wei CC, Chen CS et al. The synergistic effects of orthokeratology and atropine in slowing the progression of myopia. *J Clin Med* 2018; 7: E259.
117. Tan Q, Ng AL, Cheng GP et al. Combined atropine with orthokeratology for myopia control: study design and preliminary results. *Curr Eye Res* 2019; 44: 671–678.



# Optical mechanisms regulating emmetropisation and refractive errors: evidence from animal models

*Clin Exp Optom* 2020; 103: 55–67

DOI:10.1111/cxo.12991

**Ranjay Chakraborty\***  PhD BS

Optometry

**Lisa A Ostrin<sup>†</sup>** PhD OD FAAO

**Alexandra Benavente-Perez<sup>‡</sup>** PhD MS BS

Optometry

**Pavan Kumar Verkicharla<sup>§</sup>** PhD BS

Optometry

\*College of Nursing and Health Sciences, Optometry and Vision Science, Flinders University, Adelaide, Australia

<sup>†</sup>University of Houston College of Optometry, Houston, Texas, USA

<sup>‡</sup>State University of New York College of Optometry, New York, USA

<sup>§</sup>Myopia Research Lab, Prof. Brien Holden Eye Research Centre, LV Prasad Eye Institute, Hyderabad, India

Email: ranjay.chakraborty@flinders.edu.au

Submitted: 2 July 2019

Revised: 24 September 2019

Accepted for publication: 25 September 2019

Our current understanding of emmetropisation and myopia development has evolved from decades of work in various animal models, including chicks, non-human primates, tree shrews, guinea pigs, and mice. Extensive research on optical, biochemical, and environmental mechanisms contributing to refractive error development in animal models has provided insights into eye growth in humans. Importantly, animal models have taught us that eye growth is locally controlled within the eye, and can be influenced by the visual environment. This review will focus on information gained from animal studies regarding the role of optical mechanisms in guiding eye growth, and how these investigations have inspired studies in humans. We will first discuss how researchers came to understand that emmetropisation is guided by visual feedback, and how this can be manipulated by form-deprivation and lens-induced defocus to induce refractive errors in animal models. We will then discuss various aspects of accommodation that have been implicated in refractive error development, including accommodative microfluctuations and accommodative lag. Next, the impact of higher order aberrations and peripheral defocus will be discussed. Lastly, recent evidence suggesting that the spectral and temporal properties of light influence eye growth, and how this might be leveraged to treat myopia in children, will be presented. Taken together, these findings from animal models have significantly advanced our knowledge about the optical mechanisms contributing to eye growth in humans, and will continue to contribute to the development of novel and effective treatment options for slowing myopia progression in children.

**Key words:** accommodation, emmetropisation, form-deprivation, longitudinal chromatic aberration, myopia, peripheral defocus

Both the optical power in the anterior segment of the eye and axial length determine refractive state.<sup>1–3</sup> Emmetropisation is an active, visually guided mechanism whereby the axial length and the combined optical powers of the cornea and lens precisely match with each other to eliminate neonatal refractive errors, and bring the eye to perfect focus (also known as emmetropia). In non-accommodating emmetropic eyes, visual images of distant objects are clearly focused at the retinal photoreceptors. Any disruption to this homeostatic mechanism of ocular growth results in the development of refractive errors. In myopia, or near-sightedness, the eye is too long for the optical power of the cornea and lens, and images of distance objects focus in front of the photoreceptor plane. In hyperopia, or far-sightedness, the eye is too short for the

optics, and images of distant objects focus behind the photoreceptor plane.

This review focuses on optical mechanisms of eye growth and refractive error development. We will discuss how extensive investigations on animal models have formed our current understanding of optical mechanisms of emmetropisation, and helped in developing improved optical interventions for refractive error management.

## **Optical defocus and visual regulation of ocular growth**

The visual environment plays an important role in the regulation of ocular growth and emmetropisation. Experimental studies of myopia employ diffusers to blur the image on the retina, which induces axial

elongation, also known as form-deprivation myopia (FDM).<sup>4–8</sup> Studies also use lenses to alter the image plane with respect to the retina, resulting in image defocus that induces compensatory alterations in ocular growth, known as lens-induced myopia or hyperopia.<sup>9–15</sup> Both form-deprivation and lens-induced defocus result in abnormal eye growth and refractive error development, with associated anatomical, optical, and biochemical changes in the anterior and posterior segments of the eye (see inclusive reviews).<sup>16–18</sup> In this section, we will define the process of emmetropisation, summarise different optical aspects of FDM and lens-induced ametropias, including their similarities and differences, and describe how these experimental models have informed us about refractive error development in humans.

## Emmetropisation

At birth, most animal species typically exhibit variable degrees of hyperopia.<sup>19–26</sup> During the early period of postnatal development there is a systematic reduction in both the degree and variability of hyperopia, bringing the eye closer to emmetropia, or in some cases, low myopia.<sup>27</sup> Similar to animal models, the majority of newborn infants are born moderately hyperopic, typically in the range of +2 to +4 D, which reduces significantly during the first 18 months of life.<sup>28–30</sup> There is a concurrent rapid increase of ~2–3 mm in axial length during the first one–two years of life, primarily due to an expansion in the vitreous chamber.<sup>31–33</sup> The rapid reduction in hyperopia and the changes in axial length during the early phase of emmetropisation are strongly correlated.<sup>32,33</sup> More importantly, based on evidence from animal models, the increase in axial length during the postnatal period in infant human eyes is believed to be modulated by active visual feedback from the hyperopic refractive error.<sup>32</sup> While axial length is the primary biometric component of emmetropisation in humans, there is also a passive contribution from reductions in corneal and crystalline lens power during postnatal eye growth.<sup>31,32,34</sup>

## FDM

Form-deprivation as an experimental model of myopia was first described by Wiesel and Raviola<sup>35</sup> in neonatal monkeys with lid fusion. Soon after, FDM was successfully induced in tree shrews,<sup>36</sup> chicks,<sup>6</sup> and cats<sup>37</sup> by suturing their eyelids, and in macaque monkeys by opacifying the cornea soon after birth.<sup>38</sup> Subsequent studies imposed form-deprivation by securing translucent diffusers over the eye using a mask,<sup>2,13,39</sup> glue,<sup>40,41</sup> Velcro,<sup>4,42,43</sup> or a head-mounted pedestal.<sup>44–47</sup> These studies have consistently shown that depriving the retina of form or patterned vision produces axial myopia compared to untreated eyes, suggesting that a sharp, high-contrast retinal image is essential for normal eye growth (Figure 1). FDM is believed to be an ‘open-loop’ condition, in which myopia occurs as a result of unrestricted eye growth due to absence of visual feedback from the form-deprived retina and absence of a defined refractive endpoint.<sup>35,48</sup>

FDM is primarily a result of increased axial length, mainly an elongated vitreous chamber, and is accompanied by thinning of the choroid and sclera.<sup>4,7,10,49–54</sup> While FDM

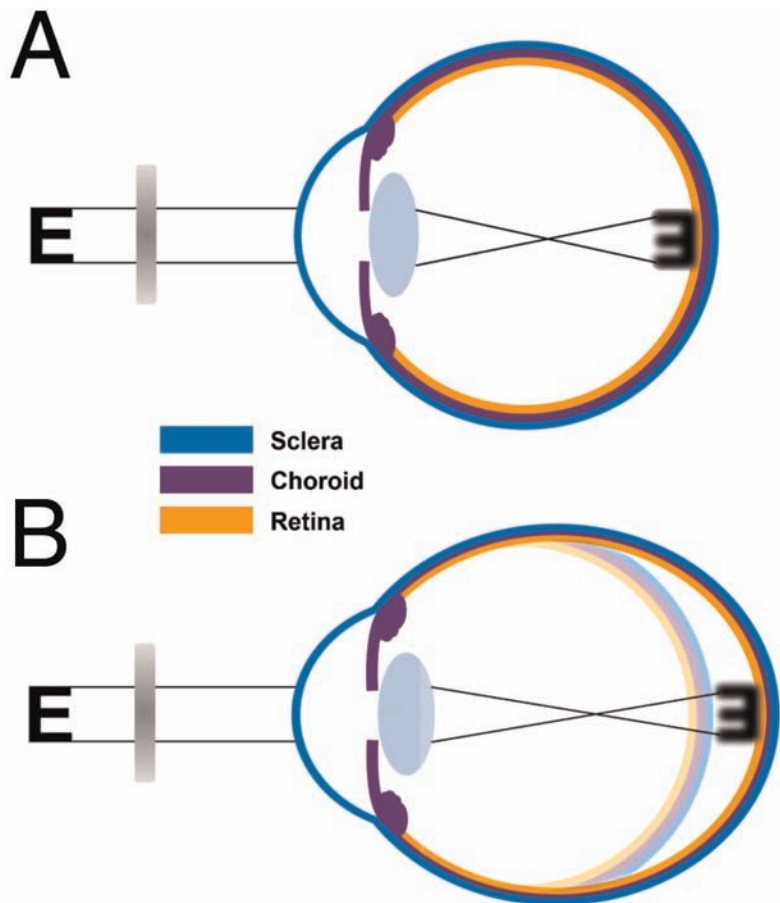


**Figure 1. Ocular compensation for form-deprivation. A: A diffuser causes non-directional blur and a reduction in contrast of the retinal image. B: The absence of visual feedback related to the effective refractive state of the eye causes a thinning of the posterior choroid and an increase in ocular growth, resulting in myopia, known as form-deprivation myopia (FDM). The blurred eye represents the original shape of the eye prior to form-deprivation.**

has been reported in a wide range of animal species, including birds,<sup>7,10,55</sup> rodents,<sup>39,56</sup> non-human primates,<sup>35,54</sup> and even fish,<sup>57</sup> the magnitude of myopia and the rate of ocular elongation varies among species. For example, chick eyes can develop myopia of up to 17 D after 10 days of form deprivation,<sup>7</sup> whereas primates develop approximately 5–6 D of myopia after 17 weeks of form-deprivation.<sup>8,58</sup> Despite quantitative differences between species, potentially due to differences in experimental paradigms and/or inherent ocular anatomical variations between animal models, these results importantly point toward a ubiquitous visual mechanism of ocular growth modulation that is conserved across species.

FDM is a graded phenomenon; the degree of axial myopia is positively correlated with the degree of reduction in retinal image contrast.<sup>54,59</sup> Therefore, even mild distortions in the quality of the retinal image may potentially lead to some degree of myopia. In any given animal model, there are significant individual (or between-subject) differences in the myopic response to form-deprivation. This suggests that both visual environment and individual genetic factors contribute to FDM,<sup>48</sup> which is consistent with our current understanding of the aetiology of myopia in humans. Furthermore, the ability of the eye to respond to form-deprivation declines with age in chicks,<sup>7,55</sup> monkeys,<sup>60</sup> tree shrews,<sup>5</sup> and marmosets.<sup>50</sup> However, older chickens<sup>55,61</sup>

and monkeys<sup>60</sup> do continue to respond to form-deprivation, albeit to a lesser magnitude, suggesting that the visual system retains some degree of plasticity even at the end of the 'initial infantile phase' of emmetropisation. Constant darkness also deprives the eye of form vision, causing ocular elongation and significant corneal flattening in chicks and monkeys.<sup>51,62,63</sup> The reduction in corneal power related to the loss of circadian cues in darkness strongly influence the refractive development of the eye, leading to more hyperopic refraction in young animals. Finally, in all animal models, removing the diffusers at the end of the form-deprivation period leads to recovery, defined by a rapid and systematic reduction in the magnitude of experimentally induced myopia.<sup>4,7,10,55</sup> The rapid deceleration in eye growth during recovery from FDM largely occurs as a result of changes in the vitreous chamber and choroidal thickness.<sup>7,10</sup> Recovery from FDM depends on the magnitude of myopia and the age at which diffusers are removed.<sup>64</sup> In animals, the ability of the eye to recover from myopia declines with age in optically mature eyes, with stable corneal and lens powers.<sup>1</sup> Interestingly, in humans, visual deprivation from ptosis,<sup>65</sup> congenital cataract,<sup>66</sup> corneal opacity,<sup>67</sup> and vitreous haemorrhage<sup>68</sup> are associated with myopia, which likely results from mechanisms similar to FDM observed in animals.

### Lens-induced refractive errors

As shown in Figure 2, a large part of our current knowledge of visual regulation of ocular growth has originated from experimental studies describing the ability of the eye to compensate for myopic or hyperopic defocus, imposed with positive or negative lenses, respectively. When defocus is induced, the eye undergoes compensatory changes in ocular growth to match its axial length to the altered focal plane, thereby decreasing or eliminating the imposed refractive error.<sup>9,16</sup> Myopic defocus induced with positive lenses leads to a thickening of the choroid which brings the retina forward, a slowing of axial elongation, and a hyperopic shift in refraction. Conversely, hyperopic defocus induced with negative lenses results in choroidal thinning which moves the retina backward, an increase in axial elongation, and a myopic shift in refraction. For either defocus condition, the change in axial length is largely attributed to the changes in the vitreous chamber.<sup>10</sup> Lens-induced defocus is a 'closed-loop' condition, in which axial growth

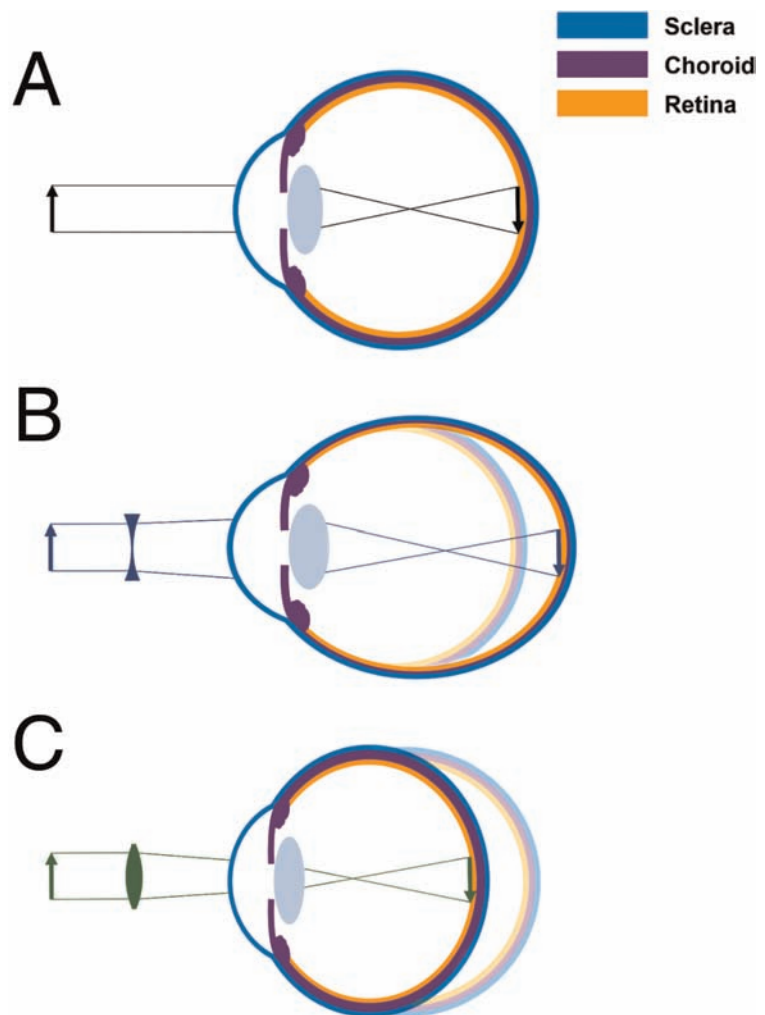


**Figure 2. Schematic of lens-induced refractive errors. A: A normal eye with no imposed lens defocus exhibits normal ocular growth and choroidal thickness. B: Hyperopic defocus induced with negative lenses (blue) results in choroidal thinning which moves the retina backward, an increase in axial elongation, and a myopic shift in refraction. C: Myopic defocus induced with positive lenses (green) leads to a thickening of the choroid which brings the retina forward, a slowing of axial elongation, and a hyperopic shift in refraction. The blurred eye in B and C represents the original shape of the eye prior to the introduction of lens defocus. Adapted from Wallman and Winawer, 2004.<sup>1</sup>**

ceases when the imposed defocus is appropriately compensated.<sup>69</sup> The effects of lens defocus on ocular growth have been demonstrated in chickens,<sup>7,9-12,70,71</sup> tree shrews,<sup>72</sup> monkeys,<sup>13,14</sup> marmosets,<sup>73</sup> guinea pigs,<sup>15</sup> and mice,<sup>49,74</sup> suggesting that this vision-dependent regulatory mechanism of eye growth is conserved across species.

Similar to FDM, there are significant interspecies differences in ocular responses to lens-induced defocus. Chick eyes can compensate for a large range of spectacle lens

powers ranging from  $-10$  to  $+20$  D,<sup>70</sup> while Old and New World monkeys' eyes exhibit a relatively smaller operating range of  $-5$  to  $+8$  D.<sup>13,75</sup> These differences in the magnitude of the response may reflect interspecies differences in refractive error, ocular anatomy, or other physiological processes, such as accommodation and vergence mechanisms. Growing eyes in young animals can fully compensate for defocus imposed by spectacle lenses as long as they are in the linear response range of their emmetropisation

mechanism.<sup>70,73</sup> Imposing higher degrees of defocus beyond the operating limits of lens compensation results in little or no change in refractive error in mice,<sup>49</sup> chicks<sup>76</sup> and primates.<sup>13</sup> When the imposed defocus is removed, all animal models show rapid recovery by reversing the changes in both choroidal thickness and axial eye growth to restore normal vision.<sup>7,10</sup> Interestingly, consistent with observations in animal models, recent studies in young adult humans have documented small, short-term bidirectional changes in axial length and choroidal thickness in response to one–two hours of imposed hyperopic and myopic defocus.<sup>77–80</sup>

During lens-imposed defocus, the sign, frequency, duration, and magnitude of defocus experienced by the eye change constantly depending on the visual scene. Therefore, the nature of vision-dependent eye growth depends on the temporal integration of visual signals over time (see reviews).<sup>16,81</sup> Previous studies have shown that the temporal integration of visual signals for ocular growth regulation is non-linear. For instance, exposing the eye to successive periods of hyperopic and myopic defocus of equal durations lead to reduced axial elongation and hyperopic refractive error in chicks.<sup>82,83</sup> Furthermore, studies in chicks have shown that myopic defocus has a greater effect on refractive development compared to hyperopic defocus, suggesting that the visual system may be using distinct visual mechanisms for ocular compensation to hyperopic and myopic defocus.<sup>81,84,85</sup> The nature of lens compensation, as well as FDM, depend on the frequency and duration of exposure, not just the total duration of exposure in a day.<sup>81,85–87</sup> In chick eyes, several brief periods of defocus throughout the day produce a larger ocular response than a single or a few longer (and less frequent) daily episodes of defocus of the same total duration.<sup>87</sup> Recent studies in chicks<sup>88</sup> and humans<sup>77</sup> have reported that ocular response to lens-induced defocus also depends on the time of day of exposure to defocus. A number of current optical treatment strategies for myopia control, such as multifocal contact lenses and orthokeratology, produce simultaneous competing hyperopic and myopic defocus signals across a large portion of the retina. In guinea pigs reared with dual-focus lenses of alternating  $-5$  D/0 D,  $+5$  D/0 D or  $-5$  D/ $+5$  D power zones, the refractive change is equivalent to the average of the two constituent powers.<sup>89</sup> In chicks<sup>90</sup> and marmosets,<sup>91</sup> the refractive compensation with dual-focus

lenses of varying powers is generally skewed toward the more positive powered lens component, leading to hyperopic refractive errors. In infant macaques, the refractive development with dual-focus lenses of concentric annular zones and alternating powers of  $-3$  D/0 D and  $+3$  D/0 D is largely dominated by the more anterior (or relatively more myopic/less hyperopic) image plane.<sup>92</sup> Spatial and temporal integration of these competing visual signals determine the overall nature and direction of refractive development. Finally, spatial integration of visual signals across the central and peripheral retina may also modulate the eye's response to lens-induced defocus (see section on peripheral defocus for details).

While both hyperopic defocus and form-deprivation induce axial myopia (discussed above), the mechanisms underlying the two experimental conditions may be different. For instance, blocking the parasympathetic innervation to the eye through ciliary ganglionectomy inhibited FDM in chicks,<sup>93</sup> but had no effect on the compensatory responses to lens-induced defocus.<sup>12</sup> Previous chick studies have reported significant differences in the inner retinal function between form-deprivation and negative lens wear.<sup>94</sup> In another study, Choh et al.<sup>95</sup> showed that in chicks with optic nerve section, the change in axial length with diffusers was about 50 per cent greater compared to the eyes experiencing lens defocus, despite similar degrees of imposed 'spatial blur' on the retina in absence of accommodation (optic nerve section eliminates active accommodation). In addition, environmental lighting manipulations have varying effects on FDM and lens-induced defocus. For instance, six days of rearing in bright lighting completely inhibited FDM in chicks, but had no effect on the refractive endpoint of negative lens-induced myopia.<sup>96</sup> Similarly, high intensity light levels eliminated the development of FDM, but only had modest effect on compensation to hyperopic defocus in chicks and macaques.<sup>97,98</sup> In another interesting study by Nickla and Totonelly, the D2 antagonist spiperone prevented the ocular growth inhibition induced by brief periods of clear vision in form-deprived eyes, but had no effect on eyes wearing negative lenses, suggesting that the dopaminergic mechanisms mediating the protective effects of brief periods of unrestricted vision may be different for form-deprivation versus lens-induced defocus conditions. These results warrant further investigation into the

differences between the two experimental conditions.

This body of work in animal models has laid a robust scientific foundation for developing optical treatments that alter retinal image quality to reduce myopia progression in young human eyes, including orthokeratology and bifocal contact lenses.<sup>99,100</sup>

## Accommodation

Accommodation is the dioptric power change of the eye to focus diverging rays on the retina, and has been implicated in myopia development. Accommodation is initiated by several cues, including retinal defocus, chromatic aberrations,<sup>101</sup> and optical vergence.<sup>102</sup> Evidence from animal studies suggests that emmetropisation is guided by retinal defocus. Speculation exists whether accommodation-related defocus plays a role in emmetropisation. Several animal models of myopia are known to show active accommodation, including the chick,<sup>9,103</sup> marmoset,<sup>104</sup> and rhesus monkey,<sup>105,106</sup> and have been utilised to examine the influence of accommodation in eye growth. Non-human primates exhibit lenticular accommodation, similar to humans. On the other hand, chicks demonstrate both corneal and lenticular accommodation.<sup>107–110</sup> Characteristics of accommodation that have been linked to emmetropisation and myopia include accommodative microfluctuations,<sup>111</sup> accommodative lag,<sup>112</sup> tonic accommodation,<sup>113,114</sup> and blur interpretation.<sup>115</sup>

Early studies that utilised minus lens-induced hyperopic defocus to induce experimental myopia were based on the belief that this affected eye growth via accommodation-related mechanisms, that is, animals wearing minus lenses could accommodate to compensate for hyperopic defocus, which would be a signal for the eye to grow.<sup>9</sup> Additionally, monocular topical application of atropine, a nonspecific muscarinic antagonist, effectively reduces experimental myopia of the treated eye in animal models. The protective effects of atropine were originally attributed to cycloplegic effects on the smooth muscle of the ciliary body, thereby eliminating accommodation.<sup>116</sup> However, several studies in animal models have shown that lens-induced defocus compensation and the mechanism of atropine in myopia control are independent of accommodation. Accommodation cues originate in the retina, and afferent

signals are carried by the optic nerve to higher brain centres. The efferent pathway travels from the Edinger-Westphal nucleus of the midbrain to the ciliary ganglion, and is ultimately carried by the ciliary nerves to the ciliary muscle of both eyes.<sup>117</sup> Accommodation signals from the Edinger-Westphal nucleus will initiate a binocular and consensual accommodation response. Lesions in either the afferent or efferent components of the accommodation pathway do not prevent lens-induced myopia.<sup>118</sup> For example, optic nerve section in rhesus monkeys,<sup>119</sup> and Edinger-Westphal nucleus lesioning and ciliary nerve section in chicks,<sup>10,12,118</sup> do not prevent defocus-induced myopia; eye growth can still be regulated via visual cues even without active accommodation. Additionally, it was shown in chicks that atropine reduces experimental myopia through non-accommodative mechanisms, as atropine has no effect on the striated muscle of the chick ciliary body.<sup>120</sup> These findings provide support that eye growth is controlled by local mechanisms within the eye. Further support that argues against a role of accommodation in defocus-induced eye growth comes from studies showing that growth in local regions of the eye can be modulated by defocus to only part of the visual field,<sup>121</sup> whereas accommodation changes focus uniformly across the visual field.

Findings that active accommodation is not necessary for experimental myopia do not preclude the presence of a role of accommodation in the development of myopia, due to its association with retinal defocus.<sup>122</sup> Studies in chicks, tree shrews, and rhesus monkeys have shown that brief periods of clear vision during a hyperopic defocus period inhibit experimental myopia development.<sup>12,123,124</sup> These findings suggest that if an animal can eliminate defocus induced from a minus lens by accommodating, a similar myopia inhibitory effect should be achieved.

Consequently, high lags of accommodation resulting in hyperopic retinal defocus would be a stimulus for the eye to grow. To test this hypothesis, Troilo et al. examined accommodative behaviour before and after the induction of experimental myopia in awake marmosets,<sup>125</sup> and found that an increased accommodative lag was present after defocus-induced myopia. However, accommodative performance before lens treatment did not predict the amount of myopia induced, suggesting that the increased lag was a consequence of myopia,

not a cause. Similarly, a recent study in chicks showed that accommodative lag does not predict the magnitude of lens-induced myopia.<sup>126</sup>

On the other hand, Diether and Wildsoet<sup>127</sup> investigated whether accommodation influenced the chick eye's ability to decode focusing errors and the relationship with spatial frequency and contrast. They found that when accommodation was eliminated through ciliary nerve section, decoding of, and compensation for, imposed defocus was impaired. Specifically, ciliary nerve section biased the eye growth response toward more myopia when competing hyperopic and myopic signals were present. The authors concluded that accommodation plays a role in decoding defocus during emmetropisation. Taken together, these results have led researchers to suggest that a complex relationship exists between accommodation and emmetropisation, involving multiple neural pathways, feedback loops, and interactions between temporal and spatial patterns of defocus (see section on peripheral defocus for details).

Studies in animal models regarding the role of accommodation in myopia have both informed and complemented studies in humans, and vice versa. Early evidence in humans linking near work to increased myopia prevalence<sup>128,129</sup> spurred much of the work regarding interactions between accommodation and experimental myopia in animal models. With the finding that hyperopic defocus in animal models produces myopia, researchers investigated whether accommodative lags in children promote myopia. However, results from various studies have shown conflicting results, such that some report increased lags exist before the onset of myopia<sup>130-132</sup> and others report that increased lags appear only after myopia onset.<sup>112</sup> Findings in animals showing that myopic defocus slows or prevents experimental myopia have provided rationale for investigating whether the use of bifocal or progressive addition lenses slow myopia progression in children; however, results have also been equivocal, showing a range of efficacy between studies from none<sup>133,134</sup> to modest levels.<sup>135,136</sup> While more recent studies show that bifocal or multifocal contact lenses more effectively slow the progression of myopia compared to spectacle lenses, the underlying mechanisms are not well understood, and may be influenced by both accommodation and peripheral defocus.

## Peripheral defocus

Emmetropisation is largely an active process guided by visual feedback that can be achieved without input from the central retina<sup>137-140</sup> or the brain,<sup>62,141,142</sup> although an intact optic nerve is required for a fine-tuned response.<sup>143,144</sup> The ability of the chick retina to selectively guide eye growth in localised areas experiencing partial retinal deprivation was a key finding by Hodos and Kuenzel,<sup>40</sup> and Wallman et al.,<sup>137</sup> later confirmed in rodents and non-human primates.<sup>139,140,145</sup> In addition to local form-deprivation, the retina can respond to regionally imposed defocus.<sup>121,146-148</sup> Chicks and non-human primates exposed to negative and positive hemi-field defocus can develop myopia and hyperopia in the corresponding retinal area.<sup>121,149</sup> Not only hemi-retinal, but also peripheral defocus can modify eye growth.<sup>91,147,148,150</sup> The compensation to negative peripheral defocus is in the same direction, but of lesser degree, than the compensation to full-field negative defocus, whereas the compensation to positive defocus is in the same direction and degree,<sup>146</sup> in some cases greater,<sup>147,148</sup> than the compensation to full-field positive defocus. In chicks, marmosets, and macaques, small treatment zones of peripheral hyperopic defocus effectively stimulate axial eye growth,<sup>91,148,151</sup> but larger treatment zones of peripheral myopic defocus are required to slow growth and significantly alter axial refraction (Figure 3).<sup>146-148</sup> In another study, Schippert and Schaeffel compared the central and peripheral (+45° and -45°) refractive development in chicks wearing either full-field spectacle lenses of +6.9 D and -7 D or lenses with central holes of 4, 6, and 8 mm diameter for four days. The study found that there was almost complete ocular compensation for full-field lenses, but no significant change in central refraction with holes in the centre of the lenses, suggesting that peripheral defocus does not necessarily affect central refractive development.<sup>152</sup> Overall, these findings provide strong evidence supporting the conservation of emmetropisation mechanisms across species, and highlight the importance of studying animal models to understand emmetropisation in humans.

For many years, the high foveal sensitivity to defocus was thought to be essential for

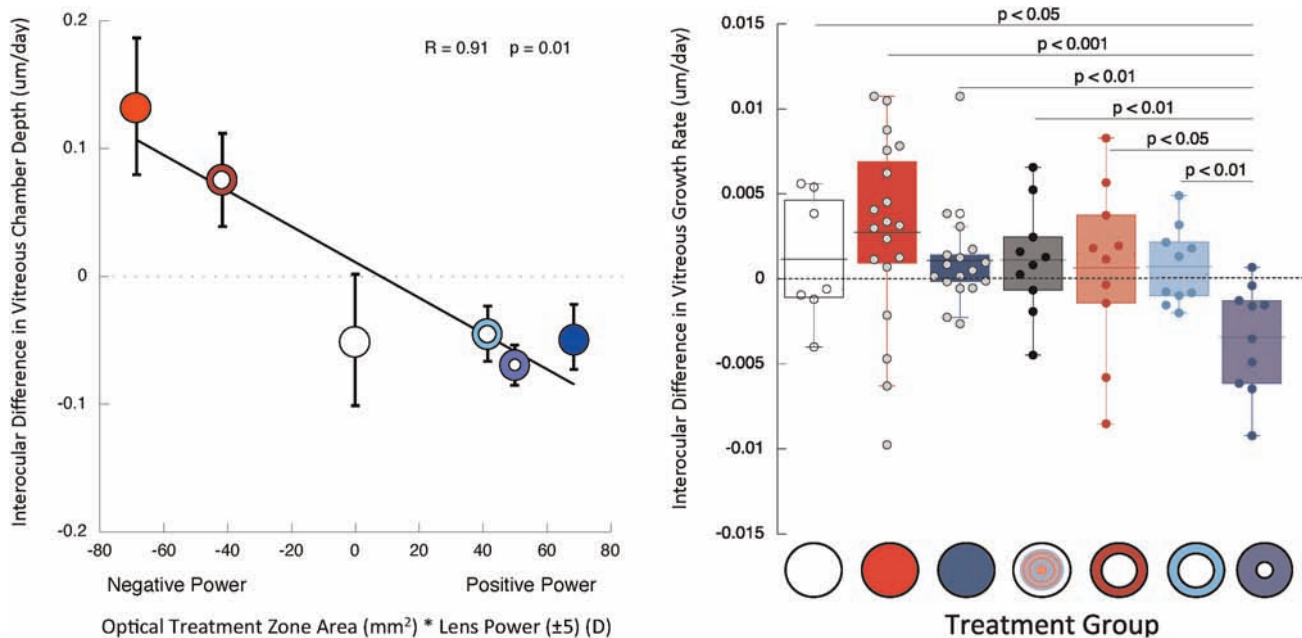


**Figure 3.** Left panel shows scatter plot showing how the inter-ocular vitreous growth differences change as a function of contact lens treatment zone area (mm<sup>2</sup>) multiplied by the power of the treatment zone (D). Right panel shows box plots describing interocular differences in ocular growth rate during treatment in untreated controls (white) and marmosets treated single-vision -5 D (dark red), single-vision +5 D (dark blue), multizone +5/-5 D (black), -5 D/3 mm (light red), +5 D/3 mm (blue) and +5 D/1.5 mm (light blue). The data shown are means  $\pm$  SE. Adapted from Benavente-Perez et al., 2014.<sup>148</sup> The Association for Research in Vision and Ophthalmology is the copyright holder of this figure.

defocus detection and emmetropisation. However, non-foveated species like the fish,<sup>57</sup> and species with comparatively low spatial resolution like chickens,<sup>7</sup> tree shrews,<sup>36</sup> and guinea pigs,<sup>4</sup> respond to form-deprivation, suggesting that the foveal contribution may not be essential. Work by Smith et al.<sup>138</sup> confirmed this hypothesis after describing how rhesus monkeys with foveal ablation emmetropised normally and compensated for form-deprivation. The peripheral retina could function alone, and an intact fovea was not essential for emmetropisation. Foveal information is also not essential for defocus compensation. The eyes of chicks and non-human primates can recover from induced refractions in the absence of foveal signals.<sup>140,153</sup> The ability of the eye to respond to localised visual manipulations confirmed that emmetropisation does not depend on a central neural mechanism, but on a local and regionally selective retinal mechanism located within the eye, which opened new avenues for eye growth manipulation in humans.

Since the mechanism of emmetropisation is contained within the eye and peripheral defocus can alter refractive development, the defocus experienced by the peripheral

retina would be expected to drive eye growth. In humans, the pattern of peripheral refraction is known to vary with central refraction; myopes tend to exhibit relative peripheral hyperopia along the horizontal axis, and hyperopes tend to exhibit relative peripheral myopia.<sup>154-156</sup> Whether the peripheral profile may be a cause or a consequence of central refractive development continues to be controversial.<sup>157</sup> In rhesus monkeys, FDM causes a shift in peripheral refraction toward relative hyperopia, which increases with the degree of central myopia.<sup>158</sup> Imposing full-field defocus on the retina of marmosets triggers compensatory changes in eye growth and refractive state that lead to asymmetries in the refraction of the peripheral retina.<sup>159</sup> In both marmosets and rhesus monkeys, the strength of the relationship between central and peripheral refraction varies with eccentricity, as does the degree of peripheral refraction asymmetry.<sup>159-161</sup> Marmosets exhibit nasal-temporal asymmetries in peripheral refraction that change with age toward relative nasal hyperopia. The changes are similar, but greater, in animals treated with full-field negative defocus, suggesting that asymmetry changes in peripheral refraction can

occur during both normal emmetropisation and lens-induced myopia.<sup>161</sup> Not only does relative peripheral refraction change toward relative hyperopia during periods of increased eye growth, there is evidence that peripheral refraction also changes when eye growth decelerates. In marmoset eyes, relative peripheral refraction changes toward relative myopia during emmetropisation periods of slower growth or recovery from visual compensation.<sup>162</sup>

The role of peripheral refraction and its interaction with the temporal properties of visually guided eye growth has also been evaluated in marmosets.<sup>163</sup> Peripheral refraction at baseline can predict the compensatory changes in eye growth only in combination with on-axis refraction, or after the eyes have begun to compensate for the imposed negative defocus. Therefore, peripheral refraction changes as a consequence of myopia development and can predict myopia progression when eyes have started to develop myopia.<sup>163</sup> These results, combined with previous results from Benavente and Troilo's group,<sup>160-163</sup> provide evidence of an interaction between the refractive asymmetry of the peripheral retina and the visual experience of the central

retina, such that peripheral refraction appears to be both cause and effect of axial growth, becoming a possible factor in the progression of myopia and offering a means to control it.

### Ocular shape and peripheral defocus

The nature of ocular growth in myopia has been described as either global, equatorial or axial, depending on the region of the eye undergoing stretching.<sup>164-166</sup> Given the magnitude of defocus depends on the location of the image with respect to the retinal plane, the shape of the retina has been investigated in association with peripheral refraction and refractive error (see review by Verkicharla et al.).<sup>166</sup> The evidence from research studies involving primates and human participants are in agreement with the hypothesis that peripheral defocus influences peripheral eye shape and myopia at large. Previous human studies have measured the shape of the retina (or the posterior eye) using magnetic resonance imaging<sup>167,168</sup> and other indirect optical methods<sup>169-173</sup> and correlated it with peripheral refraction. As shown in Figure 4, myopic eyes with steeper or prolate retinal shape exhibit relative peripheral hyperopia, whereas hyperopic or emmetropic eyes with flatter or oblate retinas exhibit relative peripheral myopia.<sup>166-168,171,174,175</sup>

In infant rhesus monkeys<sup>158,176</sup> and marmosets,<sup>177</sup> the change in peripheral refraction with form-deprivation or lens-induced defocus applied to a specific part of the visual field correlated with the interocular differences in vitreous chamber shape, as observed with magnetic resonance imaging. A large number of studies involving humans have investigated peripheral refraction, with only a few looking at peripheral refraction and retinal shape in combination. Verkicharla et al.<sup>178,179</sup> reported that peripheral refraction, peripheral eye lengths, and retinal shapes measured from partial coherence interferometry were significantly affected by race, as well as by meridian and refraction. East Asians were found to have steeper retinas and greater relative peripheral hyperopia than Caucasians, with steepness being greater along the horizontal meridian than the vertical meridian. The differences among races and meridians were attributed to structural variations of the eye between races, and more space in the orbit around the eye vertically than horizontally. Wakazono et al.<sup>180</sup>

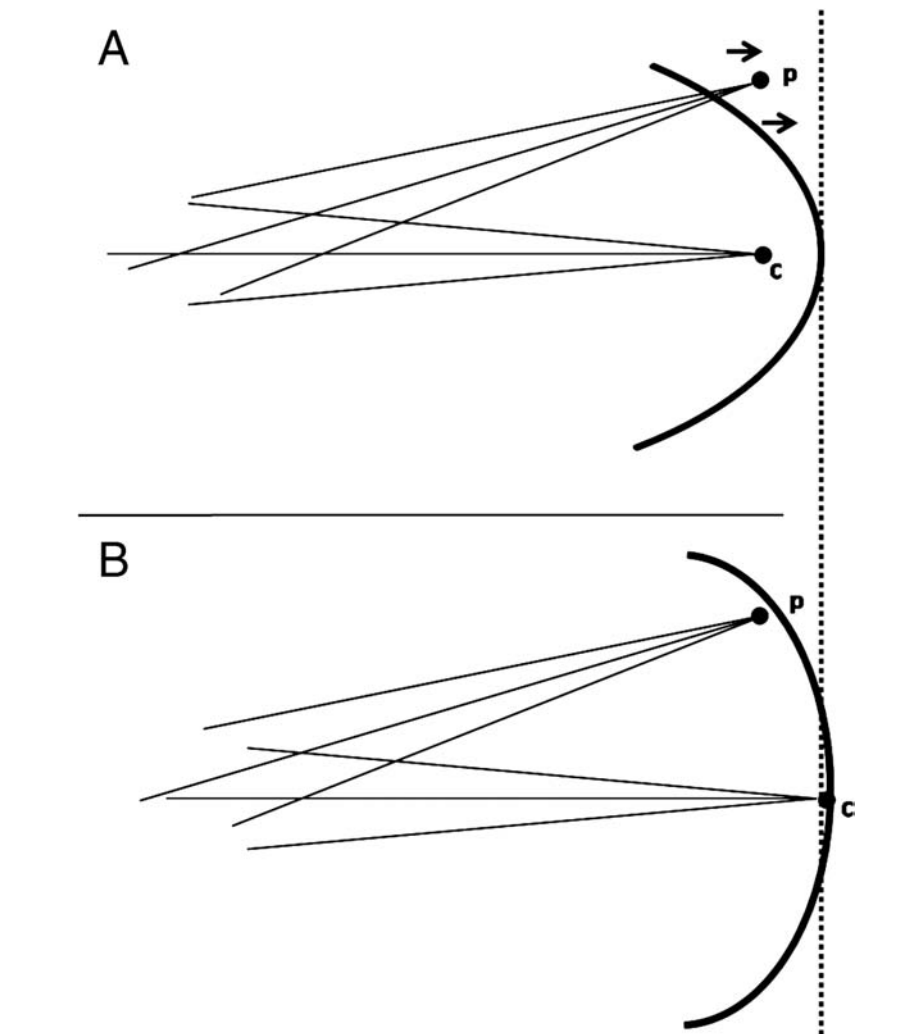


**Figure 4. Possible uncorrected image shells relative to the retina. A: Steeper or prolate myopic retina where the central refraction (c) is focused in front of the retina and the peripheral refraction at extreme point p is focused behind the retina, causing a relative peripheral hyperopia. B: Flatter or oblate emmetropic retina where the central refraction (c) is focused at the retina and the peripheral refraction at extreme point p is focused in front of the retina, causing a relative peripheral myopia. Note: this is an exaggerated view and might represent refraction beyond central 70 degrees. Adapted from Verkicharla et al., 2012, with permission.<sup>166</sup>**

assessed the posterior pole shape in highly myopic eyes by measuring the curvature of Bruch's membrane using optical coherence tomography, and reported significant protruding and undulating changes in the shape of the posterior eye with time in highly myopic eyes, indicating a potential role of the posterior eye shape in progression of high myopia.

Although various anti-myopia strategies have been designed to counteract the peripheral hyperopic defocus that are also effective in controlling myopia progression,<sup>99,181</sup> there

is now growing evidence based on the longitudinal studies conducted in Caucasian and Chinese populations indicating that peripheral hyperopic defocus may not predict the development or the progression of myopia.<sup>182-189</sup> These recent findings suggest there is a complex interaction between peripheral hyperopic defocus and myopia, and there may be a combination of optical factors that influence ocular growth associated with peripheral blur. Because retinal shape can alter the magnitude of defocus in the peripheral retina, it may play an

important role in mediating the development and progression of myopia in humans. Future studies are warranted to fully elucidate the influence of retinal shape in the pathogenesis of myopia.

### Higher order monochromatic aberrations

While the optical characteristics of the eye are largely dominated by lower order aberrations (vertical/oblique astigmatism and defocus), presence of higher order monochromatic aberrations (HOAs) can degrade retinal image quality, and therefore, may play a role in the development of refractive errors. HOAs may also interact with lower order aberrations (or spherical refractive error) and/or change the eye's depth of focus to alter the optics, and hence refractive development of the eye.<sup>190,191</sup>

Animal studies have provided important insights into the changes in HOAs during emmetropisation and how these aberrations might be involved in the development of

myopia and other refractive disorders. Studies in chicks,<sup>192</sup> marmosets,<sup>193</sup> and monkeys,<sup>194</sup> as well as humans,<sup>195</sup> have reported a systemic reduction in HOAs with age due to changes in the curvature and thickness of the cornea and the crystalline lens, as well as refractive index of the lens. Despite some interspecies differences, most animal studies have noted a relatively small influence of HOAs in age-dependent improvements in spatial vision and contrast sensitivity. It is hypothesised that a large part of the reduction in HOAs during the early postnatal period occurs passively, without any major input from the visual environment.<sup>196</sup> Animal studies have also examined the relationship between experimentally induced ametropias and HOAs. In this respect, form-deprivation and hyperopic defocus induced experimental myopias have been found to be associated with greater levels of HOAs in different animal models, albeit with minor interspecies differences.<sup>192,197,198</sup> For instance, experimental ametropias are associated with more positive spherical aberration in monkeys, but greater amounts of negative spherical

aberration in chicks. Interestingly, human myopic eyes also exhibit higher levels of positive spherical aberration.<sup>199</sup> The optical changes associated with FDM or lens-induced ametropias are believed to be a combination of changes in the curvatures and refractive index of the eye's optical components, as well as dynamic changes in the relative position of the crystalline lens with respect to the cornea.<sup>198</sup> Finally, a study by Ramamirtham et al.<sup>198</sup> found increased HOAs in both myopic and hyperopic monkey eyes that were strongly correlated with the degree of lower order aberrations and axial ametropias, suggesting that the changes in HOAs may occur as a consequence, not a cause, of refractive errors.

Previous human studies have noted that spherical aberration, coma, and trefoil are the largest contributors of HOAs in normal healthy eyes; however, there are significant inter-subject variations in the type and magnitude of HOAs in the population.<sup>190,200,201</sup> Consistent with the observation in animals, the influence of HOAs in the development of myopia is unclear, with some studies

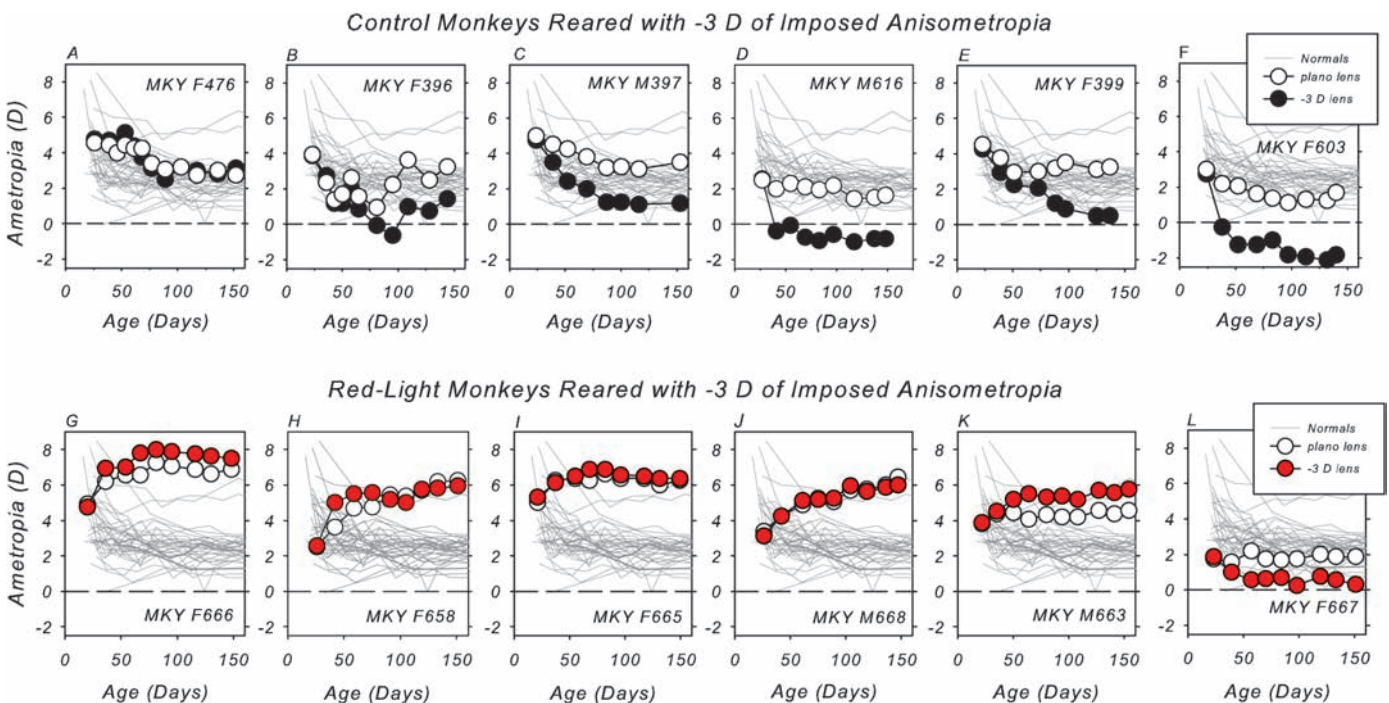


**Figure 5. Spherical-equivalent, spectacle-plane refractive corrections plotted as a function of age for the treated (filled symbols) and fellow eyes (open symbols) of representative lens-reared controls (top row) and red-light-reared monkeys (bottom row). Animals were reared with -3.0 D lenses in front of their treated eyes and plano lenses in front of their fellow eyes. The thin grey lines in each plot represent data for the right eyes of the 39 normal control monkeys. Overall, red light-rearing prevented lens-induced defocus in treated eyes, and resulted in hyperopia in both treated and fellow control eyes. Adapted from Hung et al., 2018, with permission.<sup>223</sup>**



suggesting an increase in HOAs are associated with myopia (particularly spherical aberration and coma),<sup>202,203</sup> while others reporting no significant change in ocular aberrations with myopia.<sup>204–206</sup> It is important to note that accommodation also induces changes in HOA, as well as lower order aberrations.<sup>207,208</sup> Overall, evidence from animal and human studies suggest a possible role of HOAs in visual regulation of ocular growth; however, longitudinal clinical studies during childhood are needed to confirm their role in human emmetropisation.

### Spectral and temporal characteristics of light

The spectral and temporal characteristics of light represent another optical mechanism implicated in eye growth, and includes such factors as longitudinal chromatic aberration (LCA), wavelength, intensity, and exposure time. Experiments in a laboratory setting in animal models allow these characteristics of the visual environment to be manipulated to better understand their influence on eye growth.

Evidence suggests that the eye utilises LCA to guide axial eye growth and the refractive state.<sup>209,210</sup> LCA causes long wavelengths to be focused in a more hyperopic plane than shorter wavelengths. Therefore, the eye's total refraction varies inversely with wavelength, rendering the eye relatively more hyperopic (less myopic) for long wavelength light. Broadband light results in colour fringes on the retinal image that provide a signal as to whether defocus is hyperopic or myopic.<sup>211</sup> Studies have shown that the human eye can utilise LCA as a directional cue for accommodation,<sup>101,212</sup> however, the role of LCA in emmetropisation is not fully understood. The ability of the retina to detect LCA depends on the distribution of short, medium, and long wavelength sensitive cones.<sup>213</sup> In humans, the short wavelength sensitive cones are fewest in number.<sup>214</sup> Early reports in humans suggest that there is a reduction in sensitivity of short wavelength cones in myopia when tested electrophysiologically.<sup>215,216</sup> Another mechanism by which the retina might discriminate between long and short wavelengths may be through spectral tuning of the intrinsically photosensitive retinal ganglion cells, which are most sensitive to short wavelength light.<sup>217</sup>

Animal studies have shown conflicting results across species with respect to the

influence of spectral composition of light on eye growth. In fish, chicks, and guinea pigs, eyes were less myopic when raised under short wavelength (violet and blue) light compared to those raised under longer wavelength (green or red) light.<sup>209,212,218–221</sup> In these studies, short-term eye growth matched the direction and magnitude predicted by LCA.<sup>212,222</sup> However, longer-term eye growth under these same conditions surpassed what would be predicted by LCA, indicating a more complex interaction between chromatic cues and other signals for eye growth. Jiang et al. hypothesised that blue light might preferentially stimulate the ON pathway to inhibit myopic eye growth.<sup>218</sup>

Unlike results in fish, chicks, and guinea pigs, long wavelength light rearing in non-human primates results in a decrease in eye growth.<sup>223</sup> Recent studies in rhesus monkeys have shown that animals raised with red filters over one or both eyes,<sup>224</sup> or in ambient light dominated by long wavelengths (produced by red light-emitting diodes),<sup>223</sup> demonstrate choroidal thickening and slowed eye growth, resulting in less myopic refractive errors (Figure 5). Animals raised under long wavelength light with no lens treatment demonstrate choroidal thickening in both eyes, as do animals with a +3 D or a –3 D lens over one eye. Animals, on average, maintained slightly hyperopic refractive errors. Similar effects of red light

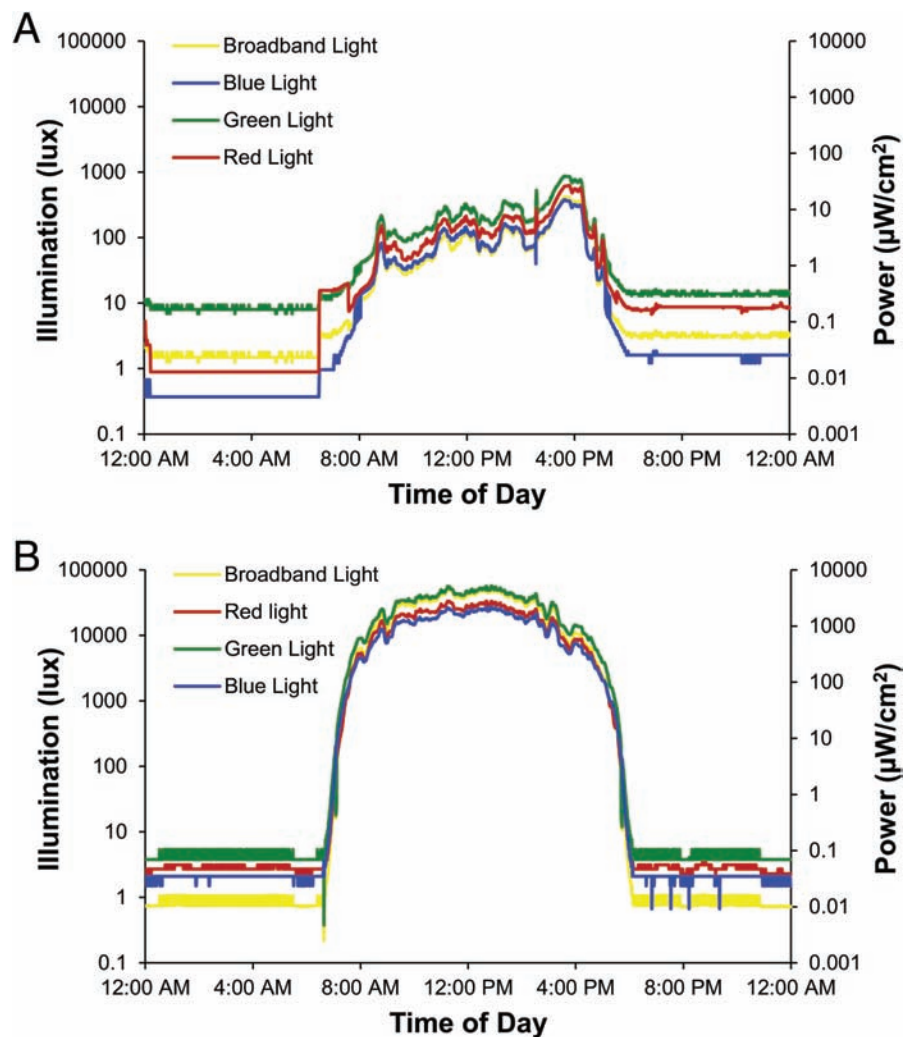


**Figure 6.** Broadband illumination in lux (yellow trace) and power in  $\mu\text{W}/\text{cm}^2$  of the blue (400–500 nm), green (500–600 nm), and red (600–700 nm) components across 24 hours of A: typical indoor lighting and B: outdoors in full sun in Houston, TX, USA. Ostrin, unpublished data.

have been shown in tree shrews.<sup>225,226</sup> Additionally, tree shrews reared in short wavelength flickering light demonstrated myopia.<sup>226</sup> The chromatic cues dominated control of eye growth such that defocus cues were largely ignored. Specifically, even animals that wore negative lenses, which would normally induce myopia, remained relatively hyperopic when reared in long wavelength light. The mechanisms of the protective effects of narrowband wavelength light on myopia remain elusive.

Numerous studies have observed that increased ambient illumination is protective for FDM in animal models,<sup>98,227,228</sup> and time outdoors is protective for myopia in children.<sup>229</sup> The mechanisms of the protective effects of light are unknown, and might include both neurochemical factors, such as alterations in melanopsin and dopamine cascades,<sup>97,230</sup> and optical factors, such as miosis-induced increased depth of field, a flatter dioptic scene, and spectral distribution of sunlight and chromatic cues. Ambient illumination outdoors ranges from 1,000 lux on a cloudy day in the shade to greater than 150,000 lux in direct sun,<sup>231</sup> and the spectral composition is comprised of a broad range of wavelengths, including ultraviolet, visible, and infrared wavelengths. Because the intensity of the entire visible spectrum exponentially increases outdoors compared to indoors (Figure 6), it is difficult to determine if the protective effects of outdoor light are attributed to a specific narrowband region of the spectrum. Another possible mechanism of the protective effect in children of time outdoors is a corresponding decrease in time spent indoors performing near tasks and being exposed to accommodation-related defocus.

Findings in animal models demonstrating that spectral and temporal properties of light affect emmetropisation have led to speculation that modifying the characteristics of indoor ambient illumination could be used as a method to prevent slow progression of myopia in children. However, conflicting results between animal models and a rudimentary understanding of mechanisms involved suggest that further studies are warranted before manipulation of indoor illumination is utilised as a treatment strategy in children.

## Conclusion

A large volume of work on animal models suggests that the visual environment exerts

a powerful influence on refractive state by controlling the axial length and overall growth of the eye during the postnatal developmental period. These studies have been instrumental to our current understanding of emmetropisation and development of refractive errors in humans. Research on birds, mammals, rodents, and non-human primates suggests that the eye uses several optical cues to modulate its growth during emmetropisation. Visual signals from active accommodation, HOAs, peripheral defocus, and chromatic aberrations could modulate the sign and magnitude of defocus on the retina, and hence refractive development of the eye. In addition, these optical mechanisms may alter the temporal and spatial integration of defocus signals across the retina. Furthermore, features of ambient lighting, such as the duration and intensity of lighting, may also affect visually guided ocular growth. Several of these findings have been successfully translated into effective optical treatment strategies for refractive error correction in humans, and will continue to aid in the development of novel and effective treatment options in the future.

## ACKNOWLEDGEMENT

Special thanks to Daniel Moderiano (Flinders University) for help generating figures.

## REFERENCES

1. Wallman J, Winawer J. Homeostasis of eye growth and the question of myopia. *Neuron* 2004; 43: 447–468.
2. Smith EL 3rd. Spectacle lenses and emmetropization: the role of optical defocus in regulating ocular development. *Optom Vis Sci* 1998; 75: 388–398.
3. van Alphen G. On emmetropia and ametropia. *Opt Acta (Lond)* 1961; 142: 1–92.
4. Howlett MH, McFadden SA. Form-deprivation myopia in the guinea pig (*Cavia porcellus*). *Vision Res* 2006; 46: 267–283.
5. Siegwart JT Jr, Norton TT. The susceptible period for deprivation-induced myopia in tree shrew. *Vision Res* 1998; 38: 3505–3515.
6. Wallman J, Turkel J, Trachtman J. Extreme myopia produced by modest change in early visual experience. *Science* 1978; 201: 1249–1251.
7. Wallman J, Wildsoet C, Xu A et al. Moving the retina: choroidal modulation of refractive state. *Vision Res* 1995; 35: 37–50.
8. Smith EL 3rd, Hung LF, Kee CS et al. Effects of brief periods of unrestricted vision on the development of form-deprivation myopia in monkeys. *Invest Ophthalmol Vis Sci* 2002; 43: 291–299.
9. Schaeffel F, Glasser A, Howland HC. Accommodation, refractive error and eye growth in chickens. *Vision Res* 1988; 28: 639–657.
10. Wildsoet C, Wallman J. Choroidal and scleral mechanisms of compensation for spectacle lenses in chicks. *Vision Res* 1995; 35: 1175–1194.
11. Irving EL, Callender MG, Sivak JG. Inducing myopia, hyperopia, and astigmatism in chicks. *Optom Vis Sci* 1991; 68: 364–368.
12. Schmid KL, Wildsoet CF. Effects on the compensatory responses to positive and negative lenses of intermittent lens wear and ciliary nerve section in chicks. *Vision Res* 1996; 36: 1023–1036.
13. Smith EL 3rd, Hung LF. The role of optical defocus in regulating refractive development in infant monkeys. *Vision Res* 1999; 39: 1415–1435.
14. Hung LF, Crawford ML, Smith EL. Spectacle lenses alter eye growth and the refractive status of young monkeys. *Nat Med* 1995; 1: 761–765.
15. Howlett MH, McFadden SA. Spectacle lens compensation in the pigmented guinea pig. *Vision Res* 2009; 49: 219–227.
16. Troilo D, Smith EL 3rd, Nickla DL et al. IMI - report on experimental models of emmetropization and myopia. *Invest Ophthalmol Vis Sci* 2019; 60: M31–M88.
17. Schaeffel F, Feldkaemper M. Animal models in myopia research. *Clin Exp Optom* 2015; 98: 507–517.
18. Smith EL 3rd, Hung LF, Arumugam B. Visual regulation of refractive development: insights from animal studies. *Eye (Lond)* 2014; 28: 180–188.
19. Bradley DV, Fernandes A, Lynn M et al. Emmetropization in the rhesus monkey (*Macaca mulatta*): birth to young adulthood. *Invest Ophthalmol Vis Sci* 1999; 40: 214–229.
20. Graham B, Judge SJ. Normal development of refractive state and ocular component dimensions in the marmoset (*Callithrix jacchus*). *Vision Res* 1999; 39: 177–187.
21. Norton TT. Animal models of myopia: learning how vision controls the size of the eye. *ILAR J* 1999; 40: 59–77.
22. Zhou X, Qu J, Xie R et al. Normal development of refractive state and ocular dimensions in guinea pigs. *Vision Res* 2006; 46: 2815–2823.
23. Norton TT, McBrien NA. Normal development of refractive state and ocular component dimensions in the tree shrew (*Tupaia belangeri*). *Vision Res* 1992; 32: 833–842.
24. Li T, Troilo D, Glasser A et al. Constant light produces severe corneal flattening and hyperopia in chickens. *Vision Res* 1995; 35: 1203–1209.
25. Schmid KL, Hills T, Abbott M et al. Relationship between intraocular pressure and eye growth in chick. *Ophthalmic Physiol Opt* 2003; 23: 25–33.
26. Pardue MT, Stone RA, Iuvone PM. Investigating mechanisms of myopia in mice. *Exp Eye Res* 2013; 114: 96–105.
27. Troilo D, Judge SJ. Ocular development and visual deprivation myopia in the common marmoset (*Callithrix jacchus*). *Vision Res* 1993; 33: 1311–1324.
28. Ingram RM, Barr A. Changes in refraction between the ages of 1 and 3 1/2 years. *Br J Ophthalmol* 1979; 63: 339–342.
29. Wood IC, Hodi S, Morgan L. Longitudinal change of refractive error in infants during the first year of life. *Eye (Lond)* 1995; 9: 551–557.
30. Cook RC, Glasscock RE. Refractive and ocular findings in the newborn. *Am J Ophthalmol* 1951; 34: 1407–1413.
31. Gordon RA, Donzis PB. Refractive development of the human eye. *Arch Ophthalmol* 1985; 103: 785–789.
32. Mutti DO, Mitchell GL, Jones LA et al. Axial growth and changes in lenticular and corneal power during emmetropization in infants. *Invest Ophthalmol Vis Sci* 2005; 46: 3074–3080.
33. Pennie FC, Wood IC, Olsen C et al. A longitudinal study of the biometric and refractive changes in full-term infants during the first year of life. *Vision Res* 2001; 41: 2799–2810.
34. Sorsby A, Leary GA, Richards MJ. Correlation ametropia and component ametropia. *Vision Res* 1962; 2: 309–313.
35. Wiesel TN, Raviola E. Myopia and eye enlargement after neonatal lid fusion in monkeys. *Nature* 1977; 266: 66–68.
36. Sherman SM, Norton TT, Casagrande VA. Myopia in the lid-sutured tree shrew (*Tupaia glis*). *Brain Res* 1977; 124: 154–157.
37. Wilson J, Sherman S. Differential effects of early monocular deprivation on binocular and monocular

- segments of cat striate cortex. *J Neurophysiol* 1977; 40: 891-903.
38. Wiesel TN, Raviola E. Increase in axial length of the macaque monkey eye after corneal opacification. *Invest Ophthalmol Vis Sci* 1979; 18: 1232-1236.
  39. Lu F, Zhou X, Zhao H et al. Axial myopia induced by a monocularly-deprived facemask in guinea pigs: a non-invasive and effective model. *Exp Eye Res* 2006; 82: 628-636.
  40. Hodos W, Kuenzel WJ. Retinal-image degradation produces ocular enlargement in chicks. *Invest Ophthalmol Vis Sci* 1984; 25: 652-659.
  41. Wallman J, Ledoux C, Friedman MB. Simple devices for restricting the visual fields of birds. *Behav Res Methods Instrum* 1978; 10: 401-403.
  42. Ashby R, Ohlendorf A, Schaeffel F. The effect of ambient illuminance on the development of deprivation myopia in chicks. *Invest Ophthalmol Vis Sci* 2009; 50: 5348-5354.
  43. Beresford JA, Crewther SG, Crewther DP. Anatomical correlates of experimentally induced myopia. *Aust N Z J Ophthalmol* 1998; 26: 584-587.
  44. Siegwart JT Jr, Norton TT. Goggles for controlling the visual environment of small animals. *Lab Anim Sci* 1994; 44: 292-294.
  45. Faulkner AE, Kim MK, Iuvone PM et al. Head-mounted goggles for murine form deprivation myopia. *J Neurosci Methods* 2007; 161: 96-100.
  46. Chakraborty R, Park H, Aung MH et al. Comparison of refractive development and retinal dopamine in OFF pathway mutant and C57BL/6J wild-type mice. *Mol Vis* 2014; 20: 1318-1327.
  47. Chakraborty R, Yang V, Park HN et al. Lack of cone mediated retinal function increases susceptibility to form-deprivation myopia in mice. *Exp Eye Res* 2019; 180: 226-230.
  48. Schaeffel F, Howland HC. Properties of the feedback loops controlling eye growth and refractive state in the chicken. *Vision Res* 1991; 31: 717-734.
  49. Tkatchenko TV, Shen Y, Tkatchenko AV. Mouse experimental myopia has features of primate myopia. *Invest Ophthalmol Vis Sci* 2010; 51: 1297-1303.
  50. Troilo D, Nickla DL, Wildsoet CF. Form deprivation myopia in mature common marmosets (*Callithrix jacchus*). *Invest Ophthalmol Vis Sci* 2000; 41: 2043-2049.
  51. Gottlieb MD, Fugate-Wentzek LA, Wallman J. Different visual deprivations produce different ametropias and different eye shapes. *Invest Ophthalmol Vis Sci* 1987; 28: 1225-1235.
  52. McBrien NA, Lawlor P, Gentle A. Scleral remodeling during the development of and recovery from axial myopia in the tree shrew. *Invest Ophthalmol Vis Sci* 2000; 41: 3713-3719.
  53. Gottlieb MD, Joshi HB, Nickla DL. Scleral changes in chicks with form-deprivation myopia. *Curr Eye Res* 1990; 9: 1157-1165.
  54. Smith EL 3rd, Hung LF. Form-deprivation myopia in monkeys is a graded phenomenon. *Vision Res* 2000; 40: 371-381.
  55. Wallman J, Adams JI. Developmental aspects of experimental myopia in chicks: susceptibility, recovery and relation to emmetropization. *Vision Res* 1987; 27: 1139-1163.
  56. Chakraborty R, Park HN, Hanif AM et al. ON pathway mutations increase susceptibility to form-deprivation myopia. *Exp Eye Res* 2015; 137: 79-83.
  57. Shen W, Vijayan M, Sivak JG. Inducing form-deprivation myopia in fish. *Invest Ophthalmol Vis Sci* 2005; 46: 1797-1803.
  58. Smith EL 3rd, Hung LF, Harwerth RS. Effects of optically induced blur on the refractive status of young monkeys. *Vision Res* 1994; 34: 293-301.
  59. Bartmann M, Schaeffel F. A simple mechanism for emmetropization without cues from accommodation or colour. *Vision Res* 1994; 34: 873-876.
  60. Smith EL 3rd, Bradley DV, Fernandes A et al. Form deprivation myopia in adolescent monkeys. *Optom Vis Sci* 1999; 76: 428-432.
  61. Papastergiou GI, Schmid GF, Laties AM et al. Induction of axial eye elongation and myopic refractive shift in one-year-old chickens. *Vision Res* 1998; 38: 1883-1888.
  62. Troilo D, Wallman J. The regulation of eye growth and refractive state: an experimental study of emmetropization. *Vision Res* 1991; 31: 1237-1250.
  63. Guyton DL, Greene PR, Scholz RT. Dark-rearing interference with emmetropization in the rhesus monkey. *Invest Ophthalmol Vis Sci* 1989; 30: 761-764.
  64. Qiao-Grider Y, Hung LF, Kee CS et al. Recovery from form-deprivation myopia in rhesus monkeys. *Invest Ophthalmol Vis Sci* 2004; 45: 3361-3372.
  65. O'Leary DJ, Millodot M. Eyelid closure causes myopia in humans. *Experientia* 1979; 35: 1478-1479.
  66. von Noorden GK, Lewis RA. Ocular axial length in unilateral congenital cataracts and blepharoptosis. *Invest Ophthalmol Vis Sci* 1987; 28: 750-752.
  67. Gee SS, Tabbara KF. Increase in ocular axial length in patients with corneal opacification. *Ophthalmology* 1988; 95: 1276-1278.
  68. Miller-Meeks MJ, Bennett SR, Keech RV et al. Myopia induced by vitreous hemorrhage. *Am J Ophthalmol* 1990; 109: 199-203.
  69. Morgan IG, Ashby RS, Nickla DL. Form deprivation and lens-induced myopia: are they different? *Ophthalmic Physiol Opt* 2013; 33: 355-361.
  70. Irving EL, Sivak JG, Callender MG. Refractive plasticity of the developing chick eye. *Ophthalmic Physiol Opt* 1992; 12: 448-456.
  71. Nickla DL, Wildsoet C, Wallman J. Visual influences on diurnal rhythms in ocular length and choroidal thickness in chick eyes. *Exp Eye Res* 1998; 66: 163-181.
  72. Norton TT, Siegwart JT Jr, Amedo AO. Effectiveness of hyperopic defocus, minimal defocus, or myopic defocus in competition with a myopiagenic stimulus in tree shrew eyes. *Invest Ophthalmol Vis Sci* 2006; 47: 4687-4699.
  73. Graham B, Judge SJ. The effects of spectacle wear in infancy on eye growth and refractive error in the marmoset (*Callithrix jacchus*). *Vision Res* 1999; 39: 189-206.
  74. Barathi VA, Boopathi VG, Yap EP et al. Two models of experimental myopia in the mouse. *Vision Res* 2008; 48: 904-916.
  75. Troilo D, Totonelly K, Harb EN. Imposed anisometropia, accommodation, and regulation of refractive state. *Optom Vis Sci* 2009; 86: 31-39.
  76. Irving EL, Callender MG, Sivak JG. Inducing ametropias in hatchling chicks by defocus-aperture effects and cylindrical lenses. *Vision Res* 1995; 35: 1165-1174.
  77. Moderiano D, Do M, Hobbs S et al. Influence of the time of day on axial length and choroidal thickness changes to hyperopic and myopic defocus in human eyes. *Exp Eye Res* 2019; 182: 125-136.
  78. Chakraborty R, Read SA, Collins MJ. Monocular myopic defocus and daily changes in axial length and choroidal thickness of human eyes. *Exp Eye Res* 2012; 103: 47-54.
  79. Chakraborty R, Read SA, Collins MJ. Hyperopic defocus and diurnal changes in human choroid and axial length. *Optom Vis Sci* 2013; 90: 1187-1198.
  80. Wang D, Chun RK, Liu M et al. Optical defocus rapidly changes choroidal thickness in schoolchildren. *PLoS One* 2016; 11: e0161535.
  81. Zhu X. Temporal integration of visual signals in lens compensation (a review). *Exp Eye Res* 2013; 114: 69-76.
  82. Zhu X, Winawer JA, Wallman J. Potency of myopic defocus in spectacle lens compensation. *Invest Ophthalmol Vis Sci* 2003; 44: 2818-2827.
  83. Winawer J, Zhu X, Choi J et al. Ocular compensation for alternating myopic and hyperopic defocus. *Vision Res* 2005; 45: 1667-1677.
  84. Zhu X, Park TW, Winawer J et al. In a matter of minutes, the eye can know which way to grow. *Invest Ophthalmol Vis Sci* 2005; 46: 2238-2241.
  85. Zhu X, Wallman J. Temporal properties of compensation for positive and negative spectacle lenses in chicks. *Invest Ophthalmol Vis Sci* 2009; 50: 37-46.
  86. Nickla DL, Sharda V, Troilo D. Temporal integration characteristics of the axial and choroidal responses to myopic defocus induced by prior form deprivation versus positive spectacle lens wear in chickens. *Optom Vis Sci* 2005; 82: 318-327.
  87. Winawer J, Wallman J. Temporal constraints on lens compensation in chicks. *Vision Res* 2002; 42: 2651-2668.
  88. Nickla DL, Thai P, Zanzerkia Trahan R et al. Myopic defocus in the evening is more effective at inhibiting eye growth than defocus in the morning: effects on rhythms in axial length and choroid thickness in chicks. *Exp Eye Res* 2017; 154: 104-115.
  89. McFadden SA, Tse DY, Bowrey HE et al. Integration of defocus by dual power Fresnel lenses inhibits myopia in the mammalian eye. *Invest Ophthalmol Vis Sci* 2014; 55: 908-917.
  90. Tse DY, Lam CS, Guggenheim JA et al. Simultaneous defocus integration during refractive development. *Invest Ophthalmol Vis Sci* 2007; 48: 5352-5359.
  91. Benavente-Perez A, Nour A, Troilo D. The effect of simultaneous negative and positive defocus on eye growth and development of refractive state in marmosets. *Invest Ophthalmol Vis Sci* 2012; 53: 6479-6487.
  92. Arumugam B, Hung LF, To CH et al. The effects of simultaneous dual focus lenses on refractive development in infant monkeys. *Invest Ophthalmol Vis Sci* 2014; 55: 7423-7432.
  93. Schmid GF, Papastergiou GI, Lin T et al. Autonomic denervations influence ocular dimensions and intraocular pressure in chicks. *Exp Eye Res* 1999; 68: 573-581.
  94. Fujikado T, Kawasaki Y, Suzuki A et al. Retinal function with lens-induced myopia compared with form-deprivation myopia in chicks. *Graefes Arch Clin Exp Ophthalmol* 1997; 235: 320-324.
  95. Choh V, Lew MY, Nadel MW et al. Effects of interchanging hyperopic defocus and form deprivation stimuli in normal and optic nerve-sectioned chicks. *Vision Res* 2006; 46: 1070-1079.
  96. Bartmann M, Schaeffel F, Hagel G et al. Constant light affects retinal dopamine levels and blocks deprivation myopia but not lens-induced refractive errors in chickens. *Vis Neurosci* 1994; 11: 199-208.
  97. Ashby RS, Schaeffel F. The effect of bright light on lens compensation in chicks. *Invest Ophthalmol Vis Sci* 2010; 51: 5247-5253.
  98. Smith EL 3rd, Hung LF, Huang J. Protective effects of high ambient lighting on the development of form-deprivation myopia in rhesus monkeys. *Invest Ophthalmol Vis Sci* 2012; 53: 421-428.
  99. Walline JJ, Lindsley K, Vedula SS et al. Interventions to slow progression of myopia in children. *Cochrane Database Syst Rev* 2011; 12: CD004916.
  100. Cho P, Cheung SW. Retardation of myopia in orthokeratology (ROMIO) study: a 2-year randomized clinical trial. *Invest Ophthalmol Vis Sci* 2012; 53: 7077-7085.
  101. Kruger PB, Mathews S, Aggarwala KR et al. Chromatic aberration and ocular focus: Fincham revisited. *Vision Res* 1993; 33: 1397-1411.
  102. Del Águila-Carrasco AJ, Marín-Franch I, Bernal-Molina P et al. Accommodation responds to optical vergence and not defocus blur alone. *Invest Ophthalmol Vis Sci* 2017; 58: 1758-1763.
  103. Ostrin LA, Liu Y, Choh V et al. The role of the iris in chick accommodation. *Invest Ophthalmol Vis Sci* 2011; 52: 4710-4716.
  104. Clarke RJ, Coimbra CJ, Alessio ML. Oculomotor areas involved in the parasympathetic control of accommodation and pupil size in the marmoset (*Callithrix jacchus*). *Braz J Med Biol Res* 1985; 18: 373-379.
  105. Ostrin LA, Glasser A. Autonomic drugs and the accommodative system in rhesus monkeys. *Exp Eye Res* 2010; 90: 104-112.




106. Croft MA, Kaufman PL, Crawford KS et al. Accommodation dynamics in aging rhesus monkeys. *Am J Physiol* 1998; 275: R1885-R1897.
107. Glasser A, Troilo D, Howland HC. The mechanism of corneal accommodation in chicks. *Vision Res* 1994; 34: 1549-1566.
108. Glasser A, Murphy CJ, Troilo D et al. The mechanism of lenticular accommodation in chicks. *Vision Res* 1995; 35: 1525-1540.
109. Troilo D, Wallman J. Changes in corneal curvature during accommodation in chicks. *Vision Res* 1987; 27: 241-247.
110. Schaeffel F, Howland HC, Farkas L. Natural accommodation in the growing chicken. *Vision Res* 1986; 26: 1977-1993.
111. Day M, Gray LS, Seidel D et al. The relationship between object spatial profile and accommodation microfluctuations in emmetropes and myopes. *J Vis* 2009; 9: 1-13.
112. Mutti DO, Mitchell GL, Hayes JR et al. Accommodative lag before and after the onset of myopia. *Invest Ophthalmol Vis Sci* 2006; 47: 837-846.
113. Gwiazda J, Bauer J, Thorn F et al. Shifts in tonic accommodation after near work are related to refractive errors in children. *Ophthalmic Physiol Opt* 1995; 15: 93-97.
114. McBrien NA, Millodot M. The relationship between tonic accommodation and refractive error. *Invest Ophthalmol Vis Sci* 1987; 28: 997-1004.
115. Gwiazda J, Thorn F, Bauer J et al. Myopic children show insufficient accommodative response to blur. *Invest Ophthalmol Vis Sci* 1993; 34: 690-694.
116. Young FA. The effect of atropine on the development of myopia in monkeys. *Am J Optom Arch Am Acad Optom* 1965; 42: 439-449.
117. Crawford K, Terasawa E, Kaufman PL. Reproducible stimulation of ciliary muscle contraction in the cynomolgus monkey via a permanent indwelling midbrain electrode. *Brain Res* 1989; 503: 265-272.
118. Schaeffel F, Troilo D, Wallman J et al. Developing eyes that lack accommodation grow to compensate for imposed defocus. *Vis Neurosci* 1990; 4: 177-183.
119. Raviola E, Wiesel TN. Neural control of eye growth and experimental myopia in primates. *Ciba Found Symp* 1990; 155: 22-38.
120. McBrien NA, Moghaddam HO, Reeder AP. Atropine reduces experimental myopia and eye enlargement via a nonaccommodative mechanism. *Invest Ophthalmol Vis Sci* 1993; 34: 205-215.
121. Diether S, Schaeffel F. Local changes in eye growth induced by imposed local refractive error despite active accommodation. *Vision Res* 1997; 37: 659-668.
122. Charman WN. Near vision, lags of accommodation and myopia. *Ophthalmic Physiol Opt* 1999; 19: 126-133.
123. Shaikh AW, Siegwart JT Jr, Norton TT. Effect of interrupted lens wear on compensation for a minus lens in tree shrews. *Optom Vis Sci* 1999; 76: 308-315.
124. Kee CS, Hung LF, Qiao-Grider Y et al. Temporal constraints on experimental emmetropization in infant monkeys. *Invest Ophthalmol Vis Sci* 2007; 48: 957-962.
125. Troilo D, Quinn N, Baker K. Accommodation and induced myopia in marmosets. *Vision Res* 2007; 47: 1228-1244.
126. Aleman A, Schaeffel F. Lag of accommodation does not predict changes in eye growth in chickens. *Vision Res* 2018; 149: 77-85.
127. Diether S, Wildsoet CF. Stimulus requirements for the decoding of myopic and hyperopic defocus under single and competing defocus conditions in the chicken. *Invest Ophthalmol Vis Sci* 2005; 46: 2242-2252.
128. Angle J, Wissmann DA. The epidemiology of myopia. *Am J Epidemiol* 1980; 111: 220-228.
129. Curtin BJ. *The Myopias: Basic Science and Clinical Management*, 1st ed. Philadelphia, PA: Harper & Row, 1985.
130. Gwiazda J, Thorn F, Held R. Accommodation, accommodative convergence, and response A/C/A ratios before and at the onset of myopia in children. *Optom Vis Sci* 2005; 82: 273-278.
131. Drobe B, de Saint-André R. The pre-myopic syndrome. *Ophthalmic Physiol Opt* 1995; 15: 375-378.
132. Goss DA. Clinical accommodation and heterophoria findings preceding juvenile onset of myopia. *Optom Vis Sci* 1991; 68: 110-116.
133. Shih YF, Hsiao CK, Chen CJ et al. An intervention trial on efficacy of atropine and multi-focal glasses in controlling myopic progression. *Acta Ophthalmol Scand* 2001; 79: 233-236.
134. Edwards MH, Li RW, Lam CS et al. The Hong Kong progressive lens myopia control study: study design and main findings. *Invest Ophthalmol Vis Sci* 2002; 43: 2852-2858.
135. Leung JT, Brown B. Progression of myopia in Hong Kong Chinese schoolchildren is slowed by wearing progressive lenses. *Optom Vis Sci* 1999; 76: 346-354.
136. Gwiazda J, Hyman L, Hussein M et al. A randomized clinical trial of progressive addition lenses versus single vision lenses on the progression of myopia in children. *Invest Ophthalmol Vis Sci* 2003; 44: 1492-1500.
137. Wallman J, Gottlieb MD, Rajaram V et al. Local retinal regions control local eye growth and myopia. *Science* 1987; 237: 73-77.
138. Smith EL 3rd, Ramamirtham R, Qiao-Grider Y et al. Effects of foveal ablation on emmetropization and form-deprivation myopia. *Invest Ophthalmol Vis Sci* 2007; 48: 3914-3922.
139. Smith EL 3rd, Huang J, Hung LF et al. Hemiretinal form deprivation: evidence for local control of eye growth and refractive development in infant monkeys. *Invest Ophthalmol Vis Sci* 2009; 50: 5057-5069.
140. Smith EL 3rd, Kee CS, Ramamirtham R et al. Peripheral vision can influence eye growth and refractive development in infant monkeys. *Invest Ophthalmol Vis Sci* 2005; 46: 3965-3972.
141. Raviola E, Wiesel TN. An animal model of myopia. *N Engl J Med* 1985; 312: 1609-1615.
142. Norton TT, Essinger JA, McBrien NA. Lid-suture myopia in tree shrews with retinal ganglion cell blockade. *Vis Neurosci* 1994; 11: 143-153.
143. Wildsoet CF. Neural pathways subserving negative lens-induced emmetropization in chicks-insights from selective lesions of the optic nerve and ciliary nerve. *Curr Eye Res* 2003; 27: 371-385.
144. Troilo D, Gottlieb MD, Wallman J. Visual deprivation causes myopia in chicks with optic nerve section. *Curr Eye Res* 1987; 6: 993-999.
145. McFadden SA. Partial occlusion produces local form deprivation myopia in the guinea pig eye. *Invest Ophthalmol Vis Sci* 2002; 43: 189.
146. Morgan IG, Ambadeniya MP. Imposed peripheral myopic defocus can prevent the development of lens-induced myopia. *Invest Ophthalmol Vis Sci* 2006; 47: 3328.
147. Liu Y, Wildsoet C. The effect of two-zone concentric bifocal spectacle lenses on refractive error development and eye growth in young chicks. *Invest Ophthalmol Vis Sci* 2011; 52: 1078-1086.
148. Benavente-Pérez A, Nour A, Troilo D. Axial eye growth and refractive error development can be modified by exposing the peripheral retina to relative myopic or hyperopic defocus. *Invest Ophthalmol Vis Sci* 2014; 55: 6765-6773.
149. Smith EL 3rd, Hung LF, Huang J et al. Effects of optical defocus on refractive development in monkeys: evidence for local, regionally selective mechanisms. *Invest Ophthalmol Vis Sci* 2010; 51: 3864-3873.
150. Liu Y, Wildsoet C. The effective add inherent in 2-zone negative lenses inhibits eye growth in myopic young chicks. *Invest Ophthalmol Vis Sci* 2012; 53: 5085-5093.
151. Smith EL 3rd, Hung LF, Huang J. Relative peripheral hyperopic defocus alters central refractive development in infant monkeys. *Vision Res* 2009; 49: 2386-2392.
152. Schippert R, Schaeffel F. Peripheral defocus does not necessarily affect central refractive development. *Vision Res* 2006; 46: 3935-3940.
153. Wildsoet CF, Schmid KL. Optical correction of form deprivation myopia inhibits refractive recovery in chick eyes with intact or sectioned optic nerves. *Vision Res* 2000; 40: 3273-3282.
154. Ferreer GR, Rand G. Interpretation of refractive conditions in the peripheral field of vision: a further study. *Arch Ophthalmol* 1933; 9: 925-938.
155. Millodot M. Effect of ametropia on peripheral refraction. *Am J Optom Physiol Opt* 1981; 58: 691-695.
156. Mutti DO, Sholtz RI, Friedman NE et al. Peripheral refraction and ocular shape in children. *Invest Ophthalmol Vis Sci* 2000; 41: 1022-1030.
157. Seidemann A, Schaeffel F, Guirao A et al. Peripheral refractive errors in myopic, emmetropic, and hyperopic young subjects. *J Opt Soc Am A Opt Image Sci Vis* 2002; 19: 2363-2373.
158. Huang J, Hung LF, Ramamirtham R et al. Effects of form deprivation on peripheral refractions and ocular shape in infant rhesus monkeys (*Macaca mulatta*). *Invest Ophthalmol Vis Sci* 2009; 50: 4033-4044.
159. Totonelly KC, Coletta NJ, Troilo D. Lens-induced refractive errors alter the pattern of peripheral refractive state in marmosets. *Invest Ophthalmol Vis Sci* 2006; 47: 3323.
160. Benavente-Perez A, Nour A, Troilo D. Peripheral refraction as a predictor for induced changes in vitreous chamber growth rates in marmosets. *Invest Ophthalmol Vis Sci* 2012; 53: 4662.
161. Benavente-Perez A, Nour A, Troilo D. Asymmetries in peripheral refraction in marmosets change with emmetropization and induced eye growth. *Invest Ophthalmol Vis Sci* 2014; 55: 2731.
162. Benavente-Perez A, Nour A, Troilo D. The role of peripheral refraction in emmetropization: evidence from marmoset studies. *Eye Vision* 2016; 3: 1-11.
163. Benavente-Perez A, Nour A, Yan L et al. The role of peripheral refraction in the temporal integration of induced eye growth in marmosets. *Ophthalmic Physiol Opt* 2013; 33: 661-674.
164. Atchison DA, Jones CE, Schmid KL et al. Eye shape in emmetropia and myopia. *Invest Ophthalmol Vis Sci* 2004; 45: 3380-3386.
165. Stone RA, Flitcroft DL. Ocular shape and myopia. *Ann Acad Med Singapore* 2004; 33: 7-15.
166. Verkharla PK, Mathur A, Mallen EAH et al. Eye shape and retinal shape, and their relation to peripheral refraction. *Ophthalmic Physiol Opt* 2012; 32: 184-199.
167. Atchison DA, Pritchard N, Schmid KL et al. Shape of the retinal surface in emmetropia and myopia. *Invest Ophthalmol Vis Sci* 2005; 46: 2698-2707.
168. Gilmartin B, Nagra M, Logan NS. Shape of the posterior vitreous chamber in human emmetropia and myopia. *Invest Ophthalmol Vis Sci* 2013; 54: 7240-7251.
169. Schmid GF. Axial and peripheral eye length measured with optical low coherence interferometry. *J Biomed Opt* 2003; 8: 655-662.
170. Schmid GF. Variability of retinal steepness at the posterior pole in children 7-15 years of age. *Curr Eye Res* 2003; 27: 61-68.
171. Atchison DA, Charman WN. Can partial coherence interferometry be used to determine retinal shape? *Optom Vis Sci* 2011; 88: 601-607.
172. Risk factors for idiopathic rhegmatogenous retinal detachment. The Eye Disease Case-Control Study Group. *Am J Epidemiol* 1993; 137: 749-757.
173. Mallen EAH, Kashyap P. Technical note: measurement of retinal contour and supine axial length using the Zeiss IOLMaster. *Ophthalmic Physiol Opt* 2007; 27: 404-411.
174. Charman WN, Radhakrishnan H. Peripheral refraction and the development of refractive error: a review. *Ophthalmic Physiol Opt* 2010; 30: 321-338.
175. Schmid GF. Association between retinal steepness and central myopic shift in children. *Optom Vis Sci* 2011; 88: 684-690.

176. Smith EL 3rd, Hung LF, Huang J et al. Effects of local myopic defocus on refractive development in monkeys. *Optom Vis Sci* 2013; 90: 1176–1186.
177. Totonelly K, Troilo D. Eye shape and off-axis refractive state following induced axial refractive errors in marmoset monkeys. *Invest Ophthalmol Vis Sci* 2008; 49: 3589.
178. Verkicharla PK, Suheimat M, Schmid KL et al. Differences in retinal shape between East Asian and Caucasian eyes. *Ophthalmic Physiol Opt* 2017; 37: 275–283.
179. Verkicharla PK, Suheimat M, Schmid KL et al. Peripheral refraction, peripheral eye length and retinal shape in myopia. *Optom Vis Sci* 2016; 93: 1072–1078.
180. Wakazono T, Yamashiro K, Miyake M et al. Time-course change in eye shape and development of staphyloma in highly myopic eyes. *Invest Ophthalmol Vis Sci* 2018; 59: 5455–5461.
181. Huang J, Wen D, Wang Q et al. Efficacy comparison of 16 interventions for myopia control in children: a network meta-analysis. *Ophthalmology* 2016; 123: 697–708.
182. Sng CC, Lin XY, Gazzard G et al. Peripheral refraction and refractive error in Singapore Chinese children. *Invest Ophthalmol Vis Sci* 2011; 52: 1181–1190.
183. Sng CC, Lin XY, Gazzard G et al. Change in peripheral refraction over time in Singapore Chinese children. *Invest Ophthalmol Vis Sci* 2011; 52: 7880–7887.
184. Mutti DO, Sinnott LT, Mitchell GL et al. Relative peripheral refractive error and the risk of onset and progression of myopia in children. *Invest Ophthalmol Vis Sci* 2011; 52: 199–205.
185. Lee TT, Cho P. Relative peripheral refraction in children: twelve-month changes in eyes with different ametropias. *Ophthalmic Physiol Opt* 2013; 33: 283–293.
186. Atchison DA, Li SM, Li H et al. Relative peripheral hyperopia does not predict development and progression of myopia in children. *Invest Ophthalmol Vis Sci* 2015; 56: 6162–6170.
187. Atchison DA, Rosén R. The possible role of peripheral refraction in development of myopia. *Optom Vis Sci* 2016; 93: 1042–1044.
188. Rotolo M, Montani G, Martin R. Myopia onset and role of peripheral refraction. *Clin Optom (Auckl)* 2017; 9: 105–111.
189. Mutti DO, Sinnott LT, Reuter KS et al. Peripheral refraction and eye lengths in myopic children in the bifocal lenses in nearsighted kids (BLINK) study. *Transl Vis Sci Technol* 2019; 8: 17.
190. Charman WN. Wavefront aberration of the eye: a review. *Optom Vis Sci* 1991; 68: 574–583.
191. Charman WN. Aberrations and myopia. *Ophthalmic Physiol Opt* 2005; 25: 285–301.
192. García de la Cera E, Rodríguez G, Marcos S. Longitudinal changes of optical aberrations in normal and form-deprived myopic chick eyes. *Vision Res* 2006; 46: 579–589.
193. Coletta NJ, Marcos S, Troilo D. Ocular wavefront aberrations in the common marmoset *Callithrix jacchus*: effects of age and refractive error. *Vision Res* 2010; 50: 2515–2529.
194. Ramamirtham R, Kee CS, Hung LF et al. Monochromatic ocular wave aberrations in young monkeys. *Vision Res* 2006; 46: 3616–3633.
195. Brunette I, Bueno JM, Parent M et al. Monochromatic aberrations as a function of age, from childhood to advanced age. *Invest Ophthalmol Vis Sci* 2003; 44: 5438–5446.
196. Artal P, Guirao A, Berrio E et al. Compensation of corneal aberrations by the internal optics in the human eye. *J Vis* 2001; 1: 1–8.
197. Kisiak ML, Campbell MC, Hunter JJ et al. Aberrations of chick eyes during normal growth and lens induction of myopia. *J Comp Physiol A Neuroethol Sens Neural Behav Physiol* 2006; 192: 845–855.
198. Ramamirtham R, Kee CS, Hung LF et al. Wave aberrations in rhesus monkeys with vision-induced ametropias. *Vision Res* 2007; 47: 2751–2766.
199. Llorente L, Barbero S, Cano D et al. Myopic versus hyperopic eyes: axial length, corneal shape and optical aberrations. *J Vis* 2004; 4: 288–298.
200. Thibos LN, Bradley A, Hong X. A statistical model of the aberration structure of normal, well-corrected eyes. *Ophthalmic Physiol Opt* 2002; 22: 427–433.
201. Castejón-Mochón JF, López-Gil N, Benito A et al. Ocular wave-front aberration statistics in a normal young population. *Vision Res* 2002; 42: 1611–1617.
202. He JC, Sun P, Held R et al. Wavefront aberrations in eyes of emmetropic and moderately myopic school children and young adults. *Vision Res* 2002; 42: 1063–1070.
203. Paquin MP, Hamam H, Simonet P. Objective measurement of optical aberrations in myopic eyes. *Optom Vis Sci* 2002; 79: 285–291.
204. Atchison DA, Schmid KL, Pritchard N. Neural and optical limits to visual performance in myopia. *Vision Res* 2006; 46: 3707–3722.
205. Carkeet A, Luo HD, Tong L et al. Refractive error and monochromatic aberrations in Singaporean children. *Vision Res* 2002; 42: 1809–1824.
206. Cheng X, Bradley A, Hong X et al. Relationship between refractive error and monochromatic aberrations of the eye. *Optom Vis Sci* 2003; 80: 43–49.
207. Lopez-Gil N, Iglesias I, Artal P. Retinal image quality in the human eye as a function of the accommodation. *Vision Res* 1998; 38: 2897–2907.
208. Vilupuru AS, Roorda A, Glasser A. Spatially variant changes in lens power during ocular accommodation in a rhesus monkey eye. *J Vis* 2004; 4: 299–309.
209. Liu R, Qian YF, He JC et al. Effects of different monochromatic lights on refractive development and eye growth in Guinea pigs. *Exp Eye Res* 2011; 92: 447–453.
210. Rucker FJ, Wallman J. Chick eyes compensate for chromatic simulations of hyperopic and myopic defocus: evidence that the eye uses longitudinal chromatic aberration to guide eye-growth. *Vision Res* 2009; 49: 1775–1783.
211. Rucker FJ. The role of luminance and chromatic cues in emmetropisation. *Ophthalmic Physiol Opt* 2013; 33: 196–214.
212. Seidemann A, Schaeffel F. Effects of longitudinal chromatic aberration on accommodation and emmetropization. *Vision Res* 2002; 42: 2409–2417.
213. Gisbert S, Schaeffel F. M to L cone ratios determine eye sizes and baseline refractions in chickens. *Exp Eye Res* 2018; 172: 104–111.
214. Roorda A, Williams DR. The arrangement of the three cone classes in the living human eye. *Nature* 1999; 397: 520–522.
215. Yamamoto S, Nitta K, Kamiyama M. Cone electroretinogram to chromatic stimuli in myopic eyes. *Vision Res* 1997; 37: 2157–2159.
216. Kawabata H, Murayama K, Adachi-Usami E. Sensitivity loss in short wavelength sensitive cones in myopic eyes. *Nippon Ganka Gakkai Zasshi* 1996; 100: 868–876.
217. Gamlin PD, McDougal DH, Pokorny J et al. Human and macaque pupil responses driven by melanopsin-containing retinal ganglion cells. *Vision Res* 2007; 47: 946–954.
218. Jiang L, Zhang S, Schaeffel F et al. Interactions of chromatic and lens-induced defocus during visual control of eye growth in guinea pigs (*Cavia porcellus*). *Vision Res* 2014; 94: 24–32.
219. Foulds WS, Barathi VA, Luu CD. Progressive myopia or hyperopia can be induced in chicks and reversed by manipulation of the chromaticity of ambient light. *Invest Ophthalmol Vis Sci* 2013; 54: 8004–8012.
220. Kröger RH, Wagner HJ. The eye of the blue acara (*Aequidens pulcher*, Cichlidae) grows to compensate for defocus due to chromatic aberration. *J Comp Physiol A* 1996; 179: 837–842.
221. Torii H, Kurihara T, Seko Y et al. Violet light exposure can be a preventive strategy against myopia progression. *EBioMedicine* 2017; 15: 210–219.
222. Rucker FJ, Osorio D. The effects of longitudinal chromatic aberration and a shift in the peak of the middle-wavelength sensitive cone fundamental on cone contrast. *Vision Res* 2008; 48: 1929–1939.
223. Hung LF, Arumugam B, She Z et al. Narrow-band, long-wavelength lighting promotes hyperopia and retards vision-induced myopia in infant rhesus monkeys. *Exp Eye Res* 2018; 176: 147–160.
224. Smith EL 3rd, Hung LF, Arumugam B et al. Effects of long-wavelength lighting on refractive development in infant rhesus monkeys. *Invest Ophthalmol Vis Sci* 2015; 56: 6490–6500.
225. Gawne TJ, Ward AH, Norton TT. Long-wavelength (red) light produces hyperopia in juvenile and adolescent tree shrews. *Vision Res* 2017; 140: 55–65.
226. Gawne TJ, Siegwart JT Jr, Ward AH et al. The wavelength composition and temporal modulation of ambient lighting strongly affect refractive development in young tree shrews. *Exp Eye Res* 2017; 155: 75–84.
227. Cohen Y, Belkin M, Yehezkel O et al. Dependency between light intensity and refractive development under light-dark cycles. *Exp Eye Res* 2011; 92: 40–46.
228. Chen S, Zhi Z, Ruan Q et al. Bright light suppresses form-deprivation myopia development with activation of dopamine D1 receptor signaling in the ON pathway in retina. *Invest Ophthalmol Vis Sci* 2017; 58: 2306–2316.
229. Xiong S, Sankaridurg P, Naduvilath T et al. Time spent in outdoor activities in relation to myopia prevention and control: a meta-analysis and systematic review. *Acta Ophthalmol* 2017; 95: 551–566.
230. Ostrin LA. The ipRGC-driven pupil response with light exposure and refractive error in children. *Ophthalmic Physiol Opt* 2018; 38: 503–515.
231. Ostrin LA. Objectively measured light exposure in emmetropic and myopic adults. *Optom Vis Sci* 2017; 94: 229–238.

## Higher order aberrations, refractive error development and myopia control: a review

*Clin Exp Optom* 2020; 103: 68–85

DOI:10.1111/cxo.12960

**Rohan PJ Hughes**  MOptom BVisSc  
**Stephen J Vincent**  PhD BAppSc (Optom)  
(Hons)  
**Scott A Read**  PhD BAppSc (Optom)  
(Hons)  
**Michael J Collins** PhD MAppSc DipAppSc  
(Optom)

Contact Lens and Visual Optics Laboratory, School of Optometry and Vision Science, Queensland University of Technology, Brisbane, Australia  
E-mail: rohan.hughes@hdr.qut.edu.au

Submitted: 31 March 2019

Revised: 1 July 2019

Accepted for publication: 28 July 2019

Evidence from animal and human studies suggests that ocular growth is influenced by visual experience. Reduced retinal image quality and imposed optical defocus result in predictable changes in axial eye growth. Higher order aberrations are optical imperfections of the eye that alter retinal image quality despite optimal correction of spherical defocus and astigmatism. Since higher order aberrations reduce retinal image quality and produce variations in optical vergence across the entrance pupil of the eye, they may provide optical signals that contribute to the regulation and modulation of eye growth and refractive error development. The magnitude and type of higher order aberrations vary with age, refractive error, and during near work and accommodation. Furthermore, distinctive changes in higher order aberrations occur with various myopia control treatments, including atropine, near addition spectacle lenses, orthokeratology and soft multifocal and dual-focus contact lenses. Several plausible mechanisms have been proposed by which higher order aberrations may influence axial eye growth, the development of refractive error, and the treatment effect of myopia control interventions. Future studies of higher order aberrations, particularly during childhood, accommodation, and treatment with myopia control interventions are required to further our understanding of their potential role in refractive error development and eye growth.

**Key words:** eye growth, higher order aberrations, myopia control, refractive error development, visual experience

The prevalence of myopia has dramatically risen over the past 60 years<sup>1</sup> with significant regional variations in myopia prevalence across the world, from approximately 15 per cent of adults in Australia,<sup>2</sup> to 70–90 per cent in South East Asian countries such as China,<sup>3</sup> South Korea,<sup>4</sup> Singapore,<sup>5</sup> and Taiwan.<sup>6</sup> By 2050, it is estimated that 50 per cent of the global population will be myopic (> -0.50 D), with one-fifth of these being highly myopic (> -5.00 D).<sup>7</sup> The numerous sight-threatening ocular conditions that are associated with myopia, including retinal detachment,<sup>8</sup> myopic maculopathy,<sup>9</sup> glaucoma,<sup>10</sup> and cataract,<sup>11</sup> represent a significant public health concern both in terms of the global economy<sup>12</sup> and the visual consequences of these ocular pathologies.<sup>13</sup>

While the aetiology of refractive error is multifactorial,<sup>14</sup> evidence from animal studies suggest that visual experience is an important factor in eye growth regulation.<sup>15</sup> Higher order aberrations (HOAs), defined as optical aberrations that remain following the optimal correction of defocus and

astigmatism with conventional spherocylindrical lenses, can significantly influence retinal image quality,<sup>16</sup> the accommodation response of the eye,<sup>17</sup> and the relative focal plane of different regions of the entrance pupil.<sup>18</sup> Therefore, there are various mechanisms through which they may play a role in guiding eye growth and the development of refractive errors. This review summarises the literature examining HOAs in animal models of refractive error development and changes in the HOA profile in humans with age, refractive error, abnormal visual development and various myopia control interventions. Additionally, possible mechanisms linking HOAs with refractive error development and the treatment effect of myopia control interventions are discussed in detail.

### Visual regulation of eye growth

During infancy and childhood, structural changes occur within the eye to minimise refractive error. Axial length increases

proportionately to a decrease in the dioptric power of the optical components of the eye, which suggests biological, passive regulation of eye growth,<sup>19</sup> a process termed emmetropisation.<sup>20</sup> Refractive errors are primarily determined by axial length changes<sup>21</sup> that are disproportionate to the change in the ocular refractive power, where a slowed and increased rate of axial eye growth results in hyperopia and myopia, respectively, due to a failure in emmetropisation.<sup>22</sup> Exposure of the eye to different visual experiences can disrupt emmetropisation, which suggests that the eye also uses visual input to actively influence eye growth in humans.<sup>23</sup>

A range of animal models have demonstrated that complete visual obscuration by lid suture (in chicks,<sup>24</sup> mice,<sup>25</sup> rabbits,<sup>26</sup> tree shrews,<sup>27</sup> marmosets<sup>28</sup> and rhesus monkeys<sup>29</sup>) or the deprivation of form vision using translucent filters (diffusers) (in fish,<sup>30</sup> mice,<sup>31</sup> guinea pigs<sup>32</sup> and rhesus monkeys<sup>33</sup>) typically results in excessive axial elongation and myopia. Similarly, humans with unilateral visual obstruction from congenital ptosis,<sup>34,35</sup> cataract,<sup>35</sup> corneal

opacity<sup>36</sup> or vitreous haemorrhage<sup>37</sup> also typically develop axial myopia due to form deprivation. First reported by Schaeffel et al.<sup>38</sup> in the chick model, imposed defocus also results in predictable bidirectional changes in eye growth in a variety of species.<sup>39</sup> Exposure to hyperopic defocus leads to an increased ocular growth rate to minimise the imposed refractive error, while the opposite occurs in response to myopic defocus, as demonstrated in chicks,<sup>38,40</sup> mice,<sup>25</sup> guinea pigs,<sup>41</sup> fish,<sup>42</sup> tree shrews,<sup>43,44</sup> marmosets<sup>45,46</sup> and rhesus monkeys.<sup>47</sup> Recently, short-term, transient, bidirectional axial length<sup>48</sup> and choroidal thickness<sup>48-50</sup> changes in response to defocus have also been reported in adult humans, but to a much smaller degree than in animal models. Insights from the chick model have shown that the response to imposed defocus occurs rapidly, within minutes of the visual stimuli being introduced.<sup>51</sup> Additionally, the sign-dependent responses to imposed defocus appear to be locally mediated,<sup>52,53</sup> which indicates that the eye can detect odd-order cues for eye growth within the retinal image. Temporal integration of these cues from the retinal image are thought to modulate scleral remodelling and axial eye growth.<sup>54</sup>

## Evidence from animal studies

During normal visual development, chick,<sup>55,56</sup> marmoset<sup>57</sup> and rhesus monkey<sup>58</sup> eyes display a decrease in HOAs over time, similar to the reduction in neonatal refractive error. A

myopigenic stimulus such as imposed hyperopic defocus<sup>55,59</sup> or form deprivation<sup>56,57,59</sup> results in significantly greater ocular HOAs associated with the development of significant ametropia compared to untreated eyes (Figure 1A); however, both the treated and untreated eyes show a reduction in HOAs over time (Figure 1B). The increase in ocular HOAs observed in chicks reared with monocularly imposed negative lenses<sup>55</sup> and diffusers<sup>56</sup> are predominantly due to changes in third order RMS (root mean square wavefront error), while fourth order<sup>55</sup> and spherical aberration<sup>56</sup> RMS were minimally affected. Similarly, the magnitude of coma and trefoil RMS (both third order terms) increased in monkeys who developed refractive errors from imposed defocus and form deprivation.<sup>59</sup> Coletta et al.<sup>57</sup> also showed strong interocular correlations for each radial order of HOAs, except third order RMS, in monocularly form-deprived marmosets.

Following removal of the visual stimuli in lens-treated and form-deprived eyes, the increase in HOAs generally reduced; however, the HOAs remained higher in the treated eyes than in the fellow untreated eyes.<sup>57,59</sup> Additionally, Ramamirtham et al.<sup>59</sup> found that some eyes showed no recovery from their experimentally induced ametropia, and in these eyes, an increase in total ocular HOAs during the recovery phase was observed, rather than a decrease. Interestingly, there was no difference in the HOA profile between the eyes that recovered and those that failed to recover from their

acquired refractive errors prior to treatment (Figure 1C).

The findings of experimentally induced ametropia in animal models suggest that the changes in HOAs associated with refractive error development are predominated by an increase in the asymmetric aberrations of the third radial order.<sup>55-57,59</sup> Eyes with experimentally acquired ametropia show increased magnitudes of coma and trefoil, therefore such asymmetric HOAs may provide a signal that influences ocular growth, which has been hypothesised based on longitudinal data from human studies.<sup>60-62</sup> Additionally, Wildsoet and Schmid<sup>63</sup> demonstrated that the chick eye is able to modulate ocular growth on the basis of optical vergence, hence it may be possible that the eye uses vergence cues from these asymmetric HOAs to influence eye growth. Furthermore, monkey eyes that developed experimentally induced hyperopia or myopia, both exhibited an increase in magnitude and inter-subject variability of HOAs compared to emmetropic eyes.<sup>59</sup> While it remains possible that an increase in HOAs provides a form deprivation-like stimulus due to a reduction in retinal image quality, or that individual HOAs produce a visual signal that promotes or inhibits ocular growth, the overall trends observed in animal studies across various species suggest that an increase in HOAs occurs coincidentally with refractive error development.

The reduction of HOAs<sup>55-58</sup> and the time course of the increase in HOAs during the

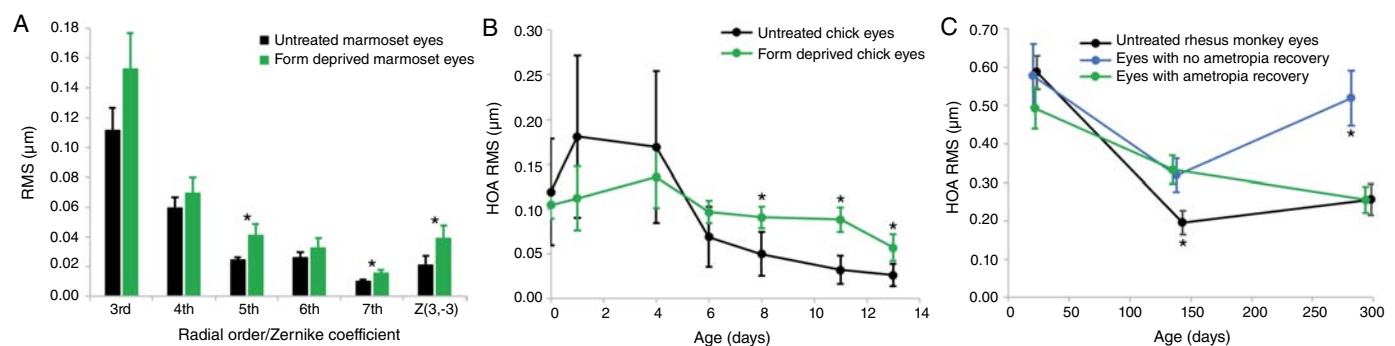


**Figure 1. Higher order aberrations (HOAs) associated with animal models of experimental myopia showing A: the greater level of HOAs during or immediately following form deprivation compared to untreated fellow eyes in marmosets (reproduced from Coletta et al.<sup>57</sup>), B: the change in HOAs in chick eyes during treatment with form deprivation compared to untreated control eyes (reproduced from Garcia de la Cera et al.<sup>56</sup>), and C: the change in HOAs in treated rhesus monkey eyes that developed form deprivation or lens-induced ametropia compared to an untreated control group (reproduced from Ramamirtham et al.<sup>59</sup>), where the three time points represent pre-treatment, immediately post-treatment and following a period of recovery in rhesus monkeys. Note that the eyes that did not recover from their experimental ametropia showed increased HOAs compared to untreated eyes and treated eyes that exhibited recovery from induced ametropia. In A, B, and C, asterisks indicate statistically significant group differences. In A and B, error bars represent the standard deviation, and in C, the standard error of the mean.**

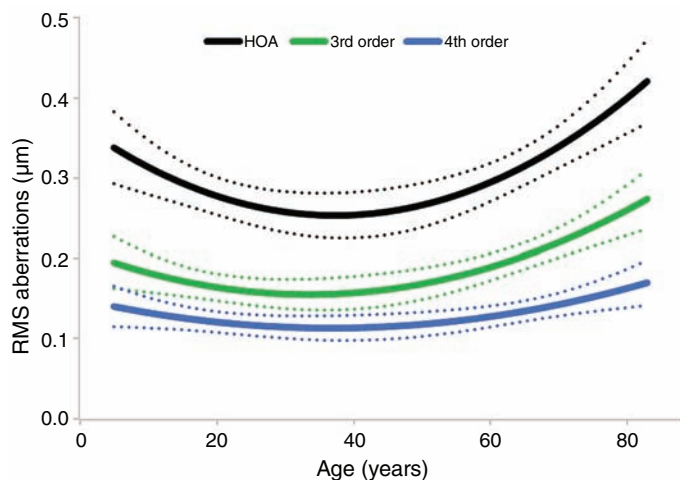


**Figure 2.** The change in higher order aberrations (HOAs), third order and fourth order root mean square wave front error (RMS) with age over a 5 mm pupil (polynomial regression functions adapted from Brunette et al.<sup>69</sup>). Dotted lines represent the 95% confidence intervals for the regression functions. HOA, third order and fourth order RMS varied in an approximate quadratic association with age, decreasing during childhood to a minimum between 30–40 years and subsequently increasing with age.

development of ametropia<sup>55–57,59</sup> suggests a passive scaling effect due to growth in ocular structures,<sup>55–58</sup> and that any increase in the level of HOAs is likely a consequence, rather than a cause, of refractive error development. However, modelling demonstrates that simple scaling of the optical components in chicks<sup>55</sup> and rhesus monkeys<sup>58</sup> cannot account for the total changes observed in HOAs, which may provide some evidence for visual, rather than entirely passive, regulation of HOAs.

## HOAs and age

### On-axis HOAs

Total ocular HOAs are influenced by the refractive elements within the eye, specifically the curvature, alignment, refractive index, and axial separation of the anterior and posterior surfaces of the cornea and crystalline lens. In humans, a partial compensatory balance exists between the anterior corneal and internal HOAs (the combination of the posterior cornea and crystalline lens), whereby the internal HOAs are of reduced magnitude and opposite in sign to the anterior corneal HOAs.<sup>64</sup>

Several studies have reported a linear increase in HOA RMS between the ages of 20 and 70 years.<sup>65–68</sup> In a cross-sectional analysis, Brunette et al.<sup>69</sup> demonstrated that

across a lifetime (six to 82 years), the change in HOA RMS was best described by a second order polynomial, where the elderly (over 60 years) displayed greater HOA RMS values than those 20 to 60 years old, with a minimum at approximately 40 years (Figure 2). Similarly, other studies have found that HOA RMS remains stable between the ages of approximately 20 and 55 years.<sup>70,71</sup> Brunette et al.<sup>69</sup> also showed that coma and spherical aberration RMS vary with age in an approximate quadratic association, reaching a minimum between 20 to 30 years, and increasing with older age.<sup>71,72</sup> Primary horizontal coma ( $Z_3^1$ ) and spherical aberration ( $Z_4^0$ ) have shown negative<sup>65</sup> and positive associations with age,<sup>71,72</sup> respectively, between approximately 20 and 70 years.

Cataract development typically causes internal ocular HOAs to increase,<sup>73–75</sup> predominantly positive shifts in coma RMS and primary spherical aberration ( $Z_4^0$ ) for cortical and nuclear cataracts, respectively.<sup>73,75</sup> Since anterior corneal HOAs exhibit negligible variation throughout adulthood<sup>68,72,76</sup> and with cataract formation,<sup>75</sup> it is likely that these age-related lenticular changes result in a breakdown of the partial internal compensation of HOAs and account for the reported changes in HOAs with age,<sup>68</sup> particularly over 60 years.<sup>69</sup>

The changes in HOAs observed during childhood are not consistent. A recent large cross-

sectional study of Chinese children ( $n = 1,634$ ) measured HOAs under cycloplegia and reported a trend of increasing HOA RMS from three to 17 years (Figure 3), primarily due to a negative shift in primary vertical coma ( $Z_3^{-1}$ ), primary spherical aberration ( $Z_4^0$ ), and secondary trefoil ( $Z_3^{-5}$ ), and positive shifts in primary trefoil ( $Z_3^{-3}$ ) and secondary astigmatism ( $Z_2^2$ ).<sup>77</sup> Conversely, Brunette et al.<sup>69</sup> examined Canadian children under cycloplegia and demonstrated a reduction in HOA RMS during childhood and suggested that HOAs are regulated similarly to lower order aberrations (spherical and astigmatic refractive errors) during emmetropisation. While this finding is consistent with various animal models,<sup>55–58</sup> their sample included only 29 subjects under the age of 20 years whereas Zhang et al.<sup>77</sup> examined over 1,600 subjects in this age group. Significant differences in the refractive error range of the examined populations of Brunette et al.<sup>69</sup> and Zhang et al.<sup>77</sup> may explain the inconsistency in their results, with  $-3.50$  to  $+3.50$  D (across all included ages from six to 82 years) and  $-10.00$  to  $+8.25$  D, respectively, although Zhang et al.<sup>77</sup> reported no significant differences in HOAs between the myopes, emmetropes and hyperopes within each age group. Additionally, Caucasian and Asian adults,<sup>78,79</sup> and Chinese and Malay children,<sup>80</sup> have been reported to exhibit HOA profile differences, particularly for primary spherical aberration ( $Z_4^0$ ); therefore, ethnic variation may also exist between the HOA profiles of Canadian and Chinese children. Given the cross-sectional designs of both studies, longitudinal studies are required to further the current understanding of the temporal variations in HOAs during childhood.

The studies of HOAs and age in adults show consistent trends in HOAs as a function of age; however, a factor which is typically neglected is the effect of natural pupil size. In adults, it is well-established that pupil size decreases with age.<sup>81,82</sup> Winn et al.<sup>81</sup> demonstrated that average pupil size at 20 years was  $\sim 4.5$  mm and decreased by  $\sim 0.02$  mm per year to  $\sim 3.2$  mm at 85 years, under typical indoor room lighting ( $\sim 263$  lux). Contrary to adults, pupil size in indoor room lighting during childhood has been shown to increase from  $\sim 5$  mm at birth to  $\sim 6.1$  mm by late adolescence; however, the exact luminance during measurement was not reported.<sup>83</sup> Each of the studies examining age-related changes in HOAs report the



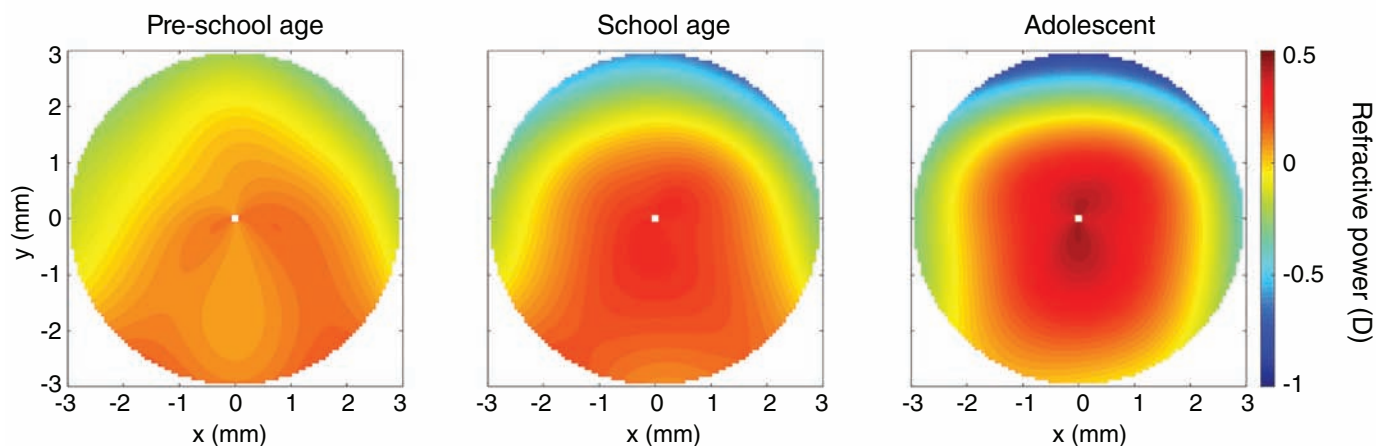


**Figure 3. Refractive power maps generated from the higher order aberrations (HOAs) (third to fifth order) in pre-school age children, school age children, and adolescents (data from Zhang et al.<sup>77</sup>). The observed changes between age groups result from positive shifts in primary trefoil ( $Z_3^{-3}$ ) and secondary astigmatism ( $Z_4^2$ ), and negative shifts in primary vertical coma ( $Z_3^{-1}$ ), primary spherical aberration ( $Z_4^0$ ) and secondary trefoil ( $Z_5^{-3}$ ), which produce the increase in positive and negative power at the centre and margin of the 6 mm pupil diameter, respectively.**

HOAs over fixed pupil diameters of greater than 4.5 mm; however, the HOA profile through the natural pupil may have differed since pupil size varies with age. Furthermore, it is possible that the consistently observed increase in HOAs reported in older adults may be offset by the natural age-related pupillary miosis, since HOAs decrease with decreasing pupil size.<sup>16</sup>

### Off-axis HOAs

Off-axis HOAs are typically of greater magnitude than on-axis HOAs, particularly for coma terms, likely as a result of the change in alignment and shape differences of the ocular refractive surfaces from off-axis incident light rays.<sup>84-87</sup> Changes in off-axis HOAs also occur with age. Emmetropic adolescents (11 to 14 years) show greater levels of off-axis HOA RMS compared to on-axis measurements,<sup>88</sup> with a magnitude similar to young adult emmetropes.<sup>85</sup> Primary vertical coma ( $Z_3^{-1}$ ) and primary horizontal coma ( $Z_3^1$ ) also increase off-axis, while primary spherical aberration ( $Z_4^0$ ) remains stable across the visual field.<sup>88</sup>

In young (20 to 30 years) and old (50 to 71 years) emmetropes, HOA RMS also varies with eccentricity in an approximate quadratic association along the horizontal and vertical meridian; however, the rate of change with eccentricity is greater in older eyes.<sup>85</sup> Additionally, Mathur et al.<sup>85</sup> found an age by

eccentricity interaction for all third and fourth order Zernike terms, except primary trefoil ( $Z_3^{-3}$ ) and quadrafoil ( $Z_4^{-4}$ ), which suggests a difference between age groups in the off-axis variation of these HOAs. However, on average, the magnitude of these HOAs across the visual field was reported to be minimal except for primary vertical ( $Z_3^{-1}$ ) and horizontal ( $Z_3^1$ ) coma, and spherical aberration ( $Z_4^0$ ).<sup>85</sup> Most significantly, the combination of the coma terms increased approximately linearly across the visual field, and older eyes exhibited a greater rate of change than younger eyes,<sup>85</sup> where the orientation of the off-axis variation of the combined coma terms aligned with the axis of the term, as expected due to the change in alignment and shape of the cornea and crystalline lens. For example, vertical coma varied across the vertical meridian, horizontal coma varied across the horizontal meridian, and the combined terms varied along oblique visual field meridians being measured. Primary spherical aberration ( $Z_4^0$ ) was stable across the visual field in each group; however, the older subjects displayed more positive values on average.<sup>85</sup> Studies of peripheral HOAs in children, in addition to longitudinal studies of off-axis HOAs, ocular biometry and refractive error are required to further examine changes in on- and off-axis HOAs with age and their potential role in eye growth and refractive error development.

## HOAs and refractive error

### Cross-sectional studies

Numerous cross-sectional studies have compared HOAs between subjects with established refractive errors; however, the results have not been consistent (Table 1). Several studies of adults have found that myopic eyes show significantly higher levels of ocular HOA RMS than emmetropic eyes,<sup>89-91</sup> but others have found no differences.<sup>92,93</sup> Llorente et al.<sup>94</sup> showed that hyperopic eyes exhibit greater HOA RMS than myopic eyes; however, this finding has not been duplicated.<sup>92</sup> Spherical aberration and coma RMS have been reported to increase with increasing levels of myopia.<sup>90</sup> Similarly, most studies have shown that third order, fourth order, and coma-like RMS values are higher in myopes than emmetropes and hyperopes,<sup>89,91</sup> but this is also not a universal finding.<sup>94</sup> While some studies have shown no trend,<sup>92,94</sup> a positive correlation between primary spherical aberration ( $Z_4^0$ ) and refractive error has been observed, whereby spherical aberration becomes more negative with increasing myopia.<sup>91,93</sup>

Cross-sectional studies of off-axis HOAs in young adults have shown that HOA RMS increases more rapidly with visual field eccentricity in myopes than in emmetropes;<sup>86</sup> however, Osuagwu et al.<sup>87</sup>

Authors	Year	N	Ages (years)	N by refractive group and range (D)	Sex	Location (ethnicity)	Measurement technique	Accommodation control	PD (mm)	HOA	3rd	4th	SA	Coma
Carkeet et al. <sup>80</sup>	2002	273	7.9–12.7	138 M 36 HM (≤ -3.00) 102 LM (-3.00 ≤ -0.5)	147 female, 126 male	Singapore (Chinese, Malay, Indian)	Hartman-Shack ray tracing	1% Cyclopentolate (3 drops)	5	M = E = H	M = E = H	HM < LM = E = H	HM < LM = E = H (same for Z <sub>2</sub> <sup>0</sup> )	M = E = H
He et al. <sup>89</sup>	2002	170	10–17	123 E (-0.5 ≤ +1.00) 12 H (≥ +1.00)	NR	China, America	Psychophysical ray tracing	Badal	≥ 6	M > E	NR	NR	NR	NR
Paquin et al. <sup>90</sup>	2002	146	18–29	87 M (≤ -0.75) 83 E (±0.50) 92 M (≤ -0.75) 54 E (±0.50)	NR	Canada	Hartman-Shack ray tracing	1% Tropicamide; 2.5% Phenylephrine	5; 9	M > E	NR	NR	↑ M / ↑ SA	↑ M / ↑ coma
Cheng et al. <sup>92</sup>	2003	162	26.1 ± 5.6 (mean ± SD)	124 M (≤ -0.75) 19 E (-0.75 ≤ +0.75) 7 E (≥ -1.00)	NR	America	Hartman-Shack ray tracing	0.5% Cyclopentolate	6	M = E = H	NR	NR	M = E = H	NR
Llorente et al. <sup>94</sup>	2004	46	23–40	19 H (≥ +0.75) 24 M (≤ -0.8) 22 H (≥ +0.5)	NR	Spain	Laser ray tracing	1% Tropicamide	6.5	M < H	H > M	NR	H > M (Z <sub>2</sub> <sup>0</sup> )	H > M
Kirwan et al. <sup>95</sup>	2006	82 (162 eyes)	4–14	25 M (≤ -0.70) 137 H (≥ +0.06)	42 female, 40 male	Ireland	Hartman-Shack ray tracing	1% Cyclopentolate	6	M > H	M = H	M > H	M = H	M > H (Z <sub>3</sub> <sup>-1</sup> )
Kwan et al. <sup>93</sup>	2009	116	19–29	86 M 30 HM (≤ -5.00) 56 MM (-5.00 ≤ -0.50)	62 female, 54 male	Hong Kong (Chinese)	Hartman-Shack ray tracing	Internal instrument fixation target	5	M = E	E = M	E > M; ↑ M / ↓ 4 <sup>th</sup>	E > M; ↑ M / ↓ SA; ↑ M / ↓ Z <sub>4</sub> <sup>0</sup>	E = M
Martinez et al. <sup>101</sup>	2009	771	5.7–7.9	30 E (≥ -0.50) 53 E (-0.50 ≤ +0.50) 718 H (≥ +0.50)	368 female, 403 male	Australia (Caucasian)	Hartman-Shack ray tracing	1% Cyclopentolate; 1% Tropicamide	5	E < H	E = H	E < H	E < H; ↓ H / ↓ Z <sub>2</sub> <sup>0</sup>	E = H
Li et al. <sup>97</sup>	2012	86	7–13	64 M 21 MM (-6.00 ≤ -3.00) 43 LM (-3.00 ≤ -0.50) 22 E (-0.50 ≤ +0.50)	45 female, 41 male	China (Chinese)	Hartman-Shack ray tracing	0.5% Tropicamide (5 drops); 1.50 D target fogging	5	M = E	M = E	M = E	M = E	Z <sub>3</sub> varied

**Table 1. Summary of cross-sectional cohort studies examining on-axis higher order aberrations between refractive error groups**

Authors	Year	N	Ages (years)	N by refractive group and range (D)	Sex	Location (ethnicity)	Measurement technique	Accommodation control	PD (mm)	HOA	3rd	4th	SA	Coma
Philip et al. <sup>99</sup>	2012	675	16-19	125 M 25 MM (< -3.00)	339 female, 336 male	Australia	Hartman-Shack	1% Cyclopentolate; 1% Tropicamide	5	MM = LM = E < H M = E < H M > E > H	MM = LM = E < H M = E < H (same for Z <sub>3</sub> <sup>1</sup> )			
				100 LM (-3.00 < -0.50)										
				197 E (-0.50 < -0.50)										
				353 H (≥ +0.50)										
Zhang et al. <sup>96</sup>	2013	148	6-16	99 PM (-4.25 ± 1.58)	NR	China (Chinese)	Hartman-Shack	1% Tropicamide	6	PM > SM	PM > SM	PM = SM		PM > SM (more -ve)
				49 SM (-3.79 ± 1.92)										
Little et al. <sup>98</sup>	2014	317	9-16	33 M (≤ -0.50)	162 female, 156 male	Northern Ireland	Hartman-Shack	1% Cyclopentolate	5	M = E = H	M = E = H	M = E = H		M = E = H
				85 E (-0.13 < +0.50)										
				199 H (≥ +0.50)										
Yazar et al. <sup>91</sup>	2014	1,034	18.3-22.1	217 M (≤ -0.50)	477 female, 530 male	Australia (85% Caucasian)	Hartman-Shack	1% Tropicamide, 10% Phenylephrine	6	M > E; ↑ M / ↑ HOA	M > E > H M > E > H			↑ M / ↑ coma
				476 E (-0.50 < +0.50)										
				314 H (≥ +0.50)										
Papmatorakis et al. <sup>100</sup>	2015	557	10-15	320 M (≤ -0.50)	266 female, 291 male	Greece	Hartman-Shack	Chart fixation (0.25 D demand)	5	NR	NR	NR		NR
				201 E (-0.50 < +0.50)										
				36 H (≥ +0.50)										
Philip et al. <sup>88</sup>	2018	618	11.09-13.9	91 M (≤ -0.50)	52 female, 39 male	Australia (Caucasian, Asian, Middle Eastern)	Hartman-Shack	1% Cyclopentolate; 1% Tropicamide	5	M = E < H	M = E = H M = E M < H E < H			NR
				166 E (-0.50 < +0.50)	77 female, 89 male									
				361 H (≥ +0.50)	179 female, 182 male									

Coma: coma RMS, E: emmetropia, H: hyperopia, HOA: higher order aberrations RMS, LM: low myopia, M: myopia, MM: moderate myopia, N: number of participants in sample/refractive group, NR: not reported, PD: pupil diameter for analysis, PM: progressive myopia, 3rd: third order RMS, 4th: fourth order RMS, SA: spherical aberration RMS, Z<sub>3</sub><sup>1</sup>: primary vertical coma, Z<sub>3</sub><sup>2</sup>: primary spherical aberration, Z<sub>3</sub><sup>3</sup>: primary horizontal coma, ↑: increase, ↓: decrease.

**Table 1. Continued**

found no significant differences between refractive error groups. Consistent with the findings of on-axis HOA studies, myopes exhibit more negative primary spherical aberration ( $Z_4^0$ ) than emmetropes,<sup>86</sup> and hyperopes display more positive primary spherical aberration ( $Z_4^0$ ) than emmetropes and myopes on average across the visual field.<sup>87</sup> Coma varies with visual field eccentricity, with primary vertical coma ( $Z_3^{-1}$ ) increasing from the superior to inferior field and primary horizontal coma ( $Z_3^1$ ) increasing from the nasal to temporal field.<sup>86,87</sup> While Mathur et al.<sup>86</sup> reported that the rate of off-axis change in coma is double in myopes than in emmetropes, this finding was not confirmed by Osuagwu et al.<sup>87</sup> across the same visual field range. This may be due to study differences in the level of myopia between the two cohorts, since axial length and corneal and retinal shape are influenced by refractive error and may affect the rates of change of off-axis HOAs.

While each of these studies measured HOAs either under cycloplegia, or using a fixed distance target or the internal fixation target of the instrument (presumably focused for relaxed accommodation), various aberration measurement techniques and instruments have been utilised which may account for the broad inconsistencies between these studies. Given that myopia typically develops during childhood and adolescence, it is difficult to draw conclusions from these cross-sectional cohort studies of adult subjects with established refractive errors and it is therefore also valuable to examine the association between refractive error and HOAs in children and adolescents.

Fewer cross-sectional studies have examined HOAs in children (mostly under cycloplegia), and like studies of adults, there is disagreement regarding the relationship between HOAs and refractive error. Kirwan et al.<sup>95</sup> examined children aged four to 14 years and found that myopic children exhibited greater HOA RMS than hyperopes. He et al.<sup>89</sup> similarly found higher levels of HOA RMS in myopes than emmetropes in children aged 10 to 17 years, measured with a natural pupil and relaxed accommodation. Further supporting a role for HOA in myopia development, Zhang et al.<sup>96</sup> examined myopes aged between six and 16 years and observed that those with a higher rate of progression (greater than 0.50 D per year) exhibited significantly higher levels of HOA,

third order and coma RMS than stable myopes. While several studies have found no difference in HOAs between refractive error groups in children,<sup>80,97,98</sup> Philip et al.<sup>99</sup> reported that low hyperopes and emmetropes exhibit increased HOAs compared to emmetropes and low myopes in a group of older adolescents aged 16 to 19 years.

Hyperopic adolescents exhibit more positive primary spherical aberration ( $Z_4^0$ )<sup>99</sup> and greater fourth order and spherical aberration RMS than myopic and emmetropic adolescents.<sup>88</sup> Additionally, and in agreement with the findings of adult studies, primary spherical aberration ( $Z_4^0$ ) tends to become more negative with increasing myopia<sup>100</sup> or decreasing hyperopia,<sup>101</sup> however, not all studies agree.<sup>80,98</sup> Myopic and hyperopic adolescent eyes also exhibit more positive and negative levels of secondary spherical aberration ( $Z_6^0$ ), respectively,<sup>99</sup> inversely associated with primary spherical aberration ( $Z_4^0$ ). This inverse association, where negative secondary spherical aberration ( $Z_6^0$ ) and positive primary spherical aberration ( $Z_4^0$ ) exist, produces greater relative positive refractive power in the periphery of the pupil and vice versa, which suggests that myopic and hyperopic eyes experience more relative negative and positive refractive power in the periphery of the pupil, respectively (Figure 4). Some researchers have found that myopic eyes exhibit higher RMS values for vertical coma ( $Z_3^{-1}$ ), horizontal coma ( $Z_3^1$ ), and third order aberrations than emmetropic<sup>89</sup> and hyperopic<sup>95</sup> eyes; however, the majority of studies report minimal differences between refractive error groups.<sup>80,98,99,101</sup> Interestingly, Zhang et al.<sup>96</sup> reported that myopes with faster progression rates exhibited more negative primary vertical coma ( $Z_3^{-1}$ ) than stable myopes.

Differences in off-axis HOAs have been reported between refractive error groups in adolescents (11 to 14 years).<sup>88</sup> Myopic eyes tend to display greater levels of HOA, third order and coma RMS than hyperopic eyes in the temporal visual field, while hyperopes exhibit higher amounts of fourth order and spherical aberration RMS than myopes. Philip et al.<sup>88</sup> also found that primary vertical coma ( $Z_3^{-1}$ ) was more negative in myopic eyes than hyperopic eyes in the temporal field, while myopes displayed more positive primary horizontal coma ( $Z_3^1$ ) than hyperopes in the inferior visual field. Like the findings for off-axis primary spherical

aberration ( $Z_4^0$ ) in young adults,<sup>86,87</sup> hyperopic eyes showed more positive values than emmetropic and myopic eyes at all observed eccentricities.<sup>88</sup>

The lack of consistency concerning on-axis HOA profiles between refractive error groups demonstrates the potential variability in the measurement of HOAs across individuals, different ethnicities and ages. Cross-sectional cohort comparison studies do not control for this individual variation and therefore longitudinal assessments of HOAs associated with changes in refractive error during childhood (repeated measures of the same children over time) may provide further insights into the relationship between HOAs and refractive error.

### Longitudinal studies

Few studies have longitudinally examined HOAs and refraction (Table 2). Philip et al.<sup>88,102</sup> tracked refractive and HOA changes over approximately five years in Australian adolescents of mixed ethnicity. Emmetropic subjects who underwent a myopic shift of at least 0.50 D during the study, exhibited a reduction in third order and coma RMS,<sup>102</sup> while an increase was reported in subjects with stable refractions.<sup>88</sup> The emmetropes,<sup>102</sup> myopes and hyperopes<sup>88</sup> who underwent a myopic shift also showed a significant negative shift in primary spherical aberration ( $Z_4^0$ ) and a reduction in fourth order and spherical aberration RMS, while the opposite was found in subjects with stable refractions.<sup>88,102</sup> Additionally, a moderate, statistically significant relationship ( $r = 0.49$ ,  $p < 0.001$ ) was observed between the changes in spherical equivalent refraction and primary spherical aberration ( $Z_4^0$ ), after adjusting for age, gender and ethnicity, whereby a myopic shift was associated with a shift toward negative primary spherical aberration ( $Z_4^0$ ).<sup>102</sup> Philip et al.<sup>88</sup> also reported small changes in off-axis primary horizontal coma ( $Z_3^1$ ) in the nasal and temporal fields of myopes, emmetropes and hyperopes who underwent a myopic shift, becoming more negative and positive, respectively. This corresponded with increases in third order, coma and HOA RMS in both horizontal peripheral locations in these subjects.

Lau et al.<sup>61</sup> reported higher spherical aberration and HOA RMS values in Hong Kong children who underwent slower axial eye growth, after controlling for factors known to affect axial elongation such as age, gender, and baseline refractive error. Reduced axial elongation was also

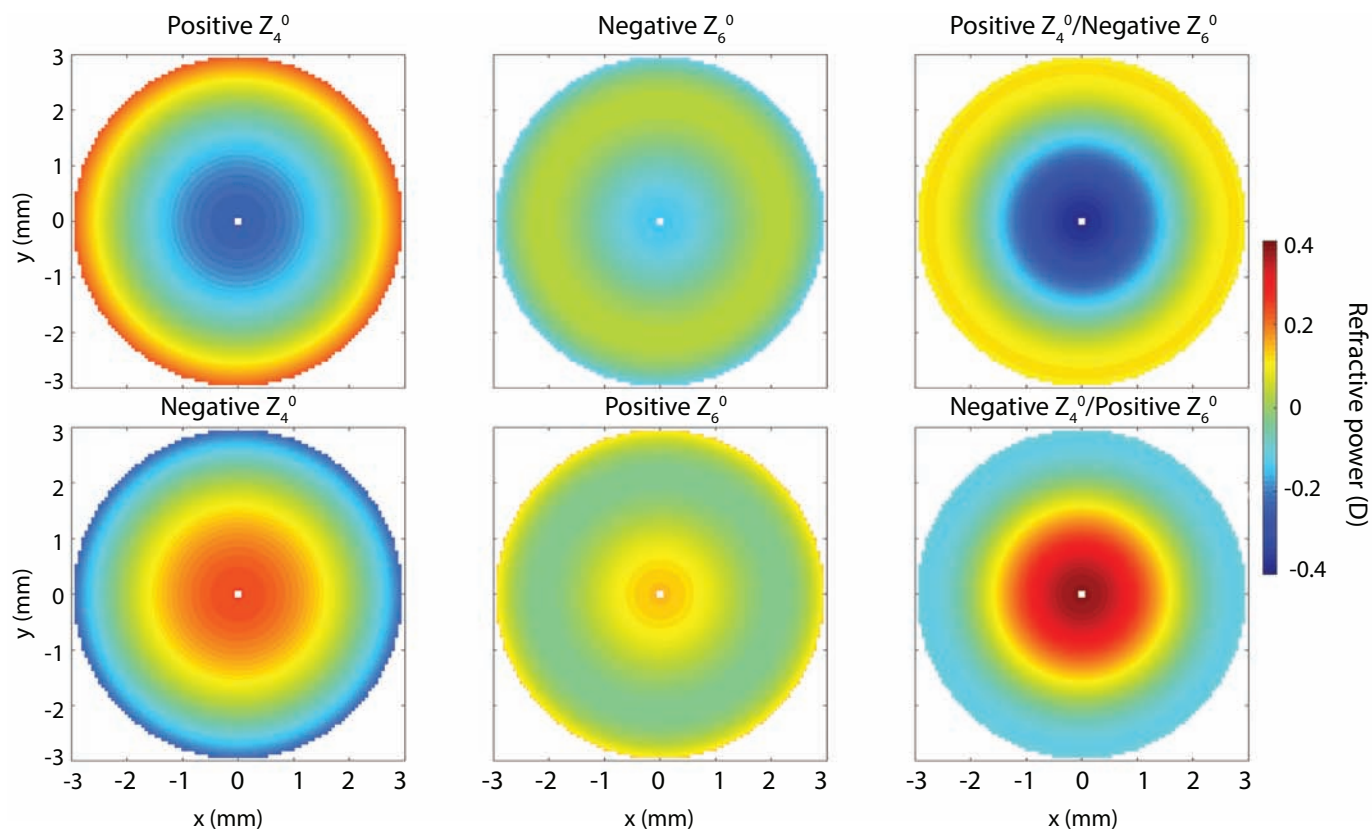


**Figure 4. Refractive power maps generated for a 6 mm pupil demonstrating the oppositely signed combinations of  $\pm 0.08 \mu\text{m}$  primary spherical aberration ( $Z_4^0$ ) and  $\pm 0.02 \mu\text{m}$  secondary spherical aberration ( $Z_6^0$ ). Note that the combination of positive primary spherical aberration ( $Z_4^0$ ) and negative secondary spherical aberration ( $Z_6^0$ ) results in more relative positive refractive power toward the pupil margin, whereas the opposite occurs for the counter-scenario.**

associated with less positive oblique trefoil ( $Z_3^2$ ), more positive primary trefoil ( $Z_3^{-3}$ ) and more positive spherical aberration ( $Z_4^0$ ), with each  $0.1 \mu\text{m}$  increment of each term associated with  $\sim 0.13$ ,  $0.11$  and  $0.11 \text{mm}$  difference in axial eye growth per year, respectively.<sup>61</sup> Interestingly, given the partial compensatory effect of anterior corneal HOAs by internal HOAs,<sup>68</sup> Hiraoka et al.<sup>103</sup> found that myopia progression and axial elongation correlate independently with many corneal HOAs, and more strongly than ocular HOAs in Japanese children. Corneal HOAs exhibited strong positive and negative correlations with refractive error shift and change in axial length, respectively, indicating that increased corneal HOAs (baseline measurement or averaged across the study) were associated with reduced myopia progression and axial elongation. The strongest correlations for individual corneal HOA terms were observed for primary vertical coma ( $Z_3^{-1}$ ), horizontal coma ( $Z_3^1$ ) and

spherical aberration ( $Z_4^0$ ). Primary vertical coma ( $Z_3^{-1}$ ) and spherical aberration ( $Z_4^0$ ) exhibited a positive and negative correlation with the change in refractive error and axial length, respectively, while the opposite trends were observed for corneal primary horizontal coma ( $Z_3^1$ ). Both ocular coma terms followed the same correlations as the corneal coma terms, but the positive correlation between ocular primary spherical aberration ( $Z_4^0$ ) and refractive change was not significant.

Greater levels of HOAs and reduced retinal image quality in myopic eyes is not a universal finding. McLellan et al.<sup>104</sup> showed that HOAs measured in myopic adults (mean age 41 years) consistently degraded the modulation transfer function less than randomly generated HOA profiles, which suggests that HOA terms are likely to be interdependent and interact to minimise the overall effect on image quality in myopic eyes. In young adults (19 to 28 years), Collins

et al.<sup>18</sup> reported greater dispersion of the point spread function, and a decreased modulation transfer function and Visual Strehl ratio in progressing myopes compared with emmetropes, at both far and near distances. Conversely, a cross-sectional study of children (nine to 10 years) and adolescents (15 to 16 years) found minimal differences in the Visual Strehl ratio between myopes, hyperopes and emmetropes; however, subject numbers varied considerably between the refractive groups.<sup>98</sup> In a cohort of emmetropic adolescents (16 to 19 years), Philip et al.<sup>102</sup> showed that the Visual Strehl ratio reduced significantly during the five-year study period, and this reduction was larger in subjects who became myopic; however, there was no difference in the Visual Strehl ratio between refractive groups at the initial visit. The inconsistent findings of these studies suggest that any differences in retinal image quality observed between refractive error groups may be related to individual variability or methodological differences

Authors	Year	N	Initial age (years)	Duration (years)	Measurement technique	Accommodation control	PD (mm)	↑ MP	↓ MP	↑ AE	↓ AE
Philip et al. <sup>102</sup>	2014	176 E	11.24–13.77	5	Hartman-Shack	1% Cyclopentolate; 1% Tropicamide	5	↓ initial 3 <sup>rd</sup> order; ↓ initial coma; ↓ Z <sub>4</sub> <sup>0</sup> (+ve); ↑ 3 <sup>rd</sup> order; ↓ 4 <sup>th</sup> order; ↑ coma; ↓ SA	↑ initial 3 <sup>rd</sup> order; ↑ initial coma; ↑ Z <sub>3</sub> <sup>-1</sup> (-ve); ↑ Z <sub>4</sub> <sup>0</sup> (+ve); ↑ 4 <sup>th</sup> order; ↑ SA	NR	NR
Hiraoka et al. <sup>103</sup>	2017	64 M	6–12	2	Hartman-Shack (ocular); Placido disc (corneal)	1% Cyclopentolate (3 drops)	6	↓ corneal HOA; ↓ corneal and ocular Z <sub>3</sub> <sup>-1</sup> ; ↑ corneal and ocular Z <sub>1</sub> <sup>1</sup> ; ↓ corneal Z <sub>4</sub> <sup>0</sup>	↑ corneal HOA; ↑ corneal and ocular Z <sub>3</sub> <sup>-1</sup> ; ↑ corneal and ocular Z <sub>1</sub> <sup>1</sup> ; ↓ corneal and ocular Z <sub>4</sub> <sup>0</sup>	↓ corneal HOA; ↓ corneal and ocular Z <sub>3</sub> <sup>-1</sup> ; ↓ corneal and ocular Z <sub>1</sub> <sup>1</sup> ; ↓ corneal and ocular Z <sub>4</sub> <sup>0</sup>	↑ corneal HOA; ↑ corneal and ocular Z <sub>3</sub> <sup>-1</sup> ; ↑ corneal and ocular Z <sub>1</sub> <sup>1</sup> ; ↑ corneal and ocular Z <sub>4</sub> <sup>0</sup>
Lau et al. <sup>61</sup>	2018	113 M; 24 H	6.1–12.6	2	Hartman-Shack	1% Cyclopentolate; 1% Tropicamide	6	NR	NR	↓ HOA; ↓ SA; ↓ Z <sub>3</sub> <sup>-3</sup> (+ve); ↓ Z <sub>4</sub> <sup>0</sup> (+ve); ↓ Z <sub>3</sub> <sup>-3</sup> (-ve)	↑ HOA; ↑ SA; ↑ Z <sub>3</sub> <sup>-3</sup> (+ve); ↑ Z <sub>4</sub> <sup>0</sup> (+ve); ↑ Z <sub>3</sub> <sup>-3</sup> (-ve)
Philip et al. <sup>88</sup>	2018	91 M; 166 E; 361 H	11.09–13.9	5	Hartman-Shack	1% Cyclopentolate; 1% Tropicamide	5	↑ 3 <sup>rd</sup> order (E); ↑ coma (E); ↓ 4 <sup>th</sup> order (M, E, H); ↓ SA (M, E, H)	↑ 4 <sup>th</sup> order (E, H); ↑ SA (E, H)	NR	NR

Coma: coma RMS, E: emmetropia, H: hyperopia, HOA: higher order aberrations RMS, M: myopia, NR: not reported, PD: pupil diameter used for analysis, SA: spherical aberration RMS, Z<sub>4</sub><sup>0</sup>: primary spherical aberration, Z<sub>3</sub><sup>-1</sup>: primary vertical coma, Z<sub>3</sub><sup>-3</sup>: primary horizontal coma, +ve: positive, -ve: negative, ↑: increase, ↓: decrease.

**Table 2. Summary of longitudinal studies examining temporal associations between on-axis higher order aberrations, myopia progression (MP) and axial elongation (AE)**

rather than a cause of refractive error development, therefore further longitudinal studies are required.

Cross-sectional cohort and longitudinal studies have demonstrated that HOAs such as coma (Z<sub>3</sub><sup>-1</sup> and Z<sub>3</sub><sup>1</sup>), vertical trefoil (Z<sub>3</sub><sup>-3</sup>) and primary spherical aberration (Z<sub>4</sub><sup>0</sup>) show relatively consistent trends between refractive error groups, and temporal variations of these terms are associated with changes in refraction and axial length, respectively. This indicates that the composition of the HOA profile (the combination or interaction of the terms) may play a more significant role in the modulation of eye growth and refractive error development rather than the magnitude of individual Zernike term co-efficients. These HOAs may provide image cues to the retina to enable the eye to rapidly and accurately respond to different visual stimuli. Wilson et al.<sup>105</sup> reported that only even, not odd, radial order HOA terms (such as fourth and sixth order), provide odd-error cues within the retinal image which may enable the correct identification of the sign of defocus.

Additionally, the accommodative response of the eye appears to be driven by the detection of optical vergence to guide direction and magnitude;<sup>106</sup> therefore, it is likely that the retina can detect relative optical vergence variations across the pupil. For example, in an eye with no HOAs, light rays from the centre and the periphery of the pupil would focus perfectly at the same retinal location; however, in the same eye with the addition of positive or negative primary spherical aberration (Z<sub>4</sub><sup>0</sup>), the peripheral light rays would be relatively convergent or divergent to the central light ray, respectively. Horizontal and vertical meridional retinal shape are non-identical<sup>107</sup> and therefore, asymmetric terms such as coma or trefoil may also produce relatively convergent or divergent light rays through different pupil positions which may be detectable by the retina.

### HOAs and abnormal visual development: anisometropia and amblyopia

#### Non-amblyopic anisometropia

Given that the fellow eyes of an individual typically display a high degree of interocular symmetry for both spherical and astigmatic refractive error (isometropia),<sup>108</sup> non-amblyopic anisometropia is a unique ocular condition in which the two eyes experience

a similar environment but develop markedly different refractive errors in the absence of ocular pathology or an amblyogenic factor, typically due to asymmetric axial eye growth.<sup>109</sup> Interestingly, the majority of HOAs are highly correlated between the eyes of both isometropes<sup>16,70,89,110,111</sup> and anisometropes.<sup>110,112,113</sup> Tian et al.<sup>112</sup> found that the more myopic eye of non-amblyopic myopic anisometropes exhibited more positive primary spherical aberration ( $Z_4^0$ ) than the fellow, less myopic eye, and suggested that this may simply be a consequence of the eye being more myopic, rather than an underlying cause of excessive eye growth. Osuagwu et al.<sup>111</sup> examined off-axis HOAs and conversely found that the less myopic eye of non-amblyopic myopic anisometropes exhibited more positive primary spherical aberration ( $Z_4^0$ ) on average across the visual field; however, there was negligible interocular difference in the rate of change with increasing eccentricity. Primary vertical coma ( $Z_3^{-1}$ ) was found to increase more rapidly from the superior to inferior visual field in the more myopic eye; however, the rate of change for primary horizontal coma ( $Z_3^1$ ) across the horizontal meridian exhibited no significant interocular difference.<sup>111</sup> These cross-sectional findings do not provide clear and consistent evidence of a solitary role for on- or off-axis HOAs in the development of non-amblyopic anisometropia and longitudinal studies are required to elucidate potential underlying mechanisms.

## Amblyopia

Unilateral amblyopia results from a significant interocular difference in image quality or visual experience during early life, typically hyperopic anisometropia,<sup>114</sup> strabismus or form deprivation.<sup>115</sup> In children, significant differences in HOAs have generally not been observed between the amblyopic and the non-amblyopic fellow eye in monocular amblyopes, whether the cause of their amblyopia is strabismic<sup>95</sup> or refractive.<sup>116</sup> In 'idiopathic' amblyopia (reduced visual acuity with no amblyogenic factor), while there was no interocular difference in the means of individual terms, interocular differences were observed in the composition of the HOA profile and the interaction between individual terms.<sup>117</sup> Vincent et al.<sup>118</sup> reported no difference in total ocular HOA RMS between the fellow eyes of adult refractive amblyopes; however, the

amblyopic eye of strabismic amblyopes, which were typically more hyperopic, exhibited a greater amount of trefoil ( $Z_3^3$ ) than the fellow non-amblyopic eyes. A weak correlation was observed between the interocular difference in primary spherical aberration ( $Z_4^0$ ) and the magnitudes of anisometropia and amblyopia, where the more hyperopic, or more amblyopic eye, had more positive primary spherical aberration ( $Z_4^0$ ). The latter finding supports the typical trend of primary spherical aberration ( $Z_4^0$ ) to be less positive (or more negative) with increasing levels of myopia. However, these cross-sectional contralateral studies do not provide convincing evidence that HOAs underpin the development of refractive error, anisometropia or amblyopia and suggest that additional factors are involved.

## HOAs during near work and accommodation

Near work has long been considered an environmental risk factor for myopia development;<sup>119,120</sup> however, this association remains contested.<sup>121,122</sup> Changes in the magnitude of HOAs have been reported to occur during near work and accommodation, which provides a potential mechanism for the reported link between myopia development and near work.

Buehren et al.<sup>123</sup> demonstrated that a two-hour reading task increased HOA RMS in both emmetropes and myopes. Myopes exhibited greater HOA RMS at both distance and near, and a larger increase in HOA RMS from distance to near fixation. Correspondingly, the increase in HOA RMS associated with the near task resulted in a reduction in retinal image quality, with myopic eyes exhibiting poorer retinal image quality at distance and near than emmetropes, and undergoing a greater reduction at near than emmetropes.<sup>18</sup> Given that near work typically involves accommodation, downgaze and convergence, it is of interest to understand the changes in HOAs that occur independently with each aspect of near work.

For a fixed pupil diameter, HOA RMS consistently increases with greater accommodation demands,<sup>124,125</sup> although some have found this occurs only with demands above 3 D.<sup>126-129</sup> The major consistent change in HOAs that occurs during accommodation is a decrease in primary spherical aberration ( $Z_4^0$ ), becoming less positive or more

negative.<sup>124-126,129-132</sup> Secondary spherical aberration ( $Z_6^0$ ) also undergoes a relatively small change,<sup>124,132</sup> but is less consistent with respect to the direction of change. Consistent with HOA differences between myopes and emmetropes, myopes exhibit less positive, or more negative, fourth order aberrations than emmetropes, and show larger fourth order aberration changes than emmetropes during accommodation.<sup>131</sup>

In a study of off-axis HOAs during accommodation, a significant interaction was reported between accommodation and eccentricity for all third and fourth order aberrations except primary trefoil ( $Z_3^{-3}$ ), secondary astigmatism ( $Z_4^{-2}$ ) and primary spherical aberration ( $Z_4^0$ ).<sup>84</sup> This suggests that accommodation produces a change in the variation of these HOAs across the visual field; however, Mathur et al.<sup>84</sup> reported these off-axis variations were of minimal magnitude except for primary horizontal coma ( $Z_3^1$ ) and spherical aberration ( $Z_4^0$ ) which became more positive and negative with accommodation, respectively, averaged across the visual field.

The on-axis HOA profile also varies during downgaze, with most of the change arising from a negative shift in primary trefoil ( $Z_3^{-3}$ ) and positive shifts in secondary spherical aberration ( $Z_6^0$ ) and primary ( $Z_3^{-1}$ ) and secondary vertical coma ( $Z_5^{-1}$ ), although significant changes also occur in secondary astigmatism ( $Z_4^{-2}$  and  $Z_4^2$ ), tetrafoil ( $Z_4^4$ ) and pentafoil ( $Z_5^{-5}$ ).<sup>132</sup> Ghosh et al.<sup>132</sup> also showed that accommodation during downgaze produced a greater negative shift in primary spherical aberration ( $Z_4^0$ ) and primary vertical coma ( $Z_3^{-1}$ ), and a greater positive shift in secondary spherical aberration ( $Z_6^0$ ) than during accommodation alone. Given these findings, and that anterior corneal HOAs<sup>133</sup> and elevation<sup>134</sup> remain stable during accommodation in primary gaze, the changes in terms such as primary vertical coma ( $Z_3^{-1}$ ) and trefoil ( $Z_3^{-3}$ ) during downgaze (and near work) are likely associated with lid-induced corneal deformation at the superior pupil margin,<sup>123,135,136</sup> while the variations in primary ( $Z_4^0$ ) and secondary ( $Z_6^0$ ) spherical aberration are likely the result of accommodation.

Subsequent studies have confirmed that typical accommodation demands (2-3 D) produce poorer retinal image quality than a 0 D accommodation demand for a fixed pupil

diameter<sup>124</sup> and Buehren et al.<sup>137</sup> also reported similar results during accommodation for a natural pupil. These findings indicate that with normal levels of accommodation during near work, even with natural accommodation-induced pupil miosis, HOAs increase and retinal image quality is reduced. Long periods of exposure to reduced retinal image quality as a result of increased HOAs or altered HOA profile during prolonged near work may therefore provide a stimulus within the retinal image to which the eye responds by increasing its axial growth.

The combination of different HOA terms can cause different effects on the quality of the retinal image. Thibos et al.<sup>138</sup> demonstrated that the combination of hyperopic defocus and negative primary spherical aberration ( $Z_4^0$ ) produces a retinal image of poorer quality than if positive primary spherical aberration ( $Z_4^0$ ) was present with hyperopic defocus. Given that myopes have been shown to exhibit higher accommodative lags<sup>139,140</sup> (producing hyperopic defocus), and primary spherical aberration ( $Z_4^0$ ) typically becomes negative with accommodation, this combination of optical changes may result in reduced retinal image quality and provide a stimulus for ocular growth. Buehren et al.<sup>141</sup> also modelled different combinations of the terms that most consistently vary with near work; positive vertical trefoil ( $Z_3^{-3}$ ), negative primary vertical coma ( $Z_3^{-1}$ ) and negative primary spherical aberration ( $Z_4^0$ ). The sphero-cylindrical correction that minimised the wavefront error and maximised retinal image quality produced by the typical combination of these terms was a low hyperopic, against-the-rule astigmatic correction. This indicates that the change in the wavefront generated during near work may mimic hyperopic defocus and provide a stimulus to the retina that promotes myopic eye growth (Figure 5).

## HOAs and myopia control interventions

The use of optical and pharmacological interventions in clinical practice to prevent or slow the progression of myopia have become more widespread in recent years;<sup>142</sup> however, the underlying mechanisms of these treatments are not fully understood. Given that most myopia control treatments alter the quality of the

retinal image, changes in the profile or magnitude of HOAs associated with these interventions may influence axial eye growth and myopia progression.

### Anti-muscarinic agents

Arguably the myopia intervention that has shown the greatest efficacy in animals<sup>143</sup> and humans<sup>144,145</sup> is the non-selective anti-muscarinic pharmacological agent, atropine. Atropine reduces myopia progression in a dose-dependent manner,<sup>144-146</sup> although, questions remain about its efficacy in slowing axial elongation, particularly for lower concentrations.<sup>146,147</sup> Given the cycloplegic effect of atropine in humans,<sup>148</sup> its mechanism of myopia control was originally thought to be related to changes in the accommodative system.<sup>149</sup> However, animal studies suggest that anti-muscarinic agents influence growth via an alternative, non-accommodative mechanism.<sup>143,149</sup> While yet to be confirmed in humans, evidence from the chick suggests that atropine binds to receptors within the retina (possibly a combination of muscarinic and non-muscarinic)<sup>149</sup> and triggers a signalling cascade to the sclera via the retinal pigment epithelium and choroid, mediated by nitric oxide.<sup>150</sup> However, the cycloplegic and mydriatic effects of atropine, which change the pupil diameter and the crystalline lens shape and thickness, alter the ocular HOA profile and may provide an optical signal which influences eye growth.

The twice-daily instillation of 1% atropine eye drops for one week in hyperopic Japanese children (three to 12 years) produced a small but significant increase of 0.044, 0.032 and 0.023  $\mu\text{m}$  in ocular HOA, coma-like and spherical-like RMS, respectively, with no demonstrable change in corneal HOAs.<sup>151</sup> Both primary horizontal coma ( $Z_3^1$ ) and spherical aberration ( $Z_4^0$ ) approximately doubled following the use of atropine, becoming more positive; however, given that the HOAs were analysed over the same fixed pupil size (6 mm) before and after atropine, the authors suggested that these changes were likely the result of the 1.18 D hyperopic shift.<sup>151</sup>

Although Hiraoka et al.<sup>151</sup> did not report on the changes in pupil size due to 1% atropine, post-hoc analysis indicated that if pupil size increased from 4 to 6 mm, HOA RMS would have increased by  $\sim 0.28 \mu\text{m}$ . Chia et al.<sup>152</sup> reported a change in photopic pupil size with 0.01%, 0.1% and 0.5% atropine from a baseline of  $\sim 4.7$  mm to 5.8, 7.4 and

7.9 mm, respectively. Based on the polynomial regression reported by Salmon and van de Pol,<sup>153</sup> HOA RMS would have increased by  $\sim 0.14$ , 0.43 and 0.54  $\mu\text{m}$  due to the pupil dilation associated with 0.01%, 0.1% and 0.5% atropine, respectively. Therefore, the change in HOA RMS resulting from pupil mydriasis is significantly greater than the change in HOAs resulting from the cycloplegic hyperopic shift. This suggests that if the effect of atropine on eye growth is mediated via a mechanism involving HOAs, it may be the result of the increased pupil size rather than the changes in HOAs associated with the hyperopic shift from cycloplegia.

The effect of other concentrations of atropine on HOAs have not been examined, although similar findings have been demonstrated following the instillation of other topical anti-muscarinic agents. In similarly aged myopic children, an increase in HOA and spherical-like RMS of 0.025 and 0.014  $\mu\text{m}$  for a 6 mm pupil, respectively, was observed following the instillation of 1% cyclopentolate eye drops.<sup>154</sup> Additionally, a positive shift in ocular primary spherical aberration ( $Z_4^0$ ) occurred coincidentally with a 0.50 D hyperopic shift, but these changes were of smaller magnitude compared to atropine and there was no change observed in coma-like RMS or primary horizontal coma ( $Z_3^1$ ).<sup>154</sup> Interestingly, 0.5% tropicamide eye drops produced a small increase of 0.017  $\mu\text{m}$  in total coma but negligible changes in HOA and spherical aberration RMS;<sup>155</sup> however, given the post-instillation interval prior to measurement was only five minutes in this study, the full manifestation of optical changes may not have been observed since maximal cycloplegia due to tropicamide occurs approximately 20 minutes post-instillation.<sup>148</sup> One per cent cyclopentolate and 0.5% tropicamide have been shown to have some<sup>156</sup> and negligible<sup>157</sup> effect in slowing myopia progression, respectively. The magnitude of the changes in HOAs with cyclopentolate and tropicamide are smaller than with atropine; therefore, this may contribute to the differences observed in their myopia control efficacy. Like atropine, the mydriasis from these pharmacological agents are likely to influence HOAs more significantly than the hyperopic shift associated with cycloplegia. Longitudinal studies are required to examine a potential link between the changes in HOAs from anti-muscarinic agents and myopia control.



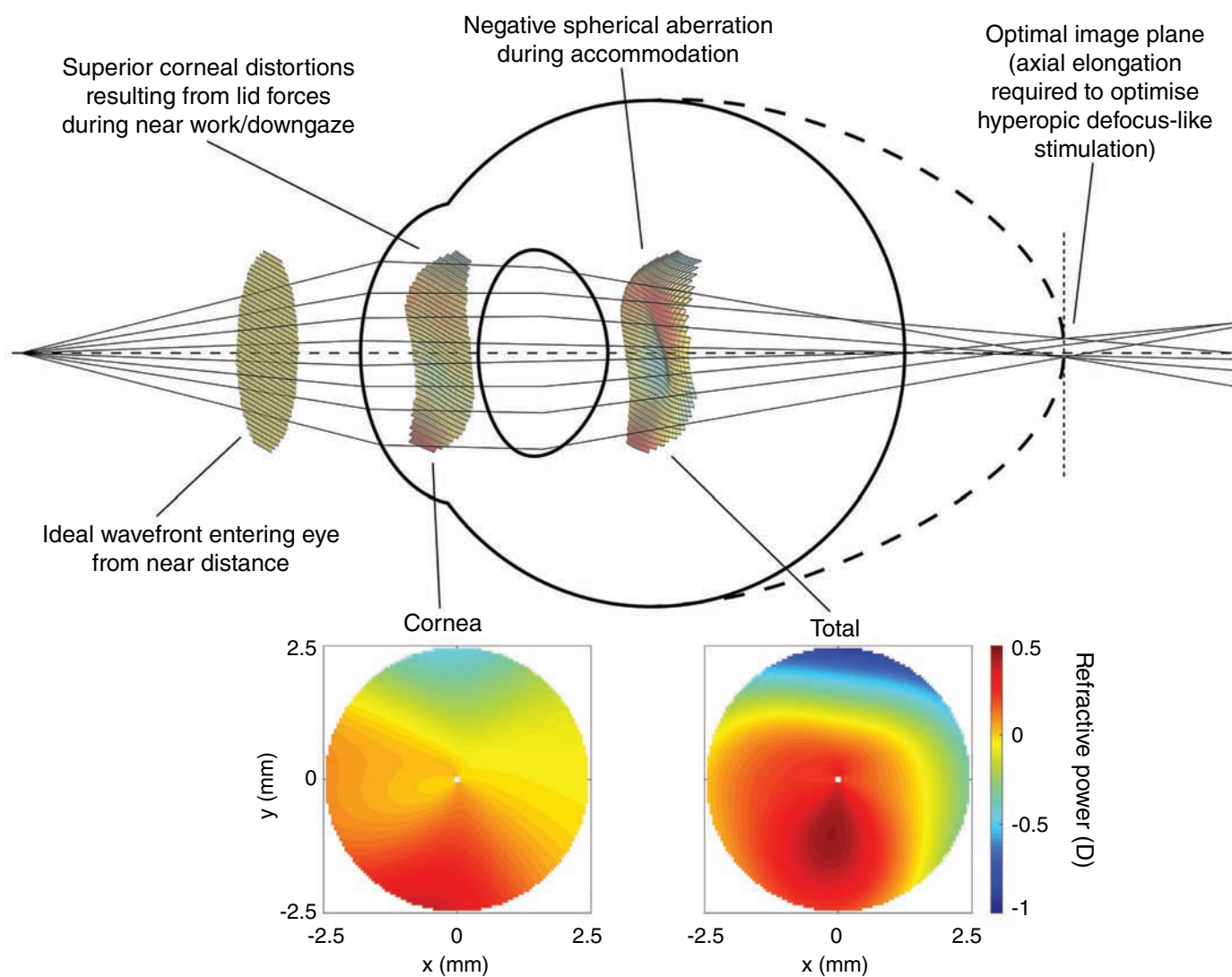


**Figure 5. Schematic of a potential mechanism between near work and myopia development involving higher order aberrations (HOAs). The increase in positive trefoil ( $Z_3^{-3}$ ) and negative primary vertical coma ( $Z_3^{-1}$ ) from lid-induced superior corneal distortion during downgaze, and increase in accommodation-induced negative primary spherical aberration ( $Z_4^0$ ) from the change in the crystalline lens results in rays from the edge of the entrance pupil exhibiting negative vergence relative to paraxial pupil rays. These rays produce a plane of best focus (optimal retinal image) posterior to the retina, emulating hyperopic defocus which may encourage axial eye growth. Note the increase in negative refractive power, particularly in the superior third of the pupil in the included corneal and total ocular refractive power maps (generated from third and fourth order HOAs for a 5 mm pupil). Figure and data adapted from Buehren et al.<sup>123,135,141</sup>**

### Spectacle lenses: bifocal and progressive addition lenses

Several optical interventions, including spectacles and contact lenses, have been developed and studied for their potential ability to slow the progression of myopia. Of the spectacle lens designs, the most promising have been progressive addition and bifocal spectacle lenses.<sup>145</sup> In comparison to single-vision designs, progressive addition lenses

reduced myopia progression over three years by approximately 14 per cent,<sup>158</sup> or 25 per cent in those with near esophoria and a lag of accommodation at near.<sup>159</sup> Bifocal lenses, with and without base-in prism in the near segment, have demonstrated a greater level of myopia control over three years, with a reduction in myopia progression of approximately 40 per cent and 50 per cent, respectively.<sup>160</sup>

Near addition lenses were originally thought to act by reducing the near accommodation demand.<sup>158-161</sup> Since the near addition zones induce localised superior relative peripheral retinal myopic defocus,<sup>162,163</sup> and the relative superior peripheral refractive shift was found to be associated with a reduction in the rate of central myopic refractive progression of a one-year period in progressive addition lens

wearers, this may be a possible alternative mechanism by which these lenses slow myopia progression.<sup>163</sup> Progressive addition and bifocal spectacle lenses will vary the optics of the eye as a result of a change in accommodation response from the near addition<sup>161,164</sup> as well as the variable optics in the periphery of the lenses.

It is currently unknown what changes occur to the HOA profile when looking through the different segments of a bifocal lens; however, the intermediate and near zones of a progressive lens produce an increase in HOA RMS of 0.119 and 0.071  $\mu\text{m}$ , respectively, relative to the distance area (for a 5 mm pupil).<sup>165</sup> Predominantly, vertical coma ( $Z_3^{-1}$ ) and trefoil ( $Z_3^{-3}$ ) exhibit changes, particularly in the lens periphery.<sup>166,167</sup> While the optics vary substantially across a progressive addition lens, it is unknown what effect this may have on the HOAs of the eye or how this may affect eye growth and refractive error development, since pupil size and accommodation during lens wear will also vary and may influence retinal image quality.

## Orthokeratology

Some contact lens designs have shown significantly greater myopia control efficacy than spectacle lenses. Overnight wear of rigid reverse-geometry lens designs, or orthokeratology, produces central corneal flattening and mid-peripheral corneal steepening. Numerous studies<sup>168–170</sup> have demonstrated a significant and repeatable slowing of axial elongation in children by approximately 45 per cent on average with orthokeratology.<sup>145</sup>

Orthokeratology produces a significant increase in on-axis HOAs, even after one night of wear.<sup>171</sup> Following seven nights of treatment, the increase in corneal HOAs ranges from 0.199  $\mu\text{m}$  over a 5 mm pupil,<sup>172</sup> to 0.71  $\mu\text{m}$  over a 6 mm pupil.<sup>173</sup> Additionally, the increase in ocular HOAs has been reported to be 0.175  $\mu\text{m}$  over a 5 mm pupil<sup>172</sup> to 0.63  $\mu\text{m}$  over a 6.5 mm pupil,<sup>174</sup> with the changes in ocular and corneal HOAs typically stabilising after 30 nights of lens wear.<sup>174</sup> The predominant changes in HOAs are positive shifts in corneal<sup>172,173</sup> and ocular<sup>171–174</sup> primary spherical aberration ( $Z_4^0$ ), and corneal<sup>173</sup> and ocular<sup>171,173,174</sup> primary horizontal coma ( $Z_3^1$ ). In addition, changes in corneal primary vertical coma ( $Z_3^{-1}$ ) have been reported.<sup>175,176</sup> The change

in primary spherical aberration ( $Z_4^0$ ) is thought to be the result of mid-peripheral corneal steepening,<sup>173</sup> and comatic changes are likely the result of lens, and therefore treatment zone, decentration.<sup>173,177</sup> While both the corneal and ocular HOAs increase, the corneal changes are substantially greater<sup>172,173</sup> which suggests some internal optical adaptation in response to the corneal modifications over time, perhaps due to an altered accommodative response.<sup>178</sup>

Significant changes in off-axis HOAs also occur as a result of orthokeratology treatment. On average, orthokeratology produces a significant increase in the magnitude and peripheral rate of change of HOA RMS across the visual field.<sup>179</sup> Typically, minimal variation in primary spherical aberration ( $Z_4^0$ ) is observed across the visual field; however, Mathur et al.<sup>179</sup> demonstrated a significant positive shift on average following orthokeratology, with one subject exhibiting a quadratic variation (more positive at the centre of the visual field) and another subject showing an overall positive shift along the horizontal meridian. Most notably, vertical coma increased from superior to inferior eccentricities and horizontal coma increased from nasal to temporal prior to treatment, which reversed post-orthokeratology.<sup>179</sup>

Hiraoka et al.<sup>60</sup> reported that the change in corneal coma-like aberrations following one year of orthokeratology in Japanese children exhibited a moderate negative linear correlation with axial elongation ( $r = -0.46$ ,  $p = 0.0003$ ), whereby less axial eye growth was associated with a larger change in coma-like aberrations. Conversely, Santodomingo-Rubido et al.<sup>175</sup> found no significant correlation between corneal HOA changes and axial elongation after three and 24 months of orthokeratology in European children. Chen et al.<sup>180</sup> found that a larger pupil size during orthokeratology treatment in Chinese children was associated with slower axial eye growth than a smaller pupil, and suggested that this is due to a greater relative peripheral myopic shift. This change in peripheral refraction was confirmed with modelling by Faria-Ribeiro et al.,<sup>181</sup> who also demonstrated that on- and off-axis HOAs, particularly primary horizontal coma ( $Z_3^1$ ) and primary spherical aberration ( $Z_4^0$ ), also increase with greater pupil size as a result of corneal topographical changes during orthokeratology. This finding may indicate that HOAs influence

the myopia control effect of orthokeratology; however, further longitudinal studies that examine the changes in on- and off-axis corneal and total ocular HOAs, pupil size and their association with eye growth before and during orthokeratology are required to provide further insights into a potential role for HOAs in the myopia control effect of orthokeratology.

## Soft contact lenses: multifocal and dual-focus

Soft contact lenses with modified refractive profiles have also shown significant efficacy in reducing myopia progression and axial eye growth. On average, multifocal and dual-focus lenses reduce myopia progression by approximately 30–50 per cent; however, there is significant inter-study variation as a result of lens design, study duration, and participant characteristics.<sup>182</sup> These lenses can be broadly categorised as multifocal or dual-focus lenses, according to how the optical profile of the lens varies across the optic zone. A multifocal or aspheric lens design provides a central zone of distance power with a progressive increase in positive power toward the edge of the optic zone. A dual-focus lens similarly has a central distance zone, surrounded by multiple concentric alternating zones of relative positive power and the central distance refraction. Given that single-vision spherical rigid<sup>183</sup> and soft contact lenses<sup>184</sup> have minimal effect on myopia progression, the modified optics must contribute to the myopia control effect of multifocal and dual-focus lenses.

The measured effect of different soft contact lens designs on HOAs are similar; however, there are some notable differences (Figure 6). Distance-centre multifocal contact lenses<sup>185,186</sup> produce significant positive shifts in primary spherical aberration ( $Z_4^0$ ) ranging from 0.125  $\mu\text{m}$  with a low (+1.50 D) to 0.245  $\mu\text{m}$  with a high add (+2.50 D) for a 5 mm pupil.<sup>185</sup> In addition, Fedtke et al.<sup>186</sup> demonstrated that primary horizontal coma ( $Z_3^1$ ) increases with multifocal contact lenses due to lens decentration. On-eye modelling of distance-centre dual-focus lenses through a schematic eye<sup>185</sup> showed that these lenses also shift primary spherical aberration ( $Z_4^0$ ) more positively when measured across a 3 mm pupil; however, primary spherical aberration ( $Z_4^0$ ) became negative when analysed over a 4 mm pupil and more so over a 5 mm pupil. This suggests that the concentric, alternating power profile of the

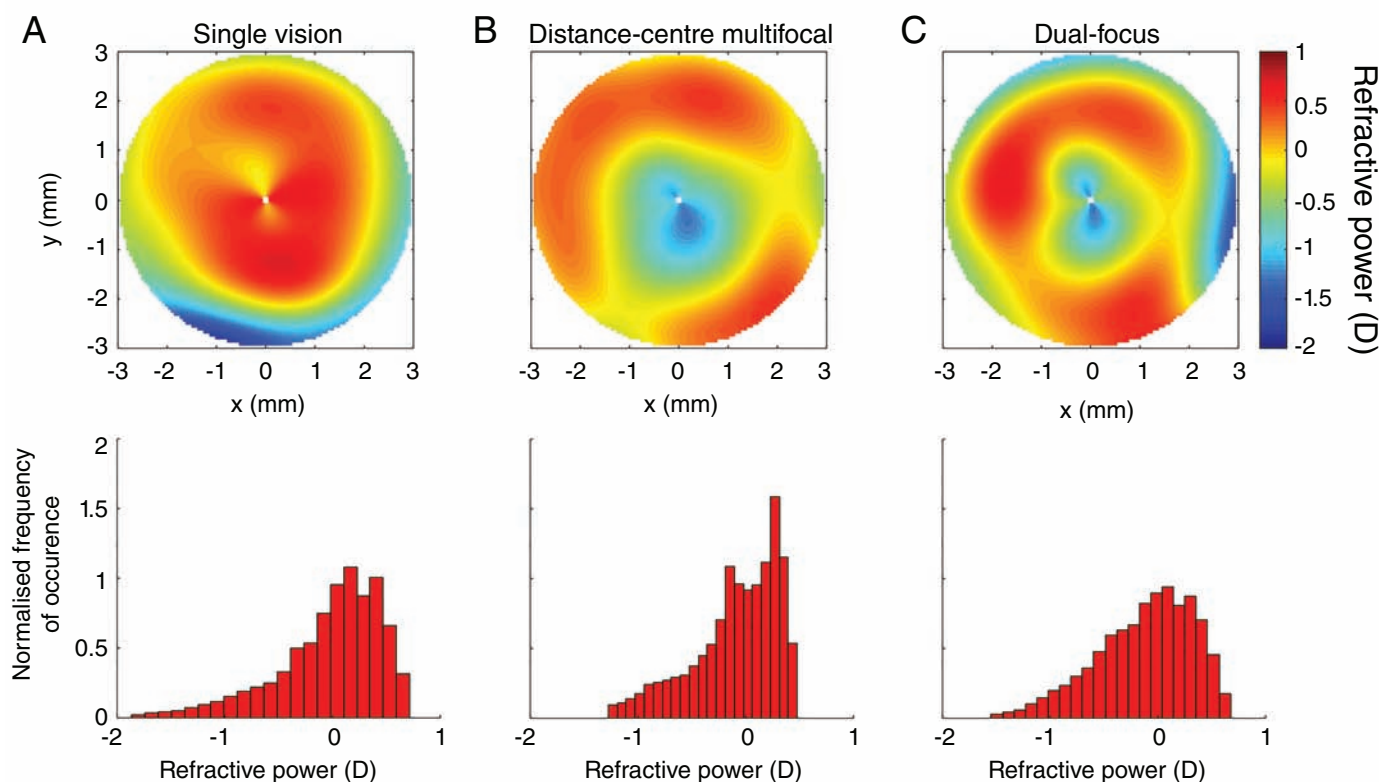


**Figure 6. Refractive power maps and associated histograms generated from the difference in ocular higher order aberrations (HOAs) (third to eighth order), measured using a commercial Hartmann-Shack wavefront sensor (COAS-HD, Wavefront Sciences) during soft contact lens wear compared to a bare eye condition in a moderately myopic young adult with normal vision for A: single-vision, B: distance-centre multifocal, and C: dual-focus soft contact lenses over a 6 mm pupil. Each lens had the same distance zone refractive power ( $-4.00$  D), with a  $+2.00$  D addition power in the distance-centre multifocal and dual-focus lens. Note that although the overall refractive power distribution is similar between the three lenses, the location of the refractive powers within the pupil plane varies between the three lenses, with an increase in positive refractive power in the mid-periphery and periphery of the dual-focus and distance-centre multifocal contact lenses compared to the single-vision lens, consistent with the differences in primary spherical aberration ( $Z_4^0$ ) between these lenses.**

lenses causes changes in HOAs that are markedly pupil-dependent. Multifocal contact lenses have been shown to affect the accommodation response;<sup>187,188</sup> however, the change in HOAs during accommodation with multifocal contact lens wear is yet to be examined. Future studies examining the change in HOAs during accommodation while wearing dual-focus and multifocal contact lenses may provide valuable insights into accommodative function during lens wear and potential mechanisms for myopia control.

A multifocal soft lens design by Sankaridurg et al.,<sup>189</sup> which incorporated  $+2.00$  D at  $4.5$  mm from the optical centre ( $9$  mm optic zone diameter), resulted in a reduction in myopia progression and axial elongation of approximately 34 per cent

over one year of wear in Chinese children. Fujikado et al.<sup>190</sup> reported on the myopia control effect of a multifocal soft contact lens which included  $+0.50$  D at  $4$  mm from the lens centre with a unique  $0.5$  mm nasal decentration of the optic zone. The decentration was designed to better align with, and produce more symmetrical optics across, the pupil, and produced a reduction in axial elongation of 47 per cent over 12 months in Japanese children but did not demonstrate a significant effect on refractive myopia progression. Another novel soft contact lens design incorporated positive spherical aberration ( $+0.175$   $\mu$ m for a  $5$  mm pupil, an amount purported by the authors to negate the accommodation-induced negative shift of spherical aberration) and resulted in a 65 per cent and 54 per cent

reduction in axial elongation and myopia progression in American children after six months, respectively; however, the efficacy reduced by 12 months to 39 per cent and 20 per cent, respectively.<sup>191</sup> A crossover study in New Zealand children examining the effect of a dual-focus lens design with  $+2.00$  D zones reported a reduction in myopia progression and axial elongation of 36 per cent and 50 per cent, respectively, over 10 months.<sup>192</sup> A recent two-year randomised, controlled trial in Chinese children<sup>193</sup> examined four novel contact lens designs, two of which incorporated peripheral positive refractive shifts of  $+1.50$  and  $+2.50$  D at  $3$  mm from the lens centre (similar to the commercial distance-centre multifocal), and two which manipulated the HOAs to improve retinal image quality at

and anterior to the retina, but diminished image quality for planes posterior to the retina. These lenses reduced myopia progression and axial elongation by ~30 per cent and 22 per cent, respectively, with negligible differences between the lens designs.<sup>193</sup>

Based on the difference in refractive power between the centre and periphery of the lenses, and calculations described by Carkeet et al.,<sup>80</sup> the lens designs by Fujikado et al.<sup>190</sup> and Sankaridurg et al.<sup>189</sup> would have produced approximately +0.055 µm of primary spherical aberration ( $Z_4^0$ ) over a 5 mm pupil, while the lens designs recently reported by Sankaridurg et al.<sup>193</sup> would have produced approximately +0.102 µm over a 5 mm pupil. The Anstice and Phillips<sup>192</sup> lens would have produced a greater level of positive spherical aberration (approximately +0.213 µm over a 4.78 mm pupil) and showed a greater reduction in myopia progression and axial elongation. This, together with the reports that commercially available soft multifocal and dual-focus lenses also produce positive spherical aberration, support a role for spherical aberration in the myopia control effect of these lenses, in what may be a magnitude-dependent manner.

## Consideration of pupil size

Although HOAs may influence refractive error development and the treatment effect of myopia control interventions via several potential mechanisms, an important consideration is the effect of pupil size. Most studies typically report HOAs over a fixed pupil size of 5 mm or greater; however, this may not be a realistic pupil size for children across a range of visual tasks and environments, and accommodation demands.<sup>194</sup> Pupil size is dynamic and influenced by several factors, including age,<sup>81,82</sup> ambient illumination,<sup>81,194</sup> and accommodation.<sup>137,194</sup> Exposure to photopic illumination conditions, such as bright outdoor lighting, is likely to reduce the pupil diameter to under 3–4 mm and may result in HOAs of negligible magnitude (diffraction-limited pupil size, or Marechal criterion). It is possible that the reduced HOAs in bright outdoor lighting may explain the reduced axial elongation in non-myopic and myopic children<sup>195</sup> as a result of the improved retinal image quality. Further research is required to examine pupil size dynamics and HOAs under varying levels and

combinations of illumination and accommodation, and how these factors may temporally interact to influence eye growth and refractive development.

## Conclusion

Several plausible theories based on retinal image quality and vergence cues suggest that HOAs may play a role in the development and control of refractive error and eye growth. However, animal studies suggest that changes in the HOA profile may simply be a consequence of experimentally induced refractive error rather than a cause. Likewise, variations in the HOA profile between myopic, hyperopic and emmetropic eyes in both children and adults have not produced clear, consistent, and reliable evidence to substantiate these theories. Characteristic temporal variations and changes during near work and accommodation provide some evidence of a role for certain HOAs, such as primary spherical aberration ( $Z_4^0$ ) coma ( $Z_3^{-1}$  and  $Z_3^1$ ) and trefoil ( $Z_3^{-3}$  and  $Z_3^3$ ); however, longitudinal studies examining the changes in HOAs during infancy, childhood and adolescence, and their association with refractive error and ocular structural development are required to comprehensively investigate these theories. Additionally, further longitudinal studies of the changes in HOAs before and after the introduction of various pharmacological and optical interventions for the control of myopia progression are necessary to establish a clearer link between the optical changes associated with these treatments and their demonstrated efficacy.

## REFERENCES

- Dolgin E. The myopia boom. *Nature* 2015; 519: 276–278.
- Attebo K, Ivers R, Mitchell P. Refractive errors in an older population - the Blue Mountains eye study. *Ophthalmology* 1999; 106: 1066–1072.
- Chen M, Wu A, Zhang L et al. The increasing prevalence of myopia and high myopia among high school students in Fenghua City, eastern China: a 15-year population-based survey. *BMC Ophthalmol* 2018; 18: 1–10.
- Han SB, Jang J, Yang HK et al. Prevalence and risk factors of myopia in adult Korean population: Korea National Health and Nutrition Examination Survey 2013–2014 (KNHANES VI). *PLoS ONE* 2019; 14: e0211204.
- Koh V, Yang A, Saw SM et al. Differences in prevalence of refractive errors in young Asian males in Singapore between 1996–1997 and 2009–2010. *Ophthalmic Epidemiol* 2014; 21: 247–255.
- Lin LL, Shih YF, Hsiao CK et al. Prevalence of myopia in Taiwanese schoolchildren: 1983 to 2000. *Ann Acad Med Singapore* 2004; 33: 27–33.

- Holden BA, Fricke TR, Wilson DA et al. Global prevalence of myopia and high myopia and temporal trends from 2000 through 2050. *Ophthalmology* 2016; 123: 1036–1042.
- Lam DS, Fan DS, Chan WM et al. Prevalence and characteristics of peripheral retinal degeneration in Chinese adults with high myopia: a cross-sectional prevalence survey. *Optom Vis Sci* 2005; 82: 235–238.
- Chen SJ, Cheng CY, Li AF et al. Prevalence and associated risk factors of myopic maculopathy in elderly Chinese: the Shihpai eye study. *Invest Ophthalmol Vis Sci* 2012; 53: 4868–4873.
- Shen L, Melles RB, Metlapally R et al. The association of refractive error with glaucoma in a multiethnic population. *Ophthalmology* 2016; 123: 92–101.
- Pan CW, Cheng CY, Saw SM et al. Myopia and age-related cataract: a systematic review and meta-analysis. *Am J Ophthalmol* 2013; 156: 1021–1033.
- Zheng YF, Pan CW, Chay J et al. The economic cost of myopia in adults aged over 40 years in Singapore. *Invest Ophthalmol Vis Sci* 2013; 54: 7532–7537.
- Ohno-Matsui K, Lai TY, Lai CC et al. Updates of pathologic myopia. *Prog Ret Eye Res* 2016; 52: 156–187.
- Flitcroft DL. The complex interactions of retinal, optical and environmental factors in myopia aetiology. *Prog Ret Eye Res* 2012; 31: 622–660.
- Troilo D. Neonatal eye growth and emmetropisation - a literature review. *Eye* 1992; 6: 154–160.
- Liang J, Williams DR. Aberrations and retinal image quality of the normal human eye. *J Opt Soc Am A Opt Image Sci Vis* 1997; 14: 2873–2883.
- Plainis S, Ginis HS, Pallikaris A. The effect of ocular aberrations on steady-state errors of accommodative response. *J Vis* 2005; 5: 466–477.
- Collins MJ, Buehren T, Iskander DR. Retinal image quality, reading and myopia. *Vision Res* 2006; 46: 196–215.
- Mutti DO, Mitchell GL, Jones LA et al. Axial growth and changes in lenticular and corneal power during emmetropization in infants. *Invest Ophthalmol Vis Sci* 2005; 46: 3074–3080.
- Brown NP, Koretz JF, Bron AJ. The development and maintenance of emmetropia. *Eye* 1999; 13: 83–92.
- Saw S-M, Gazzard G, Shin-Yen EC et al. Myopia and associated pathological complications. *Ophthalmic Physiol Opt* 2005; 25: 381–391.
- Flitcroft DL. Emmetropisation and the aetiology of refractive errors. *Eye* 2014; 28: 169–179.
- Wildsoet CF. Active emmetropization - evidence for its existence and ramifications for clinical practice. *Ophthalmic Physiol Opt* 1997; 17: 279–290.
- Wallman J, Turkel J, Trachtman J. Extreme myopia produced by modest change in early visual experience. *Science* 1978; 201: 1249–1251.
- Barathi VA, Boopathi VG, Yap EP et al. Two models of experimental myopia in the mouse. *Vision Res* 2008; 48: 904–916.
- Verolino M, Nistri G, Sellitti L et al. Axial length increase in lid-sutured rabbits. *Surv Ophthalmol* 1999; 44: 103–108.
- Sherman SM, Norton TT, Casagrande VA. Myopia in the lid-sutured tree shrew (*Tupaia glis*). *Brain Res* 1977; 124: 154–157.
- Troilo D, Judge SJ. Ocular development and visual deprivation myopia in the common marmoset (*Callithrix jacchus*). *Vision Res* 1993; 33: 1311–1324.
- Wiesel TN, Raviola E. Myopia and eye enlargement after neonatal lid fusion in monkeys. *Nature* 1977; 266: 66–68.
- Shen W, Vijayan M, Sivak JG. Inducing form-deprivation myopia in fish. *Invest Ophthalmol Vis Sci* 2005; 46: 1797–1803.
- Schaeffel F, Burkhardt EV, Howland HC. Measurement of refractive state and deprivation myopia in two strains of mice. *Optom Vis Sci* 2004; 81: 99–110.
- Howlett MH, McFadden SA. Form-deprivation myopia in the Guinea pig (*Cavia porcellus*). *Vision Res* 2006; 46: 267–283.

33. Smith EL III, Hung LF. Form-deprivation myopia in monkeys is a graded phenomenon. *Vision Res* 2000; 40: 371–381.
34. O'Leary DJ, Millodot M. Eyelid closure causes myopia in humans. *Experientia* 1979; 35: 1478–1479.
35. van Noordten GK, Lewis RA. Ocular axial length in unilateral congenital cataracts and blepharoptosis. *Invest Ophthalmol Vis Sci* 1987; 28: 750–752.
36. Gee KS, Tabbara KF. Increase in ocular axial length in patients with corneal opacification. *Ophthalmology* 1988; 95: 1276–1278.
37. Miller-Meeks MJ, Bennett SR, Keech RV et al. Myopia induced by vitreous hemorrhage. *Am J Ophthalmol* 1990; 102: 199–203.
38. Schaeffel F, Glasser A, Howland HC. Accommodation, refractive error and eye growth in chickens. *Vision Res* 1988; 28: 639–657.
39. Wallman J, Winawer J. Homeostasis of eye growth and the question of myopia. *Neuron* 2004; 43: 447–468.
40. Diether S, Schaeffel F. Local changes in eye growth induced by imposed local refractive error despite active accommodation. *Vision Res* 1997; 37: 659–668.
41. Howlett MH, McFadden SA. Spectacle lens compensation in the pigmented Guinea pig. *Vision Res* 2009; 49: 219–227.
42. Shen W, Sivak JG. Eyes of a lower vertebrate are susceptible to the visual environment. *Invest Ophthalmol Vis Sci* 2007; 48: 4829–4837.
43. Shaikh AW, Siegwart JT, Norton TT. Effect of interrupted lens wear on compensation for a minus lens in tree shrews. *Optom Vis Sci* 1999; 76: 308–315.
44. Norton TT, Siegwart JT, Amedo AO. Effectiveness of hyperopic defocus, minimal defocus, or myopic defocus in competition with a myopiagenic stimulus in tree shrew eyes. *Invest Ophthalmol Vis Sci* 2006; 47: 4687–4699.
45. Graham B, Judge SJ. The effects of spectacle wear in infancy on eye growth and refractive error in the marmoset (*Callithrix jacchus*). *Vision Res* 1999; 39: 189–206.
46. Troilo D, Totonelly K, Harb E. Imposed anisometropia, accommodation, and regulation of refractive state. *Optom Vis Sci* 2009; 86: E31–E39.
47. Smith EL III, Hung LF. The role of optical defocus in regulating refractive development in infant monkeys. *Vision Res* 1999; 39: 1415–1435.
48. Read SA, Collins MJ, Sander BP. Human optical axial length and defocus. *Invest Ophthalmol Vis Sci* 2010; 51: 6262–6269.
49. Chiang ST-H, Phillips JR, Backhouse S. Effect of retinal image defocus on the thickness of the human choroid. *Ophthalmic Physiol Opt* 2015; 35: 405–413.
50. Wang D, Chun RK, Liu M et al. Optical defocus rapidly changes choroidal thickness in schoolchildren. *PLoS ONE* 2016; 11: e0161535.
51. Zhu X, Park TW, Winawer J et al. In a matter of minutes, the eye can know which way to grow. *Invest Ophthalmol Vis Sci* 2005; 46: 2238–2241.
52. Wallman J, Gottlieb MD, Rajaram V et al. Local retinal regions control local eye growth and myopia. *Science* 1987; 237: 73–77.
53. Miles FA, Wallman J. Local ocular compensation for imposed local refractive error. *Vision Res* 1990; 30: 339–349.
54. Rada JA, Shelton S, Norton TT. The sclera and myopia. *Exp Eye Res* 2006; 82: 185–200.
55. Kisilak ML, Campbell MC, Hunter JJ et al. Aberrations of chick eyes during normal growth and lens induction of myopia. *J Comp Physiol A Neuroethol Sens Neural Behav Physiol* 2006; 192: 845–855.
56. García de la Cera E, Rodríguez G, Marcos S. Longitudinal changes of optical aberrations in normal and form-deprived myopic chick eyes. *Vision Res* 2006; 46: 579–589.
57. Coletta NJ, Marcos S, Troilo D. Ocular wavefront aberrations in the common marmoset *Callithrix jacchus*: effects of age and refractive error. *Vision Res* 2010; 50: 2515–2529.
58. Ramamirtham R, Kee CS, Hung LF et al. Monochromatic ocular wave aberrations in young monkeys. *Vision Res* 2006; 46: 3616–3633.
59. Ramamirtham R, Kee CS, Hung LF et al. Wave aberrations in rhesus monkeys with vision-induced ametropias. *Vision Res* 2007; 47: 2751–2766.
60. Hiraoka T, Kakita T, Okamoto F et al. Influence of ocular wavefront aberrations on axial length elongation in myopic children treated with overnight orthokeratology. *Ophthalmology* 2015; 122: 93–100.
61. Lau JK, Vincent SJ, Collins MJ et al. Ocular higher-order aberrations and axial eye growth in young Hong Kong children. *Sci Rep* 2018; 8: 6726.
62. Kim J, Lim DH, Han SH et al. Predictive factors associated with axial length growth and myopia progression in orthokeratology. *PLoS ONE* 2019; 14: e0218140.
63. Wildsoet CF, Schmid KL. Emmetropization in chicks uses optical vergence and relative distance cues to decode defocus. *Vision Res* 2001; 41: 3197–3204.
64. Artal P, Guirao A, Berrio E et al. Compensation of corneal aberrations by the internal optics in the human eye. *J Vis* 2001; 1: 1–8.
65. Atchison DA, Markwell EL. Aberrations of emmetropic subjects at different ages. *Vision Res* 2008; 48: 2224–2231.
66. McLellan JS, Marcos S, Burns SA. Age-related changes in monochromatic wave aberrations of the human eye. *Invest Ophthalmol Vis Sci* 2001; 42: 1390–1395.
67. Wang L, Koch DD. Ocular higher-order aberrations in individuals screened for refractive surgery. *J Cataract Refract Surg* 2003; 29: 1896–1903.
68. Artal P, Berrio E, Guirao A et al. Contribution of the cornea and internal surfaces to the change of ocular aberrations with age. *J Opt Soc Am A Opt Image Sci Vis* 2002; 19: 137–143.
69. Brunette I, Bueno JM, Parent M et al. Monochromatic aberrations as a function of age, from childhood to advanced age. *Invest Ophthalmol Vis Sci* 2003; 44: 5438–5446.
70. Levy Y, Segal O, Avni I et al. Ocular higher-order aberrations in eyes with supernormal vision. *Am J Ophthalmol* 2005; 139: 225–228.
71. Radhakrishnan H, Charman WN. Age-related changes in ocular aberrations with accommodation. *J Vis* 2007; 7: 1–21.
72. Amano S, Amano Y, Yamagami S et al. Age-related changes in corneal and ocular higher-order wavefront aberrations. *Am J Ophthalmol* 2004; 137: 988–992.
73. Rocha KM, Nosé W, Bottós K et al. Higher-order aberrations of age-related cataract. *J Cataract Refract Surg* 2007; 33: 1442–1446.
74. Fujikado T, Kuroda T, Maeda N et al. Light scattering and optical aberrations as objective parameters to predict visual deterioration in eyes with cataracts. *J Cataract Refract Surg* 2004; 30: 1198–1208.
75. Kuroda T, Fujikado T, Maeda N et al. Wavefront analysis in eyes with nuclear or cortical cataract. *Am J Ophthalmol* 2002; 134: 1–9.
76. Wang L, Dai E, Koch DD et al. Optical aberrations of the human anterior cornea. *J Cataract Refract Surg* 2003; 29: 1514–1521.
77. Zhang N, Liu L, Yang B et al. Higher-order aberrations in children and adolescents of Southwest China. *Optom Vis Sci* 2018; 95: 53–59.
78. Cerviño A, Hosking SL, Ferrer-Blasco T et al. A pilot study on the differences in wavefront aberrations between two ethnic groups of young generally myopic subjects. *Ophthalmic Physiol Opt* 2008; 28: 532–537.
79. Lim KL, Fam HB. Ethnic differences in higher-order aberrations: spherical aberration in the south east Asian Chinese eye. *J Cataract Refract Surg* 2009; 35: 2144–2148.
80. Carkeet A, Luo HD, Tong L et al. Refractive error and monochromatic aberrations in Singaporean children. *Vision Res* 2002; 42: 1809–1824.
81. Winn B, Whitaker D, Elliott DB et al. Factors affecting light-adapted pupil size in normal human subjects. *Invest Ophthalmol Vis Sci* 1994; 35: 1132–1137.
82. Birren JE, Casperson RC, Botwinick J. Age changes in pupil size. *J Gerontol* 1950; 5: 216–221.
83. Silbert J, Matta N, Tian J et al. Pupil size and anisocoria in children measured by the plusoptix photoscreener. *J AAPOS* 2013; 17: 609–611.
84. Mathur A, Atchison DA, Charman WN. Effect of accommodation on peripheral ocular aberrations. *J Vis* 2009; 9: 1–11.
85. Mathur A, Atchison DA, Charman WN. Effects of age on peripheral ocular aberrations. *Opt Express* 2010; 18: 5840–5853.
86. Mathur A, Atchison DA, Charman WN. Myopia and peripheral ocular aberrations. *J Vis* 2009; 9: 1–12.
87. Osuagwu UL, Suheimat M, Atchison DA. Peripheral aberrations in adult hyperopes, emmetropes and myopes. *Ophthalmic Physiol Opt* 2017; 37: 151–159.
88. Philip K, Sankaridurg PR, Ale JB et al. Profile of off-axis higher order aberrations and its variation with time among various refractive error groups. *Vision Res* 2018; 153: 111–123.
89. He JC, Sun P, Held R et al. Wavefront aberrations in eyes of emmetropic and moderately myopic school children and young adults. *Vision Res* 2002; 42: 1063–1070.
90. Paquin MP, Hamam H, Simonet P. Objective measurement of optical aberrations in myopic eyes. *Optom Vis Sci* 2002; 79: 285–291.
91. Yazar S, Hewitt AW, Forward H et al. Comparison of monochromatic aberrations in young adults with different visual acuity and refractive errors. *J Cataract Refract Surg* 2014; 40: 441–449.
92. Cheng X, Bradley A, Hong X et al. Relationship between refractive error and monochromatic aberrations of the eye. *Optom Vis Sci* 2003; 80: 43–49.
93. Kwan WCK, Yip SP, Yap MKH. Monochromatic aberrations of the human eye and myopia. *Clin Exp Optom* 2009; 92: 304–312.
94. Llorente L, Barbero S, Cano D et al. Myopic versus hyperopic eyes: axial length, corneal shape and optical aberrations. *J Vis* 2004; 4: 288–298.
95. Kirwan C, O'Keefe M, Soeldner H. Higher-order aberrations in children. *Am J Ophthalmol* 2006; 141: 67–70.
96. Zhang N, Yang XB, Zhang WQ et al. Relationship between higher-order aberrations and myopia progression in schoolchildren: a retrospective study. *Int J Ophthalmol* 2013; 6: 295–299.
97. Li T, Zhou X, Chen Z et al. Relationship between ocular wavefront aberrations and refractive error in Chinese school children. *Clin Exp Optom* 2012; 95: 399–403.
98. Little JA, McCullough SJ, Breslin KM et al. Higher order ocular aberrations and their relation to refractive error and ocular biometry in children. *Invest Ophthalmol Vis Sci* 2014; 55: 4791–4800.
99. Philip K, Martinez AA, Ho A et al. Total ocular, anterior corneal and lenticular higher order aberrations in hyperopic, myopic and emmetropic eyes. *Vision Res* 2012; 52: 31–37.
100. Papamastorakis G, Panagopoulou S, Tsilimbaris MK et al. Ocular higher-order aberrations in a school children population. *J Optom* 2015; 8: 93–100.
101. Martinez AA, Sankaridurg PR, Naduvilath TJ et al. Monochromatic aberrations in hyperopic and emmetropic children. *J Vis* 2009; 9: 1–14.
102. Philip K, Sankaridurg P, Holden B et al. Influence of higher order aberrations and retinal image quality in myopisation of emmetropic eyes. *Vision Res* 2014; 105: 233–243.
103. Hiraoka T, Kotsuka J, Kakita T et al. Relationship between higher-order wavefront aberrations and natural progression of myopia in schoolchildren. *Sci Rep* 2017; 7: 7876.
104. McLellan JS, Prieto PM, Marcos S et al. Effects of interactions among wave aberrations on optical image quality. *Vision Res* 2006; 46: 3009–3016.
105. Wilson BJ, Decker KE, Roorda A. Monochromatic aberrations provide an odd-error cue to focus direction. *J Opt Soc Am A Opt Image Sci Vis* 2002; 19: 833–839.
106. Del Águila-Carrasco AJ, Marín-Franch I, Bernal-Molina P et al. Accommodation responds to optical

- vergence and not defocus blur alone. *Invest Ophthalmol Vis Sci* 2017; 58: 1758-1763.
107. Atchison DA, Pritchard N, Schmid KL et al. Shape of the retinal surface in emmetropia and myopia. *Invest Ophthalmol Vis Sci* 2005; 46: 2698-2707.
108. Huynh SC, Wang XY, Ip J et al. Prevalence and associations of anisometropia and aniso-astigmatism in a population based sample of 6 year old children. *Br J Ophthalmol* 2006; 90: 597-601.
109. Vincent SJ, Collins MJ, Read SA et al. Myopic anisometropia: ocular characteristics and aetiological considerations. *Clin Exp Optom* 2014; 97: 291-307.
110. Hartwig A, Atchison DA, Radhakrishnan H. Higher-order aberrations and anisometropia. *Curr Eye Res* 2013; 38: 215-219.
111. Osuagwu UL, Suheimat M, Atchison DA. Mirror symmetry of peripheral monochromatic aberrations in fellow eyes of isomyopes and anisomyopes. *Invest Ophthalmol Vis Sci* 2016; 57: 3422-3428.
112. Tian Y, Tarrant J, Wildsoet CF. Optical and biometric characteristics of anisomyopia in human adults. *Ophthalmic Physiol Opt* 2011; 31: 540-549.
113. Vincent SJ, Collins MJ, Read SA et al. Interocular symmetry in myopic anisometropia. *Optom Vis Sci* 2011; 88: 1454-1462.
114. Weakley DR Jr. The association between non-strabismic anisometropia, amblyopia, and subnormal binocularity. *Ophthalmology* 2001; 108: 163-171.
115. Smith EL III, Hung LF, Arumugam B et al. Observations on the relationship between anisometropia, amblyopia and strabismus. *Vision Res* 2017; 134: 26-42.
116. Kirwan C, O'Keefe M. Higher order aberrations in children with amblyopia. *J Pediatr Ophthalmol Strabismus* 2008; 45: 92-96.
117. Prakash G, Sharma N, Saxena R et al. Comparison of higher order aberration profiles between normal and amblyopic eyes in children with idiopathic amblyopia. *Acta Ophthalmol* 2011; 89: e257-e262.
118. Vincent SJ, Collins MJ, Read SA et al. Monocular amblyopia and higher order aberrations. *Vision Res* 2012; 66: 39-48.
119. Goss DA. Nearwork and myopia. *Lancet* 2000; 356: 1456-1457.
120. Sorsby A. School myopia. *Br J Ophthalmol* 1932; 16: 217-222.
121. Jones-Jordan LA, Sinnott LT, Graham ND et al. The contributions of near work and outdoor activity to the correlation between siblings in the collaborative longitudinal evaluation of ethnicity and refractive error (CLEERE) study. *Invest Ophthalmol Vis Sci* 2014; 55: 6333-6339.
122. Mutti DO, Zadnik K. Has near work's star fallen? *Optom Vis Sci* 2009; 86: 76-78.
123. Buehren T, Collins MJ, Carney LG. Near work induced wavefront aberrations in myopia. *Vision Res* 2005; 45: 1297-1312.
124. Li YJ, Choi JA, Kim H et al. Changes in ocular wavefront aberrations and retinal image quality with objective accommodation. *J Cataract Refract Surg* 2011; 37: 835-841.
125. Iida Y, Shimizu K, Ito M et al. Influence of age on ocular wavefront aberration changes with accommodation. *J Refract Surg* 2008; 24: 696-701.
126. Cheng H, Barnett JK, Vilupuru AS et al. A population study on changes in wave aberrations with accommodation. *J Vis* 2004; 4: 272-280.
127. Zhou XY, Wang L, Zhou XT et al. Wavefront aberration changes caused by a gradient of increasing accommodation stimuli. *Eye* 2015; 29: 115-121.
128. He JC, Burns SA, Marcos S. Monochromatic aberrations in the accommodated human eye. *Vision Res* 2000; 40: 41-48.
129. Ninomiya S, Fujikado T, Kuroda T et al. Changes of ocular aberration with accommodation. *Am J Ophthalmol* 2002; 134: 924-926.
130. Atchison DA, Collins MJ, Wildsoet CF et al. Measurement of monochromatic ocular aberrations of human eyes as a function of accommodation by the Howland aberroscope technique. *Vision Res* 1995; 35: 313-323.
131. Collins MJ, Wildsoet CF, Atchison DA. Monochromatic aberrations and myopia. *Vision Res* 1995; 35: 1157-1163.
132. Ghosh A, Collins MJ, Read SA et al. The influence of downward gaze and accommodation on ocular aberrations over time. *J Vis* 2011; 11: 1-13.
133. Read SA, Buehren T, Collins MJ. Influence of accommodation on the anterior and posterior cornea. *J Cataract Refract Surg* 2007; 33: 1877-1885.
134. He JC, Gwiazda J, Thorn F et al. Change in corneal shape and corneal wave-front aberrations with accommodation. *J Vis* 2003; 3: 456-463.
135. Buehren T, Collins MJ, Carney L. Corneal aberrations and reading. *Optom Vis Sci* 2003; 80: 159-166.
136. Vincent SJ, Read SA, Collins MJ et al. Corneal changes following near work in myopic anisometropia. *Ophthalmic Physiol Opt* 2013; 33: 15-25.
137. Buehren T, Collins MJ. Accommodation stimulus-response function and retinal image quality. *Vision Res* 2006; 46: 1633-1645.
138. Thibos LN, Bradley A, Liu T et al. Spherical aberration and the sign of defocus. *Optom Vis Sci* 2013; 90: 1284-1291.
139. Gwiazda J, Thorn F, Bauer J et al. Myopic children show insufficient accommodative response to blur. *Invest Ophthalmol Vis Sci* 1993; 34: 690-694.
140. Gwiazda J, Bauer J, Thorn F et al. A dynamic relationship between myopia and blur-driven accommodation in school-aged children. *Vision Res* 1995; 35: 1299-1304.
141. Buehren T, Iskander DR, Collins MJ et al. Potential higher-order aberration cues for spherocylindrical refractive error development. *Optom Vis Sci* 2007; 84: 163-174.
142. Walline JJ. Myopia control: a review. *Eye Contact Lens* 2016; 42: 3-8.
143. McBrien NA, Moghaddam HO, Reeder AP. Atropine reduces experimental myopia and eye enlargement via a nonaccommodative mechanism. *Invest Ophthalmol Vis Sci* 1993; 34: 205-215.
144. Chia A, Lu QS, Tan D. Five-year clinical trial on atropine for the treatment of myopia 2: myopia control with atropine 0.01% eyedrops. *Ophthalmology* 2016; 123: 391-399.
145. Huang J, Wen D, Wang Q et al. Efficacy comparison of 16 interventions for myopia control in children: a network meta-analysis. *Ophthalmology* 2016; 123: 697-708.
146. Yam JC, Jiang Y, Tang SM et al. Low-concentration atropine for myopia progression (LAMP) study myopia control. *Ophthalmology* 2018; 126: 113-124.
147. Bullimore MA, Berntsen DA. Low-dose atropine for myopia control: considering all the data. *JAMA Ophthalmol* 2018; 136: 303.
148. Gettes BC. Drugs in refraction. *Int Ophthalmol Clin* 1961; 1: 237-248.
149. McBrien NA, Stell WK, Carr B. How does atropine exert its anti-myopia effects? *Ophthalmic Physiol Opt* 2013; 33: 373-378.
150. Carr BJ, Stell WK. Nitric oxide (NO) mediates the inhibition of form-deprivation myopia by atropine in chicks. *Sci Rep* 2016; 6: 9.
151. Hiraoka T, Miyata K, Nakamura Y et al. Influences of cycloplegia with topical atropine on ocular higher-order aberrations. *Ophthalmology* 2013; 120: 8-13.
152. Chia A, Chua WH, Cheung YB et al. Atropine for the treatment of childhood myopia: safety and efficacy of 0.5%, 0.1%, and 0.01% doses (atropine for the treatment of myopia 2). *Ophthalmology* 2012; 119: 347-354.
153. Salmon TO, van de Pol C. Normal-eye zernike coefficients and root-mean-square wavefront errors. *J Cataract Refract Surg* 2006; 32: 2064-2074.
154. Hiraoka T, Miyata K, Nakamura Y et al. Influence of cycloplegia with topical cyclopentolate on higher-order aberrations in myopic children. *Eye* 2014; 28: 581-586.
155. Amirshakarizadeh N, Hashemi H, Jafarzadehpur E et al. Higher-order aberrations after cyclopentolate, tropicamide, and artificial tear drops application in normal eyes. *Eye Contact Lens* 2018; 44: 109-112.
156. Yen MY, Liu JH, Kao SC et al. Comparison of the effect of atropine and cyclopentolate on myopia. *Ann Ophthalmol* 1989; 21: 180-187.
157. Shih YF, Chen CH, Chou AC et al. Effects of different concentrations of atropine on controlling myopia in myopic children. *J Ocul Pharmacol Ther* 1999; 15: 85-90.
158. Gwiazda J, Hyman L, Hussein M et al. A randomized clinical trial of progressive addition lenses versus single vision lenses on the progression of myopia in children. *Invest Ophthalmol Vis Sci* 2003; 44: 1492-1500.
159. Gwiazda J, Chandler DL, Cotter SA et al. Progressive-addition lenses versus single-vision lenses for slowing progression of myopia in children with high accommodative lag and near esophoria. *Invest Ophthalmol Vis Sci* 2011; 52: 2749-2757.
160. Cheng D, Woo GC, Drobe B et al. Effect of bifocal and prismatic bifocal spectacles on myopia progression in children. *JAMA Ophthalmol* 2014; 132: 258-264.
161. Cheng D, Schmid KL, Woo GC. The effect of positive-lens addition and base-in prism on accommodation accuracy and near horizontal phoria in Chinese myopic children. *Ophthalmic Physiol Opt* 2008; 28: 225-237.
162. Smith EL III, Campbell MC, Irving E. Point-counterpoint. Does peripheral retinal input explain the promising myopia control effects of corneal reshaping therapy (CRT or ortho-K) & multifocal soft contact lenses? *Ophthalmic Physiol Opt* 2013; 33: 379-384.
163. Berntsen DA, Barr CD, Mutti DO et al. Peripheral defocus and myopia progression in myopic children randomly assigned to wear single vision and progressive addition lenses. *Invest Ophthalmol Vis Sci* 2013; 54: 5761-5770.
164. Schilling T, Ohlendorf A, Varnas SR et al. Peripheral design of progressive addition lenses and the lag of accommodation in myopes. *Invest Ophthalmol Vis Sci* 2017; 58: 3319-3324.
165. Ghosh A, Collins MJ, Read SA et al. Measurement of ocular aberrations in downward gaze using a modified clinical aberrometer. *Biomed Opt Express* 2011; 2: 452-463.
166. Villegas EA, Artal P. Spatially resolved wavefront aberrations of ophthalmic progressive-power lenses in normal viewing conditions. *Optom Vis Sci* 2003; 80: 106-114.
167. Blendowske R, Villegas EA, Artal P. An analytical model describing aberrations in the progression corridor of progressive addition lenses. *Optom Vis Sci* 2006; 83: 666-671.
168. Cho P, Cheung SW, Edwards M. The longitudinal orthokeratology research in children (LORIC) in Hong Kong: a pilot study on refractive changes and myopic control. *Curr Eye Res* 2005; 30: 71-80.
169. Cho P, Cheung SW. Protective role of orthokeratology in reducing risk of rapid axial elongation: a reanalysis of data from the ROMIO and TO-SEE studies. *Invest Ophthalmol Vis Sci* 2017; 58: 1411-1416.
170. Lin HJ, Wan L, Tsai FJ et al. Overnight orthokeratology is comparable with atropine in controlling myopia. *BMC Ophthalmol* 2014; 14: 1-8.
171. Stillitano I, Chalita MR, Schor P et al. Corneal changes and wavefront analysis after orthokeratology fitting test. *Am J Ophthalmol* 2007; 144: 378-386.
172. Gifford P, Li M, Lu H et al. Corneal versus ocular aberrations after overnight orthokeratology. *Optom Vis Sci* 2013; 90: 439-447.
173. Lian Y, Shen M, Huang S et al. Corneal reshaping and wavefront aberrations during overnight orthokeratology. *Eye Contact Lens* 2014; 40: 161-168.
174. Stillitano I, Schor P, Lipener C et al. Long-term follow-up of orthokeratology corneal reshaping using wavefront aberrometry and contrast sensitivity. *Eye Contact Lens* 2008; 34: 140-145.

175. Santodomingo-Rubido J, Villa-Collar C, Gilmartin B et al. Short- and long-term changes in corneal aberrations and axial length induced by orthokeratology in children are not correlated. *Eye Contact Lens* 2016; 43: 358–363.
176. Santodomingo-Rubido J, Villa-Collar C, Gilmartin B et al. The effects of entrance pupil centration and coma aberrations on myopic progression following orthokeratology. *Clin Exp Optom* 2015; 98: 534–540.
177. Hiraoka T, Mihashi T, Okamoto C et al. Influence of induced decentered orthokeratology lens on ocular higher-order wavefront aberrations and contrast sensitivity function. *J Cataract Refract Surg* 2009; 35: 1918–1926.
178. Tarrant J, Liu Y, Wildsoet CF. Orthokeratology can decrease the accommodative lag in myopes. *Invest Ophthalmol Vis Sci* 2009; 50: 4294.
179. Mathur A, Atchison DA. Effect of orthokeratology on peripheral aberrations of the eye. *Optom Vis Sci* 2009; 86: E476–E484.
180. Chen Z, Niu L, Xue F et al. Impact of pupil diameter on axial growth in orthokeratology. *Optom Vis Sci* 2012; 89: 1636–1640.
181. Faria-Ribeiro M, Navarro R, González-Méjome JM. Effect of pupil size on wavefront refraction during orthokeratology. *Optom Vis Sci* 2016; 93: 1399–1408.
182. Li SM, Kang MT, Wu SS et al. Studies using concentric ring bifocal and peripheral add multifocal contact lenses to slow myopia progression in school-aged children: a meta-analysis. *Ophthalmic Physiol Opt* 2017; 37: 51–59.
183. Walline JJ, Jones LA, Mutti DO et al. A randomized trial of the effects of rigid contact lenses on myopia progression. *Arch Ophthalmol* 2004; 122: 1760–1766.
184. Walline JJ, Jones LA, Sinnott L et al. A randomized trial of the effect of soft contact lenses on myopia progression in children. *Invest Ophthalmol Vis Sci* 2008; 49: 4702–4706.
185. Bakaraju RC, Ehrmann K, Ho A et al. Inherent ocular spherical aberration and multifocal contact lens optical performance. *Optom Vis Sci* 2010; 87: 1009–1022.
186. Fedtke C, Ehrmann K, Thomas V et al. Peripheral refraction and aberration profiles with multifocal lenses. *Optom Vis Sci* 2017; 94: 876–885.
187. Gong CR, Troilo D, Richdale K. Accommodation and phoria in children wearing multifocal contact lenses. *Optom Vis Sci* 2017; 94: 353–360.
188. Kang P, Wildsoet CF. Acute and short-term changes in visual function with multifocal soft contact lens wear in young adults. *Cont Lens Anterior Eye* 2016; 39: 133–140.
189. Sankaridurg P, Holden B, Smith EL III et al. Decrease in rate of myopia progression with a contact lens designed to reduce relative peripheral hyperopia: one-year results. *Invest Ophthalmol Vis Sci* 2011; 52: 9362–9367.
190. Fujikado T, Ninomiya S, Kobayashi T et al. Effect of low-addition soft contact lenses with decentered optical design on myopia progression in children: a pilot study. *Clin Ophthalmol* 2014; 8: 1947–1956.
191. Cheng X, Xu J, Chehab K et al. Soft contact lenses with positive spherical aberration for myopia control. *Optom Vis Sci* 2016; 93: 353–366.
192. Anstice NS, Phillips JR. Effect of dual-focus soft contact lens wear on axial myopia progression in children. *Ophthalmology* 2011; 118: 1152–1161.
193. Sankaridurg P, Bakaraju RC, Naduvilath T et al. Myopia control with novel central and peripheral plus contact lenses and extended depth of focus contact lenses: 2 year results from a randomised clinical trial. *Ophthalmic Physiol Opt* 2019; 39: 294–307.
194. Gislén A, Gustafsson J, Kröger RH. The accommodative pupil responses of children and young adults at low and intermediate levels of ambient illumination. *Vision Res* 2008; 48: 989–993.
195. Read SA, Collins MJ, Vincent SJ. Light exposure and eye growth in childhood. *Invest Ophthalmol Vis Sci* 2015; 56: 6779–6787.

## Peripheral refraction and higher order aberrations

*Clin Exp Optom* 2020; 103: 86–94

DOI:10.1111/cxo.12943

**Dmitry Romashchenko\***  MSc

**Robert Rosén†** PhD

**Linda Lundström\***  PhD

\*Department of Applied Physics, Royal Institute of Technology, Stockholm, Sweden

†R&D, Johnson & Johnson Vision, Groningen, The Netherlands

E-mail: dmitry.romashchenko@biox.kth.se

This is an open access article under the terms of the Creative Commons Attribution-NonCommercial License, which permits use, distribution and reproduction in any medium, provided the original work is properly cited and is not used for commercial purposes.

Submitted: 28 March 2019

Revised: 18 June 2019

Accepted for publication: 18 June 2019

Peripheral image quality influences several aspects of human vision. Apart from off-axis visual functions, the manipulation of peripheral optical errors is widely used in myopia control interventions. This, together with recent technological advancements enabling the measurement of peripheral errors, has inspired many studies concerning off-axis optical aberrations. However, direct comparison between these studies is often not straightforward. To enable between-study comparisons and to summarise the current state of knowledge, this review presents population data analysed using a consistent approach from 16 studies on peripheral ocular optical quality (in total over 2,400 eyes). The presented data include refractive errors and higher order monochromatic aberrations expressed as Zernike co-efficients (reported in a subset of the studies) over the horizontal visual field. Additionally, modulation transfer functions, describing the monochromatic image quality, are calculated using individual wavefront data from three studies. The analysed data show that optical errors increase with increasing eccentricity as expected from theoretical modelling. Compared to emmetropes, myopes tend to have more hypermetropic relative peripheral refraction over the horizontal field and worse image quality in the near-periphery of the nasal visual field. The modulation transfer functions depend considerably on pupil shape (for angles larger than 30°) and to some extent, the number of Zernike terms included. Moreover, modulation transfer functions calculated from the average Zernike co-efficients of a cohort are artificially inflated compared to the average of individual modulation transfer functions from the same cohort. The data collated in this review are important for the design of ocular corrections and the development and assessment of optical eye models.

**Key words:** myopia, ocular modulation transfer function, peripheral higher order aberrations, peripheral refraction, retinal image quality

This review summarises the results of earlier studies on the peripheral optical errors of the human eye. Knowledge of the peripheral optical quality is of importance to several fields within optometry and ophthalmology:<sup>1</sup> development of technical aids with intact or improved perception and mobility; correction of peripheral optical errors to improve vision for various ocular diseases; and manipulation of peripheral image quality to halt progressing myopia.

Many activities in everyday life require sufficient image quality on the peripheral retina. Unlike central vision, designed primarily for resolution tasks, peripheral vision is responsible for various forms of detection. Even though peripheral high-contrast resolution is limited by the sampling density of the retina, both detection and low-contrast resolution depend on the quality of the peripheral image.<sup>2–8</sup> It has been demonstrated that peripheral vision is essential for driving,<sup>9–11</sup> and several studies have

reported that mobility, including the risk of falling, is also highly dependent on vision beyond the fovea.<sup>12,13</sup> Further, limiting off-axis vision can affect the performance of search tasks, where well-controlled saccadic eye movements are required.<sup>14</sup>

Knowledge of the peripheral retinal image quality can be useful for the development of optical aids for patients with reduced retinal functionality (for example, due to age-related macular degeneration), retinitis pigmentosa, and glaucoma. For instance, patients with central visual field loss have shown improved visual performance with optical corrections that enhance the image contrast on the peripheral retina.<sup>15–17</sup> Treating pseudophakic patients can also be challenging since intraocular lenses, currently available on the market, can decrease peripheral retinal image quality.<sup>18</sup> Thus, explicit knowledge of the peripheral ocular aberrations and image quality may be highly beneficial from a clinical and research perspective.

It has also been suggested that manipulating peripheral image quality might prevent myopia onset or slow down its progression.<sup>19–23</sup> In recent years the prevalence of myopia has continued to increase and currently affects approximately 30 per cent of the population worldwide.<sup>19,21,24</sup> This is of serious concern, because high myopia is a risk factor for severe ocular pathologies (such as myopic macular degeneration<sup>25</sup>) and therefore, many research studies have been dedicated to myopia control. Studies in chickens,<sup>26,27</sup> monkeys<sup>28–31</sup> and guinea pigs<sup>32</sup> have shown that peripheral image quality has the potential to drive myopia development; but the entire mechanism as yet is not completely understood. Nevertheless, specific peripheral aberration patterns are already implemented in myopia control methods through different types of multifocality. However, all of the available optical treatments (including multifocal soft contact lenses, spectacles that alter peripheral



Study	Measurements technique	Subjects	Horizontal VF	Used data	Comments
Lotmar and Lotmar <sup>38</sup>	Retinoscopy	363, all emmetropes	20°, 40°, 60° in nasal and temporal VF	J <sub>0</sub>	J <sub>0</sub> calculated from interval Sturm
Millodot <sup>39</sup>	Topcon refractor	62 subjects (13 emmetropes, 30 myopes, 19 hypermetropes)	(−60; +60)° in 10° steps	RPR, J <sub>0</sub>	J <sub>0</sub> calculated from interval Sturm
Mutti et al. <sup>40</sup>	Canon R-1 autorefractor	822 children aged 5 to 14 years	Foveal and 30° nasal VF of the right eye	RPR, J <sub>0</sub>	J <sub>0</sub> calculated from cylinder power
Gustafsson et al. <sup>41</sup>	Double-pass technique	20 emmetropes, either left or right eye measured per subject	(−60; +60)° in 10° steps	RPR, J <sub>0</sub>	
Seidemann et al. <sup>42</sup>	PowerRefractor and double-pass technique	31 young adult subjects: 8 emmetropic, 18 myopic, 5 hypermetropic	0°, 15°, (20°), 30°, (40°), 45° nasal VF	RPR, J <sub>0</sub>	J <sub>0</sub> calculated from interval Sturm
Atchison et al. <sup>43</sup>	Shin-Nippon SRW-5000	116 subjects, emmetropes and myopes	(−35; +35)° in 5° steps	RPR, J <sub>0</sub>	Polynomial fit to the graphs
Shen et al. <sup>44</sup>	COAS	34 adult subjects: 8 emmetropes, 26 myopes	(−30; +30)° horizontal VF	M, J <sub>0</sub>	Polynomial fit to the graphs
*Lundström et al. <sup>45</sup>	Laboratory Hartmann-Schack wavefront sensor	43 subjects	0°, 20° and 30° nasal VF	Zernike co-efficients up to 9 <sup>th</sup> order	J <sub>0</sub> calculated from C22
*Mathur et al. <sup>46</sup>	COAS-HD	19 subjects: 10 emmetropes, 10 myopes (raw data available for 20 subjects)	(−21; +21)° (colour map)	Zernike co-efficients up to 6 <sup>th</sup> order	Polynomial fit to colour maps
Baskaran et al. <sup>47</sup>	COAS-HD VR	30 younger and 30 older emmetropes	(−40; +40)° in 10° steps	RPR, J <sub>0</sub> , C(4,0), C(1,3)	J <sub>0</sub> calculated from C22
*Jaeken and Artal <sup>48</sup>	Scanning wavefront sensor	202 eyes of 101 subjects: 64 non-myopes and 37 myopes	(−40; +40)° at 1° intervals	Zernike co-efficients up to 3 <sup>rd</sup> order	J <sub>0</sub> calculated from C22
Bakaraju et al. <sup>53</sup>	BHVI-EyeMapper	26 participants, emmetropes and myopes	(−50; 50)° horizontal VF	M, J <sub>0</sub> , C(1,3), C(3), C(4,0)	M and J <sub>0</sub> as polynomial fit to the graphs
Osuagwu et al. <sup>49</sup>	COAS-HD	29 subjects, 19 isomyopic (anisometropia < 1 D)	(−20; +20)° (colour maps)	2 <sup>nd</sup> and 3 <sup>rd</sup> order Zernike co-efficients, C(4,0)	1. Polynomial fit to colour maps 2. Only right eyes data used
Osuagwu et al. <sup>50</sup>	COAS-HD	49 young adults: 9 hypermetropes, 20 emmetropes, 20 myopes	(−21; +21)° (colour maps)	RPR, J <sub>0</sub> , C(3,−3), C(3,−1), C(1,3), C(4,0)	1. Polynomial fit to colour maps 2. Emmetropes: SE (−0.5; +0.75) D
Philip et al. <sup>51</sup>	COAS	678 adolescents: 176 emmetropic, 96 myopic and 375 hypermetropic	Foveal and 30° nasal and temporal VF	M, J <sub>0</sub> , 3 <sup>rd</sup> and 4 <sup>th</sup> orders of Zernike co-efficients	
Osuagwu et al. <sup>52</sup>	COAS-HD	37 eyes: 18 Caucasians, 19 East Asians	(−21; +21)° (colour maps)	RPR, J <sub>0</sub> , C(3,−1), C(1,3), C(3), C(4,0)	Polynomial fit to colour maps

The first group contains studies with only J<sub>0</sub> and relative peripheral refraction available, the second group shows those containing Zernike co-efficients, and the asterisk (\*) marks studies for which raw wavefront data were available. The table contains only the details relevant to the analysis over the horizontal visual field (VF) of this review. See Table S1 for full details of the studies.

M: mean sphere, RPR: relative peripheral refraction.

**Table 1. List of studies from which the data were extracted**

defocus, and orthokeratology) are only partially effective and subject-dependent.<sup>33,34</sup> This suggests that peripheral aberrations as well as their effect on the development

and progression of myopia need to be further investigated.

Despite the importance of peripheral aberrations, direct access to population data on

retinal image quality is limited and the comparison between different studies is often not straightforward. Even though there are guidelines for reporting ocular aberrations,<sup>35–37</sup>

they do allow some freedom for data representation. One of the possible discrepancies between studies is the difference in pupil size and shape (spherical or elliptical) over which peripheral Zernike co-efficients are calculated. Confusion can also arise from different data types (for instance,  $J_0$ /Cylinder/C(2,2) for astigmatism), visualisation styles (table/chart/colour map) and the sign convention used to encode the angles of the visual field.

This paper is therefore intended to provide a comprehensive overview of results from previously published studies of peripheral ocular aberrations. An analysis of ocular modulation transfer functions (MTF) is also presented, which is essential to estimate the effect of the optical aberrations on central and peripheral vision. The data presented in this review have potential use in both research and clinical applications, including the design of optical eye models and the development of optical corrections.

### Peripheral ocular aberrations data

Peripheral ocular aberrations and their effect on retinal image quality were assessed using data from 16 articles, listed in Table 1.<sup>38-53</sup> For three studies, marked with an asterisk, wavefront data for each individual subject were generously shared by the authors.<sup>45,46,48</sup> The full list of articles considered for this review is provided in Table S1. The final decision to include an article was governed by the following criteria: (1) available data in multiple eccentricities over the horizontal visual field (VF); (2) wavefront data represented as a set of Zernike co-efficients; and (3) the number of participants in the study (at least 20).

All processing and analyses presented were conducted using the following guidelines.

- If the angular steps in data representations were denser than in the original publication, available data was linearly interpolated.
- No additional recalculations for the wavelength were made. Defocus data were unchanged from the original publications, assuming these measurements already compensated for any differences between the measurement wavelength and the visible spectrum wavelengths.
- The ocular wavefront measurements are represented as standard Zernike co-efficients for a 4 mm circular pupil so that comparison between different studies can be made.<sup>1,35-37,45</sup>

- If the relative peripheral refraction over the horizontal VF was not readily available in the article, it was calculated from Zernike co-efficients using the following formulas:

$$M = -\frac{4\sqrt{3}}{r_{pupil}^2}c_2^0 + \frac{12\sqrt{5}}{r_{pupil}^2}c_4^0 \quad [1]$$

Relative Peripheral Refraction =  $M(\theta) - M(\theta = 0)$ , where  $\theta$  is the angle in horizontal VF (negative for temporal VF).

- If astigmatism was not readily available as the horizontal Jackson cross cylinder ( $J_0$ ), it was calculated using one of the following methods (also see 'Comments' column in Table 1):

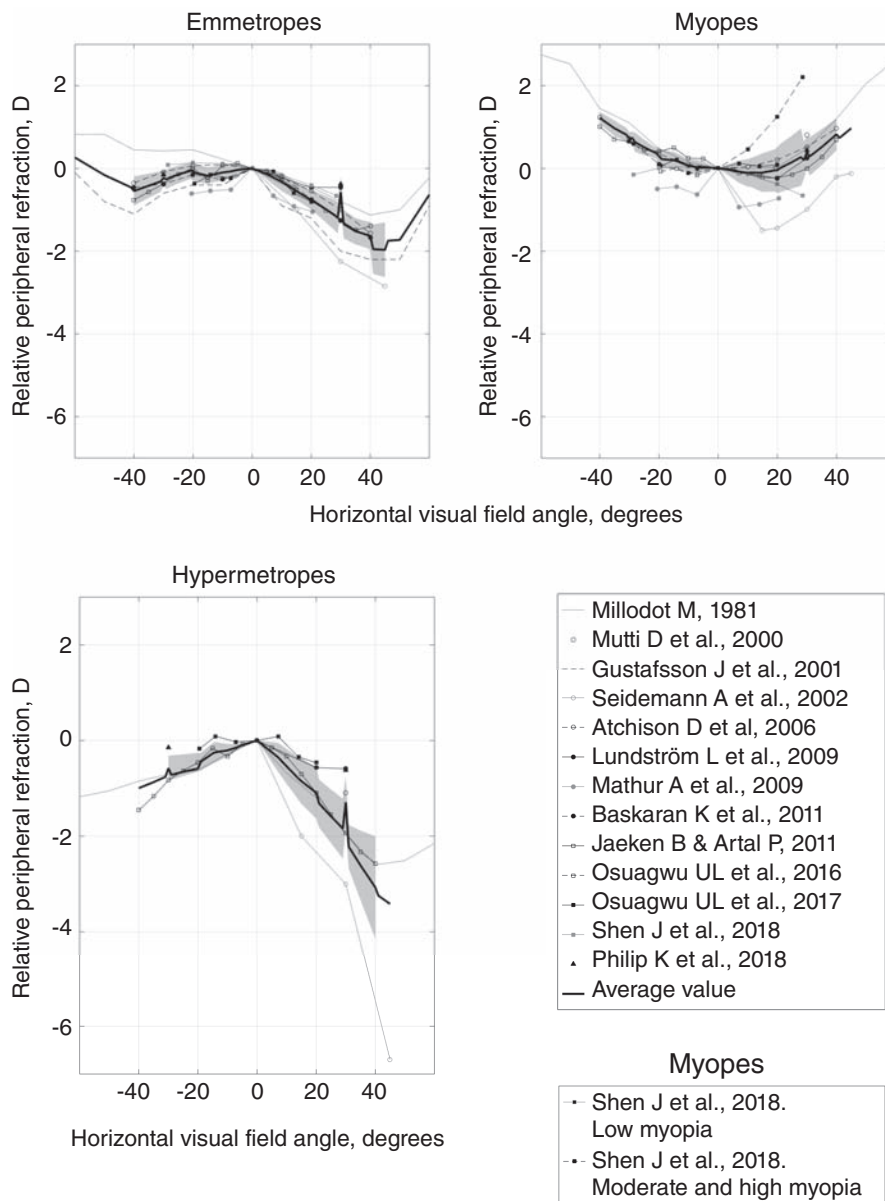


**Figure 1. Relative peripheral refraction in dioptres for emmetropes (top, left; 1,098 subjects), myopes (top, right; 427 subjects; weighted average spherical equivalent =  $-3.17 \pm 0.98$  D) and hypermetropes (bottom; 482 subjects; weighted average spherical equivalent =  $+1.25 \pm 0.49$  D). Negative visual angles correspond to the temporal visual field (nasal retina).**

- from Zernike co-efficients:

$$J_0 = -\frac{2\sqrt{6}}{r_{pupil}^2}c_2^2 + \frac{6\sqrt{10}}{r_{pupil}^2}c_4^2 \quad [2]$$

- using Sturm interval (taking half of the dioptric difference between the two line foci assuming  $J_{45} = 0$ );
- $J_0$  from cylinder power assuming  $J_{45} = 0$ :

$$J_0 = \frac{\text{Cylinder}}{2} \quad [3]$$

- Relative peripheral refraction data were divided into three refractive groups: myopes, emmetropes and hypermetropes. If not specified in the original article, the classification was made using these refractive error intervals: foveal refractive error  $\leq -0.50$  D for myopes;  $-0.50$  D < foveal refractive error <  $+0.50$  D for emmetropes; and foveal refractive error  $\geq +0.50$  D for hypermetropes.

- The population average optical errors, both in tables and figures, were calculated taking the number of subjects into consideration (that is, weighted average).

The combined effect of ocular aberrations on retinal image quality was assessed by calculating the monochromatic MTFs using all available Zernike co-efficients for each individual subject from three studies, marked with an asterisk in Table 1.<sup>45,46,48</sup> The average MTF curves presented in this review refer to the average of individual MTFs (not MTFs derived from Zernike co-efficients averaged across a cohort of individuals). For the off-axis horizontal VF MTF calculations, the elliptical shape of the pupil was taken into account by scaling the horizontal radius of the pupil by  $\cos(\theta)$ , where  $\theta$  is the angle in the horizontal VF.<sup>54</sup> The MTFs were represented and analysed as 2-D functions obtained as an average of the original MTF curves over all pupil meridians.

## Results

The subject group in this review is the combination of those for the studies listed in Table 1. Overall, it can be described as follows:

- 2,492 phakic subjects, both male and female
- no reported ocular conditions or surgeries
- 60 per cent emmetropes, 20 per cent myopes (weighted average spherical equivalent

$-2.90 \pm 1.10$  D), and 20 per cent hypermetropes (weighted average spherical equivalent  $+1.35 \pm 0.69$  D)

- age range five to 58 years
- except one study (Bakaraju et al.<sup>53</sup>) no pupil dilation, cycloplegia or fogging
- ethnicity not reported, but the studies have been conducted in Europe, Northern America and Australia.

The number of subjects and the amount of available data vary among the included studies (refer to the figures captions). Therefore, the sample size for each individual type of analysis may differ from the total number of

subjects. For more specific information, refer to the 'Subjects' and 'Used data' columns of Table 1.

Figures 1–3 show the population average defocus (relative peripheral refraction), horizontal astigmatism ( $J_0$ ), primary spherical aberration, and horizontal coma across the horizontal VF. The weighted average curves, represented by the thick lines, were calculated for the areas where data from more than one study were available. The shaded areas show  $\pm$  one standard deviation for regions with data from at least three studies. In Figure 1, relative peripheral refraction

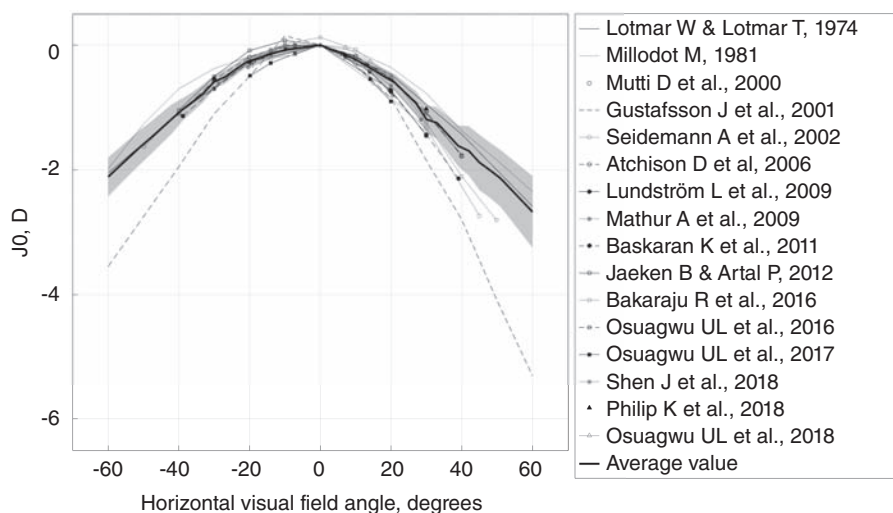


**Figure 2.  $J_0$  in dioptres for all subjects. Sample size: 2,493 subjects. Negative visual angles correspond to the temporal visual field (nasal retina).**

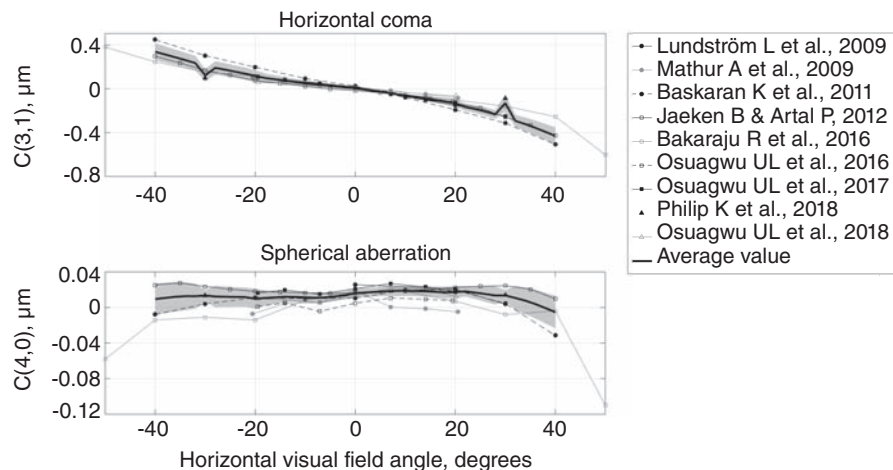
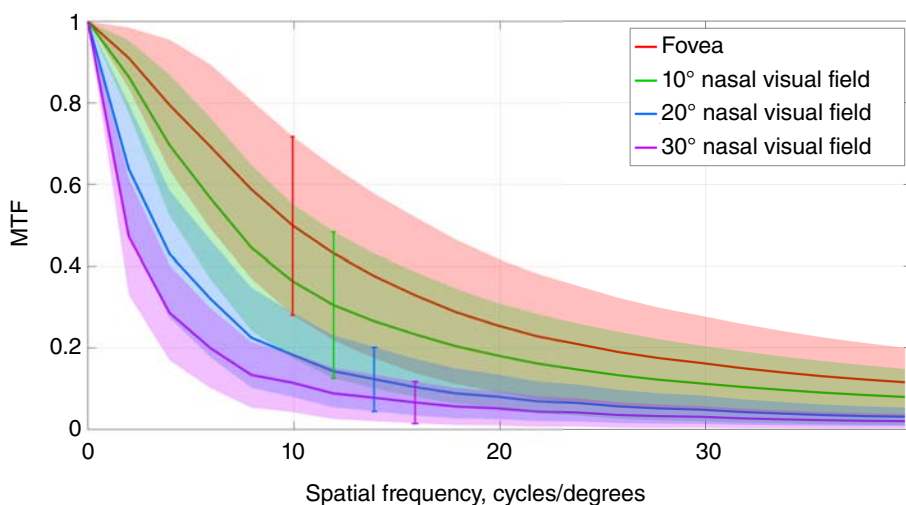


**Figure 3. Horizontal coma C(3,1) and primary spherical aberration C(4,0) in  $\mu\text{m}$  for all subjects (for a 4 mm pupil diameter). Sample size: 1,045 subjects. Negative visual angles correspond to the temporal visual field (nasal retina).**

is represented separately for emmetropes (top, left), myopes (top, right) and hypermetropes (bottom). Horizontal astigmatism (Figure 2) was not divided into subgroups because there was no correlation between off-axis astigmatism and central refractive error. Figure 3 represents Zernike coefficients for primary horizontal coma (top) and primary spherical aberration (bottom).

Population weighted average Zernike coefficients for the horizontal VF are listed in Table 2. The values were obtained using all studies from Table 1 with available wavefront data.<sup>45-53</sup> Calculations for each angular position were made for a 4 mm pupil diameter using the full extent of available wavefront data, that is all Zernike coefficients and all angles reported. However, it is important to mention that all of these studies contained measurements for different angular extents.

The MTF curves for the emmetropic subjects, obtained using the three studies marked in Table 1 with an asterisk,<sup>45,46,48</sup> are plotted in Figure 4 for four angles in the horizontal VF. The calculations were carried out for the following sample sizes: 84 subjects for fovea, 71 subjects for 10°, 84 subjects for 20°, and 74 subjects for 30°. The table below the figure shows the average MTF value ± standard deviation for six different spatial frequencies. As can be seen, the MTF monotonically decreases with the off-axis angle.



Angle, degrees	Spatial frequency, cycles/degrees					
	5	10	15	20	25	35
0	0.74 ± 0.18	0.50 ± 0.22	0.35 ± 0.20	0.25 ± 0.16	0.20 ± 0.14	0.13 ± 0.10
10	0.63 ± 0.18	0.36 ± 0.19	0.25 ± 0.16	0.18 ± 0.13	0.14 ± 0.11	0.09 ± 0.08
20	0.37 ± 0.15	0.18 ± 0.10	0.11 ± 0.07	0.08 ± 0.05	0.06 ± 0.04	0.04 ± 0.03
30	0.24 ± 0.11	0.11 ± 0.07	0.07 ± 0.05	0.05 ± 0.04	0.04 ± 0.03	0.02 ± 0.02

**Figure 4. Average modulation transfer function (MTF), calculated from available Zernike co-efficients,<sup>45,46,48</sup> for emmetropes in four angles of the nasal visual field (shown as solid lines). The shaded areas represent the standard deviation at each eccentricity. Sample sizes: 84 subjects for fovea, 71 subjects for 10°, 84 subjects for 20°, and 74 subjects for 30° of the nasal visual field. The table at the bottom shows average ± standard deviation for each curve at spatial frequencies up to 35 cycles/degree.**

## Discussion

This analysis pools peripheral ocular aberration data from a number of published studies to summarise the current understanding of optics and image quality across the horizontal VF in the human eye. All reviewed studies clearly show an increase in ocular optical errors with increasing off-axis angle, consistent with optical theory.

### Defocus

To be able to compare the peripheral spherical equivalent between different refractive error groups, relative peripheral refraction is often used. The relative peripheral refraction not only depends on the optical aberration field curvature (due to the oblique incidence of light), but also on the ocular shape. Therefore, both hypermetropes and emmetropes on average have a negative relative peripheral refraction (myopic, with the peripheral image in front of the retina), whereas myopes tend to have positive relative

peripheral refraction (hypermetropic, with the peripheral image behind the retina) due to the elongated shape of the eye (Figure 1).

### Astigmatism

As predicted by Coddington's equations,<sup>55</sup> astigmatism ( $J_0$ ) increases with increasing horizontal off-axis angle (Figure 2), best described by a quadratic function. Thus, second order polynomials can be fitted to the average curve in the figure (equation [4];  $\theta$  in degrees will give  $J_0$  in dioptres). This nature of peripheral astigmatism also dictates that the vertical astigmatism is rather small in the horizontal VF (for 20° nasal VF:  $J_0 = [-0.57 \pm 0.13]$  D,  $J_{45} = [0.06 \pm 0.07]$  D). With this in mind, Figure 2 illustrates that

for the horizontal VF the refractive error in the horizontal (tangential) meridian is noticeably more negative than in the vertical (sagittal) meridian. Thus, for the majority of the horizontal VF, the vertical line focus is located more anterior to the peripheral retina, whereas the horizontal line focus is closer to the retina.

### Spherical aberration

Both primary and higher order spherical aberrations are present for on-axis as well as for the off-axis object points (Table 2). However, for most of the VF primary spherical aberration C(4,0) is dominant. Figure 3 (top) shows that, on average, primary spherical aberration does not change

$$\begin{cases} J_0 = - (5.23 \cdot 10^{-4}) \cdot \theta^2 + (5.05 \cdot 10^{-3}) \cdot \theta, \theta \leq 0 \text{ (fitting error RMS = 0.037D),} \\ J_0 = - (3.17 \cdot 10^{-4}) \cdot \theta^2 - (5.05 \cdot 10^{-3}) \cdot \theta, \theta > 0, \text{ (fitting error RMS = 0.059D)} \end{cases} \quad [4]$$

Zernike term	Off-axis angle (negative angles correspond to temporal VF and positive to nasal VF)						
	-30°	-20°	-10°	0°	10°	20°	30°
C(2,-2)	+0.116 ± 0.227	+0.035 ± 0.136	0 ± 0.116	-0.038 ± 0.125	-0.057 ± 0.128	-0.047 ± 0.154	-0.126 ± 0.251
C(2,2)	+0.341 ± 0.366	+0.030 ± 0.239	-0.059 ± 0.214	-0.030 ± 0.223	+0.070 ± 0.217	+0.296 ± 0.349	+0.823 ± 0.547
C(3,-3)	+0.009 ± 0.040	-0.009 ± 0.040	-0.014 ± 0.031	-0.019 ± 0.044	-0.013 ± 0.033	-0.007 ± 0.037	+0.008 ± 0.065
C(3,-1)	+0.011 ± 0.069	+0.015 ± 0.046	0.010 ± 0.039	+0.007 ± 0.044	-0.003 ± 0.036	+0.001 ± 0.038	-0.001 ± 0.050
C(3,1)	+0.204 ± 0.107	+0.108 ± 0.066	+0.048 ± 0.042	+0.006 ± 0.041	-0.059 ± 0.041	-0.125 ± 0.076	-0.252 ± 0.136
C(3,3)	+0.037 ± 0.042	+0.012 ± 0.039	+0.009 ± 0.031	0 ± 0.036	-0.007 ± 0.030	-0.018 ± 0.045	-0.054 ± 0.084
C(4,-4)	+0.004 ± 0.011	+0.002 ± 0.016	0.003 ± 0.009	+0.002 ± 0.015	+0.001 ± 0.008	+0.002 ± 0.011	+0.007 ± 0.022
C(4,-2)	-0.002 ± 0.012	-0.001 ± 0.008	-0.001 ± 0.005	0 ± 0.009	-0.001 ± 0.006	0 ± 0.009	0 ± 0.016
C(4,0)	+0.014 ± 0.026	+0.009 ± 0.020	+0.010 ± 0.018	+0.015 ± 0.020	+0.017 ± 0.018	+0.016 ± 0.019	+0.013 ± 0.029
C(4,2)	+0.005 ± 0.018	0 ± 0.011	0 ± 0.010	0 ± 0.012	+0.001 ± 0.010	+0.002 ± 0.013	-0.001 ± 0.027
C(4,4)	+0.004 ± 0.011	+0.001 ± 0.010	+0.002 ± 0.012	+0.001 ± 0.013	+0.002 ± 0.010	+0.003 ± 0.012	-0.003 ± 0.263
C(5,-5)		0 ± 0.002	0 ± 0.001	0 ± 0.004	0 ± 0.002	-0.001 ± 0.005	-0.002 ± 0.009
C(5,-3)		0 ± 0.001	0 ± 0.001	+0.001 ± 0.004	0 ± 0.001	-0.001 ± 0.004	0 ± 0.006
C(5,-1)		0 ± 0.001	0 ± 0.001	0 ± 0.003	0 ± 0.001	-0.002 ± 0.004	-0.004 ± 0.007
C(5,1)		-0.001 ± 0.003	-0.001 ± 0.002	0 ± 0.003	0 ± 0.002	+0.001 ± 0.005	+0.004 ± 0.010
C(5,3)		0 ± 0.001	0 ± 0.001	0 ± 0.003	0 ± 0.001	+0.001 ± 0.003	+0.002 ± 0.081
C(5,5)		0 ± 0.002	0 ± 0.002	0 ± 0.003	0 ± 0.001	+0.001 ± 0.005	+0.003 ± 0.012
C(6,-6)		0 ± 0.001	0 ± 0.001	-0.001 ± 0.005	0 ± 0.001	+0.001 ± 0.005	-0.002 ± 0.004
C(6,-4)		0 ± 0.001	0 ± 0.001	0 ± 0.002	0 ± 0.001	0 ± 0.002	0 ± 0.004
C(6,-2)		0	0	0 ± 0.001	0 ± 0.001	0 ± 0.001	0 ± 0.003
C(6,0)		0 ± 0.001	0 ± 0.001	-0.001 ± 0.003	0 ± 0.001	0 ± 0.003	0 ± 0.006
C(6,2)		0 ± 0.001	0 ± 0.001	0 ± 0.001	0 ± 0.001	0 ± 0.002	+0.001 ± 0.004
C(6,4)		0 ± 0.001	0 ± 0.001	0 ± 0.001	0 ± 0.001	0 ± 0.002	+0.001 ± 0.004
C(6,6)		0 ± 0.001	0 ± 0.001	0 ± 0.002	0 ± 0.001	0 ± 0.003	+0.001 ± 0.004

Table 2. Population weighted average ± standard deviation of Zernike co-efficients (in micrometres for a 4 mm circular pupil) over the horizontal visual field (VF) from the studies marked in Table 1 with an asterisk<sup>45,46,48</sup>

much over the horizontal VF; however, there is some variation throughout the population.

### Horizontal coma

Foveal coma is usually small, and horizontal coma is dominant for purely horizontal off-axis angles. Primary horizontal coma shows a clear increase with increasing eccentricity (Figure 3, bottom) while the standard deviation for the average curve remains relatively low. A linear function can be fitted to the average curve in the figure ( $\theta$  in degrees will give the horizontal coma in  $\mu\text{m}$  for a 4 mm pupil diameter):

$$C(3,1)(\theta) = - (7.80 \cdot 10^{-3}) \cdot \theta - 1.420 \cdot 10^{-2}. \tag{5}$$

Using a third order polynomial would only improve the fitting root-mean-square-error by 0.016  $\mu\text{m}$  (from 0.040 to 0.0249  $\mu\text{m}$ ).

### Calculation of the ocular MTF

The central and peripheral MTFs in Figure 4 are calculated by averaging curves for all pupil meridians. Because of off-axis astigmatism across the majority of the horizontal VF, objects with horizontal lines are associated with better image quality than those with vertical lines. Therefore, the calculated MTFs represent the average retinal image quality for a stimulus containing details with all possible orientations. Apart from that, the shape of the ocular MTF itself depends on several parameters as well as the method of calculation.

### EFFECT OF NUMBER OF ZERNIKE TERMS ON MTF

By definition, Zernike series have an infinite number of elements; in practice the decomposition of a wavefront is more limited. Although the residual error is generally small, in some cases it can have a noticeable effect on the shape of the ocular MTF. In particular, accurate individual MTFs require more Zernike terms than population average curves. This can be illustrated by comparing the MTFs (1) for the full available extent of Zernike terms, and (2) for Zernike terms up to the third order and primary spherical aberration. While the average difference between these MTFs is close to zero, in individual cases it can be rather high (standard deviation of difference in MTFs = 0.05 @ 20 cycles/degree, for studies marked with an asterisk in Table 1, fovea).

### EFFECT OF PUPIL SHAPE ON MTF

For large off-axis angles the elliptical shape of the pupil affects the appearance of the ocular MTF curve. The difference in MTFs calculated using a 4 mm cosine-scaled elliptical pupil and a circular pupil becomes considerable for eccentricities of 30° and higher (standard deviation of difference in MTFs = 0.05 @ two cycles/degree, for studies marked with asterisk in Table 1, 30° horizontal VF).

### EFFECT OF AVERAGING METHODS ON MTF

In Figure 5 the average MTF and the MTF from average Zernike co-efficients are based on different mathematical approaches. The calculation of the average MTF consists of obtaining individual MTF curves calculated separately for each set of Zernike co-efficients of each subject, and then averaging these MTF curves. In contrast, the MTF from average Zernike co-efficients implies calculation of only one MTF curve from the set of already-averaged Zernike co-efficients. Figure 5 contains MTFs for four VF angles calculated with both described routines using available raw data for emmetropic subjects.<sup>45,46,48</sup> For each angle, the MTF from average Zernike co-efficients shows unrealistically high values. It is also worth noting that this difference is largest in the central VF and gradually decreases towards the periphery. This is because the

average peripheral optical errors are large compared to their intrasubject variation.

### Retinal image quality and myopia

The connection between myopia development and peripheral image quality in the human eye is not straightforward. Hoogerheide et al.<sup>56</sup> once suggested that relative peripheral hypermetropia is a risk factor for myopia development, but this conclusion was made without considering the change in ocular shape with ocular growth.<sup>57</sup> More recent studies show that relative peripheral hypermetropia is most likely a consequence of myopia and not its precursor.<sup>58,59</sup> That is, relative peripheral refraction depends on the degree of myopia.<sup>43</sup> This is also observed in the available raw data for 62 myopic subjects<sup>45,48</sup> (Figure 6). However, substantial differences in relative peripheral refraction for different degrees of myopia start appearing only at rather high eccentricities of the VF (20° and higher). It should further be mentioned that, as suggested earlier, comparison of relative peripheral refraction in the horizontal VF is most representative beyond 40° of eccentricity.<sup>60</sup>

Nevertheless, many reasonably effective myopia control interventions rely on manipulating the peripheral retinal image quality; the optical treatments with the highest efficacy are orthokeratology and multifocal soft

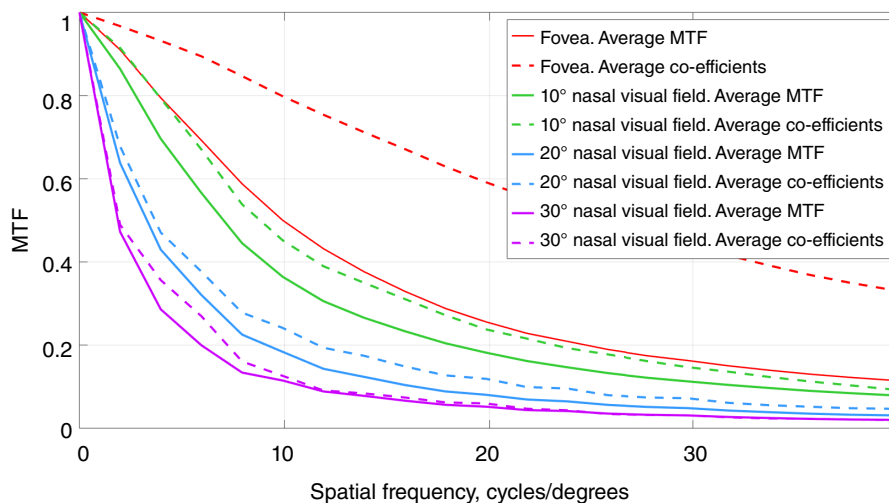


**Figure 5. Average modulation transfer function (MTF) and MTF from average Zernike co-efficients for four angular positions in the nasal visual field (VF) for the emmetropic cohort with available data.<sup>45,46,48</sup> Average MTF is calculated by averaging curves from individual Zernike data sets; MTF from average Zernike co-efficients is obtained by averaging individual Zernike data sets and subsequent MTF calculation. Sample sizes: 84 subjects for fovea, 71 subjects for 10°, 84 subjects for 20°, and 74 subjects for 30° of the nasal VF.**

contact lenses.<sup>33,35</sup> In orthokeratology, a reverse geometry rigid contact lens worn overnight flattens the central cornea, which decreases the overall optical power of the eye. However, this flattening in conjunction with relative steepening of the mid-peripheral cornea also results in increased off-axis astigmatism and inverted coma.<sup>61,62</sup> Currently available multifocal soft contact lens corrections impose a large depth of focus in the periphery.<sup>63,64</sup>

In order to further develop these optical myopia control interventions, it is important to compare peripheral image quality between myopes and emmetropes. Figure 7 shows the average MTFs for emmetropes and myopes with simulated central refractive error correction: foveal defocus and primary astigmatism were subtracted from every individual set of Zernike co-efficients (central and peripheral). As can be seen, the average MTF for myopic subjects is generally lower than that of emmetropic subjects over the horizontal VF. However, this difference becomes less prominent with increasing eccentricity and disappears at about 20° off-axis angle. Nonetheless, the results of Figure 7 need to be interpreted with caution, because there were cases with myopic subjects having better image quality than emmetropic ones (standard deviation not shown on the figure).

## Conclusion

This paper summarises the findings of 16 recent publications on the peripheral refractive errors and higher order aberrations in the horizontal VF. The presented data demonstrate an increase in aberrations with off-axis angle, well predicted by the optical aberrations theory.

Increasing amounts of the peripheral horizontal astigmatism and coma lead to an asymmetric profile of peripheral retinal image quality. Furthermore, the horizontal meridian (vertical line focus) is more myopic than the vertical meridian (horizontal line focus). Comparison between the different refractive groups shows that relative peripheral refraction is positive for myopic subjects while being negative for emmetropic and hypermetropic subjects.

Additionally, with ideal foveal refractive correction, myopes tend to have worse MTFs than emmetropes; this effect is less prominent for high eccentricities. The shape of MTF curve itself depends on the number

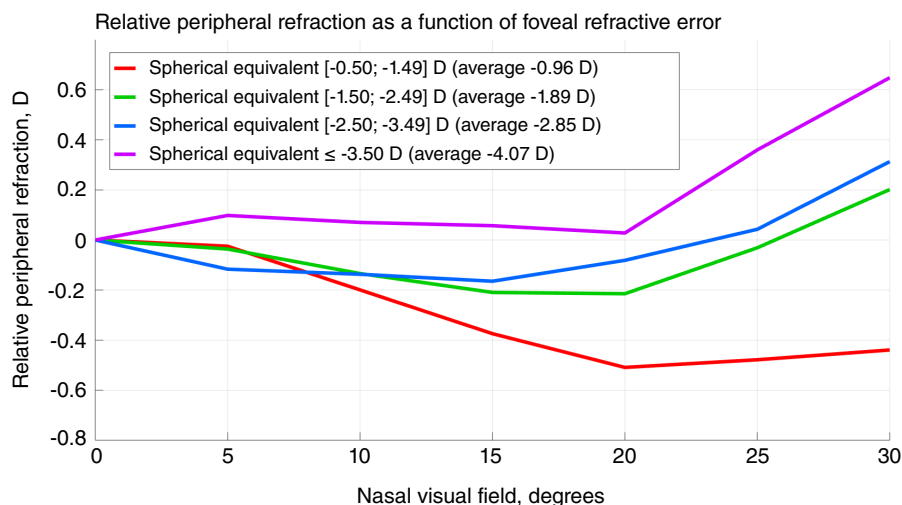


**Figure 6.** Relative peripheral refraction as a function of foveal refractive error across the nasal visual field. The curves are obtained using data from the three studies, marked in Table 1 with an asterisk.<sup>45,46,48</sup> Sample sizes: 19 subjects with spherical equivalent (−0.50; −1.49 D), 17 subjects with spherical equivalent (−1.50; −2.49 D), 17 subjects with spherical equivalent (−2.50; −3.49 D), nine subjects with spherical equivalent ≤ −3.50 D.

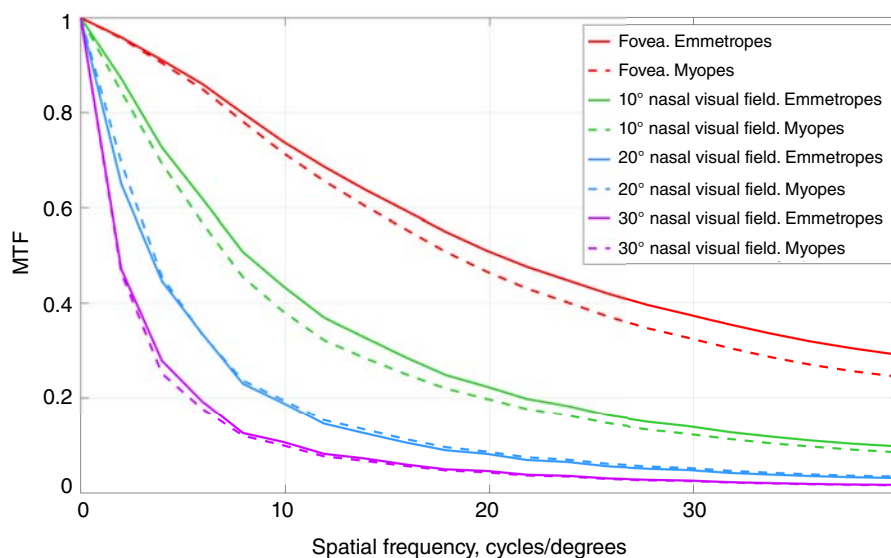


**Figure 7.** Average modulation transfer function (MTF) for emmetropes and myopes (with ideal central refractive correction) from the three studies marked in Table 1 with an asterisk<sup>45,46,48</sup> for four angular positions in the nasal visual field (0°, 10°, 20°, and 30°). Sample sizes: 84 emmetropes and 72 myopes for fovea; 71 emmetropes and 47 myopes for 10°; 84 emmetropes and 72 myopes for 20°; 74 emmetropes and 62 myopes for 30°. Weighted average spherical equivalent of the whole myopic group −2.41 ± 0.55 D.

of Zernike terms used (mostly in the fovea) and the shape of the pupil (at angles ≥ 30°). A considerable difference was also found between the average MTF and the MTF

from average Zernike co-efficients with the latter demonstrating artificially high retinal image quality, especially in the central VF.

## ACKNOWLEDGEMENTS

The authors would like to gratefully acknowledge Professor David Atchison, Doctor Karthikeyan Baskaran, Professor Pablo Artal, and Doctor Bart Jaeken for providing data essential for this article. This review was supported by the MyFUN project, that receives funding from the European Union's Horizon 2020 Research and Innovation Programme under the Marie Skłodowska-Curie grant agreement No 675137.

## REFERENCES

- Lundström L, Rosén R. Peripheral aberrations. In: Artal P, ed. *Handbook of Visual Optics*, Vol. 1, 1st ed. Boca Raton, FL: CRC Press, 2017. pp. 313–335.
- Lundström L, Manzanera S, Prieto PM et al. Effect of optical correction and remaining aberrations on peripheral resolution acuity in the human eye. *Opt Express* 2007; 15: 12654–12661.
- Thibos LN, Cheney FE, Walsh DJ. Retinal limits to the detection and resolution of gratings. *J Opt Soc Am A* 1987; 4: 1524–1529.
- Thibos LN, Still DL, Bradley A. Characterization of spatial aliasing and contrast sensitivity in peripheral vision. *Vision Res* 1996; 36: 249–258.
- Williams DR, Coletta NJ. Cone spacing and the visual resolution limit. *J Opt Soc Am A* 1987; 4: 1514–1523.
- Wang YZ, Thibos LN, Bradley A. Effects of refractive error on detection acuity and resolution acuity in peripheral vision. *Invest Ophthalmol Vis Sci* 1997; 38: 2134–2143.
- Rosén R, Lundström L, Unso P. Influence of optical defocus on peripheral vision. *Invest Ophthalmol Vis Sci* 2011; 52: 318–323.
- Venkataraman AP, Papadogiannis P, Romashchenko D et al. Peripheral resolution and contrast sensitivity: effects of monochromatic and chromatic aberrations. *J Opt Soc Am A* 2019; 36: B52–B57.
- Owsley C, McGwin G. Vision impairment and driving. *Surv Ophthalmol* 1999; 43: 535–550.
- Wetton MA, Horswill MS, Hatherly C et al. The development and validation of two complementary measures of drivers' hazard perception ability. *Accid Anal Prev* 2010; 42: 1232–1239.
- Wood JM, Troutbeck R. Effect of restriction of the binocular visual field on driving performance. *Ophthalmic Physiol Opt* 1992; 12: 291–298.
- Patino CM, McKean-Cowdin R, Azen SP et al. Central and peripheral visual impairment and the risk of falls and falls with injury. *Ophthalmology* 2010; 117: 199–206.e1.
- Berenci A, Ishihara M, Imanaka K. The functional role of central and peripheral vision in the control of posture. *Hum Mov Sci* 2005; 24: 689–709.
- Dakin S, Fiser J, Pasquale LR et al. Effects of peripheral visual field loss on eye movements during visual search. *Front Psychol* 2012; 3: 1–13.
- Lewis P, Venkataraman AP, Lundström L. Contrast sensitivity in eyes with central scotoma. *Optom Vis Sci* 2018; 95: 354–361.
- Baskaran K, Rosén R, Lewis P et al. Benefit of adaptive optics aberration correction at preferred retinal locus. *Optom Vis Sci* 2012; 89: 1417–1423.
- Lundström L, Gustafsson J, Unso P. Vision evaluation of eccentric refractive correction. *Optom Vis Sci* 2007; 84: 1046–1052.
- Jaeken B, Mirabet S, Marín JM et al. Comparison of the optical image quality in the periphery of phakic and pseudophakic eyes. *Invest Ophthalmol Vis Sci* 2013; 54: 3594–3599.
- Holden BA, Mariotti SP, Kocur I et al. Impact of increasing prevalence of myopia and high myopia. In: Holden BA, ed. *Report of the Joint World Health Organization - Brien Holden Vision Institute Global Scientific Meeting on Myopia*. Sydney: University of New South Wales, 2015.
- Flitcroft DL. The complex interactions of retinal, optical and environmental factors in myopia aetiology. *Prog Retin Eye Res* 2012; 31: 622–660.
- Holden B, Sankaridurg P, Smith E et al. Myopia, an underrated global challenge to vision: where the current data takes us on myopia control. *Eye* 2014; 28: 142–146.
- Goldschmidt E, Jacobsen N. Genetic and environmental effects on myopia development and progression. *Eye* 2014; 28: 126–133.
- Wallman J, Winawer J. Homeostasis of eye growth and the question of myopia. *Neuron* 2004; 43: 447–468.
- Williams KM, Bertelsen G, Cumberland P et al. Increasing prevalence of myopia in Europe and the impact of education. *Ophthalmology* 2015; 122: 1489–1497.
- Verkicharla PK, Ohno-Matsui K, Saw SM. Current and predicted demographics of high myopia and an update of its associated pathological changes. *Ophthalmic Physiol Opt* 2015; 35: 465–475.
- Schaeffel F, Glasser A, Howland HC. Accommodation, refractive error and eye growth in chickens. *Vision Res* 1988; 28: 639–657.
- Irving EL, Sivak JG, Callender MG. Refractive plasticity of the developing chick eye: a summary and update. *Ophthalmic Physiol Opt* 2015; 35: 600–606.
- Hung L-F, Crawford MJ, Smith EL. Spectacle lenses alter eye growth and the refractive status of young monkeys. *Nat Med* 1995; 1: 761–765.
- Smith EL 3rd, Kee C-S, Ramamirtham R et al. Peripheral vision can influence eye growth and refractive development in infant monkeys. *Invest Ophthalmol Vis Sci* 2005; 46: 3965–3972.
- Benavente-Pérez A, Nour A, Troilo D. Axial eye growth and refractive error development can be modified by exposing the peripheral retina to relative myopic or hyperopic defocus. *Invest Ophthalmol Vis Sci* 2014; 55: 6765–6773.
- Whatham AR, Judge SJ. Compensatory changes in eye growth and refraction induced by daily wear of soft contact lenses in young marmosets. *Vision Res* 2001; 41: 267–273.
- McFadden SA, Howlett MHC, Mertz JR. Retinoic acid signals the direction of ocular elongation in the Guinea pig eye. *Vision Res* 2004; 44: 643–653.
- Huang J, Wen D, Wang Q et al. Efficacy comparison of 16 interventions for myopia control in children: a network meta-analysis. *Ophthalmology* 2016; 123: 697–708.
- Smith EL III, Campbell MCW, Irving E. Does peripheral retinal input explain the promising myopia control effects of corneal reshaping therapy (CRT or ortho-K) & multifocal soft contact lenses? *Ophthalmic Physiol Opt* 2013; 33: 379–384.
- American National Standard for Ophthalmics: Methods for Reporting Optical Aberrations of Eyes; ANSI Z80.28–2004. Merrifield, VA: Optical Laboratory Association, 2004.
- Ophthalmic Optics and Instruments - Reporting Aberrations of the Human Eye*, ISO 24157:2008, 1st ed. Case postale 56 CH-1211 Geneva 20: International Organization for Standardization, 2008.
- Thibos L, Applegate RA, Schwiegerling JT et al. Standards for reporting the optical aberrations of eyes. *J Refract Surg* 2002; 18: S652–S660.
- Lotmar W, Lotmar T. Peripheral astigmatism in the human eye: experimental data and theoretical model predictions. *J Opt Soc Am* 1974; 64: 510–513.
- Millodot M. Effect of ametropia on peripheral refraction. *Am J Optom Physiol Opt* 1981; 58: 691–695.
- Mutti DO, Sholtz RI, Friedman NE et al. Peripheral refraction and ocular shape in children. *Invest Ophthalmol Vis Sci* 2000; 41: 1022–1030.
- Gustafsson J, Terenius E, Buchheister J et al. Peripheral astigmatism in emmetropic eyes. *Ophthalmic Physiol Opt* 2001; 21: 393–400.
- Seidemann A, Schaeffel F, Guirao A et al. Peripheral refractive errors in myopic, emmetropic, and hyperopic young subjects. *J Opt Soc Am A* 2002; 19: 2363–2373.
- Atchison DA, Pritchard N, Schmid KL. Peripheral refraction along the horizontal and vertical visual fields in myopia. *Optom Vis Sci* 2006; 46: 1450–1458.
- Shen J, Spors F, Egan D et al. Peripheral refraction and image blur in four meridians in emmetropes and myopes. *Clin Ophthalmol* 2018; 12: 345–358.
- Lundström L, Gustafsson J, Unso P. Population distribution of wavefront aberrations in the peripheral human eye. *J Opt Soc Am A* 2009; 26: 2192–2198.
- Mathur A, Atchison DA, Charman WN. Myopia and peripheral ocular aberrations. *J Vis* 2009; 9: 1–12.
- Baskaran K, Unso P, Gustafsson J. Influence of age on peripheral ocular aberrations. *Optom Vis Sci* 2011; 88: 1088–1098.
- Jaeken B, Artal P. Optical quality of emmetropic and myopic eyes in the periphery measured with high-angular resolution. *Invest Ophthalmol Vis Sci* 2012; 53: 3405–3413.
- Osugwu UL, Suheimat M, Atchison DA. Mirror symmetry of peripheral monochromatic aberrations in fellow eyes of isomyopes and anisomyopes. *Invest Ophthalmol Vis Sci* 2016; 57: 3422–3428.
- Osugwu UL, Suheimat M, Atchison DA. Peripheral aberrations in adult hyperopes, emmetropes and myopes. *Ophthalmic Physiol Opt* 2017; 37: 151–159.
- Philip K, Sankaridurg PR, Ale JB et al. Profile of off-axis higher order aberrations and its variation with time among various refractive error groups. *Vision Res* 2018; 153: 111–123.
- Osugwu UL, Verkicharla P, Suheimat M et al. Peripheral monochromatic aberrations in young adult Caucasian and East Asian eyes. *Optom Vis Sci* 2018; 95: 234–238.
- Bakaraju RC, Fedtke C, Ehrmann K et al. Peripheral refraction and higher-order aberrations with cycloplegia and fogging lenses using the BHVI-EyeMapper. *J Optom* 2016; 9: 5–12.
- Mathur A, Gehrman J, Atchison DA. Pupil shape as viewed along the horizontal visual field. *J Vis* 2013; 13: 1–8.
- Freeman MH, Hull CC. *Optics*, 11th ed. Oxford: Butterworth-Heinemann, 2003. pp. 250–251.
- Hoogerheide J, Rempt F, Hoogenboom WP. Acquired myopia in young pilots. *Ophthalmologica* 1971; 163: 209–215.
- Rosén R, Lundström L, Unso P et al. Have we misinterpreted the study of Hoogerheide et al. (1971)? *Optom Vis Sci* 2012; 89: 1235–1237.
- Atchison DA, Li SM, Li H et al. Relative peripheral hyperopia does not predict development and progression of myopia in children. *Invest Ophthalmol Vis Sci* 2015; 56: 6162–6170.
- Mutti DO, Sinnott LT, Mitchell GL et al. Relative peripheral refractive error and the risk of onset and progression of myopia in children. *Invest Ophthalmol Vis Sci* 2011; 52: 199–205.
- Mathur A, Atchison DA. Peripheral refraction patterns out to large field angles. *Optom Vis Sci* 2013; 90: 140–147.
- Mathur A, Atchison D. Effect of orthokeratology on peripheral aberrations of the eye. *Optom Vis Sci* 2009; 86: E476–E484.
- Gonzalez-Mejome JM, Faria-Ribeiro MA, Lopes-Ferreira DP et al. Changes in peripheral refractive profile after orthokeratology for different degrees of myopia. *Curr Eye Res* 2016; 41: 199–207.
- Rosén R, Jaeken B, Lindskoog-Petersson A et al. Evaluating the peripheral optical effect of multifocal contact lenses. *Ophthalmic Physiol Opt* 2012; 32: 527–534.
- Ji Q, Yoo Y-S, Alam H et al. Through-focus optical characteristics of monofocal and bifocal soft contact lenses across the peripheral visual field. *Ophthalmic Physiol Opt* 2018; 38: 326–336.

## Supporting information

Additional supporting information may be found in the online version of this article at the publisher's website:

**Table S1.** List of studies on peripheral refraction and higher order aberrations.



## Aberrations and accommodation

*Clin Exp Optom* 2020; 103: 95–103

DOI:10.1111/cxo.12938

**Antonio J Del Águila-Carrasco\*** PhD

**Philip B Kruger<sup>†</sup>** PhD OD

**Francisco Lara<sup>‡</sup>** PhD

**Norberto López-Gil<sup>‡</sup>** PhD

\*Eye and Vision Research Group, School of Health Professions, University of Plymouth, Plymouth, UK

<sup>†</sup>College of Optometry, The State University of New York, New York, NY, USA

<sup>‡</sup>Vision Science Research Group (CIVIUM), Instituto Universitario de Investigación en Envejecimiento (IUIE), University of Murcia, Murcia, Spain  
E-mail: norberto@um.es

Submitted: 30 March 2019

Revised: 22 May 2019

Accepted for publication: 23 May 2019

**Key words:** aberrations, accommodation, dynamic accommodation

Accommodation can be thought of as a natural adaptive optics mechanism to improve the retinal image quality of objects placed at different distances. It was Thomas Young who demonstrated at the beginning of the 19th century that the change in refractive power of the eye is due to the crystalline lens.<sup>1,2</sup> Currently, it is well known that there are no significant changes in corneal power during accommodation,<sup>3,4</sup> and only small changes have been observed in the sclera.<sup>5</sup> In addition to this, Young realised that the refractive power in the periphery of his pupil was greater than in the centre, and when he accommodated, the refractive power distribution was opposite.<sup>1,2</sup> This was the first observation that proved that the spherical aberration (SA) of the eye changed its sign with accommodation.

Two centuries after Young's discoveries, the measurement of spherical and other aberrations of the accommodated eye can be performed *in vivo* using wavefront sensors. As accommodation dynamically changes,<sup>6,7</sup> fast wavefront sensors, such as a Hartmann-Shack need to be used.<sup>8,9</sup> The experimental system should include the

Modern methods of measuring the refractive state of the eye include wavefront sensors which make it possible to monitor both static and dynamic changes of the ocular wavefront while the eye observes a target positioned at different distances away from the eye. In addition to monitoring the ocular aberrations, wavefront refraction methods allow measurement of the accommodative response while viewing with the eye's habitual chromatic and monochromatic aberrations present, with these aberrations removed, and with specific aberrations added or removed. A large number of experiments describing the effects of accommodation on aberrations and vice versa are reviewed, pointing out the implications for fundamental questions related to the mechanism of accommodation.

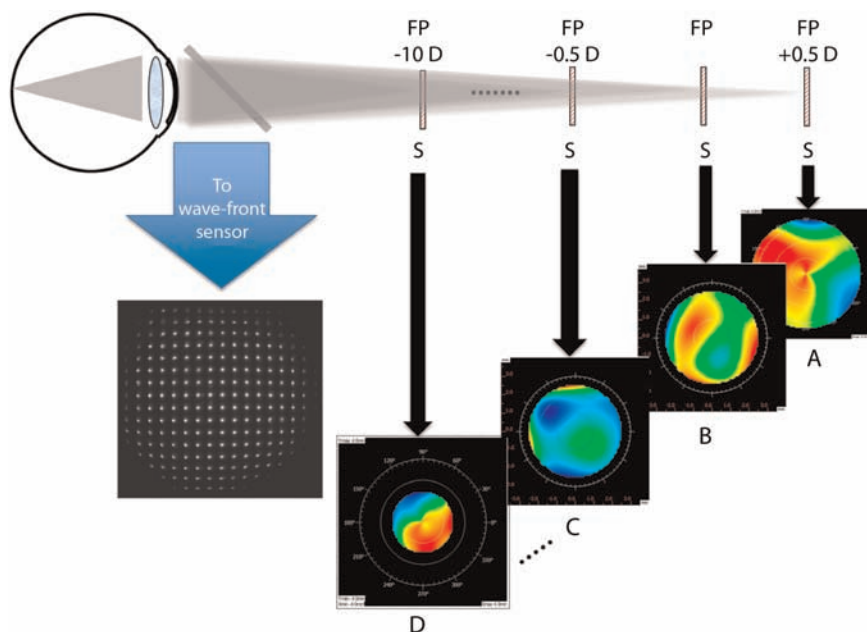
possibility of changing the vergence of the target (by changing the distance between the eye and the target, or by adding lenses), to stimulate the subject's accommodation. There are several commercially available devices that can measure aberrations while stimulating accommodation (for example, iRX3, COAS-HD, WASCA, iTrace) as well as custom-built systems.<sup>10</sup>

Figure 1 shows a schematic of the methodology typically used to measure ocular aberrations during accommodation in a static procedure. A Badal lens (not shown) is usually used so the target always subtends the same visual angle regardless of its optical vergence.<sup>11</sup> After each change in vergence the target remains static for some time before the wavefront is measured to allow time for the subject to accommodate. Step changes in vergence (0.5 D in Figure 1), far point (FP), maximum vergence, and target configuration (for example, monochromatic/polychromatic, spatial frequency content) vary depending on the study. For dynamic studies, the target vergence is usually continuously modified, following a pre-determined vergence function such as a sinusoidal or a random step function.

Besides the changes of ocular aberrations due to the change in curvature of the external surfaces of the crystalline lens of the eye,<sup>12</sup> the ocular wavefront may also change due to:

- displacement and tilt of the lens<sup>13</sup>
- pupil changes (accommodative miosis)<sup>13</sup>
- torsions on the eye globe produced by binocular convergence<sup>14</sup>
- changes of the internal iso-indicial surfaces of the lens.<sup>15</sup>

The study of accommodation and its relationship with aberrations can be carried out through two time domains: static and dynamic. The term static accommodation refers to the steady state condition of accommodation while viewing a stationary target at a fixed distance from the eye. But accommodation is never really static, instead fluctuating continuously over a small range. These small microfluctuations<sup>6,7</sup> of accommodation are a dynamic characteristic of accommodation even under static steady state conditions. Dynamic accommodation refers to the change in ocular focus that occurs in response to changes in accommodative demand, including sudden step changes from one target distance to another, sinusoidal



**Figure 1. Schematic of the methodology for measuring aberrations during accommodation.** In this example, the stimulus (S) is initially placed 0.50 D beyond the subjective far point (FP) (FP +0.50 D), where a wavefront A is measured. Then, it can be moved to the FP, where wavefront B is now obtained. The same procedure is repeated (wavefront C) until the stimulus vergence reaches the maximum vergence to be measured corresponding in this case to 10.00 D closer than the FP (FP –10.00 D), giving the wavefront D. To cover all the intervals of accommodation it is assumed that the largest vergence (10.00 D) is closer than the subject’s near point.

changes, and unpredictable sum-of-sines changes in target distance. Finally, dynamic accommodation also refers to the ongoing microfluctuations of accommodation.<sup>6,7</sup>

Knowledge of how aberrations vary with static accommodation provides information about the shape of the surface of the lens<sup>12</sup> as well as information about its internal structure.<sup>15</sup> Dynamic accommodation studies usually shed light on fundamental questions such as which cues trigger the accommodation system to accurately change the power of the lens and accommodate in the right direction,<sup>10,16–19</sup> which is of particular interest concerning myopia development.<sup>20–22</sup> From an applied science perspective, knowledge of how aberrations change with accommodation can lead to improved designs of multifocal and accommodative intraocular lenses, which imitate the profile of ocular aberrations during accommodation. Knowing the effect of aberrations on accommodation can also lead to new contact and intraocular lens designs with customised aberration profiles that extend the depth of field.<sup>23–25</sup>

This review examines the relationship between accommodation and ocular aberrations in detail. Given the differences in methodologies and the different types of aberrations considered by different authors, this manuscript treats static and dynamic accommodation, and the effect of monochromatic and chromatic aberrations separately.

### The influence of aberrations on the subjective and objective amplitude of accommodation

The amplitude of accommodation (AA) can be measured objectively as the dioptric change between the FP and the near point (NP). However, the eye does not present a constant refractive power across the whole pupil due to astigmatism and other higher-order aberrations (HOAs), and theoretically numerous FPs and NPs exist depending on the region of interest examined within the pupil. Therefore, HOAs influence the AA. A number of objective methods (metrics) for determining accommodation or AA from

wavefront analysis have been applied.<sup>26,27</sup> All of them show smaller objective AA values than the subjective AA obtained as the dioptric difference between the subjective far and NPs. Three optical reasons have been proposed to explain such differences.

Typically, subjective AA is measured after correcting any distance ametropia and computed as the inverse of the distance to the NP with respect to the spectacle plane. However, using this reference plane without performing the corresponding mathematical correction overestimates subjective AA, especially in young myopic subjects.<sup>28</sup>

The metric chosen to calculate the subjective AA can cause a false accommodative error. For instance, positive SA (typical in an unaccommodated eye) can cause the objective measurement of the FP to be more myopic than the subjective one,<sup>29,30</sup> and as a consequence an accommodative lead will be observed (Figure 2). On the other hand, negative SA (typical in the accommodating eye), can result in a smaller objective maximum accommodation than observed with the subjective method, which translates to an apparent accommodative lag<sup>12,29,31,32</sup> (Figure 2).

It has been demonstrated that the eye uses its depth of field both in far and near vision in order to increase the subjective AA.<sup>33</sup> In addition to the limitation imposed by photoreceptor sampling and photonic noise, depth of field occurs because of the presence of HOAs when the pupil is larger during relaxed accommodation,<sup>24</sup> and as a consequence of the accommodative miosis.<sup>34</sup>

### Monochromatic aberrations and static accommodation

During accommodation, not only is the defocus term modified, but other monochromatic aberrations vary too. The change in monochromatic aberrations during accommodation has been extensively studied.<sup>29,35–38</sup> In general, all monochromatic aberrations change with accommodation; however, this change is generally small and subject-dependant.<sup>37</sup>

The change in astigmatism is generally small,<sup>39</sup> although there are some exceptions where the magnitude and axis vary significantly with accommodation.<sup>40,41</sup> Changes in astigmatism with accommodation may be due to an increase in lens tilt caused by the combined effects of a slacker zonular tension and gravity.<sup>42</sup> Astigmatism can also change with accommodative miosis in the presence of HOA, although this potential explanation has not been verified to date.

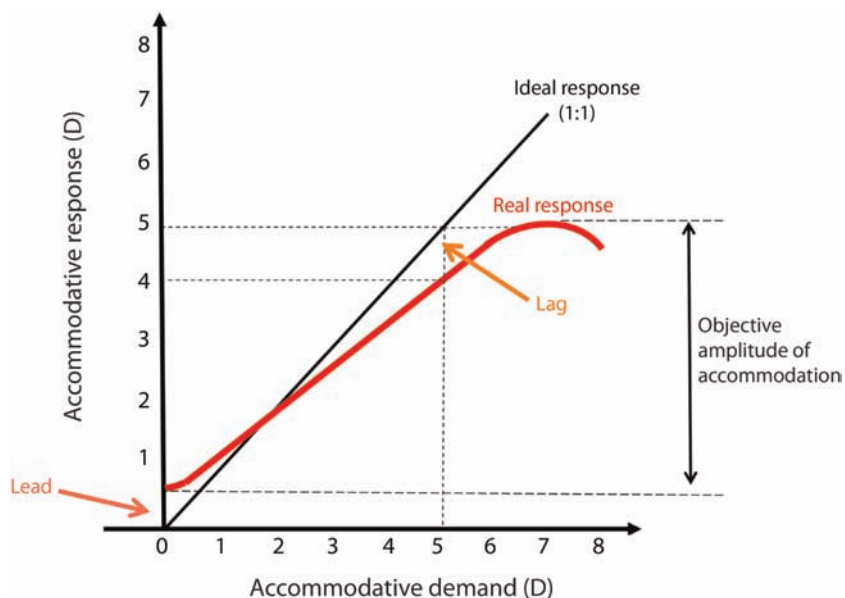


**Figure 2. Typical accommodative response. For an accommodative demand of 0 D, that is, when the stimulus is at the far point (FP) accommodation of the eye should be relaxed, but usually presents an accommodative lead. For vergences larger than 2.00 D, the eye typically presents an accommodative lag. Objective amplitude of accommodation is found as the dioptric range between the minimum and the maximum accommodation response.**

Third-order aberrations (that is, coma and trefoil) may also vary during accommodation, but not systematically,<sup>36,37</sup> and in many eyes these aberrations remain relatively stable over the range of accommodation demands.<sup>35,42,43</sup>

In the case of fourth-order SA, there is agreement between numerous studies about its well-defined trend, becoming less positive (or more negative) with increasing accommodation.<sup>29,35,36</sup> As mentioned earlier, this was originally discovered by Young,<sup>1,2</sup> although he did not give it the name of SA. After Young, many others reported this change,<sup>29,35,36</sup> which has been proven to be generated because of the hyperbolic shape of the surfaces of the crystalline lens.<sup>12</sup> Usually, in the relaxed eye corneal positive SA is larger than the absolute value of the crystalline lens SA (negative value), so the total eye has a slight positive SA. However, when the eye accommodates the crystalline lens increases its SA negative value, and the total SA of the eye becomes negative (see Figure 3). Therefore, generally speaking, the relaxed eye has positive SA and the accommodated eye has negative SA. However, there are exceptions to this rule. For instance, the eye may have negative SA when relaxed which becomes more negative

during accommodation; or it may have a large positive value of SA which decreases during accommodation but never becomes negative. But in any case, SA decreases with accommodation for a fixed pupil size.

There are no other systematic changes in any HOA except sixth-order SA, which increases during accommodation.<sup>12,44</sup> However, the values of that aberration are usually very small, and in many cases fall below the experimental errors.

There are a few studies that have shown how some aberrations influence static accommodation. In particular, Khosravi<sup>45</sup> showed that the accommodation response to a grating stimulus in the presence of astigmatism depends on the orientation of the grating, but for multiple orientations, the accommodation response usually corresponds with the circle of least confusion. A different study used adaptive optics to study the effect of one micron of coma or fourth-order SA on the accommodation response, finding that those aberrations may increase the accommodation error, especially when positive SA was induced.<sup>46</sup> The effect of fourth- and six-order SA on the accommodation response has also been studied theoretically by other researchers<sup>32</sup> with the

hypothesis that the change of SA during accommodation may play a role in myopia development. Their explanation is based on the fact that the combination of negative SA (typical in the accommodated eye) with negative defocus (hyperopic image, or lag of accommodation) increases visual detection of the letters although it reduces image contrast, which may promote growth of the eye.

### Chromatic aberration and static accommodation

In a non-cycloplegic eye, even when the target vergence is kept constant, the level of accommodation fluctuates continuously over a small range of approximately  $\pm 0.50$  D at temporal frequencies ranging up to a few cycles per second.<sup>6,7</sup> Chromatic dispersion of light by the optical components of the eye<sup>47-49</sup> results in retinal images of polychromatic objects with subtle colour fringes at the edges that reliably indicate whether the image is focused behind or in front of the retina.<sup>47-49</sup> These colour fringes change substantially when the eye changes focus (Figure 4). When red light is focused on the retina, blue light is focused in front of the retina, and a fuzzy blue colour fringe is formed at the image edge, so under-accommodation (hyperopic defocus) is characterised by a red colour fringe, while over-accommodation (myopic defocus) results in a blue colour fringe. These colour cues provide reliable directional signals for accommodation.<sup>50-54</sup>

Fincham<sup>50</sup> was the first investigator to remove the effects of chromatic aberration by using monochromatic light and by placing a specially designed achromatising lens in front of the eye. He used a coincidence optometer to measure accommodation while trial lenses were placed in front of the subject's eye and found that accommodation was impaired in some subjects when chromatic aberration was removed. By the mid-1980s high-speed recording of accommodation was available<sup>55</sup> to test Fincham's hypothesis that chromatic aberration provides a cue for static accommodation. Subjects viewed stationary targets at 0 D, 2.5 D and 5 D in white and monochromatic light, and in white light with chromatic aberration reversed by a specially designed lens.<sup>52</sup> When chromatic aberration was removed, some subjects had difficulty accommodating and when chromatic aberration was reversed, so that blue light focused further back in the eye than red light, accommodation was severely impaired, and some subjects accommodated in the wrong

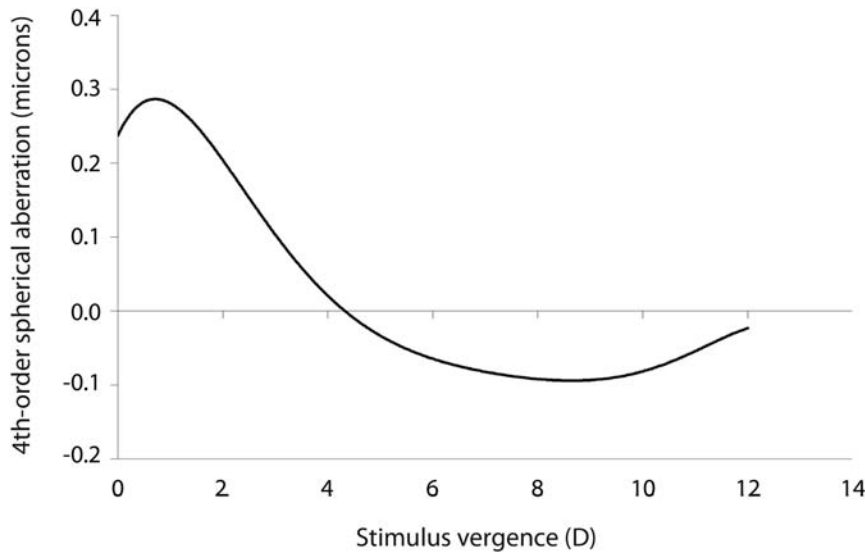


**Figure 3.** Example of the change of fourth-order spherical aberration with accommodation in a young subject with an amplitude of accommodation (AA) > 12.00 D. In the relaxed eye the value is positive decreasing with accommodation and becoming negative. For large values of accommodation demand, spherical aberration tends to zero because the subject's pupil becomes small.

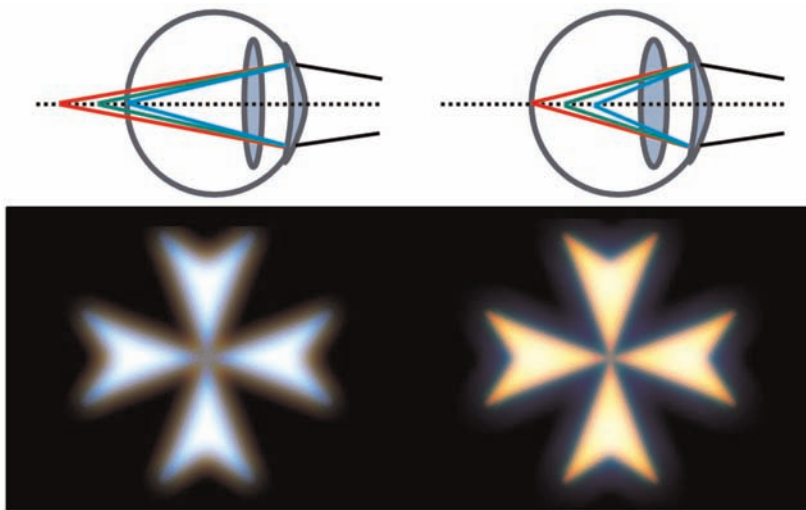


**Figure 4.** Ray diagrams illustrate under-accommodation (hyperopic defocus) on the top left side of the figure and over-accommodation (myopic defocus) on the top right side. In the presence of chromatic aberration, under-accommodation produces blur spread-functions with a red colour fringe, whereas over-accommodation produces blur spread-functions with a blue colour fringe, as can be seen in the bottom row. Adapted from Del Águila-Carrasco.<sup>66</sup>

direction when chromatic aberration was reversed.

Next, computer-generated images that simulated hyperopic and myopic defocus with and without the effects of longitudinal

chromatic aberration (LCA)<sup>53</sup> or transverse chromatic aberration (TCA)<sup>54</sup> were used to drive accommodation for near and far distances. These simulated images were viewed through small pinhole pupils to

eliminate the normal blur feedback from trial-and-error microfluctuations<sup>6,7</sup> of accommodation that were believed to be essential for effective accommodation. Accommodation responded readily to these static simulations of LCA, and accommodation was not adversely affected by simulations of LCA that included typical amounts of TCA.

Some authors have argued that chromatic aberration does not play a role in accommodation because when an isoluminant target is used (that is, a red target on a green background or vice versa, both with the same luminance), accommodation is not induced.<sup>56,57</sup> However, this conclusion may not be valid<sup>58</sup> since colour and luminance signals are mixed in a single neural channel rather than separate channels.<sup>59,60</sup> Furthermore, it is well known that many other visual functions fail under isoluminant target conditions, including form, colour, motion, and depth perception.<sup>59,61,62</sup> Further investigations are required in this field.

The magnitude of LCA depends on the refractive index and dispersive power of the ocular media. The crystalline lens of the eye has a gradient refractive index structure (GRIN) with maximum refractive index at the centre and a minimum at the periphery.<sup>63-65</sup> During accommodation it becomes more convex, especially the anterior lens surface, and there is also a change in the distribution of the gradient refractive index that produces a small increase in the equivalent refractive index of the whole lens. The increase in the equivalent refractive index is approximately 0.0013 per dioptre of accommodation.<sup>63-65</sup> This is accompanied by a small increase of the chromatic aberration of the eye amounting to approximately three per cent per dioptre of accommodation.<sup>49</sup> Charman measured an increase of approximately 0.2 dioptres of chromatic aberration between 422 nm and 633 nm when accommodating six dioptres.<sup>49</sup>

In another study, Jaskulski et al.<sup>66</sup> studied the accommodation response to three target vergences for three different wavelengths and white light, all having the same luminance. They found a shift in refractive error for each colour condition corresponding to the defocus shift created by the LCA, but the accommodation responses did not significantly change. However, Kruger et al. found some subjects accommodated less accurately in monochromatic light when stationary targets were positioned significantly closer or further away than the subject's resting position of accommodation.<sup>52</sup>

## Monochromatic aberrations and dynamic accommodation

How does the visual system know when to accommodate or disaccommodate and by how much? Researchers have been trying to answer this fundamental question for a long time, and still there is not a completely satisfactory answer. It is well known that the visual system makes use of information from the outside world, such as the intensity and wavelength of light reflected from objects, as well as information about the interaction of light with the optics of the eye itself, such as the effects of inaccurate refraction and chromatic dispersion. This information that the visual system uses in order to change the accommodation state accordingly is typically referred to as 'cues' for accommodation.<sup>67</sup> For example, from the disparity between the two signals, or images, formed by the two eyes, the visual system is able to interpret depth,<sup>68</sup> and depth perception guides accommodation.<sup>50,69</sup> Nonetheless, most people are able to accommodate correctly under monocular conditions. The reason for this is that the visual system can extract depth information from monocular cues. Some of these monocular cues are apparent distance,<sup>70,71</sup> changing size,<sup>72-74</sup> and interposition of objects.<sup>71</sup> But even when all these monocular cues that allow the visual system to interpret depth are removed, many people are still able to appropriately change their accommodation state. How is this possible with the lack of external cues? In this case, the visual system uses information extracted from the image formed on the retina, or from the way light rays reach the retina (optical cues for accommodation). It is known that an out-of-focus retinal image of a perfect eye without astigmatism and HOAs can trigger accommodation.<sup>75</sup> However, there are other optical cues that are based on the fact that images formed at the retina differ if they are focused in front (myopic defocus) or behind the retina (hyperopic defocus) (see upper part of Figure 5). Even-order monochromatic aberrations, which generate different images for different signs of defocus<sup>16,76</sup> may also play a role. Irregularly shaped pupils,<sup>16,77</sup> and the Stiles-Crawford effect,<sup>78-80</sup> can lead to different retinal images of the object depending upon if they are formed in front of or behind the retina.<sup>16</sup>

One aberration that has always been linked to accommodation has been spherical defocus. Phillips and Stark<sup>75</sup> demonstrated that blur alone could trigger accommodation with a remarkable experiment using a sophisticated system at the time. In their

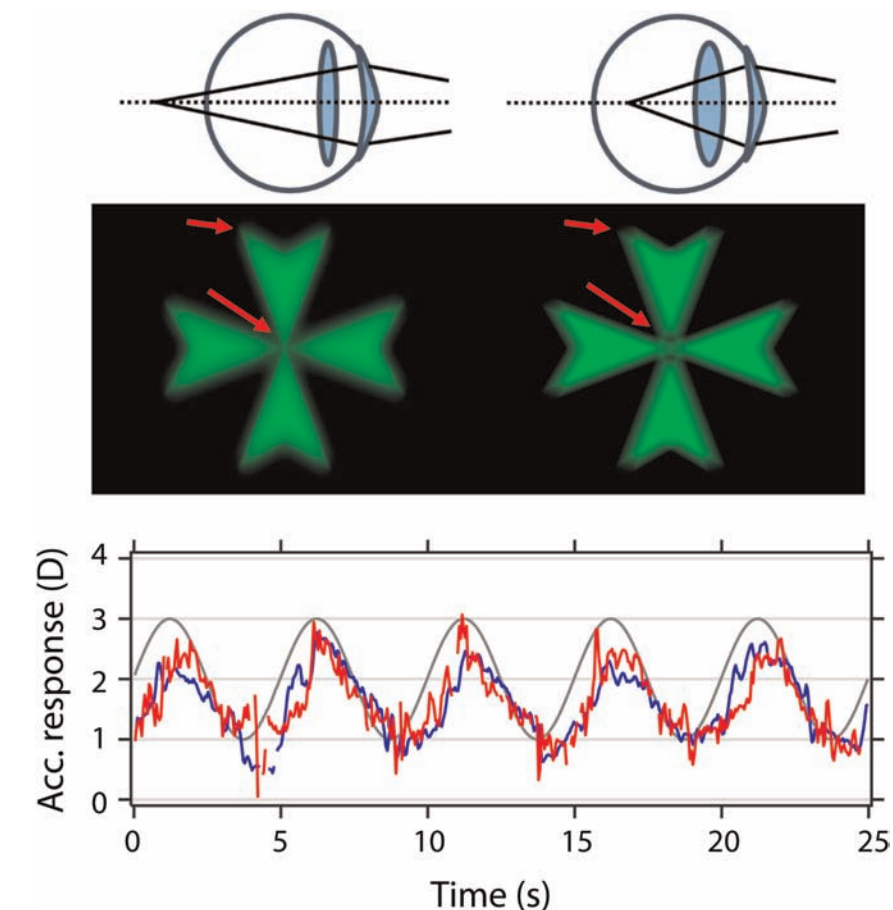


**Figure 5.** Ray diagrams illustrate under-accommodation (hyperopic defocus) on the top left side of the figure and over-accommodation (myopic defocus) on the top right side. In the presence of monochromatic aberrations, under-accommodation and over-accommodation produce different retinal images. Red arrows indicate some of the differences between the images. The bottom row shows dynamic accommodation response for one subject while viewing a Maltese cross target in a Badal optical system moving sinusoidally toward and away from the eye at 0.2 Hz, oscillating between one and three dioptres (grey line) with natural aberrations present (blue line) and with all aberrations corrected except for defocus (red line). Adapted from Del Águila-Carrasco.<sup>55</sup>

experiment, the only way in which the eye could accommodate was by trial-and-error, or how Phillips and Stark referred to it, the eye was constantly 'hunting', searching for the correct direction of accommodation. The recorded responses were at times in the wrong direction, and then changed rapidly toward the correct direction. However, their main conclusion that blur alone drives accommodation seems too far-fetched from their measurement in a single subject who usually responded in the wrong direction to a sudden change in target vergence. Recent work by Del Águila-Carrasco et al.<sup>10</sup> suggests that accommodation responds to the actual

changes in target vergence, and not changes in blur alone. A similar experiment<sup>19</sup> to that of Phillips and Stark agreed somewhat with their results; nevertheless, when target blur was changed quickly, some participants' accommodation was worse or even absent. An interesting conclusion of this work is that accommodation works much better when changes in light vergence were present than when there were only changes in target blur.

The majority of studies about the effect of monochromatic aberrations on dynamic accommodation have been carried out recently, thanks to the development and implementation of adaptive optics (AO) in

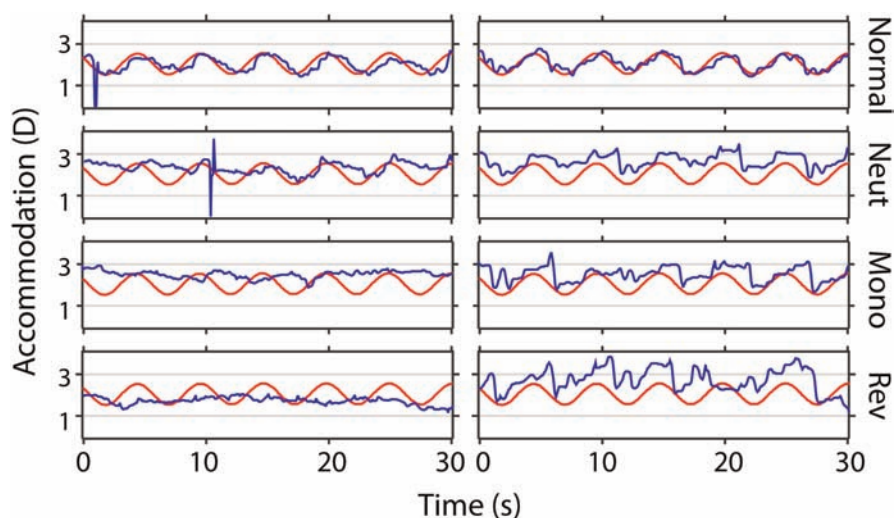


**Figure 6.** Dynamic accommodation responses for two subjects while viewing a Maltese cross target in a Badal optical system moving sinusoidally toward and away from the eye at 0.2 Hz, oscillating between one and three dioptres (red line) with chromatic aberration of the eye normal, neutralised, with monochromatic light and reversed chromatic aberration. Accommodation (blue line) responded well with normal chromatic aberration (first row); the response was reduced with chromatic aberration neutralised by an achromatising lens (second row), and with monochromatic light (third row); and the response was severely impaired when chromatic aberration was reversed (fourth trace). Adapted from Kruger et al.<sup>58</sup>

vision.<sup>81,82</sup> Using AO technology, some or all the aberrations of the eye can be corrected, or different amounts of them can be induced in real time. Since some of the ocular monochromatic aberrations change with accommodation,<sup>29,35–37</sup> it is essential that their correction is performed in real time. By correcting particular monochromatic aberrations and evaluating the accommodative response of the eye, it is possible to assess the effect of these aberrations on accommodation, if any. Recent studies manipulating the eye's natural aberrations suggest that the eye does not use monochromatic aberrations for accommodation,<sup>17,83–85</sup> since no significant differences were found between the response with natural aberrations present, or corrected. In a recent experiment,<sup>17</sup> the accommodative response of two out of eight subjects seemed to increase slightly when astigmatism was present while other monochromatic aberrations were corrected. A different approach has been used to elucidate whether certain monochromatic aberrations do provide a cue for dynamic accommodation.<sup>18</sup> The approach consists of blurring the target computationally using different combinations of the subject's own monochromatic aberrations together with defocus, and

measuring the accommodation response in open-loop conditions (without feedback). Results from these simulation experiments suggest that the eye does not use monochromatic aberrations to detect the sign of defocus, since a large number of participants did not respond to the simulations, and the few who showed some response, could not properly follow the changes in blur.<sup>18</sup> Nevertheless, these studies were carried out on relatively small populations, thus larger sample sizes need to be evaluated in order to draw firm conclusions.

### Chromatic aberration and dynamic accommodation: the chromatic cue

Fincham's original findings<sup>50</sup> were confirmed in monkeys<sup>86</sup> and in a series of experiments in humans in which the LCA of the eye was doubled, neutralised and reversed<sup>58,73,74</sup> while a Maltese cross target, viewed in a Badal optical system, moved sinusoidally toward and away from the eye at 0.2 Hz oscillating between one and three dioptres of accommodative demand (Figure 6). Doubling the amount of chromatic aberration had no adverse effect on accommodation, neutralising chromatic

aberration reduced the response for most subjects, and reversing chromatic aberration so that red light focused further forward in the eye than blue light severely impaired the dynamic accommodative response (Figure 6). Subjects accommodated poorly to sinusoidally moving targets in narrowband monochromatic light; their response improved as the bandwidth of the light increased, and the response was best in broadband 'white' light.<sup>51,87,88</sup>

Using sinusoidally moving sine-wave grating targets, accommodation responded to an intermediate band of spatial frequencies between one and eight cycles/degree, with peak sensitivity to the effects of chromatic aberration between three and five cycles/degree.<sup>89,90</sup> Even very small amounts of normal chromatic aberration (for example, 0.25 D) improved dynamic accommodation gain, while small amounts of chromatic aberration in the reversed direction significantly impaired the dynamic response.<sup>91</sup> It was also established that both dynamic gain and the accuracy of static accommodation were improved by the presence of chromatic aberration.<sup>52</sup>

All of these dynamic accommodation experiments were performed under normal 'closed-loop' conditions where blur feedback from small oscillations of accommodation was available. But the presence of blur feedback can mask the true nature of the stimulus cue, and it was important to repeat these experiments under 'open-loop' conditions without blur feedback from oscillations of accommodation and without trial-and-error changes in focus. Effective dynamic accommodation responses with high dynamic gains in the absence of blur feedback confirmed that chromatic aberration provides a highly reliable directional signal for dynamic accommodation.<sup>92</sup>

This series of dynamic accommodation experiments established that ratios of the contrasts of the red, green and blue components of the retinal image provide the optical signals that drive accommodation. Calculations of the cone contrasts measured by long- middle- and short-wavelength-sensitive cones<sup>93</sup> and empirical tests of this theory<sup>94</sup> proved that it was ratios of L-, M- and S-cone contrasts that provide the directional signals that drive dynamic accommodation in two colour directions: red-green and blue-yellow.

Another series of experiments showed that isolated short-wavelength-sensitive cones (S-cones) drive dynamic accommodation on their own, without any input from L-cones or M-cones.<sup>95–97</sup> In the first of these

experiments, accommodation was monitored continuously to a sine-wave grating target (three cycles/degree; 0.53 contrast) moving with an unpredictable sum-of-sines motion in a Badal stimulus system under two experimental conditions: a 'blue' condition (420 nm blue grating +580 nm intense yellow homogeneous adapting field) and a 'white' condition (broadband white grating). Mean dynamic gains for eight subjects were reduced by 50 per cent in the 'blue' condition compared to the 'white' condition.<sup>95</sup> Both S-cones and LM-cones mediate static and signed step accommodation responses to changes in accommodation demand.<sup>96</sup> S-cone contrast drives accommodation strongly for near, resulting in significant over-accommodation of more than one dioptre, but the S-cone response is too slow to influence step dynamics when LM-cones participate. The latencies and time constants for the accommodation response mediated by S-cones alone to step changes in optical vergence are two to three times longer than the latencies and time constants for accommodation mediated by LM-cones.<sup>96</sup> Thus the slow accommodation response from S-cones actually reduces dynamic gain to sinusoidal target motion at 0.2 Hz.<sup>97</sup> The directional signal from the chromatic mechanism that compares S- and LM-cone contrasts ( $S - [L + M]$ ) cannot assist accommodation to sinusoidally moving targets.<sup>97</sup>

Finally, L-cones on their own and M-cones on their own can mediate both static and dynamic accommodation: L-cone contrast reduces the mean accommodation level, while M-cone contrast increases the mean accommodation level.<sup>98</sup> Mean accommodation level is decreased when L-cone contrast is higher than M-cone contrast, and increased when M-cone contrast is higher than L-cone contrast.<sup>98</sup> In summary, L-cones reduce accommodation while both M-cones and S-cones increase accommodation.<sup>98,99</sup> The same chromatic cues, cone contrasts and neural mechanisms that control everyday focusing of the human eye, also control long-term emmetropisation and development of myopia in animals.<sup>100</sup>

### Future directions

The interaction between aberrations and ocular accommodation has been studied extensively. Nevertheless, there are still a number of questions that need to be resolved and the possibilities for future research on the topic are almost countless. Some areas need further work. For instance,

more detailed studies about the optics of the crystalline lens and its change during accommodation are needed, in particular, those corresponding to the changes in its internal structure (iso-indicial surfaces) during accommodation<sup>15</sup> and their effects on the accommodation response. More detail about the shape of the back surface of the lens and its change during accommodation are also needed since current data are not precise enough. New imaging technology devices based on optical coherence tomography probably combined with other wavefront technologies will likely allow more accurate determination of these types of lenticular changes in the near future. Further investigation into the change in monochromatic aberrations during accommodation may lead to improved designs of intraocular and contact lenses to compensate for presbyopia.

Another interesting area of research is to determine how the visual system is able to detect the sign of defocus, and thus appropriately accommodate. There are still many fundamental research studies to perform in this regard. For example, it has not been investigated whether not having a perfectly circular pupil is used by the visual system as a directional cue for accommodation. Moreover, in the last five years theoretical studies have been carried out to determine if the sign of defocus can be detected by particular structures of the retinal anatomy.<sup>101,102</sup> In particular, Vohnsen et al. have carried out computational simulations to show that there are different distributions of the electromagnetic field along the cone when light is focused either before or after the photoreceptor entrance plane, which may produce different cone signals.<sup>101</sup> López-Gil et al. have taken a different geometric optics approach based on different shadows that are cast by retinal vessels in the peripheral retina when light is focused in front, on, or behind the blood vessel plane.<sup>102</sup> Further experiments in humans should be conducted to test these theoretical hypotheses of optical vergence detection by the retina. The long-term goal of this fundamental research is to extend what we have learned about cues for everyday accommodation to the long-term focusing mechanism called emmetropisation, which operates to avoid the development of refractive errors.

### Conclusions

Accommodation not only changes the refractive power of the eye to improve the retinal

image quality of objects located at different distances, but also modifies its aberrations. Reciprocally, aberrations may influence the accommodation response, increasing, for instance, the lag of accommodation. The most significant change in HOA during accommodation is that experienced by fourth-order SA, which decreases during accommodation, usually changing its value from positive to negative, while chromatic aberration changes very little during accommodation. Dynamic accommodation studies have shown that monochromatic aberrations do not seem to play a role in accommodation. On the contrary, LCA provides a strong signed cue that reliably guides accommodation.

### ACKNOWLEDGEMENTS

Part of the studies presented have been performed by some of the authors who want to acknowledge their funding resources:

- European Research Council Starting Grant (ERC-2012-StG-309416-SACCO)
- Universitat de València (UV-INV-PREDOC14-179135)
- European Research Council Marie Curie ITN grant ("AGEYE" 608049)
- Ayudas para la realización de proyectos de investigación, Spain (grants: 05832/PI/07 and 15312/PI/10)
- National Eye Institute of NIH (EYO5901).

### REFERENCES

1. Young T. The Bakerian Lecture on the mechanism of the eye. *Philos Trans R Soc London* 1801; 91: 23–88.
2. Atchison DA, Charman WN. Thomas Young's contributions to geometrical optics. *Clin Exp Optom* 2011; 94: 333–340.
3. He JC, Gwiazda J, Thorn F et al. Change in corneal shape and corneal wave-front aberrations with accommodation. *J Vis* 2003; 3: 1.
4. Sisó-Fuertes I, Domínguez-Vicent A, del Águila-Carrasco A et al. Corneal changes with accommodation using dual Scheimpflug photography. *J Cataract Refract Surg* 2015; 41: 981–989.
5. Consejo A, Radhakrishnan H, Iskander DR. Scleral changes with accommodation. *Ophthalmic Physiol Opt* 2017; 37: 263–274.
6. Charman WN, Heron G. Fluctuations in accommodation: a review. *Ophthalmic Physiol Opt* 1988; 8: 153–164.
7. Charman WN, Heron G. Microfluctuations in accommodation: an update on their characteristics and possible role. *Ophthalmic Physiol Opt* 2015; 35: 476–499.
8. Platt BC, Shack R. History and principles of Shack-Hartmann wavefront sensing. *J Refract Surg* 2001; 17: S573–S577.
9. Thibos LN, Hong X. Clinical applications of the Shack-Hartmann aberrometer. *Optom Vis Sci* 1999; 76: 817–825.
10. Del Águila-Carrasco AJ, Marín-Franch I, Bernal-Molina P et al. Accommodation responds to optical vergence and not defocus blur alone. *Invest Ophthalmol Vis Sci* 2017; 58: 1758.
11. Atchison DA, Bradley A, Thibos LN et al. Useful variations of the Badal optometer. *Optom Vis Sci* 1995; 72: 279–284.

12. López-Gil N, Fernández-Sánchez V. The change of spherical aberration during accommodation and its effect on the accommodation response. *J Vis* 2010; 10: 12–12.
13. El Hage S, Le Grand Y. *Physiological optics*. New York: Springer, 1980.
14. Fincham EF, Walton J. The reciprocal actions of accommodation and convergence. *J Physiol* 1957; 137: 488–508.
15. Navarro R, López-Gil N. Impact of internal curvature gradient on the power and accommodation of the crystalline lens. *Optica* 2017; 4: 334.
16. López-Gil N, Rucker FJ, Stark LR et al. Effect of third-order aberrations on dynamic accommodation. *Vision Res* 2007; 47: 755–765.
17. Bernal-Molina P, Marín-Franch I, Del Águila-Carrasco AJ et al. Human eyes do not need monochromatic aberrations for dynamic accommodation. *Ophthalmic Physiol Opt* 2017; 37: 602–609.
18. Esteve-Taboada JJ, Del Águila-Carrasco AJ, Bernal-Molina P et al. Dynamic accommodation without feedback does not respond to isolated blur cues. *Vision Res* 2017; 136: 50–56.
19. Marín-Franch I, Del Águila-Carrasco AJ, Bernal-Molina P et al. There is more to accommodation of the eye than simply minimizing retinal blur. *Biomed Opt Express* 2017; 8: 4717–4728.
20. Goss DA. Nearwork and myopia. *Lancet* 2000; 356: 1456–1457.
21. Chen JC, Schmid KL, Brown B. The autonomic control of accommodation and implications for human myopia development: a review. *Ophthalmic Physiol Opt* 2003; 23: 401–422.
22. Weizhong L, Zhikuan Y, Wen L et al. A longitudinal study on the relationship between myopia development and near accommodation lag in myopic children. *Ophthalmic Physiol Opt* 2008; 28: 57–61.
23. Benard Y, López-Gil N, Legras R. Subjective depth of field in presence of 4th-order and 6th-order Zernike spherical aberration using adaptive optics technology. *J Cataract Refract Surg* 2010; 36: 2129–2138.
24. Benard Y, López-Gil N, Legras R. Optimizing the subjective depth-of-focus with combinations of fourth- and sixth-order spherical aberration. *Vision Res* 2011; 51: 2471–2477.
25. Yi F, Robert Iskander D, Collins M. Depth of focus and visual acuity with primary and secondary spherical aberration. *Vision Res* 2011; 51: 1648–1658.
26. López-Gil N, Fernández-Sánchez V, Thibos LN et al. Objective amplitude of accommodation computed from optical quality metrics applied to wavefront outcomes. *J Optom* 2009; 2: 223–234.
27. Tarrant J, Roorda A, Wildsoet CF. Determining the accommodative response from wavefront aberrations. *J Vis* 2010; 10: 4.
28. Bernal-Molina P, Vargas-Martín F, Thibos LN et al. Influence of Ametropia and its correction on measurement of accommodation. *Invest Ophthalmol Vis Sci* 2016; 57: 3010.
29. Plainis S, Ginis HS, Pallikaris A. The effect of ocular aberrations on steady-state errors of accommodative response. *J Vis* 2005; 5: 7.
30. Rocha KM, Vabre L, Chateau N et al. Expanding depth of focus by modifying higher-order aberrations induced by an adaptive optics visual simulator. *J Cataract Refract Surg* 2009; 35: 1885–1892.
31. López-Gil N, Martín J, Liu T et al. Retinal image quality during accommodation. *Ophthalmic Physiol Opt* 2013; 33: 497–507.
32. Thibos LN, Bradley A, López-Gil N. Modelling the impact of spherical aberration on accommodation. *Ophthalmic Physiol Opt* 2013; 33: 482–496.
33. Bernal-Molina P, Montés-Micó R, Legras R et al. Depth-of-field of the accommodating eye. *Optom Vis Sci* 2014; 91: 1208–1214.
34. Charman WN, Radhakrishnan H. Accommodation, pupil diameter and myopia. *Ophthalmic Physiol Opt* 2009; 29: 72–79.
35. He J, Burns S, Marcos S. Monochromatic aberrations in the accommodated human eye. *Vision Res* 2000; 40: 41–48.
36. Atchison DA, Collins MJ, Wildsoet CF et al. Measurement of monochromatic ocular aberrations of human eyes as a function of accommodation by the Howland aberroscope technique. *Vision Res* 1995; 35: 313–323.
37. López-Gil N, Fernández-Sánchez V, Legras R et al. Accommodation-related changes in monochromatic aberrations of the human eye as a function of age. *Invest Ophthalmol Vis Sci* 2008; 49: 1736–1743.
38. Cheng H, Barnett JK, Vilupuru AS et al. A population study on changes in wave aberrations with accommodation. *J Vis* 2004; 4: 3.
39. Liu T, Thibos LN. Variation of axial and oblique astigmatism with accommodation across the visual field. *J Vis* 2017; 17: 24.
40. Hofstetter HW. The correction of astigmatism for near work. *Optom Vis Sci* 1945; 22: 121–134.
41. Bannon RE. A study of astigmatism at the near point with special reference to astigmatic accommodation. *Optom Vis Sci* 1946; 23: 53–72.
42. Radhakrishnan H, Charman WN. Changes in astigmatism with accommodation. *Ophthalmic Physiol Opt* 2007; 27: 275–280.
43. Ukai K, Ichihashi Y. Changes in ocular astigmatism over the whole range of accommodation. *Optom Vis Sci* 1991; 68: 813–818.
44. Ninomiya S, Fujikado T, Kuroda T et al. Changes of ocular aberration with accommodation. *Am J Ophthalmol* 2002; 134: 924–926.
45. Khosravi B. *The Influence of Ocular Astigmatism on Accommodation (Monograph on the Internet)*. Manchester, UK, 1992.
46. Gamba E, Sawides L, Dorronsoro C et al. Accommodative lag and fluctuations when optical aberrations are manipulated. *J Vis* 2009; 9: 1–15.
47. Wald G, Griffin DR. The change in refractive power of the human eye in dim and bright light. *J Opt Soc Am* 1947; 37: 321–336.
48. Bedford RE, Wysecki G. Axial chromatic aberration of the human eye. *J Opt Soc Am* 1957; 47: 564–565.
49. Charman WN, Tucker J. Accommodation and color. *J Opt Soc Am* 1978; 68: 459–471.
50. Fincham EF. The accommodation reflex and its stimulus. *Br J Ophthalmol* 1951; 35: 381–393.
51. Aggarwala KR, Kruger ES, Mathews S et al. Spectral bandwidth and ocular accommodation. *J Opt Soc Am A* 1995; 12: 450–455.
52. Kruger PB, Aggarwala KR, Bean S et al. Accommodation to stationary and moving targets. *Optom Vis Sci* 1997; 74: 505–510.
53. Lee JH, Stark LR, Cohen S et al. Accommodation to static chromatic simulations of blurred retinal images. *Ophthalmic Physiol Opt* 1999; 19: 223–235.
54. Stark LR, Lee RS, Kruger PB et al. Accommodation to simulations of defocus and chromatic aberration in the presence of chromatic misalignment. *Vision Res* 2002; 42: 1485–1498.
55. Kruger PB. Infrared recording retinoscope for monitoring accommodation. *Am J Optom Physiol Opt* 1979; 56: 116–123.
56. Wolfe JM, Owens DA. Is accommodation colorblind? Focusing chromatic contours. *Perception* 1981; 10: 53–62.
57. Switkes E, Bradley A, Schor C. Readily visible changes in color contrast are insufficient to stimulate accommodation. *Vision Res* 1990; 30: 1367–1376.
58. Kruger PB, Mathews S, Aggarwala KR et al. Chromatic aberration and ocular focus: Fincham revisited. *Vision Res* 1993; 33: 1397–1411.
59. Logothetis NK, Schiller PH, Charles ER et al. Perceptual deficits and the activity of the color-opponent and broad-band pathways at isoluminance. *Science* 1990; 247: 214–217.
60. Gur M, Akri V. Isoluminant stimuli may not expose the full contribution of color to visual functioning: spatial contrast sensitivity measurements indicate interaction between color and luminance processing. *Vision Res* 1992; 32: 1253–1262.
61. Livingstone M, Hubel D. Segregation of form, color, movement, and depth: anatomy, physiology, and perception. *Science* 1988; 240: 740–749.
62. Troscianko T, Fahle M. Why do isoluminant stimuli appear slower? *J Opt Soc Am A* 1988; 5: 871–880.
63. Dubbelman M, Van der Heijde GL, Weeber HA. Change in shape of the aging human crystalline lens with accommodation. *Vision Res* 2005; 45: 117–132.
64. Bahrami M, Heidari A, Pierscionek BK. Alteration in refractive index profile during accommodation based on mechanical modelling. *Biomed Opt Express* 2016; 7: 99–110.
65. Khan A, Pope JM, Verkharla PK et al. Change in human lens dimensions, lens refractive index distribution and ciliary body ring diameter with accommodation. *Biomed Opt Express* 2018; 9: 1272–1282.
66. Jaskulski M, Marín-Franch I, Bernal-Molina P et al. The effect of longitudinal chromatic aberration on the lag of accommodation and depth of field. *Ophthalmic Physiol Opt* 2016; 36: 657–663.
67. Del Águila-Carrasco A. *Light Vergence Detection in Monocular and Monochromatic Accommodation (Monograph on the Internet)*. Valencia, Spain; 2017. Available from <http://roderic.uv.es/handle/10550/59161>.
68. Qian N. Binocular disparity and the perception of depth. *Neuron* 1997; 18: 359–368.
69. Wheatstone CXVIII. Contributions to the physiology of vision. —part the first. On some remarkable, and hitherto unobserved, phenomena of binocular vision. *Philos Trans R Soc London* 1838; 128: 371–394.
70. Ittelson WH, Ames A. Accommodation, convergence, and their relation to apparent distance. *J Psychol* 1950; 30: 43–62.
71. Takeda T, Iida T, Fukui Y. Dynamic eye accommodation evoked by apparent distances. *Optom Vis Sci* 1990; 67: 450–455.
72. Kruger PB, Pola J. Changing target size is a stimulus for accommodation. *J Opt Soc Am A* 1985; 2: 1832–1835.
73. Kruger PB, Pola J. Stimuli for accommodation: blur, chromatic aberration and size. *Vision Res* 1986; 26: 957–971.
74. Kruger PB, Pola J. Dioptic and non-dioptic stimuli for accommodation: target size alone and with blur and chromatic aberration. *Vision Res* 1987; 27: 555–567.
75. Phillips S, Stark L. Blur: a sufficient accommodative stimulus. *Doc Ophthalmol* 1977; 43: 65–89.
76. Wilson BJ, Decker KE, Roorda A. Monochromatic aberrations provide an odd-error cue to focus direction. *J Opt Soc Am A* 2002; 19: 833.
77. Wyatt HJ. The form of the human pupil. *Vision Res* 1995; 35: 2021–2036.
78. Kruger PB, López-Gil N, Stark LR. Accommodation and the Stiles-Crawford effect: theory and a case study. *Ophthalmic Physiol Opt* 2001; 21: 339–351.
79. Kruger PB, Stark LR, Nguyen HN. Small foveal targets for studies of accommodation and the Stiles-Crawford effect. *Vision Res* 2004; 44: 2757–2767.
80. Stark LR, Kruger PB, Rucker FJ et al. Potential signal to accommodation from the Stiles-Crawford effect and ocular monochromatic aberrations. *J Mod Opt* 2009; 56: 2203–2216.
81. Roorda A. Adaptive optics for studying visual function: a comprehensive review. *J Vis* 2011; 11: 6.
82. Marín-Franch I, Del Águila-Carrasco AJ, Levecq X et al. Drifts in real-time partial wavefront correction and how to avoid them. *Appl Optics* 2017; 56: 3989–3994.
83. Chen L, Kruger PB, Hofer H et al. Accommodation with higher-order monochromatic aberrations corrected with adaptive optics. *J Opt Soc Am A* 2006; 23: 1–8.
84. Chin SS, Hampson KM, Mallen EAH. Role of ocular aberrations in dynamic accommodation control. *Clin Exp Optom* 2009; 92: 227–237.



85. Chin SS, Hampson KM, Mallen EAH. Effect of correction of ocular aberration dynamics on the accommodation response to a sinusoidally moving stimulus. *Opt Lett* 2009; 34: 3274–3276.
86. Flitcroft DI, Judge SJ. The effect of stimulus chromaticity on ocular accommodation in the monkey. *J Physiol* 1988; 398: 36.
87. Aggarwala KR, Nowbotsing S, Kruger PB. Accommodation to monochromatic and white-light targets. *Invest Ophthalmol Vis Sci* 1995; 36: 2695–2705.
88. Kotulak JC, Morse SE, Billock VA. Red-green opponent channel mediation of control of human ocular accommodation. *J Physiol* 1995; 482: 697–703.
89. Stone D, Mathews S, Kruger PB. Accommodation and chromatic aberration: effect of spatial frequency. *Ophthalmic Physiol Opt* 1993; 13: 244–252.
90. Mathews S, Kruger PB. Spatiotemporal transfer function of human accommodation. *Vision Res* 1994; 34: 1965–1980.
91. Kruger PB, Nowbotsing S, Aggarwala KR et al. Small amounts of chromatic aberration influence dynamic accommodation. *Optom Vis Sci* 1995; 72: 656–666.
92. Kruger PB, Mathews S, Katz M et al. Accommodation without feedback suggests directional signals specify ocular focus. *Vision Res* 1997; 3: 2511–2526.
93. Flitcroft DI. A neural and computational model for the chromatic control of accommodation. *Vis Neurosci* 1990; 5: 547–555.
94. Kruger PB, Mathews S, Aggarwala KR et al. Accommodation responds to changing contrast of long, middle and short spectral-waveband components of the retinal image. *Vision Res* 1995; 35: 2415–2429.
95. Rucker FJ, Kruger PB. Isolated short-wavelength sensitive cones can mediate a reflex accommodation response. *Vision Res* 2001; 41: 911–922.
96. Rucker FJ, Kruger PB. The role of short-wavelength sensitive cones and chromatic aberration in the response to stationary and step accommodation stimuli. *Vision Res* 2004; 44: 197–208.
97. Kruger PB, Rucker FJ, Hu C et al. Accommodation with and without short-wavelength-sensitive cones and chromatic aberration. *Vision Res* 2005; 45: 1265–1274.
98. Rucker FJ, Kruger PB. Accommodation responses to stimuli in cone contrast space. *Vision Res* 2004; 44: 2931–2944.
99. Graef K, Schaeffel F. Control of accommodation by longitudinal chromatic aberration and blue cones. *J Vis* 2012; 12: 1–14.
100. Rucker FJ, Wallman J. Chick eyes compensate for chromatic simulations of hyperopic and myopic defocus: evidence that the eye uses longitudinal chromatic aberration to guide eye-growth. *Vision Res* 2009; 49: 1775–1783.
101. Vohnsen B. Directional sensitivity of the retina: a layered scattering model of outer-segment photoreceptor pigments. *Biomed Opt Express* 2014; 5: 1569–1587.
102. López-Gil N, Jaskulski MT, Vargas-Martín F et al. Retinal blood vessels may be used to detect the sign of defocus. *Invest Ophthalmol Vis Sci* 2016; 57: 3958.

## Blur adaptation: clinical and refractive considerations

*Clin Exp Optom* 2020; 103: 104–111

DOI:10.1111/cxo.13033

**Matthew P Cufflin** PhD

**Edward AH Mallen** PhD

School of Optometry and Vision Science, University of  
Bradford, Bradford, West Yorkshire, UK

E-mail: e.a.h.mallen@bradford.ac.uk

Submitted: 19 July 2019

Revised: 8 November 2019

Accepted for publication: 13 November 2019

**Key words:** adaptation, blur, defocus

### Blur adaptation

#### Definition of blur adaptation

Blur can be defined as a degradation of image quality due to a number of influences including optical aberrations, diffusion, and spatial filtering. For example, the introduction of myopic defocus diminishes the visual clarity of a scene and induces the awareness of 'blur' in the observer. If the presence of blur persists, the visual system quickly begins to re-calibrate to these changes in an attempt to partially recover vision. Several minutes later, the deleterious effects of blur (such as reduced high-contrast visual acuity [VA]) imposed on vision will have lessened. This compensatory effect has been termed blur adaptation, which is defined as an improvement in visual resolution, without alteration of refractive error or pupil size, following exposure to a blur stimulus.<sup>1</sup> There are a number of visual adaptive processes that help to improve function and perceived image quality. Such adaptive processes are essential in overcoming the many imperfections of the human eye. This article will review studies of blur adaptation in human vision with an emphasis on the clinical manifestations of this phenomenon. We have used electronic databases and library resources to identify relevant articles and have attempted to group these elements in a manner that we hope will help the reader

The human visual system is amenable to a number of adaptive processes; one such process, or collection of processes, is the adaptation to blur. Blur adaptation can be observed as an improvement in vision under degraded conditions, and these changes occur relatively rapidly following exposure to blur. The potential important future directions of this research area and the clinical implications of blur adaptation are discussed.

to navigate this area of vision research. We have not conducted a systematic review.

#### Blur adaptation using different methods of generating blur

##### Refractive manipulation REMOVING MYOPIC REFRACTIVE CORRECTION

In response to anecdotal reports of vision improving after periods of uncorrected vision, Pesudovs and Brennan<sup>2</sup> removed the optical correction from 10 myopic participants for a period of 90 minutes. Seven of the 10 observers displayed a small improvement in unaided acuity. The overall mean improvement was in the order of two letters, which was statistically significant yet clinically less significant and within the test-retest variability (TRV) of high-contrast VA charts.<sup>3</sup> Rosenfield et al.<sup>4</sup> used the same method but extended the adaptation period to three hours, observing a much greater mean improvement in unaided acuity of 0.23 logMAR units. The disadvantage of this method of blur production is the lack of a constant level of uncorrected lower-order aberrations (myopic defocus and astigmatism) across all participants. In addition, neither study controlled for entrance pupil size, which also impacts on the attenuating ability of retinal defocus on the modulation transfer function (MTF).<sup>5</sup>

##### ADDING CONVEX LENSES

Mon-Williams et al.<sup>1</sup> added +1.00 D convex lenses to the distance view of 15 emmetropes. This allowed for a similar level of myopic defocus to be applied across all participants, and for the adaptation effects to be investigated in non-myopes, who had not been habitually exposed to previous myopic defocus. While one dioptre of myopic defocus may initially reduce VA by 0.35–0.40 logMAR units on an Early Treatment Diabetic Retinopathy Study chart,<sup>6</sup> the blur adaptation effect may result in a recovery of approximately 0.07–0.17 logMAR units over a 30- to 45-minute adaptation period.<sup>1,7</sup> Significantly increasing the levels of myopic defocus up to +3.00 D yielded only a moderate increase in the adaptive VA improvement to 0.20–0.26 logMAR units<sup>8</sup> in a group of myopes and emmetropes. The use of convex lenses to induce myopic defocus in myopes and emmetropes gives equal initial reduction in visual performance under conditions of cycloplegia.<sup>9</sup>

During these experiments, participants were instructed to view videos presented at close to optical infinity. This stimulus method provides an approximation of real-world vision and the usual visual diet of spatial frequencies, as well as minimising boredom.<sup>10</sup> The importance of fully correcting any residual defocus and astigmatism prior to the addition of convex lenses should be noted, as any residual refractive errors will lead to

inconsistencies in the level of blur experienced by participants. An under-corrected myope for example, may undergo blur adaptation before the commencement of an experiment, thus limiting the measurable effects of experimentally induced adaptation.

### SPATIAL FREQUENCY MANIPULATION

The perception of blur may also be produced by manipulation of the spectral characteristics of a stimulus.<sup>11</sup> When viewing a natural scene the eye receives visual information coded across a range of spatial frequencies. For a natural scene there is a greater low spatial frequency content, with the amplitude of each contributing frequency believed to fall as frequency increases.<sup>12</sup> Consequently, a log amplitude versus log frequency plot of a natural scene will have a gradient of approximately  $-1.00$ .<sup>13</sup> Webster et al.<sup>14</sup> have applied amplification factors to increase the gradient of this graph, which will in turn accentuate the contribution of the lower spatial frequencies. Once the image is recombined, there will be an attenuation of high spatial frequency information similar to that seen when myopic defocus is applied to an image.<sup>5</sup> An increase in the negative slope of the power spectrum of  $-0.50$  has an equivalent effect on image clarity to the addition of  $1.50$  D of myopic defocus.<sup>15</sup>

### USING SCATTER FILTERS

An alternative approach to the generation of blur is to apply a filter, as employed by Vera-Diaz et al.<sup>16</sup> This allows for the perception of blurred vision to be produced without altering the vergence of an accommodative target. Vera-Diaz et al.<sup>16</sup> employed a  $0.2$  Bangerter occlusion foil which reduced contrast by approximately 75 per cent and attenuated the MTF to 50 per cent and 20 per cent of pre-blur levels for spatial frequencies of  $\geq 0.25$  and  $\geq 1.25$  cycles per degree (cpd) respectively. The blur produced by Bangerter foils differs from that produced by optical defocus – for example, Bangerter foils generate monotonically increasing attenuation of high spatial frequency content, whereas the attenuation effects of optical defocus on higher spatial frequencies is more irregular.<sup>17</sup>

### EMPLOYING ADAPTIVE OPTICS TO MANIPULATE HIGHER-ORDER ABERRATIONS

Adaptive optics (AO) is a versatile technique for the manipulation of image quality (see

Marcos et al.<sup>18</sup> for review) and has many applications across the field of optics from astronomy to retinal imaging. An AO system comprises a device for measurement of the quality of an image, a method for the manipulation of image quality (for example a deformable mirror), and a control system. AO can be used to induce many different types of blur, via the facility of, for example, a deformable mirror to change individual aberration terms (for example defocus, astigmatism, spherical aberration, and coma aberrations) in isolation or in combination. In the study of blur adaptation, AO can be used to present the visual system with a highly flexible array of stimuli, and has the added capability of using the participant's natural aberrations to contribute to the stimulus. For example, the coma-type aberrations of the eye could be manipulated (for example rotated by some amount) and this used as a blur adapting stimulus. Thus, AO offers a whole range of experimental options for the study of the impact of blur on visual function. Sawides et al.<sup>19</sup> applied AO to study the perceived best focus of the human visual system. It has been demonstrated that the point of best focus across a range of blur levels are biased toward the natural aberrations for a given individual. This gives evidence for the adaptation of the human visual system to its own aberration pattern, thus maximising spatial vision performance.

### INTRODUCING ASTIGMATIC BLUR

The effects of blur adaptation produced by other lower-order aberrations have also been examined. Sawides et al.<sup>20</sup> assessed the impact of two minutes of adaptation to images simulating vertical or horizontal astigmatic errors in focus. Adaptation to defocus caused a shift in the perceived isotropic blurring of images and this aftereffect transferred across a range of stimuli, such as faces and flowers. For example, adaptation to vertical blurring caused an isotropically blurred test image to appear horizontally blurred. This orientation-specific aspect of adaptation suggests that observers adapt to uncorrected astigmatic errors, such as those present in the correction of low-level astigmats with spherical soft contact lenses. Ohlendorf et al.<sup>21</sup> measured the effect on vision of astigmatic blur generated optically (trial case lenses) versus blur generated by computer modelling (ZEMAX). The computer-generated blur had a greater deleterious effect on visual

function compared to optical blur. This is an important point to note when comparing across studies that may use different methods of generating blur.

## Quantifying the effects of blur adaptation

As well as differing methods of blur production, blur adaptation investigations have utilised many methods to quantify this change in blur perception both pre- and post-adaptation. These methods include standard optometric acuity tests of letter-based optotypes, grating acuity, as well as measures of contrast sensitivity and direct measures of blur sensitivity.

### High-contrast VA

High-contrast logMAR VA charts have been used widely in the measurement of blur adaptation changes during and following exposure to defocus.<sup>1,2,4,7,22–25</sup> VA with myopic defocus in place is measured to provide an insight into the changes in resolution that occur during blur adaptation. The logMAR acuity charts have an advantage over Snellen charts in that the visual task and crowding effects remain constant for all acuity levels.<sup>26</sup> Table 1 summarises the blurred VA (BVA) improvements observed following various durations of blur adaptation.

Prolonged exposure to myopic defocus has been shown to gradually improve blurred VA by between  $0.04$  and  $0.27$  logMAR units. The use of BVA to monitor changes in visual resolution has the advantage of speed and ease of performance and understanding for both the observer and examiner. However, the measurement of BVA does have a major disadvantage, namely the variability of VA measurements is known to increase in the presence of blur.<sup>3,29</sup> Carkeet et al.<sup>29</sup> found that optical defocus extended the probit interval, and thus reduced the accuracy of the endpoint of high-contrast VA measurements. Similarly, Rosser et al.<sup>3</sup> found an increase in the TRV of VA measurements under conditions of induced myopic defocus.

The time elapsed between the end of the adaptation task and the measurement of visual function is small, with most studies reporting immediate measures of VA upon completion of the adaptation period. In addition, these studies did not employ top-up periods of adaptation during the

Study	Subject refractive status	Level of defocus	Duration of adaptation	Blurred acuity improvement
Mon-Williams et al. <sup>1</sup>	Emmetropes	+1.00 D	30 minutes	RE 0.12 logMAR LE 0.09 logMAR BE 0.09 logMAR
George and Rosenfield <sup>10</sup>	Emmetropes under cycloplegia	+2.00 D	30 minutes	0.26 logMAR
	Emmetropes	+2.50 D	Two hours	0.13 logMAR
	Myopes	+2.50 D	Two hours	0.27 logMAR
Wang et al. <sup>22</sup>	Myopes	+2.50 D	One hour	0.16 logMAR
Pesudovs and Brennan <sup>2</sup>	Uncorrected myopes	0.25 to 2.00 D	90 minutes	0.04 logMAR
Rosenfield et al. <sup>27</sup>	Uncorrected myopes	1.50 to 3.00 D	Three hours	0.21 logMAR
Rosenfield et al. <sup>4</sup>	Uncorrected myopes	1.00 to 3.50 D	Three hours	0.23 logMAR
Cufflin et al. <sup>7</sup>	Emmetropes			0.06 logMAR
	Early-onset myopes	+1.00 D	30 minutes	0.07 logMAR
	Late-onset myopes			0.07 logMAR
Cufflin and Mallen <sup>23</sup>	Emmetropes			0.08 logMAR
	Early-onset myopes	+3.00 D	30 minutes	0.26 logMAR
	Late-onset myopes			0.18 logMAR
Poulere et al. <sup>25</sup>	Emmetropes	+2.00 D	One hour	0.10 logMAR 0.09 (Landolt C)
	Myopes			0.07 logMAR 0.13 (Landolt C)
Khan et al. <sup>28</sup>	Emmetropes	+1.00 D	30 minutes	0.17 logMAR
		+3.00 D		0.16 logMAR
	Myopes	+1.00 D	0.20 logMAR	
		+3.00 D	0.23 logMAR	
Ghosh et al. <sup>24</sup>	Emmetropes	+2.00 D	One hour	0.05 logMAR
	Myopes			0.07 logMAR

BE: both eyes, BVA: blurred visual acuity; LE: left eye, RE: right eye.

**Table 1. Summary of the BVA improvements seen following adaptation to myopic defocus (induced by lenses over optimal correction or removal of myopic correction)**

measurement of VA. However, top-up periods have been employed in studies examining the effects of blur adaptation on contrast sensitivity and the subjective point of best focus.

**Grating VA**

Rosenfield et al.<sup>4</sup> determined the effect of three hours of uncorrected myopic vision on the grating acuity of 22 young myopes. Randomly orientated sine wave gratings were presented at contrasts of between 2.5 and 40 per cent in a three-alternative forced-choice paradigm to find the spatial frequency threshold. The grating acuity improved at all contrasts following 30 minutes without optical correction, and this improvement continued for the remainder of the three-hour adaptation period. George and Rosenfield<sup>10</sup> extended the study of grating VA and blur adaptation by adding

contrasts of 63 per cent and 98 per cent to the testing in a group of emmetropes and myopes. The same method of acuity assessment was employed, but the level of myopic defocus was standardised to 2.50 D across the entire subject cohort.

**Contrast sensitivity measures**

In addition to the significant changes in BVA, adaptation has been shown to influence contrast sensitivity. The introduction of defocus will reduce contrast levels across a range of spatial frequencies, with this attenuating effect enhanced as spatial frequency increases.<sup>30</sup> The effects of blur adaptation on the contrast sensitivity function (CSF) can be measured with and without blur in place.

The original study of refractive blur adaptation effects on contrast sensitivity was undertaken by Mon-Williams et al.,<sup>1</sup> with 2.00 D

myopic defocus and a 30-minute adaptation time. The CSF was measured under defocused conditions for some observers and without defocus for others, and no top-up adaptation was included. The authors observed a reduction in contrast sensitivity for all frequencies between 5 and 25 cpd following blur adaptation. The sensitivity of spatial frequencies at 2 and 4 cpd was found to be unaffected by blur adaptation.

Rajeev and Metha<sup>31</sup> employed a similar method (30-minute adaptation to 2.00 D of myopic defocus), but CSF was measured with defocus in place. The results showed an increase in sensitivity for 8 and 12 cpd, and a reduction in sensitivity for 0.5 cpd. This study also underlines the importance of top-up adaptation during CSF testing. When top-up images between test stimuli were removed, then adaptive effects on the CSF were negligible.

Venkataraman et al.<sup>32</sup> investigated the effects of 7.5° and 42° adapting stimuli on the foveal and peripheral (10° from fixation) CSF. A myopic defocus level of 2.00 D and an adaptation period of 30 minutes was employed. This adaptation generated an increase in sensitivity for 3 and 4 cpd only. In this study, the CSF measures were undertaken under clear conditions and without top-up of adaptation. Due to the time taken to measure the CSF, it is important to consider the use of top-up periods of adaptation, as the decay of the effect may mask the true effects.

These reports indicate that blur adaptation influences the CSF. There is evidence to suggest that the sensitivity to medium<sup>32</sup> and high spatial frequencies<sup>31</sup> is increased post-adaptation in response to their attenuation by defocus. The reduction of medium and higher spatial frequency contrast will bias the image further toward low frequency content. Webster<sup>33</sup> has demonstrated that brief adaptation to scenes with a bias toward low spatial frequency content can lead to a reduction in contrast sensitivity for low spatial frequencies. Webster's observations are also consistent with the preceding work by Webster and Miyahara,<sup>34</sup> where adaptation to increasingly blurred images reduced the contrast sensitivity at low frequencies only.

### Subjective point of best focus

A number of studies have examined the effect of blur adaptation on the positioning of the subjective point of best focus.<sup>14,35,36</sup> Manipulation has been performed to accentuate either the low or high spatial frequency content present in a series of images. Biasing image content toward the low spatial frequencies caused an image to appear blurred, while emphasising the high spatial frequency information caused the sharp transitions present in the image to appear 'too sharp'.<sup>14</sup> Both pre- and post-adaptation, the subjects viewed an assortment of images of varying degrees of spatial frequency filtering. A staircase method was used to determine the subject point of best focus, where images were not too sharp and not blurred. Adaptation to blur was found to significantly shift this null point toward a level that was described as blurred prior to adaptation. The opposite occurred with adaptation to sharpened images, with the point of best focus translated so that images previously acknowledged as 'too sharp' were now perceived as optimally

focused. This blur adaptation change was present in both young and old observers.<sup>35</sup>

### Blur sensitivity

Rather than using an indirect measure of blur sensitivity, Wang et al.<sup>22</sup> employed an ascending method of adjustment to directly determine the blur sensitivity pre- and post-blur adaptation. Unlike VA, the presence of defocus reduces subjective blur sensitivity thresholds and reduces the variability of the response.<sup>37</sup> After positioning a target at the position of subjective best focus, myopic defocus was added at a rate of 0.1 D/sec. The observer was instructed to indicate the levels of defocus required to induce just noticeable blur, bothersome level of blur and non-resolvable blur. The authors defined bothersome blur as where the 'blur of the target became just bothersome or annoying to look at'. This is a highly subjective criterion, and requires the criteria of annoyance to remain constant throughout the adapting period. It was observed that following blur adaptation, the subjective sensitivity to all three levels of blur was increased for a single letter target, but not for an extract of text. It is suggested that the larger visual angle and reduction in peripheral blur sensitivity are responsible for the discrepancy between a single letter and text stimulus behaviour.<sup>38</sup>

Conversely, Cufflin et al.<sup>7</sup> measured blur sensitivity and blur discrimination thresholds before and after blur adaptation in emmetropes, youth onset myopes, and young adult onset myopes using similar methods of adjustment. Thresholds for blur detection and discrimination were found to be elevated (that is observers were less sensitive to blur) following adaptation, with this effect being greatest in the youth onset myopes.

### Assessing the accommodation response

Blur is a cue to accommodation, and any changes in the ability of the visual system to detect blur may have consequences for the control and accuracy of this response. Le et al.<sup>39</sup> measured accommodation and pupil responses before, during and after a period of blur adaptation. An increase in accommodation response variability of around 17 per cent was observed in both emmetropic and myopic participants following blur adaptation. Following a wash-out period without blur adaptation, accommodation response parameters returned to the pre-adaptation levels. Cufflin and Mallen<sup>23</sup> observed

increases in accommodation response time to stepwise stimulus changes following blur adaptation. There was also an increase in accommodation response phase lag when tracking a sinusoidally moving accommodative stimulus. Adaptation to blur induced by Bangerter diffusing filters has also been shown to increase the magnitude of the accommodative response following three minutes of adaptation in myopic adult observers,<sup>16</sup> although others have found little effect of prior adaptation to myopic defocus on the accommodation response.<sup>8</sup>

## Characteristics of the blur adaptation effect

### Time period of blur adaptation

Significant changes in the perception of blur have been observed following as little as three minutes of blur adaptation.<sup>14</sup> Ohlendorf et al.<sup>21</sup> observed adaptation to astigmatic blur (produced by either lenses or simulated by image manipulation) after a 10-minute adaptation period.

Khan et al. documented significant improvements in VA within four minutes of the introduction of 1.00 D or 3.00 D of myopic defocus in young adult observers.<sup>28</sup> High-contrast VA was measured at two-minute intervals for a period of 30 minutes, and the rate of VA improvement slowed considerably following the first six minutes. Figure 1 shows an example plot of the time course of adaptation to 1.00 D of myopic blur (from Khan et al.<sup>28</sup>).

The longest duration of adaptation period used in studies that generated blur using myopic defocus was three hours.<sup>4</sup> The levels of VA improvement in myopes observed here were similar to those seen by studies employing a significantly shorter adaptation period of 30 minutes.<sup>23,28</sup> This suggests that once blur adaptation has been established, extending the adaptation period from minutes to hours does not produce additional improvements in VA.

The persistence of the adaptation effect has also been investigated. Delshad et al.<sup>40</sup> observed a mean improvement of 0.16 logMAR units in 26 adults following 60 minutes exposure to 3.00 D of myopic defocus. Following 20 further minutes of clear vision, an improvement of 0.11 logMAR units persisted, meaning that over two-thirds of the improvements accrued during adaptation were retained in the short term. There is also evidence of adaptive effects persisting

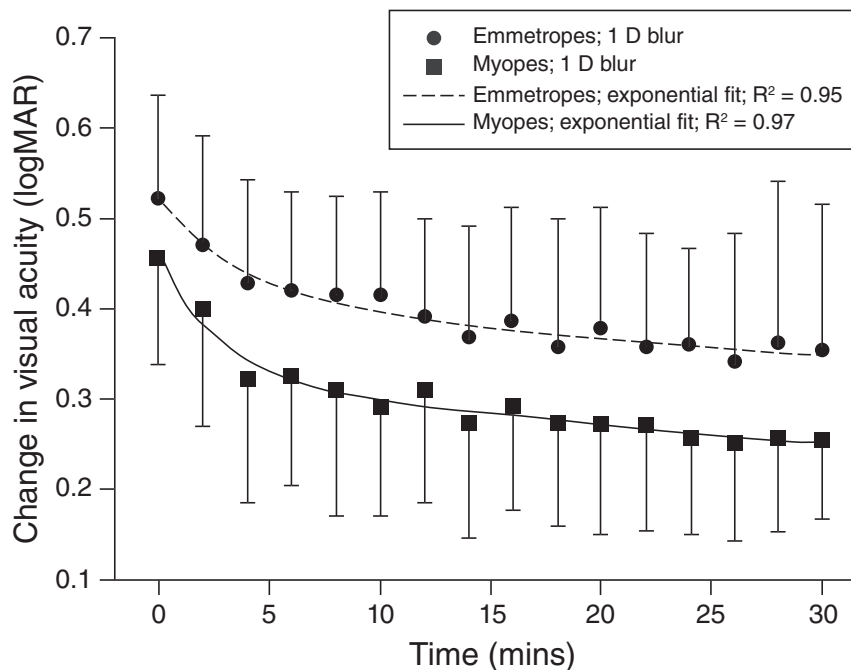


**Figure 1. Time course of blur adaptation, taken from Khan et al.<sup>28</sup>**

further than this. Following an adaptation period of three hours of uncorrected myopic vision, refractive corrections were returned to a group of subjects and their unaided acuities were checked six times over the subsequent 48 hours.<sup>27</sup> The majority of the unaided VA improvement accrued during the adaptation period was still present after two days of optimally focused vision. However, it must be noted that no control groups were included in this investigation.

### Resilience of adaptation

Khan et al.<sup>41</sup> demonstrated that improvements in defocused VA can occur even through a disrupted period of exposure to myopic blur. Equivalent improvements in VA were seen in young adults when a 15-minute adaptation period consisted of alternating short (seven-second) periods of blurred or clear vision was compared to a 15-minute period of sustained myopic defocus. Blur adaptation effects induced by convex lens additions were also found to withstand intervening periods of clear vision lasting one, five or 10 minutes in duration with no reduction in acuity effects.<sup>42</sup>

### Adaptation to higher-order aberrations

There is evidence to suggest that the visual system also adapts to higher-order

aberrations, such as coma and spherical aberration, in order to reduce their detrimental effects on visual resolution. Artal et al.<sup>43,44</sup> used AO to recreate and manipulate the higher-order aberrations present in a subject's vision. This allowed for a direct comparison of the visual resolution both with habitual aberrations in place and in the presence of abnormal aberrations. The initial magnitude of these abnormal aberrations was identical to the habitual state, although the orientation of these abnormal aberrations had been altered. The observer was required to vary the magnitude of the rotated aberrations until the image quality matched that of the habitual image. The observers consistently reduced the magnitude of the rotated aberrations in order to match the perception of the habitual aberration condition. This suggests that neural adaptation had acted to reduce the impact of the habitual aberrations on the visual perception, and this had resulted in improved visual resolution under habitual conditions.

### Blur adaptation in peripheral vision

Mankowska et al.<sup>45</sup> investigated the ability of the parafoveal region to adapt to defocus.

This region experiences moderately altered refraction, a decrease in neural receptor density, and a reduction in sensitivity to high spatial frequency stimuli. Myopic defocus of 1.00 D was added to the optimal refraction of a group of emmetropes and myopes for an adaptation period of 30 minutes. VA was measured at 2° intervals from 0° to 10° into the temporal visual field. Blur adaptation was found to occur across all locations measured and was found to be independent of eccentricity. As the capability to detect high spatial frequencies declines with increasing eccentricity, yet the adaptation effects were unaffected, this may indicate that recalibration of the sensitivity to high spatial frequencies may only play a limited role in blur adaptation. Vera-Diaz et al.<sup>46</sup> also found that eccentricity had little impact on the ability of blur adaptation to shift the point of subjective neutrality – the adaptive effects were similar when normally sighted observers saw a target straight-on, or when looking up to 10° past its edge.

The visual field is exposed to varying degrees of defocus as we move away from the optical axis. Venkataraman et al.<sup>47</sup> assessed the effects of a 60-second adaptation period to 2.00 D of non-optical defocus on the perceived neutral focus (PNF). The PNF is analogous to the subjective point of best focus and was measured in 0.01 D steps, with responses from participants indicating whether or not a test image was 'blurred' or 'sharp'. It was measured at the fovea, but a range of adapting stimuli combinations were examined, including a blurred parafovea (4°–20°) with a clear central area (0°–4°) and vice versa. Adaptation to a clear image at the fovea slightly reduced the defocus required at the PNF, regardless of whether the parafovea simultaneously had adapted to a grey, blurred or sharply focused image. Similarly, foveal adaptation to blurred central images increased the PNF regardless of the stimuli in the 4°–20° region. This indicates that the fovea may dominate when adapting to defocus, although the PNF was only measured foveally, so we have no indication of the effect on PNF other parts of the retina. Ghosh et al.<sup>24</sup> also investigated blur adaptation foveally and at 10° in the periphery, employing AO to correct for higher-order aberrations. Following 60 minutes of adaptation to 2.00 D of myopic defocus, myopes were found to experience a greater degree of BVA improvement compared to emmetropes, but only at the 10° temporal retinal location – equivalent levels of

adaptation were seen foveally. In another study, extending the blur stimulus to 42° from 7.5° was found to minimise the effects of blur adaptation on the CSF which were present when the smaller target was employed.<sup>32</sup>

## The mechanism of blur adaptation

Blur adaptation yields significant changes in blur perception and improvements in BVA. A reduction in pupil size or hyperopic shift in refractive error during the adaptation period would account for these improvements. However, evidence has shown there is no change in pupil size, refractive error or crystalline lens thickness following adaptation to blur.<sup>2</sup> Webster et al. attributed the changes in vision following blur adaptation to temporary recalibrations of the neural response to blur.<sup>14</sup> Mon-Williams et al.<sup>1</sup> suggested that the contrast constancy theory of Georgeson and Sullivan<sup>48</sup> may explain the adaptation-induced changes in visual resolution. Georgeson and Sullivan<sup>48</sup> observed the ability to accurately perceive contrast levels for a wide range of spatial frequencies, even those severely affected by optical aberrations.

The fall-off in contrast sensitivity at spatial frequencies beyond the peak sensitivity frequency has been attributed to the combined effects of optical and neural limitations of the human visual system.<sup>49</sup> This attenuation in the MTF of the eye at higher spatial frequencies impacted on contrast detection thresholds, yet the effect of these limitations on a suprathreshold contrast matching task was minimal.<sup>48</sup> Georgeson and Sullivan<sup>48</sup> instructed observers to vary the contrast of a grating until it appeared to match the contrast of a standard grating of 5 cpd. This was repeated for standard grating contrasts of up to 90 per cent (Michelson contrast) and spatial frequencies of 0.25 to 25 cpd. The marked reduction in contrast sensitivity at the higher spatial frequencies failed to impact on the contrast matching ability, with accurate contrast matching performed up to 25 cpd. The authors proposed that a compensation process occurred to counteract the optical and neural attenuation of high spatial frequencies by the human eye and restore the clarity of the image. This was termed contrast constancy.<sup>48</sup>

The visual system is known to process visual information in a series of spatial

frequency-specific channels in the visual cortex.<sup>50</sup> It was proposed that the gains of these channel outputs are variable and can be altered in response to the attenuation of high spatial frequencies by the human eye.<sup>48</sup> This attenuation also occurs in the presence of defocus, which increasingly attenuates content as spatial frequency increases. Georgeson and Sullivan<sup>48</sup> suggested that continuous feedback from the visual system would allow the determination of the attenuating factor for a certain channel. A correction factor could be derived to instigate an increase in gain from the affected channel, thus restoring perceived clarity.<sup>14</sup>

More recently, contrast constancy has been shown to withstand the effects of a 3.00 D level of defocus. The investigators suggested that contrast amplification of the blurred stimuli allowed for the maintenance of the contrast constancy effect.<sup>51</sup>

At present, this deblurring mechanism described by Georgeson and Sullivan<sup>48</sup> is the most likely mechanism for blur adaptation. The gains of the spatial frequency channels could be modified in order to compensate for defocus and restore visual resolution back to pre-blur levels. There are three ways of reducing the effect of blur on vision.

1. Increase the sensitivity to high spatial frequency content. This will partially reverse the drop in high spatial frequency sensitivity that occurs immediately on insertion of myopic defocus. This is supported by the work of Subramanian and Mutti.<sup>52</sup>
2. Decrease the gain of the low spatial frequency-sensitive channels. In the presence of blur the ability of the low spatial frequency content to mask the high spatial frequency content is increased. This is due to the relative weakness of high spatial frequency content under the influence of blur. Reduction in the gain of the low spatial frequency channels will cause an 'unmasking' effect<sup>1</sup> which will restore the relative contributions of the low and high spatial frequency channels back toward pre-blur levels.
3. A combination of both high spatial frequency gain increase and unmasking could be employed to maximise the deblurring effect. This mechanism is supported by Mon-Williams et al.<sup>1</sup> The deblurring process is believed to take place in central binocular cells of the visual cortex, due to the inter-ocular

transfer of blur adaptation that has been observed.<sup>1</sup>

## Blur adaptation and myopia

Myopes will be exposed to myopic defocus at the fovea whenever they remove their refractive correction, which is likely to give them a greater lifetime exposure to myopic defocus than emmetropes. It is perhaps reasonable to expect that myopes will draw on this experience when adapting to myopic defocus. There is also evidence that myopes have reduced blur sensitivity compared to emmetropes.<sup>53</sup>

Thorn et al.<sup>54</sup> suggested that the myopes in their study performed better (than emmetropes) in the presence of defocus due to their increased experience of defocused vision. George and Rosenfield examined the effect of equivalent levels of blur on defocused VA between emmetropes and myopes.<sup>10</sup> They found that the improvement in high-contrast BVA following blur adaptation was significant and equivalent for the two refractive groups. The effect of blur adaptation on grating BVA was also investigated for contrasts of between 2.5 per cent and 98 per cent. The emmetropes showed no change in grating acuity following adaptation, whereas the myopes showed significant improvements in grating acuity, but only at contrasts ≤ 16 per cent. This improved performance at low contrast suggests that there may be subtle differences in the myopic adaptation response to defocus.

Pouleret et al.<sup>25</sup> found that myopes were affected less by blur, compared to emmetropes, and this differential effect was more obvious with letter targets compared to Landolt Cs. There was a correlation between refractive error and change in VA following imposition of blur, with emmetropes showing a larger reduction in vision than myopes, and the change in vision becoming smaller with the higher myopes. However, no difference in the magnitude of blur adaptation effects was evident between refractive groups. Ghosh et al.<sup>24</sup> also observed higher levels of blur adaptation in myopes compared to emmetropes, but only at 10° in the peripheral field – no difference between groups was observed at the fovea.

The visual diet presented to the human visual system has undergone considerable change in the last decade, with increasing reliance on handheld devices for work,

communication and entertainment. Such devices can expose the eyes to stimuli that differ from natural images in terms of spatial frequency content and chromatic spectrum. This offers the potential of a chronic blur stimulus, which may induce adaptive effects. In the area of myopia management, the role of relative myopic retinal blur as a 'stop' signal for eye growth is building in the evidence base of clinical effectiveness. Radhakrishnan et al.<sup>55</sup> examined the effect of simultaneous vision from a bifocal correction. Shifts in the perception of blur were observed with simultaneous vision bifocal designs, and the magnitude of the shifts in perception were related to the proportions of defocus. The impact of chronic exposure to myopic defocus provides considerable opportunity for the study of blur adaptation. It may be the case that blur adaptation has a role to play in the refinement of myopia management strategies.

### Blur adaptation in disease

Vera-Diaz et al.<sup>46</sup> assessed blur adaptation (using the method described by Webster et al.<sup>14</sup> and Vera-Diaz et al.<sup>36</sup>) in a small number of patients with central vision loss compared with normally sighted controls. Blur adaptation was evident in the peripheral field of normal observers and those with central vision loss. It was found that adaptation to short-term blur was evident in the participants with vision loss, despite their long-term reduced vision; blur adaptation processes appear intact and robust following pathology. There was no correlation between the degree of adaptation to blur and VA.

### Clinical implications of blur adaptation

The clinical ramifications of blur adaptation could be directly relevant to the refraction process during an eye examination. Lengthy exposure to blur during refraction may induce blur adaptation in patients. Confirmation tests of the refractive end point which rely on responses to a blurred stimulus, specifically the '+1.00 D blur test', may yield a better than expected level of vision. Given the relatively short onset time of blur adaptation effects, care should be taken to limit a patient's exposure to blur during the refraction process. Patients being examined for their first myopic correction, for example at a level of myopia

of around 1.00 to 2.00 D, may show elevated performance in terms of unaided vision. It is possible that the uncorrected myope could be in a chronic state of blur adaptation, with the well-documented effects impacting upon clinical measurements. A similar effect may be seen in presbyopic patients wearing monovision correction, due to the chronic myopic blur presenting to the 'near vision' eye during distance vision.

The changes induced by blur adaptation are unlikely to be confined to the visual function alone. Read et al.<sup>56</sup> observed small, but statistically significant changes in axial length following one hour of exposure to myopic and hyperopic defocus while viewing a distance target. A mean ( $\pm 1$  SD) decrease in axial length of  $13 \pm 14 \mu\text{m}$  was observed following exposure to 3.00 D of myopic defocus, while similar exposure to hyperopic defocus induced a mean increase of  $8 \pm 14 \mu\text{m}$  in a group of young adults. Adaptation to 1.50 D of myopic defocus was also found to reduce the amplitude of the daily changes in sub-foveal and parafoveal choroidal thickness, as well as shifting the timing of the maximum and minimum values.<sup>57</sup> Effects of myopic and hyperopic defocus on choroidal thickness have also been observed in myopic school children.<sup>58</sup> These changes were induced under experimental conditions that are very similar to those used to study blur adaptation to refractive defocus. Therefore, there are likely to be changes occurring in the ocular structures as well as the changes in visual function that we see in blur adaptation.

Blur adaptation may have relevance to myopia management procedures where a lens with a relative positive addition places an image shell in front of the retina. The likely increase in the number of patients being prescribed myopia management interventions will drive the need for a fuller understanding of blur adaptation processes, and any impact on other processes, such as accommodation function. In the eye corrected with a conventional spectacle lens, Lin et al.<sup>59</sup> demonstrated a significant level of relative hypermetropic blur away from the visual axis. Study of any adaptation to this form of blur may provide useful insight into myopia progression.

### Summary

In summary, prolonged exposure to blur significantly improves visual performance after

a period of adaptation, with effects being observed in the contrast and blur sensitivities of adapted observers, in addition to performance on high-contrast acuity charts. This effect is likely due to compensatory changes in spatial frequency detection channels at the level of the visual cortex and may include both low and high spatial frequencies. Additionally, changes in ocular anatomy may be observed, particularly since recent advances in methods of biometric measurement, for example, axial length and enhanced depth imaging ocular coherence tomography. Evidence suggests that myopes may display a slightly higher propensity for this blur adaptation improvement. As exposure to defocus is being established as a myopia management strategy, the impact of chronic blur on the structure and function of the visual system is ripe for further investigation.

### REFERENCES

1. Mon-Williams M, Tresilian JR, Strang NC et al. Improving vision: neural compensation for optical defocus. *Proc Biol Sci* 1998; 265: 71–77.
2. Pesudovs K, Brennan NA. Decreased uncorrected vision after a period of distance fixation with spectacle wear. *Optom Vis Sci* 1993; 70: 528–531.
3. Rosser DA, Murdoch IE, Cousens SN. The effect of optical defocus on the test-retest variability of visual acuity measurements. *Invest Ophthalmol Vis Sci* 2004; 45: 1076–1079.
4. Rosenfield M, Hong SE, George S. Blur adaptation in myopes. *Optom Vis Sci* 2004; 81: 657–662.
5. Charman WN, Jennings JA. The optical quality of the monochromatic retinal image as a function of focus. *Br J Physiol Opt* 1976; 31: 119–134.
6. Radhakrishnan H, Pardhan S, Calver RI et al. Effect of positive and negative defocus on contrast sensitivity in myopes and non-myopes. *Vision Res* 2004; 44: 1869–1878.
7. Cufflin MP, Mankowska A, Mallen EA. Effect of blur adaptation on blur sensitivity and discrimination in emmetropes and myopes. *Invest Ophthalmol Vis Sci* 2007; 48: 2932–2939.
8. Cufflin MP, Hazel CA, Mallen EA. Static accommodative responses following adaptation to differential levels of blur. *Ophthalmic Physiol Opt* 2007; 27: 353–360.
9. Radhakrishnan H, Pardhan S, Calver RI et al. Unequal reduction in visual acuity with positive and negative defocusing lenses in myopes. *Optom Vis Sci* 2004; 81: 14–17.
10. George S, Rosenfield M. Blur adaptation and myopia. *Optom Vis Sci* 2004; 81: 543–547.
11. Schmid KL, Iskander DR, Li RWH et al. Blur detection thresholds in childhood myopia: single and dual target presentation. *Vision Res* 2002; 42: 239–247.
12. Field DJ. Relations between the statistics of natural images and the response properties of cortical cells. *J Opt Soc Am A* 1987; 4: 2379–2394.
13. Tolhurst DJ, Tadmor Y, Chao T. Amplitude spectra of natural images. *Ophthalmic Physiol Opt* 1992; 12: 229–232.
14. Webster MA, Georgeson MA, Webster SM. Neural adjustments to image blur. *Nat Neurosci* 2002; 5: 839–840.
15. Tadmor Y, Tolhurst DJ. Discrimination of changes in the second-order statistics of natural and synthetic images. *Vision Res* 1994; 34: 541–554.
16. Vera-Diaz FA, Gwiazda J, Thorn F et al. Increased accommodation following adaptation to image blur in myopes. *J Vis* 2004; 4: 1111–1119.



17. Pérez GM, Archer SM, Artal P. Optical characterization of Bangerter foils. *Invest Ophthalmol Vis Sci* 2010; 51: 609–613.
18. Marcos S, Werner JS, Burns SA et al. Vision science and adaptive optics, the state of the field. *Vision Res* 2017; 132: 3–33.
19. Sawides L, de Gracia P, Dorronsoro C et al. Vision is adapted to the natural level of blur present in the retinal image. *PLoS One* 2011; 6: e27031.
20. Sawides L, Marcos S, Ravikumar S et al. Adaptation to astigmatic blur. *J Vis* 2010; 10: 22.
21. Ohlendorf A, Taberner J, Schaeffel F. Neuronal adaptation to simulated and optically-induced astigmatic defocus. *Vision Res* 2011; 51: 529–534.
22. Wang B, Ciuffreda KJ, Vasudevan B. Effect of blur adaptation on blur sensitivity in myopes. *Vision Res* 2006; 46: 3634–3641.
23. Cufflin MP, Mallen EA. Dynamic accommodation responses following adaptation to defocus. *Optom Vis Sci* 2008; 85: 982–991.
24. Ghosh A, Zheleznyak L, Barbot A et al. Neural adaptation to peripheral blur in myopes and emmetropes. *Vision Res* 2017; 132: 69–77.
25. Poulere E, Moschandreas J, Kontadakis GA et al. Effect of blur and subsequent adaptation on visual acuity using letter and Landolt C charts: differences between emmetropes and myopes. *Ophthalmic Physiol Opt* 2013; 33: 130–137.
26. Ferris FL 3rd, Kassoff A, Bresnick GH et al. New visual acuity charts for clinical research. *Am J Ophthalmol* 1982; 94: 91–96.
27. Rosenfield M, Portello JK, Hong SE et al. Decay of blur adaptation. *Invest Ophthalmol Vis Sci* 2003; 44: 4315.
28. Khan KA, Dawson K, Mankowska A et al. The time course of blur adaptation in emmetropes and myopes. *Ophthalmic Physiol Opt* 2013; 33: 305–310.
29. Carkeet A, Lee L, Kerr JR et al. The slope of the psychometric function for Bailey-Lovie letter charts: defocus effects and implications for modeling letter-by-letter scores. *Optom Vis Sci* 2001; 78: 1113–1121.
30. Smith G. Ocular defocus, spurious resolution and contrast reversal. *Ophthalmic Physiol Opt* 1982; 2: 5–23.
31. Rajeev N, Metha A. Enhanced contrast sensitivity confirms active compensation in blur adaptation. *Invest Ophthalmol Vis Sci* 2010; 51: 1242–1246.
32. Venkataraman AP, Winter S, Unsbo P et al. Blur adaptation: contrast sensitivity changes and stimulus extent. *Vision Res* 2015; 110: 100–106.
33. Webster MA. Contrast sensitivity under natural states of adaptation. *Proc SPIE* 1999; 3644: 58–70.
34. Webster MA, Miyahara E. Contrast adaptation and the spatial structure of natural images. *J Opt Soc Am A Opt Image Sci Vis* 1997; 14: 2355–2366.
35. Elliott SL, Hardy JL, Webster MA et al. Aging and blur adaptation. *J Vis* 2007; 7: 8.
36. Vera-Diaz FA, Woods RL, Peli E. Shape and individual variability of the blur adaptation curve. *Vision Res* 2010; 50: 1452–1461.
37. Jacobs RJ, Smith G, Chan CD. Effect of defocus on blur thresholds and on thresholds of perceived change in blur: comparison of source and observer methods. *Optom Vis Sci* 1989; 66: 545–553.
38. Wang B, Ciuffreda KJ. Blur discrimination of the human eye in the near retinal periphery. *Optom Vis Sci* 2005; 82: 52–58.
39. Le R, Bao J, Chen D et al. The effect of blur adaptation on accommodative response and pupil size during reading. *J Vis* 2010; 10: 1.
40. Delshad S, Collins MJ, Read SA et al. The time course of blue adaptation and its persistence. In: *The Association for Research in Vision and Ophthalmology (ARVO) - Asia Meeting*. Brisbane, Qld: Brisbane Convention & Entertainment Centre, 2017.
41. Khan KA, Cufflin MP, Mallen EA. The effect of interrupted defocus on blur adaptation. *Ophthalmic Physiol Opt* 2016; 36: 649–656.
42. Portello J, Rosenfield M. Effect of intervening periods of clear vision on blur adaptation. *Optom Vis Sci* 2002; 79: 24.
43. Artal P, Chen L, Fernández EJ et al. Adaptive optics for vision: the eye's adaptation to point spread function. *J Refract Surg* 2003; 19: S585–S587.
44. Artal P, Chen L, Fernández EJ et al. Neural compensation for the eye's optical aberrations. *J Vis* 2004; 4: 281–287.
45. Mankowska A, Aziz K, Cufflin MP et al. Effect of blur adaptation on human parafoveal vision. *Invest Ophthalmol Vis Sci* 2012; 53: 1145–1150.
46. Vera-Diaz FA, Woods RL, Peli E. Blur adaptation to central retinal disease. *Invest Ophthalmol Vis Sci* 2017; 58: 3646–3655.
47. Venkataraman AP, Radhakrishnan A, Dorronsoro C et al. Role of parafovea in blur perception. *Vision Res* 2017; 138: 59–65.
48. Georgeson MA, Sullivan GD. Contrast constancy: deblurring in human vision by spatial frequency channels. *J Physiol* 1975; 252: 627–656.
49. Campbell FW, Green DG. Optical and retinal factors affecting visual resolution. *J Physiol* 1965; 181: 576–593.
50. Blakemore C, Campbell FW. On the existence of neurons in the human visual system selectively sensitive to the orientation and size of retinal images. *J Physiol* 1969; 203: 237–260.
51. Comerford JP, Thorn F, Chuang J. Contrast constancy with refractive blur. *Invest Ophthalmol Vis Sci* 2002; 43: 4719.
52. Subramanian V, Mutti DO. The effect of blur adaptation on contrast sensitivity. *Invest Ophthalmol Vis Sci* 2005; 46: 5604.
53. Rosenfield M, Abraham-Cohen JA. Blur sensitivity in myopes. *Optom Vis Sci* 1999; 76: 303–307.
54. Thorn F, Cameron L, Arnel J et al. Myopia adults see through defocus better than emmetropes. In: Tokoro T, ed. *Myopia Updates Proceedings of the 6th International Conference on Myopia*. Tokyo: Springer, 1998, pp. 368–374.
55. Radhakrishnan A, Dorronsoro C, Sawides L et al. Short-term neural adaptation to simultaneous bifocal images. *PLoS One* 2014; 9: e93089.
56. Read SA, Collins MJ, Sander BP. Human optical axial length and defocus. *Invest Ophthalmol Vis Sci* 2010; 51: 6262–6269.
57. Chakraborty R, Read SA, Collins MJ. Monocular myopic defocus and daily changes in axial length and choroidal thickness of human eyes. *Exp Eye Res* 2012; 103: 47–54.
58. Wang D, Chun RK, Liu M et al. Optical defocus rapidly changes choroidal thickness in schoolchildren. *PLoS One* 2016; 11: e0161535.
59. Lin Z, Martinez A, Chen X et al. Peripheral defocus with single-vision spectacle lenses in myopic children. *Optom Vis Sci* 2010; 87: 4–9.

## Adaptive optics imaging of the retinal microvasculature

*Clin Exp Optom* 2020; 103: 112–122

DOI:10.1111/cxo.12988

**Phillip Bedgood** BOptom PhD  
**Andrew Metha** BSc BSc (Optom)  
PGCertOcTher PhD

Department of Optometry and Vision Sciences, The  
University of Melbourne, Melbourne, Australia  
E-mail: pabedg@unimelb.edu.au

Submitted: 3 July 2019

Revised: 17 September 2019

Accepted for publication: 20 September  
2019

The eye has long been recognised as the window to pathological processes occurring in the brain and other organs. By imaging the vasculature of the retina we have improved the scientific understanding and clinical best practice for a diverse range of conditions, ranging from diabetes, to stroke, to dementia. Mounting evidence suggests that damage to the smallest and most delicate vessels in the body, the capillaries, is the first sign in many vasculopathies. These are the most critical vessels involved in the exchange of metabolites with tissue. Accurate assessment of retinal capillary structure and function would therefore be of great benefit across a broad range of disciplines in medical science; however, their small size does not make this an easy task. This has led to the development of high-resolution adaptive optics imaging methods to non-invasively explore retinal microvascular networks in living human eyes. This review describes the present state of the art in the field, the scientific breakthroughs that have been made possible in the understanding of vessel structure and function in health and disease, and future directions for this emerging technology.

**Key words:** adaptive optics, blood flow, capillaries, diabetes, retina

### **Microvasculature as a window to systemic and central nervous system pathology**

The retina is the only tissue for which the body's deep vasculature can be visualised directly and non-invasively, offering a unique avenue for the assessment of vascular health in major systemic conditions such as diabetes,<sup>1</sup> hypertension<sup>2</sup> and coronary heart disease.<sup>3</sup> Being neural tissue, retinal observation of blood vessels is also uniquely relevant to important neurovascular conditions such as stroke, Alzheimer's disease and other dementias.<sup>3,4</sup>

The vasculature can be thought of as an interconnected network of distribution pipes the function of which is, essentially, to deliver a reliable flow of blood through the entire body. Within the blood are the required nutrients, gases, hormones, and immune agents which must be delivered to tissue, while at the same time removing the waste products of metabolism. Using standard ophthalmoscopy methods, the most readily visualised vessels in colour fundus photographs of the retina are ~75–150 µm wide. Vessels as small as 30 µm can sometimes be resolved, and from close observations at this scale we have learnt much about the structure and some of the functional workings of the vascular supply

and drainage networks. However, the critical activities of the vascular system described above take place on a smaller scale, within networks of capillaries on the order of 5–10 µm wide. This is so for a variety of reasons. The narrow capillary lumen forces blood cells to be marshalled through in single file, deforming into elongated shapes.<sup>5,6</sup> Resistance to flow is high, comprising ~1/4 to 1/3 of the vascular total; flow is accordingly slower which enables sufficient time for exchange of metabolites.<sup>5</sup> Metabolite exchange is further facilitated by the increased cell-wall contact area, reduced average distance between cell contents and tissue, and much thinner capillary wall.<sup>5,6</sup> The sheer abundance of capillaries provides closer average proximity to all cell types in the body, particularly neurons.<sup>6,7</sup> Despite lacking a muscular coat, capillaries are capable of active local flow regulation by way of contractile pericyte cells distributed within their walls.<sup>7</sup> In addition to their importance to overall vascular function, being vastly more numerous, they offer greater redundancy compared with large vessels and so are statistically more likely to reveal the earliest, pre-clinical hallmarks of pathology. For all these reasons, it makes sense to pay attention to the smallest vessels, as well as the large.

As technology has improved and enabled the microvasculature to be assessed in human

disease, small vessels have indeed been observed to affect and be affected by pathological processes early in diverse conditions including diabetes, hypertension, coronary heart disease, cerebral ischaemia-reperfusion injury, stroke or brain haemorrhages, dementia, demyelinating disease, and sepsis.<sup>7,8</sup> The most well-understood example is diabetic vasculopathy which begins with loss of pericytes, thickening of the endothelial basement membrane<sup>9</sup> and eventual development of microaneurysms. Dysfunction of endothelial and/or pericyte cells and associated disruption of the blood-brain barrier lead to leakage and impaired local regulation of flow. Various combinations of these processes are thought to be compromised in a range of diseases.<sup>7,8</sup> The term 'small vessel disease' has been proposed as a common microvasculopathy manifesting in heart (leading to ischaemic heart disease), brain (leading to stroke and dementia), retina and kidneys.<sup>10</sup>

### **Challenges in study of the smallest vessels**

Is studying individual vessels of the microvasculature worthwhile? Each one does not get very much of the overall flow; what flow they do get is hard to interpret as it is

extremely heterogenous, changing markedly over time and between neighbouring capillaries in seemingly unpredictable fashion. In some ways capillaries appear uninteresting, with no muscular coat or a tunica media or adventitia at all. They are small and accordingly difficult to study; they are typically about 25 per cent narrower than the blood cells they permit,<sup>6</sup> forcing most to undergo significant deformation which alters resistance in a poorly understood manner.<sup>11</sup> Resistance is also increased by significant interaction between blood cells and the endothelial glycocalyx; these factors are tempered by formation of a relatively large plasma layer which effectively lubricates the flow.<sup>12</sup> Thus the flow state is complex and not easy to describe with simple models of fluid mechanics. Small changes in vessel morphology, endothelial cell function, basement membrane thickness, local blood composition, cell aggregation and other rheological factors could all have significant effects on capillary flow. Thus, while study of capillary function may provide very sensitive indicators of pathology, there is still much to learn.

The retina may be the best place in the body to improve our understanding of microvascular flow phenomena, given the transparency of the ocular media and the ability to image repeatedly and non-invasively in living human subjects. The first challenge is spatial resolution: as mentioned above, vessels below about 30 µm diameter cannot be seen by conventional or 'flood' illumination ophthalmoscopy (where the entire field is imaged simultaneously by brief flashes of light). Rather than size per se though, the main limitation is low contrast (because light is absorbed by only a thin column of haemoglobin, and veiled by other intra-ocular scatter) combined with imperfect focusing of the eye (aberrations). Methods to address these limitations include the following:

- Contrast agents introduced intravenously or orally. Fluorescein angiography can facilitate flow measurements in some individual capillaries without adaptive optics,<sup>13</sup> although the lifetime of useful fluorescence is limited, normal cell rheology may be disrupted, and intravenous injection of dyes is somewhat invasive which precludes routine use.
- Confocal methods,<sup>14</sup> which image a small point or line that is rapidly scanned across the retina to construct each frame. An aperture blocks light from scattering

interactions outside the plane of interest, improving axial resolution and minimising veiling glare. Manipulation of the aperture can reject directly returned light so that the signal only shows scatter from multiple structures; such scatter requires a change in refractive index, rendering otherwise transparent objects.<sup>15</sup> The chief limitation of confocal scanning is the lower frame rate as time is required to form the image; however, scanning can be 'frozen' on a cross-section of a single vessel to afford extremely rapid serial reconstruction of flow.<sup>16</sup>

- Interferometry for example, optical coherence tomography (OCT), which generates contrast from optical path differences as small as tens of nanometres to enable visualisation of otherwise transparent structures. Coherent light imaging 'gates' information to a particular range in depth, providing high axial resolution and minimising veiling glare. Entire tissue volumes are acquired which provides unique three-dimensional profiling of tissue. However, signal acquisition is time-consuming relative to the speed of blood flow. This means that, despite recent claims,<sup>17</sup> transverse flow velocity cannot be determined – the sampling requirements for this are described further below. Without the ability to track flow, and again despite recent claims, crossings cannot be differentiated from vessel branches to learn network connectivity.<sup>18</sup> Axial velocity can be measured using the Doppler effect, but only a small proportion of retinal micro-vessels are oriented axially.<sup>19</sup> Another limitation of OCT is that acquisition is time-consuming relative to the incessant motion of the eye, meaning that no two OCT scans look exactly the same. The inherent distortion degrades local structural measures such as diameter and branching angle and, while useful global metrics can still be determined, individual vessels or micropathology may be missed entirely due to a sudden jump in the eye's position.<sup>20</sup>
- Changes over time of recorded image data occur due to movement of blood constituents with different absorption and/or refractive index characteristics. Repeated observations of the same point on the retina can generate high contrast from these differences; in lower frame rate devices this creates perfusion maps of the vasculature; in higher frame rate devices, flow in individual vessels can be tracked.

- Choice of imaging wavelengths to maximise back-reflection from tissue posterior to the vasculature, and absorption by the vasculature relative to other absorbers such as the lens, macular pigment or melanin. If a narrow bandwidth is used, the light is partially coherent and so contrast may be generated by complex interference effects including defocused phase contrast.<sup>21</sup>
- Adaptive optics (AO) which, combined with other methods described above, compensates for the distorted shape of light waves returning from the eye to enable resolution of cellular structures. The downsides are that the superior resolution is afforded over a limited field of view, for example 1–2°,<sup>22</sup> and that increased cost and complexity have historically limited widespread clinical adoption.

## State of the art in AO imaging of the human retinal microvasculature

### Vascular structure

Adaptive optics was invented to compensate for atmospheric turbulence encountered by ground-based telescopes. The technology was extended to retinal imaging over two decades ago for study of the cone photoreceptor mosaic, by combining conventional flash or 'flood' fundus photography with AO.<sup>23</sup> The shadows of blood vessels were noted during the first AO studies of the *in vivo* photoreceptor mosaic and used to aid repeated retinal alignment,<sup>24</sup> but it was not until AO was combined with confocal scanning methods that images directly focused on vasculature structure were demonstrated.<sup>14</sup> Later strategies computed intensity variations in time to generate label-free, high-contrast perfusion maps of the lumens of the smallest retinal vessel networks.<sup>25,26</sup> Figure 1 shows a perfusion map (B) generated by our flood AO system with methods recently described,<sup>27</sup> overlaid on a commercial OCT angiography (OCT-A) scan used to guide imaging (A).

Both the blood column and vessel wall itself are composed of largely transparent cells which nonetheless differ in refractive index from surrounding tissue. Collecting indirectly scattered light from these structures allows them to be visualised using 'offset aperture' methods akin to darkfield microscopy.<sup>28,29</sup> A related variation of this imaging modality, known as 'split-detector',

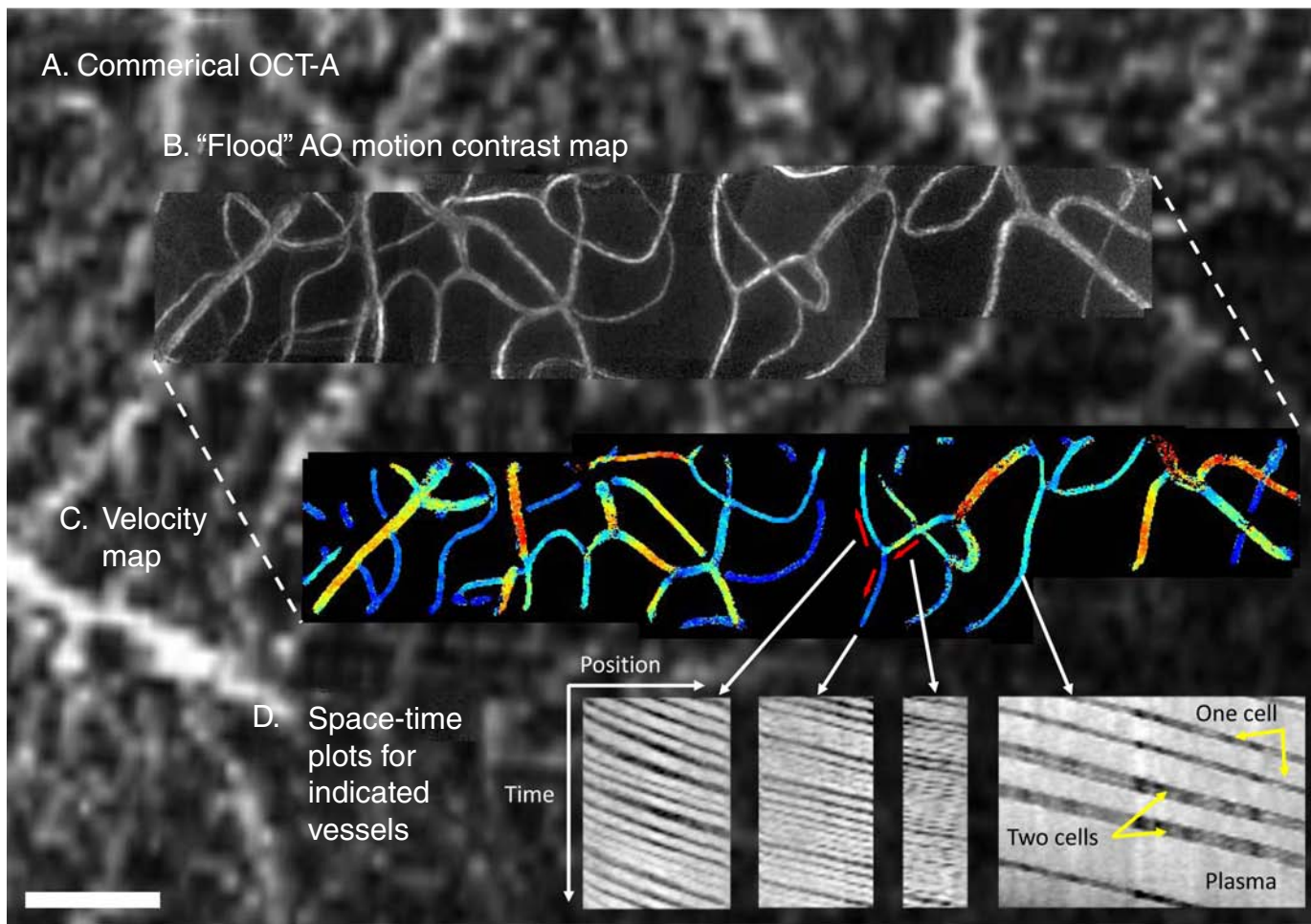


**Figure 1.** Mapping capillary flow in a human subject with type I diabetes. **A:** Background acquired with a commercial optical coherence tomography angiography (OCT-A) device (Heidelberg Spectralis). **B:** Motion contrast montage acquired with our ‘flood’ adaptive optics (AO) system at 400 fps with 593 nm light. **C:** Velocity mapping using pixel intensity cross-correlation, in the same region as B. Red arrows indicate flow direction for three segments at an arterial junction, referenced in D. **D:** Spatiotemporal plots over a 200 ms period for vessels indicated by white arrows, showing the alternating single-file passage of cells (black) and plasma (white). The right-most plot has much lower haematocrit despite being of comparable diameter and flow velocity. Scale bar is 100  $\mu\text{m}$ . Velocity colour map ranges from 0 to 4.5 mm/s.

ignores the directly scattered, confocally imaged rays while collecting and contrasting light landing on either side of the confocal image point.<sup>30</sup> Such methods are sensitive to refractive index (phase) changes in the direction of the offset or split, although at the cost of some lateral resolution. A programmable aperture can be used to explore structure oriented in arbitrary directions.<sup>31</sup> Recently developed darkfield methods may be able to reveal similar details for flood-based illumination geometries.<sup>32</sup>

### Vascular function

The first label-free investigations of capillary flow in the living human retina were achieved by tracking the shadows of individual

leukocytes, with their relative scarcity in the bloodstream allowing unambiguous tracking of each cell.<sup>33–35</sup> Similarly, the tendency of cell aggregates and/or lengthy sections of plasma to form in certain vessels allows unambiguous tracking of those aggregates.<sup>36</sup> An alternate strategy is to ‘freeze’ the scanning raster on a cross-section of a single vessel of interest.<sup>16</sup> This allows extremely rapid (kilohertz) measurement of the flow profile across a single vessel; smaller vessels are precluded due to difficulties in compensating for motion of the eye. More recent strategies have extended this approach to individual capillaries in anaesthetised rodents, allowing the counting of individual red cells, white cells and platelets as well as accurate

measurements of velocity, cell shape and lumen diameter.<sup>37,38</sup> Example data from this method are shown in Figure 2, courtesy of Dr Jesse Schallek’s laboratory, University of Rochester.

For assessment of contemporaneous flow velocity across the capillary network, deviations from the traditional point-scanning approaches are required. This includes high frame rate ‘flood’ illumination imaging, which affords direct visualisation and tracking of individual cells traversing the network<sup>21,39</sup> line scanning technology which strikes a balance between confocality and rapidity of acquisition,<sup>40</sup> or dual-channel point scanning with a very small temporal offset between channels, allowing pairwise cell displacements to be calculated.<sup>41</sup>

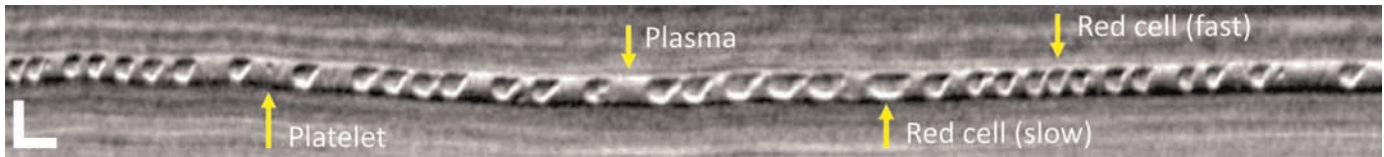


**Figure 2.** Fast cross-sectional imaging for reconstruction of capillary contents. A 1D scan line is ‘frozen’ along a cross-section perpendicular to the lumen of a target capillary, and rapidly sampled over time (15 kHz). The resulting space–time image is depicted here with time horizontal and shows the ability to count different blood components and measure their velocity, shape and packing arrangement. Data were acquired in an anaesthetised rodent at 796 nm with split-detection adaptive optics scanning laser ophthalmoscopy (AOSLO). Scale bars: horizontal = 10 ms, vertical = 5  $\mu\text{m}$ . Image supplied courtesy of Dr Jesse Schallek’s laboratory, University of Rochester.

The resulting datasets afford detailed analysis of flow patterns across the capillary network. Figure 1C shows a map of average velocity calculated by ‘flood’ AO at 400 fps, using pixel intensity cross-correlation.<sup>27</sup>

In recent years, the advent of new methods to analyse variations in amplitude and phase information in OCT data (OCT-A) have allowed commercial OCT systems to provide high-contrast, noninvasive perfusion maps of the retinal vasculature.<sup>42</sup> The same methods have been applied to improve AO-OCT perfusion mapping,<sup>43,44</sup> including visualisation of the choriocapillaris.<sup>45</sup> The combination of AO and OCT-A significantly improves both transverse and axial resolution, with recorded vessel diameters according with histology and the distinct anatomical beds appearing better separated. AO-OCT-A perfusion maps now rival those generated by other AO modalities. Given the recent successes of AO-OCT in visualising fine transparent structure such as ganglion cell somas and axons,<sup>46</sup> advances in visualisation of vascular support cells with AO-OCT-A may lie in the near future. The AO procedure itself can in principle be achieved in software alone with swept source OCT, due to the simultaneous acquisition of phase-stable information.<sup>47</sup>

### Scientific advances with AO imaging: vessel structure

The above developments have improved our understanding of the normal structure of the retinal microvasculature, and how this becomes altered in various disease processes.

#### Lumen and vessel wall

One of the most significant indicators for prognosis of hypertension is structural adaptation to sustained high blood pressure, which results in narrowing of the

lumen and thickening of the vessel wall, that is an increase in the wall-to-lumen ratio (WLR). This is hard to assess with standard clinical retinal photography or other *in vivo* methods; the gold standard is a subcutaneous biopsy which is invasive and may not be entirely representative of neural tissue.<sup>48</sup>

Using AO retinal imaging, WLR can be measured non-invasively and has been shown to increase with mean blood pressure, body mass index and age.<sup>49–52</sup> The WLR in healthy individuals is highly predictable from the size of the vessel, with a strong linear relationship ( $R^2 \sim 0.98$ ) between lumen and total diameter for the gamut of vessels spanning from 10 to 150  $\mu\text{m}$  in size (that is, all except the capillaries).<sup>53</sup> In hypertension the correlation remains strong but some vessels show significant departures from the predicted relationship, with narrowing of the lumen and concomitant thickening of the wall. Evaluation of deviations from the normally tight coupling observed may provide a statistically powerful biomarker for disease. It has recently been shown that WLR as measured with AO is responsive to both short-term (dilation of the lumen) and long-term (lumen dilation and reduction of wall thickening) pharmacological treatment of hypertension.<sup>54</sup>

Remodelling affecting WLR has also been noted in diabetes. While reports have been mixed on whether microvascular diameter increases or decreases in diabetes, likely due to differential effects at different stages of the disease,<sup>55</sup> AO-enabled studies point to wall thickening in those vessels large enough to have a substantive wall<sup>56</sup> together with narrowing of the lumen.<sup>57</sup> Figure 3 shows images captured with both offset-pinhole AO scanning laser ophthalmoscopy (AOSLO) (A–C, courtesy of Dr Stephen Burns, Indiana University) and flood AO (D–E, using our system), revealing alterations to the vessel wall in diabetes.

#### Branching

There is strong coupling expected between the diameter of parent and daughter branches at vascular junctions, based on minimisation of energy expended in transporting and supporting the blood volume. This is expressed by Murray’s law, which states that the sum of the cubes of the daughter radii should equal that of the parent.<sup>58</sup> The majority of vessels across various tissues and species conform well to this law, including the largest retinal vessels imaged with conventional retinal fundus photography.<sup>19</sup>

However, AO imaging of healthy vessels < 100  $\mu\text{m}$  in diameter has demonstrated significant departures from the expected cubic relationship, with exponents around two or less in veins of diameter 20–100  $\mu\text{m}$  and in arteries 20–50  $\mu\text{m}$ .<sup>59</sup> Departures from Murray’s law are expected where the underlying assumptions no longer hold, that is, that resistance no longer varies inversely with the fourth power of vessel radius. Such departures may occur for example where the underlying flow is turbulent, where blood viscosity and/or vessel stiffness change significantly across a junction, or in dynamic states where flow is redistributed across the network.<sup>58,59</sup> Further study is needed to develop our theories of capillary flow in light of the measurements now afforded by AO imaging technology; this is discussed further below in the section on vessel function.

#### Tortuosity

AO-based investigations have demonstrated that small vessel tortuosity is increased in diabetes, even in eyes with no clinically detectable retinopathy.<sup>56,60</sup> Adaptations include the formation of small, sharp loops and sprouts in the capillaries, analogous to the clinically familiar presentation of intraretinal microvascular abnormalities (IRMA) in larger retinal vessels. An example of

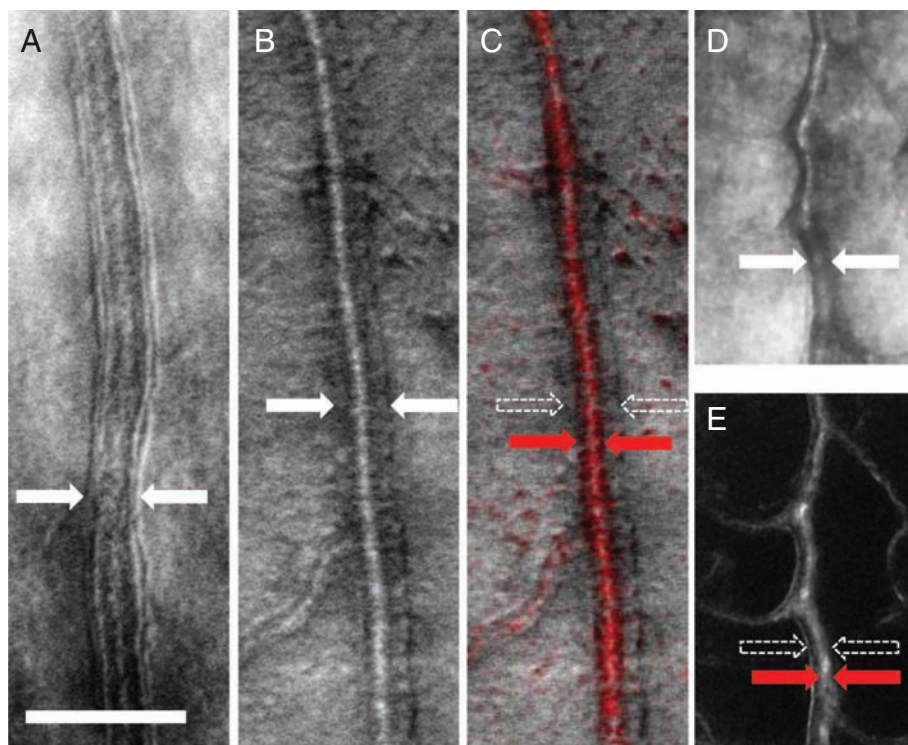


**Figure 3.** Visualisation of vessel wall and lumen in human diabetic retina. **A:** Adaptive optics scanning laser ophthalmoscopy (AOSLO) reflectance image with horizontal offset of the pinhole, revealing vessel wall fine structure in the horizontal direction. Focal constriction is evident in this vessel (arrows). **B:** AOSLO reflectance image in a different subject who shows thickening of the wall (arrows). **C:** The same data from **B** with motion contrast overlay (red), revealing that the wall (white arrows) is substantially thicker than the lumen (red arrows), especially on the right-hand side. **D:** Flood AO reflectance image of an arteriole. The vessel edge is indicated (arrows). **E:** Motion contrast of the area in **D**, demonstrating a large dark (non-perfused) region on the left side of the vessel. Extent of the functional lumen (red arrows) is much smaller than the total vessel diameter (white arrows), especially on the left side. Scale bar is 100  $\mu\text{m}$ . AOSLO images supplied courtesy of Dr Stephen Burns, Indiana University; flood AO images acquired with our system.

unusual vessel malformations in diabetes can be seen in Figure 4, with B-C showing a 'knot' structure, D-E showing a hairpin loop (white arrows) and F-G showing a tortuous vessel (white arrows) which feeds a microaneurysm. Microaneurysms are discussed further below.

AO imaging data has shown that tortuosity changes in diabetes occur preferentially in the arteriovenous channels, which are the widest and most direct path between arterial and venous systems and are hence preferred by the larger leukocytes.<sup>60</sup> It has been proposed that, following these structural changes, leukocytes become re-routed into the surrounding capillaries which would otherwise be relied upon to traffic large numbers of red cells. This disrupts metabolic

exchange between red cells and tissue, leading to further ischaemia and channel closure in a vicious cycle. The result is widespread capillary dropout and other later stage complications of diabetic retinopathy.

### Microaneurysms and other lesions in diabetes

Microaneurysms can be rendered in exquisite detail with AO imaging, identifying unique morphological classes not previously known.<sup>61</sup> Previous knowledge regarding the details of microaneurysm formation comes from histology, where sample sizes are limited and it is impossible to track lesions over time. Using AO, microaneurysm shapes have been shown to be predictive of surrounding disorganisation of the inner retina.<sup>62</sup>

Figure 4A shows a large microaneurysm (red arrow) imaged with offset-pinhole AOSLO (courtesy of Dr Stephen Burns, Indiana University), with surrounding large cysts (white arrows) and mottled microcystic appearance of the inner retina. Other panels show microaneurysms (red arrows) imaged with our flood AO system.

Lesions identified with AO can be repeatedly targeted with longitudinal follow-up, allowing study of the natural history of formation, progression and resolution of individual microaneurysms and other pathology.<sup>61,63,64</sup> Further studies are needed to determine whether microaneurysms give way to or are caused by other structural abnormalities, such as highly tortuous capillaries. Regardless, the rate of microaneurysm turnover is known to be a strong biomarker for development of future sight-threatening complications.<sup>65</sup> However, microaneurysms exhibit wide variation in their size (for example, compare lesion sizes in Figure 4A and 4D) and perfusion status (for example compare motion contrast in Figure 4E and 4G). This means that non-AO-enabled systems without a contrast agent are liable to miss more than half of microaneurysms.<sup>66</sup>

The detailed characterisation of lesion shape is critical information required for computational fluid models which can predict the dynamics of flow through affected regions of the retina. This allows the calculation of otherwise unmeasurable parameters such as wall shear stress and perfusion pressure. This information, if estimated accurately, would prove indispensable in deciding the likelihood that a given vessel or lesion will progress to lack of perfusion or development of other abnormalities.<sup>67,68</sup> Such techniques can similarly be applied to study less severe structural abnormalities described above such as altered tortuosity or branching.<sup>69</sup>

In addition to microaneurysms, AO can be used to image other characteristic pathologies with high resolution, such as neovascularisation, hard exudates, haemorrhages, cotton wool spots, and intraretinal cysts.<sup>70</sup>

### Other focal vascular abnormalities

In addition to diffuse changes to the vessel wall and lumen in hypertension, noted above, microvascular remodelling underpins more familiar clinical signs such as arteriovenous (A/V) nicking and focal arteriolar narrowing. Focal narrowing has been

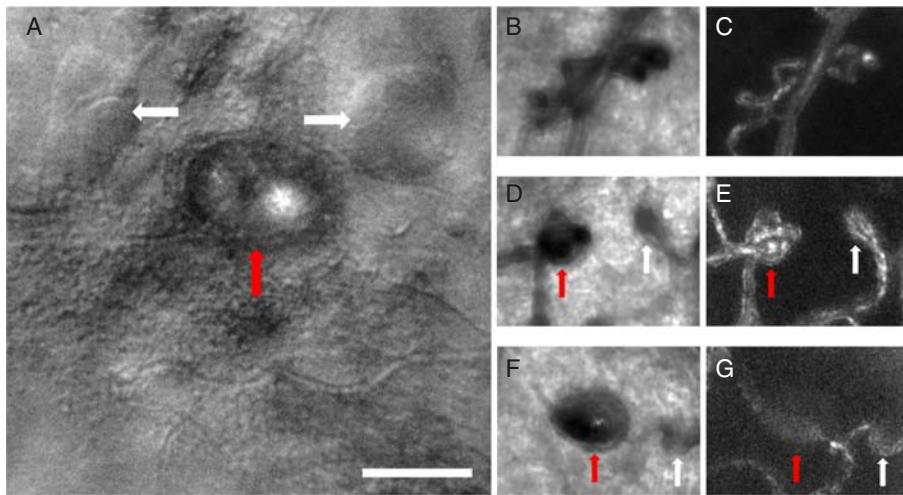


**Figure 4. Examples of gross structural abnormalities of the retinal microvasculature in diabetes. A: Offset-pinhole adaptive optics scanning laser ophthalmoscopy (AOSLO) showing an area containing a large microaneurysm (red arrow) and adjacent cysts (white arrows). Retina surrounding the lesion is disrupted (mottled appearance) which may indicate microcysts. B: Flood AO reflectance image showing a highly tortuous 'knot' structure. C: Motion contrast of the area in B. D: Flood AO reflectance image showing a microaneurysm (red arrow) alongside a hairpin loop (white arrow). E: Motion contrast of the area in D, revealing the perfused structure of the lesions. F: Another microaneurysm (red arrow), fed by a tortuous vessel (white arrow). G: Motion contrast of the area in F, revealing poor perfusion of this microaneurysm (compared to strong perfusion of the lesion in E). Scale bar is 100  $\mu\text{m}$ . AOSLO images courtesy of Dr Stephen Burns, Indiana University; flood AO images acquired with our system.**

observed to form and disappear over time and does not appear to be associated with a thicker wall, suggesting chronic over-constriction as the cause.<sup>71</sup> Similarly, AV nicking has been shown not to indicate physical compression by the arteriole, rather being produced by independent constriction of the vein.<sup>49,72</sup>

In cases of retinal vasculitis, focal compression of vessels, opacification of perivascular tissue<sup>73</sup> and increased scatter arising from infiltrates (groups of extravasating leukocytes) in post-capillary venules have been demonstrated and tracked over time with AO imaging.<sup>71</sup> The microvasculature has also been studied in branch venous occlusions, where precise longitudinal tracking of vessels can be used to infer the ischaemic status of the retina.<sup>64</sup>

### Choriocapillaris

AO-OCT-A is currently the best modality for quantitative imaging of choriocapillaris morphology,<sup>45</sup> which is very difficult with other modalities due not only to the small capillary diameter but also to the intervening retinal pigment epithelium and tight

vessel density/connectivity. This advance was achieved with various optical, hardware, and software improvements to AO-OCT systems. The choriocapillaris is of central importance for a number of disease processes, notably age-related macular degeneration.<sup>74</sup>

### Scientific advances with AO imaging: vessel function

In addition to improving understanding of normal microvascular morphology and the development of structural malformations, AO retinal imaging has facilitated significant advances in our understanding of vascular function. Vascular function can be thought about in terms of flow at 'rest', as well as 'dynamic' changes which are brought about in response to some stimulus.

#### 'Resting' flow state

By freezing the AOSLO scanning raster on a particular vessel as described above,<sup>16</sup> the cross-sectional velocity of small retinal vessels can be measured and its evolution

tracked rapidly over time. The method is best suited to vessels in the 30–80  $\mu\text{m}$  range due to the significant, incessant movement of the eye;<sup>16</sup> however, it can in principle be applied to individual capillaries.<sup>37</sup> In many of the larger vessels in the body, idealised approximations of fluid mechanics hold and a parabolic velocity profile is expected. It has now been shown that in the small retinal vessels these approximations begin to break down; the profile becomes flatter with decreasing vessel diameter and, in arterioles, depends dynamically on the phase of the cardiac cycle.<sup>38,75</sup> These departures from idealised models of fluid mechanics may reflect changes in viscosity, and/or easier cell aggregation at slower flow speeds and as lumen size becomes comparable to cell size.<sup>75</sup> The method has also been used to study complex flow dynamics such as mixing of flow downstream from a venous confluence;<sup>75</sup> this phenomenon has been replicated in a number of studies.<sup>28,37</sup>

The tendency of blood cells to aggregate within retinal capillaries could be a potent biomarker given the suspected importance of aggregation in a range of disease processes including hypertension, diabetes, metabolic syndrome, coronary disease, stroke, infectious disease and haematological disease.<sup>76</sup> Cell aggregation is typically measured with a blood panel, by necessity a proxy for true *in vivo* cell behaviour, but it can be studied directly with AO. For example, long 'tails' form within certain vessels in AOSLO video sequences and are seen to elongate over time. These are believed to represent dynamically aggregating groups of cells. Some vessels show much higher tendency to form or traffic aggregates in a way that depends upon their particular morphology.<sup>77</sup> The tendency to form aggregates may therefore be altered in disease processes that cause structural adaptations; this has been confirmed in diabetes, where aggregates are seen to accrete more rapidly prior to the development of clinically detectable retinopathy; and in eyes with retinopathy, the increased aggregation is even more pronounced.<sup>78</sup>

Individual platelets, which are low contrast and in humans only 2.5–3  $\mu\text{m}$  in diameter, have been resolved in rodents using AOSLO by reconstruction of high-speed capillary cross-sections.<sup>37</sup> Data from this group are shown in Figure 2 and demonstrate the potential for accurate characterisation of red cell shape and packing arrangement as well. Platelet aggregation is a key predictor

for occlusive vessel disease such as myocardial infarction;<sup>79</sup> however, it is typically measured by mixing a clotting agent with spun blood. As it has been established that the natural movement and shear forces that platelets are exposed to are the predominant factor in driving aggregation,<sup>80</sup> the typical measurement process may not reflect the natural state; the potential for a non-invasive, *in vivo* blood panel afforded by AO imaging may be far more sensitive than currently available tests.

Just as vessels can undergo periods whereby cell aggregates are passed with no discernible plasma gaps, some vessels undergo repeated periods of low haematocrit or acellularity, causing them to transiently disappear from motion contrast maps.<sup>56,81</sup> To illustrate variations in haematocrit, Figure 1D shows the evolution in vessel appearance over time for four segments in a diabetic subject imaged with our flood AO system. The right-most panel passes long sections of plasma (bright) broken up sporadically by cells (dark), indicating a low haematocrit; a more typical haematocrit of ~50 per cent is evident in the other three panels. These variations in cellular perfusion occurred despite comparable diameter (Figure 1B) and flow speed (Figure 1C) between the vessels. Figure 2 also depicts moment-to-moment variations in capillary haematocrit. Persistence of low haematocrit states has obvious implications for metabolism and could prove a useful signpost for disease processes; early intermittent drops in perfusion may presage more pronounced capillary dropout later in disease. AO imaging has been used to track the appearance of non-perfused capillaries over time, primarily in diabetes.<sup>63,64,82</sup> By combining structural and motion contrast imaging, it is possible to identify 'ghost' capillaries which are present but not perfused by cells; such vessels have been observed to occur more frequently in diabetic eyes.<sup>20,56</sup>

The above discussion highlights the importance of repeated observation to learn the true patency of a vessel. This is relevant to OCT-A perfusion mapping which has recently seen widespread adoption as a clinical and research tool for identification of capillary dropout. Multiple OCT-A scans are recommended to ensure that the wide variations in capillary haematocrit, noted above, do not masquerade as dropout (a similar argument can be made regarding the potential for eye movements to skip some vessels or lesions entirely). Variation in the local haematocrit is also a major confounder for

attempts to infer capillary flow velocity from the decorrelation computations employed for OCT-A.<sup>17</sup>

The above discussion deals primarily with lower frame rate imaging of the microvasculature; other approaches allow imaging of the capillary network full-field at high speed, in order to simultaneously determine velocity in multiple micro-vessels.<sup>21,27,39-41</sup> This allows investigation of the distribution of flow across the microvascular network in space and time. In our experience, even with the high transverse resolution of vessel structure afforded by AO, it is only with flow information that we are able to unambiguously map network connectivity (that is, separate crosses from true branches); without this information, the task can probably only be done with histology.<sup>83</sup> Figure 1C illustrates the spatial flow mapping that can be achieved with AO imaging.

Using AO, it has now been established that the cardiac imprint is very pronounced even at the capillary level, with essentially all capillaries undergoing pulsatile variations in velocity between systole and diastole.<sup>27,37,38,40,41</sup> However, superimposed on this pattern are complex changes which occur due to variations in cell 'traffic', in particular with the passage of leukocytes and large aggregates of erythrocytes. Figure 5 demonstrates examples of two patterns of flow: segment '1' (red solid line) undergoes rhythmic flow variations in line with the expected cardiac pattern (red dotted line). In comparison, segment '2' (solid blue line) appears hindered from following its expected cardiac pattern (dotted blue line), being especially slowed at one of the systolic peaks (arrow). The reason for this disruption to flow is evident in the corresponding single frame shown in Figure 5B, where a fat, dark cell aggregate is seen within segment 2. These examples underscore the ability of AO imaging to facilitate accurate measurement of vessel diameter and other morphology, flow velocity, and contents of the blood column to allow investigation of the 'rules' governing the normal trafficking of blood constituents across the capillary network. Despite their fundamental importance, these rules have hitherto remained poorly understood due to the lack of accessibility to capillary networks operating in their natural state.

In addition to observing pulsatility of flow velocity in individual vessels, it may be possible to measure propagation of the pulse wave itself, that is to measure how quickly

changes in pressure at one part of the microvascular network are propagated downstream. In a completely rigid vessel the pulse wave would travel at the speed of sound; real vessels have some degree of compliance, which buffers pressure changes and accordingly slows propagation of the pulse wave. Loss of compliance (increased stiffness) in large vessels such as the aorta, measured as more rapid propagation of the pulse wave through these vessels, is a major risk factor for the development of coronary heart disease and stroke.<sup>84</sup> It is possible that the pulse wave in smaller vessels is also important; however, the high speeds and short distances involved have precluded direct measurement. In the retina, indirect methods have produced conflicting estimates of normal pulse wave velocity which range from 20 to 600 mm/second.<sup>85,86</sup> However, direct observation of the pulse wave may be possible with modern AO imaging. Extrapolating sampling requirements for measurement of cell velocity,<sup>27,40</sup> frame rates in the range 2,000 to 60,000 fps are suggested. Such sampling rates are on the order of the line scan rate employed by current AO scanning systems.<sup>38,41,87</sup>

Understanding normal capillary flow may be a particularly fruitful field of study because the introduction of aberrant flow dynamics may precede (or cause) the formation of structural abnormalities. A particularly simple area to study would be the vessels along the edge of the foveal avascular zone (FAZ), as they comprise only a single layer in depth. Since this area is also often an early casualty in disease, due perhaps to the reliance of diffusion from the edge of the FAZ to locations within the central fovea,<sup>67,88</sup> it marks an excellent place to undertake a thorough characterisation of normal network flow dynamics and changes throughout various stages of disease.

### Stimulus-evoked changes in flow

The retina is the most metabolically active tissue in the body.<sup>89</sup> The inner retinal blood supply supports fundamental visual processing performed by the bipolar and ganglion cells; as the patterns of light falling on the retina change in space or time, the need for information processing increases which causes large variations in metabolic activity. The autoregulation of blood flow to match the ever-changing neuronal activity is termed 'neurovascular coupling'. A major contribution to this process comes from the



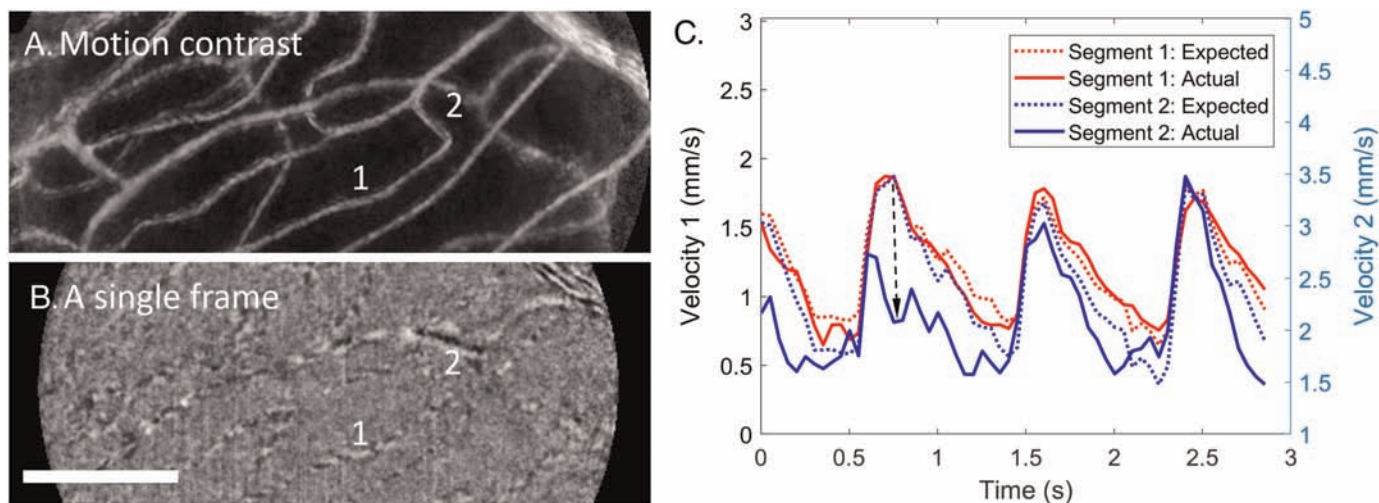


**Figure 5. Patterns of variation in capillary flow over time. A:** Motion contrast image generated with flood adaptive optics (AO) at 300 fps over three seconds, using 750 nm light. Two example segments are labelled ('1', '2'). **B:** One frame from the sequence, showing normal single-file flow through segment 1, and the passage of a large cell aggregate through segment 2. Frame coincides with the systolic peak and to the arrow in C. **C:** Velocity over time for segment 1 (solid red line) and segment 2 (solid blue line), alongside scaled averages for the field (matching dotted lines) which show the pattern expected from variations in cardiac output. At the time point indicated by the arrow, segment 2 is significantly slowed, coinciding with the presence of the fat, dark aggregate within this segment as seen in B. Scale bar is 100  $\mu\text{m}$ .

capillaries themselves by way of stimulation of the contractile pericyte cells contained within their walls. Pericytes respond by various pathways in a feed-forward manner triggered by neurotransmitter release.<sup>7</sup>

Neurovascular coupling may be implicated in a number of conditions. Pericyte cells are among the first damaged in diabetes,<sup>9</sup> and impaired vascular autoregulation is thought to play a major role in dementia and stroke.<sup>7</sup> The retina makes particularly fertile ground for study of neurovascular coupling in such conditions.<sup>4</sup> With conventional fundus imaging, the neurovascular response to full-field flickering light has been explored in the large retinal vessels, eliciting changes in diameter of the order of a few percent for healthy vessels.<sup>90</sup> As expected, deficits in the stimulus-evoked flow response have been noted in a variety of disease processes.<sup>90</sup>

Advances in AO imaging have extended the study of neurovascular coupling to measurement of flow changes elicited for retinal vessels in the 30–80  $\mu\text{m}$  range.<sup>91</sup> Using a local stimulation protocol has highlighted the local redistribution of flow to match neuronal activity, with flow increasing only when the stimulated retina lies within the feeding area of a small arteriole, and progressively greater changes in flow occurring the wider the area stimulated.

More recently, neurovascular coupling has been studied in healthy vessels < 30  $\mu\text{m}$  wide, by measuring changes in vessel diameter in response to locally delivered flickering light in a spot  $\sim 1^\circ$  across.<sup>92</sup> Proportional changes observed were much larger in these vessels, under local stimulation, than previously reported for the larger vessels under full-field stimulation ( $\sim 30$  per cent for capillaries of < 10  $\mu\text{m}$  diameter and  $\sim 12$  per cent for vessels of 10–30  $\mu\text{m}$  diameter, as opposed to a few per cent for large retinal vessels<sup>90</sup>). This confirms the key role played by the smallest vessels in local redistribution of flow and suggests that exploring flow regulation in these vessels may provide an even more sensitive stress test for the study of pathological processes.

In addition to the surprisingly large changes in diameter elicited, the above work showed that dilations tended to be focally distributed (that is, non-uniform) along many vessels, which further implicates pericytes as the agents for change in accordance with their intermittent positioning along vessels of the calibre studied.<sup>92</sup> Additional unique observations made were the ability of post-capillary venules to dilate, which was not predicted based on previous *ex vivo* animal work, and constriction of some vessels in response to the stimulus which indicates targeted redistribution of

flow. This work is still in its infancy, with many unanswered questions including the relationship between diameter changes and flow, the manner in which the vascular autoregulation signal is propagated along the vascular tree,<sup>8</sup> and whether deficits in autoregulation precede the formation of structural abnormalities.

In contrast to the flicker-evoked changes described above, a similar protocol exploring the influence of altered blood gas (hyperoxia or hypercapnia) produced changes in vessel size of comparable degree to those obtained with flicker, but these were not focally distributed, indicating a different mechanism of action as predicted based on current theories of the key pathways involved.<sup>93</sup>

Both pericytes and glial cells are thought to form a key component of the neurovascular unit. The magnitude of response and location of any deficits should ideally be co-localised with the presence and morphology of these important cells. This now appears to be possible with both mural cells and glial cell end-feet visualised by appropriate manipulation of AOSLO detection geometry.<sup>15,29,31</sup> Pericytes in particular could represent a very sensitive biomarker for diabetes due to their central role in pathophysiology of vascular changes in that condition.

## Future directions

Many investigations that have been carried out by AO retinal imaging research laboratories are not yet amenable to routine clinical assessment in large numbers of patients. Factors limiting the broader applicability of AO imaging include: the cost, complexity and immobility of the systems; specialist expertise required in hardware deployment and operation; lack of standardised software; small fields imaged; small fixational eye movements (which are large relative to the objects of interest); sensitivity to scatter or distorted ocular media; and need for manually assisted analysis of data including identification of novel lesion types. Nonetheless, inroads have been made in deploying the technology in clinical paradigms. For example, there is a clinical device available from Imagine Eyes (the 'rx1'), with some 257 citable entries returned by Google Scholar from 2010 to 2018 for the terms 'rx1' and 'Imagine Eyes'. However, routine deployment in clinical practice is unlikely to come until there is widespread uptake in ophthalmic research, which may be several years away as the limitations identified above are gradually overcome. Developments in commercial instrumentation such as OCT-A have greatly assisted research in AO imaging, offering readily accessible widefield and depth information to inform targeted study of smaller areas with AO.

In contrast to widespread clinical adoption of AO technology, there are many exciting avenues for further development of AO imaging methods as a research tool to develop scientific understanding of retinal vascular structure and function, on the cellular scale, in health and disease. Precise and repeatable measurements facilitate longitudinal study of various disease processes as highlighted above. Recent improvements in technology allow faster frame rates which have revealed elaborate flow patterns across the microvascular network; this information could be used to seed models which identify aberrant flow profiles in individual vessels, revealing which vessels in which patients will give way to non-perfusion and eventually more widespread disease complications. Rapid imaging also has the potential to observe propagation of the pulse wave in retinal micro-vessels, which would provide crucial and otherwise unobtainable information on microvascular compliance (or stiffness) relevant to stroke and coronary

heart disease. Full-field approaches may allow for study of the propagation of vascular autoregulation signals across the vascular tree. Clever manipulation of detection geometry in scanning modalities continues to reveal previously invisible structures such as pericytes and glial cells, which could be co-localised with flow deficits and so offer greater explanatory power and more sensitive biomarkers for disease; developments in AO-OCT promise to reveal still further details of 'invisible' cell classes. Multispectral methods may facilitate oximetry for individual capillaries and even individual blood cells.

The ultimate goal is for quick, broadly applicable, non-invasive, high spatiotemporal resolution observation of retinal vasculature structure and function to robustly determine an individual's vascular health in its natural state.<sup>8</sup> Adaptive optics extends the vessels that can be imaged to the finest capillary networks. Detailed measurement of structure, function and stimulus-evoked changes will allow better understanding of normal microvascular function as well as the natural history of disease, including pre-clinical variations which may predict the development of severe complications of both retinal disease and systemic co-morbidities. Such investigations, if successful, would have major impacts on early diagnosis and accurate prognosis for individual patients, and offer sensitive, non-invasive, longitudinally accessible biomarkers for clinical trials of novel therapies targeting the vasculature to facilitate optimal capillary perfusion.

## ACKNOWLEDGEMENTS

The authors would like to thank Dr Stephen Burns (Indiana University) and Dr Jesse Schallek (University of Rochester) for supplying sample AOSLO image data presented in this review.

Research supported by Australian Research Council Discovery Project ARC DP180103393.

## REFERENCES

- Cheung N, Wong TY. Diabetic retinopathy and systemic vascular complications. *Prog Retin Eye Res* 2008; 27: 161-176.
- Ong Y-T, Wong TY, Klein R et al. Hypertensive retinopathy and risk of stroke. *Hypertension* 2013; 62: 706-711.
- Witt N, Wong TY, Hughes AD et al. Abnormalities of retinal microvascular structure and risk of mortality from ischemic heart disease and stroke. *Hypertension* 2006; 47: 975-981.
- Cheung CY-I, Ikram MK, Chen C et al. Imaging retina to study dementia and stroke. *Prog Ret Eye Res* 2017; 57: 89-107.

- Burton AC. *Physiology and Biophysics of the Circulation: An Introductory Text*. Chicago: Year Book Medical Publishers, 1972.
- Snyder GK, Sheafar BA. Red blood cells: centerpiece in the evolution of the vertebrate circulatory system. *Am Zool* 1999; 39: 189-198.
- Hamilton NB, Attwell D, Hall CN. Pericyte-mediated regulation of capillary diameter: a component of neurovascular coupling in health and disease. *Front Neuroenergetics* 2010; 2: 5.
- Bosetti F, Galis ZS, Bynoe MS et al. 'Small blood vessels: big health problems?': scientific recommendations of the National Institutes of Health workshop. *J Am Heart Assoc* 2016; 5: e004389.
- Cogan DG, Toussaint D, Kuwabara T. Retinal vascular patterns: IV. Diabetic retinopathy. *Arch Ophthalmol* 1961; 66: 366-378.
- Berry C, Sidik N, Pereira AC et al. Small-vessel disease in the heart and brain: current knowledge, unmet therapeutic need, and future directions. *J Am Heart Assoc* 2019; 8: e011104.
- Dintenfass L. Inversion of the Fahraeus-Lindqvist phenomenon in blood flow through capillaries of diminishing radius. *Nature* 1967; 215: 1099.
- Fahraeus R, Lindqvist T. The viscosity of the blood in narrow capillary tubes. *Am J Physiol* 1931; 96: 562-568.
- Wolf S, Arend O, Reim M. Measurement of retinal hemodynamics with scanning laser ophthalmoscopy: reference values and variation. *Surv Ophthalmol* 1994; 38: S95-S100.
- Roorda A, Romero-Borja F, Donnelly WJ III et al. Adaptive optics scanning laser ophthalmoscopy. *Opt Express* 2002; 10: 405-412.
- Burns SA, Elsner AE, Sapoznik KA et al. Adaptive optics imaging of the human retina. *Prog Retin Eye Res* 2019; 68: 1-30.
- Zhong Z, Petrig BL, Qi X et al. In vivo measurement of erythrocyte velocity and retinal blood flow using adaptive optics scanning laser ophthalmoscopy. *Opt Express* 2008; 16: 12746-12756.
- Wang RK, Zhang Q, Li Y et al. Optical coherence tomography angiography-based capillary velocimetry. *J Biomed Opt* 2017; 22: 066008.
- Nesper PL, Fawzi AA. Human parafoveal capillary vascular anatomy and connectivity revealed by optical coherence tomography angiography. *Invest Ophthalmol Vis Sci* 2018; 59: 3858-3867.
- Riva CE, Grunwald JE, Sinclair SH et al. Blood velocity and volumetric flow rate in human retinal vessels. *Invest Ophthalmol Vis Sci* 1985; 26: 1124-1132.
- Mo S, Krawitz B, Efsthadiadis E et al. Imaging foveal microvasculature: optical coherence tomography angiography versus adaptive optics scanning light ophthalmoscope fluorescein angiography. *Invest Ophthalmol Vis Sci* 2016; 57: OCT130-OCT140.
- Bedggood P, Metha A. Analysis of contrast and motion signals generated by human blood constituents in capillary flow. *Opt Lett* 2014; 39: 610-613.
- Bedggood P, Daaboul M, Ashman RA et al. Characteristics of the human isoplanatic patch and implications for adaptive optics retinal imaging. *J Biomed Opt* 2008; 13: 024008.
- Liang J, Williams DR, Miller DT. Supernormal vision and high-resolution retinal imaging through adaptive optics. *J Opt Soc Am A* 1997; 14: 2884-2892.
- Roorda A, Williams DR. The arrangement of the three cone classes in the living human eye. *Nature* 1999; 397: 520.
- Tam J, Martin JA, Roorda A. Noninvasive visualization and analysis of parafoveal capillaries in humans. *Invest Ophthalmol Vis Sci* 2010; 51: 1691-1698.
- Chui TY, Zhong Z, Song H et al. Foveal avascular zone and its relationship to foveal pit shape. *Optom Vis Sci* 2012; 89: 602.
- Bedggood P, Metha A. Mapping flow velocity in the human retinal capillary network with pixel intensity cross correlation. *PLoS One* 2019; 14: e0218918.



28. Chui TY, VanNasdale DA, Burns SA. The use of forward scatter to improve retinal vascular imaging with an adaptive optics scanning laser ophthalmoscope. *Biomed Opt Express* 2012; 3: 2537–2549.
29. Chui TY, Gast TJ, Burns SA. Imaging of vascular wall fine structure in the human retina using adaptive optics scanning laser ophthalmoscopy. *Invest Ophthalmol Vis Sci* 2013; 54: 7115–7124.
30. Sulai YN, Scoles D, Harvey Z et al. Visualization of retinal vascular structure and perfusion with a nonconfocal adaptive optics scanning light ophthalmoscope. *J Opt Soc Am A* 2014; 31: 569–579.
31. Sapoznik KA, Luo T, De Castro A et al. Enhanced retinal vasculature imaging with a rapidly configurable aperture. *Biomed Opt Express* 2018; 9: 1323–1333.
32. Gofas-Salas E, Mece P, Mugnier L et al. Near infrared adaptive optics flood illumination retinal angiography. *Biomed Opt Express* 2019; 10: 2730–2743.
33. Martin JA, Roorda A. Pulsatility of parafoveal capillary leukocytes. *Exp Eye Res* 2009; 88: 356–360.
34. Tam J, Roorda A. Speed quantification and tracking of moving objects in adaptive optics scanning laser ophthalmoscopy. *J Biomed Opt* 2011; 16: 036002.
35. Martin JA, Roorda A. Direct and noninvasive assessment of parafoveal capillary leukocyte velocity. *Ophthalmology* 2005; 112: 2219–2224.
36. Arichika S, Uji A, Hangai M et al. Noninvasive and direct monitoring of erythrocyte aggregates in human retinal microvasculature using adaptive optics scanning laser ophthalmoscopy. *Invest Ophthalmol Vis Sci* 2013; 54: 4394–4402.
37. Guevara-Torres A, Joseph A, Schallek J. Label free measurement of retinal blood cell flux, velocity, hematocrit and capillary width in the living mouse eye. *Biomed Opt Express* 2016; 7: 4228–4249.
38. Joseph A, Guevara-Torres A, Schallek J. Imaging single-cell blood flow in the smallest to largest vessels in the living retina. *Elife* 2019; 8: e45077.
39. Bedggood P, Metha A. Direct visualization and characterization of erythrocyte flow in human retinal capillaries. *Biomed Opt Express* 2012; 3: 3264–3277.
40. Gu B, Wang X, Twa MD et al. Noninvasive in vivo characterization of erythrocyte motion in human retinal capillaries using high-speed adaptive optics near-confocal imaging. *Biomed Opt Express* 2018; 9: 3653–3677.
41. de Castro A, Huang G, Sawides L et al. Rapid high resolution imaging with a dual-channel scanning technique. *Opt Lett* 2016; 41: 1881–1884.
42. Gorczynska I, Migacz JV, Zawadzki RJ et al. Comparison of amplitude-decorrelation, speckle-variance and phase-variance OCT angiography methods for imaging the human retina and choroid. *Biomed Opt Express* 2016; 7: 911–942.
43. Salas M, Augustin M, Ginner L et al. Visualization of micro-capillaries using optical coherence tomography angiography with and without adaptive optics. *Biomed Opt Express* 2017; 8: 207–222.
44. Zawadzki RJ, Choi SS, Jones SM et al. Adaptive optical coherence tomography: optimizing visualization of microscopic retinal structures in three dimensions. *J Opt Soc Am A* 2007; 24: 1373–1383.
45. Kurokawa K, Liu Z, Miller DT. Adaptive optics optical coherence tomography for morphometric analysis of choriocapillaris. *Biomed Opt Express* 2017; 8: 1803–1822.
46. Liu Z, Tam J, Saeedi O et al. Trans-retinal cellular imaging with multimodal adaptive optics. *Biomed Opt Express* 2018; 9: 4246–4262.
47. Hillmann D, Spahr H, Hain C et al. Aberration-free volumetric high-speed imaging of in vivo retina. *Sci Rep* 2016; 6: 35209.
48. Rizzoni D, Agabiti-Rosei E. Structural abnormalities of small resistance arteries in essential hypertension. *Intern Emerg Med* 2012; 7: 205–212.
49. Koch E, Rosenbaum D, Broly A et al. Morphometric analysis of small arteries in the human retina using adaptive optics imaging: relationship with blood pressure and focal vascular changes. *J Hypertens* 2014; 32: 890.
50. Meixner E, Michelson G. Measurement of retinal wall-to-lumen ratio by adaptive optics retinal camera: a clinical research. *Graefes Arch Clin Exp Ophthalmol* 2015; 253: 1985–1995.
51. Arichika S, Uji A, Ooto S et al. Effects of age and blood pressure on the retinal arterial wall, analyzed using adaptive optics scanning laser ophthalmoscopy. *Sci Rep* 2015; 5: 12283.
52. Rosenbaum D, Kachenoura N, Koch E et al. Relationships between retinal arteriole anatomy and aortic geometry and function and peripheral resistance in hypertensives. *Hypertens Res* 2016; 39: 536.
53. Hillard JG, Gast TJ, Chui TY et al. Retinal arterioles in hypo-, normo-, and hypertensive subjects measured using adaptive optics. *Transl Vis Sci Technol* 2016; 5: 16.
54. Rosenbaum D, Mattina A, Koch E et al. Effects of age, blood pressure and antihypertensive treatments on retinal arterioles remodeling assessed by adaptive optics. *J Hypertens* 2016; 34: 1115–1122.
55. Burgansky-Eliash Z, Barak A, Barash H et al. Increased retinal blood flow velocity in patients with early diabetes mellitus. *Retina* 2012; 32: 112–119.
56. Burns SA, Elsner AE, Chui TY et al. In vivo adaptive optics microvascular imaging in diabetic patients without clinically severe diabetic retinopathy. *Biomed Opt Express* 2014; 5: 961–974.
57. Lombardo M, Parravano M, Serrao S et al. Analysis of retinal capillaries in patients with type 1 diabetes and nonproliferative diabetic retinopathy using adaptive optics imaging. *Retina* 2013; 33: 1630–1639.
58. Sherman TF. On connecting large vessels to small. The meaning of Murray's law. *J Gen Physiol* 1981; 78: 431–453.
59. Luo T, Gast TJ, Vermeer TJ et al. Retinal vascular branching in healthy and diabetic subjects. *Invest Ophthalmol Vis Sci* 2017; 58: 2685–2694.
60. Tam J, Dhamdhare KP, Tiruveedhula P et al. Disruption of the retinal parafoveal capillary network in type 2 diabetes before the onset of diabetic retinopathy. *Invest Ophthalmol Vis Sci* 2011; 52: 9257–9266.
61. Dubow M, Pinhas A, Shah N et al. Classification of human retinal microaneurysms using adaptive optics scanning light ophthalmoscope fluorescein angiography. *Invest Ophthalmol Vis Sci* 2014; 55: 1299–1309.
62. Lammer J, Karst SG, Lin MM et al. Association of Microaneurysms on adaptive optics scanning laser ophthalmoscopy with surrounding Neuroretinal pathology and visual function in diabetes. *Invest Ophthalmol Vis Sci* 2018; 59: 5633–5640.
63. Chui TYP, Pinhas A, Gan A et al. Longitudinal imaging of microvascular remodelling in proliferative diabetic retinopathy using adaptive optics scanning light ophthalmoscopy. *Ophthalmic Physiol Opt* 2016; 36: 290–302.
64. Chui TY, Mo S, Krawitz B et al. Human retinal microvascular imaging using adaptive optics scanning light ophthalmoscopy. *Int J Retina Vitreous* 2016; 2: 11.
65. Nunes S, Pires I, Rosa A et al. Microaneurysm turnover is a biomarker for diabetic retinopathy progression to clinically significant macular edema: findings for type 2 diabetics with nonproliferative retinopathy. *Ophthalmologica* 2009; 223: 292–297.
66. Schreier V, Domanian A, Liefers B et al. Morphological and topographical appearance of microaneurysms on optical coherence tomography angiography. *Br J Ophthalmol* 2019; 103: 630–635.
67. Fu X, Gens JS, Glazier JA et al. Progression of diabetic capillary occlusion: a model. *PLoS Comput Biol* 2016; 12: e1004932.
68. Bernabeu MO, Lu Y, Abu-Qamar O et al. Estimation of diabetic retinal microaneurysm perfusion parameters based on computational fluid dynamics modeling of adaptive optics scanning laser ophthalmoscopy. *Front Physiol* 2018; 9: 989.
69. Lu Y, Bernabeu MO, Lammer J et al. Computational fluid dynamics assisted characterization of parafoveal hemodynamics in normal and diabetic eyes using adaptive optics scanning laser ophthalmoscopy. *Biomed Opt Express* 2016; 7: 4958–4973.
70. Karst SG, Lammer J, Radwan SH et al. Characterization of in vivo retinal lesions of diabetic retinopathy using adaptive optics scanning laser ophthalmoscopy. *Int J Endocrinol* 2018; 2018: 7492946.
71. Paques M, Meimon S, Rossant F et al. Adaptive optics ophthalmoscopy: application to age-related macular degeneration and vascular diseases. *Prog Retin Eye Res* 2018; 66: 1–16.
72. Paques M, Broly A, Benesty J et al. Venous nicking without arteriovenous contact: the role of the arteriolar microenvironment in arteriovenous nickings. *JAMA Ophthalmol* 2015; 133: 947–950.
73. Errera M-H, Coisy S, Fardeau C et al. Retinal vasculitis imaging by adaptive optics. *Ophthalmology* 2014; 121: 1311–1312.e2.
74. McLeod DS, Grebe R, Bhutto I et al. Relationship between RPE and choriocapillaris in age-related macular degeneration. *Invest Ophthalmol Vis Sci* 2009; 50: 4982–4991.
75. Zhong Z, Song H, Chui TYP et al. Noninvasive measurements and analysis of blood velocity profiles in human retinal vessels. *Invest Ophthalmol Vis Sci* 2011; 52: 4151–4157.
76. Baskurt OK, Meiselman HJ. Erythrocyte aggregation: basic aspects and clinical importance. *Clin Hemorheol Microcirc* 2013; 53: 23–37.
77. Arichika S, Uji A, Ooto S et al. Adaptive optics-assisted identification of preferential erythrocyte aggregate pathways in the human retinal microvasculature. *PLoS One* 2014; 9: e89679.
78. Arichika S, Uji A, Murakami T et al. Retinal hemorheologic characterization of early-stage diabetic retinopathy using adaptive optics scanning laser ophthalmoscopy. *Invest Ophthalmol Vis Sci* 2014; 55: 8513–8522.
79. Trip MD, Cats VM, van Capelle FJ et al. Platelet hyperreactivity and prognosis in survivors of myocardial infarction. *N Engl J Med* 1990; 322: 1549–1554.
80. Nesbitt WF, Westein E, Tovar-Lopez FJ et al. A shear gradient-dependent platelet aggregation mechanism drives thrombus formation. *Nat Med* 2009; 15: 665.
81. Pinhas A, Razeen M, Dubow M et al. Assessment of perfused foveal microvascular density and identification of nonperfused capillaries in healthy and vasculopathic eyes. *Invest Ophthalmol Vis Sci* 2014; 55: 8056–8066.
82. Tam J, Dhamdhare KP, Tiruveedhula P et al. Subclinical capillary changes in non proliferative diabetic retinopathy. *Optom Vis Sci* 2012; 89: E692.
83. Chandrasekera E, An D, McAllister IL et al. Three-dimensional microscopy demonstrates series and parallel Organization of Human Peripapillary Capillary Plexuses. *Invest Ophthalmol Vis Sci* 2018; 59: 4327–4344.
84. Mattace-Raso FU, van der Cammen TJ, Hofman A et al. Arterial stiffness and risk of coronary heart disease and stroke. *Circulation* 2006; 113: 657–663.
85. Li Q, Li L, Fan S et al. Retinal pulse wave velocity measurement using spectral-domain optical coherence tomography. *J Biophoton* 2018; 11: e201700163.
86. Spahr H, Hillmann D, Hain C et al. Imaging pulse wave propagation in human retinal vessels using full-field swept-source optical coherence tomography. *Opt Lett* 2015; 40: 4771–4774.
87. Lu J, Gu B, Wang X et al. Adaptive optics parallel near-confocal scanning ophthalmoscopy. *Opt Lett* 2016; 41: 3852–3855.
88. Alibhai AY, Moulton EM, Shahzad R et al. Quantifying microvascular changes using OCT angiography in diabetic eyes without clinical evidence of retinopathy. *Ophthalmol Retina* 2018; 2: 418–427.
89. Wangsa-Wirawan ND, Linsenmeier RA. Retinal oxygen: fundamental and clinical aspects. *Arch Ophthalmol* 2003; 121: 547–557.
90. Riva CE, Logean E, Falsini B. Visually evoked hemodynamic response and assessment of

- neurovascular coupling in the optic nerve and retina. *Prog Retin Eye Res* 2005; 24: 183–215.
91. Zhong Z, Huang G, Chui TYP et al. Local flicker stimulation evokes local retinal blood velocity changes. *J Vis* 2012; 12: 3.
92. Duan A, Bedggood PA, Bui BV et al. Evidence of flicker-induced functional hyperaemia in the smallest vessels of the human retinal blood supply. *PLoS One* 2016; 11: e0162621.
93. Duan A, Bedggood PA, Metha AB et al. Reactivity in the human retinal microvasculature measured during acute gas breathing provocations. *Sci Rep* 2017; 7: 2113.

# The influence of orthokeratology compression factor on ocular higher-order aberrations

*Clin Exp Optom* 2020; 103: 123–128

DOI:10.1111/cxo.12933

Jason K Lau\*  BOptom  
Stephen J Vincent†  PhD  
Sin-Wan Cheung\* PhD  
Pauline Cho\* PhD

\*Centre for Myopia Research, School of Optometry,  
The Hong Kong Polytechnic University, Hong Kong  
Special Administrative Region, China

†Contact Lens and Visual Optics Laboratory, School of  
Optometry and Visual Science, Queensland University  
of Technology, Brisbane, Queensland, Australia  
E-mail: kklau@polyu.edu.hk

**Background:** To investigate the influence of compression factor upon changes in ocular higher-order aberrations (HOAs) in young myopic children undergoing orthokeratology treatment.

**Methods:** Subjects aged between six and < 11 years, with low myopia (0.50–4.00 D inclusive), low astigmatism ( $\leq 1.25$  D), and anisometropia ( $\leq 1.00$  D), were randomly assigned to wear orthokeratology lenses of different compression factors in each eye (one eye 0.75 D and the fellow eye 1.75 D). HOAs were measured weekly over one month of lens wear. Wavefront analysis was conducted over a 5-mm pupil using a sixth order Zernike polynomial expansion. Linear mixed models were used to examine the individual Zernike coefficients and specific root-mean-square (RMS) error (spherical, comatic, total HOAs) metrics and their changes between the two eyes during the study period.

**Results:** Twenty-eight myopic (mean manifest spherical equivalent refraction:  $-2.10 \pm 0.58$  D) children (median [range] age: 9.3 [7.8–11.0] years) were analysed. Significant interocular differences in HOAs at baseline were observed for  $Z_6^{-6}$  and  $Z_6^{-4}$  only (both  $p < 0.05$ ). During the lens wear period, eyes fitted with the increased compression factor showed greater changes in primary spherical aberration ( $Z_4^0$ ,  $p = 0.04$ ) and RMS values for spherical and total HOAs (both  $p < 0.01$ ). Considering data from both eyes together, after adjusting for the paired nature of the data, some other Zernike terms ( $Z_3^1$  and  $Z_6^0$ , both  $p < 0.01$ ) and the RMS value of comatic aberrations ( $p < 0.001$ ) significantly increased after one month of orthokeratology treatment. The increase in primary spherical aberration ( $Z_4^0$ ) was positively correlated with the reduction in spherical equivalent refractive error, but only in eyes fitted with the increased compression factor ( $r = 0.69$ ,  $p < 0.001$ ).

**Conclusions:** Increasing the orthokeratology compression factor by 1.00 D significantly altered some HOAs, particularly spherical aberration. Given the association between positive spherical aberration and eye growth in children, further research investigating the influence of orthokeratology compression factor on axial eye growth is warranted.

Submitted: 16 March 2019

Revised: 20 May 2019

Accepted for publication: 21 May 2019

**Key words:** compression factor, higher-order aberrations, orthokeratology

Orthokeratology is an established treatment for paediatric myopia control<sup>1–3</sup> and is popular among both practitioners<sup>4</sup> and parents.<sup>5,6</sup> It utilises reverse geometry rigid gas permeable lenses worn overnight which flatten the central cornea and steepen the mid-peripheral cornea,<sup>7</sup> resulting in daytime myopia correction and provides children with an increased quality of life due to improved unaided vision and convenience.<sup>5,6</sup> However, upon lens removal in the morning, the induced corneal changes begin to regress and may result in approximately 0.50–0.75 D under-correction toward the end of the day.<sup>8–11</sup> Therefore, most orthokeratology lens manufacturers incorporate an extra

correcting factor, known as the compression factor (that is, the Jessen factor), in addition to the correction for myopia, to counteract this refractive regression to ensure good unaided vision and patient satisfaction throughout the entire day.

Despite the use of a conventional compression factor (0.75 D), under-correction of myopia (of about 0.50–0.75 D) has been reported<sup>10–13</sup> and researchers have postulated that the correcting factor was most likely underestimated. Chan et al.<sup>14</sup> analysed the refractive outcome of their myopic children and suggested that an additional 1.00 D should be incorporated (that is, a 1.75 D compression factor) to achieve

full correction; however, currently no studies have investigated the feasibility, safety, or optical outcomes of increasing the compression factor by 1.00 D in children.

As the corneal shape is altered during orthokeratology treatment, both corneal and ocular aberrations, primarily spherical and comatic aberrations, significantly increase.<sup>15–21</sup> Hiraoka et al.<sup>22</sup> investigated the correlations between ocular aberrations and axial elongation in 55 children (mean age:  $10.3 \pm 1.4$  years) undergoing orthokeratology treatment for one year and showed that children with greater increases in the root-mean-square (RMS) error values for spherical, comatic, and total higher-order aberrations (HOAs) exhibited slower

axial eye growth. Theoretically, a greater change in HOAs should be induced during orthokeratology treatment when the amount of myopia corrected is higher, as a greater change in corneal shape is necessary to achieve the desired refractive correction (that is, more reduction in corneal sphericity).<sup>23</sup>

Kang et al.<sup>24</sup> attempted to alter corneal HOAs by changing the optic zone diameter (from 6 mm to 5 mm) and the peripheral tangent (from  $\frac{1}{4}$  to  $\frac{1}{2}$ ) while controlling for lens centration and refractive correction; however, no significant difference in spherical aberration ( $Z_4^0$ ) was found. Chen et al.<sup>25</sup> also hypothesised that modifying the lens diameter may be useful to alter the HOA profile, particularly vertical coma, but to date no studies have systematically examined the effect of total lens diameter on the changes induced in corneal optics.

The aim of this study was therefore to compare the changes in ocular HOAs in young myopic children wearing orthokeratology lenses of different compression factors in the two eyes over a one-month period.

## Methods

### Study design

This was a double-blind, contralateral, self-controlled study investigating the effect of different orthokeratology compression factors (0.75 D and 1.75 D) on the changes in ocular HOAs. The procedures followed the Declaration of Helsinki and the study was approved by the Departmental Research Committee of the School of Optometry at The Hong Kong Polytechnic University. Informed consent of the parents was obtained after thorough explanation of the nature and possible consequences of the study. The study was registered at ClinicalTrials.gov (NCT02643875).

### Subjects

Chinese subjects aged between six and < 11 years, with low myopia (0.50–4.00 D), low astigmatism ( $\leq 1.25$  D), and anisometropia  $\leq 1.00$  D, were recruited. Those with high corneal toricity ( $\geq 2.00$  D), a history of previous myopia control treatments, any ocular or systemic diseases that may affect refractive development or contact lens wear, or were non-compliant with lens wear or related procedures, were excluded. Lenses were only ordered if the subjects demonstrated good lens-handling skills.

### Lenses and solutions

Four-zone orthokeratology lenses (Menicon Z Night or Menicon Z Night Toric lenses; NKL Contactlinsen B.V., Emmen, The Netherlands) with a Dk of 163 (ISO unit) were used. Either spherical or toric lenses, based on the manufacturer's software (Easyfit, version 2013; NKL Contactlinsen B.V.), were fitted to each subject (that is, the same lens design was used for both eyes). An extra 1.00 D was added to the target for myopia correction in eyes randomised to wear the increased compression factor (1.75 D) lens, while the fellow eyes wore lenses with the default compression factor of 0.75 D.

Subjects were required to wear the lenses every night, and to perform daily cleaning and disinfection and weekly protein removal procedures (cleaning: Menicon Spray and Clean; rinsing: Ophthecs cleadew; disinfection: Menicare Plus; protein removal: Menicon Progent). Artificial tears (Precilens Aquadrop+) were also provided to avoid bubbles trapped underneath the lens and facilitate lens removal when necessary.

### Examination visits

Lenses were delivered at the baseline visit and subsequent weekly data collection visits over one month were scheduled at a similar time of day ( $\pm$ two hours) to avoid the potential influence of diurnal variation on outcome measures. The early morning visit (within two hours after waking) after the first overnight lens wear and any additional unscheduled visits were arranged when necessary to maintain good vision and ocular health throughout the study period.

### Data collection

High-contrast visual acuity (Early Treatment Diabetic Retinopathy Study charts, 90 per cent contrast; Precision Vision, Woodstock, IL, USA), non-cycloplegic subjective refraction, slit-lamp biomicroscopy, and Medmont corneal topography were conducted at each visit to monitor lens performance, ocular health, and vision. External ocular health conditions were graded according to the Efron grading system.

Ocular HOAs were measured from each eye using a Shack-Hartmann aberrometer (COAS; Wavefront Sciences Ltd., Albuquerque, NM, USA) through natural pupils under scotopic conditions (five lux) with the fellow eye occluded. A Badal optometer,<sup>26</sup> mounted on the COAS machine, was set with the spherical equivalent refraction of the subject to control for accommodation. For each eye,

125 measurements of monochromatic HOAs were acquired (555 nm wavelength), and later averaged.

### Wavefront analysis

The wavefront data acquired from COAS was fitted with a sixth order polynomial and the Zernike co-efficients were rescaled to a 5-mm pupil through interpolation. The RMS of spherical ( $Z_4^0$  and  $Z_6^0$  combined), comatic ( $Z_3^{-1}$ ,  $Z_3^1$ ,  $Z_5^{-1}$ , and  $Z_5^1$  combined), and total HOAs (from third to sixth radial orders, inclusive) were also calculated. The signs of Zernike terms ( $Z_3^1$ ,  $Z_3^3$ ,  $Z_4^{-4}$ ,  $Z_4^{-2}$ ,  $Z_5^1$ ,  $Z_5^3$ ,  $Z_5^5$ ,  $Z_6^{-6}$ ,  $Z_6^{-4}$ , and  $Z_6^{-2}$ ) for the left eyes were reversed to account for enantiomorphism (mirror symmetry) between the two eyes.<sup>27,28</sup>

### Sample size determination

The sample size was calculated with G\*Power (version 3.1.9.2; Kiel University, Kiel, Germany) based on the average apical corneal power difference anticipated between the two eyes during orthokeratology treatment. A minimum interocular difference of 0.50 D was expected with a within-subject standard deviation of 0.70 D.<sup>18</sup> Therefore, a minimum of 18 subjects were required to provide 80 per cent power to detect a significant difference with an alpha level of 0.05.

### Statistical analyses

All statistical analyses were performed using SPSS version 23 (IMB Corp., Armonk, NY, USA). The normality of the baseline demographics, ocular HOA Zernike co-efficients, and their changes at the one-month visit were checked with Shapiro-Wilk tests. Paired t-tests or Wilcoxon tests, where appropriate, were used to compare the baseline differences or changes (at the one-month visit) between eyes. Linear mixed models were used to assess the effect of different compression factors on HOAs over time, with restricted maximum likelihood estimation and a first-order autoregressive covariance structure.

Estimated marginal means, adjusted with Bonferroni corrections, are presented for significant between-eye differences; otherwise, the results are presented considering both eyes together, after adjustment for paired-eye data. Changes in the Zernike co-efficients and RMS values from baseline at each visit were also compared between the two eyes using paired t-tests or equivalent (for significant terms in the linear mixed

models). Pearson or Spearman correlations, when appropriate, were then used to assess the associations between changes in these Zernike co-efficients and changes in spherical equivalent refraction. A p-value of less than 0.05 was considered statistically significant.

## Results

Thirty-six subjects were randomised and completed the baseline data collection. However, eight subjects were excluded due to failure to adapt to lens wear (one), broken lens (one), poor vision (one), and loss to follow-up (two). An additional three subjects were excluded because of a poor lens fit, leaving 28 subjects included in the final analyses, consisting of 12 boys and 16 girls, with median (range) age of 9.3 (7.8–11.0) years. Eighteen subjects were fitted with spherical lenses and 10 with toric lenses.

Table 1 displays the mean baseline visual acuities, refraction, and ocular HOAs for the two eyes. There were no significant baseline interocular differences for refraction, unaided visual acuities, or best-corrected visual acuities (all  $p > 0.05$ ). Significant interocular differences were observed at the baseline visit for some higher-order Zernike terms ( $Z_6^{-6}$  and  $Z_6^{-4}$ , both  $p < 0.05$ ).

### Effect of compression factor

After one week of lens wear, eyes fitted with the increased compression factor showed a greater initial refractive reduction than the fellow eyes by  $0.44 \pm 0.66$  D ( $p = 0.001$ ). However, this difference diminished with time (mean differences: week two:  $0.39 \pm 0.65$  D, week three:  $0.31 \pm 0.54$  D; both  $p < 0.01$ ), with no significant difference in refractive correction observed between the eyes at the one-month visit (mean spherical equivalent reduction: increased compression factor:  $2.58 \pm 0.89$  D, conventional compression factor:  $2.36 \pm 0.83$  D; mean difference:  $0.22 \pm 0.68$  D,  $p = 0.10$ ).

Figure 1 shows the changes in Zernike co-efficients and RMS values with significant differences between the two eyes during the study period. Eyes fitted with the increased compression factor showed a significantly greater increase in primary spherical aberration ( $Z_4^0$ , mean difference:  $0.089 \pm 0.139 \mu\text{m}$ ,  $p = 0.002$ ), the RMS of spherical aberrations (mean difference:  $0.094 \pm 0.120 \mu\text{m}$ ,  $p < 0.001$ ) and total HOAs (mean difference:

	Compression factor		p-value
	1.75 D	0.75 D	
Visual acuities, logMAR			
Unaided	0.63 ± 0.29	0.65 ± 0.31	0.387 <sup>†</sup>
Best-corrected	0.00 ± 0.04	0.00 ± 0.05	0.678 <sup>†</sup>
Refraction, D			
Myopia	-2.09 ± 0.97	-2.12 ± 0.94	0.714 <sup>†</sup>
Astigmatism	-0.50 (-1.25, 0.00)	0.00 (-1.25, 0.00)	0.080 <sup>‡</sup>
SER	-2.30 ± 1.03	-2.27 ± 0.99	0.646 <sup>†</sup>
Individual Zernike terms, $\mu\text{m}$			
$Z_3^{-3}$	0.025 ± 0.080	0.012 ± 0.071	0.327 <sup>†</sup>
$Z_3^{-1}$	-0.019 ± 0.114	0.000 ± 0.113	0.185 <sup>†</sup>
$Z_3^1$	0.002 (-0.094, 0.110)	-0.013 (-0.104, 0.083)	0.425 <sup>‡</sup>
$Z_3^3$	-0.008 ± 0.066	-0.009 ± 0.059	0.938 <sup>†</sup>
$Z_4^{-4}$	0.022 ± 0.022	0.020 ± 0.025	0.604 <sup>†</sup>
$Z_4^{-2}$	-0.014 (-0.030, 0.026)	-0.006 (-0.039, 0.027)	0.053 <sup>‡</sup>
$Z_4^0$	0.057 (-0.019, 0.212)	0.067 (-0.020, 0.376)	0.633 <sup>‡</sup>
$Z_4^2$	-0.003 ± 0.028	-0.006 ± 0.031	0.468 <sup>†</sup>
$Z_4^4$	0.007 ± 0.022	0.013 ± 0.024	0.146 <sup>†</sup>
$Z_5^{-5}$	0.002 (-0.017, 0.038)	0.001 (-0.020, 0.031)	0.964 <sup>‡</sup>
$Z_5^{-3}$	-0.003 (-0.043, 0.020)	-0.004 (-0.070, 0.012)	0.585 <sup>‡</sup>
$Z_5^{-1}$	0.009 (-0.015, 0.069)	0.007 (-0.018, 0.035)	0.076 <sup>‡</sup>
$Z_5^1$	0.001 (-0.014, 0.013)	0.001 (-0.046, 0.011)	0.633 <sup>‡</sup>
$Z_5^3$	0.001 ± 0.005	0.002 ± 0.005	0.449 <sup>†</sup>
$Z_5^5$	0.002 (-0.015, 0.031)	0.004 (-0.013, 0.047)	0.982 <sup>‡</sup>
$Z_6^{-6}$	0.002 (-0.005, 0.009)	-0.001 (-0.012, 0.020)	<b>0.031<sup>‡</sup></b>
$Z_6^{-4}$	-0.003 ± 0.002	-0.001 ± 0.003	<b>&lt; 0.001<sup>†</sup></b>
$Z_6^{-2}$	0.000 (-0.008, 0.007)	0.000 (-0.006, 0.018)	0.274 <sup>‡</sup>
$Z_6^0$	-0.005 (-0.016, 0.026)	-0.005 (-0.016, 0.100)	0.633 <sup>‡</sup>
$Z_6^2$	-0.001 (-0.026, 0.010)	0.000 (-0.021, 0.024)	0.274 <sup>‡</sup>
$Z_6^4$	0.001 (-0.006, 0.015)	-0.001 (-0.067, 0.023)	0.106 <sup>‡</sup>
$Z_6^6$	-0.002 ± 0.004	-0.001 ± 0.006	0.330 <sup>†</sup>
Root-mean-squares (RMS), $\mu\text{m}$			
RMS SA	0.057 (0.004, 0.213)	0.068 (0.006, 0.389)	0.187 <sup>†</sup>
RMS coma	0.116 ± 0.064	0.107 ± 0.059	0.411 <sup>†</sup>
RMS HOAs	0.194 (0.102, 0.316)	0.175 (0.098, 0.536)	0.439 <sup>†</sup>

Bold value indicates statistically significant value.  
 HOA: higher-order aberrations; RMS: root-mean-square; RMS coma:  $Z_3^{-1}$ ,  $Z_3^1$ ,  $Z_5^{-1}$ , and  $Z_5^1$  combined; RMS HOAs: from third to sixth orders (inclusive); RMS SA:  $Z_4^0$  and  $Z_6^0$  combined; SA: spherical; SER: spherical equivalent refraction.  
<sup>†</sup>Paired t-test.  
<sup>‡</sup>Wilcoxon test.

**Table 1. Baseline refraction and ocular aberrations, mean ± SD or median (min, max), of the eyes fitted with different orthokeratology compression factors**

$0.147 \pm 0.176 \mu\text{m}$ ,  $p < 0.001$ ) after one week of lens wear. These terms and RMS values stabilised and no significant changes over time were observed for both eyes (all  $p > 0.05$ ). At the one-month visit, eyes fitted with the increased compression factor also

displayed greater increases in these terms and RMS values than the fellow eyes by  $0.076 \pm 0.142 \mu\text{m}$ ,  $0.083 \pm 0.124 \mu\text{m}$ , and  $0.096 \pm 0.141 \mu\text{m}$ , respectively (all  $p < 0.01$ ).

Despite the statistically significant difference in unaided visual acuities between

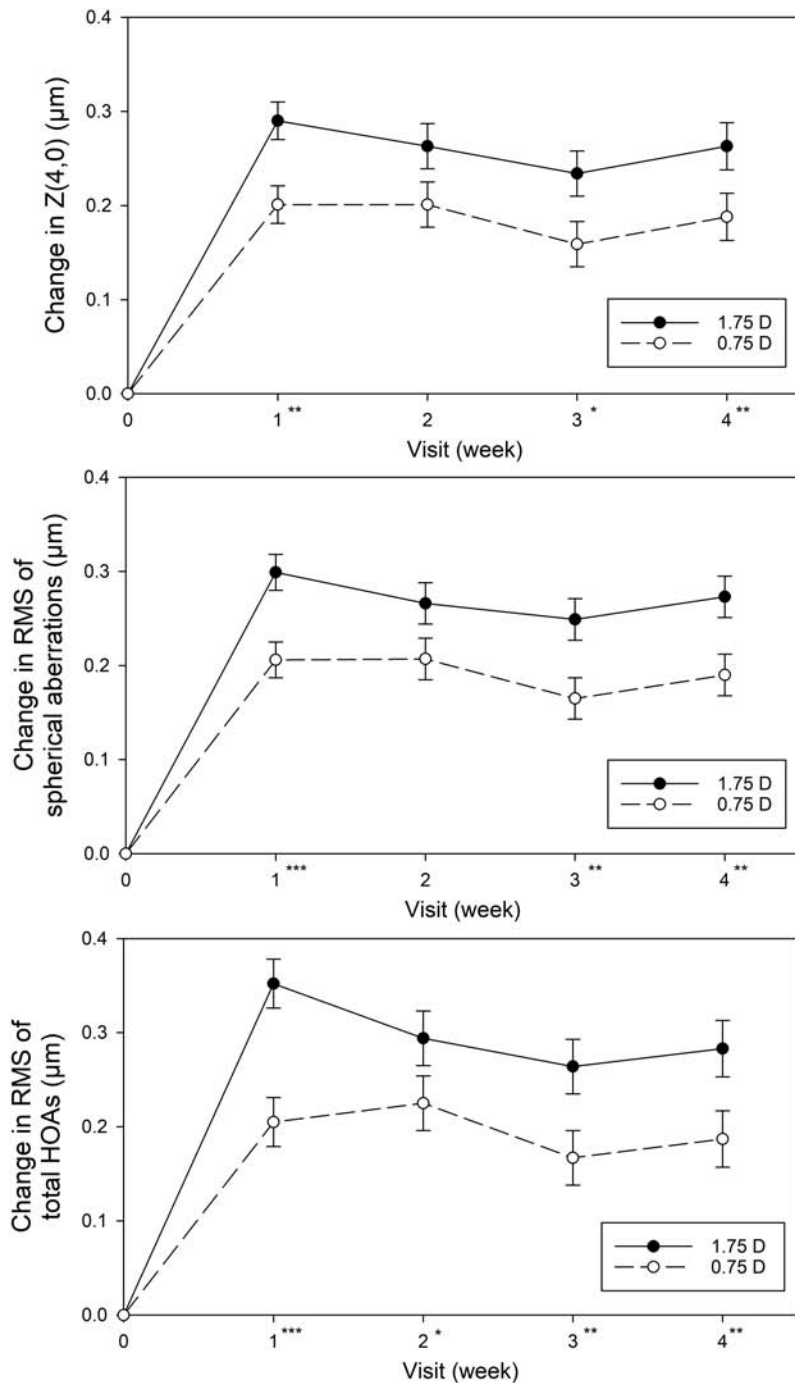


**Figure 1.** The mean change in primary spherical aberration ( $Z_4^0$ ) and root-mean-square (RMS) error for spherical aberrations and total higher-order aberrations (HOAs) in eyes fitted with orthokeratology lenses of increased compression factor (1.75 D, black circles) and conventional compression factor (0.75 D, white circles) during one-month orthokeratology lens wear. Each error bar represents one standard error of the mean. Asterisks represent significant differences between eyes (\* $p < 0.05$ ; \*\* $p < 0.01$ ; \*\*\* $p < 0.001$ ).

eyes (increased compression factor: 0.02 [-0.08 to 0.34] logMAR, conventional compression factor: -0.01 [-0.10 to 0.32] logMAR;  $p = 0.04$ ) at the one-month visit, clinically this difference was minimal (that is, 2–3 letters difference on average). There were no significant differences in best-corrected visual acuities between the two eyes (increased compression factor: -0.04 [-0.14 to 0.18] logMAR, conventional compression factor: -0.02 [-0.14 to 0.08] logMAR;  $p = 0.87$ ).

### Changes in other HOAs over time

Some other HOA terms and RMS values were also altered after orthokeratology treatment, despite no significant differences in the changes over time between the two eyes. Adjusting for using paired-eye data, after one week of lens wear, primary horizontal coma ( $Z_3^1$ ) and secondary spherical aberration ( $Z_6^0$ ) increased by  $0.117 \pm 0.116 \mu\text{m}$  and  $0.024 \pm 0.032 \mu\text{m}$ , respectively (both  $p < 0.001$ ). No further changes in these terms or significant between-eye differences were observed thereafter (all  $p > 0.05$ ). At the one-month visit, tertiary horizontal astigmatism ( $Z_6^2$ ) decreased, but the change was minimal (mean change:  $-0.012 \pm 0.016 \mu\text{m}$ ,  $p = 0.006$ ).

### Correlation analysis for primary spherical aberration ( $Z_4^0$ )

Since primary spherical aberration ( $Z_4^0$ ) was the only Zernike co-efficient (unlike unsigned RMS metrics, individual Zernike co-efficient provides directional information) found to be significant in both the linear mixed model (a significant increase during orthokeratology treatment) and higher in eyes fitted with the increased compression factor, correlation analyses were performed. Examining data from each eye separately revealed a positive association between the change in spherical equivalent refraction and the change in spherical aberration ( $Z_4^0$ ) (Figure 2). However, this relationship was only significant for the eyes fitted with the increased compression factor ( $r = 0.69$ ,  $p < 0.001$ ).

### Discussion

This is the first prospective study to examine the influence of compression factor on the changes in ocular HOAs during orthokeratology treatment. In theory, increasing



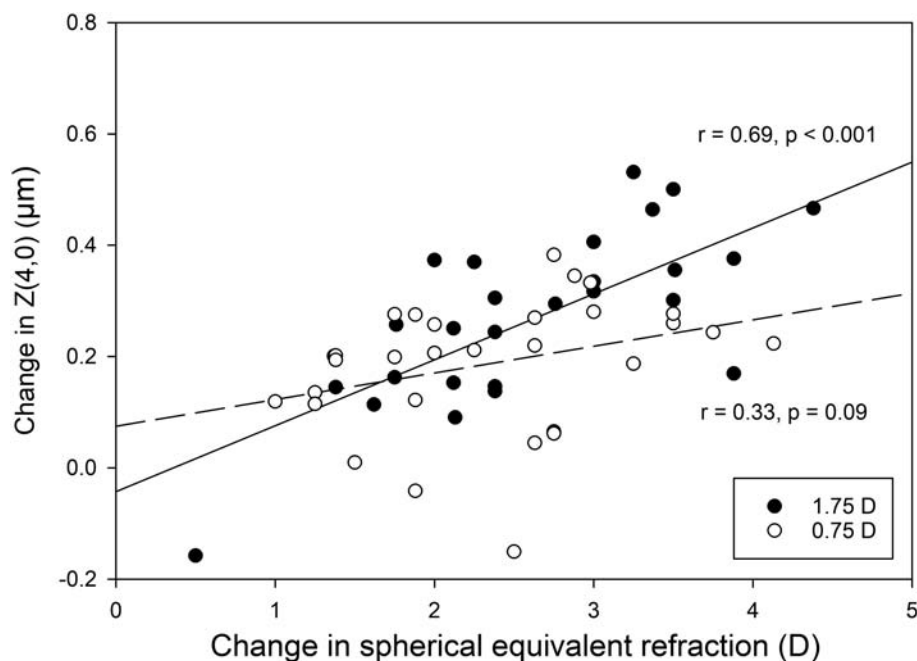


**Figure 2.** A scatter plot showing the correlation between the change in primary spherical aberration ( $Z_4^0$ ) and the change in spherical equivalent refraction for eyes fitted with orthokeratology lenses of increased compression factor (1.75 D, black circles) and conventional compression factor (0.75 D, white circles). Regression lines show the co-efficients of the Pearson correlation (1.75 D: solid line; 0.75 D: dashed line).

the compression factor by 1.00 D should lead to an increase in specific HOA terms and RMS metrics, particularly for spherical aberration, which was confirmed in this short-term study. A contralateral self-controlled design was used to provide improved control over intrinsic ocular variables of individuals, such as corneal tangent modulus,<sup>29</sup> refractive error, and the HOA profile, to minimise possible confounders.

The concept of an increased compression factor (1.75 D) was introduced in an attempt to induce additional myopic correction to negate the under-correction typically observed with the conventional compression factor (0.75 D) used by most manufacturers. However, no clinically significant effect (< 0.25 D) of compression factor on changes in corneal apical power or subjective refraction following one month of lens wear was found. Lam et al.<sup>29</sup> previously analysed the influence of corneal biomechanical properties on orthokeratology treatment outcomes and found that greater corneal flattening was associated with lower corneal hysteresis and higher tangent modulus. Since a randomised, self-controlled study

design was applied in the current study, the intrinsic corneal properties of an individual should apply equally between eyes (for example, corneal hysteresis).<sup>30</sup> The results of the current study suggest that a simple alteration of the design of the initial lens (by increasing the compression factor by 1.00 D) did not significantly alter the central subjective spherical equivalent outcome compared to the conventional compression factor. This implies that other factors (such as corneal biomechanical properties) influence the final refractive outcomes.

In addition, the changes in subjective refraction mainly reflect the image quality subjectively perceived by the individuals at the foveal region while the changes in HOAs were objectively analysed over a fixed pupil diameter (5 mm in this study), which could be a reason for the discrepancy between the magnitude of change observed in subjective refraction and ocular aberrations between the fellow eyes.

Regarding the HOAs, in the current study, eyes fitted with orthokeratology lenses of increased compression factor demonstrated more primary spherical aberration ( $Z_4^0$ ) and

higher RMS values for spherical aberrations and total HOAs after one month of lens wear as anticipated.

Only a few researchers have attempted to deliberately alter the ocular HOA profile to control myopia progression. Cheng et al.<sup>31</sup> showed that children wearing a soft contact lens with additional positive spherical aberration had 39 per cent slower axial eye growth compared to children fitted with conventional single-vision contact lenses over one year. The spherical aberration incorporated in this lens design was about 0.175  $\mu\text{m}$  over a 5-mm pupil, whereas the change in spherical aberration due to orthokeratology in the current study (both compression factors) at the one-month visit was approximately 1.4 times greater (about 0.250  $\mu\text{m}$  for a 5-mm pupil). In addition, the magnitude of the positive shift in spherical aberration in eyes fitted with the increased compression factor was 40 per cent more than those fitted with the conventional compression factor.

The relationship between HOAs and axial eye growth has recently been investigated in spectacle-wearing children.<sup>32,33</sup> Hiraoka et al.<sup>32</sup> indicated that higher levels of vertical coma ( $Z_3^{-1}$ ) and spherical aberration ( $Z_4^0$ ) were correlated with slower axial eye growth, whereas Lau et al.<sup>33</sup> demonstrated that oblique trefoil ( $Z_3^3$ ) and spherical aberration ( $Z_4^0$ ) were associated with slower axial elongation, after accounting for confounding variables.

A number of studies have also investigated the association between the changes in ocular HOAs induced by orthokeratology and axial eye growth during childhood. After one year of orthokeratology, Hiraoka et al.<sup>22</sup> observed significant correlations between axial eye growth and the changes in the RMS of spherical, comatic aberrations, and total HOAs, but not for primary spherical aberration ( $Z_4^0$ ). The authors speculated that asymmetric, rather than symmetric, changes in corneal shape might be an inhibitory factor to axial elongation in orthokeratology-treated eyes. However, their study used a simple correlation analysis, which did not account for the effect of other known contributors to eye growth, such as baseline refractive error, age, and sex. If total HOAs contribute to axial elongation in children, increasing the compression factor by 1.00 D, which significantly increased the magnitude of total HOAs and spherical aberration with minimal influence on the

refractive outcome and visual acuity, may be a potential method to increase the myopia control efficacy of orthokeratology.

While increased levels of HOAs after orthokeratology treatment are associated with decreased visual acuity, particularly in low-contrast environments,<sup>34</sup> increasing the compression factor by 1.00 D resulted in comparable unaided visual acuities between eyes wearing orthokeratology lenses of different compression factors (on average a difference of a few letters), in spite of the significant increase in some Zernike terms and total HOAs. However, visual performance was not measured under low lighting conditions in this study.

## Conclusions

Increasing the orthokeratology compression factor by 1.00 D significantly increased primary spherical aberration and the RMS values of spherical and total HOAs, but not for other Zernike co-efficients or the RMS of comatic aberrations. Given the mounting evidence of the potential influence of HOAs, particularly spherical aberration, upon axial eye growth in childhood, the authors hypothesise that increasing the compression factor of a specific lens design may improve the myopia control efficacy of orthokeratology without compromising visual performance. However, further longitudinal investigations are required before firm conclusions can be drawn.

## ACKNOWLEDGEMENTS

The authors thank Mr Kin Wan for his kind assistance in data collection. This study was supported by a collaborative research agreement between The Hong Kong Polytechnic University (PolyU) and Menicon

Co. Ltd., Japan (ZG3Z) and the Research Residency Scheme of the School of Optometry, PolyU provided to J.K. Lau. The rinsing solutions were sponsored by Ophtecs Co., Japan and the artificial tears were supported by Precilens Ltd., France, respectively.

## REFERENCES

1. Cho P, Cheung SW. Retardation of myopia in orthokeratology (ROMIO) study: a 2-year randomized clinical trial. *Invest Ophthalmol Vis Sci* 2012; 53: 7077–7085.
2. Chen C, Cheung SW, Cho P. Myopia control using toric orthokeratology (TO-SEE study). *Invest Ophthalmol Vis Sci* 2013; 54: 6510–6517.
3. Charm J, Cho P. High myopia-partial reduction ortho-k: a 2-year randomized study. *Optom Vis Sci* 2013; 90: 530–539.
4. Wolffsohn JS, Calossi A, Cho P et al. Global trends in myopia management attitudes and strategies in clinical practice. *Cont Lens Anterior Eye* 2016; 39: 106–116.
5. Cheung SW, Lam C, Cho P. Parents' knowledge and perspective of optical methods for myopia control in children. *Optom Vis Sci* 2014; 91: 634–641.
6. Hiraoka T, Okamoto C, Ishii Y et al. Patient satisfaction and clinical outcomes after overnight orthokeratology. *Optom Vis Sci* 2009; 86: 875–882.
7. Zhong Y, Chen Z, Xue F et al. Central and peripheral corneal power change in myopic orthokeratology and its relationship with 2-year axial length change. *Invest Ophthalmol Vis Sci* 2015; 56: 4514–4519.
8. Mountford J. Retention and regression of orthokeratology with time. *Int Contact Lens Clin* 1998; 25: 59–64.
9. Johnson KL, Carney LG, Mountford JA et al. Visual performance after overnight orthokeratology. *Cont Lens Anterior Eye* 2007; 30: 29–36.
10. Sorbara L, Fonn D, Simpson T et al. Reduction of myopia from corneal refractive therapy. *Optom Vis Sci* 2005; 82: 512–518.
11. Nichols JJ, Marsich MM, Nguyen M et al. Overnight orthokeratology. *Optom Vis Sci* 2000; 77: 252–259.
12. Rah MJ, Jackson JM, Jones LA et al. Overnight orthokeratology: preliminary results of the lenses and overnight Orthokeratology (LOOK) study. *Optom Vis Sci* 2002; 79: 598–605.
13. Tahhan N, Du Toit R, Papas E et al. Comparison of reverse-geometry lens designs for overnight orthokeratology. *Optom Vis Sci* 2003; 80: 796–804.
14. Chan B, Cho P, Mountford J. The validity of the Jessen formula in overnight orthokeratology: a retrospective study. *Ophthalmic Physiol Opt* 2008; 28: 265–268.
15. Hiraoka T, Matsumoto Y, Okamoto F et al. Corneal higher-order aberrations induced by overnight orthokeratology. *Am J Ophthalmol* 2005; 139: 429–436.
16. Stiltiano IG, Chalita MR, Schor P et al. Corneal changes and wavefront analysis after orthokeratology fitting test. *Am J Ophthalmol* 2007; 144: 378–386.
17. Lian Y, Shen M, Huang S et al. Corneal reshaping and wavefront aberrations during overnight orthokeratology. *Eye Contact Lens* 2014; 40: 161–168.
18. Sun Y, Wang L, Gao J et al. Influence of overnight orthokeratology on corneal surface shape and optical quality. *J Ophthalmol* 2017; 2017: 3279821.
19. Berntsen DA, Barr JT, Mitchell GL. The effect of overnight contact lens corneal reshaping on higher-order aberrations and best-corrected visual acuity. *Optom Vis Sci* 2005; 82: 490–497.
20. Gifford P, Li M, Lu H et al. Corneal versus ocular aberrations after overnight orthokeratology. *Optom Vis Sci* 2013; 90: 439–447.
21. Joslin CE, Wu SM, McMahon TT et al. Higher-order wavefront aberrations in corneal refractive therapy. *Optom Vis Sci* 2003; 80: 805–811.
22. Hiraoka T, Kakita T, Okamoto F et al. Influence of ocular wavefront aberrations on axial length elongation in myopic children treated with overnight orthokeratology. *Ophthalmology* 2015; 122: 93–100.
23. Moreno-Barriuso E, Lloves JM, Marcos S et al. Ocular aberrations before and after myopic corneal refractive surgery: LASIK-induced changes measured with laser ray tracing. *Invest Ophthalmol Vis Sci* 2001; 42: 1396–1403.
24. Kang P, Gifford P, Swarbrick H. Can manipulation of orthokeratology lens parameters modify peripheral refraction? *Optom Vis Sci* 2013; 90: 1237–1248.
25. Chen Q, Li M, Yuan Y et al. Interaction between corneal and internal ocular aberrations induced by orthokeratology and its influential factors. *Biomed Res Int* 2017; 2017: 1–8.
26. Atchison DA, Bradley A, Thibos LN et al. Useful variations of the Badal Optometer. *Optom Vis Sci* 1995; 72: 279–284.
27. Gatineau D, Delair E, Abi-Farah H et al. Distribution and enantiomorphism of higher-order ocular optical aberrations. *J Fr Ophthalmol* 2005; 28: 1041–1050.
28. Porter J, Guirao A, Cox IG et al. Monochromatic aberrations of the human eye in a large population. *J Opt Soc Am A* 2001; 18: 1793–1803.
29. Lam AK, Leung SY, Hon Y et al. Influence of short-term orthokeratology to corneal tangent modulus: a randomized study. *Curr Eye Res* 2018; 43: 474–481.
30. Vincent SJ, Collins MJ, Read SA et al. Interocular symmetry in myopic anisometropia. *Optom Vis Sci* 2011; 88: 1454–1462.
31. Cheng X, Xu J, Chehab K et al. Soft contact lenses with positive spherical aberration for myopia control. *Optom Vis Sci* 2016; 93: 353–366.
32. Hiraoka T, Kotsuka J, Kakita T et al. Relationship between higher-order wavefront aberrations and natural progression of myopia in schoolchildren. *Sci Rep* 2017; 7: 7876.
33. Lau JK, Vincent SJ, Collins MJ et al. Ocular higher-order aberrations and axial eye growth in young Hong Kong children. *Sci Rep* 2018; 8: 6726.
34. Hiraoka T, Okamoto C, Ishii Y et al. Contrast sensitivity function and ocular higher-order aberrations following overnight orthokeratology. *Invest Ophthalmol Vis Sci* 2007; 48: 550–556.

# WILEY

## **PUBLISHER**

*Clinical and Experimental Optometry* is published by John Wiley & Sons Australia, Ltd  
42 McDougall Street, Milton, QLD 4064, Australia  
Tel: +61 (0)7 3859 9755

## **Production Editor**

Simon Tan (email: [ceptom@wiley.com](mailto:ceptom@wiley.com))

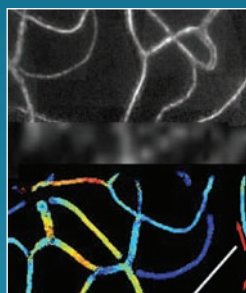
## **Copyright and Copying (in any format)**

Copyright © 2020 Optometry Australia. All rights reserved. No part of this publication may be reproduced, stored or transmitted in any form or by any means without the prior permission in writing from the copyright holder. Authorization to copy items for internal and personal use is granted by the copyright holder for libraries and other users registered with their local Reproduction Rights Organisation (RRO), e.g. Copyright Clearance Center (CCC), 222 Rosewood Drive, Danvers, MA 01923, USA ([www.copyright.com](http://www.copyright.com)), provided the appropriate fee is paid directly to the RRO. This consent does not extend to other kinds of copying such as copying for general distribution, for advertising or promotional purposes, for republication, for creating new collective works or for resale. Permissions for such reuse can be obtained using the RightsLink "Request Permissions" link on Wiley Online Library. Special requests should be addressed to: [permissions@wiley.com](mailto:permissions@wiley.com).

CLINICAL AND EXPERIMENTAL  
**OPTOMETRY**

Vol. 103 No.1 JANUARY 2020

**Visual Optics: Looking Beyond 2020 issue co-ordinated by  
Associate Professors Stephen Vincent and Scott Read**



GUEST EDITORIAL

- 1 Looking and seeing beyond 2020

INVITED REVIEWS

- 3 Modern spectacle lens design  
11 Stand magnifiers for low vision: description, prescription, assessment  
21 Correction of presbyopia: old problems with old (and new) solutions  
31 Customised aberration-controlling corrections for keratoconic patients using contact lenses  
44 Optical changes and visual performance with orthokeratology  
55 Optical mechanisms regulating emmetropisation and refractive errors: evidence from animal models  
68 Higher order aberrations, refractive error development and myopia control: a review  
86 Peripheral refraction and higher order aberrations  
95 Aberrations and accommodation  
104 Blur adaptation: clinical and refractive considerations  
112 Adaptive optics imaging of the retinal microvasculature

INVITED RESEARCH

- 123 The influence of orthokeratology compression factor on ocular higher-order aberrations

**iOS App**  
**Android App**

**Current subscribers**

Download the app from iTunes or Google Play store and log in free through your association or institution

**New subscribers**

Subscribe through the app

**Website**

[wileyonlinelibrary.com/journal/cxo](http://wileyonlinelibrary.com/journal/cxo)